Proceedings

MEA Meeting 2012

July 10 - July 13, 2012, Reutlingen, Germany

8th International Meeting on Substrate-Integrated Microelectrode Arrays

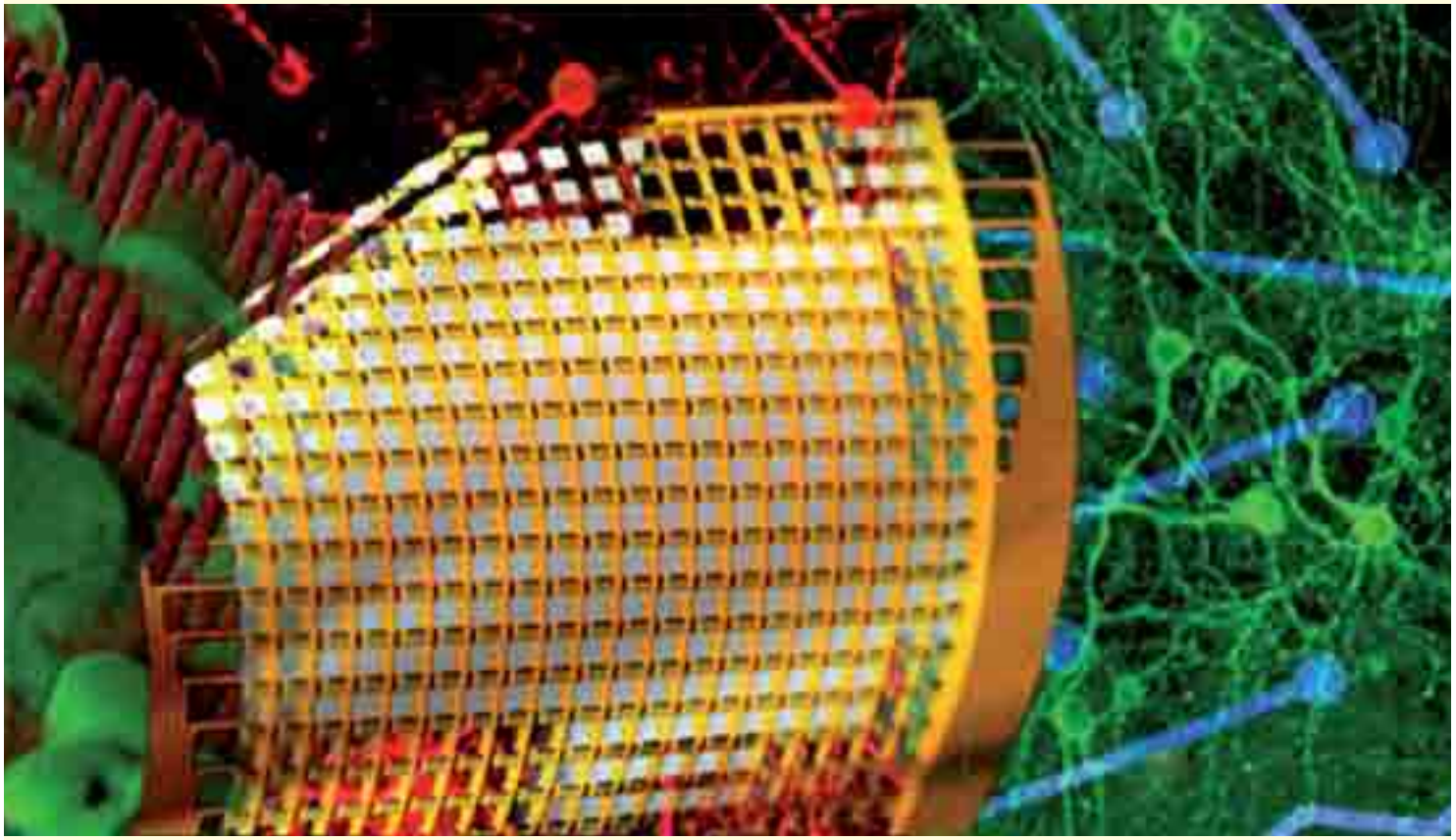

Bernstein Center Freiburg

NMI achieving results

NMI
achieving results

Benefit from your own MEA design!

NMI Natural and Medical Sciences Intsitute at the University of Tübingen

Our 25 years' experience in development and manufacturing stand us in good stead in the production of microelectrode arrays for applications in neuroscience, cardiovascular research and neurotechnology. Many publications refer to them as MCS MEAs.

>> MEAs at your option

- Application-specific and custom-made designs on glass and polyimide for *in vitro* and *in vivo* electrophysiology
- arrays with high-quality surfaces and electrodes, applied and validated by hundreds of scientists
- short time-to-application through routine production of small batches
- assured delivery of arrays with constantly-high quality, in numbers matching your needs
- layouts and electrode performance fully compatible with the Multi Channel Systems MCS hardware.

Contact
mea@nmi.de

NMI
Markwiesenstr. 55
72770 Reutlingen, Germany

Best Pictures for Cover Image

Substrate-Integrated Microelectrode Arrays:
Electrophysiological Tools for Neuroscience, Biotechnology and Biomedical Engineering

8th International Meeting on Substrate-Integrated Microelectrode Arrays, July 10 - July 13, 2012, Reutlingen, Germany

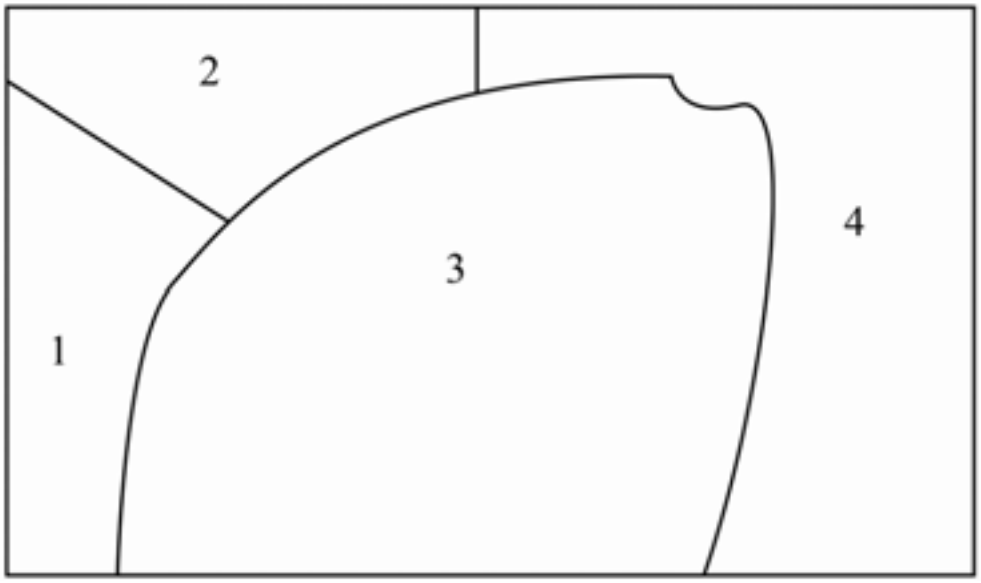

Cover images by courtesy of:

1. Roland Huys et al.: Single cell recording and stimulation using a 0.18 µm CMOS chip with 16,384 electrodes. *p. 288*
2. Tom Reimer et al.: Spontaneous activity patterns of cortical in vitro networks depend on cellular network composition. *p. 98*
3. Dae-Hyeong Kim et al.: High density micro-electrocorticography (µECoG) using flexible silicon electronics. *p. 368*
4. Tom Reimer et al.: Spontaneous activity patterns of cortical in vitro networks depend on cellular network composition. *p. 98*

Conference Proceedings of the
8th International Meeting on Substrate-Integrated Microelectrode Arrays
July 10 - July 13, 2012, Reutlingen, Germany

Meeting Organisation and Imprint

Organiser	NMI Natural and Medical Sciences Institute at the University of Tuebingen Markwiesenstrasse 55, 72770 Reutlingen, Germany Phone: +49 7121 - 51 530 -0; Fax: +49 7121 - 51 530 16; E-Mail: info@nmi.de Internet: www nmi.de
Publisher	NMI Natural and Medical Sciences Institute at the University of Tuebingen Markwiesenstrasse 55, 72770 Reutlingen, Germany Phone: +49 7121 - 51 530 -0; Fax: +49 7121 - 51 530 16; E-Mail: info@nmi.de Internet: www nmi.de
Editors	Dr. Alfred Stett and Dr. Günther Zeck
Co-organiser	Bernstein Center Freiburg Hansastraße 9, 79104 Freiburg, Germany Tel.: +49 (0)761 203 9549 ; Fax: +49 (0)761 203 9559 ; E-Mail: contact@bcf.uni-freiburg.de Internet: www.bcf.uni-freiburg.de
Organisation Team	Karla Burgert, Ira Digel, Nadja Gugeler, Priscilla Herrmann E-Mail: meameeting@nmi.de Internet: http://www.nmi.de/meameeting2012/
Scientific Programme Committee	Prof. Andreas Hierlemann, Swiss Federal Institute of Technology, Basel, Switzerland Prof. Bruce Wheeler, University of Florida, USA Prof. Cornelius Schwarz, University of Tübingen, Germany Prof. Gaute Einevoll, Norwegian University of Life Sciences (UMB) Prof. Michele Giugliano, University of Antwerp, Belgium Dr. Michela Chiappalone, Italian Institute of Technology, Genova, Italy Prof. Sven Ingebrandt, University of Applied Sciences, Kaiserslautern, Germany Prof. Sergio Martinoia, University of Genova, Italy Dr. Thomas Meyer, Multi Channel Systems MCS GmbH, Reutlingen, Germany Dr. Udo Kraushaar, NMI Natural and Medical Sciences Institute, Reutlingen, Germany Prof. Ulrich Egert, University of Freiburg, Germany Prof. Wim L.C. Rutten, University of Twente, The Netherlands Prof. Yael Hanein, Tel-Aviv University, Israel Prof. Yong S. Goo, Chungbuk National University, South Korea
Conference Chairs	Dr. Alfred Stett and Dr. Günther Zeck, NMI Natural and Medical Sciences Institute, Reutlingen, Germany
Sponsor	Multi Channel Systems MCS GmbH, Reutlingen, Germany (www.multichannelsystems.com)
Cover	MaLdesign, Büro für Gestaltung, Baltmannsweiler, Germany
Production	IVS Abele GmbH in Deizisau, Germany
ISSN	2194-5519

NMI Natural and Medical Sciences Institute at the University of Tuebingen

Bernstein Center Freiburg

Multi Channel Systems MCS GmbH

Foreword

Substrate-Integrated Microelectrode Arrays:
Electrophysiological Tools for Neuroscience, Biotechnology and Biomedical Engineering

8th International Meeting on Substrate-Integrated Microelectrode Arrays, July 10 - July 13, 2012, Reutlingen, Germany

Forty years ago, in 1972, Thomas et al. introduced the use of planar microelectrode arrays (MEAs) as a "*convenient non-destructive method for maintaining electrical contact with an individual culture, at a large number of points, over periods of days or weeks.*" [1]

Since then, the number of users is growing continuously. Thanks to the worldwide MEA community and its creative drive, a broad spectrum of applications employing MEAs has been established. Currently, 630 members subscribe to the MEA user group, the web-based scientific discussion group for MEA users[2].

Equipped with outstanding hard- and software, MEAs contribute to the unravelling of fundamental physiological functions of the brain, such as memory, learning, circadian rhythms, and neuronal development. Through MEAs, we have begun to understand cognitive diseases, such as Alzheimer's disease and epilepsy, better. Furthermore, cardiovascular, stem cell, and retina research also benefit from the advancements in MEAs. An ever increasing number of excellent scientific publications proves the maturity of MEA systems: they are now routine tools in extracellular electrophysiology and, in the pharmaceutical industry, they have been applied successfully in tests of efficacy and safety.

The broad range of applications is rooted in the broad spectrum of customized hardware. Today's electrode arrays comprise between 30 and 30,000 recording sites embedded in glass, silicon or a flexible polymer, with electrodes made of either titanium nitride, field effect transistors or futuristic carbon nanotubes.

It is again an honour and a great pleasure for the NMI and the Bernstein Center Freiburg, our co-organizer, to be able to host the eighth edition of the MEA meeting. This year we welcome more than 280 students and senior researchers, MEA developers, as well as new and experienced MEA users. Several hundred authors and co-authors from 23 countries have submitted abstracts for 28 oral and 130 poster presentations.

The topics of the meeting range from sub-cellular analyses to the newly introduced session of *in vivo* applications. Special emphasis is given to technological developments. The proceedings book offers a representative overview of current techniques and applications.

microelectrode array

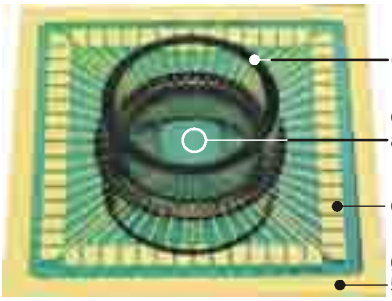

Standard Microelectrode Array (MEA). The substrate-integrated electrodes in the centre of the dish can be used both for stimulating and recording cultured cells and tissue. MEAs are being used to address numerous questions in neuroscience, neurotechnology and cardiovascular research, as well as for drug testing in the pharmaceutical industry.

A scientific committee was set up to review each of the submitted abstracts and to select the best ones for oral presentations. We would like to thank them for their support and also for selecting figures for the best-picture award. This year's cover collage reflects the application range, from cellular analysis to *in vivo* applications using flexible arrays.

We welcome you wholeheartedly to Reutlingen and we are looking forward to an exciting meeting with lively and stimulating discussions – with old and new friends and colleagues.

Enjoy the meeting!

Dr. Alfred Stett, Dr. Günther Zeck
Conference chairs, NMI, Reutlingen

Prof. Dr. Ulrich Egert
Co-Organizer, Bernstein Center Freiburg

[1] Thomas, C. A. Jr. et al. A miniature microelectrode array to monitor the bioelectric activity of cultured cells. Exp Cell Res. 1972;74(1):61-66

[2] http://tech.groups.yahoo.com/group/mea-users/

Programm at a Glance

Tuesday, July 10	
13:00 – 16:30	MEA Workshop: “Meet the Expert”-Sessions (at NMI, Reutlingen)
19:00 – 20:00	Welcome Addresses and Opening Lecture Wireless and implantable multielectrode devices interfaced to brain circuits - clinical prospects (A. Nurmikko, Brown University)
20:00	Opening Reception

Wednesday, July 11	
8:30 - 10:30	Session: New Materials and MEA Design
10:30 – 11:00	Coffee Break
11:00 – 12:20	Session: Multi-Electrode Probes for In Vivo Applications
12:20 – 14:10	Lunch Break
14:10 – 15:50	Session: Neural Dynamics and Plasticity
15:50 – 16:20	Coffee break
16:20 – 17:00	Session: Signal Analysis and Statistics
17:00 – 17:40	Session: Applications in System Neuroscience
18:30	Social event: Punt ride on the river Neckar in Tübingen

Thursday, July 12	
8:30 – 15:00	Poster Sessions
15:00 – 16:00	Coffee Break
16:00 – 17:20	Session: Heart
18:30	Social event: Conference Dinner at Urach Residential Palace

Friday, July 13	
8:30 – 10:10	Session: Electrical Stimulation
10:10 – 10:50	Coffee Break
10:50 – 12:10	Session: Pharmacology, Toxicology, and Drug Screening
12:10 – 12:30	Closing remarks
12:30	Farewell lunch

Contents

Applications in Systems Neuroscience — 111

Opening Lecture

Wireless and implantable multielectrode arrays interfaced to brain circuits

Arto V. Nurmikko[1*], Ming Yin[1], David Borton[1], and Juan Aceros[1]

1 School of Engineering, Brown University, Providence, RI , USA 02912
* Corresponding author. E-mail address: Arto_Nurmikko@brown.edu

Abstract
The development of implantable devices which enable fully wireless transmission of brain signals, recorded by microelectrode arrays (MEA) as dynamical neural circuit information, is one important goal for advancing human neuroprostheses. Current brain sensing research for prostheses via first clinical trials is offering tantalizing glimpses for the future, even if these technologies are cumbersome, percutaneous, and limited in their scalability for larger cortical coverage. Here we summarize some engineering challenges and constraints that apply to the design and fabrication of active electronic microcircuits in wireless devices, be embedded in the head area below the skin of a subject, which take their input from cortical MEAs. We demonstrate a hermetically sealed chronic, subcutaneous implant realized in our laboratories which has been implanted into mobile pigs and primates for high-speed digital, radio-frequency transmission or neural data to nearby receivers and neural decoders.

1 Overview

In this presentation we review current work where the question is addressed how to extract and electronically transport large amounts of neural data wirelessly from microelectrode arrays (MEA) to computational tools and assistive devices for a mobile disabled subject. Recent clinical trial work in tetraplegic and other seriously neurologically impaired humans [1], [2] provides the motivation for this engineering research for the emerging field of neural prosthetics. The clinical trials have culminated in demonstrations of brain (motor) control of robotic arms/hands and communication devices but have limitations due to percutaneous electronic cables which tether subjects to buly external electronics.

Here we summarize one particular approach developed in the authors‘ laboratory where an implantable compact electronic module enables the wireless transmission of the neural broadband signals captured by an intracortical MEA as a high speed digital data stream (tens of Mbits/sec) via a microwave frequency link. The module has been implanted into pigs and primates to show the performance and viability under chronic conditions. Neural broadband equates here with simultaneous acquisition over, say 100 channels of spike waveforms (action potentials at single neuron level of spatial resolution) to lower frequencies such as emanating from local field potentials (LFPs) and brain rhythms. The implant to be described below is but one example efforts by several groups to develop headmounted wireless neural interfaces for primates, most notably by Shenoy an collaborators [3-7]. Our system is distinct in several ways, including its packaging to a fully bicompatible subcutanous hermetic titanium enclosure and scalability to multiple MEAs at different cortical locations [8]. For fundamental brain science, an implanted wireless neural interfaces enable access cortical microcircuits in freely moving primates to increase our understanding of the role of dynamical brain states that guide e.g. motor planning and action.

Most present recording systems require a multiwire percutaneous connection between the MEAs and head mounted electronics to external instrumentation which restricts the subject’s mobility, present a liability for infection, and cause potential contamination of the weak electronic signals due to external noise/interference. Any wireless system that might be implanted within the body’s protective skin envelope must fulfill multiple stringent requirements for biomedical engineering and considerations. From the implantable systems point of view, challenges include ultralow-power integrated circuit design, hermetically sealed device packaging, large bandwidth wireless telemetric capability (including anticipation of 100 Mb/sec and beyond), and compatibility with surgical implantation procedures.

2 A Hermetically Sealed Implantable 100 channel Broadband Wireless Neural Interface Device

Fig.1 shows a photograph of the completed wireless neural recording prototype device. In this device, the neural 100-electrode sensor (Blackrock MEA [9]) is located at the distal end of a bundle of 100 gold wires. The proximal end of the wirebundle is connected to a hermetically sealed subcutaneous module that is implanted below the skin of the subject.

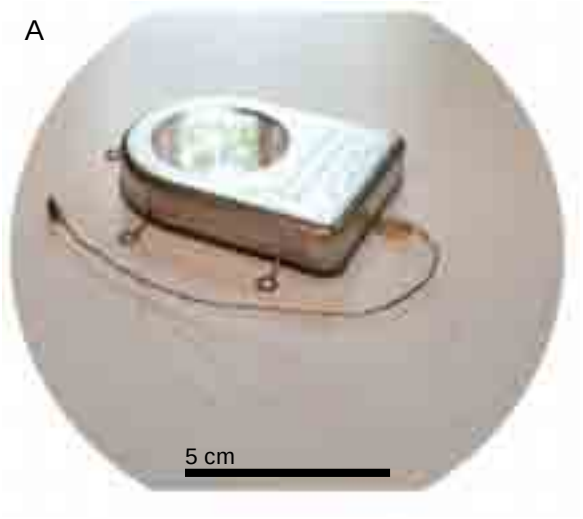

Figure 1: A wireless neural interface, hermetically sealed, MEA-microelectronic package for mobile use. (The device is placed in special holder for sterilization and transport to the operating room). The standard 10 x 10 element microelectrode array (Blackrock Microsystems) can be seen exiting the enclosure in a wirebundle.

The subcutaneous module hosts all active electronics within a two-piece titanium enclosure that is hermetically sealed by welding. The "top" section has a brazed single-crystal sapphire window for electromagnetic transparency that facilitates (i) low loss wireless transmission of RF and/or IR neural data from the device and (ii) inductively coupling wireless power into the device for recharging the embedded battery power supply. The "bottom" section of the titanium enclosure contains a high density array of Pt/Ir feedthrough pins embedded in metal-ceramic seals that can be made possible with advanced manufacturing techniques. To facilitate electrical connections from the individual wires of the gold wirebundle to the feedthroughs, a flexible Kapton parallel-interface-plate (PIP) is used to fan out the wires from the bundle onto the feedthroughs. The individual 25 μm diameter gold wires are wire bonded to PIP sites that connect by printed wiring to holes aligned with the feedthrough pins. The actual connection to the pins is made with lead-free solder. The PIP is overmolded with biocompatible silicone for protection from ionically conductive body fluids.

2.1 Fabrication and Performance Summary of the Prototype Wireless Device

The cortical signals from the MEAs enter as inputs to the Ti-enclosure where key active microelectronic integrated circuits are as follows [10]: A 100-Ch preamplifier (≈ 4 μV of RMS noise per channel) and a digital controller ASIC were fabricated in a 0.5μm 3M2P standard CMOS process and measure $5.2\times4.9mm^2$ and $2\times2mm^2$ respectively. The electronics are mounted on thin flexible circuit boards and tightly packed in the case along with a medical grade rechargeable battery. A inductively coupled coil and a onmidirectional RF chip antenna are placed directly below the sapphire window. Inductive power transfer efficiency at 5mm distance is 32%. There is less than 50% RF signal transmission loss. We note that in the prototype version, temperature increase due to charging (eddy currents in Ti-can) are a concern. The FDA mandates that a device has to meet the ISO standard requiring no outer surface of a device rise more than 2C˚ above body temperature (37C˚). We have performed finite element modeling and *in vivo* measurements to characterize heat generation. Optimizations have been implemented in the RF power link to reduce heating. The key overall electronic performance parameters of the 100-channel prototype of the broadband wireless NI implant are: Total power consumption of less than 100 mW during continuous operation, individual preamplifier noise floor of 4 μV RMS, an FSK modulated RF transmitter outputting ~ 4 mW power in the range of 3-4 GHz (with a superheterodyne custom receiver not described here). The wireless link can be designed to cover a transmission frequency range from 3.0- 4.0 GHz. The 45 gram total weight NI implant will use an approximately 250 mA-hour medical grade battery to enable one charge cycle for up to 8 hour operation. From only electronic point of view, and with the rational assumption that the system lifetime will be limited by number of battery charging cycles, operation for multiple years of continued mobile use is achievable (for >2000 recycles). We note that due to other portable consumer electronic device technologies (e.g. smartphones, iPads, PCs), there is a huge worldwide push to improve the current Li-ion based battery technologies.

2.2 In Vivo Animal Experiments in Mobile Pig and Monkey Model

The full functionality of the entire wireless neural recording system was first validated on the bench (MEA in saline with electrical injection of "pseudospike trains") and then implanted in two adult awake Yorkshire pigs and two primates, respectively. In the primates the devices have been operating over a period of about 9 months (at this writing), yielding useful neural data.

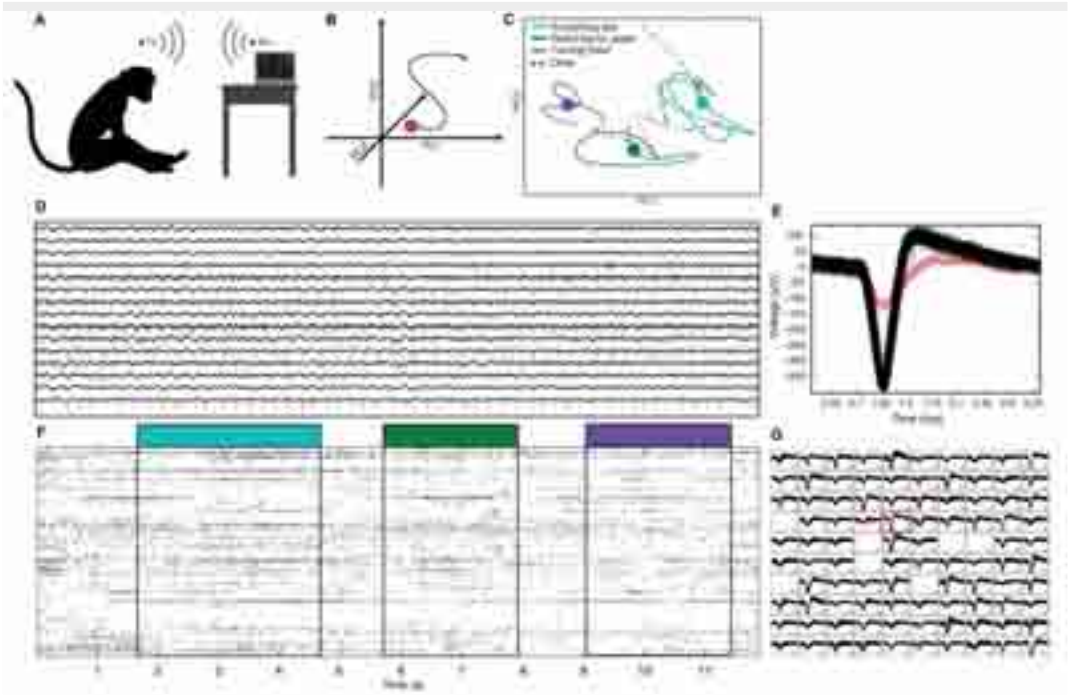

Figure 2: Wirelessly recorded 100-channel data from implanted neural interface in non-human primates. (a) A schematized depiction of a recording session in primate experiments. The implant was charged for up to one hour prior to recordings. Monkeys were then returned to their home-cage and recordings were made as the animal moved freely in its environment. Data was constantly transmitted at 3.2-3.8 GHz to a receiver for demodulation where it was then outputted to an x86 PC over USB 2.0. (b-c) Threshold crossings across multiple (all) channels can be reduced to a low-dimensional state space through principal component analysis (among others). The evolution over time of the first three dimensions of such a space is plotted, as a neural trajectory. We present such neural trajectories produced during free movement of monkey JR: scratching eye (blue), touching an apple (green) and turning head (purple). Circles represent centroids of trajectory during each movement. (d) A selection of 15/100 broadband recording channels demonstrating heterogeneity of the neural signals and the richness of high-sample rate data collection (20 Ksps). (e) Enlarged single channel showing two isolatable neurons near one microelectrode in the array. While all data analysis using APs was here performed by using "threshold crossings," it is an important characteristic of our neural interface to have the resolution and fidelity for unit isolation. (f) A raster plot (12 s) marking threshold-crossing timestamps for all input channels and behavior is indicated by color: scratching eye (blue), touching an apple (green) and turning head (purple). (g) Extracted spike, i.e. action potential (AP) waveforms from all 100 input channels or a 10x10 element microelectrode array recorded over a period of 10 s. (Blocks with no APs simply state that no single units were detected, however all 100 channels showed robust field potential modulation)

Fig. 2 demonstrates the prototype NI device's ability to record cortical spikes (as well as LFPs, β-bands etc; not shown here but used by us e.g. in ongoing studies of brain states under different anesthetic agents in monkeys), from a large fraction of total channels in a *freely moving monkey*. Neural data is streamed via the 3.2 GHz wireless link to an adjacent laptop, which detects and sorts spikes. The new NI is an advance over other externally headmounted_wireless units [2-6] given its full 100 channel continuous neural broadband recording capability, in addition to the implantable hermetically sealed Ti-enclosure.This prototype NI platform is the starting point for the BRP renewal proposal, for further advances and innovations on our path to initial human sub-acute trials, to culminate in a new class of chronic human neuroprostheses.

3 Conclusion

We have presented the prototype implementation of a 100 channel fully implantable wireless broadband neural recording system with inductively rechargeable battery and RF/IR data transfer for behavioral neuroscience research and potential brain disease diagnosis applications. The functionality of the device has been demonstrated through *in vivo* implants in pigs and primates. Robust neural spikes and LFP signals were recorded from cortical circuits. We are currently working on furthering this device approach towards transitioning in human clinical applications while continuing to testing in non-human primate models in freely moving behavioral research. Initial trials in such mobile primate brain science research have been productive and will be reported in detail elsewhere.

Acknowledgment

The authors acknowledge the role of Cirtec Medical Inc, Microconnex Inc, CV Inc, and Blackrock Microsystems Inc, in their important role for fabricating specific components of the implantable device. We thank Drs. James Barrese, Sydney Cash, Leigh Hochberg, and Moses Goddard, for their surgical and neurological expertise. We acknowledge Kineteks Inc for fabricating the sterilizable and ESD-proof holder for devices through a constructive collaboration. Many members of the Brown University Neuroengi-

neering Laboratory made key contributions: we especially thank William Patterson, Christopher Bull, and Naubahar Agha. The expertise and dedication of the staff of the Brown University Animal Care Facility was invaluable, and we thank Dr, James Harper, Veronica Budz, Roxanne Burrill, and Pamela Norberg. All animal experiments were conducted according to Institutional Animal Care and Use Committee guidelines and the USDA under protocol #0911091. This work was supported in part by the National Institute of Health (NIBIB and NCMRR/NICHD, 1R01EB007401-01), the National Science Foundation under the EFRI Program (#0937848), and DARPA Repair Program.

References

[1] Hochberg, L.R. *et al.* Reach and grasp by people with tetraplegia using a neurally controlled robotic arm. *Nature* 485, 372-375 (2012).

[2] J.D. Simeral, S.P. Kim, M.J. Black, J.P. Donoghue, and L.R. Hochberg, "Neural control of cursor trajectory and click by a human with tetraplegia 1000 days after implant of an intracortical microelectrode array," *Journal of Neural Engineering* 2011. 8(2) 025027.

[3] R.R. Harrison, R.J. Kier, C.A. Chestek, V. Gilja, P. Nuyujukian, S. Ryu, B. Greger, F. Solzbacher, and K.V. Shenoy, "Wireless neural recording with single low-power integrated circuit," *IEEE Trans. Neural Syst. Rehab. Eng.*, vol. 17, no.4, pp. 322-329, Aug. 2009.

[4] A. Avestruz, W. Santa, D. Carlson, R. Jensen, S. Stanslaski, A. Helfenstine, and T. Denison, "A 5 μW/channel spectral analysis IC for chronic bidirectional brain–machine interfaces," *IEEE Journal of Solid-State Circuits*, vol. 43, no. 12, pp. 3006-3024, Dec. 2008.

[5] H. Miranda, V. Gilja, C.A. Chestek, K. V. Shenoy, and T. H. Meng, "HermesD: A high-rate long-range wireless transmission system for simultaneous multichannel neural recording applications," *IEEE Trans. Biomed. Circuits Syst.*, vol. 4, no. 3, pp. 181-191, Jun. 2010.

[6] M. Rizk, C.A. Bossetti, T.A. Jochum, S.H. Callender, M.A.L. Nicolelis, D.A. Turner, and P.D. Wolf, "A fully implantable 96-channel neural data acquisition system," *J. Neural Eng.*, vol. 6, no. 2, art. 026002, Apr. 2009.

[7] M. Yin and M. Ghovanloo, "A low-noise clockless simultaneous 32-channel wireless neural recording system with adjustable resolution," *Analog Integrated Circuits and Signal Proc.*, vol. 66, no. 3, pp. 417-431, Mar. 2011.

[8] A 100-Channel Hermetically Sealed Implantable Device for Wireless Neurosensing Applications, Ming Yin, David A. Borton, Juan Aceros, William R. Patterson, and Arto V. Nurmikko, International Symposium on Circuits and Systems (ISCAS) Seoul (2012)

[9] Jones, K.E., Campbell, P.K. & Normann, R.A. A glass/silicon composite intracortical electrode array. *Annals of Biomedical Engineering* 20, 423-437 (1992). Blackrock Microsystems, Cereport multiport array, http://www.blackrockmicro.com/en/micro-electrode-arrays-products.html#mult

[10] J. Aceros, M. Yin, D.A. Borton, W.R. Patterson, and A.V. Nurmikko, "A 32-channel fully implantable wireless neurosensor for simultaneous recording from two cortical regions," *Proc. IEEE 33th Eng. in Med. and Biol. Conf.*, pp. 2300-2306, Aug. 2011

Neural Dynamics and Plasticity

Cortical-thalamic co-cultures coupled to a dual compartment MEA-based system: investigation of network dynamics and connectivity

Paolo Massobrio[1*], Thirukumaran Kanagasabapathi[2], Mariateresa Tedesco[1], Michel M. J.Decre[2], Sergio Martinoia[1]

1 Neuroengineering and Bio-nano Technology Group (NBT), Department of Informatics, Bioengineering, Robotics, System Engineering (DIBRIS), University of Genova, Genova, Italy.
2 Minimally Invasive Healthcare Department, Philips Research, High Tech Campus, Eindhoven, The Netherlands.
* Corresponding author. E-mail address: paolo.massobrio@unige.it

Abstract
Co-cultures containing dissociated cortical and thalamic cells may provide a unique model for understanding the pathophysiology in the respective neuronal sub-circuitry. In addition, developing an *in vitro* dissociated co-culture model offers the possibility to study the system without influence from other neuronal sub-populations. In this work, we demonstrated a dual compartment system coupled to Micro-Electrode Arrays (MEAs) for co-culturing and recording spontaneous activities from neuronal sub-populations.

1 Introduction

The interactions between thalamus and cortex has been extensively studied both *in vivo* [1] and *in vitro* [2]. The significance of the thalamus in the brain circuitry can be well understood considering that almost all neuronal signals from the sensory and motor periphery reach the cortex *via* the thalamus [3]. Thalamic neurons receive strong input from cortico-thalamic feedback neurons thereby allowing the context to communicate continuously through the thalamus during sensory processing. This implies that cortical neurons can dynamically modulate the thalamic processing function, and ultimately shape the nature of its own input [4]. These connectivity pathways between cortex and thalamus are also responsible for generating rhythmic neuronal network oscillations. To better understand the interplay between thalamus and cortex, the development of *in vitro* systems utilizing dissociated cells offer a complementary approach to *in vivo* studies. In this work, we considered both experiments and simulations to investigate specific interaction mechanisms between thalamic and cortical populations. We characterized the dynamics of such co-cultures by means of first-order statistics to investigate the influence of cortical cell dynamics in thalamic network activity and *vice versa*. Then, we inferred the functional connectivity maps between the two populations, and the directionality in the burst propagation. The main result is that a reciprocal connectivity between the cortical and thalamic region was found. Burst events originate in the cortical region and the presence of strong cortico-thalamic connections drives the thalamic network to discharge bursts while reciprocal weak thalamo-cortical connections play a salient role in the cortical network by modulating the duration of the burst event. Finally, to further validate such connectivity schemes, we developed a model of two large-scale neuronal interconnected populations mimicking the cortical and thalamic dynamics.

2 Materials and Methods

2.1 Dual-compartment device

The micro-fluidic compartments (Fig. 1A) of 1.5 mm width, 8mm length and 100μm in height are interconnected by means of microchannels of 10μm height, 3μm width and 150 μm length that are spaced at regular intervals of 50 μm (there are about 120 microchannels connecting the two compartments).

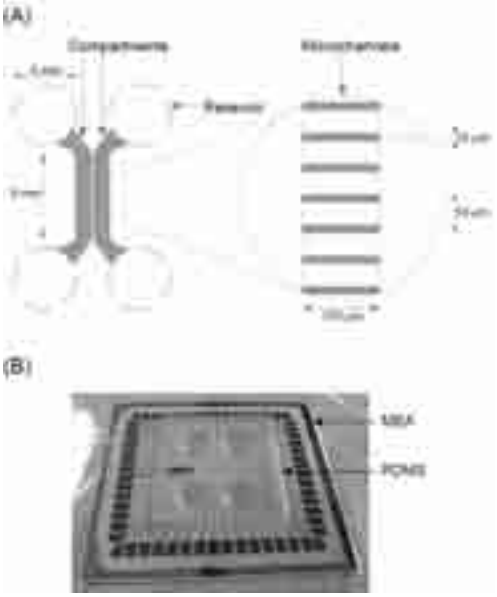

Fig. 1. (A) Layout of the dual-compartment device. (B) MEA substrate with the dual compartment device. Adapted from [5].

The small cross-section of the microchannels prevents the movement of cells between compartments while allowing neurites to cross-over to the adjacent compartment and form a functional network [5]. The compartmented PDMS device (Fig. 1B) was selectively oxygen-plasma treated to render the compartments and microchannels hydrophilic while preserving hydrophobic contact surface. The oxygen-plasma treated device was reversibly bonded to Micro-Electrode Arrays (MEA) substrate (Multi Channel Systems, Reutlingen, Germany). Prior to bonding, MEA substrates were coated overnight with polyethylenimine (PEI) solution at a concentration of 40 µg/ml.

2.2 Co-culture preparation

Primary cultures of Wistar rat embryonic cortical and thalamic neurons were prepared by Trypsine (GIBCO, Invitrogen, USA) digestion of day-18 embryonic rat whole cortices and ventral basal thalamus. The dissociated cortical cells were cultured in neurobasal medium (Lonza lifesciences, USA) and the dissociated thalamic cells were cultured in similar medium supplemented with an additional 3% Fetal bovine serum (FBS) and 1% Horse serum (HS). On the day of the experiment, PEI coated MEA substrates were rinsed 3x times in sterile water prior to bonding with PDMS device. After bonding PDMS and MEA substrate, dissociated cells were platted at a concentration of ~ 2 x 10^5 cells / cm^2 in both the compartments. The devices were then incubated in a humidified incubator at 37° C supplied with 5% CO_2. The presence of serum in the culture medium for thalamic cells (3%FBS+1%HS) was maintained for at least 5 days in vitro (DIV). The serum dosage was reduced during the following days to 2%FBS+0.5%HS and finally completely eliminated after DIV 9 to avoid the glia overgrowth during long term culture.

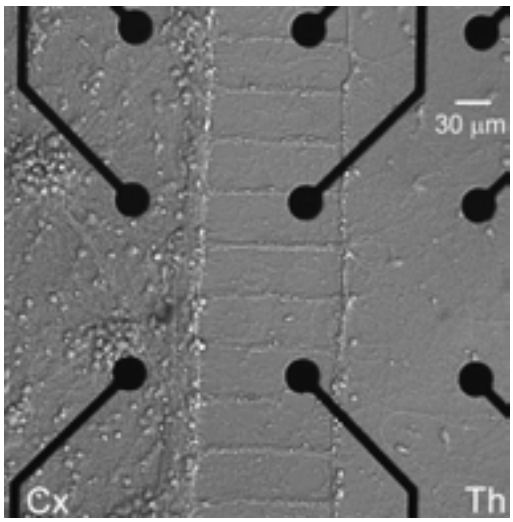

Fig. 2. Cortical-thalamic co-culture coupled to a MEA.

2.3 Data analysis

Network activity has detected by using threshold based 'Precise Timing Spike Detection' (PTSD) algorithm [6]. Bursts and network bursts are detected by using the algorithm devised by Pasquale et al. [7].

Cross-Correlation (CC) function was built by considering the spike trains of two recording site [8]. From the CC, we estimated the functional connectivity maps by considering only the strongest links to avoid any possible false positive connection and to focus on the most reliable connections. In particular, we considered the 20 strongest connections intra-cluster (i.e., cortico-cortical, or thalamo-thalamic connections), and the 10 inter-cluster (i.e., cortico-thalamic, or thalamo-cortical connections).

2.4 Computational model

A neuron model based on the Izhikevich equations [9] was used to simulate the dynamics of cortical-thalamic networks. Graph theory was used to represent the network connectivity. The structure of the graph is described by the graph's adjacency matrix, a square matrix of size equal to the number of nodes N with binary entries. If the element $a_{ij} = 1$, a connection is present between the node j to i, while $a_{ij} = 0$ means no connection between the two nodes. All the auto-connections are avoided. Following this approach, two independent networks made up of 512 nodes each, one for the cortical, and one for the thalamic network were realized. Both the networks are fully connected, as found experimentally, and the average degree was set at 1500 ± 97. The interconnections between the two sub-populations were modeled as follows: the presynaptic neurons in a compartment were chosen among the ones that establish the strongest connections within the same cluster; the targets were randomly chosen in the other compartments. In the simulated model, 10% strongest connections was set from cortical to thalamic compartment, while 5% of strongest connection was set from thalamic to cortical compartment [10].

3 Results

3.1 Cortical-thalamic dynamics

To analyze the influence between the two cultures we investigate the time of initiation of network bursts in both compartments of Cx-Th co-cultures. The obtained results shown that in the Cx-Th co-cultures network bursts were observed to originate in the Cx compartment in majority of the cases closely followed by thalamic bursts. Finally we look at the burst duration by hypothesizing a possible feed-back influence of the thalamic population on the behavior of cortical cells. The duration of cortical bursts in the co-culture

is elongated (Fig. 3) with an average burst duration of 389.17 ± 23.61 ms (mean ± standard error), when compared to the cortical bursts in isolation - with an average duration of 246.48 ± 3.82 ms, ($p < 0.01$, Kruskal-Wallis nonparametric test). In addition, also the burst duration of the thalamic subpopulation is modulated by the presence of cortical neurons: when thalamic neurons are cultured alone, they display a burst duration equal to 397.41 ± 1.70 ms, which is reduced to 280.66 ± 3.60 when cultured with cortical neurons.

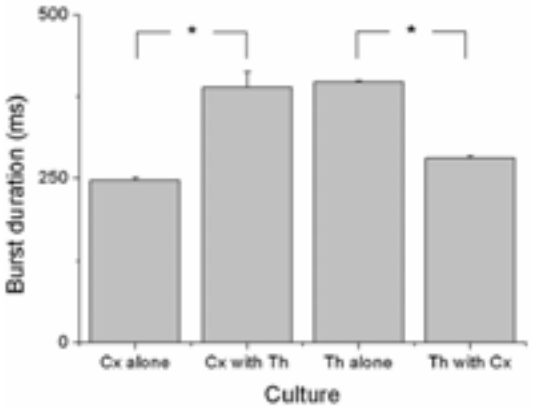

Fig. 3. Burst duration for cortical and thalamic cultures alone and when co-cultured ($p < 0.01$, Kruskal-Wallis, non parametric test).

3.2 Cortical-thalamic connectivity

The interplay between cortico-thalamic and thalamo-cortical populations have been investigated, by estimating the functional connectivity between the two populations. An example of functional connectivity map evaluated by considering the strongest 20 intra-cluster and 10 inter-cluster connections is shown in Fig. 4A.

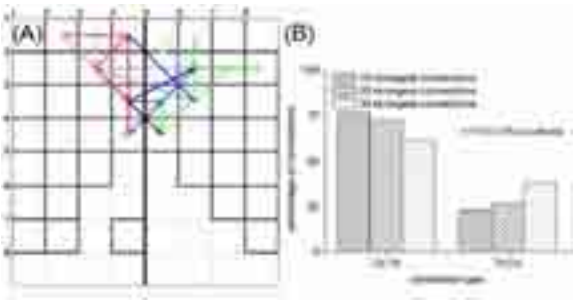

Fig. 4. (A) Example of a functional connectivity map. (B) Distribution of the inter-cluster connections evaluated over 5 cortical-thalamic co-cultures.

Direction of the links is derived by the peak latency of the cross-correlogram and allows to estimate the weight of the reciprocal influence of the two co-cultured populations. By considering 5 co-cultures used in this analysis, it was observed that ~ 77% of the connections are cortico-thalamic, while ~ 23% was thalamo-cortical. By varying the number of connections (i.e., from 10 to 30), an increase in the fraction of thalamo-cortical links was observed indicating that the strongest connections are from cortical to thalamic population (Fig. 4B).

3.3 Simulated models

Finally, to support the experimentally interplay between the cortical and thalamic populations, an Izhikevich based neuronal network model was developed to specifically study network dynamics in the two sub-populations (cortical and thalamus), influenced by the presence or absence of reciprocal connections. In this model, three different configurations were simulated: (i) populations of cortical and thalamic cells in isolated conditions; (ii) interconnected cortical-thalamic populations with unidirectional cortical to thalamic inter-connections, and (iii) interconnected populations with bidirectional strong cortico-thalamic and weak thalamo-cortical inter-connections (resembling the actual experimental situation). For each configuration, 300 seconds of spontaneous activity were simulated, and analyzed by using the same metrics adopted from the experimental data.

We computed the burst duration of cortical neurons by sweeping the percentage of the inter-connections between the two populations (Fig. 5).

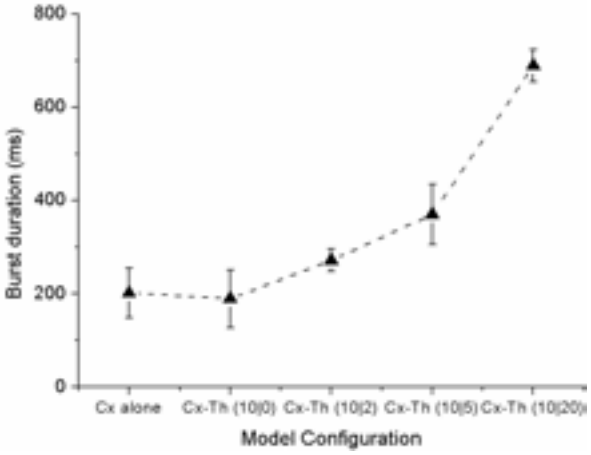

Fig. 5. Simulated Burst durations of cortical neurons, as a function of the percentage of the inter-compartment connections

It can be noticed that if we consider only a pool of cortico-thalamic connections (unidirectional inter-compartment connectivity) equal to 10% of the total connections within the cortical compartment (second bar of Fig. 5), burst durations are close to those obtained in an isolated cortical population (first bar). Increasing the percentage of thalamo-cortical projections, the mean burst duration of cortical population also increases (third bar of figure 8 with 10% cortico-thalamic and 2% thalamo-cortical connections), and resembles the experimental values when thalamo-cortical links are 5% of the intra-compartment connections (fourth bar). Finally, if the percentage of the thalamo-cortical inter-connections is greater than cortico-thalamic connections (last bar), the mean burst duration assumes implausible large values (more than 600 ms). These results are qualitatively in agreement

with functional connectivity analysis in Cx-Th devices, in which the ratio of cortico-thalamic functional connections were experimentally observed to be much higher compared to the thalamo-cortical connections.

4 Conclusions

A novel dual compartment micro-fluidic system for co-culturing dissociated cortical-thalamic cells was demonstrated in our current study allowing investigation of specific interactions between the two populations. We demonstrate that functional connectivity is re-established in dissociated cortical and thalamic cells indicating a natural inclination of the system to form reciprocal interconnections.

In a dual compartment device with cortical cells in both compartments [5], although functionally connected, the cells in individual compartments appear to exhibit network bursting behavior independent of the other compartment. In our current work with cortical-thalamic co-cultures, reciprocal connections between the cortical and thalamic region were observed. Burst events for the vast majority originate in the cortical region and the presence of strong cortico-thalamic connections drives the network and in-turn, the thalamic cells discharge bursts. On the other hand, reciprocal weak thalamo-cortical connections were observed to play a relevant role in cortical behavior by modulating the duration of burst events. Thalamic cells are mainly characterized by a tonic firing both in isolation and when co-cultured with cortical cells. However, the presence of cortical projections produces burst events in the thalamic culture with features that resemble the cortical ones. This influence is reciprocal and, in the average found behavior in cortical-thalamic co-cultures, the burst duration in the cortical region is elongated by about 57%, while the burst duration in the thalamic region shortened by about 29%. Simulated neuronal network models, based on Izhikevich equations, further confirms the necessity of bi-directional cortico-thalamic connections to drive the network dynamics as observed experimentally.

The analysis presented in this work confirms the recent findings that cortical region is the site of initiation of burst firing events while reciprocal thalamo-cortical connections are required to maintain a prolonged synchronized bursting pattern in the cortical culture [2].

References

[1] Crunelli V., Errington A. C., Hughes S. W. and Toth T. I. (2011). The thalamic low-threshold Ca(2+) potential: a key determinant of the local and global dynamics of the slow (< 1 Hz) sleep oscillation in thalamocortical networks. *Philosophical Transactions Of The Royal Society A-Mathematical Physical And Engineering Sciences*, 369,1952, 3820-3839.

[2] Adams B. E. L., Kyi M., Reid C. A., Myers D. E., Xu S., Williams D. A. and O'Brien T. J. (2011). Seizure-like thalamocortical rhythms initiate in the deep layers of the cortex in a co-culture model. *Experimental Neurology*, 227, 203-209.

[3] Jones E. G. (1985). The Thalamus. *New York: Plenum Press*,

[4] Briggs F. and Usrey W. M. (2008). Emerging views of cortico-thalamic function. *Current Opinion In Neurobiology*, 18,4, 403-407.

[5] Kanagasabapathi T. T., Ciliberti D., Martinoia S., Wadman W. J. and Decre M. M. J. (2011). Dual compartment neurofluidic system for electrophysiological measurements in physically segregated and functionally connected neuronal cell culture. *Frontiers in Neuroengineering*, 4,

[6] Maccione A., Gandolfo M., Massobrio P., Novellino A., Martinoia S. and Chiappalone M. (2009). A novel algorithm for precise identification of spikes in extracellularly recorded neuronal signals. *Journal of Neuroscience Methods*, 177,1, 241-249.

[7] Pasquale V., Martinoia S. and Chiappalone M. (2009). A self-adapting approach for the detection of bursts and network bursts in neuronal cultures. *Journal of Computational Neuroscience*, 29,1-2, 213-29.

[8] Garofalo M., Nieus T., Massobrio P. and Martinoia S. (2009). Evaluation of the performance of information theory-based methods and cross-correlation to estimate the functional connectivity in cortical networks. *PLoS ONE*, 4,8, e6482.

[9] Izhikevich E. M. (2003). Simple model of spiking neurons. *IEEE Transactions on Neural Networks*, 6, 1569-1572.

[10] Kanagasabapathi T. T., Massobrio P., Barone R. A., Tedesco M., Martinoia S., Wadman W. J. and Decre M. M. J. (2012). Functional connectivity and dynamics of cortical-thalamic networks co-cultured in a dual compartment device. *Journal of Neural Engineering*, in press.

Astrocytes drive neural network synchrony

N. Levine-Small[1,2,6], R.J. Guebeli[3], M. Goddard[1,2], A.Yang[4,5], A.S. Chuong[4,5], B. Chow[4,5], E.S. Boyden[4,5], W. Weber[3], U. Egert[1,2*]

1 Biomicrotechnology, Dept. of Microsystems Engineering, Univ. Freiburg, Freiburg, Germany.
2 Bernstein Center Freiburg, Univ. Freiburg, Freiburg, Germany
3 Faculty of Biology, Centre for Biological Signaling Studies (BIOSS) and Spemann Graduate School of Biology and Medicine (SGBM),Univ. Freiburg, Freiburg, Germany.
4 The MIT Media Laboratory, Synthetic Neurobiology Group and Dept. of Biological Engineering, Massachusetts Institute of Technology,Cambridge, MA, USA
5 McGovern Inst. for Brain Research and Dept. of Brain and Cognitive Sciences, Massachusetts Institute of Technology, Cambridge, MA, USA
6 Faculty of Biology, Univ. Freiburg, Freiburg, Germany
*Correspondence to: egert@imtek.uni-freiburg.de

Abstract
While astrocytes have been repeatedly shown to play a functional and developmental role at the synapse, it remains unclear whether these cells contribute to neuronal network state and processing. Calcium imaging in conjunction with the extracellular recording of hundreds of neurons revealed complex relationships between the network activity of neurons and astrocytes. Using GFAP-Melanopsin, a light activated calcium channel, we induced transient calcium concentration increases in astrocytes, which led to prolonged periods (several seconds) of sustained, enhanced synchronized firing (spontaneous periods of bursts of bursts) in neurons throughout the network. The spatiotemporal properties of this behaviour indicate that astrocytes can modulate the overall state of synchronicity in neuronal networks.

1 Introduction

The neuroscience community is largely divided over the role of astrocytes in the brain's ability to process and store information. Several studies *(1–3)* cast doubt on the assertion that astrocytes serve a meaningful role in encoding by neural ensembles. While *(4–7)* among others argue that there is clear evidence that astrocytes are crucial players in computation, encoding and storage. We assert that the brain's functionality is a manifestation of the activity of networks of neurons (rather than the action of individual cells). Microelectrode arrays (MEAs) allowed us to measure the spiking activity of distal neurons while simultaneously observing calcium-related activity in astrocytes through live Ca^{2+} imaging. Since the network role of astrocytes is yet unclear and the functioning of the brain is achieved through the complex activity of neural ensembles, we sought to elucidate the contribution, if any, of astrocytes to the activity of groups of neurons.

2 Methods

Melanopsin was mammalian codon-optimized, and was synthesized by Genscript (Genscript Corp., USA). All constructs were verified by sequencing. Human embryonic kidney cells (HEK-293T *(8)*) were cultured in advanced DMEM (Invitrogen, Germany) supplemented with 2 % fetal calf serum (FCS, PAN Biotech GmbH, Germany), 10 µM cholesterol (Sigma-Aldrich, USA), 10 µM egg lecithin (Serva Electrophoresis GmbH, Germany) and 1 % chemically defined lipid concentrate (Invitrogen, Germany). For the production of lentiviral particles, 500,000 HEK-293T cells were seeded in 2 ml medium 24 h before transfection. 100 µl of 0.25 M $CaCl_2$, 25 µM chloroquine (Sigma-Aldrich, Germany) containing 2 µg of the lentiviral expression vector fgfa2-melanopsin-mCherry and 1 µg of each helper plasmid (pCD/NL-BH**(9)* and pLTR-G *(10)* were mixed with 100 µl 2x-HBS solution (100 mM HEPES, 280 mM NaCl, 1.5 mM Na_2HPO_4, pH 7.1) and added to the cells. The medium was replaced after 5 h and viral particles were produced for 48 h. The cell culture supernatant containing the viral particles was collected, filtrated through a 0.45 µm filter (Schleicher & Schuell GmbH, Germany,) and stored at -80 °C. For transduction, 200 µl of thawed viral particles were added to a primary cortical culture in 2ml of MEM medium and incubated for 1 day followed by exchange to new MEM medium.

Rhodamine-3 (Invitrogen, Germany) was used according to the manufactures instructions. Calcium imaging was undertaken while the culture was maintained at 37°C (TC02, Multi Channel Systems, Germany) 5% CO_2 and pH 7.4. Ca-imaging was performed using a Zeiss Z1 Examiner microscope with an excitation wavelength of 550nm. To stimulate GFAP-Melanopsin, cultures were exposed to approximately 2 lm of 470 nm light at 100ms duty cycles.

Ca imaging movies were preprocessed with ImageJ, where regions-of-interest (ROI) were defined manually. Astrocyte traces were selected based on calcium-transient properties described in *(11, 12)*. The traces were then filtered to remove noise using a Savitzky-Golay filter *(13)* with a kernel width of 21 and a first degree polynomial. Slow trends were removed with an equiripple high-pass filter (sampling frequency:12.5 Hz, stop-band frequency: 0.0008 Hz, pass-band frequency: 0.008 Hz. amplitude attenuation: 20 db).

Spike data was sampled at 10 Khz, per channel (20 ms cut outs around threshold (at 5.5 standard deviations from average signal). The raw electrode data was imported into Matlab (Mathworks, USA) using the open-source software, Neuroshare *(14)* and spikes were detected using the wavelet packet discrimination algorithm described in *(15, 16)*. The spike times were then stored for each channel.

3 Results

All of the neural networks exhibited spontaneous activity with global network coordination manifested by the generation of bursting events – short time windows during which most of the neurons participate in more rapid neuronal firings. The time-averaged network firing rates in the baseline were the same as in the experiments (during Ca imaging or optogenetic stimulation). All the networks shared characteristic neuronal firing rates, inter-burst-intervals (IBI) distributions and burst width distributions in the baseline (data not shown). Calcium transients of astrocytes within a view field were comparable to astrocyte calcium dynamics observed in vivo and in slices. These calcium traces were observed to be coordinated with each other and with neurons throughout the network (even at great distances). The synchronized nature of the neuronal firing and the coincidence of astrocyte Ca increases with these bursts led us to investigate the functional relationship between these cell types as characterized by their observed activity. This analysis revealed, by the structure apparent in the dendrogram ordered correlation matrix *(17)*, the existence of correlated astrocytic “patches” (figure 1B). These patches have been reported in other works as being the result of either transmitted calcium through gap junctions *(4)* or through shared neuronal input *(5)*. The neural network activity showed variable coordination with astrocyte activity – that is, some astrocytic transients appeared to correspond to the network firing rate whereas other astrocytes appeared less well coordinated (figure 1A). The mix of similar and dissimilar calcium signals among different astrocytes within a view field and the fact that subsets of astrocyte traces appeared to be related to the neural network firing rate, suggests that astrocytes form functionally relevant ensembles. This complex structure of interactions between the two cell types led us to question whether astrocytes were simply responding to neural input or, as suggested by the synaptic studies *(4–7)*, capable of modulating the activity of neural networks.

Cortical cultures of neurons and glia, where exclusively astrocytes expressed Melanopsin, demonstrated a dramatic neuronal response upon stimulation. During stimulation, prolonged periods (several seconds long) of intense synchronized firing occurred across the neural network (Fig. 1D-F). That is, though the overall firing rate remained constant, the maximum burst duration during astrocyte stimulation increased considerably. This neuronal response to astrocyte stimulation was not observed to be sharply correlated in time with the 470 nm pulse nor did it show strong dependence on light intensity, exposure time or pulse rate. However, the network-wide super-bursting began shortly after stimulation and persisted only a short time following the end of stimulation.

To exclude neuronal expression of Melanopsin we performed immunohistochemistry (IHC). IHC revealed that astrocytoma cells that do not express GFAP and neurons labeled with anti-MAP2 antibodies both fail to immunoreact with Anti-OPN4 (anti-melanopsin) antibodies (data not shown). Cultures infected with GFAP-Mcherry only or not infected did not superburst in response to 470 nm light pulses (data not shown).

4 Discussion

Whether or not astrocytes have the potential to change a neural network’s state is crucial in determining their relevance to the aspects of brain function that, to date, have been solely considered neuronal. Using optogenetic tools, we prompted calcium transients in astrocytes (and only astrocytes). These cells, activated through Ca-influx, induced a state change in the neural network leading to repeated, highly synchronized super-bursts. Astrocytes are thus capable of not only modulating neuronal activity but changing a network’s overall working mode. Since astrocyte proliferation is a hallmark of various brain diseases, for example, gliosis is typical of epileptic foci *(18)*, our results suggest that this astrocytic potential to modulate network states may contribute to highly-active super-synchronized epileptic episodes.

Acknowledgments

Supported by the German BMBF (FKZ 01GQ0830) and Minerva Stiftung. We thank Ms. Ute Riede and Mr. Patrick Pauli for technical assistance.

References

[1] C. Agulhon et al., What is the role of astrocyte calcium in neurophysiology?, *Neuron* **59**, 932-46 (2008).

[2] T. a Fiacco et al., Selective stimulation of astrocyte calcium in situ does not affect neuronal excitatory synaptic activity., *Neuron* **54**, 611-26 (2007).

[3] G. Perea, M. Navarrete, A. Araque, Tripartite synapses: astrocytes process and control synaptic information., *Trends in neurosciences* **32**, 421-31 (2009).

[4] K. Smith, Settling the great glia debate*Science* **468**, 8-10 (2010).

[5] V. Parpura, P. G. Haydon, Physiological astrocytic calcium levels stimulate glutamate release to modulate adjacent neurons, **97**, 8629-8634 (2000).

[6] A. Araque, G. Carmignoto, P. G. Haydon, Dynamic signaling between astrocytes and neurons., *Annual review of physiology* **63**, 795-813 (2001).

[7] S. Hülsmann, Y. Oku, W. Zhang, D. W. Richter, Metabolic coupling between glia and neurons is necessary for maintaining respiratory activity in transverse medullary slices of neonatal mouse., *The European journal of neuroscience* **12**, 856-62 (2000).

[8] B. Mitta et al., Advanced modular self-inactivating lentiviral expression vectors for multigene interventions in mammalian cells and in vivo transduction., *Nucleic acids research* **30**, e113 (2002).

[9] H. Mochizuki, J. P. Schwartz, K. Tanaka, R. O. Brady, J. Reiser, High-titer human immunodeficiency virus type 1-based vector systems for gene delivery into nondividing cells., *Journal of virology* **72**, 8873-83 (1998).

[10] J. Reiser et al., Transduction of nondividing cells using pseudotyped defective high-titer HIV type 1 particles., *Proceedings of the National Academy of Sciences of the United States of America* **93**, 15266-71 (1996).

[11] Y. Ikegaya, M. Le Bon-Jego, R. Yuste, Large-scale imaging of cortical network activity with calcium indicators., *Neuroscience research* **52**, 132-8 (2005).

[12] N. Takahashi, T. Sasaki, A. Usami, N. Matsuki, Y. Ikegaya, Watching neuronal circuit dynamics through functional multineuron calcium imaging (fMCI)., *Neuroscience research* **58**, 219-25 (2007).

[13] U. Egert et al., MEA-Tools: an open source toolbox for the analysis of multi-electrode data with matlab, *Journal of Neuroscience Methods* **117**, 33-42 (2002).

[14] R. Meier, U. Egert, A. Aertsen, M. P. Nawrot, FIND--a unified framework for neural data analysis., *Neural networks : the official journal of the International Neural Network Society* **21**, 1085-93 (2008).

[15] E. Hulata, A method for spike sorting and detection based on wavelet packets and Shannon's mutual information, *Journal of Neuroscience Methods* **117**, 1-12 (2002).

[16] E. Hulata, R. Segev, Y. Shapira, M. Benveniste, E. Ben-Jacob, Detection and sorting of neural spikes using wavelet packets., *Physical review letters* **85**, 4637-40 (2000).

[17] R. Segev, I. Baruchi, E. Hulata, E. Ben-Jacob, Hidden Neuronal Correlations in Cultured Networks, *Physical Review Letters* **92**, 23-26 (2004).

[18] G. Seifert, K. Schilling, C. Steinhäuser, Astrocyte dysfunction in neurological disorders : a molecular perspective, *Neuroscience* **7**, 194-206 (2006).

Modular topology introduces gating in neuronal networks through excitation-inhibition balance

Mark Shein-Idelson[1*], Eshel Ben-Jacob[2,3], Yael Hanein[1]

1 School of Electrical Engineering, Tel-Aviv University, Tel-Aviv 69978, Israel
2 School of Physics and Astronomy, Tel-Aviv University, Tel-Aviv 69978, Israel
3 Sagol School of Neuroscience, Tel Aviv University, Tel Aviv 69978, Israel
* Corresponding author. E-mail address: markshei@post.tau.ac.il

Abstract
Functional neuronal networks reliably transmit information from specific inputs to specific outputs. While it is widely accepted that network topology plays an important role in controlling activity, it is still unknown how network topology gives rise to routing and whether the topological properties of the network may be utilized to allow activity gating. To systematically study these questions we utilized an in-vitro cell patterning technique to induce self-organization of networks into connected clusters with a modular topology. We found that the modular architecture gave rise to conditional activity propagation between sub populations. Network bursts (NBs) initiated in "sending" clusters did not always propagate to the "receiving" clusters. The propagation was conditioned by the activity intensity in the sending cluster and was characterized by long delays. This conditional activation was also observed in large networks of many connected clusters where it is manifested as events initiating at different network locations and propagating to different distances. Interestingly, such conditional activation could also be turned on and off by excitation-inhibition imbalance.

1 Introduction

One of the basic tasks of a functional neuronal network is to reliably transmit information from input to output. Even in simple feed-forward networks, this is a highly non-trivial operation. All the more so when the transmission takes place in a recurrent network where multiple pathways are embedded within the same network of connected neurons. One way to restrict the propagation of activity to specific pathways is by utilizing a gating mechanism between connected neurons and sub-populations. A basic question in this context is what part does the network topology play in controlling activity propagation and routing and whether the topological properties of the network may be utilized to allow such activity gating?

Topology has an immense impact on various network activity properties [*1*]. In particular, modular topology was suggested to play a major role in determining the activity properties of neuronal circuits. Indeed, theoretical studies indicated that modular organization, with highly connected sub-populations which are loosely coupled to each other, is most beneficial for efficient information processing (for review see [*2*]). Foremost, network synchronization is highly affected by circuit modularity which enables the transition from a local to a global activation [*3*, *4*]. In the former, synchronized activity is confined to single module, while in the latter it spreads to other modules in the network. In addition, a modular network, being a subclass of small world networks, is more efficient in generating coherent oscillations [*5*]. Finally, modularity can give rise to time-scale separation between fast intra-modular and slow inter-modular processing [*6*]. These properties enhance the complexity of the network dynamics [*4*, *7*, *8*] and support control over activity spread.

Taking into account the compartmentalization of the brain into neuronal subpopulations of different spatial scales [*9*, *10*], it is tempting to suggest that the functional features of such networks are affected by their topological characteristics. However, topology-activity relations are hard to study in-vivo due to the limited accessibility of complete circuits and the lack of control over their connectivity patterns. Foremost, brain circuits are not prone to design, preventing the possibility of systematic studies. Finally, the connectivity maps of neural circuits are highly untraceable in the three dimensional architecture.

To overcome these limitations we utilized an in-vitro cell patterning technique to control neuronal network architecture [*11*]. We used soft lithography of Poly-D-Lysine (PDL) islands to induce self-organization of networks into connected clusters with a modular topology. These networks were patterned on top of multi-electrode arrays (MEAs) allowing long term recording of their activity. We found that the activity within each cluster is characterized by network bursts (NBs), activating the whole cluster synchronously. When examining pairs of connected clusters, we found that the modular topology gave rise to conditional activation, activation asymmetry and long delays. These features were also observed in large networks of many connected clusters. Interestingly, by breaking the inhibition-excitation

balance in these networks, it was possible to erase the unique features of the modularity: the conditional activation was replaced by network-wide synchronized events.

2 Methods

2.1 Cell culturing

Entire cortices of Sprague Dawley rat embryos (E18) were removed, chemically digested and mechanically dissociated by trituration. Dissociated cells were suspended in a modified essential medium with Eagle's salts (Biological Industries, Kibbutz Beit Haemek, Israel, Cat. No. 01-025-1), 5% horse serum (Biological Industries, Kibbutz Beit Haemek, Israel, Cat. No. 04-004-1), 5 mg/ml gentamycin (Biological Industries, Kibbutz Beit Haemek, Israel, Cat. No. 03-035-1), 50 μM glutamine (Biological Industries, Kibbutz Beit Haemek, Israel, Cat. No. 03-020-1) and 0.02 mM glucose (BDH, Cat. No. 101174Y), and plated onto patterned substrates at a density of 700 cells/mm^2. To promote the long-term viability of the cells on the isolated islands it was crucial to use a ''feeder'' colony of cells. The mitotic inhibitor, FuDr (80 mM FuDr, Sigma, Cat. No. F0503 and 240 mM Uridine, Sigma, Cat. No. U3303) was added once after four days in culture. The cultures were maintained at 37°C with 5% CO_2 and 95% humidity. The growth medium was partially replaced every 3–4 days.

2.2 Patterning

Poly-D-Lysine (PDL) islands were patterned on top of MEAs by soft lithography using polydimethylsiloxane (PDMS) stencils [*12*]. An SU8-2075 (Micro Chem) mold 120 μm in thickness was patterned on a silicon wafer. This pattern was in accordance with the electrode array arrangement. The stencil was prepared by spin coating the wafer with PDMS. After detaching the PDMS membrane from the mold, the stencil was placed on commercial MEAs (multi-channel systems) in alignment with the electrode locations. PDL solution was dripped onto the PDMS stencil and the PDL was dried on a hot plate at 37°C. The PDMS stencil was removed before cell plating. For uniform network, PDL was applied uniformly to the MEA and washed after 4-8 hours with distilled water.

2.3 Analysis

Activity intensity traces were extracted from recorded voltage traces and burst peaks were identified in individual clusters using a previously described method [*13*]. To calculate the propagation direction, the sample cross-correlation function between clusters was calculated on 1s time windows around each burst peak. The center of mass of the cross-correlation function was used to evaluate the propagation direction. For the results presented in figure 1, only bursts with clearly identified propagation directionality were considered (center of mass > 20ms).

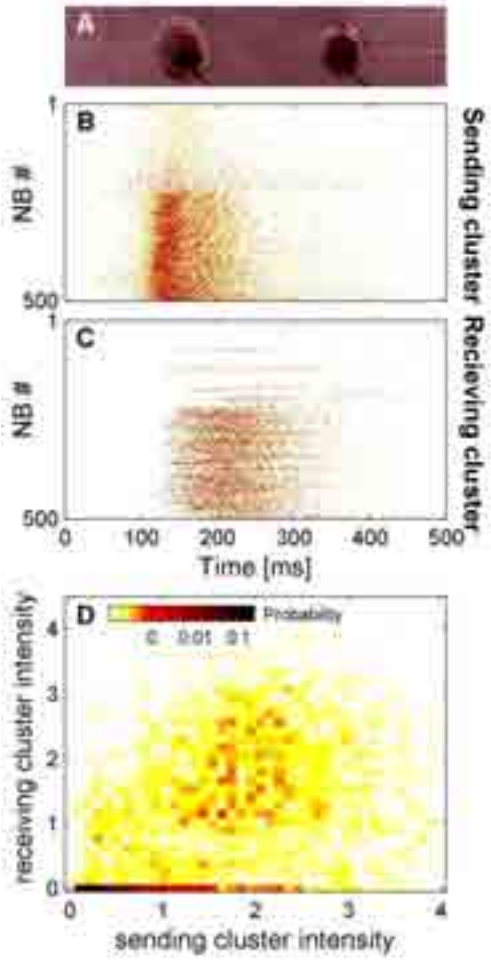

Fig. 2. Conditional activation in two connected clusters. (A) A bright-field image of two clusters within an engineered chain of clusters. (B,C) Activity intensity of 500 consecutive bursts recorded from two connected clusters along the cluster chain (one cluster defined as the sending cluster and the other as the receiving cluster). Only bursts propagating from the sending to the receiving cluster are shown. Bursts were ordered according to the overall burst intensity in the sending cluster. (D) The probability of occurrence for bursts with different total intensities in the receiving cluster as a function of the sending cluster (calculated on 4435 consecutive bursts propagating from the sending to the receiving cluster). Burst intensity was normalized to the standard deviation of intensities in each cluster separately. Colour code is show in a logarithmic scale.

3 Results

As many past experiments have shown, the activity of uniform, developing networks in culture is characterized by stereotipic network-wide bursting patterns [*14*]. These network bursting (NB) events are highly robust [*15*, *16*] and do not fundamentally change as a function of the network size or density [*17*]. In fact, small populations of several tens of cells are already enough to sustain such bursting patterns [*13*]. To examine how these bursting patterns propagate between connected sub-populations, we engineered networks in which two highly connected sub populations were weakly coupled to each other through bundles of extensions (Fig. 1A). Such connec-

tivity patterns can be induced in culture using soft lithography of PDL [*13*]. The population activity of pairs of clusters emmbedded within larger clustered networks (Fig 1A) was recorded using MEAs.

Neurons within each cluster were synchornously recruited to fire in network bursts, similary to the activity of neurons in large uniform networks and in isolated clusters (Fig 1B,C and Fig 2A). In contrast, activation of neurons belonging to different (yet connected) clusters did not always synchronize over neighboring clusters (Fig 1B,C). Larger networks of either one-dimensional cluster chains (Fig 2A) or two dimensional connected clusters [*17*], fired bursts which were initiated at different clusters propagated to a varying number of connected clusters. Thus, each network exhibited a wide spectrum of burst activation profiles, from segregated activation in individual clusters to integrated activation of the whole network.

To examine the conditional activation between connected cluster pairs, we identified consecutive bursts in one of the two connected clusters and termed this cluster as the "sending" cluster. Next, from within this burst pool we selected only the ones that propagated from the sending cluster to the connected cluster (see Methods), termed here as the "recieving" cluster. An example of such 500 consecutive bursts from two connected clusters is shown in Figures 1B and 1C (bursts were ordered according to the total activity intensity in the sending cluster, activity intensity is defined in Ref. [13]). Clearly, the stronger bursts have a higher probability to propagate to the recieving cluster. This is also evident from the joint probability of burst intensities, calculated on a large pool of bursts (Fig 1D). Here, weak bursts in the sending cluster did not yield strong responses in the recieving cluster. This is in contrast to bursts with high intensities which activated strong responses in the recieving cluster.

The propagation direction between connected cluster pairs was often asymettric. In the example shown in figure 1, 4435 bursts propagated from the sending cluster to the recieving cluster while only 776 bursts propagated in the opposite direction. We found that such asymettery was dependend on the topology of the embedding network, but was also observed in smaller networks of only two connected clusters (data not shown). For cases in which bursts propagated to connected clusters, this propagation was characterized by long delays on the order of several tens of milliseconds (67 ms on average in the example in figure 1). Such long delays are on the same temporal order of the recruitment time of the whole network in isolated clusters and uniform networks [*13*, *18*].

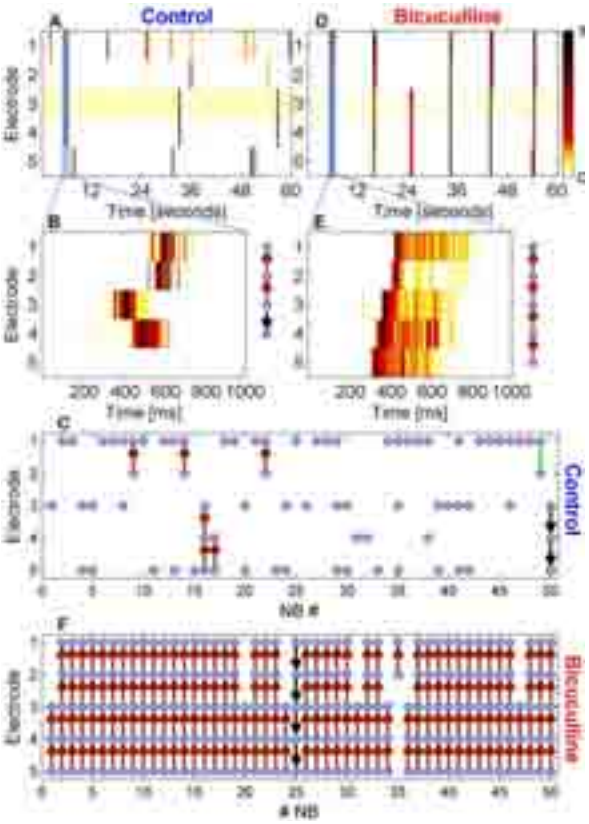

Fig. 2. Propagation in modular networks with unbalanced inhibition. Activity patterns in a chain of five connected clusters were analyzed before (A,B,C) and after (D,E,F) inhibition block by 30μM Bicuculline. (A,D) Activity intensity in the clusters as a function of time (colour coded). (B,E) Zoom into a single network burst from (A) and (D) (marked by the blue rectangle). A schematic representation of network burst propagation is shown on the right. Red and black arrows represent upward and downward propagation along the cluster chain. Green line represents simultaneous activation. Blue full circles represent activation of the cluster during the burst. (C,F) Schematic representation of the propagation (see B,E) in 50 consecutive bursts. In control conditions (C), the network shows both segregated activation (activation of single clusters or a subset of the clusters) and integrated activation (activation of the whole network). After inhibitory block (F), only integrated activation is observed. This activation is typified by a clear and dominant activation focus (cluster 5).

Next, we examined if conditional activation can be gated by an external parameter. More specifically, since inhibition and excitation are carefully balanced in neuronal networks [*15*], we investigated whether breaking this balance, by applying 30 μM Bicuculline, may change the transfer probability of bursts between connected clusters. Indeed, following the application of Bicuculline, the segregated activation of bursts in chained clusters (Fig. 2A) was replaced by mostly integrated activation of the whole network (Fig 2D). To examine the burst propagation between clusters, we identified single bursts in the network (Fig B,E) and calculated the propagation direction between all active clusters within the same time window (see Methods). Such activation sequence can be schematically represented by dots that mark the activation of individual clusters in the chain and arrows marking the propagation direction. This is shown for single bursts in figure 2B and 2E, and is

calculated for many consecutive bursts as shown in figure 2C and 2F. Interestingly, in addition to the global synchrony that is triggered by unbalancing inhibition, a clear initiation-like focus emerges (Fig. 2F).

3 Discussion

Using patterned networks of interconnected clusters we were able, for the first time, to systematically study how network topology affects activity transmission. We found that modular topology gives rise to conditional activation, activation asymmetry and long delays. The delays result in temporal separation between intra and inter cluster activation which may be important for separating different functional processes in the network. The activation asymmetry may be important for controlling propagation directionality.The conditional activation observed in the study highlights a possible mechanism for restricting activity propagation and controlling the degree of the network synchrony. Evidently, while connected clusters have the potential to synchronize, they also exhibit segregated activity in which NBs are confined to one or a limited number of clusters.

Most interestingly, the topology-related conditional activation reported here may be gated by the balance between excitation and inhibition in the network. When inhibition is unbalanced, the network's activity shifts to synchronous activation, typified by a clear activity initiation focus. Such activity patterns may be relate to pathological conditions observed during epileptic seizures [*19*].

Acknowledgement

We thank Inna Brainis and Moshe David-Pur for their technical assistance.

References

[1] Boccaletti, S., Latora, V., Moreno, Y., Chavez, M., and Hwang, D. U. (2006) Complex networks: Structure and dynamics. *Physics reports 424*, 175-308.

[2] Meunier, D., Lambiotte, R., and Bullmore, E. T. (2011) Modular and hierarchically modular organization of brain networks. *Front Neurosci 4*, 200.

[3] Kaiser, M. (2007) Brain architecture: a design for natural computation. *Philosophical Transactions of the Royal Society a-Mathematical Physical and Engineering Sciences 365*, 3033-3045.

[4] Shanahan, M. (2008) Dynamical complexity in small-world networks of spiking neurons. *Physical Review E 78*,

[5] Lago-Fernández, L. F., Huerta, R., Corbacho, F., and Sigüenza, J. A. (2000) Fast response and temporal coherent oscillations in small-world networks. *Physical review letters 84*, 2758-61.

[6] Pan, R. K., and Sinha, S. (2009) Modularity produces small-world networks with dynamical time-scale separation. *Epl 85*.

[7] Shanahan, M. (2010) Metastable chimera states in community-structured oscillator networks. *Chaos 20*, 013108.

[8] Sporns, O., Tononi, G., and Edelman, G. M. (2000) Connectivity and complexity: the relationship between neuroanatomy and brain dynamics. *Neural networks 13*, 909-22.

[9] Mountcastle, V. B. (1997) The columnar organization of the neocortex. *Brain 120*, 701-722.

[10] Bullmore, E., and Sporns, O. (2009) Complex brain networks: graph theoretical analysis of structural and functional systems. *Nat Rev Neurosci 10*, 186-198.

[11] Wheeler, B. C., and Brewer, G. J. (2010) Designing Neural Networks in Culture. *Proceedings of the Ieee 98*, 398-406.

[12] Sorkin, R., Gabay, T., Blinder, P., Baranes, D., Ben-Jacob, E., and Hanein, Y. (2006) Compact self-wiring in cultured neural networks. *J Neural Eng 3*, 95-101.

[13] Shein Idelson, M., Ben-Jacob, E., and Hanein, Y. (2010) Innate synchronous oscillations in freely-organized small neuronal circuits. *PloS one 5*, e14443.

[14] Ben-Ari, Y. (2001) Developing networks play a similar melody, *Trends Neurosci 24*, 353-360.

[15] Wilson, N. R., Ty, M. T., Ingber, D. E., Sur, M., and Liu, G. (2007) Synaptic reorganization in scaled networks of controlled size. *J Neurosci 27*, 13581-13589.

[16] Shein, M., Volman, V., Raichman, N., Hanein, Y., and Ben-Jacob, E. (2008) Management of synchronized network activity by highly active neurons. *Phys Biol 5*, 36008.

[17] Shein-Idelson, M., Ben-Jacob, E., and Hanein, Y. (2011) Engineered Neuronal Circuits: A New Platform for Studying the Role of Modular Topology. *Frontiers in Neuroengineering 4*, 1-8.

[18] Eytan, D., and Marom, S. (2006) Dynamics and effective topology underlying synchronization in networks of cortical neurons. *J Neurosci 26*, 8465-8476.

[19] Treiman, D. M. (2001) GABAergic mechanisms in epilepsy. *Epilepsia 42 Suppl 3*, 8-12.

Structural and functional identification of sub-networks in dissociated neuronal cultures: an automated multimodal analysis combining high density MEA and fluorescence imaging

Alessandro Maccione[1,*], Simona Ullo[2], Alessandro Simi[1], Thierry Nieus[1], Diego Sona[2], Alessio Del Bue[2], Vittorio Murino[2], Luca Berdondini[1]

1 Dep. Neuroscience and Brain Technologies, Istituto Italiano di Tecnologia, Genova, Italy
2 Pattern Analysis & Computer Vision, Istituto Italiano di Tecnologia, Genova, Italy
* Corresponding author. E-mail address: alessandro.maccione@iit.it

Abstract
High density MEAs provides improved capabilities in spatially and temporally resolving network activity patterns at the resolution of single cell, becoming more and more a standard technology in unravelling neuronal signal processing. In combination with fluorescence imaging, these devices open new perspective in finely identify structural and functional network properties. In this paper we present an automated analysis able to correlate the network topology extracted from fluorescence imaging of specific sub populations (e.g. inhibitory neurons), with high density electrophysiological recordings, paving the way to finely correlate functional activity with morphological spatial composition of dissociated neuronal cultures.

1 Introduction

High density MEAs are opening new perspectives to investigate how neuronal networks are functionally self-organized. By recording from the whole array of 4096 electrodes, these devices provide an improved capability to spatially and temporally resolving network activity patterns [1-2]. Further, network-wide activity parameters can be computed with a better statistical significance then from acquisitions obtained from low-resolution MEAs [3]. Interestingly, coupled with low-density cultures, high-resolution MEAs can resolve network activity at single-neuron resolution. This fine network-wide functional description [4] can be completed by structural data acquired with fluorescent imaging of specific cellular constituents of the network. Indeed, given the heterogeneous cell-type composition of neuronal networks, this multimodal approach would allow studying dissociated cultures not as undefined "black-boxes", but as a defined distributed processing architecture where each specific neuronal types (e.g. inhibitory) contributes to the orchestrated collective behavior. The overall aim of this work is to develop adapted hardware and analysis tools to enable the investigation of neuronal networks at cellular resolution with such a multimodal imaging methodology.

2 Materials and Methods

2.1 Cell culture and experimental protocol

Primary hippocampal neurons at E18 were dissociated and seeded at low density concentration (100-150cell/µL, 30-50µL drop) on high-resolution MEAs (BioCam4096 platform from 3Brain Gmbh, www.3brain.com). Cell cultures were recorded at 18-21DIVs for multiple phases of 15 min in spontaneous condition and under BIC chemical modulation. Successively cultures were immunoprobed for β3-tubulin and NeuN. GAD staining was also used to identify the family of GABAergic neurons (i.e. the inhibitory population). Images were acquired with a custom epifluorescence upright microscope setup and stitched together to observe the entire active area of the MEA (2.6 x 2.6 mm^2).

2.2 Data analysis

Neuronal nuclei identification

Fluorescent imaging where analyzed to identify the precise position of neurons respect to the electrode array. Neuronal nuclei were identified by adapting the Circular Hough Transform algorithm [5]. The identification of the electrode array consisted of: i) detection of visible electrodes by computing a correlation with an electrode image template, ii) an interpolation phase to estimate the position of the occluded ones by applying the RANSAC algorithm [6]. Fig 1 shows an example of nuclei and electrodes identification, grey

electrodes are considered active channels, i.e. they recorded a spiking activity > 0.1 spike/sec (see *Statistical analysis*).

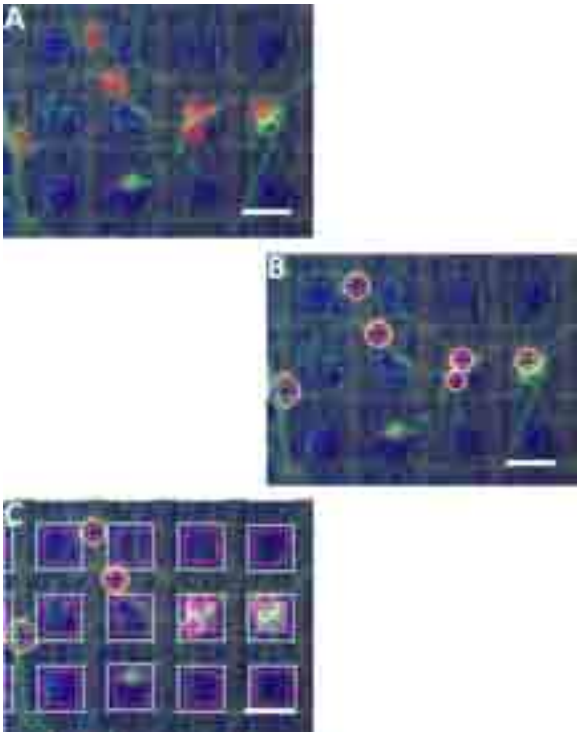

Fig. 1. a) close up of a portion of the low density culture grown on the electrode array (red - NeuN, green - β3-tubulin), **b)** neuronal nuclei identification by means of adapted Circular Hough Transform algorithm, **c)** superimposition of the electrode grid detected by correlating an electrode template image (scalebar 21 μm)

Statistical analysis

Electrophysiological recordings were analyzed by using the BrainWave software tool (3Brain Gmbh). Event detection was based on the Precise Timing Spike Detection (PTSD) algorithm [7]; only channels with a firing rate > 0.1 spike/sec have been taken into account. Based on analysis *presented in Neuronal nuclei identification*, we further filtered active channels by taking only the subset presenting a single neuron on top of them. We computed the Mean Firing Rate (MFR) and the Mean Inter Spike Interval (MISI) by dividing the network in two distinct populations (inhibhitory vs not inhibitory neurons) by considering GAD staining as shown in fig 2.

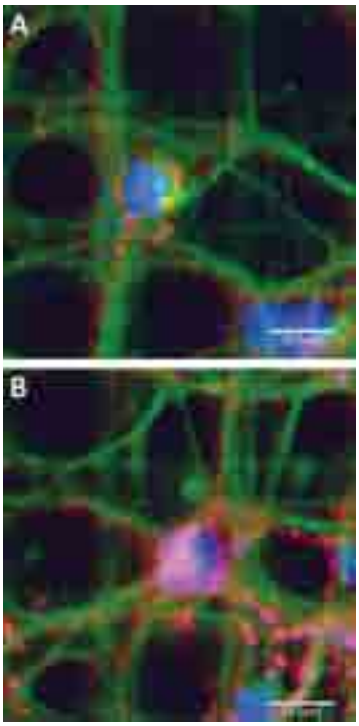

Fig. 2. Example of a single inhibitory (**a**) and excitatory (**b**) neuron on an electrode. Fluorescence colormap: green indicates B3-tubulin, blue NeuN and pink GAD.

3 Results

Here we present combined high resolution electrophysiological recordings and fluorescence imaging data emerging from low-density hippocampal cultures. This allows to approach a one-to-one neuron-electrode coupling and to identify specific network cellular constituents. To join optical and electrical datasets we introduce an automated computer vision approach able to precisely identify and localize each neuron over the array. This neuron-electrode mapping merged with electrophysiological MEA recordings allows associating to each neuron type its own activity. Staining of GABAergic neurons is used to separate the activity of inhibitory and excitatory populations and to study the behavior of the two subnetworks. As shown in Fig 3, the MFR of both populations exhibits different electrical behaviours under basal and chemically manipulated conditions. BIC induces an increasing in firing rate for both subnetworks still maintaining a difference in the firing dynamic.

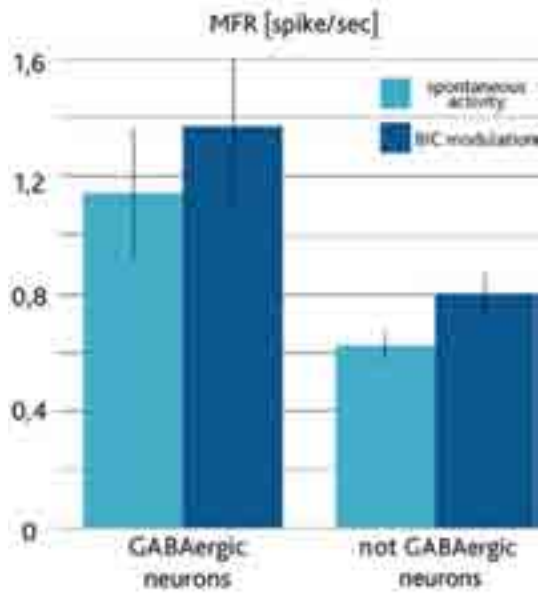

Fig. 3. Population specific mean firing rates (MFR) and STDerror calculated for GABAergic and not GABAergic sub-populations of the network.

This is also evident in table 1, where MFR and MISI are calculated for the two sub-networks and considered all together. It is clear that averaging the two sub-populations, is a strong approximation of the real functional dynamics occurring within neuronal networks.

4 Discussion

Our results demonstrate that it is possible to investigate neuronal networks at cellular resolution with cell-type information content. Under chemical stimulation, this allowed identifying electrical activity of inhibitory and excitatory sub-populations. The extension of the cross-correlation based functional connectivity algorithm [4] to the detection of functional inhibitory connections is undergoing and will allow to better characterize network processing. The advantages and limits of the overall methodology will be discussed during the presentation.

Tab. 1. MFR and MISI, with their respective stdErr, calculated averaging all active channels and considering the GABaergic (inhibitory) and not GABAergic (not inhibitory) classification.

References

[1] Berdondini, L., et al., *Active pixel sensor array for high spatio-temporal resolution electrophsyiological recordings from single cell to large scale neuronal networks.* Lab On A Chip, 2009. **9**: p. 2644–2651.

[2] Gandolfo, M., et al., *Tracking burst patterns in hippocampal cultures with high-density CMOS-MEAs.* J Neural Eng, 2010. **7**(5): p. 056001.

[3] Maccione, A., et al., *Experimental Investigation on Spontaneously Active Hippocampal Cultures Recorded by Means of High-Density MEAs: Analysis of the Spatial Resolution Effects.* Front Neuroeng, 2010. **3**: p. 4.

[4] Maccione, A., et al., *Multiscale functional connectivity estimation on low-density neuronal cultures recorded by high-density CMOS Micro Electrode Arrays.* J Neurosci Methods, 2012. **207**(2): p. 161-171.

[5] Ballard, D.H., *Generalizing the hough transform to detect arbitrary shapes*, in *Pattern recognition* 1981.

[6] Fischler, M.A. and R.C. Bolles, *Random sample consensus: a paradigm for model fitting with applications to image analysis and automated cartography*, Morgan Kaufmann Publishers Inc., Editor. 1987: San Francisco. p. 726-740.

[7] Maccione, A., et al., *A novel algorithm for precise identification of spikes in extracellularly recorded neuronal signals.* Journal of Neuroscience Methods, 2009. **177**(1): p. 241-249.

The neural code in developing cultured networks: Experiments and advanced simulation models

W.L.C. Rutten, T.A. Gritsun, I. Stoyanova and J. leFeber

Neural Engineering Dept., University of Twente, Enschede, The Netherlands

1 Background

Understanding the neural code of cultured neuronal networks may help to forward our understanding of human brain processes.The most striking property of spontaneously firing cultures is their regular bursting activity, a burst being defined as synchronized firing of groups of neurons spread throughout the entire network. The regularity of bursting may change gradually with time, typically being stable over hours (Stegenga et al. 2008). Cultured cortical networks composed of many thousands of neurons show bursting behavior starting from the end of the first week in vitro. Bursts can be characterized by both intraburst parameters (burst shape, maximum firing rate, leading and trailing edge steepness, etc.) and interburst parameters (statistics, stability of burst rates) (Van Pelt et al. 2004; Wagenaar et al. 2006). Not only the temporal burst characteristics develop with time. Also, spatial burst propagation patterns, socalled ‘’burst waves”, change with age of the network.

2 Methods

In (Gritsun et al. 2010) we modeled the intraburst phenomena, whereas in (Gritsun et al. 2011) we focused on the interburst intervals (IBIs). The spiking activity model used basically consists of the ‘’Izhikevich neuron” model, for individual neurons and a connectivity matrix of randomly positioned neurons. These two studies showed that random recurrent network activity models generate intra- and inter- bursting patterns similar to experimental data. The networks were noise or pacemaker-driven and had Izhikevich-neuronal elements with only short-term plastic (STP) synapses (so, no LTP included). However, elevated pre-phases (burst leaders) and after-phases of burst main shapes, that usually arise during the development of the network, were not yet simulated in sufficient detail. Recently, by adding a biologically realistic neuronal growth model (with and without field-guided axonal bundling) we structured the position and outgrowth of neurons (Gritsun et al. 2012). By integrating the growth-spatial model with the spiking activity model, we modeled the development of bursting behavior, both in time and space, for networks with 50000 neurons or more.

3 Results

The integrated model yielded realistic topology of young cultured networks (figure 1) and their activity , such as bursting patterns, developing with time up to three weeks. The model contains noise triggering and 5% large GABA-ergic neurons (which are excitatory in the first three weeks) with short term plastic (STP) properties (Gupta et al., 2000). Bursting activity (their spread, as well as their development in time) was validated against experimental recordings obtained from cortical neuronal cultures. This integrated network model enabled us also to visualize the 'wave-like' spatial propagation of bursts (figure 2). Depending on network size, wave reverberation mechanisms were seen along the network boundaries. These reverberations may explain the generation of phases of elevated firing before and after the main phase of the burst shape (figure 3) and they may explain the occurrence of very short inter-burst intervals.

In summary, the results show that adding topology and growth explain burst shapes in great detail in networks with STP neurons. Future work must reveal whether long term plastic properties (LTP) add and explain more details or may be ignored in these young cultures.

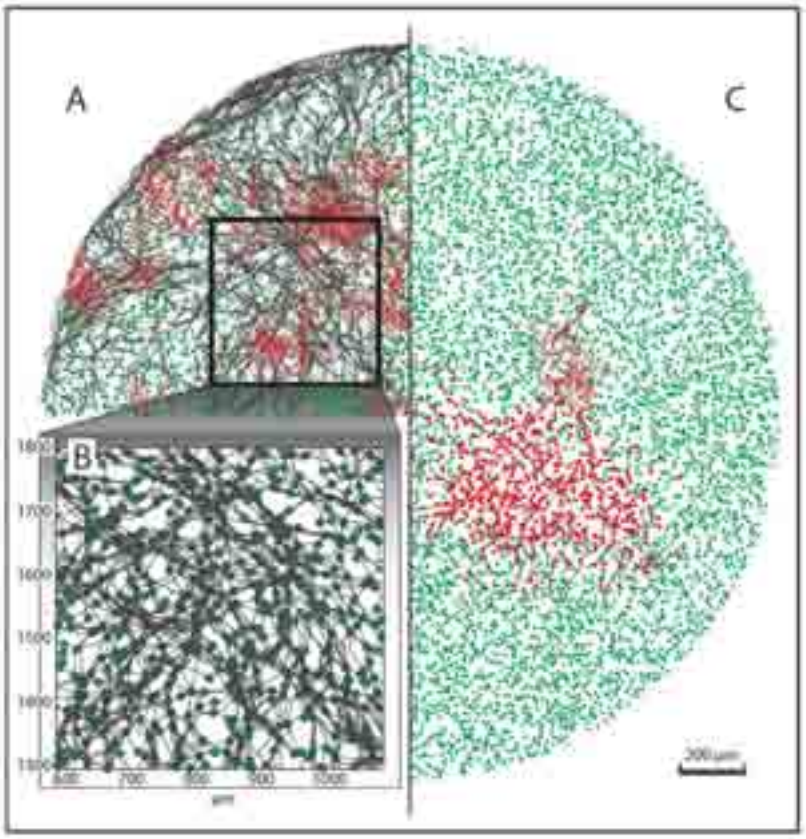

Figure 1. Simulation of neurite morphology in the field guided network of 10,000 neurons. A: The neuronal somas are indicated in green. For 0.5% of these neurons, marked with a large black dot, the neurite structures are shown: axons (black) and dendrites (red). B: Close-up of A, showing bundles of axons that occur in field guided growth models. C: Axon (black line) and dendritic tree (red lines) of a pyramidal neuron (large black dot). Neurons that receive input from this pyramidal neuron are indicated by blue dots.

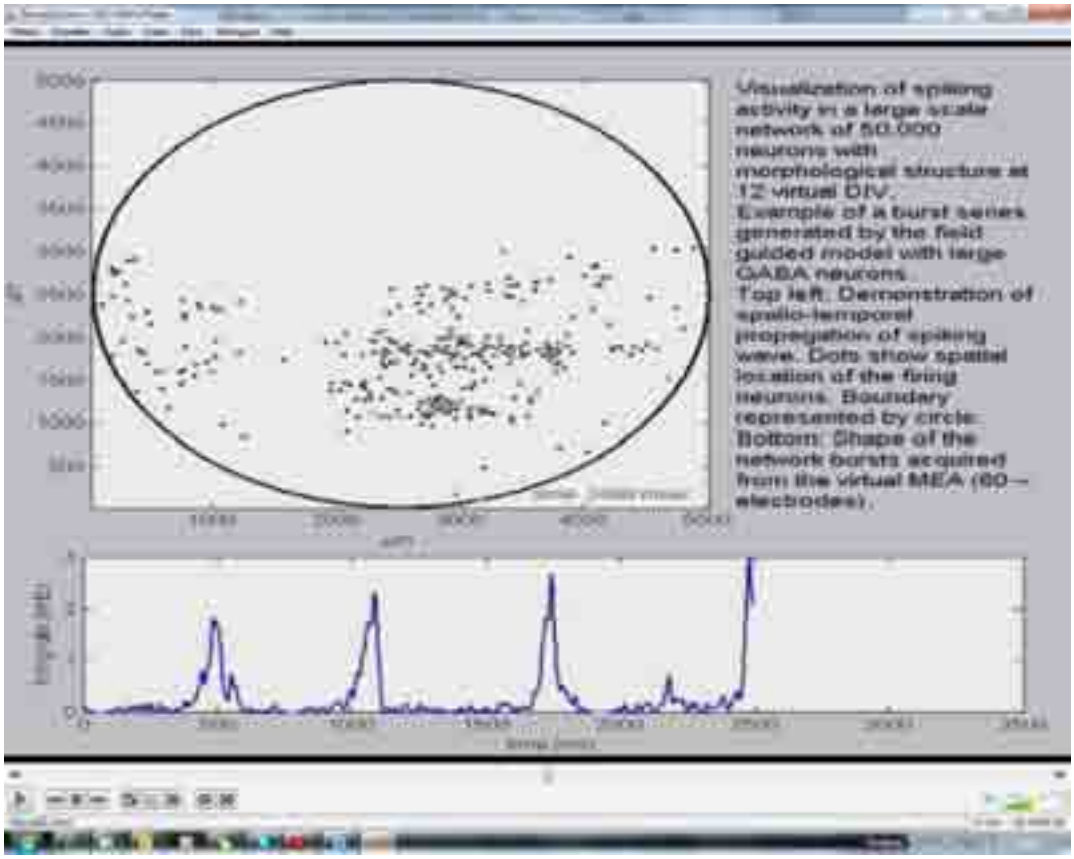

Figure 2. The integrated model at work: snapshot at time 2500 ms of a visualization movie of a burst wave.

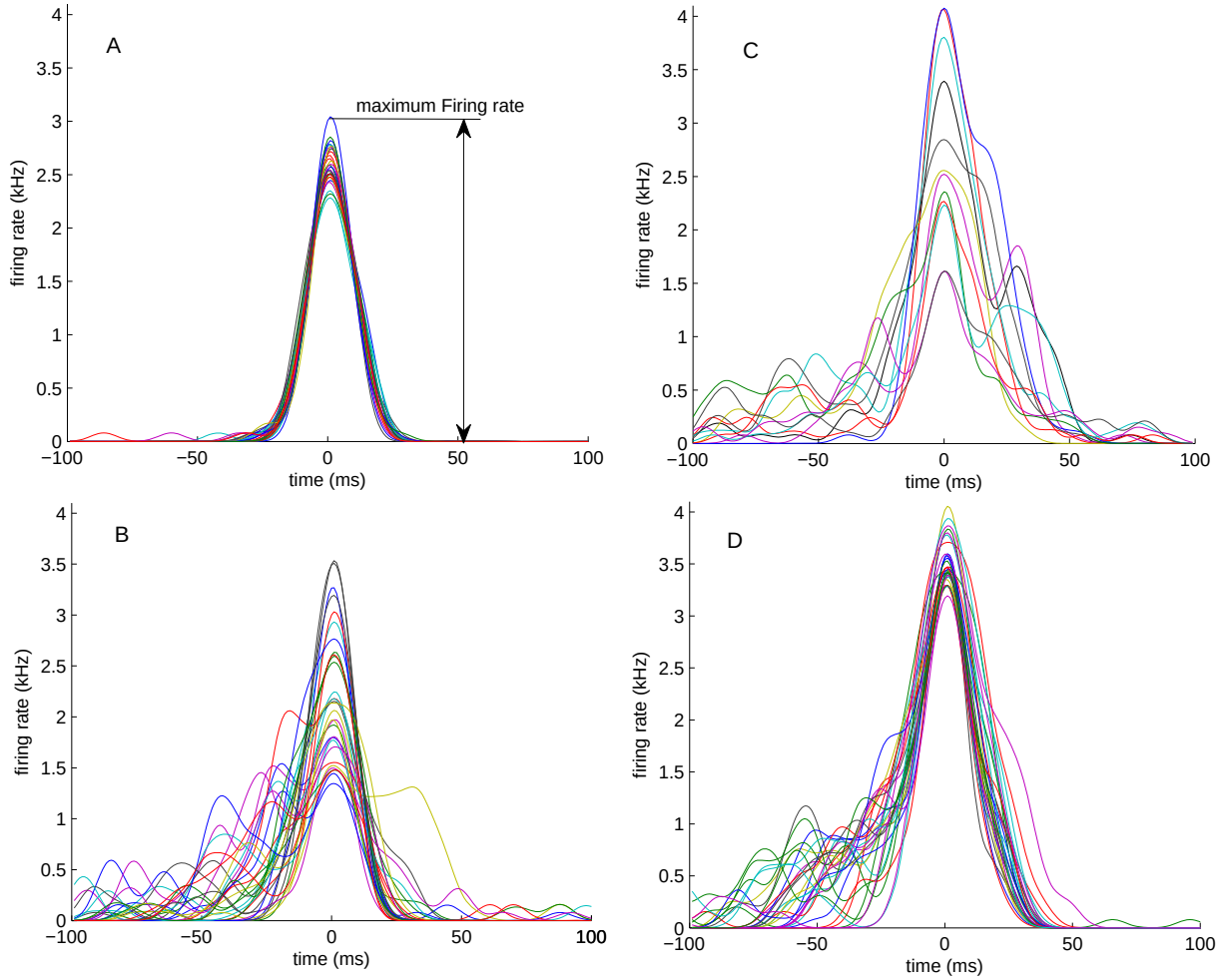

Figure 3. Typical network burst profiles. Networks consisted of 10,000 (A and B) or 50,000 neurons (C) and were wired using the field guided approach with large GABA-ergic neurons. D: example of experimental bursts taken from previous study (Gritsun et al 2011, culture # 4) . Bursts were detected in the recorded or simulated activity acquired from the networks of the same (virtual) age (12th vDIV for A and C, and 19th (v)DIV for B and D), and aligned by their peaks.

References

[1] Stegenga J, le Feber J, Marani E, Rutten WLC (2008) Analysis of cultured neuronal networks using intra-burst firing characteristics. IEEE Trans Biomed Eng 55(4):1382–1390

[2] Van Pelt J, Wolters PS, Corner MA, Rutten WLC, Ramakers GJA (2004) Long-term characterization of firing dynamics of spontaneous bursts in cultured neural networks. IEEE Trans Biomed Eng 51:2051–2062

[3] Wagenaar DA, Pine J, Potter SM (2006) An extremely rich repertoire of bursting patterns during the development of cortical cultures. BMC Neurosci 7:11

[4] Gritsun TA, le Feber J, Stegenga J, Rutten WLC (2010) Network bursts in cortical cultures are best simulated using pacemaker neurons and adaptive synapses. Biol Cybern 102:1–18

[5] Gritsun TA, leFeber J, Stegenga J and Rutten WLC (2011) Experimental analysis and computational modeling of inter-burst intervals in spontaneous activity of cortical neuronal cultures, Biol Cybern 105:197-210.

[6] Gritsun TA, leFeber J and Rutten WLC (2012) Growth dynamics explain the development of connectivity and spatiotemporal burst activity of young cultured neuronal networks in detail . PlosOne, in press.

[7] Gupta A, Wang Y, Markram H (2000) Organizing principles for a diversity of GABAergic interneurons and synapses in the neocortex. Science 287: 273-278.

Three-dimensional quantitative analysis of the dorsal-root-ganglia neuron-electrode interface

João Fernando Mari [1,2], Amanda Ferreira Neves [3,5], José Hiroki Saito [2,4], Celina M. C. Lotufo [5], João-Batista Destro-Filho [3], Ariadne A.B. Oliveira[5]

1 Institute of Exact Sciences and Technology - Federal University of Vicosa - Campus Rio Paranaíba - BRAZIL
2 Department of Computer Science - Federal University of Sao Carlos - BRAZIL.
3 School of Electrical Engineering - Federal University of Uberlandia - Campus Santa Monica - BRAZIL
4 Faculty of Campo Limpo Paulista - BRAZIL.
5 Dept. of Physiological Science - Institute of Biomedical Sciences - Federal Univ. of Uberlandia - BRAZIL.
* Corresponding author. E-mail address: joaofmari@gmail.com

Abstract
Microelectrode arrays (MEAs) can stimulate and record extracellular electrical activities from neurons in culture over long periods and neuronal arrangements can greatly influence the electrical activity recorded by MEAs. Using images obtained by confocal fluorescence microscopy, we suggest methodological tools aimed at quantitatively studying neural network topology on microelectrodes, based on a three-dimensional perspective. Thus, it is possible to characterize the neuron-electrode interface, so that to enable efficient electrical activity recordings.

1 Introduction

Microelectrode Arrays (MEAs) allow studying the distributed patterns of electrical activities in dissociated cultures of brain tissues, composed by neurons and glia [1]. Confocal microscopy imaging allows monitoring the three-dimensional cell morphology and even the cell culture topology, it still permits to investigate the relation between cell and electrode, critical to recording a good-quality signal [2]. We propose a system that generates 3D polygonal cell models, which is capable to perform a fully-automated quantitative analysis, applied to dorsal root ganglia (DRG) cultures.

2 Methods

2.1 Cell Culture and Imaging

Dissociated DRG cell cultures were prepared from Wistar young rats, anesthetized with CO_2 and sacrificed by decapitation in accordance with the IASP and approved by the local Ethic Committee of Animal Experiments (CEUA/UFU). Dissociated cells were then plated on 60-channel MEAs ((*30* μm diameter, *200* μm spacing; *Multichannel Systems*). Cells were incubated with DiBAC4(3) and imaged under a laser scanning confocal microscope (*Zeiss LSM 510 META*). Images were acquired in two channels, a fluorescence channel and a light-transmission one. The transmission-light channel was used to assess the position of the microelectrodes.

2.2 Neuron 2D Manual Assessment

The number of microelectrodes and neurons on images were counted, but considering only cells located at most 100 μm radius far from electrode center, and neurons were classified according to their distance to microelectrode (D) as potentially connected (D < 30 μm); neighboring (30<D<60 μm), and distant (D>60 μm). From the results, we calculated the mean distances (D') between microelectrodes and the neurons standing within its recording area. Thus, simple geometric 2D measurements were calculated as the mean surface area and the mean membrane perimeter of all neurons individually, as well as the mean Feret's diameter.

2.3 Automated 3D Quantification System

The preprocessing applied to volumetric images aims to reduce noise, to improve images contrast, and to avoid the mistakes of sub-segmentation.

In order to obtain a polygonal representation of the cells surfaces from the volumetric images, it was used an implementation of the "marching-cubes" algorithm [3], that is implemented in the "3D Viewer" software [4], an *ImageJ* plug-in (http://imagej.nih.gov/ij/). Due to the presence of noise and residues in the culture, even after the preprocessing stage, a large number of the generated polygonal surfaces do not correspond to neurons, i.e. "false positives". In order to reduce them, a semi-automatic classification method is proposed. An interactive tool was developed to identify and eliminate the remaining false positives.

The polygonal surfaces produced in the previous step and the information about the position of the microelectrodes are processed in order to automatically calculate a series of quantitative measures: (a) number of cells presents in the image; (b) surface area of each cell (in μm^2); (c) the distances between the cells, in

the 3D-space and 2D- plane; (d) the distances between the microelectrodes and the cells. These measures are important for monitoring the development of the neurons plated on MEA; and to study the relationship among electrophysiological activities recorded by the electrodes. The classification steps, 3D visualization and automated quantitative analysis were developed using Java and the VTK library (www.vtk.org).

3 Results and Discussion

In order to evaluate the system performance, three volumetric images obtained from two different cultures were considered. Images 1 and 2 were observed from a cell-high-density region in Culture 1 and 2, respectively. Image 3 was observed from a cell-low-density region in culture 2.

3.1 Neuron 2D Manual Quantification

Each image presented different patterns of neuron adhesion. Most part of neurons were classified as distant from microelectrode and few neurons were found either neighboring or connected with them. This result was expected since we did not use any technique to guide neuronal growth.

Table 1 shows the neurons classified according to their distance to microelectrode, where *E* is the number of electrodes; *C/E* is the cell electrode ratio; *CC*, *CN* and *CD* are the number of connected, neighbouring and distant cells respectively, and *D'* is the mean distance between electrodes and cells within its recording area.

Table 1 – 2D-manual classification of neurons according to their distance to microelectrodes

I	*E*	*C/E*	*CC*	*CN*	*CD*	*D' (μm)**
1	1	4.0	0	0	4	92.5 ± 12.9
2	9	3.1	2	7	19	73.4 ± 28.2
3	1	2.0	0	2	0	39.6 ± 1.2

* Data are reported as mean ± standard deviation.

3.2 Neuron 3D Manual Quantification

The surface reconstruction step generates 100, 246, and 32 polygonal surfaces, where 80, 218 and 30 are respectively false-positives. The semi-automatic classification was able to remove 67(83%), 190(87%), and 30(100%) false-positives results, remaining only 13, 28 and 0 objects to be manually removed by the interactive tool, considering the images 1, 2, and 3, respectively. The system allows visualizing neurons as well as the electrodes three-dimensionally by any angle of view and zooming level. Fig. 1 shows the 3D visualization of DRG culture in Image 2.

Table 2 summarize the measures obtained in the automated quantitative analysis, where *S'* is the mean cells surface area. *DC' 2D* and *3D* are the mean distance between the pairs of cells in 2D and 3D, respectively. *DE'* is the mean distance between electrodes and cells

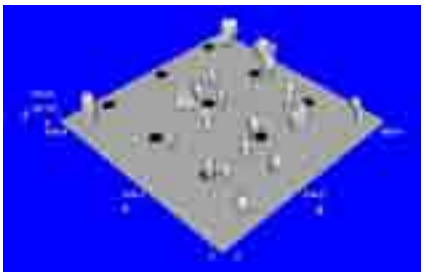

Fig. 1. 3D visualization of DRG culture present in image 2.

Table 2. The measures obtained in the automated quantitative analysis

I.	*S' (μm^2)**	*DC' 3D (μm)**	*DC' 2D (μm)**	*DE' 2D (μm)**
1	1641± 890	124 ± 58	124 ± 58	173 ± 55
2	6932 ± 4223	303 ± 152	303 ± 58	323 ± 155
3	8094 ± 1722	34 ± 0	34 ± 0	39 ± 1

* Data are reported as mean ± standard deviation.

4 Conclusion

As a result we found more neurons located within the microelectrode recording area (100 μm) in cultures with a high-cell-density then in low-cell-density condition. To propose better approaches for studies with electrophysiological and image processing, a high concentration of DRG cells must be added on MEAs in order to enhance the acquisition of electrophysiological signals. Consequently, cultures with high-cell-density require automated and semi-automated systems to identify, and calculate quantitative measures. The proposed system efficiently eliminates false positives in a semi-automatic way, and automatically computes quantitative measures. The distance among cells is very important, since it may describe the topology of cell distribution within the culture, and the distance between the microelectrodes and the cells provides a way to infer the relationship of the electrophysiological activity of the neural cells and the signal recorded by MEA.

Acknowledgement

The authors want to thank CNPq (558114/2010-5, A.F. Neves), FAPEMIG (TEC- APQ-02143-10), Genova Univ. and *Multichannel Systems Inc.*, *DE*, for providing us with MEA devices, and Mariane Silva and to Prof. M.E. Beletti (Histology Dept. - UFU.

References

[1] Potter, S.M. (2001). Distributed processing in cultured neuronal networks. In: Nicolelis, M.A.L. (Ed) Progress in Brain Research, 130, 49-62.

[2] Van Pelt, J., Wolters, P.S., Corner, M.A., Rutten, W.L., Ramakers, G.J. (2004). Long-term characterization of firing dynamics of spontaneous bursts in cultured neural networks. *IEEE T. Bio-Med Eng.*, 51(11), 2051-2062.

[3] Lorensen, W.E., Line, H.E. (1987). Marching cubes: a high-resolution 3D surface reconstruction algorithm. *Computer Graphics*, 21(4), 163-169.

[4] Schmid, B. et al. (2010). A high-level 3D visualization API for Java and ImageJ. *BMC Bioinformatics*, 11(274).

Formation of neuronal networks *in vitro* and analysis of neuronal avalanches

Miho Goto[1]*, Lui Yoshida[1], Atsushi Saito[1], Aki Saito[1], Yuzo Takayama[2], Hiroyuki Muriguchi[1], Kiyoshi Kotani[1] and Yasuhiko Jimbo[1]

1 Graduate School of Frontier Sciences, the University of Tokyo, Japan
2 Graduate School of Information Science and Technology, the University of Tokyo, Japan
* Corresponding author. E-mail address: goto@bmpe.k.u-tokyo.ac.jp

Abstract
To analyse network dynamics, neuronal avalanches are quite interesting phenomena. Recently, it was reported that neuronal avalanches were power-law distributed in a slice cortex of a rat, which is an important index representing a network criticality and its efficiency of information transition. In this study, extracellular electrical activities were measured using Microelectrode Array (MEA) measurement system, and the temporal changes of the power-law behaviour in neuronal avalanches were studied for cultured neuronal networks.

1 Introduction

To analyse network dynamics, neuronal avalanches are quite interesting phenomena. Neuronal avalanche is the phenomena where neuronal firing spreads spatially and temporally in the duration from several tens of ms to several hundreds of ms in the neuronal networks [1]. Recently, it was reported that neuronal avalanches were power-law distributed in a slice cortex of a rat [1] and cultured neuronal networks [2], which attracted attention because power law has been proposed as an indicator of self-organized criticality by P. Bak et al. [3]. Furthermore, C. Haldeman et al. reported that the numbers of particular repeating signal patterns which occur more frequent than incidental firing were maximized at the critical point [4]. In this study, extracellular electrical activities were measured using Microelectrode Array (MEA) measurement system, and the temporal changes of the power-law behaviour in neuronal avalanches were studied for cultured neuronal networks.

2 Materials and methods

Neuronal cells of cerebral cortex derived from 18-day-old embryo rat were dissociated by trypsinization. Cell suspension was prepared with standard culture medium at the cell concentration of 5×10^6 cells/ml. Cells were cultured on the MEA substrate for more than 48 days *in vitro* (DIV). The temporal changes of electrical signals were amplified to 10000 times and converted into digital signals with a resolution of 12 bit and 25 kHz of sampling rate. Electrical signals larger than five times of standard deviation of the noise were considered as action potentials from neuronal cells. An avalanche was detected in the same ways as described in previous report [2]. Briefly, Potential peak times of each electrode were divided by 0.6 ms window and distinguished as active frames, where at least one electrode detected the potential peaks, or non-active frames, where any electrode did not detect the potential peaks. An avalanche was defined as continuous flames separated by non-active frames [1]. The probability distribution of avalanche size was plotted in log-log coordinates [2].

3 Results and Discussion

Power-law behaviour in neuronal avalanches, indicating self-organized criticality, was traced over the period of 5-48 DIV. The plot was divided into two parts, linearly-approximated component and peak component. About linearly-approximated component, the probability was power-law distributed in the latter DIV as reported previously [1, 2]. On the other hand, in the early DIV, the probability was not power-law distributed (Fig. 1 (A, B)). This indicates that there is a transient period toward the matured stage of neuronal network. Especially, in phase II (16 DIV~ 19 DIV), drastic change in the shape of probability was found (Fig. 1 (C)). It was reported that a distribution of avalanches with shuffled data did not follow a power-law distribution [2], thus phase (II) was the period for formation of proper and functional networks. Furthermore, the fraction of peak component to linearly-approximated component (P/L) changed in the same way with the analysis about linear components (Fig. 2). This indicates that peak components also contribute the network maturation.

4 Conclusion and Future Perspective

Electrical activities of cultured neuronal networks on MEA *in vitro* were measured. Power-law behavior in neuronal avalanches, indicating self-organized criticality, was traced over the period of 5-48 DIV. In the early DIV, the probability was not power-law distributed. This indicates that there is a transient period to-

ward the matured stage of neuronal network. To understand the transient phase (II), it is useful to study these avalanche of network patterned into arbitrary configuration. Thus, in the next step, we study the temporal changes of the power-law behavior in neuronal avalanches for normally cultured neuronal networks and patterned ones.

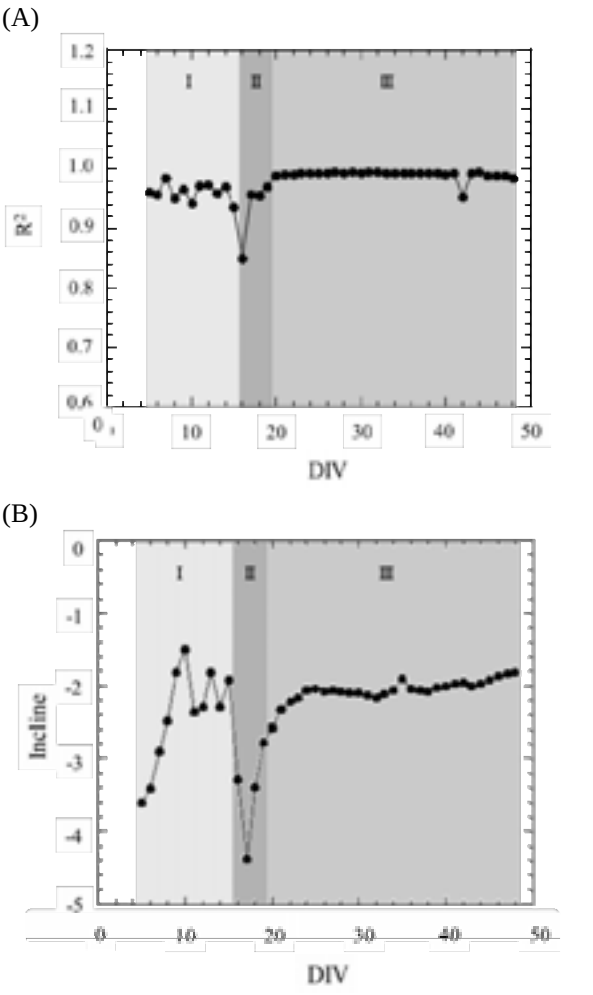

Fig. 1. Temporal changes of R^2 value (A) and incline (B). The time course could be divided into three phases, (I) 5 -15 DIV, (II) 16-24 DIV, (III) 25-48 DIV. Temporal changes of avalanche plots in phase II (C). In early stage, the size distribution of avalanches did not follow power law, indicating that there was the transient period moving on to the critical point.

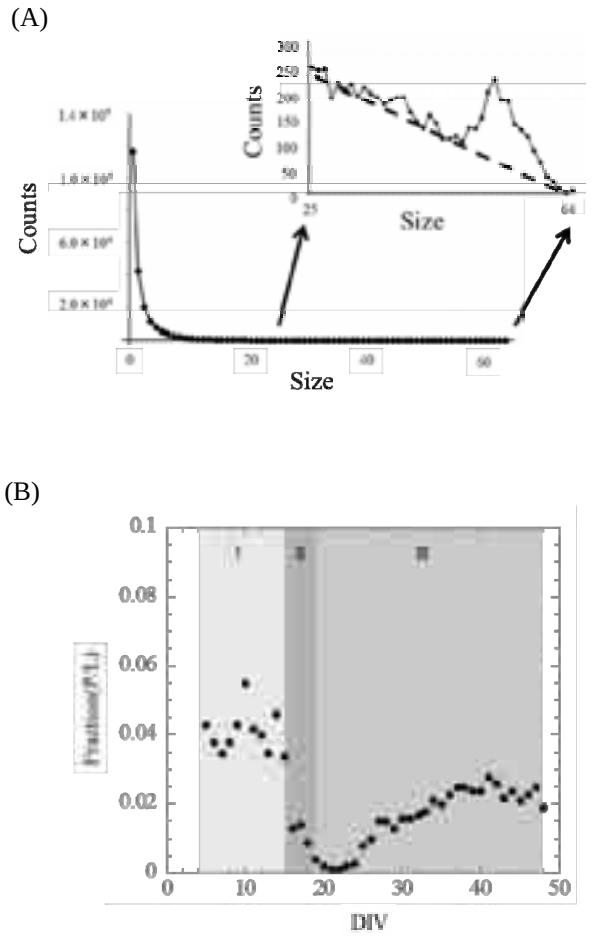

Fig. 2. Analysis including the components of peaks. (A) Intensity of counts with size 25~64 was composed of linear component, i.e. background, and peak component. The background was Peak was approximated by trapezoidal shape. (B) The change of fraction of P/L was plotted. Peak component was also changed with three periods, thus peak component also contributes to neuronal network maturation.

Acknowledgement

This work was supported in part by Japan Society for the Promotion of Science.

References

[1] Beggs J. M. and Planz D. (2003), Neuronal Avalanches in Neocorti-cal Circuits., *Journal of Neuroscience*, 23, 35, 11167-11177.

[2] Pasquale V., Massobrio P., Bologna L. L., Chiappalone M. and Martinoia S. (2008), *Neuroscience*, 153, 1354-1369.

[3] Bak P., Tang C., and Wiesenfeld K. (1987), Self-Organized Criticality: An Explanation of 1/f Noise., *Physical Review Letter*, 59, 4, 381-384.

[4] Harris T. E. (1963), The Theory of Branching Process, *New York: Dover Publications*.

Clustered network structure promotes spontaneous burst initiation in vitro

Samora Okujeni[1,2,3*], Nila Mönig[2], Steffen Kandler[1,2,3], Oliver Weihberger[1,2,3], Ulrich Egert[1,3]

1 Bernstein Center Freiburg, University Freiburg, Freiburg, Germany
2 Faculty of Biology, University Freiburg, Germany
3 Biomicrotechnology, Dept. Microsystems Engineering – IMTEK, University Freiburg, Germany
* Corresponding author. E-mail address: okujeni@bcf.uni-freiburg.de

Abstract
To assess dependencies between evolving connectivity and emerging network dynamics we modified connectivity in developing networks of cortical neurons in vitro by pharmacological manipulation of morphological differentiation processes. Our data suggests that clustering of neurons and fasciculation of neurites increases the ability of cultured networks to spontaneously initiate synchronous network bursts.

1 Introduction

Synchronous bursting events (SBE) are widely observed in developing neuronal systems, suggesting that the ability to spontaneously initiate these dynamics reflects a crucial, though transient feature of forming networks. Similarly, SBE dynamics robustly emerge as the predominant type of activity in networks of cultured neurons in vitro. We suggest that general neuronal mechanisms might guide network self-organization in a way that establishes these dynamics. Interestingly, theoretical models have shown that hierarchical network structures embedding clusters of strongly inter-connected neurons are optimal for initiating and sustaining spontaneous activity [1] and clustered network structure typically emerges in networks forming in vitro [2] and in vivo [3]. We speculate that activity-dependent structural plasticity, being a principal driving force of network self-organization, establishes clustered network structures and thereby promotes spontaneous activity levels. Previous studies have shown that protein kinase C (PKC) inhibition promotes dendritic outgrowth and arborization [4], and impairs pruning [5], linking this protein closely to structural plasticity. To test our hypothesis, we thus inhibited PKC in developing networks of cortical neurons in vitro to modify network structure.

2 Materials and Methods

Primary cortical cell cultures were prepared as described previously [6]. Cells were extracted from cortices of newborn rats by mechanical and enzymatic dissociation and plated onto polyethyleneimine-coated micro-electrode arrays (6x10 with 0.5mm and 32x32 electrodes with 0.3mm spacing; Multichannel Systems). Cultures developed in growth medium (MEM) supplemented with heat-inactivated horse serum (5%), L-glutamine (0.5mM), glucose (20mM) and gentamycin (10µg/ml) under 5% CO2 and 37°C incubator conditions. PKC inhibitor Gö6976 1µM was applied starting from the 1st day in vitro (DIV). Staining against MAP2 protein was performed for morphological analysis of dendrites. Recordings were performed under culture conditions (MEA1600-BC and MEA30-1024, Multichannel Systems).

3 Results

We show that developmental inhibition of PKC in cortical cell cultures increased dendritic outgrowth, impaired neurite fasciculation and clustering, and abolished network pruning. This resulted in more homogeneous and potentially better connected networks. In consequence, SBEs propagated faster and in more regular wave fronts. Yet, in agreement with our hypothesis, SBEs were triggered from fewer sites and at lower rates suggesting that these homogeneous networks embedded fewer SBE initiation zones. We tested if the homogeneous networks were able to support higher SBE rates by providing additional input by electrical stimulation. Interestingly, homogeneous networks achieved higher SBE rates when electrically stimulated compared to the more clustered control networks. Our data suggests that activity-dependent structural plasticity promotes network clustering and thereby spontaneous SBE initiation during development. Based on recent evidence for a reciprocal scaling between synaptic strength and number of neuronal partners in vitro [7], we propose that locally more confined synaptic targeting within neuronal clusters promotes stronger and more recurrent coupling of neurons. The resulting connectivity structure could thereby more easily amplify spontaneous excitation locally beyond a critical threshold necessary for SBE initiation.

4 Conclusion

Our results indicate that activity-dependent structural plasticity promotes neuronal clustering and thereby the ability of in vitro networks to spontaneously initiate SBEs. We propose that this might be part of a general strategy pursued by neuronal networks to establish this crucial activity pattern during development.

Acknowledgements

We thank Patrick Pauli and Ute Riede for technical assistance. The neuroanatomy Freiburg is gratefully acknowledged for their helpful support. Funded by the German BMBF (FKZ 01GQ0420 & FKZ 01GQ0830) and by the EC (NEURO, No. 12788).

References

[1] Kaiser M, Hilgetag CC (2010) Optimal hierarchical modular topologies for producing limited sustained activation of neural networks. *Front Neuroinformatics 4:8.:8.*

[2] Kriegstein AR, Dichter MA (1983) Morphological classification of rat cortical neurons in cell culture. *J Neurosci 3:1634-1647.*

[3] Song S, Sjostrom PJ, Reigl M, Nelson S, Chklovskii DB (2005) Highly nonrandom features of synaptic connectivity in local cortical circuits. *PLoS Biol 3:e68.*

[4] Metzger F, Kapfhammer JP (2000) Protein kinase C activity modulates dendritic differentiation of rat Purkinje cells in cerebellar slice cultures. *Eur J Neurosci 12:1993-2005.*

[5] Kano M, Hashimoto K, Chen C, Abeliovich A, Aiba A, Kurihara H, Watanabe M, Inoue Y, Tonegawa S (1995) Impaired synapse elimination during cerebellar development in PKC gamma mutant mice. *Cell 83:1223-1231.*

[6] Shahaf G, Marom S (2001) Learning in networks of cortical neurons. J Neurosci 21:8782-8788.

[7] Wilson NR, Ty MT, Ingber DE, Sur M, Liu G (2007) Synaptic reorganization in scaled networks of controlled size. *J Neurosci 27:13581-13589.*

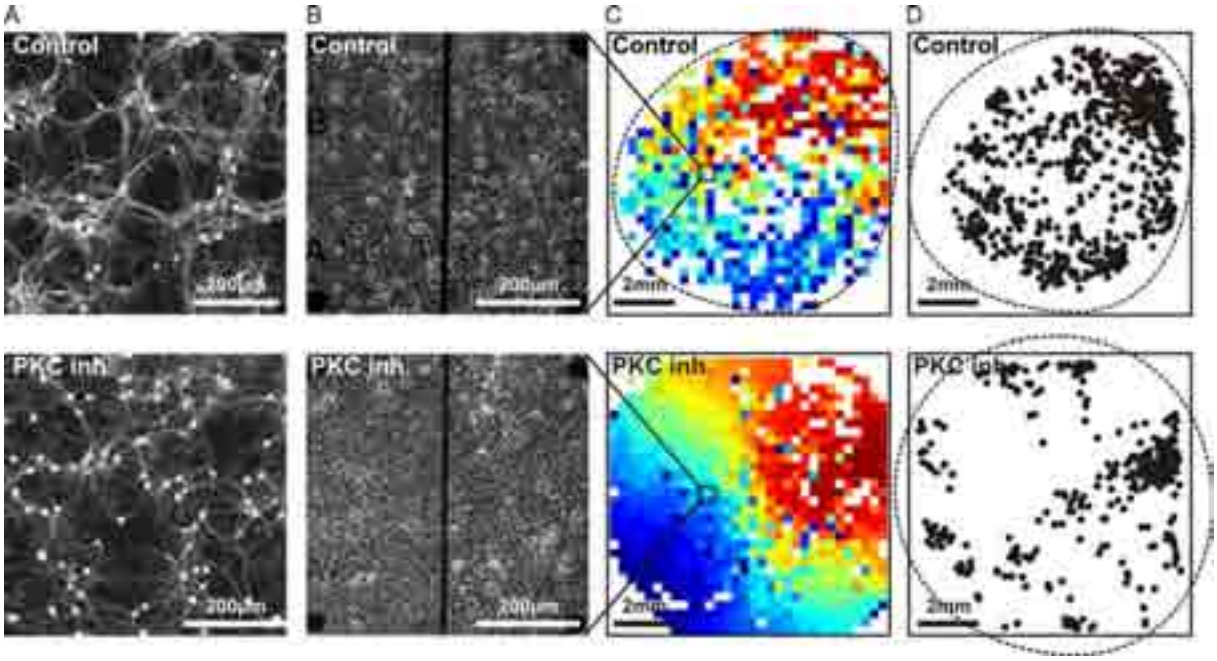

Fig. 1. Structure and dynamics in cortical cell cultures

A) MAP2 Staining against dendrites and somata in low density cultures (~200 neurons/mm2) after 42DIV. PKC inhibition impaired neuronal clustering and reduced dendritic fasciculation in developing networks which suggests more homogeneous connectivity.

B) Dense cultures (~2000 neurons/mm2) were grown on MEAs and documented by phase contrast microscopy. More homogenous networks had formed under impaired PKC activity at 44DIV.

C) Propagation of activity during SBE was assessed with 1024 electrode MEAs (32x32) that spanned almost the entire area of cultured networks (corners lack neurons). The pseudo-color map depicts the first spike rank order (from early in red to late blue; white indicates no activity) of during exemplary SBEs. PKC inhibited networks showed more regular propagation patterns indicating more homogeneous connectivity. The zoom-in gives an impression of the size of neurons, networks and MEA.

D) SBE initiation zones were identified as median coordinate position of the first percent of active sites during single SBEs, respectively. Network boundaries (dashed circle) were generally more susceptible to initiate SBEs. More homogeneous networks forming under impaired PKC embedded fewer initiation sites than controls and triggered SBEs at lower rates (Controls N=807 SBEs in 60min; PKC inhibited N=676 SBEs in 140min).

Developmental changes in temporal coordination of network activity in neuronal cultures

Arthur Bikbaev[1*], Renato Frischknecht[2], Martin Heine[1]

1 RG Molecular Physiology, Leibniz Institute for Neurobiology, Magdeburg, Germany
2 RG Extracellular Matrix, Leibniz Institute for Neurobiology, Magdeburg, Germany
* Corresponding author. E-mail address: bikbaev@yahoo.com

Abstract
Synchronisation of neuronal activity is known to play a pivotal role in activity-dependent changes that mediate plasticity in the brain. Neuronal cultures represent relatively simple neuronal networks that are isolated from sensory inputs present in intact brain, and therefore thought to be a suitable subject for studying the mechanisms of self-organisation of the network level. In present study, we monitored the spontaneous neuronal activity in hippocampal cultures grown on microelectrode arrays during development and analysed the changes in temporal coordination of activity. In line with earlier reports, we found that bursting becomes a dominant pattern of neuronal activity during development. Further, we found that maturation of neuronal cultures is associated with dramatic improvement of temporal precision of bursting correlated between spatially remote network locations, thus indicating facilitation of burst propagation across the network. Our results demonstrate that developmental period after synaptogenesis is characterised by optimisation of network interaction even in the absence of external sensory input.

1 Introduction

Neuronal cultures belong to widely used preparations in molecular biology and represent relatively simple neuronal networks. Due to isolation from sensory input, which is known to play a crucial role for neural development [1], a developmental arrest occurs in cultures from 3rd to 4th weeks of development [2, 3]. However, such absence of sensory drive provides an opportunity to elucidate intrinsic mechanisms of self-organisation of neuronal activity that are masked by various factors in intact brain. In order to characterize the changes in temporal coordination of the network activity associated with maturation of neuronal cultures, we monitored the spontaneous neuronal activity of dissociated hippocampal cultures at different developmental stages.

2 Experimental procedures

Neuronal cultures

Dissociated neuronal cultures prepared from embryonic (E18) rat hippocampi were plated on 60-channel microelectrode arrays (MultiChannel Systems, Reutlingen, Germany) and incubated at 37°C for at least 28 days *in vitro* (DIV) with culture medium being partially exchanged on a weekly basis. All experimental procedures were carried out in accordance with the EU Council Directive 86/609/EEC and were approved and authorised by the local Committee for Ethics and Animal Research.

Recording and analysis of the network activity

Spontaneous neuronal activity of each culture (n=5) was recorded at DIV14, DIV21 and DIV28 under conditions (temperature, humidity and gas composition) identical to those during incubation. The analysis was performed on 10-min long recorded sessions for each culture at each time-point, and included threshold-based (±5SD) spike detection followed by burst identification (5 or more spikes with inter-spike interval <100 ms). Obtained spike and burst time-stamps were used for a general evaluation of the spiking and bursting activity. Due to relatively low level of the network activity at DIV14, data for each culture were normalised to respective values at DIV28 (taken as 100%). Further, to evaluate the changes in the network interaction that take place during development, we analysed network (population) bursts (NBs), i.e. episodes of correlated (coincident) bursting in two or more channels. For each NB, participating channels were ranked by burst onset time, hence representing propagation of bursting across the network. Next, we analysed the duration of NB episodes, number of participating channels per NB, as well as the delays between bursting onset in channels with neighbouring ranks (burst onset lag for individual channel pairs) and for each channel in a given NB (NB recruitment lag relative to NB onset). For statistical analysis, Kruskal-Wallis rank ANOVA was used. The effect of the temporal factor and differences between groups was considered as significant at $p<0.05$.

3 Results

General evaluation of neuronal activity revealed that developmental changes within observed period were related predominantly to the bursting activity (Fig. 1). Although, a trend towards an increase of spiking was evident, the effects were non-significant. Maturation of neuronal cultures was found however to be associated with strong enhancement and generalisation of bursting activity, reflected by significantly bigger number of bursting channels (*time*: $p<0.01$) and the number of bursts per session (*time*: $p<0.05$), which corresponded to a gradual decrease of inter-burst interval (*time:* $p<0.05$). Furthermore, this shift of the network activity pattern towards bursting mode was associated with marked decrease of the mean inter-spike interval during bursts (*time:* $p<0.05$).

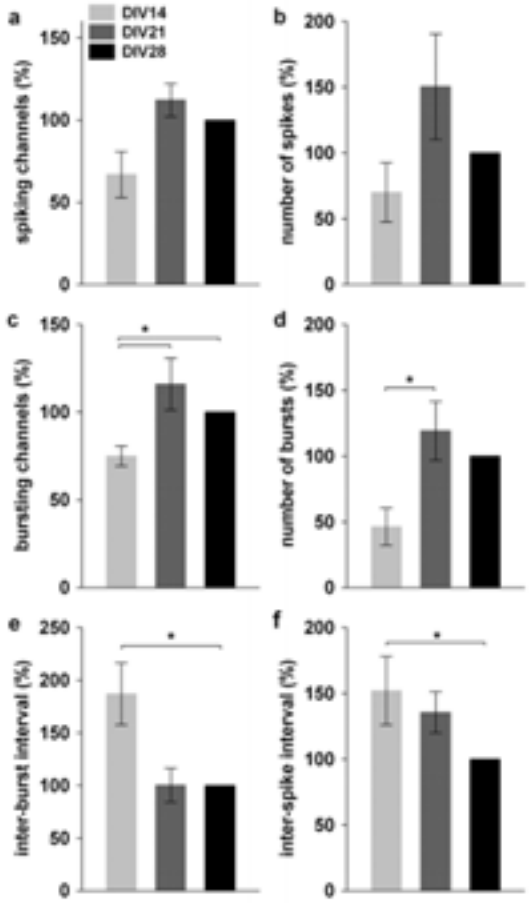

Fig. 1. Maturation of neuronal cultures is associated with enhancement and generalisation of bursting activity. A trend towards facilitation of spiking was evident for the number of spiking channels and the number of spikes per session (**a,b**), but effects did not reach significance. (**c-f**) After synaptogenesis, bursting becomes a preferential pattern of activity in neuronal cultures. Data are represented as mean ± s.e.m. Asterisks denote significant between-group differences at $p<0.05$.

The results of analysis of network bursts demonstrated dramatic changes in temporal precision of correlated bursting between spatially remote neuronal clusters that occurred after DIV14 (Fig. 2). Albeit, the duration of NBs was significantly shorter at DIV21 and DIV28 in comparison to DIV14 (*time:* $p<0.001$), such episodes of network interaction involved bigger number of channels (*time:* $p<0.01$). Importantly, burst onset lag decreased linearly along the development and was markedly shorter at DIV28, when compared to DIV14 (*time:* $p<0.001$), reflecting facilitation of sequential recruitment of network locations into correlated bursting. Furthermore, significantly shorter NB recruitment lags (*time:* $p<0.001$) that were found in mature cultures indicate a higher probability of bursting propagation and generalisation across the network.

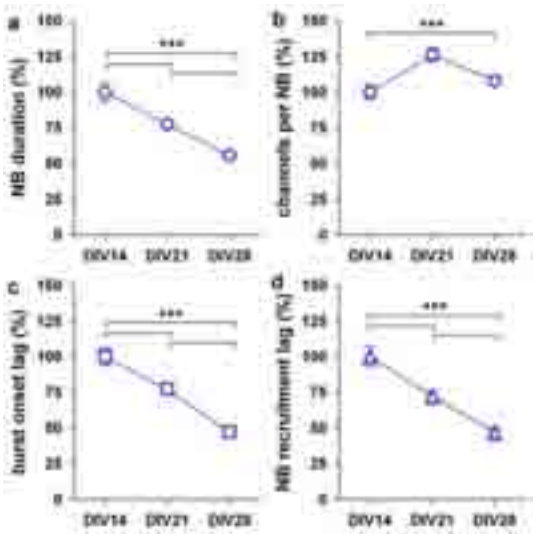

Fig. 2. Facilitation of correlated bursting in neuronal cultures during development. Despite striking decrease of NB duration (**a**), synchronous bursting in mature cultures involves bigger number of channels (**b**). (**c,d**) Maturation of neuronal cultures is characterised by significant decrease of bursting onset lags between remote network locations. Data are represented as mean ± s.e.m. Asterisks denote significant between group differences at $p<0.001$.

Taken together, our findings suggest that maturation of neuronal cultures is associated with self-organization of the network activity and optimization of network interaction.

Acknowledgement

This study was supported by the Federal State of Saxony-Anhalt (LSA RG Molecular Physiology) and DFG (grant HE-3604/2-1).

References

[1] Ben-Ari Y. (2001). Developing networks play a similar melody. *Trends Neurosci.*, 24(6), 353-360.

[2] Marom S., Shahaf G. (2002). Development, learning and memory in large random networks of cortical neurons: lessons beyond anatomy. *Quart. Rev. Biophys.* 35, 63-87.

[3] van Pelt J., Wolters P.S., Corner M.A., Rutten W.L., Ramakers G.J. (2004). Long-term characterization of firing dynamics of spontaneous bursts in cultured neural networks. *IEEE Trans. Biomed. Eng.* 51(11), 2051-2062.

How to link neuronal network activity to robot behavior

Suguru N. Kudoh* and Hidekatsu Ito

Lab. for Neuronal Intelligence Engineering, Dep. Human System Interaction,
School of Science and Technology, Kwansei Gakuin University, 2-1 Gakuen, Sanda, 669-1337, Japan
* Corresponding author. E-mail address: snkudoh@kwansei.ac.jp

Abstract
The rat hippocampal neurons were cultured on a dish with 64 planer micro electrodes array (MEA). Neurons reorganized a functional network, and an external inputs form outer world elicited a reproducible, particular spatiotemporal pattern of evoked action potentials. We integrated a living hippocampal network and a small moving robot as a body to contact with outside world. The neurorobot is a suitable test environment for embodiment of neuronal information processing. We call the system "Vitroid", meaning a robot as a test tube for neuronal intelligence science. Here we propose behavior-generating system for Vitroid using self-organization map (SOM), which perform regulation of robot and learning at the same time.

1 Background/Aims

Dissociated neurons elongate neurites on a multielectrodes array (MEA) probe and reconstruct a network structure. This structure is not regulated by developmental process and there is no particular genetically controlled circuit. Autonomously composed network is achieved by the functions intrinsic in individual neurons. Therefore this reconstructed network may include primitive basic mechanism of information processing, just like a neuronal system of a primitive animal. We expect a certain type of information processing to emerge in this semi-artificial neuronal network by interaction between the neuronal circuit and outer environment via an interface system. A neurorobot with hippocampal dissociated culture system is a suitable test environment for embodiment of neuronal information processing (Fig.1). We call the system "Vitroid", meaning a robot as a test tube for neuronal intelligence science [1]. In the system, interface systems for interaction between neurons and outer world can be evaluated. As an example of such interface system, we previously reported a pattern recognition method with simplified fuzzy reasoning [1]. The system is enough worth, but it is difficult to perform learning and generation of the robot behaviour simultaneously. Here we propose a robot behaviour generating system with self-organization map (SOM), which perform regulation of robot and learning at the same time.

2 Materials and Methods

2.1 Preparation of living neuronal network

Rat hippocampal neuronal cells were dissociated and cultured on MEA dish in conventional method [1].

Briefly, The hippocampal region of brain was cut off from Wistar rat on embryonic day 17-18 (E17-18). Hippocampal neuronal cells were dissociated by 0.175% trypsin (Invitrogen-Gibco, Carlsbad, California, U.S.A.) in Ca^{2+}- and Mg^{2+}-free phosphate-buffered saline (PBS^{-}) supplemented with 10 mM glucose at 37 ℃ for 10 min. Then neuronal cells were

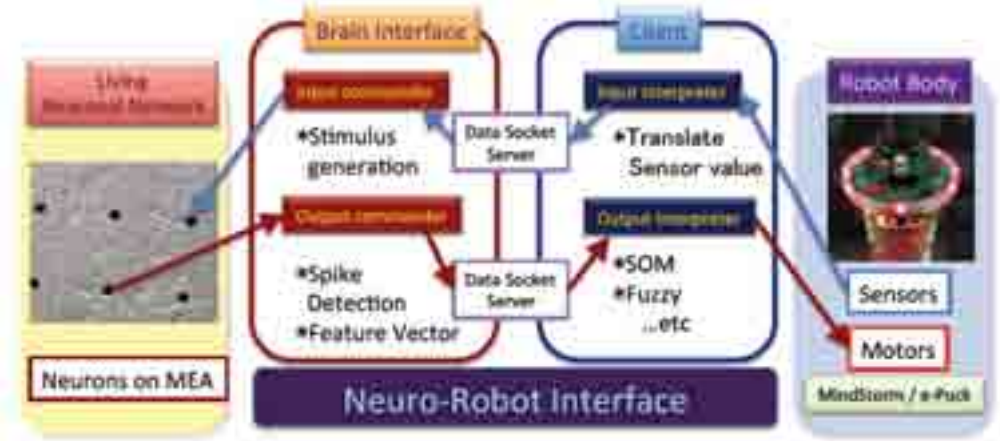

Fig. 1. schematic diagram of neuro robot system "Vitroid"

cultured on a multielectrodes array dish (MED probe, alpha-MED scientific, Japan). We used MED probes that the distance between an electrode (center to center) was 450 μ m. The density of seeded cells was 7800 cells/mm^2. Cell density is higher comparing to the conventional condition, because the reproducibility and stability of spontaneous electrical activity increased in such high-density condition. Culture medium consisted of 45% Ham's F12, 45% Dulbecco's modified minimum essential medium (Invitrogen-Gibco, California, U.S.A.), 5% horse serum (Invitrogen-Gibco, California, U.S.A.), and 5% fetal calf serum (Invitrogen-Gibco, California, U.S.A.), 100 U/ml penicillin, 100 μ g/ml streptomycin (Invitrogen-Gibco, Carlsbad, California, U.S.A.), and 5 μ g/ml insulin (Sigma-Aldrich, US). The MED prove was previously coated with 0.02 % poly-ethylene-imine (Sigma-Aldrich, US). Neurons were cultured at 37 ^{o}C in 5 % CO_2 / 95 % air at saturating humidity. The conduct of all experimental procedures was governed by the “Kwansei Gakuin University Regulations for Animal Experimentation".

2.2 Neurorobot with SOM interpreter

Electrical activity pattern at a certain time window was represented as a feature vector of which 64 elements were spike numbers detected at each electrode. SOM is a kind of unsupervised neural networks proposed by Kohonen [2]. The input layer with 64 nodes has been provided to input feature vector. A two-dimensional output layer with 10 x 10 nodes has been provided. The function of SOM is dimension reduction. SOM picks up a winner node in output layer against input vector. Winner node is located in 2D map, so a 64-dimentional vector is mapped to a two-dimensional position vector of the winner node. This two-dimensional SOM reduce the dimension of a feature vector from 64 to 2 without a loss of information. Each node has a reference vector (weight vector). Euclidean distance between an input feature vector and a reference vector of each node is calculated and node with shortest Euclidean distance is selected as a winner for the input vector. The reference vector of the winner is updated to be closer to input vector. Simultaneously, the reference vector of the neighbor nodes of winner node also updated to be slightly closer to input vector. This procedure gathers nodes with similar reference vectors in neighbor. As a result of that, spacial relationship among nodes in the output layer corresponds to the relationship among input vectors coupled with nodes in the output layer. Our purpose is to extract a reproducible pattern as a representation of certain information in the living neuronal network. Gathered nodes coupled with similar feature vectors means that the similar spacial patterns of network activity gathered each other. In the case that electrical stimulation is applied at a certain electrode, let say E1, as an input from robot sensor, a winner node should be located at a certain position in the output layer. If a winner against other neuronal activity evoked by E2 stimulation is located near the winner against the activity evoked E1, outputs of the living neuronal network against the E1 and E2 inputs are similar each other. In other words, the decisions against these inputs from E1 and E2 are almost same. The spacial distribution of the winner depends on the initial state of reference vectors. At generation of the behavior of the robot, premise behaviors should be designed as the instinct such as collision avoidance. To design such a behavior, winner distribution should be restricted. If the position of representative winner for the E1 input can be specified, the suitable behavior for the E1 input can be defined. For example, if E1 input is applied as the signal of obstacle at the left side of the robot, the robot should be turn to the right, so the left motor speed should be set at the higher value than right motor. To restrict the winner against a particular input, the winner for that input should be fixed at a seed node and E1 input should be applied repeatedly during initial learning process (Fig. 2).

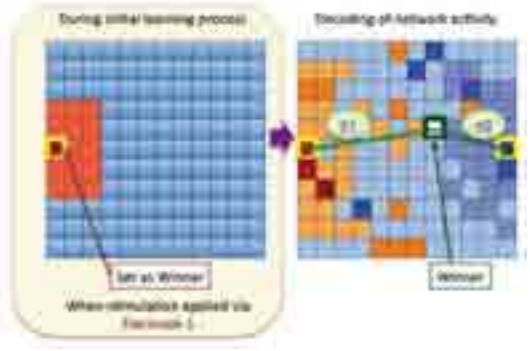

Fig.2 Generation of robot behavior with SOM.

After that, winners against E1 input are expected to be gathered near the seed node. The robot control is performed depending on the position of the winner for the inputted activity. For example, speeds for left and right motors are calculated by weighted average of total network activity, which weights is defined depending on the Euclidian distances between the winner and the E1 seed node or the E2 seed node. We confirmed that this seeding approach could perform separated map around the seed nodes of each input.

Acknowledgement

This research is supported by the Ministry of Education, Culture, Sports, Science, and Technology of Japan under Grant-in-Aid for Scientific Research #24300091.

References

[1] Kudoh SN, Tokuda M, Kiyohara A, Hosokawa C, Taguchi T, Hayashi I (2011), Vitroid - The Robot System with an Interface Between a Living Neuronal Network and Outer World, International Journal of Mechatronics and Manufacturing System, Vol.4, No.2, pp.135-149.

Modeling the dynamics of excitability and its temperature sensitivity

Willem Wybo[1], Rocco A. Barone[1], Daniele Linaro[1] and Michele Giugliano[1,2,3]

1 Theoretical Neurobiology & Neuroengineering, Dept. of Biomedical Sciences, Univ. of Antwerp, Belgium
2 Dept. of Computer Sciences, University of Sheffield, Sheffield, United Kingdom
3 Brain Mind Institute, Swiss Federal Institute of Technology, Lausanne, Switzerland

1 Background/Aims

(Sub)cellular mechanisms underlying action potential (AP) generation in neurons grown on substrate arrays of microelectrodes (MEAs) were recently shown to display extremely rich dynamical properties [1]. Upon repeated electrical stimulation, antidromically evoked APs show instability, fluctuations, and intermittency, whose features are unexpected from conventional biophysical models.

A novel and more accurate quantitative description of excitability is then imperative, if neural dynamics and plasticity have to be captured *in silico* [2] for very large-scale neocortical simulations [3].

Here, we replicate the experiments of [1], and define a mathematical neuron model, introducing non-conventional state-dependent inactivation descriptions of sodium currents [4]. We qualitatively compare model and experiments under the same stimulation paradigm, and specifically use the model to predict the dependency of the stability and intermittency of evoked APs on temperature. We speculate that, by employing temperature as a global modulator of subcellular kinetics, access to complementary information on the excitability processes can be readily gained.

2 Methods

Rat cortical neurons were dissociated and plated, at 3000 cells/mm^2, over titanium nitride microelectrodes arrays (MEAs; 200 μm spacing, 30 μm electrode diameter) whose surface was previously treated by polyethylenimine (10 mg/ml) and laminin (0.02 mg/ml). Neurons were incubated at 37°C - 5% CO_2 [5] in culture medium (Neurobasal by 2% B-27, 10% serum, 1% L-glutamine, and 1% Penicillin-Streptomycin) that was changed 3 times a week.

Recordings were performed by a MCS1060BC amplifier at 25 kHz, in a low-humidity incubator with 5% CO_2 atmosphere, and at 35°C, 37°C, or 39°C. Thirty minutes before each recording session, synaptic receptors antagonists (i.e. 20 ⌠M AP-V, 10 ⌠M CNQX, 10 ⌠M SR-95531) were bath applied to block spontaneous activity. Changes of the incubating temperature were followed by an accommodation interval of at least 20 min, before data recording. Repetitive biphasic pulses (±0.8 V, 200 msec) were generated (STG1002) at 1-20 Hz, and delivered by one extracellular electrode, employed in monopolar configuration [6]. MC_Rack software was used for data acquisition. Offline high-pass filtering (400 Hz) and analysis were performed to extract the occurrence time of evoked APs.

A deterministic, single-compartment conductance-based mathematical model derived from the Connor-Stevens model [2] was developed and computer simulated in NEURON [7]. Briefly, the model includes a sodium current and delayed-rectifier and A-type potassium currents [4]. The sodium current was modified from the fast-inactivating description [2] to incorporate state-dependent inactivation as in [6] (Fig. 1A). The effect of temperature on the transition rates was accounted for by a multiplicative factor $Q_{10} = 3$ [2].

3 Results

- APs complex past-history dependence, first described in [1], is experimentally reproduced;
- APs latency and instability are highly temperature-sensitive, over a small range (±2°C);
- A novel biophysical model, based on state-dependent inactivation of sodium-currents (Fig. 1A), qualitatively captures the experimental data (Fig. 1D).
- The model predicts a latency decrease (~0.1-0.2 msec/°C) with increasing temperature, and an increase of the time-scales associated to APs generation instability (Fig.1B).
- Preliminary experiments reveal good agreement with both model predictions (Fig. 1C-D).

4 Conclusion/Summary

We replicated a recently proposed experimental paradigm, enabling to probe neuronal excitability over extended time-scales [1]. We formulated a novel mathematical model of AP generation to reproduce qualitatively the experimental data, with in mind its incorporation in large-scale simulations [3]. The same model allows us to make predictions on how temperature affects the dynamics of excitability. In fact, temperature has a global influence on the kinetics of a variety of sub-cellular phenomena, directly and indirectly related to excitability. Temperature might thus serve as a control signal, to extract

complementary information and to validate the model description. When model predictions were tested experimentally, a qualitatively good agreement was found, confirming non-trivial consequences on APs latency and APs generation instability. In conclusion, the recently disclosed dynamical complexity of single-cell excitability, and its accurate biophysical modeling, are of great impact for the study of emergence of activity-dependent correlations, long-lasting plasticities, information encoding and, ultimately, for behaviorally relevant time-scales.

References

[1] Gal A, Eytan D, Wallach A, Sandler M, Schiller J, Marom S (2010) *J. Neurosci*. 30(48):16332-42.

[2] Sterratt D, Graham B, Gillies A, Willshaw D, (2011) Cambridge University Press.

[3] Markram H (2006) *Nature Rev. Neurosci.* 7:153-60.

[4] Gilboa G, Chen R, Brenner N (2005) *J. Neurosci*. 25(28):6479-89.

[5] Potter S, DeMarse T (2001) *J. Neurosci. Methods* 110:17-24.

[6] Wagenaar D, Pine J, Potter S (2004) *J. Neurosci. Methods* 138: 27-7.

[7] Carnevale NT, Hines ML (2006) The NEURON book, Cambridge University Press.

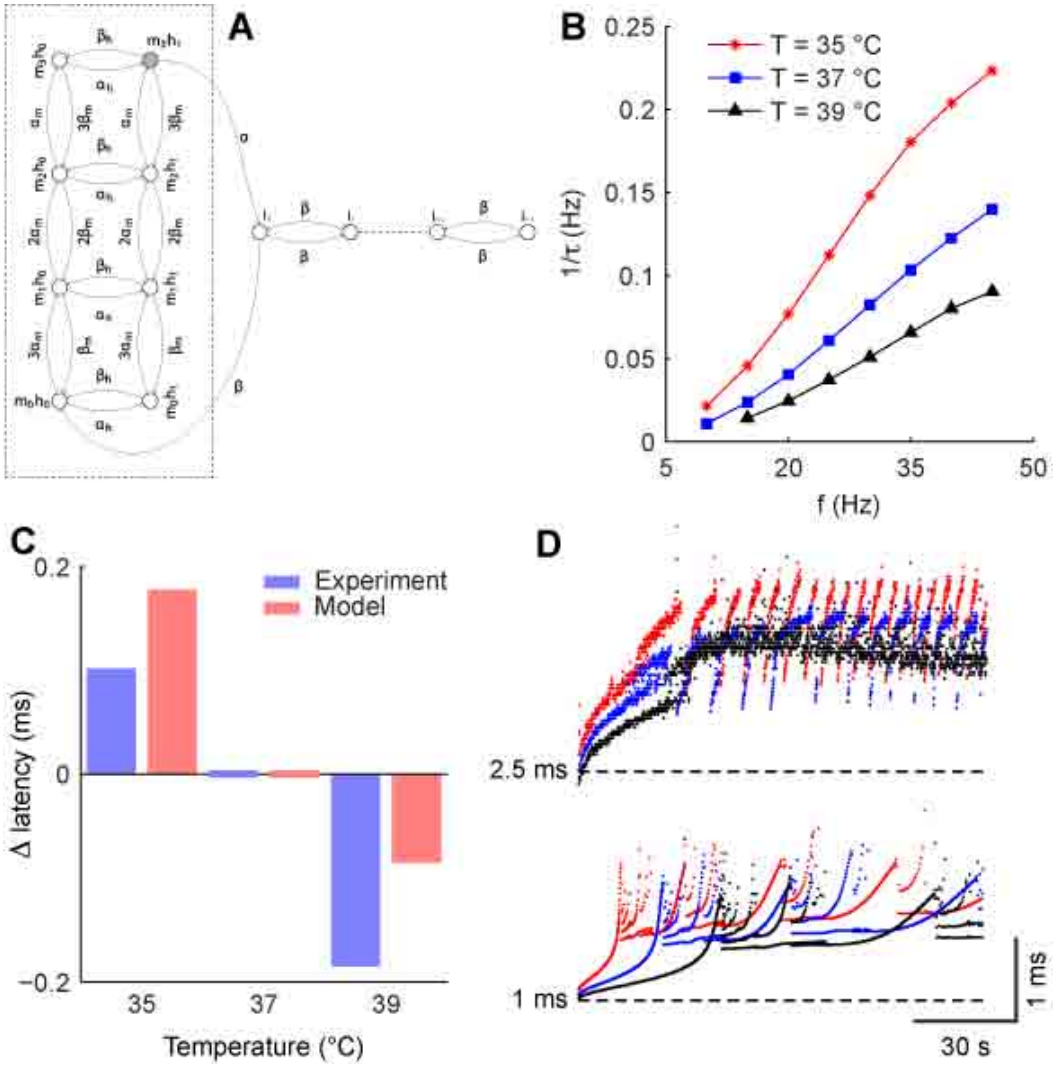

Figure 1: A standard sodium current model is altered as in [4], to include state-dependent inactivation in its kinetic description (**A**). When computer simulated, the model neuron replicates APs generation instability and intermittency, as well as a decrease in the time of intermittency onset for increasing stimulation frequencies (**B**). For a limited temperature range, the model predicts an overall speed-up of evoked APs (**C**), and a substantial increase in instability time-scales with increasing temperature (**D**). Preliminary experiments qualitatively confirm model predictions (**C**-**D**).

Adaptive learning protocol in cultured networks

Gladkov Arseniy[1*], Pimashkin Aleksey[1], Mukhina Irina[1,3], Ekaterina Koryagina[1,3], Kazantsev Victor[1,2]

1 Department of Neurodynamics and Neurobiology, Lobachevsky State University of Nizhny Novgorod, Nizhny Novgorod, Russia
2 Laboratory of Nonlinear Processes in Living Systems, Institute of Applied Physics RAS, Nizhny Novgorod, Russia
3 Normal Physiology Department, Nizhny Novgorod State Medical Academy, Nizhny Novgorod, Russia
* Corresponding author. E-mail address: gladkov@neuro.nnov.ru

Abstract

Dissociated neuronal cultures grown on multielectrode arrays can be used as a simple in vitro model for learning [1]. In closed-loop conditions the culture networks can be trained to increase evoked spiking rate response in selected electrode in predefined time window after a stimulus. We show that the learning protocol [1] can be enhanced to achieve learning criteria for any desired electrode in the system..

1 Methods

1.1 Cell Culturing

Hippocampal neural cells from mice embryos at 18-th prenatal day were plated on 64-electrode arrays (Alpha MED Science, Japan) (Fig. 1). The final density of cellular cultures was about 1600-2000 cells/mm^2. Cells were stored in culture Neurobasal medium (Invitrogen 21103-049) with B27 (Invitrogen 17504-044), Glutamine (Invitrogen 25030-024) and fetal calf serum (PanEco K055), under constant conditions of 37˚C, 100% humidity, and 5% CO_2 in air in an incubator (MCO-18AIC, SANYO). No antibiotics or antimycotics were used.

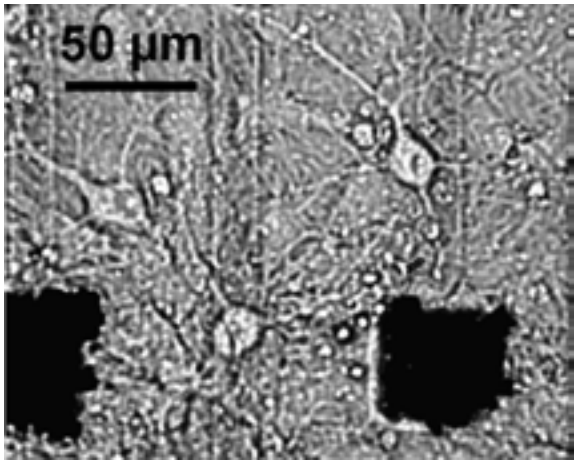

Fig. 1. Fragment of hippocampal culture network on multielectrode array. Scale bar, 50 µm..

1.2 Stimulation

Electrophysiological signals were recorded with 20 KHz samplerate. Threshold of spike detection was set at a factor of 8 times the median of absolute signal from the electrode (see Pimashkin, 2011 [2] for more details). Stimuli were generated (±600mV, 300ms, 0,06-0,1 Hz) using a four channels stimulator (Multi Channel Systems, Germany). Response-to-stimulus (R/S) ratio was measured as number of evoked spikes in 40-80 ms post-stimulus time interval per each 10 stimuli. Control stimulation was performed during 80 min (10 min - stimulation, 5 min – rest). Closed-loop real-time signal processing with feedback was performed using custom made software in Labview®. If the R/S value during learning reaches a threshold value then the stimulation stops for 5 min.

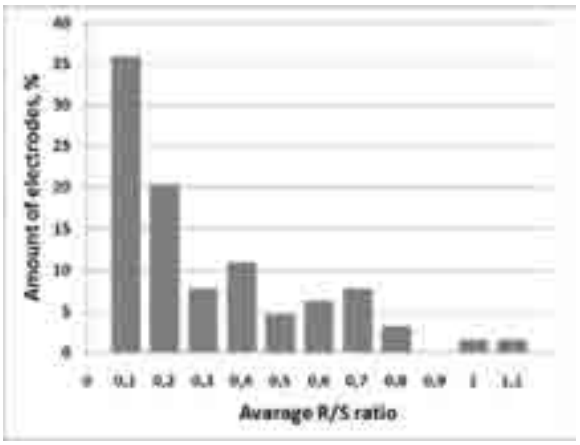

Fig. 2. R/S ratio distribution for all electrodes during trial stimulation for one experiment.

2 Results

In earlier studies [1, 3, 4] the electrodes with R/S=0,1 were selected for learning protocol. For R/S=0,2 taken as a threshold the stimulation was stopped for 5 min. In our experiments we found that 38,2±8,4% of the electrodes had $0<R/S\leq0,1$ during control stimulation. The number of electrodes with $0<R/S\leq0,5$ was 67,3±11,4% (Fig. 2). We successfully performed learning protocol for selected electrodes having R/S in the range of 0,1-0,5 in control stimula-

tion. Threshold for learning was set to upper 80% of R/S values distribution for selected electrode (Fig. 3). We found that such R/S selection was effective in 5 of 9 cultures (55%). Thus the enhanced protocol efficiency was similar as in the previous studies.

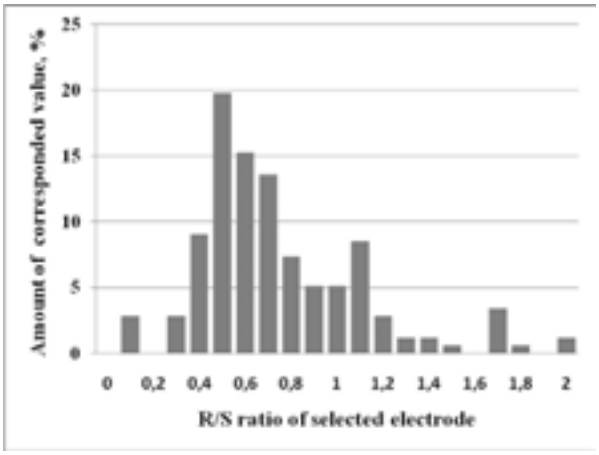

Fig. 3. R/S ratio distribution for single electrode during control stimulation.

3 Conclusion

We showed that learning in networks of hippocampal cells can be performed using R/S ratio of order of 0,5. It permits to apply the learning protocol to many different electrodes. Moreover in the enhanced protocol the learning threshold is estimated automatically based on response variability in control stimulation.

Acknowledgement

This work is supported by the Russian Foundation for Basic Research (Grant No 11-04-12144), by Russian Federal Program (No 16.512.11.2136), by MCB RAS Program and by the Russian President grant MD-5096.2011.2.

References

[1] Shahaf G., Marom S. (2001). Learning in networks of cortical neurons. *J Neurosci* , 21, 8782–8788.

[2] Pimashkin A, Kastalskiy I, Simonov A, Koryagina E, Mukhina I and Kazantsev V (2011) Spiking signatures of spontaneous activity bursts in hippocampal cultures. Front. Comput. Neurosci. 5:46. doi: 10.3389/fncom.2011.00046

[3] le Feber J., Stegenga J., Rutten WLC (2010). The Effect of Slow Electrical Stimuli to Achieve Learning in Cultured Networks of Rat Cortical Neurons. *PLoS ONE*, 5(1): e8871.

[4] Li Y., Zhou W., Li X., Zeng S., Liu M., et al. (2007). Characterization of synchronized bursts in cultured hippocampal neuronal networks with learning training on microelectrode arrays. *Biosens. Bioelectr*., 22, 2976–2982.

Are bursting neurons interneurons?

Tom Reimer[1], Werner Baumann[1], Jan Gimsa[1]*

1 University of Rostock, Chair for Biophysics, Gertrudenstrasse 11a, 18057 Rostock, Germany
* corresponding author, jan.gimsa@uni-rostock.de

Abstract
Spontaneous electrical activity of cortical in vitro networks has mostly been described as synchronized population bursts. It is assumed that this activity is exhibited by pyramidal cells that account for the majority (about 80%) of neurons in the networks. We analyzed the morphology of axons of parvalbumin-positive interneurons and their spontaneous activity patterns in cortical networks cultivated on MEA glass-neurochips. The axons were strongly ramified and covered wide areas of the MEAs. From axons arising from parvalbumin-marked cell bodies, only bursting activities were registered. We conclude that parvalbumin-positive interneurons are capable of burst generation and suggest that interneurons rather than pyramidal cells are the sources of synchronous bursting.

1 Background

Network bursts – the temporal and spatial clustering of action potentials – are typical for the spontaneous activity of *in vitro* networks and has been found in invertebrates and vertebrates [1]. The origins and functions of this kind of neuronal activity are not well understood. Spontaneous activity of *in vitro* networks has often been described as synchronized population bursts that are characterized by the collective synchronized bursting of numerous neurons [2]. Here we focus at the question if bursting activity arises from pyramidal cells, interneurons or both in cortical *in vitro* networks.

2 Methods

Cortices were prepared from embryonic mice (E16) followed by enzymatic dissociation. Cells were plated at a density of 1200 cells/mm^2 on poly-D-lysine/laminin coated miniaturized (16x16mm²) glass – neurochips (developed at the Chair for Biophysics, University of Rostock) with integrated 52-microelectrode MEAs and on coverslips. The culture areas were 20 mm^2. Cell cultures were incubated at 10% CO_2 and 37°C for four weeks. Half of the medium was replaced thrice a week. Recordings were performed with our modular glass chip system (MOGS) coupled to a preamplifier and data acquisition software (Plexon Inc., Dallas,TX,USA). For morphological characterization, networks were fixed with paraformaldehyd and immunohistochemically stained against parvalbumin, a marker for chandelier and basket cells [3] and neurofilament 200 kD before confocal laser scanning microscopy. We were able to identify the activity patterns of parvalbumin-positive interneurons by correlating the electric activity patterns with the microscopic morphology data.

3 Results

Parvalbumin-positive interneurons accounted for about 10-30% of the neurons in our networks. Their strongly ramified axons covered extensive areas of coverslip and MEA surfaces (Fig.1). The parvalbumin-positive interneurons were correlated to the activity patterns recorded before staining (Fig.2). A correlation was possible only for MEA electrodes that were not covered by a dense axonal clutter (Fig.3). A further precondition was that the course of an axon arising from a parvalbumin-positive interneuron could be microscopically traced. In any case, the spontaneous activity recorded from MEA pads with parvalbumin-positive interneurons was bursting.

4 Conclusion

Our results suggest that parvalbumin-positive interneurons, rather than pyramidal cells, are the source of the synchronous bursting activity which is characteristic for cortical networks. Further analysis of the spontaneous electrical activity of the different cortical neuron types is needed to confirm our conclusion and to understand the relationship between network cytoarchitectonics and electrical activity.

Fig. 1. Two parvalbumin-positive neurons of a 4 week old network cultivated on a coverslip. Parvalbumin is mainly expressed in cell bodies. The axons are strongly ramified, covering a wide surface area. Blue: DNA; green: parvalbumin; red: neurofilament 200; bar: 20µm.

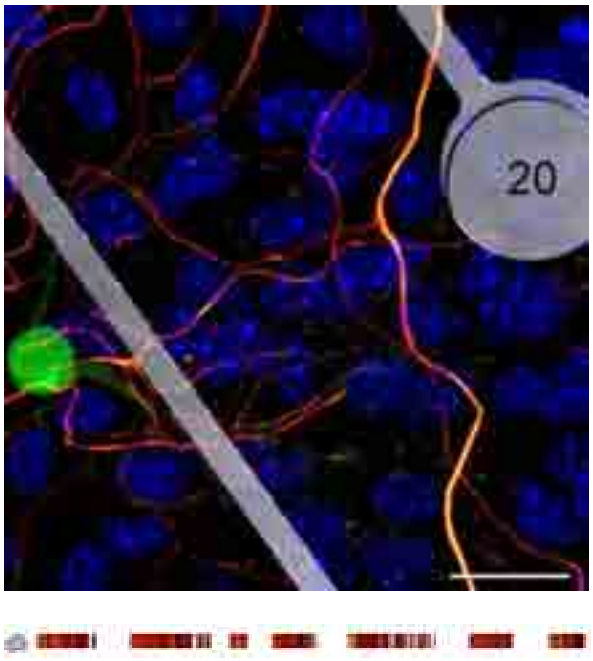

Fig. 2. Parvalbumin-positive interneuron near electrode 20 of the MEA. With electrode 20 superbursting activity was recorded, visualized as timestamps over a time period of 50 sec. Blue: DNA; red: neurofilament 200; green: parvalbumin; grey: electrode and pad connector; bar: 20 µm.

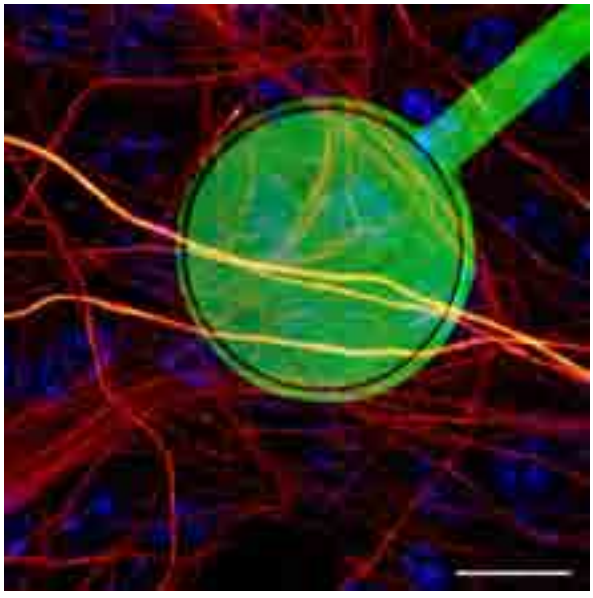

Fig. 3. Single MEA pad covered by a dense axonal clutter preventing a correlation of neuron type with the activity pattern. Green: electrode; red: neurofilament 200; blue: DNA; bar: 15 µm.

Acknowledgements

This work was supported by the DFG-research training group *welisa* 1505/1.

References

[1] Gross G.W. (1994). Internal dynamics of randomized mammalian neuronal networks in culture. *Enabling technologies for cultured neural networks*, Academic press, 277-317

[2] Wagenaar D.A., Pine J. & Potter S.M. (2006). An extremely rich repertoire of bursting patterns during the development of cortical cultures. *BMC Neuroscience*, **7**, 11

[3] De Felipe J. (2002). Cortical interneurons: from Cajal to 2001. *Prog. Brain Res*. 126, 215-238

Enhanced maturation of human pluripotent stem cell derived neuronal networks

Laura Ylä-Outinen[1,2,*], Marja Pajunen[1,2], Juha Heikkilä[1,2], Riikka Äänismaa[1,2], Susanna Narkilahti[1,2]

1 NeuroGroup, Institute of Biomedical Technology, University of Tampere, Tampere, Finland
2 BioMediTech, Tampere, Finland

* Corresponding author. E-mail address: laura.yla-outinen@uta.fi

Abstract
Nowadays, it is possible to form functional neural networks from human pluripotent stem cells. At the moment, the network formation process is quite time consuming. Moreover, in culture these cells divide vigorously and the culture plates quickly grow confluent. These matters slow down the progress in the research and long-term *in vitro* experiments are practically impossible to conduct. Here, the neuronal cells derived from human pluripotent stem cells were cultured on microelectrode array plates and their maturation was enhanced using cell cycle blocker aphidicolin. Microelectrode array measurements showed that aphidicolin increased the electrical activity of the neuronal networks during the exposure period and, with suitable concentration, did not increase notably the cell death.

1 Introduction

Human pluripotent stem cell (hPSC) derived neuronal cells are a potential tool in the areas of developmental biology, neurotoxicology, drug screening/development and in regenerative medicine [1, 2, 3]. These human derived neuronal cells resemble their *in vivo* counterparts many ways; they develop into action firing neurons and can form spontaneously active neuronal networks [4]. The formation of these human neuronal networks is, however, rather slow process *in vitro*; it typically takes 4 to 5 weeks to get neuronal networks with synchronous bursting behaviour on a microelectrode array (MEA) dish [4]. For many applications it would, indeed, be beneficial if these networks could be formed more rapidly.

In this study, the aim was to evaluate whether chemical cell cycle blocker aphidicolin (APC) fastens the maturation process of hPSC derived neuronal networks.

2 Methods

Human embryonic stem cells (hESCs) and human induced pluripotent stem cells were (hiPSCs) were differentiated into neuronal progenitor cells in suspension culture in presence of fibroblast growth factor (FGF). Cells were plated on MEA plates (Multichannel Systems GmbH) and allowed to form spontaneous neuronal networks for 14 days. Thereafter, the networks were exposed to APC at concentrations 0, 1, or 3 µg/ml for 7 days. The cells were observed twice a week with contrast phase microscopy and MEA measurements were performed during exposure period and up to 5 weeks after the exposure. The viability of the cells was evaluated with live/dead analysis (viability/cytotoxicity kit, Invitrogen) and the proliferation with BrdU kit (Roche). MEA data was analysed using MATLAB software with tailor-made analysis methods for burst detection [5]. The statistical analyses were performed using at least 5 parallel samples with Kruskall-Wallis analysis followed by Mann-Whitney U-test.

3 Results

APC, at the concentration 1 µg/ml, decreased the cell proliferation significantly compared to control cells according to BrdU-analysis (Figure 1.).

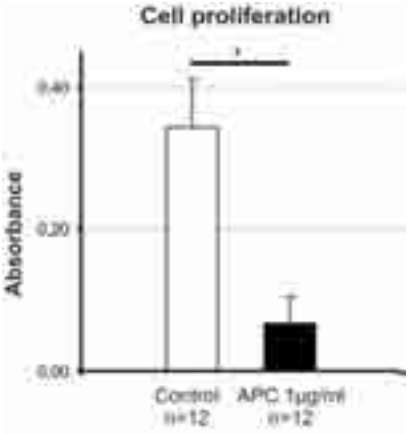

Fig. 1. Cell proliferation was measured using BrdU proliferation assay. Bars represent background corrected absorbance and error bars represent SD. Control cells proliferated significantly more compared to APC treated (1 µg/ml) cells ($p < 0.05$).

The cell viability decreased due to APC treatment compared to control cells. Still, this phenomenon was not significant (Figure 2.).

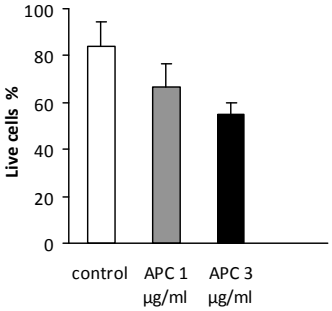

Fig. 2. Cell viability according to live/dead analysis. Live and dead cells were calculated from the populations and the results are represented as percentage of live cells from the population. Error bars represent SD.

The 1 µg/ml APC exposure increased the spontaneous activity of the hESC derived neuronal networks during the exposure period whereas concentration of 3 µg/ml inhibited the activity permanently (Figure 3.).

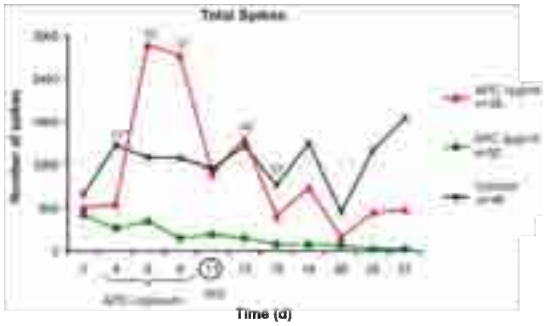

Fig. 3. The number of total spikes per MEA for 0, 1, and 3 µg/ml APC treatment. APC exposure period is marked, and the circle marks the APC washout day (WO). 1)** on day 4 significant difference between control and APC 3 µg/ml, 2)* on day 5 significant difference between control and APC 1 µg/ml, 3)* on day 8 significant difference between control and APC 1 µg/ml, and between control and APC 3 µg/ml, 4)* on day 13 significant difference between control and APC 3 µg/ml, 5)* on day 15 significant difference between control and APC 3 µg/ml. * = $p< 0.05$, ** = $p<0.005$.

The bursting activity did not increase due to the APC exposure, i.e. the network did not show more mature activity pattern during or after the APC exposure (Figure 4.).

APC is potential cell cycle inhibitor that blocks proliferation of hPSCs derived neural cells without affecting the viability of the cells on low concentrations. Simultaneously, APC exposure increased the spontaneous activity of the network. Nevertheless, the activity returned back to baseline level after washout. Thus, it might be beneficial to prolong the exposure to gain permanent effects.

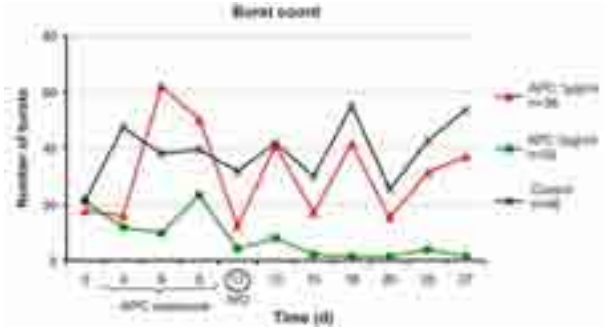

Fig. 4. Burst activity of APC 1 µg/ml, APC 3 µg/ml and control. The activity pattern of APC 1 µg/ml and control seem to follow a similar trend. The burst activity of APC 3 µg/ml starts to decline after the APC exposure period. APC exposure period is marked, and the circle marks the APC washout day (WO).

4 Conclusion

APC inhibited efficiently the cell proliferation. It also affected the hPSC derived neuronal network signalling during the exposure; by increasing the activity in smaller concentration and decreasing the activity with bigger concentration.

Acknowledgement

This work was supported by the Academy of Finland, the Finnish Funding Agency for Technology and Innovation, and the Kordelin Foundation.

References

[1] Lappalainen R.S., Salomäki M., Ylä-Outinen L., Heikkilä T. J., Hyttinen , J.A.K., Pihlajamäki H., Suuronen R., Skottman H., and Narkilahti S. (2010): Similarly derived and cultured hESC lines show variation in their developmental potential towards neuronal cells in long-time culture. *Regen. Med.* 5, 749.

[2] Ylä-Outinen L., Heikkilä J., Skottman H., Suuronen R., Äänismaa R., Narkilahti S. (2010): Human cell-based micro electrode array platform for studying neurotoxicity. *Front. Neuroeng*, 3:111

[3] Li J.-Y., Christophersen N., Hall V., Soulet D., and Brundin P. (2008) : Critical issues of clinical human embryonic stem cell therapy for brain repair. *Trends in neurosciences* 31, (3):146-53

[4] Heikkilä T.J., Ylä-Outinen L., Tanskanen J. M. A., Lappalainen R., Skottman H., Suuronen R., Mikkonen J.E., Hyttinen J.A.K., and Narkilahti S. (2009): Human embryonic stem cell-derived neuronal cells form spontaneously active neuronal networks *in vitro*. *Exp. Neurol.* 218, 109.

[5] Kapucu F.E., Tanskanen J.M.A., Mikkonen J.E., Ylä-Outinen L., Narkilahti S., Hyttinen J.A.K. (2012) Burst analysis tool for developing neuronal networks exhibiting highly varying action potential dynamics. *Front Comput Neurosci. Under revision.*

Selectivity of neural responses to electrical stimulus location in dissociated hippocampal cultures grown on multielectrode arrays

Pimashkin Alexey[1,2*], Gladkov Arseniy[1], Mukhina Irina[1,3], Kazantsev Victor[1,2]

1 Department of Neurodynamics and Neurobiology, Lobachevsky State University of Nizhny Novgorod, Nizhny Novgorod, Russia
2 Laboratory of Nonlinear Processes in Living Systems, Institute of Applied Physics RAS, Nizhny Novgorod, Russia
3 Normal Physiology Department, Nizhny Novgorod State Medical Academy, Nizhny Novgorod, Russia
* Corresponding author. E-mail address: aspimashkin@mail.ru

Abstract
Network activity patterns formed in neuronal cultures can be monitored by multielectrode arrays (MEAs). It has been demonstrated in many studies that spontaneous and stimulus evoked spike sequences can be organized as repeatable population bursts with précised spike timings. In this study we show that different input signals induce statistically distinguishable changes in the spiking patterns and, hence, the culture networks can generate selective evoked responses.

1 Methods

Dissociated hippocampal cells were grown on microelectrode arrays (MED64, Alpha MED Science, Japan). 64 micro-electrodes with 50μm x 50μm shape and 150 μm spacing were used for recording electrophysiological signals at 20kHz sample rate. Threshold detection was set at a factor of 8 times the median of absolute signal from the electrode (see Quiroga R., 2004; Pimashkin, 2011 for more details).

Electrical low-frequency stimulation (0.05-0.3 Hz) of pairs of nearby electrodes (stimulation sites) was applied using a stimulus generator (MultiChannel Systems). The stimulation consisted of bipolar pulse train with 600 μV and 500 μs applied to two stimulation sites. Each site was stimulated for 10 min. Electrical stimuli evoked population spiking response in most of the electrodes. The response from single electrode during 200-300 ms after stimulus artifact is shown in Fig. 1. Selectivity was considered as an ability of the neurons to generate different responses to different stimulation sites. To estimate statistical difference of the responses we used two basic characteristics of the evoked neural activity: timing of the first spikes (Marom S., 2008) and spiking rate. These parameters can be associated with information encoding in neural networks. The spiking rate of the response was defined as the total number of spikes within 200 ms of post stimulus activity. Measure of the selectivity from single electrode considered as statistical difference in responses to two stimulation sites were estimated by Mann-Wittney ranksum test.

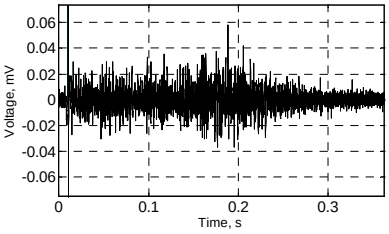

Fig. 1. Post-stimulus response recorded from single electrode. Time axis represent latency of recorded signal relatively to stimulus artifact.

2 Results

We found that the cultured network naturally contains a small fraction of neurons with high sensitivity (selectivity) to electrical stimulation site. Such high selectivity of the neurons on individual electrodes was verified using first spike timing and total spike rate (see methods). Time course of the first spike timings of the responses to two stimulation sites recorded from selective electrode is shown in Fig. 2 A, and spike rate of the responses to two stimulation sites recorded from selective electrode is shown in Fig. 2 B (black line - response to stimulation site 1, red line - stimulation site 2). We also demonstrated that in average (6 cultures) the number of electrodes with statistically high selectivity using total spike rate characteristics is greater than number of electrodes using first spike timing characteristics but not significantly (Fig.2 C).

3 Conclusion

We found that culture networks can respond selectively to electrical stimuli applied to different spatial sites. This selectivity appears in particular electrode (e.g. neuron groups) that can reliably distinguish the type of the stimulus in its spatial location. We also proved that spiking rate characteristics of the response can be more efficient to estimate the selectivity than precise first spike timing.

The evoked response dynamics found eventually indicates that culture networks contain different signaling pathways activated selectively by appropriate stimulus. The response selectivity with robust statistical characteristics can be further used to the design of closed-loop solutions of culture network based control systems (e.g. neuroanimats) where the selective electrodes generated distinguishable responses are associated with different sensory signals.

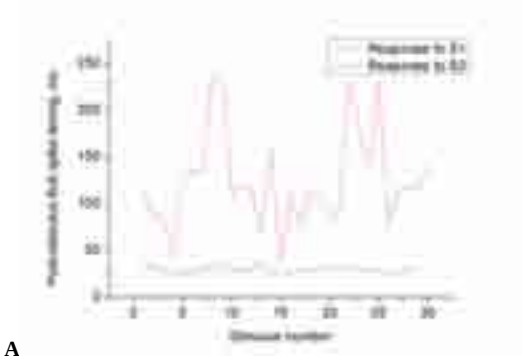

A

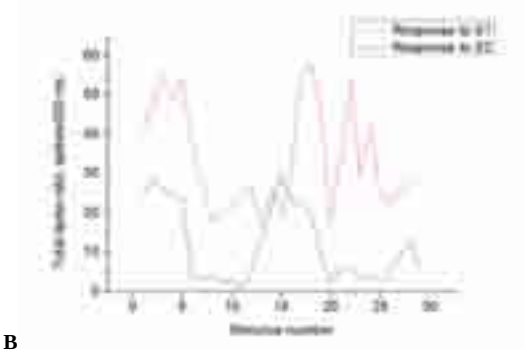

B

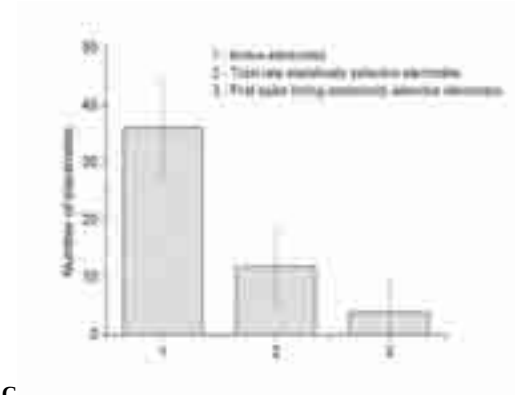

C

Fig. 2. Time course of the first spike timings of responses to two stimulation sites recorded from selective electrode (A), the spike rate of responses to two stimulation sites recorded from selective electrode (B) (black line - response to stimulation site 1, red line - stimulation site 2). (C) Average number of electrodes responded to more than 80% of stimuli, average number of electrode statistically selective to stimulus source using total spike rate and first spike timing as response characteristics.

Acknowledgement

This work is supported by the Russian Foundation for Basic Research (Grant No 11-04-12144), by Russian Federal Program (No 16.512.11.2136), by MCB RAS Program and by the Russian President grant MD-5096.2011.2.

References

[1] Shahaf, G., Eytan, D., Gal, A., Kermany, E., Lyakhov, V., Zrenner, C.,and Marom, S. (2008). Order-based representation in random networks of cortical neurons. PLoS Comput. Biol. 4, e1000228. doi:10.1371/journal.pcbi.1000228

[2] Quiroga R., Nadasdy Q., Ben-Shaul, Y. (2004). Unsupervised Spike Detection and Sorting with Wavelets and Superparamagnetic Clustering. *Neural Computation* (16) 1661-1688.

[3] Bologna l. L., Nieus T., Tedesco M., Chiappalone M., Benfenati F., Martinoia S., Low-frequency stimulation enhances burst activity in cortical cultures during development. Neuroscience 165 (2010) 692–704

[4] Pimashkin A, Kastalskiy I, Simonov A, Koryagina E, Mukhina I and Kazantsev V (2011) Spiking signatures of spontaneous activity bursts in hippocampal cultures. Front. Comput. Neurosci. 5:46. doi: 10.3389/fncom.2011.00046

Simulation of a neuronal network with 10,000 neurons using OpenCL and GPU

Kay Barthold[1], Barbara Priwitzer[1*]

1 Faculty of Engineering and Computer Science, Lausitz University of Applied Sciences, Senftenberg, Germany
* Corresponding author. E-mail address: barbara.priwitzer@hs-lausitz.de

Abstract
In an in vitro experiment about 10,000 neurons can be counted on a multielectrode array (MEA) neurochip. In the past we have developed a model called INEX which shall be used to run such a simulation of a MEA neurochip experiment with 10,000 neurons.
Similar to processors on a CPU which can be represented by number of cores, the GPU provides a certain number of so called shaders. Since recently, it is possible to run complex algorithms on these shaders which can be controlled via interfaces like OpenCL and CUDA. Using this method can significantly decrease the run time of algorithms.

1 Background/Aims

In an *in vitro* experiment about 10,000 neurons can be counted on a multielectrode array (MEA) neurochip. In the past we have developed a model called INEX [1] which shall be used to run a simulation of a MEA neurochip experiment with 10,000 neurons.

General Purpose Computation on Graphics Processing Units (GPGPU) describes a system for massively parallel processing of computer algorithms. Similar to processors on a CPU which can be represented by number of cores, the GPU provides a certain number of so called shaders. In the past these shaders were used for projection and manipulation of geometric data on the computer screen. Since recently, it is possible to run complex algorithms on these shaders which can be controlled via interfaces like OpenCL [2] and CUDA [3]. Using this method can significantly decrease the run time of algorithms.

2 Methods

The INEX model is based on an inhomogeneous Poisson process to simulate neurons which are active without external input or stimulus as observed in neurochip experiments. It is accomplished using an Ising model with Glauber dynamics. The INEX model is implemented in C++.

For parallelisation the OpenCL1.1 interface of the Khronos Group was used. All runs were performed on an Intel I7 930 Nehalem CPU and a NVIDIA GTX460 GF104@1024MB GPU. The splitting of the algorithm follows the network volume (in this case up to over 10,000 neurons). Take note that CPU and GPU are designed for different use cases. A combination of these two platforms would exhibit negative impact on the performance.

To compare the run times of this simulation with the single core GPU implementation we realized the model algorithm also on a single core CPU. To make the run times and results comparable, the parameter sets of the model, which are usually chosen randomly, were fixed. Thus, two identical spike trains, each with a length of 30 minutes, were separately generated with GPU and CPU. The algorithm was run simulating for 10 to 10240 neurons in eleven steps, always doubling the number of neurons (Table 1).

3 Results and Discussions

With increasing number of neurons the GPU implementation shows a clear run time advantage (Table 1, Figure 1) compared to CPU. The run times for 2560, 5120 and 10240 neurons had to be extrapolated for the CPU variant. GPU as well as CPU exhibit an exponentially increase of run time. However, it grows much slower in case of the GPU. For 10240 neurons the GPU was almost 12 times faster than the CPU. For the GPU, the relatively constant development of the run time up to 320 neurons is justifiable with the high maintenance workload which is due to transport to the GPU and back in the system. This effort can be ignored with increasing number of neurons because the algorithm itself needs significant more run time.

4 Conclusion

The developed OpenCL algorithm is very performant in the current version. The usage of multicore processors or shaders requires higher maintenance efforts; therefore their positive effect on run time is best observed for large networks.

Table. 1. Performance comparison between single core CPU and single core GPU with increasing number of neurons; run time in minutes.

Number of Neurons	CPU	GPU
10	0.067	2.772
20	0.110	2.586
40	0.203	2.693
80	0.425	3.142
160	1.018	4.026
320	3.079	5.882
640	10.588	9.247
1280	101.505	20.229
2560	415.119	56.343
5120	1,823.782	192.688
10240	8,502.237	721.584

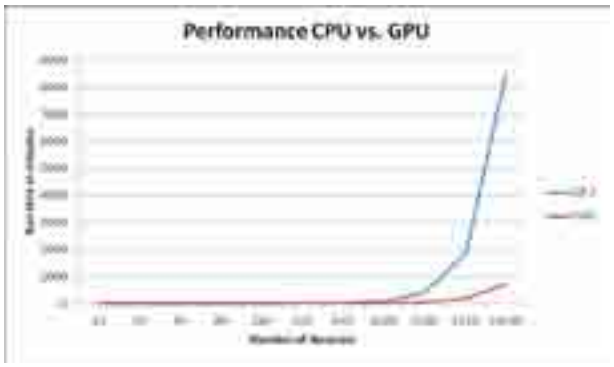

Fig. 1. Visualisation of Table 1: Performance comparison between single core CPU and single core GPU with increasing number of neurons.

Acknowledgement

We thank Kerstin Lenk (Lausitz University of Applied Sciences, Senftenberg, Germany) for her continuous support.

References

[1] Lenk, K. (2011). "A simple phenomenological neuronal model with inhibitory and excitatory synapses" in *Advances in Nonlinear Speech Processing*, ed. C. Travieso-González and J Alonso-Hernández (Berlin/Heidelberg:Springer), 232-238.

[2] Mutch, J., Knoblich, U.,Paggio, T. (2010): CNS: a GPU-based framework for simulating cortically-organized networks. *http://dspace.mit.edu/bitstream/handle/1721.1/51839/MIT-CSAIL-TR-2010-013.pdf*. Accessed 31 Oct 2010.

[3] Nowotny, T. (2010): Parallel Implementation of a Spiking Neuronal Network Model of Unsupervised Olfactory Learning on NVidia® CUDA ™. Proceedings, The 2010 International Joint Conference on Neural Networks (IJCNN), 1-8.

Analysis of gene expression underlying network activity during long-term development of rat cortical cultured neurons

Daisuke Ito[1,2*], Keiko Yokoyama[2,3], Kazutoshi Gohara[3]

1 Division of Functional Life Science, Faculty of Advanced Life Science, Hokkaido University, Sapporo, Japan
2 Research Fellow of the Japan Society for the Promotion of Science
3 Division of Applied Physics, Faculty of Engineering, Hokkaido University, Sapporo, Japan
* Corresponding author. E-mail address: ditoh@mail.sci.hokudai.ac.jp

Abstract
Molecular mechanisms underlying the generation of synchronized bursts during long-term development remain unclear. In order to clarify the mechanisms of this phenomenon at a molecular level, we cultured rat cortical neurons for 1 month and analyzed the gene expression involved in the changes in network activity. Synchronized bursts were observed starting at approximately 2 weeks and the rate increased gradually during the culture periods. Reverse transcription PCR analysis revealed that the transcription factor gene *creb* were found to be consistently expressed during the culture period. However, the expression level of immediate early gene *arc* increased up to 1-month culture period. These results suggest that the generation of synchronized bursts is correlated with the increase in immediate early gene expression during long-term development of cultured neuronal networks.

1 Introduction

Recently, molecules involved in higher functions of the nervous system, such as memory and learning, have begun to be identified. At the network level, exhaustive analysis of gene expression has been performed during pharmacologically induced neuronal plasticity [1]. However, the molecules involved in network construction and the generation of synchronized bursts during long-term development remain unclear. We previously presented changes in synaptic density (both excitatory and inhibitory) and electrical activity during long-term development [2]. In addition to these methods, we performed gene analysis to link gene expression to network activity. Expression levels of the transcription factor gene *creb* and immediately early gene *arc* were investigated during 1-month culture periods.

2 Materials & Methods

Cell culture, electrical activity recordings, and immunofluorescence staining were performed as described previously [3]. We cultured cortical neurons derived from Wistar rats at embryonic day 17 for 1 month. The spontaneous electrical activity of cortical culture was recorded using MED64 extracellular recording system (Alpha MED Scientific) and immunofluorescence staining was performed using antibodies against anti-microtubule associated protein 2 (MAP2), anti-vesicular glutamate transporter 1 (VGluT1), and anti-vesicular transporter of γ-aminobutyric acid (VGAT). Gene expression was analyzed by reverse transcription PCR (RT-PCR) using gene-specific primers. Total RNA was extracted from the cultures every week during the 1-month culture period. RNA was then reverse transcribed and 40 cycles of PCR were performed.

3 Results & Discussion

Figure 1A shows the developmental changes in network activity of rat cortical cells cultured for 1 month. Synchronized bursts were observed starting at approximately 2 weeks and the rate increased gradually during the culture period. Immunofluorescence staining of MAP2, VGluT1, and VGAT revealed that both excitatory and inhibitory synaptic boutons increased around the dendrites and somata over 1 month (Fig. 1B). To analyze specific gene expression during these periods, we performed RT-PCR using *gapdh*, *creb*, and *arc* primers (Fig. 1C). Both the housekeeping gene *gapdh* and transcription factor gene *creb* were found to be consistently expressed during the culture period. However, the immediately early gene *arc* was not identified at 1-7 DIV, but the expression level increased up to 28 DIV. In addition, the increase in the expression of *arc* resembles the increase in the synchronized burst rate (Fig. 1A). Since *arc* mRNA expression is known to be induced by increased levels of synaptic activity [4], these results suggest that the generation of synchronized bursts is correlated with the increase in *arc* expression during the culture period. Based on these results, we have begun to quan-

tify the expression level of *arc* and investigate the expression of other genes.

Acknowledgement

This work was supported in part by Grants-in-Aid for Scientific Research from the Japan Society for the Promotion of science to K. Gohara (Nos. 20240023 and 21650049) and D. Ito (No. 23700523).

References

[1] Pegoraro S., Broccard F. D., Ruro M. E., Bianchni D., Avossa D., Pastore G., Bisson G., Altafini C., Torre V. (2010). Sequential steps underlying neuronal plasticity induced by a transient exposure to Gabazine. *J. Cell. Physiol.*, 222, 713-728.

[2] Ito D., Komatsu T., Tamate H., Gohara K. (2010). Long-term measurement of excitatory and inhibitory synapse densities with electrical activity during development of cultured rat cortical networks. *Proc. MEA Meeting 2010*, 20-23.

[3] Ito D., Tamate H., Nagayama M., Uchida T., Kudoh S. N., Gohara K. (2010). Minimum neuron density for synchronized bursts in a rat cortical culture on multi-electrode arrays. *Neuroscience*, 171, 50-61.

[4] Plath N., Ohana O., Dammermann B., Errington M. L., Schmitz D., Gross C., Mao X., Engelsberg A., Mahlke C., Welzl H., Kobalz U., Stawrakakis A., Fernandez E., Waltereit R., Bick Sander A., Therstappen E., Cokke S. F., Blanquet V., Wurst W., Salmen B., Bosl M. R., Lipp H. P., Grant S. G. N., Bliss T. V. P., Wolfer D. P., Kuhl D. (2006). Arc/Arg3.1 is essential for the consolidation of synaptic plasticity and memories. *Neuron*, 52, 437-444.

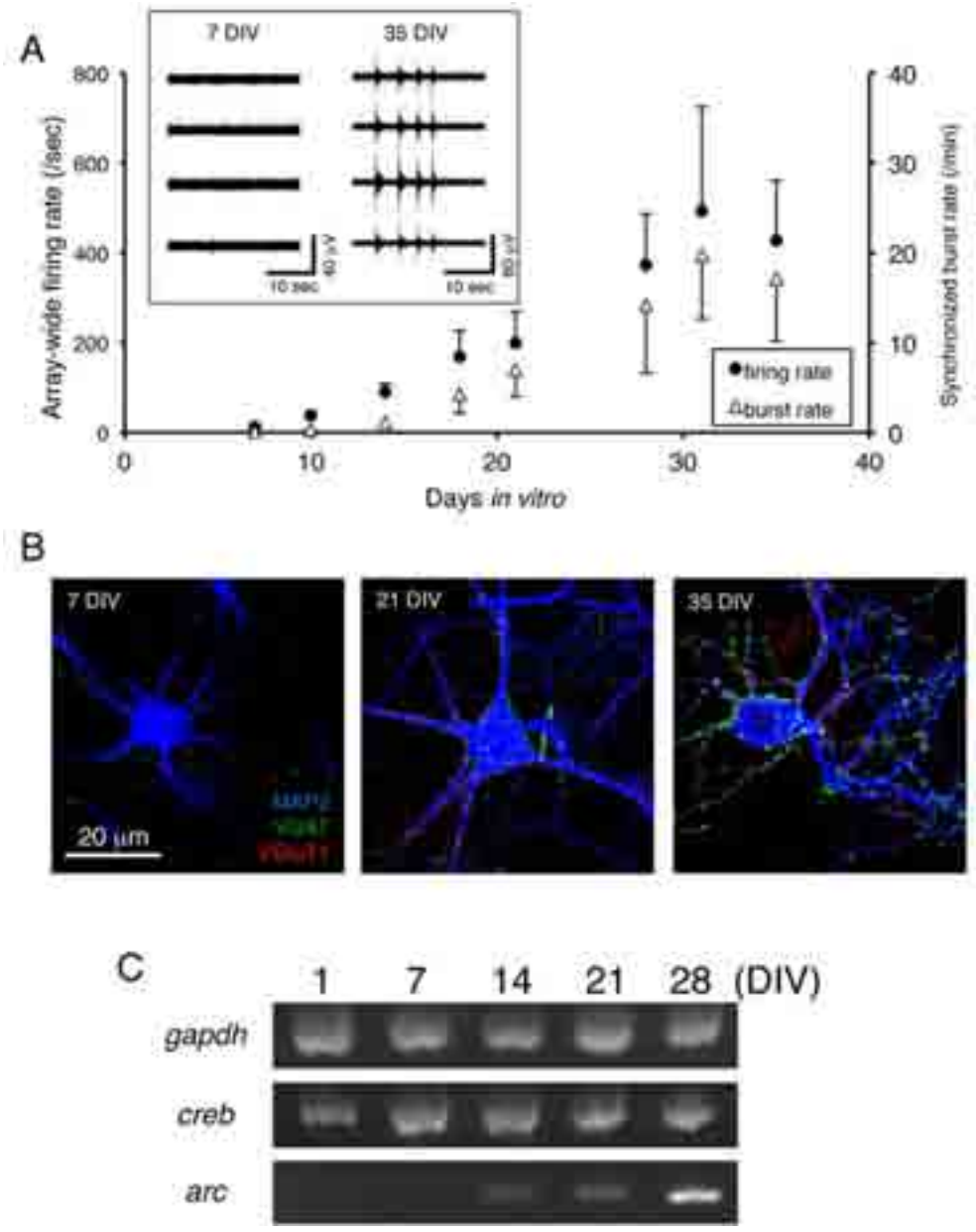

Fig. 1. (A) Changes in network activity during long-term development of rat cortical cultured neurons. The upper left frame shows the extracellular potential traces recorded in each electrode. Firing rate data are shown as the mean + standard error of the mean (SEM), whereas the synchronized burst rate are shown as the mean – SEM (for both n = 6). (B) Immunofluorescence micrographs of cultured cortical neurons. Blue color indicates MAP2. Green color indicates VGAT. Red color indicates VGluT1. (C) Electrophoresis of gapdh, creb, and arc genes extracted from cultures every week during a 1-month culture period. The genes were amplified by RT-PCR using gene-specific primers.

Effect of low and high frequency electric stimulation on plasticity in primary dissociated mice hippocampal neuronal cultures

Burtsev Mikhail[1,2*], Sukhanova Anna[1], Mineeva Olga[1,2,3], Kiselev Ilya[1], Azieva Asya[1], Anokhin Konstantin[1,2,3]

1 Neuroscience Department, Kurchatov NBIC Centre, Moscow, Russia
2 Department of Systemogenesis, P.K. Anokhin Institute of RAMS, Moscow, Russia
3 Institute of Higher Nervous Activity and Neurophysiology of RAS, Moscow, Russia
* Corresponding author. E-mail address: burtsev.m@gmail.com

1 Background/Aims

Plasticity in primary dissociated neuronal cultures can be induced by both low [1] or high [2,3] frequency stimulation. We compare effects of both stimulation types by estimating values of expression of gene *c-fos*. It is so called immediate early gene coding for a transcription factor which participates in the process of neuronal plasticity.

2 Methods/Statistic

Dissociated hippocampal cultures were obtained from P0 BALB/c mice and grown on microelectrode arrays to 21 DIV. Electric stimulation was applied for 10 minutes. Two protocols of electric stimulation were used: low frequency (single pulses at 0.1 Hz) or high frequency (bursts of 6 pulses spaced at 10 ms with 300 ms interburst intervals) stimulation. Each group, as well as a control group (without stimulation), consisted of 3 neuronal cultures. In 2.5 hours after beginning of stimulation cultures were fixed and c-Fos expression was detected using immunofluorescence microscopy.

3 Results

Low and high frequency of electric stimulation resulted in significant increase of c-Fos expression in neuronal cultures (5.5 or 4-fold, respectively, $p < 0.001$), compared to non-stimulated samples (Fig.1). However, no significant difference was found between stimulation protocols.

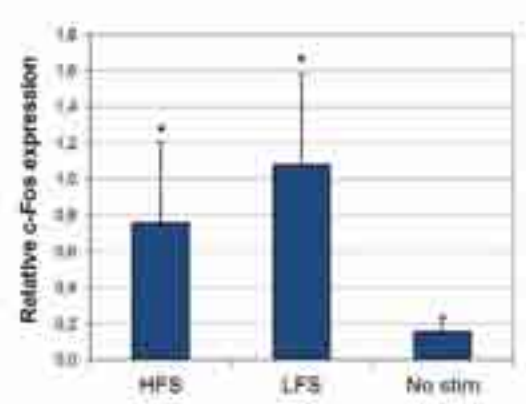

Fig. 1. Mean intensity of c-Fos immunofluorescence normalized to intensity of Hoechst staining (nuclei). HFS, high frequency stimulation; LFS, low frequency stimulation; No stim, non-stimulated cells.

4 Conclusion/Summary

Our results demonstrate that high as well as low frequency stimulation induce comparable levels of c-Fos expression. Considering c-Fos as a molecular marker of neuronal plasticity both protocols effectively produce modifications of neural networks in vitro.

Acknowledgement

This work was supported by the Ministry of Education and Science of Russian Federation cont. #16.512.11.2134.

References

[1] Shahaf G., Marom S. (2001): Learning in Networks of Cortical Neurons. *The Journal of Neuroscience*, 21, 22, 8782-8788

[2] Novellino A. et al. (2007): Connecting Neurons to a Mobile Robot: An In Vitro Bidirectional Neural Interface. *Computational Intelligence and Neuroscience*, 2007, 1-13.

[3] Bakkum D.J., Chao Z.C., Potter S.M. (2008): Spatio-temporal electrical stimuli shape behavior of an embodied cortical network in a goal-directed learning task. *Journal of Neural Engineering*, 5, 310.

Methods for long-term high-resolution characterization of *in vitro* developing neuronal networks grown over high-density CMOS-based microelectrode arrays

Milos Radivojevic[1], David Jäckel[1], Jan Müller[1], Michele Fiscella[1], Urs Frey[2], Branka Roscic[1], Andreas Hierlemann[1], Douglas Bakkum[1]

1 Bio Engineering Laboratory, D-BSSE, ETH Zürich, Basel, Switzerland

2 RIKEN Quantitative Biology Center, Kobe, Japan

* Corresponding author. E-mail address: milos.radivojevic@bsse.ethz.ch

Abstract

High-resolution assessment of how the electrical properties and physical motility of multiple individual neurons contribute to the organization of a network *in vitro* requires a neuron-electrode interface that provides single cell accessibility and high spatial resolution. Here we present a method to trace the spatial distribution of average spike shapes (footprints) of the same cell during its development on a high-density complementary metal–oxide–semiconductor (CMOS) based microelectrode array (MEA) and demonstrate changes in its footprint over time.

1 Introduction

Examination of developing neuronal cultures in vitro reveals morphological and electrical phenomena, at the cellular and network level that lead to stable functional and structural relations among neuronal cells in a mature culture [1]. Neuronal cell migration, axonal pathfinding, and synaptic pruning represent constitutive processes of neuronal development. Besides its role in development, neuronal motility plays a role in regeneration of nervous system in vivo [2] and in cortical neuronal networks *in vitro* [3]; moreover, synaptic rewiring represents a basis for activity-dependent structural plasticity in the developing and adult brain [4]. Many of these phenomena can be investigated at the morphological and molecular level of a single cell, nevertheless it is challenging to trace electrical activity of multiple individual neurons during *in vitro* development. To circumvent this limitation we utilized a high-density complementary metal–oxide–semiconductor (CMOS) based microelectrode array (MEA) [5] for long-term recording of neuronal activity during development; principal component analysis (PCA) based spike sorting was used to identify the respective cells.

2 Material and Methods

2.1 Cell culture preparation

Sparse cultures (1000 cells/mm2) of neocortical cells were grown on high-density MEAs and were maintained in Jimbo medium at 37 ° C and 5% CO2. One third of the medium (300 µl) was replaced on a daily basis after each recording session. In order to prevent contamination, culture chambers were sealed with lids, covered with a fluorinated ethylene-propylene membrane [6].

2.2 Recordings

A High-density CMOS-based MEA that comprises 11,011 platinum electrodes and 126 recording channels was utilized for long-term recording (35 days *in vitro* (DIV)) of electrical activity of developing networks. Two sets of 126-electrode configurations were used for the recordings: (i) A sequence of 95 configurations, each with randomly selected electrodes, to sample general network activity over consecutive days, and (ii) a sequence of 147 overlapping high-density configuration blocks to extract clusters of extracellular signals produced by individual cells.

2.3 Statistics

Self-organization of the network architecture, followed by the characteristic development of general network activity distribution, are presented as topographically mapped electrical “images” extracted from median spike heights and firing rates throughout the 3.5 mm^2 array on the successive days, over three different developmental periods (Fig.1). From the data, which were recorded in a series of 102-electrode high-density configuration blocks, we extracted clusters of extracellular electrical signals and assigned them to individual cells using PCA/clustering-based spike sorting.

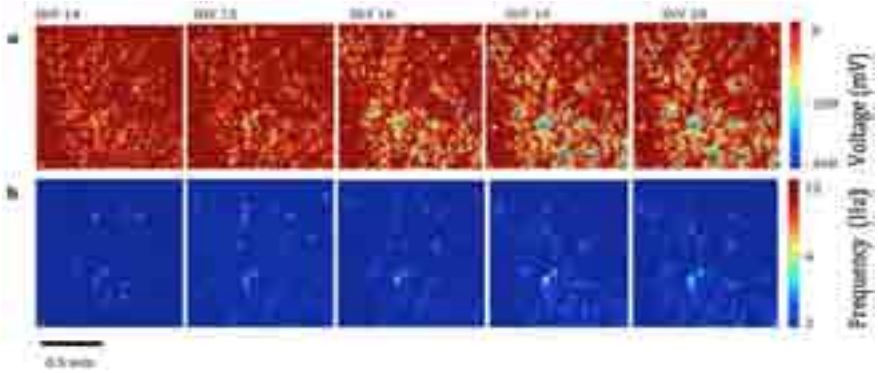

Fig. 1. Topographically mapped electrical "images" reconstructed from the neural activity, recorded with 95 configurations, each with 126 randomly selected electrodes, over a duration of 60 sec per configuration. Color bars represent the median amplitude of recorded spikes (*a*) and firing rates (*b*).

2.4 Immunocytochemistry

The cortical neurons cultured on MEAs were fixed with 4% formaldehyde at 35 DIV. After permeabiliztion with 0.25% Triton X-100 in phosphate buffered saline (PBS) for 10 min, the cultures were incubated with PBS containing 0.1% Tween20 for 30 min. The cultures were incubated with primary antibodies (anti-GABA IgG rabbit (Sigma-Aldrich), anti-MAP2 IgG chicken (Sigma-Aldrich), anti-tau-1 IgG mouse (Millipore)) overnight at 4ºC and then incubated with secondary antibodies (anti-IgG rabbit, anti-IgG chicken and anti-IgG mouse (Invitrogen)) for 1 h at room temperature. Fluorescence observation was performed using a Leica DM6000 FS fluorescence microscope.

3 Results

We were able to trace the spatial distribution of average spike shapes of the same cell (footprints) during the developmental process, perceiving fine changes in its extracellular spike waveforms (Fig.2). For validation of our results, we immunostained two of the cultures and assigned the obtained spike waveform footprints to the imaged cells.

4 Conclusions

Network and single-cell electrophysiological analysis of growing neuronal networks on high-density CMOS-based arrays can be performed in combination with PCA/clustering-based spike sorting at a much greater level of detail than with conventional multi-electrode arrays. Long-term maintenance of neuronal cultures together with continuous collection of electrophysiological data with this system offer a valuable approach to investigate the network structural and functional dynamics and development of cortical neuronal cultures in vitro.

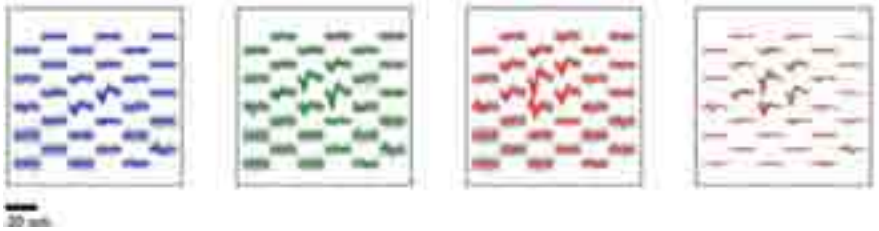

Fig. 2. Tracing the footprints of a preselected cell over three consecutive days (blue - DIV 6, green – DIV 7, red – DIV8).

Acknowledgement

We acknowledge Financial support from the Swiss National Science Foundation (SNF) through the Ambizione program.

References

[1] D. A. Wagenaar, J. Pine and S. M. Potter. (2006). An extremely rich repertoire of bursting patterns during the development of cortical cultures. *BMC Neuroscience 7:11.*

[2] Sundholm-Peters NL, Yang HK, Goings GE, Walker AS, Szele FG. (2005). Subventricular zone neuroblasts emigrate toward cortical lesions. *J Neuropathol Exp Neurol 64(12):1089–1100.*

[3] M. A. Haas, J. A. Chuckowree, R. S. Chung, J. C. Vickers, and T. C. Dickson. (2007). Identification and Characterization of a Population of Motile Neurons in Long-Term Cortical Culture. *Cell Motility and the Cytoskeleton. 64, 274–287.*

[4] M. Butz, F. Wörgötter, A. van Ooyen. (2009). Activity-dependent structural plasticity. Brain Research Reviews. 60, 287-305.

[5] U. Frey, J. Sedivy, F. Heer, R. Pedron, M. Ballini, J. Mueller, D. Bakkum, S. Hafizovic, F. D. Faraci, F. Greve, K.-U. Kirstein, and A. Hierlemann. (2010). Switch-matrix-based high-density microelectrode array in CMOS technology. *IEEE Journal of Solid-State Circuits*. 45, 467–482.

[6] S. M. Potter and T. B. DeMarse. (2001). A new approach to neural cell culture for long-term studies. *Journal of Neuroscience Methods. 110, 17–24.*

Memory in cultured cortical networks

Joost le Feber[1*], Tim Witteveen[1], Irina Stoyanova[1] and Wim Rutten[1]

1 Biomedical Signals and Systems, University of Twente, the Netherlands
* Corresponding author. E-mail address: j.lefeber@utwente.nl

Abstract
Tetanic stimulation was applied to affect network connectivity, as assessed by conditional firing probabilities. We showed that the first period(s) of titanic stimulation at a certain electrode significantly alters functional connectivity, but subsequent, identical stimuli do not. These findings support the hypothesis that isolated networks develop an activity-connectivity balance, and that electrical stimulation pushes a network out of this equilibrium. Networks then develop a new balance that supports the activity patterns in response to the stimulus. Accordingly, subsequent stimuli no longer disturb the equilibrium. Similar results were obtained with slow pulses (~0.2 Hz) instead of tetani, suggesting that connectivity changes are driven by network activation, rather than the tetanus itself.

1 Background/Aims

A well-known method in plasticity research is tetanic stimulation, traditionally applied intracellular to induce long term potentiation. Recent studies [3,4] showed that extracellular tetanic stimulation affects network connectivity, whereas other studies found it difficult to detect changes on a network scale [6]. The monitored parameters like e.g. network wide firing rates, which may have been too global, may explain this discrepancy. Alternatively, intrinsic activity may exert uncontrolled influence on network connectivity, and mask induced changes. Here, we used cultured neuronal networks to study the effect of repeated periods of tetanic stimulation. We hypothesize that the existing balance between activity and connectivity is diturbed by the applied stimulation. The network adapts and develops a new balance that supports the induced activity patterns. Thus, reapplying the same input will not disturb the new balance; the network memorizes the input.

2 Methods/Statistic

To detect stimulus induced changes we estimated functional connectivity, through Conditional Firing Probability (CFP) analysis [1]. CFP describes the probability that neuron j fires at t= , given that i fired at t=0. CFP's are used to express functional connections between two neurons by a strength and a latency. We studied the effect of repeated periods of tetanic stimulation (2-15 min), separated by 1h periods of no stimulation. We analysed periods of spontaneous activity to obtain an estimate for functional connectivity. Stimulation periods were repeated at least four times. We calculated the change in functional connectivity by comparing the strengths of all persisting connections before and after stimulation. To quantify changes we calculated the fraction of significantly changed connections (FSCS), as well as the mean magnitude of change ($|\overline{\Delta}|$). We calculated the plasticity index (PI) [2] to assess the change in functional connectivity: $PI=FSCS \cdot |\overline{\Delta}|$.

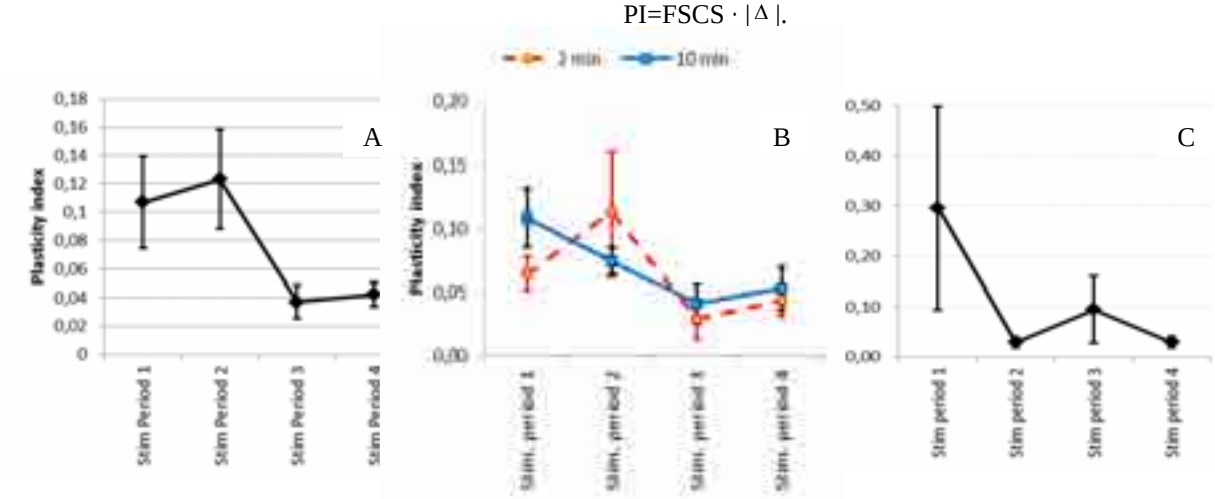

Fig 1. Plasticity index (PI) across four subsequent periods of stimulation. $PI=FSCS \cdot |\Delta|$, where *FSCS* is fraction of significantly changes connections, and $|\overline{\Delta}|$ equals the average absolute strength change of these connections. **A.** shows that PI is ~3 times higher in the around the first two periods of tetanic stimulation than around later periods. **B**. shows that experiments with long periods of tetanic stimulation (10 min) resulted in the first PI to be highest, whereas shorter periods (2 min) in a highest 2nd PI. **C.** Periods of similar duration with slow pulse stimulation (0.2-0.3Hz) yielded very similar development of PI.

3 Results

In twelve experiments, the PI's around the first periods of tetanic stimulation (PI~0.11) were significantly higher than control values (PI~0.035) around periods of no stimulation, (2-tailed t-test: p=0.04). Two-way ANOVA revealed that PI's significantly decreased around subsequent stimulation periods (p=0.03), differences between cultures were not significant. Changes in functional connectivity were the largest around the first two periods of stimulation (Fig 1a), three times higher than controls. Here, the differences between individual experiments were the largest. In experiments with long periods of stimulation, the first PI was highest whereas short periods of stimulation led to the 2nd PI being highest (Fig 1b). Three experiments with slow pulse trains during periods of similar duration (0.2-0.3Hz) showed the same effect ((t-test p>0.70, see Fig. 1c). Subsequent stimulation at a second electrode (four experiments) showed a similar tendency of decreasing PIs, however, differences were much smaller, and also absolute values did not exceed spontaneous PIs. Return to the first stimulation electrode showed PIs at the level of spontaneous fluctuations (see Fig. 2).

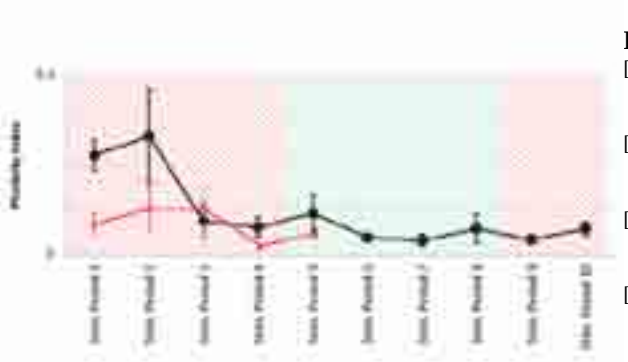

Fig 2. Development of plasticity index upon stimulation at two different electrodes (black line, ●) or across periods with no stimulation (n=10; red line, ▵). Hatched areas indicate stimulation at electrode A (stim period 1-4 and 9-10; ▨) or electrode B (stim. period 5-8; ▨)

4 Conclusion/Summary

PI's around the first stimulation period were significantly higher than those around periods of no stimulation, showing that tetanic stimulation did affect functional connectivity. Interesting however, are the lower PI's around subsequent stimulation periods, which indicate that these periods had less effect on functional connectivity. We hypothesize that the first period of tetanic stimulation pushed the network out of its existing balance between activity and connectivity. This balance causes stable activity patterns, at least on a timescale of several hours [5]. Because the evoked activity patterns are different from spontaneous patterns, synaptic connections will change. The network then develops a new balance between activity and connectivity, which now supports the stimulus induced patterns. Therefore, differences in activity patterns will be smaller when the same stimulus is re-applied in subsequent periods, yielding smaller changes in connectivity. The effect of stimulation at a second electrode hardly exceeded spontaneous fluctuations, it may have been too close to the first stimulation in time and/or space. Slow pulses yielded very similar results, suggesting that the effects are caused by network activation rather than by the tetanus itself.

References

[1] J. le Feber, et al. Conditional firing probabilities in cultured neuronal networks: a stable underlying structure in widely varying spontaneous activity patterns. J Neural Eng, 2007.

[2] J. le Feber, et al. The Effect of Slow Electrical Stimuli to Achieve Learning in Cultured Networks of Rat Cortical Neurons. PloS ONE, 2010.

[3] Y. Jimbo et al. Simultaneous induction of pathway-specific potentiation and depression in networks of cortical neurons.Biophys J, 1999.

[4] M. E. Ruaro et al. Towards the neurocomputer: Image processing and pattern recognition with neuronal cultures.IEEE Trans Biomed Eng, 2005.

[5] J. Stegenga et al. Analysis of cultured neuronal networks using intra-burst firing characteristics.IEEE Trans Biomed Eng, 2008.

[6] D.A. Wagenaar et al. Searching for plasticity indissociated cortical cultures on multi electrode arrays. J Neg Res Biomed 5(16), 2006.

Analysis of time-varying connection properties of cultured neuronal network under diverse conditions of electrical stimuli

Tatsuya Haga[1*], Yuzo Takayama[1,2], Osamu Fukayama[1], Takafumi Suzuki[3], Kunihiko Mabuchi[1]

1 Graduate School of Information Science and Technology, The University of Tokyo, Tokyo, Japan
2 Research Fellow of the Japan Society for the Promotion of Science, Tokyo, Japan.
3 Center for Information and Neural Networks, National Institute of Information and Communications Technology, Osaka, Japan
* Corresponding author. E-mail address: Tatsuya_Haga@ipc.i.u-tokyo.ac.jp

Abstract
Plasticity of neuronal networks is thought to be the basis of memory and learning in the brain and the relationship between inputs and plasticity has been of interest. Previous studies have revealed that different frequency or location of stimuli make various effects to the network but few studies have quantitatively evaluated in detail how these factors affect to network plasticity. Therefore we investigated changes of connection properties of living neuronal networks cultured on Multi-Electrode Array applying diverse conditions of electrical stimuli. We investigated how various conditions of stimuli changes connection strength of cultured neuronal network. As a result, both potentiation and depression of connectivity were observed under condition of stimuli and the most significant change was observed 100 Hz stimulation from only one electrode.

1 Background/Aims

Plasticity of neuronal networks is thought to be the basis of memory and learning in the brain and the relationship between inputs and plasticity has been of interest. Previous studies have revealed that different frequency or location of stimuli make various effects to the network [1] but few studies have quantitatively evaluated in detail how these factors affect to network plasticity. Therefore we investigated changes of connection properties of living neuronal networks cultured on Multi-Electrode Array applying diverse conditions of electrical stimuli.

2 Methods/Statistics

We cultured cortical neurons obtained from Wister rat embryos on MED210A (Alpha MED Scientific Inc.), which has 8 × 8 indium–tin–oxide (ITO) electrodes coated with platinum black. Each electrode on MED was 20μm square and the distance between the centres of the electrodes was 200μm. A culture in 24DIV was used in the experiment.

The experiment was constructed of 24 sessions. In each session, 30 sets of stimuli were induced at ten-second interval. A set was constructed of ten biphasic pulses induced at frequency different according to sessions. Amplitude of a pulse was 1.5V, and it lasted for 100μs in +/- phase respectively. 24 conditions were combinations of twelve frequencies of electrical stimuli (1Hz, 5Hz, 10Hz, 20Hz, …, 90Hz, 100Hz) and a choices of two electrodes to induce stimuli (electrodes A and B, illustrated in Fig. 1). We inserted 60-minute intervals before the start of the stimulation and between sessions.

Connection properties were estimated from spike trains obtained from recorded signal in real-time. We derived the probabilistic model from leaky integrate and fire model with multi-timescale adaptive threshold [2] including post-synaptic potentials (PSP) as synaptic interactions between neurons, and estimated them using extended kalman filter regarding the model as a state-space model. Maximum heights of estimated PSP were showed as connectivity strength.

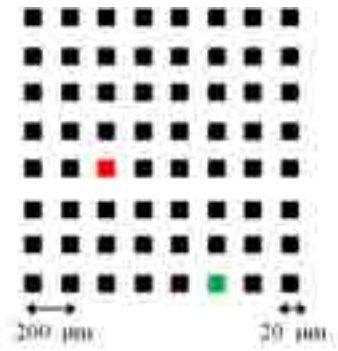

Fig. 1. The diagram of electrodes embedded on MEA. The electrode A and the electrode B is showed as the red square and the green square respectively.

3 Results

We extracted only connections that had PSP stronger than 2mV (the network diagram is illustrated

as Fig. 2). Some changes were observed in strength of extracted connections (Fig. 3). The most significant change occurred in 800 minutes after the start of the experiment, it is just after 100 Hz stimulation from electrode A was induced (Fig. 4). Besides, we calculated changes of connections strength induced by one session of stimuli by subtracting strength at the start of the session from strength at the start of the next session. It indicates that one condition of stimuli evoked both potentiation and depression to the network (Fig. 5), and different conditions of stimuli evoked different effects (potentiation, depression or no change) to the same connection (Fig. 6).

4 Conclusion/Summary

We investigated how various conditions of stimuli changes connection strength of cultured neuronal network. As a result, both potentiation and depression of connectivity were observed under one condition of stimuli and different conditions of stimuli evoked variant changes of one connection. These results indicate possibility of controlling connections by induction of appropriate stimuli.

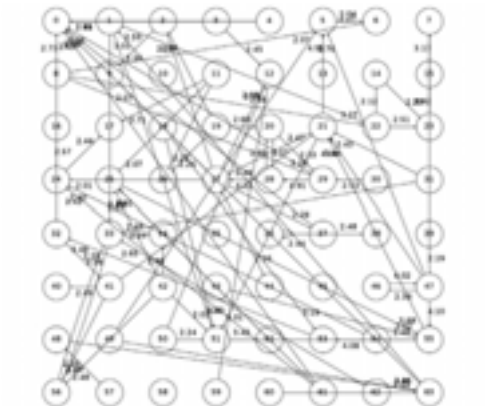

Fig. 2. Network estimated from spike trains recorded from MEA (only connections that had PSP stronger than 2mV are showed).

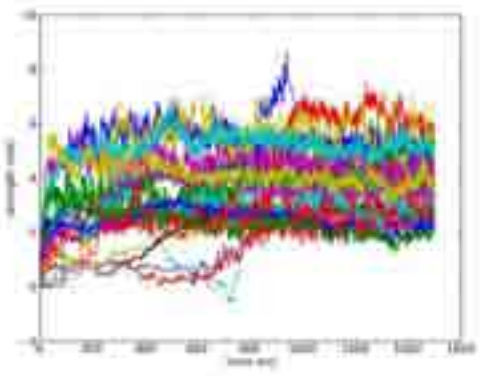

Fig. 3. Time series variations of strength of connections.

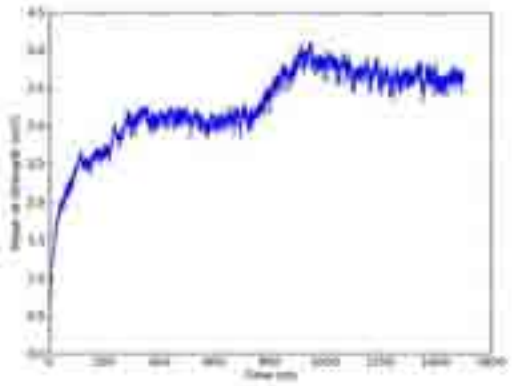

Fig.4. Time series variations of mean strength of all connections.

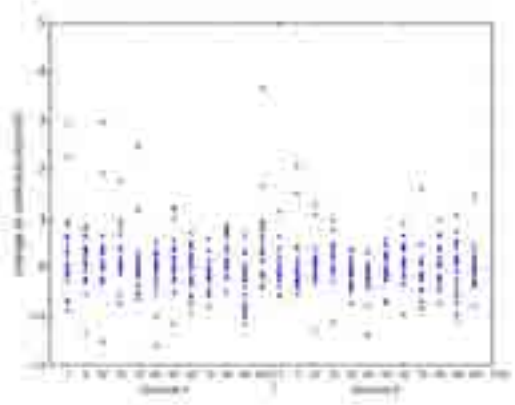

Fig.5. Changes of connection strength induced by different conditions of stimuli (one point corresponds to one connection).

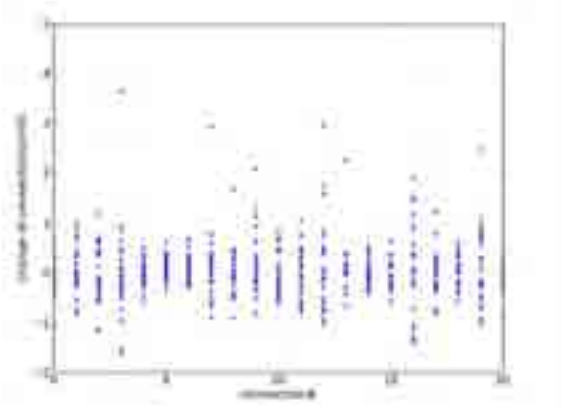

Fig. 6. Changes of each connection (one point corresponds to one condition of stimuli).

References

[1] Chiappalone, M. and Bove, M. and Vato, A. and Tedesco, M. and Martinoia, S.(2006) Dissociated cortical networks show spontaneously correlated activity patterns during in vitro development, Brain research, vol. 1093, No. 1, 41-53.

[2] Kobayashi R. and Tsubo Y. and Shinomoto S.(2009) Made-to-order spiking neuron model equipped with a multi-timescale adaptive threshold, *Frontiers in computational neuroscience, vol. 3, article 9.*

Hysteresis of evoked activity pattern in cultured neuronal network

Hidekatsu Ito and Suguru N. Kudoh*

School of Science and Technology, Kwansei Gakuin University, 2-1 Gakuen, Sanda, Japan
* Corresponding author. E-mail address: snkudoh@kwansei.ac.jp

Abstract
In order to elucidate dynamics of a neuronal network, dissociated culture system is adequate. The rat hippocampal neurons were cultured on a multi electrode array (MEA) dish. We applied shots of electrical stimuli in several types of inter-stimulus intervals and analysed evoked responses. We found that the response pattern of evoked electrical activity was affected by existence of prestimulation in the case that interval between the first stimulation and second paired stimulation was within 2 s. These results suggest that an origin of the hysteresis is transition of the internal state of the network, undertaken by synaptic transmissions. This "memory" like hysteresis function was observed even in stimulus-evoked electrical activity of a semi-artificial neuronal network on MEA.

1 Introduction

Cultured neurons reorganized complex networks on a multi-electrodes array dish, and spontaneous electrical activity has been observed [1, 2]. Spontaneous activity pattern changes depending on the culture days and the network structure is modified by inputs from outer world in activity dependent manner. The synchronized electrical activity has been confirmed also in cortical dissociated culture system [3, 4], suggesting the phenomenon is a common feature of reconstructed network on a culture dish. As for temporal structure of the firing-rate, the burst period was reported to continue from 14 DIV to 30 DIV, though the burst activity fragments over 30 DIV [5, 6]. Spontaneous activity in neuronal network may form various "states" of the network. This state also influenced on the spike activity pattern evoked by an electrical stimulation. Even a single shot of the stimulation is expected to change the internal state of the network, similar as spontaneously evoked activity. So we investigated the feature of evoked activity pattern and here we report a "memory" like function observed in stimulus evoked electrical activity of neuronal network cultured on MEA probe.

2 Materials and methods

2.1 Rat hippocampal dissociated culture

Culture method is previously described conventional one [7]. Briefly, rat hippocampal Neurons were dissociated and placed in an arranged cloning ring with a diameter of 7 mm at the center of a MEA dish (MED probe, Alfa-MED scientific, Japan), preventing from adhesion of cells on the reference electrodes located on near border of the culture area. The density of seeded cells was 7800 cells/mm2. Culture medium consists of 45% Ham's F12, 45% Dulbecco's modified minimum essential medium (Invitrogen-Gibco, California, U.S.A.), 5% horse serum (Invitrogen-Gibco, California, U.S.A.), 5% fetal calf serum (Invitrogen-Gibco, California, U.S.A.), 100 U/ml penicillin, 100 μg/ml streptomycin (Invitrogen-Gibco, Carlsbad, California, U.S.A.), and 5 μg/ml insulin (Sigma-Aldrich, US). The conduct of all experimental procedures was governed by the "Kwansei Gakuin University Regulations for Animal Experimentation".

2.2 Electrophysiological experiments by MEA

Extracellular potentials were collected by the MED64 integrated system (Alfa-MED scientific, Japan). A/D conversion of measured signals was carried out at a sampling rate of 20 kHz and quantization bit rate of 16 bit. The data were stored at a hard disk of a PC/AT computer. The system was controlled by recording software, MED Conductor 3.1(Alfa-MED scientific, Japan). Electrical activity spikes were detected and analysed, using MEDFAUST software, which we developed. We applied sequential shot of electrical stimuli to the neuronal network cultured on MEA dish via a selected electrode. The interval of the consecutive electrical stimuli was set to 1 s, 2 s, 2.5 s, 5 s and 10 s. Electrical stimuli were applied 4 times at a trial. First 2 stimuli, stim1 and stim2, were single-shot stimuli with an enough inter-stimulus interval (ISI, usually more than 60 s) for recovering a state of network activity. These stimuli were for a control experiment. Then a paired stimulation set with short ISI (stim4 with stim3 as pre-stimulation) was applied. This experimental procedure of a sweep was performed repeatedly for 30 times. Inter-sweep-interval was 50 s. The 60 s delay after the stim1 and 50 s of inter-sweep-interval were determined according to our previous result that effect of an electrical stimulation

on spontaneous activity diminished within approximately 60 s.

2.3 Elucidation distance of similarity of activity pattern

Firstly, the feature vector which components were number of detected spikes at each electrode within a 50 ms time window was synthesized repeatedly. Then, to elucidate similarity between the spatio-temporal pattern of evoked activity, we calculated Euclidian distances between feature vector of electrical spike patterns along time axis.

3 Result and Discussions

Fig.1 upper panel indicates Euclidean distances between the pattern by a single stimulation and by a paired stimulation in 23-26 DIV. There is no obvious differences in the case of ISI are 1s to 10s. Lower panel indicates Euclidean distances is obviously long at immediately after the paired stimulation, and then gradually reduces. The hysterical effect on the activity gradually reduces depending on increasing of the ISI. The long distances indicates that response pattern was quite different between a single stimulation and a paired stimulation, if ISI is enough short. Normalization is achieved by dividing the distances between the pattern by a single stimulation and a paired stimulation by the distances between the patterns by single stimulations.

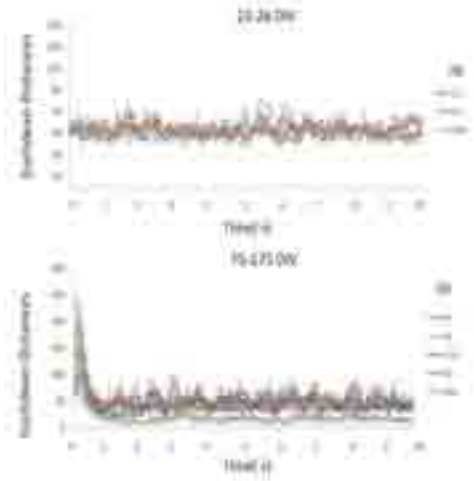

Fig.1 Panels indicate Euclidean distances calculated from activity in a same single culture.

Transitions of Euclidean distance between activity evoked by the single stimulation and activity by the paired stimulation. Upper panel indicate transitions of Euclidean distance in 23-26 DIV and Lower panel indicate the 75-175 DIV. The hysteresis was remarkable only in 75-175 DIV.

Fig.2 upper panel indicates that there is no obvious differences at all ISI in the case of short-term cultures (DIV < 30). In lower panel, the state with long distances by a paired stimulation with 1s ISI last for approximately 1 s. In addition, there are some peaks of long distances, corresponding to second peaks. These results indicate that the differences were significant only in 75-175 DIV.

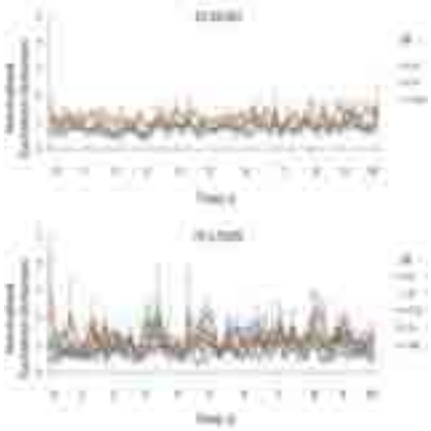

Fig.2 Panels indicate normalized Euclidean distances calculated from activity in a same single culture. These results show that large values of normalized Euclidean distances appear immediately after 1s ISI paired stimulation in a culture of 75-175 days. However, the tendency is not seen in 23-36 DIV culture.

4 Conclusion

The cultured network can memorize that there had been a previous stimulation several seconds before the second stimulation. Network hysteresis is expected to depend on internal state of the network.

Acknowledgement

This research is supported by the Ministry of Education, Culture, Sports, Science, and Technology of Japan under Grant-in-Aid for Scientific Research #24300091.

References

[1] Gross GW, Rieske E, Kreutzberg GW and Meyer A (1977) A new fixed-array multimicroelectrode system designed for long-term recording. Neurosci Lett 6:101-105

[2] Pine J (1980) Recording action potentials from cultured neurons with extracellular microcircuit electrodes. J Neurosci Methods 2:19-31

[3] Eytan D, Marom S (2006) Dynamics and effective topology underlying synchronization in networks of cortical neurons. J of Neurosci 26:8465-8476

[4] Wagenaar DA, Pine J, Potter SM (2006) An extremely rich repertorie of bursting patterns during the development of cortical cultures. BMC Neurosci 7:11.

[5] van Pelt J, Wolters PS, Corner MA, Rutten WLC, Ramarkers GJA (2004) Long-term characterization of firing dynamics of spontaneous bursts in cultured neural networks. IEEE Trans Biomed Eng 51:2051-2062

[6] Chiappalone M, Bove M, Vato A, Tedesco M, Martinoia S (2006) Dissociated cortical networks show spontaneously correlated activity pattern during in vitro development. Brain Res 1093:41-53

[7] Kudoh SN, Tokuda M, Kiyohara A, Hosokawa C, Taguchi T, Hayashi I (2011), Vitroid - The Robot System with an Interface Between a Living Neuronal Network and Outer World, International Journal of Mechatronics and Manufacturing System, Vol.4, No.2, pp.135-149.

A flexible system to provide sub-millisecond feedback stimulation loops between multiple sets of individually identifiable neurons

Jan Müller[1*], Douglas J. Bakkum[1], Branka Roscic[1], Andreas Hierlemann[1]

1 ETH Zurich, Bio Engineering Laboratory, Department of Biosystems Science and Engineering, Basel, Switzerland
* Corresponding author E-mail address: jan.mueller@bsse.ethz.ch

Abstract
A system to provide an artificial synapse between cultured neurons is presented. A complementary metal-oxide-semiconductor (CMOS)-based MEA provides high resolution bidirectional access to record from and stimulate individual neurons in a cell culture. In conjunction with a field-programmable gate array (FPGA), this system allows to identify single neurons and to apply closed-loop feedback stimulation cycles within as little as 200 µs. Computing the cross-correlation between the neurons before, during, and after the feedback stimulation provides a measure for closed-loop induced plasticity.

1 Background and Aims

It is believed that memory and learning processes in the brain are, among other factors, governed by the relative timing of the activity between different neurons. Applying an artificial synapse between two or more neurons allows the experimental manipulation of connectivity in the neural network under study, as predicted by spike-timing dependent plasticity rules [1]. Here, we present a system for sub-millisecond real-time closed-loop feedback to record from and subsequently stimulate individual neurons, cultured on a high-density (3150 electrodes per mm2) CMOS (Complementary Metal Oxide Semiconductor) microelectrode array (MEA) [2].

2 Methods

We grew cultures of E18 rat cortical neurons over 11,011-electrode CMOS arrays. The CMOS MEA features 126 on-chip amplifiers (0-80dB) and analog-to-digital converters (8bit, 20 kHz), which can be connected to an arbitrary subset of 126 electrodes. The digitized traces are streamed to a field-programmable gate array (FPGA), which performs band pass filtering (0.5-1.8kHz) and subsequent threshold detection to assign events. After the detection of an event, a pre-programmed stimulation waveform is triggered on an arbitrary electrode(s), which can reliably evoke action potentials in a defined subset of neurons, located at other electrodes. The delay between the trigger spike and the stimulation is programmable in a range from 200 µs to seconds. Due to the small electrode pitch of 17 µm, sub-cellular-resolution measurements are possible, and individual neurons can be identified by scanning through the 11,011 electrodes using high-resolution blocks or random configurations of 126 electrodes. Functional connectivity between identified neurons was computed using a custom-designed cross-correlation algorithm. The flexibility of the electrode selection allows for searching through the whole culture and for specifically targeting, e.g., two neurons, which are not or only weakly connected with each other.

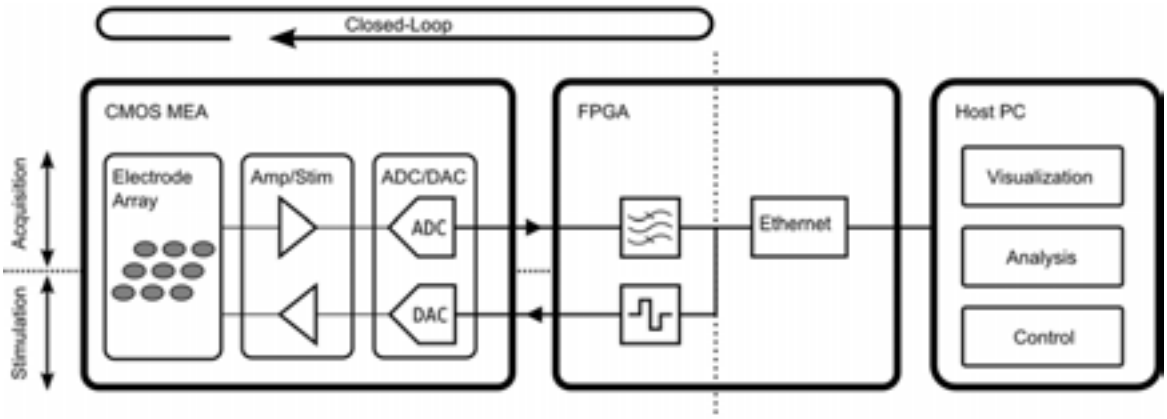

Fig. 1. Overview of the main components of the system. The feedback stimulation loop is closed around the CMOS MEA device and the FPGA.

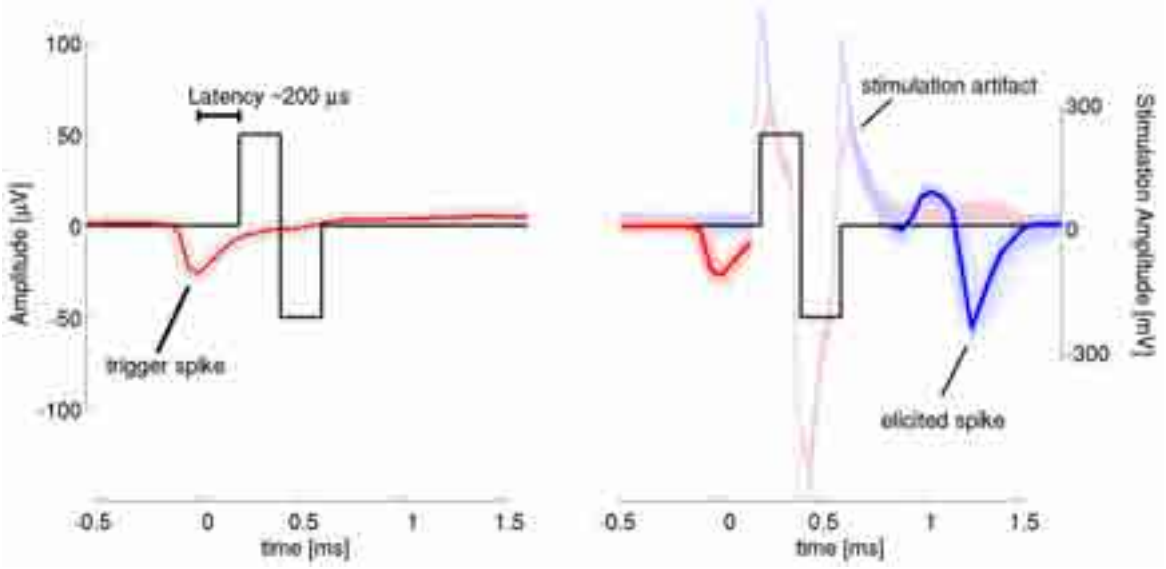

Fig. 2. Representation of 140 unfiltered raw traces of recorded action potentials (red). They reliably triggered a stimulation pulse after 200 µs. In the figure on the left, the stimulation channel was disconnected from the electrode to avoid artifacts for a clearer figure, whereas on the right it was connected and elicited spikes. The black bar shows the latency between the averaged negative peak of the recorded action potentials and the onset of the triggered stimulation pulse. The stimulation pulse reliably triggered action potentials on a different electrode (blue), on average after 0.5 ms. The distance from the electrode that recorded the elicited spikes to the stimulation site was 140 µm, and that to the trigger electrode 168 µm; the trigger electrode was at 185 µm distance from the stimulation site. Obtaining reliable recordings was not possible during the occurrence of the stimulation pulse due to the presence of artifacts, but was possible immediately afterwards (within less than 200 µs).

3 Results

The system was successfully applied to a neuronal network grown over the array. We were able to detect individual neurons and to provide an "artificial synapse" between some of them. By using an FPGA in between the chip and a PC to do the filtering, spike detection and stimulation, feedback cycles as short as 200 µs with a jitter below 50 µs were achieved (Figure 1). Most of the delay between the actual spike and the stimulation pulse comes from a two tab Butterworth band-pass filter. Due to the parallel nature of processing in FPGAs, many feedback loops can be applied simultaneously without introducing additional latency.

4 Conclusion

Closing the loop around the CMOS MEA and the FPGA allows for fast and precise feedback as a consequence of the deterministic nature of the FPGA design and provides a new tool to study information processing and learning in neuronal networks. The system has been implemented and verified here, and future plans include examining how individual cells respond to various closed-loop protocols, designed to alter functional connectivity. Moreover we will investigate how this response propagates into the rest of the network.

Acknowledgements

This work was financially supported by the FP7 of the European Community through the ERC Advanced Grant 267351 "NeuroCMOS".

References

[1] Bi G-Q, Poo M-M (1998). Synaptic Modifications in Cultured Hippocampal Neurons: Dependence on Spike Timing, Synaptic Strength, and Postsynaptic Cell Type. *J. Neurosci, 77: 551-555.*

[2] Frey U, Egert U, Heer F, Hafizovic S, Hierlemann A (2009). Microelectronic system for high-resolution mapping of extracellular electric fields applied to brain slices. *Biosensors and Bioelectronics* 24: 2191–2198.

Tracking the evolution of neural network activity in uninterrupted long-term MEA recordings

Aurel Vasile Martiniuc[1*], Dirk Saalfrank[2], Francesco Difato[3], Francesca Succol[3], Marina Nanni[3], Alois Knoll[1], Sven Ingebrandt[2], Axel Blau[3]

1 Computer Science Department VI, Technical University Munich, 85748 Garching , Germany, www.in.tum.de * Corresponding author's email address: martiniv@in.tum.de
2 Dept. of Informatics and Microsystem Technology, University of Applied Sciences Kaiserslautern, 66482 Zweibrücken, Germany, www.fh-kl.de
3 Dept. of Neuroscience and Brain Technologies (NBT), Fondazione Istituto Italiano di Tecnologia (IIT), Via Morego 30, 16163 Genoa, Italy, www.iit.it

Abstract
Most cell culture studies rely on taking representative, quasi-static data snapshots during limited time windows. To permit continuous experimentation, we devised an automated perfusion system based on microfluidic cell culture chambers for microelectrode arrays (MEAs). The design is based on a perfusion cap fabricated in replica-molding technology and on a hermetically shielded, gravity-driven perfusion mechanism. Network activity from neurons on MEAs was continuously recorded outside of a CO_2 incubator at ambient conditions over one month under stabilized temperature, osmolarity and pH conditions. Our analysis exemplarily focused on the evolution of paired spiking (PS) activity consisting of two spikes separated by 2 ms in spontaneously active hippocampal cultures. It started as early as 10 days *in vitro* (DIV) and triggered patterns of network-wide spreading activity that persisted until the end of the recording session lasting 32 days. We hypothesize that paired-spike activity is a general coding phenomenon that is conserved in spontaneously active *in vitro* networks. In lack of *in vivo*-like sensory stimuli, cultured neurons may use it to substitute for natural stimuli.

1 Introduction

The common approach of performing snapshot experiments bears several risks: each time, data is collected at different physiological cellular 'response states', which might furthermore be affected by non-reproducible variations in cell culture handling during their transfer from the incubator to the experimental setup. Furthermore, datasets are fragmented by lack of observation continuity. We therefore tested a simple gravity-driven perfusion concept to uninterruptedly record spike trains from neural cultures on MEAs over several weeks. The setup allowed us to investigate and compare the activity evolution in two separate cortical cultures over 32 days (hippocampal) and 59 days (cortical), respectively. We briefly discuss the evolution of paired-spike activity in the hippocampal culture.

2 Methods

2.1 Cell culture and perfusion setup

Hippocampal neurons (Sprague-Dawley rat, E17, ~50,000 cells/dish) were plated on Ti/TiN 30/200iR MEAs coated with poly-D-lysine/laminin (0.1 mg/ml; 5 µg/ml) and cultured in serum-free, pH-buffered medium (NBM, 2% B27, 2 mM AlaGlu, 100 U/ml Pen-Strep, 10 mM histidine/HEPES) following published protocols. They were kept 7 days in a humidified incubator before being transferred onto the 60 channel amplifier (Multi Channel Systems, Reutlingen, Germany) with T-control (36.5 °C). A polydimethylsiloxane (PDMS) perfusion cap based on a previously published design [1] featured ID 1.8 mm Teflon® tubing with in- and outlet silicone septa. Supply and waste Teflon tubing could be reversibly connected to these septa by OD 0.7 mm syringe needles. A pinch-valve (Velleman relay card K8056, Profilab) at the outlet tubing allowed timed gravity-driven medium exchange (~200 µl every 8 hours; relative positions with respect to tabletop: supply: 520 mm, MEA: 320 mm, valve: 10 mm, waste: - 300 mm; Fig. 1). Extracellularly recorded spikes were detected at 5.5 STDV from p-p noise and extracted (but not sorted) for time-stamp-based analysis.

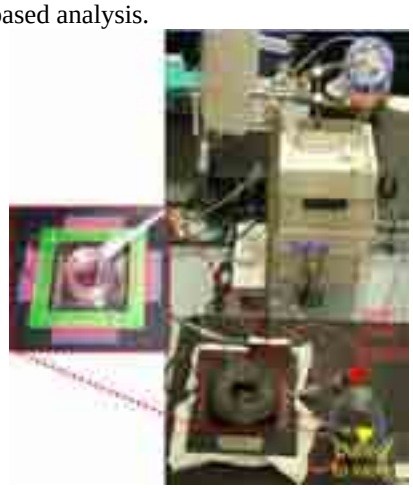

Fig. 1 Perfusion setup and PDMS cap (inset).

2.2 Paired spiking (PS) versus bursting activity at individual sites

We defined paired-spikes (PS) as the neural activity consisting of two spikes recorded from the same electrode that were separated by an interval of 2 ms followed by an inter-paired-spike interval (IPSI) larger than 50 ms. Bursting activity at individual sites was defined as events with more than 10 spikes separated by an interval lower than 100 ms followed by an interburst interval (IBI) larger than 200 ms.

3 Results and Discussion

In vivo, paired-spike (PS) enhancement plays a crucial role in information processing at different hierarchical stages within the nervous system [2, 3]. While spike pairing was very low at the early DIVs, it consistently increased after 3-4 weeks *in vitro* (WIV) (Fig. 2).

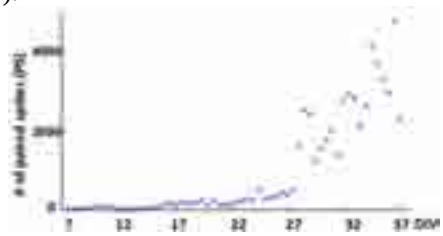

Fig. 2 Network-wide number of paired spikes (PS) recorded at different developmental stages.

Activity patterns consisting of PS separated by 2 ms were rarely encountered at the very beginning of the recordings. Instead, random isolated spikes rather than synchronized rapid firing dominated neural activity [4]. During the first 3 WIVs, the IPSI was very large (up to 170 s) and fluctuated highly with a low number of repetitions at individual sites, denoting that PS was not yet robust (Fig. 3a & b, first period).

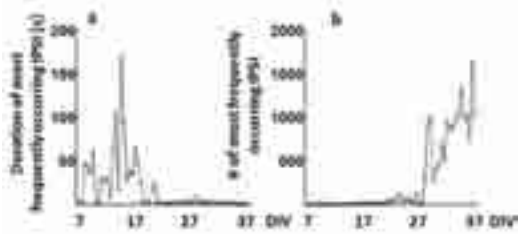

Fig. 3 a) Plot of the duration of the most frequent IPSI in a certain 12-hours interval over DIVs: the distribution can be separated into two distinct periods with fluctuating high values during the first 3 WIVs and a second period with an almost constant value of 2-3 s. **b**) Inversely, the overall number of the most frequently occurring IPSI in 12 hours was low during the first period while it increased during the second period.

After 3 WIVs, the IPSI dramatically decreased to 2-3 s and remained robust up to the end of the recording session. In the same period, the number of the most frequently occurring IPSI increased consistently. Furthermore, PS patterns that repeated at 2-3 s IPSI stayed associated to individual sites within the network as pointed out by the purple circles in Fig. 4. Moreover, in most cases, PS were recorded from those electrodes that also recorded bursting activity as shown in Fig. 5a & b. The network location with dominant PS and bursting activity could change over the days, though (Fig. 5b).

Acknowledgement

IIT intramural funding for this research line is greatly appreciated.

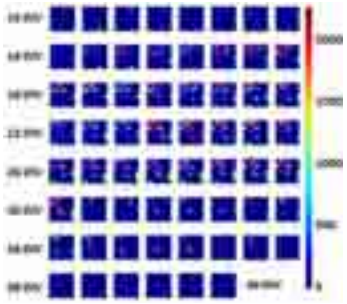

Fig. 4 Cumulative number of PS and its distribution over an 8 x 8MEA at different DIVs in 12-hours intervals. The purple ellipse points out a robust PS pattern.

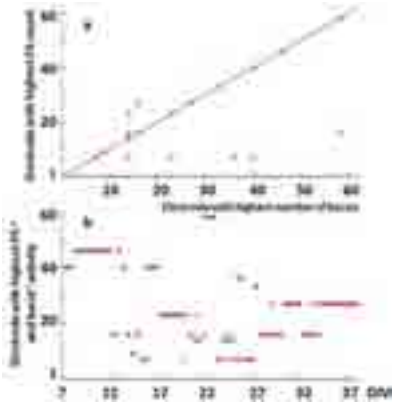

Fig. 5 a) In most cases, the highest number of PS (y axis) were recorded from the same electrode from which the highest number of bursts (x axis) were recorded **b)** The network location with highest PS (blue circle) and bursting (red dot) activity changed over time.

4 Conclusions

We uninterruptedly recorded spontaneous activity from cultured neurons over 32 DIVs. Our findings show that PS activity becomes more robust after about 3 WIVs. PS might thus be used as an indicator for network maturity. The findings also suggest that neurons in culture use PS to replace the missing stimuli found in natural conditions within the nervous system. This hypothesis will be tested in future experiments.

References

[1] A. Blau, T. Neumann, C. Ziegler, F. Benfenati (2009) Replica-molded poly(dimethylsiloxane) culture vessel lids attenuate osmotic drift in long-term cell culturing, *J. Biosci.*, 34, 59-69.

[2] W. M. Usrey, J. B. Reppas, R. C. Reid (1998) Paired-spike interactions and synaptic efficacy of retinal inputs to the thalamus, *Nature*, 395, 384-387.

[3] E. Salinas, T. J. Sejnowski (2001) Correlated neuronal activity and the flow of neural information, *Nat Rev Neurosci*, 2, 539-550.

[4] J. Van Pelt, P. S. Wolters, M. A. Corner, W. L. C. Rutten, G. J. A. Ramakers (2004) Long-term characterization of firing dynamics of spontaneous bursts in cultured neural networks, *IEEE Transaction on Biomedical Engineering*, 51, 2051-2062.

Return map analysis of synchronized bursts in cultured neuronal networks

Keiko Yokoyama[1, 2*], Daisuke Ito[2, 3], Kazutoshi Gohara[1]

1 Division of Applied Physics, Faculty of Engineering, Hokkaido University, Sapporo, Japan
2 Research Fellow of the Japan Society for the Promotion of Science, Tokyo, Japan
3 Division of Functional Life Science, Faculty of Advanced Life Science, Hokkaido University, Sapporo, Japan
* Corresponding author. E-mail address: yoko.k@eng.hokudai.ac.jp

Abstract

The aim of this study was to verify whether return map analysis is an effective method of evaluation of the temporal dynamics underlying sequences of synchronized bursts (SBs) in neurons. The spike events of a single neuron and the time events of SBs were derived from electrical data of neuronal networks cultured on multi-electrode arrays (MEAs). The distribution of points on a return map, corresponding to the sequences of SBs, exhibited an "L-shaped" cluster. This is similar to the observation in a previous study of the spike events of a single neuron. In agreement with the previous study, one of the neurons in the network used here showed a similar L-shaped cluster of spike events on a return map. These results expand the possibilities of the use of return map analysis for clarification of the temporal dynamics of SBs through comparison of the phenomenon at different scales, such as an entire network *versus* a single neuron.

1 Introduction

Synchronized bursts (SBs) in neuronal networks are important phenomena in the brain. Recent work using multi-electrode arrays (MEAs) revealed a variety of burst patterns throughout the development of neuronal networks. However, the detailed temporal dynamics, including specific characteristics underlying the sequences of SBs, have not been precisely elucidated. In dynamic systems, return map analysis is a useful tool for understanding the temporal dynamics of complex phenomena. Such analysis can aid in the understanding of unresolved phenomena because of its ability to clarify the universal dynamics, regardless of the scale of the phenomena. This is evident from the fact that return map analysis has been applied to various complex phenomena, such as individual fluctuations and climate variation, and has demonstrated excellent resolution of the temporal dynamics. Many studies of neuronal firing patterns using return maps have focused on a single neuron [1-4]. On the other hand, some studies had applied the method to the firing patterns of collective neurons, such as SBs [5], but the universal dynamics underlying the network were not demonstrated clearly. In this study, we examined the efficacy of return map analysis for evaluation of the temporal dynamics of SBs in neuronal networks cultured on MEAs.

2 Methods

2.1 Cell culture

Cerebral cortices derived from Wistar rats at embryonic day 17 were dissociated on multi-electrode dish (MED) probes and cultured for 1-2 months. Spontaneous electrical activity on the 64-electrode arrays (8×8) was recorded several times during these periods using an MED64 extracellular recording system (Alpha MED Scientific, Osaka, Japan) at a sampling rate of 20 kHz. Immediately after electrical recording, immunofluorescence staining was performed directly on the MEAs [6]. Figure 1a shows an immunofluorescence micrograph of cortical cultures on MEAs.

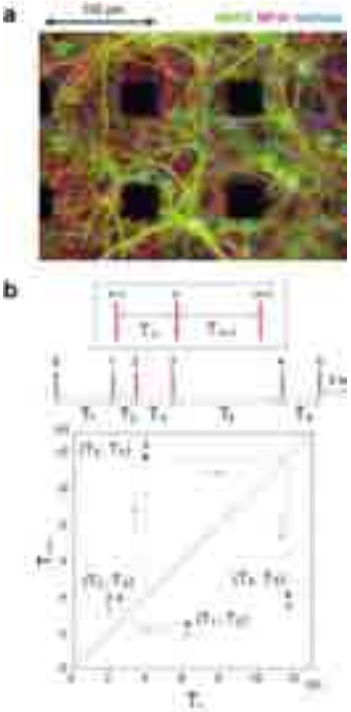

Fig. 1: a. Immunofluorescence micrograph of cortical cultures on multi-electrode arrays. **b.** Sample return map, illustrating the relations between time intervals (see section 2.3 for a detailed explanation).

2.2 Spike and synchronized burst detection

In the electrical recordings, spikes were identified when the amplitude exceeded a noise-based threshold. The correlation values among spikes were calculated, and a group of spikes showing high correlation was regarded as the activity of one neuron. These processes were performed about each electrode. SB events were identified when the rate of firing rate during a 100-ms time bin exceeded a threshold (*e.g.*, Figure 2b).

2.3 Return map

The abscissa and ordinate on a map indicate the time intervals Tn and Tn+1, respectively. As indicated in the upper box in Figure 1b, Tn and Tn+1 are defined as the time intervals between events n-1 and n, and n and n+1, respectively. Thus, one point on a map shows the temporal relations among three events. A sample map is shown in Figure 1b, in which time intervals among six time events are shown as four points.

3 Results

Figures 2a and 2b show, respectively, a raster plot of a single neuron and its firing rate over a 10-min period. The time events corresponding to the SBs of Figures 2a and 2b are shown in the upper panel of Figure 2c, and the return map of the data is shown in the left panel of Figure 2d. The distribution of points on the return map exhibits an "L-shaped'' cluster, such as has been previously observed for a single neuron [1-3]. This similarity in the return map of a network compared with that of a single neuron is confirmed in our data; Figure 2d shows the return map for the individual spike events of a single neuron, which are shown in the lower panel of Figure 2c over 11 s, including one SB.

4 Conclusion

We applied return map analysis, which has the ability to reveal the temporal dynamics underlying SBs, to neuronal networks cultured on MEAs. As a result, a cluster on a return map of SBs exhibited the same tendency as that of spikes from a single neuron. This suggests that return map analysis can effectively reveal the temporal dynamics of SBs through comparison of the phenomenon at different scales, such as over a network versus a single neuron.

Acknowledgement

This work has been supported in part by Grant-in-Aid for Scientific Research from the Japan Society for the Promotion of Science (20240023, 23700523 and 11J04016).

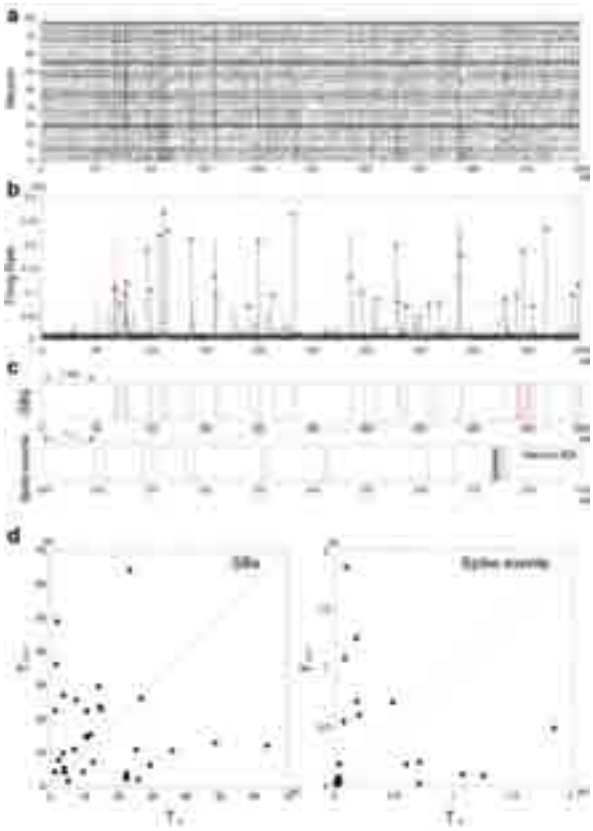

Fig. 2: Return map analysis of synchronized bursts (SBs) (data from one culture, 31 DIV, 10 min) **a.** A raster plot of 78 single neurons over 10 min. **b.** Time series of the firing rate of all neurons during a 100-ms time bin. Dashed line shows the threshold that defines SBs. **c.** Time events of SBs and spikes. Upper panel: SB events marked as red points in Figure 1b. Lower panel: Spike events of neuron number 25 over 11 s, including one SB indicated by the red-dash box in the upper panel. **d.** Return maps of SBs generated from the network (left), and of spike events generated by a single neuron (right).

References

[1] Segundo J. (2003). Nonlinear dynamics of point process systems and data. *International Journal of Bifurcation and Chaos*, 13, 2035-2116.

[2] Segundo J., Vibert J., and Stiber M. (1998). Periodically-modulated inhibition of living pacemaker neurons-III. The heterogeneity of the postsynaptic spike trains, and how control parameters affect it. *Neuroscience*, 87, 15-47.

[3] Segundo J., Sugihara G., Dixon P., Stiber M., and Bersier L. (1998). The spike trains of inhibited pacemaker neurons seen through the magnifying glass of nonlinear analyses. *Neuroscience*, 87, 741-766.

[4] Szücs A., Pinto R., Rabinovich M., Abarbanel H., and Selverston A. (2003). Synaptic modulation of the interspike interval signatures of bursting pyloric neurons. *Journal Neurophysiology*, 89, 1363-1377.

[5] Wagenaar D., Nadasdy Z., and Potter S. (2006). Persistent dynamic attractors in activity patterns of cultured neuronal networks. *Physical Review E*, 73, 051907.

[6] Ito D., Tamate H., Nagayama M., Uchida T., Kudoh S. N., Gohara K. (2010). Minimum neuron density for synchronized bursts in a rat cortical culture on multi-electrode arrays. *Neuroscience*, 171, 50-61.

Identifying activity perturbations that trigger homeo-static synaptic plasticity

Ming-fai Fong[1,2*], Jonathan P. Newman[2], Peter Wenner[1], Steve M. Potter[2]

1 Department of Physiology, Emory University School of Medicine, Atlanta, GA, USA
2 Laboratory for Neuroengineering, Department of Biomedial Engineering, Georgia Institute of Technology and Emory University School of Medicine, Atlanta, GA, USA
* Corresponding author. E-mail address: ming-fai.fong@emory.edu

Abstract

Homeostatic synaptic scaling is a form plasticity whereby chronic reduction or elevation of activity elicits a compensatory shift in the amplitude of synaptic currents. While homeostatic changes in synaptic strength have been well-described both *in vitro* and *in vivo* using pharmacological treatments to manipulate activity, network spiking is rarely monitored during these manipulations. In this study we used microelectrode array (MEA) recordings to monitor activity through chronic pharmacological blockade of spiking or fast excitatory transmission, and assessed subsequent changes in synaptic strength. We found that the direction, but not the magnitude, of synaptic scaling could be predicted by changes in spiking activity that occurred during the treatment.

1 Introduction

Homeostatic plasticity provides a set of mechanisms for maintaining appropriate levels of spiking activity in developing neural circuits. For example, when spiking in a cultured cortical network was blocked for 2 days, there was a compensatory increase in excitatory synaptic strength (synaptic scaling) [1]. Upward scaling also occurred when AMPAergic transmission was blocked. Here, we examined the relationship between changes in network activity and synaptic strength that follow chronic blockade of spiking or AMPAergic transmission.

2 Methods

2.1 Cell culture and drug treatments

Primary neuronal cultures were derived from E18 rat cortex and grown on polyethyleneimine- and laminin-coated MEAs. Serum-containing growth medium was changed every 3 days. During the second week *in vitro*, cultures were treated for 2 days with tetrodoxin (TTX, 1µM) to block spiking, or 6-cyano-7-nitroquinoxaline-2,3-dione (CNQX, 20µM) to block AMPAergic transmission. MEA recordings were used to monitor activity during the treatments, and whole-cell recordings were used to measure synaptic strength after washing the drug.

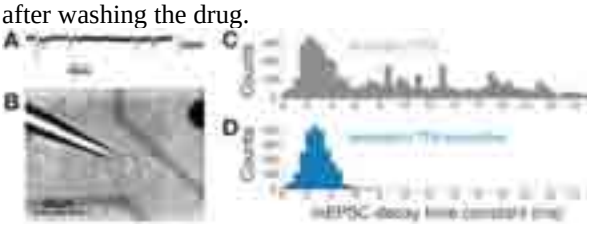

Fig. 1: Measuring AMPAergic synaptic strength. (A) Sample mEPSCs trace. **(B)** Pyramidal-shaped cell in cultured cortical network grown on MEA. **(C)** Histogram of decay time constants for glutamatergic and GABAergic mEPSCs recorded in the presence of TTX, or **(D)** TTX and bicuculline.

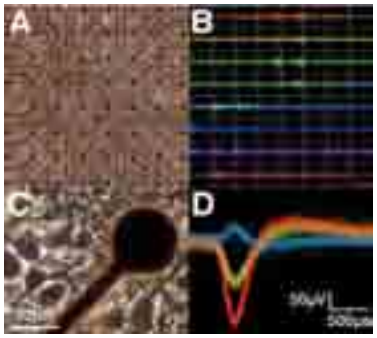

Fig. 2: Monitoring network and individual neuron activity. (A) Phase-contrast micrograph of dissociated cortical culture on MEA. Electrode spacing, 200µm. **(B)** Voltage traces recorded on each electrode using Neurorighter. **(C)** Magnified view of (A) showing neurons near an MEA electrode. **(D)** Sorted spike waveforms recorded on a single MEA electrode.

2.2 MEA electrophysiology

Extracellular action potentials were continuously recorded from 59-electrode MEAs (MCS 200/30iR-Ti-pr) using the Neurorighter acquisition system (www.sites.google.com/site/neurorighter). Recordings were performed at 35°C and 5% CO_2 in standard growth medium. Network firing rate was computed by taking a time histogram of all spikes across the array.

2.3 Whole-cell electrophysiology

Miniature excitatory postsynaptic currents (mEPSCs) were recorded from pyramidal-shaped cells in a continuous perfusion of artificial cerebrospinal fluid containing TTX (1µM) and bubbled with 95% O_2 and 5% CO_2. mEPSCs were recorded using a HEKA EPC8 amplifier and analyzed using MiniAnalysis (Synaptosoft). AMPAergic mEPSCs were isolated pharmacologically using bicuculline (20µM) to eliminate GABAergic currents, or by decay kinetics ($\tau \leq 6$ms) (Fig. 1C,D). Amplitude of AMPAergic mEPSCs is a measure of excitatory synaptic strength.

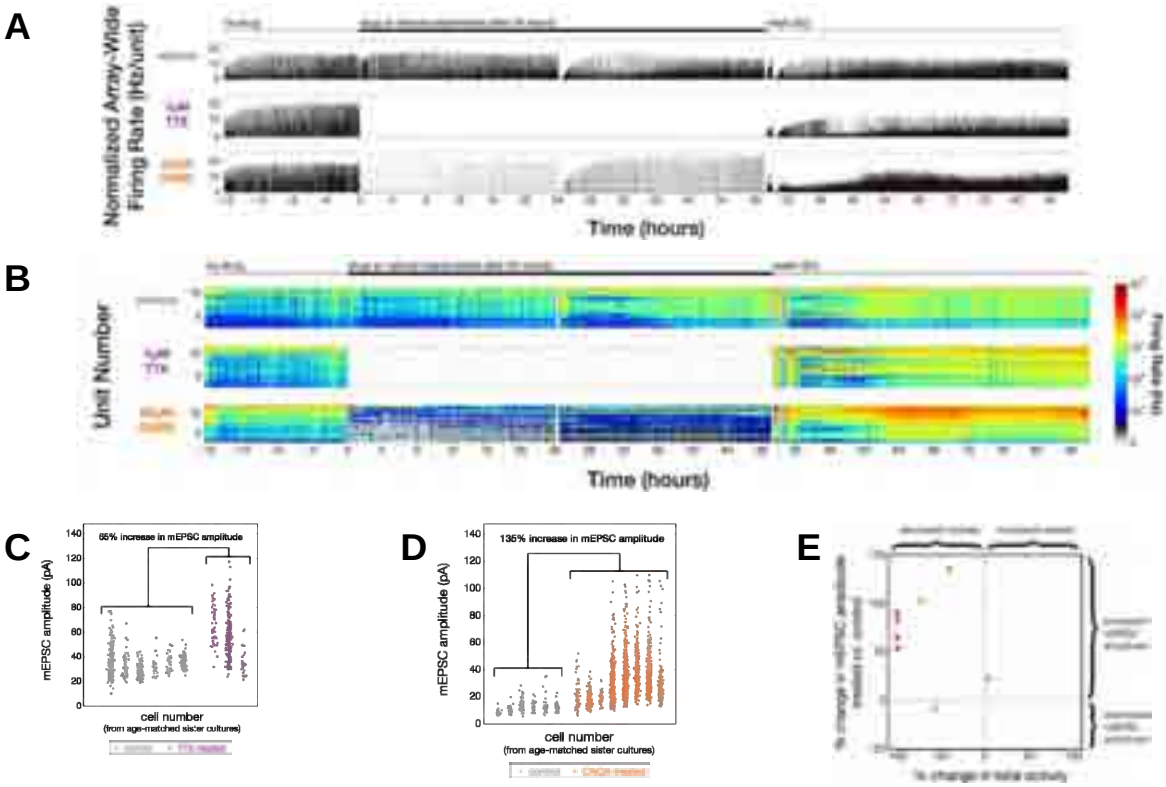

Fig. 3: Relating network spiking activity to changes in synaptic strength after chronic TTX or CNQX treatment. (A) Unit-normalized firing rate for three sister cultures chronically treated with vehicle, TTX, or CNQX. TTX completely eliminates spiking while CNQX elicits a moderate reduction that slowly recovers. **(B)** Firing rate for individual units before, during, and after treatment with vehicle, TTX, or CNQX. Recovery of spiking after CNQX is mediated both by increased firing rates in individual units, as well as a general elevation in firing rate across all units as seen in the vehicle-treated culture. After the wash, firing rate is especially heightened in the CNQX-treated culture. **(C)** mEPSC amplitudes for 3 cells from a TTX-treated culture (purple) and 6 cells from a vehicle-treated sister control culture (grey). **(D)** mEPSC amplitudes for 8 cells from a CNQX-treated culture (orange) and 6 cells from a vehicle-treated sister control culture (grey). **(E)** Percent change in mEPSC amplitude as a function of percent change in MEA-recorded activity. The percent change in mEPSC amplitude was computed for each TTX- and CNQX-treated culture by comparing to vehicle-treated age-matched sister control cultures.

3 Results

Under pre-drug or vehicle-treated conditions, the vast majority of spikes occurred within synchronous network-wide discharges or "bursts". TTX effectively abolished spiking and bursting activity during the 2-day treatment window (Fig. 3A, middle). Meanwhile, CNQX reduced overall spiking and initially eliminated bursting; surprisingly, over the course of the 2-day CNQX treatment, bursting gradually recovered (Fig. 3A, bottom). After the drugs were washed, both TTX and CNQX-treated cultures showed increased unit and network spiking activity compared to the vehicle-treated sister controls (Fig. 3A,B). Both treatments were accompanied by compensatory increases in mEPSC amplitude (Fig. 3C,D). Interestingly, some CNQX-treated cultures exhibited a greater degree of synaptic scaling than TTX-treated cultures even though CNQX was less effective at blocking spiking. While most cultures exhibited upward scaling with TTX or CNQX treatment, the degree of synaptic scaling was poorly correlated with the overall reduction in network spiking activity (Fig. 3E).

4 Conclusions

MEAs provide excellent tools for studying the activity dependence underlying mechanisms of homeostatic synaptic plasticity at the level of individual units and small neural circuits. In this study, continuous MEA recordings revealed a homeostatic recovery of bursting activity during CNQX treatment. This suggests that another form of excitatory transmission may emerge when AMPAergic transmission is impaired. Further, MEA recordings followed by whole-cell patch clamp revealed a poor correlation between network spiking and the degree of synaptic scaling. This raises questions about what type of activity is monitored within neural circuits to trigger compensatory changes in synaptic strength.

Acknowledgements

We thank J.T. Shoemaker for assistance with tissue harvests. This work was funded by the NIH NINDS Grant R01NS065992 to P.W., the NSF EFRI COPN Grant 0836017 to S.M.P., the NSF GRFP 09-603 Fellowship and Emory NI SPINR Fellowship to M.F., and the NSF GRFP Fellowship 08-593 to J.P.N.

References

[1] Turrigiano GG, Leslie KR, Desai NS, Rutherford LC, Nelson SB (1998). Activity-dependent scaling of quantal amplitude in neocortical neurons. *Nature* 391:892-895.

Structural changes in cultured neuronal networks during development

Song Hao[1], Huang Yu-Ting[1,2], Chan C. K.[1*]

1 Institute of Physics, Academia Sinica, Taipei, Taiwan
2 Department of Physics, National Central University, Chungli, Taiwan
* Corresponding author. E-mail address: ckchan@gate.sinica.edu.tw

Abstract
Structural changes were identified in cultured neuronal networks during development. Removal of magnesium or addition of BMI changes the characteristics and duration of spontaneous synchronized bursting. Spike sorting analysis suggests that these changes are related to the change of number of links between neuron clusters and change of spike patterns in the neuronal networks. Simulation results base on Volman model also generate similar changes when we change some parameters controlling the firing efficacy and number of links between neuron cells.

1 Introduction

Spontaneous synchronized bursting is a fundamental feature of developing neuronal cultures and the characteristic of the bursts (Figure1) is a function of DIV[1]. The origin of the bursting and its time dependence are still unknown. The most interesting observation from the measurements of the histograms is that there are periodic structures[2]; suggesting that there is reverberations in the network. However, it can be seen that the periodic structures of the histogram disappear as the culture mature. Since the cultures are growing at different DIVs, intuitively these changes should be related to the changes in structures during the growth. An interesting question is how to relate the changes in the characteristics of the bursts with the effective structure of the network which also changes with DIV.

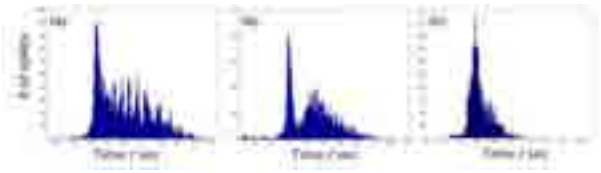

Figure 1. Histograms within a spontaneous burst with a 5ms time bin at a) 10DIV, b) 17DIV and c) 20DIV.

2 Materials and Methods

Spontaneous synchronized activities in cultures of rat cortical neurons are recorded in an MEA system. The bursts are characterized by the histogram of the spike timing within a burst (Figure 1). Effective structure of the network is modified by the help of pharmacology. We study how these histograms change with the addition of bicucumlin bicuculline methiodide (BMI, used to suppress inhibitory connections) or removal of magnesium (enhancement of excitability) in the culture media. Spike sorting algorithms are used to analyse the number of links and spike patterns. We also worked on simulations based on Volman *et al.*[3] and compare with the experiment results.

3 Result and Discussions

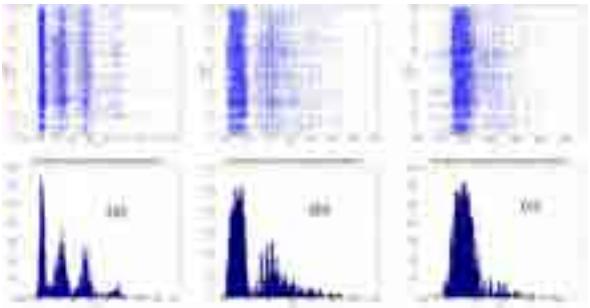

Figure 2. Effects of different [$Mg2^{+}$] on bursting behavior of neuronal cultures. The upper panel is rastor plots and the lower panel is histograms within a burst. Signals were measured in rat cortical cultures at 29 DIV with [$Mg2^{+}$] (a) 0 mM, (b) 1.0mM, and (c) 2.0mM

We found that the effective structure of the network is modified by the help of pharmacology. We studied how these histograms change with removal of magnesium (enhancement of excitability) or the addition of BMI (bicuculline, suppression of inhibitory connections) in the culture media.

It is known that Mg ion can block the NMDA (excitable) receptors of neurons. Therefore, an addition or removal of Mg ions can reduce or enhance network connectivity. In Figure 3 we show the effects of [Mg^{2+}] on the burst histogram. It can be seen from Figure 3 that the removal of Mg ion will enhance the coherence of the reverberation while the addition of Mg^{2+} destroys such coherence. These results suggest that the connectivity of the network can be studied through the coherence of the histogram.

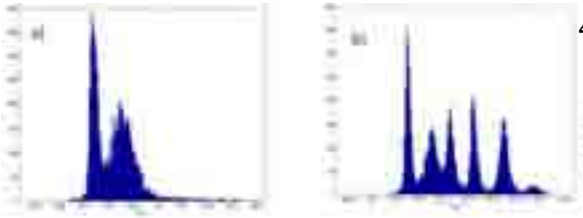

Figure 3. a) Histograms within a burst in 17 DIV culture for a) 0 μM and b) 0.5 μM of BMI.

The drug BMI is a blocker for inhibitory connections. Therefore, the addition of BMI should be similar to the removal of Mg^{2+}. As shown in Figure 3, with the addition of BMI, the distribution and duration of bursts are found to change significantly. The number of peaks in the histogram increased; suggesting a more coherent dynamics.

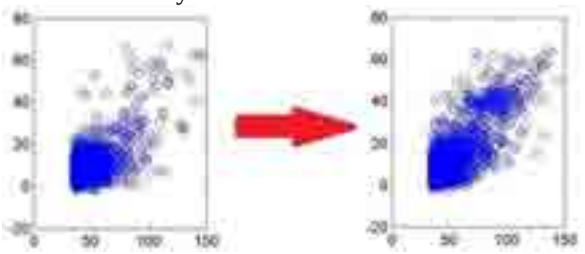

Figure 4. After the addition of BMI, more spike patterns were found near one electrode. X-axis is the measured voltage amplitude and Y-axis is the rising slope of the action potential. This was measured in rat cortical cultures at 24 DIV.

In Figure 4 we show the result of spike sorting results. More spike patterns are found near one electrode after the addition of BMI. Similar results are also found with the removal of magnesium. The spike sorting result suggests that these changes are probably related to the change of number of links between neuron clusters and the change of spike patterns in the neuronal network.

We compared those results with simulation results based on Volman, *et al.*[3]. As shown in Figure 5, the upper-left burst histogram is similar to that in Figure 3(a). When the value u, which describes the firing efficacy, increases from 0.05 to 0.20, burst histogram has more periodic structures and becomes similar to Figure 3(c) and 3(d). In Figure 6, we show the histogram change with increasing network size. When the number of cells increases from 40 to 100, the burst histogram has a longer duration and more periodical structures. Our simulation results support the idea that increase of connectivity can lead to more coherent reverberations.

4 Summary

With removal of magnesium or the addition of

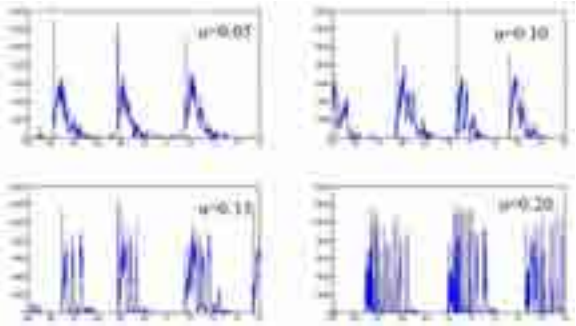

Figure 5. Bursting histograms from simulation. The u value which describes the firing efficacy changes from 0.05 to 0.20 with the same network size of 80 cells. Time duration of each figure is 10s.

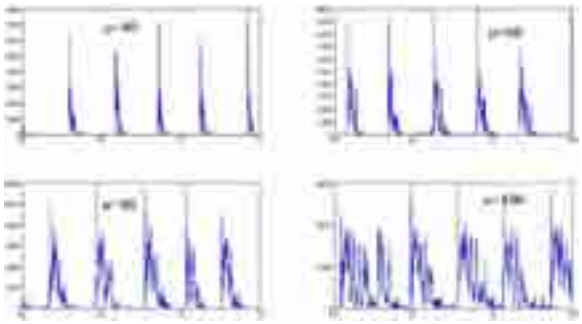

Figure 6. Bursting histograms from simulation. The network size changes from 40 to 100 cells with the same firing efficacy u. Time duration of each figure is 15s.

BMI in the culture medium, changes in the characteristics and duration of spontaneous synchronized bursting have been measured in rat cortical cultures grown on an MEA system. Our spike sorting result suggests that these changes are probably related to the change of number of links between neuron clusters and the change of spike patterns in the neuronal network. Simulation results also confirm the relation of the structure of the neuronal network and the spontaneous synchronized bursting.

Acknowledgement

The authors would like to thank Yu-Lin Cheung, Pin-Han Chen, and Chun-Chung Chen. This work is supported by the National Science Council (NSC99-2112-M-001-026-MY3), Taiwan.

References

[1] Segal, M., et al., *Determinants of spontaneous activity in networks of cultured hippocampus.* Brain Research, 2008. **1235**: p. 21-30.

[2] Bi, G.Q. and P.M. Lau, *Synaptic mechanisms of persistent reverberatory activity in neuronal networks.* Proceedings of the National Academy of Sciences of the United States of America, 2005. **102**(29): p. 10333-10338.

[3] Volman, V., *et al.*, *Calcium and synaptic dynamics underlying reverberatory activity in neuronal networks*. PHYSICAL BIOLOGY, 2007. **4** (2007) 91–103.

Spontaneous reverberation in developing neuronal culture networks

Yu-Ting Huang [1,2], Yu-Lin Cheung [1], Hao Song [1], Pik-Yin Lai [2], C. K. Chan [1*]

1 Institute of Physics, Academia Sonic, Nankang, Taipei, Taiwan
2 Department of Physics, National Central University, Chungli, Taiwan
* Corresponding author. E-mail address: ckchan@gate.sinica.edu.tw

Abstract
Firing patterns of a growing neuronal network are studied in a multi-electrode array system. Synchronized bursting is observed in the cultures a few days after plating. We find that the synchronization of spikes within the bursts can be understood as network reverberations which have a time scale of 100 ms while the time scale of the synchronization of the network is set by the depletion of neuronal vesicles which can be of the order of seconds. However, as the cultures mature, the reverberation of the spikes within the burst disappear indicating that there is either a change of intrinsic property of neurons or a change of the network structure. Results from simulation and pharmacological studies of reverberation model suggest that the disappearance of spike synchronization is related to a change in the network structure

1 Introduction

Spontaneous synchronized activity is an important phenomenon in neuronal cultures, which can be detected at about 7 DIV for developing cultures. As the cultures develop, the synchronous firing patterns change with DIV[1]. Recent studies revealed that the firing patterns play an important role in the network developing and memory. It is believed the dynamic of firings are related to network structures. However, it is still unclear how the firing patterns related to network structure. In this study, we measure the firing patterns of cultures in a MEA system at different DIV to study the relation between dynamics and structures with the help of pharmacology.

2 Materials and Methods

Primary cortical cell (E17) were dissociated and plated on to polyethyleneimine coated micro electrode arrays (8x8 with 200um spacing; Ayanda Biosystem) with cell density of 3000cells/mm^2. Cultures developed in DMEM with 5% horse serum and 5% Fetal bovine serum and incubated in 5% CO_2 and 37°C. The activities of neurons were recorded for 10 minute by MEA 1060-INC-BC (Multi Channel System) with a sampling rate of 20Hz in 37 ℃ and 5% CO_2 . Spikes were detected when the signal is greater than seven times of standard deviation of noise.

A synchronized burst is characterized by the histogram of spiking time averaged over the 60 electrodes with 5ms time bin. These histograms are studied as a function of DIV (Figure 1) and pharmacology (Figure 2). Histograms are measured under different buffer solutions: magnesium free buffer, bicuculline methiodide (BMI) containing buffer and Glutamate containing buffer.

3 Result and Discussions

3.1 Effect of DIV

Synchronized bursts with duration of the time scale of seconds can be observed one week after plating. As the cultures mature, the time interval between burst and burst duration become shorter. At early DIV, the structure of the histograms show that the neurons are firing more or less periodically within a burst with the time interval of 100ms; similar to reverberation[2]. Figure 1 shows the changes of the histograms as a function of DIV. It can be seen that the periodic structures of the histogram disappear around 12 DIV which can be cultures dependent.

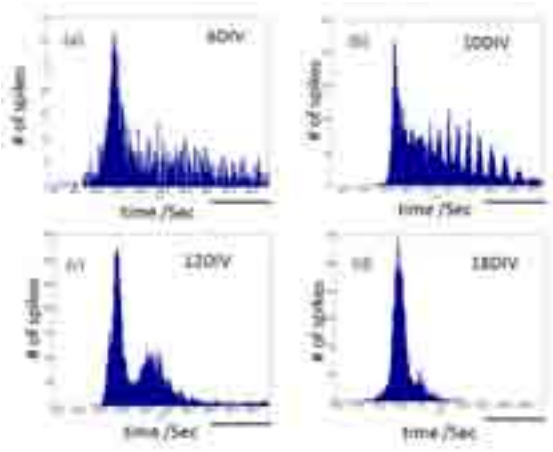

Figure 1. Histograms of spontaneous activities within synchronized burst at a) 6 DIV, b) 10 DIV, c) 12 DIV and d) 18 DIV. Scale bar is 200ms.

3.2 Effect of bicuculline methiodide

Bicuculline is a blocker of inhibitory transmission (GABA A receptor antagonist). Figure 2 (a) and (b) are the histograms before and after additional BMI. It shows that blocking inhibitory transmission enhanced the reverberation and extended the burst duration time.

3.3 Effect of Magnesium

The concentration of magnesium is related to the synaptic connectivity of the cultures[3] ; a decrease of [Mg] can be considered as an increase of network connection. Figure 2 (c) and (d) shows that the reverberation can be induced by the removal of magnesium from the buffer.

3.4 Effect of Glutamate

The addition of glutamate is used to increase the random firings of neurons to simulate an increase of environment noise. Figure 2 (e) and (f) show the reverberation is suppressed by the addition of Glu.

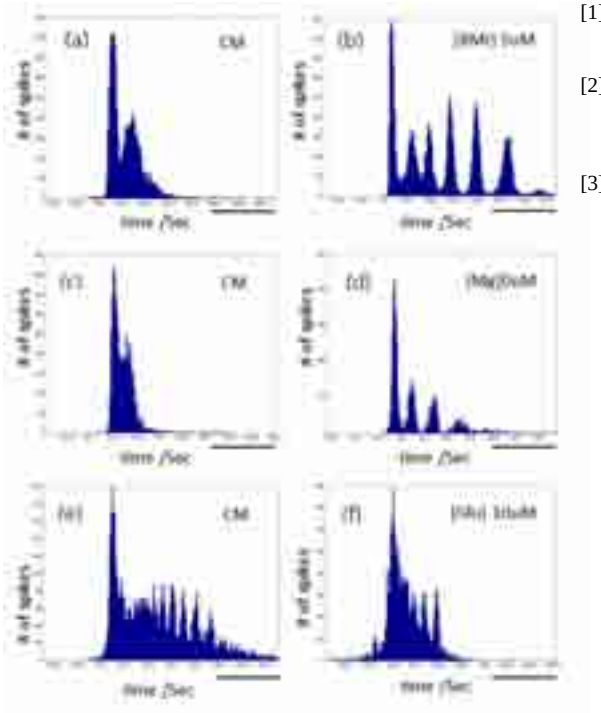

Figure 2. Results of pharmacology studies of spontaneous activities within a synchronized burst. a) and b) are the histograms with 0 and 5uM BMI respectively at 24 DIV. c) and d) are the histograms in culture medium and BSS with no Mg respectively at 27 DIV. e) and f) are the histograms with 0 and 10uM glutamate respectively at 10 DIV. Scale bar is 200ms.

4 Summary

1. Our experiments show that network activities change during network development.
2. Reverberation can only be observed at 13±3 DIV.
3. Results of BMI and Mg suggest that the reverberation is the result of a better connected network.
4. Result of glutamate experiments show that an increase of system noise effectively reduces the connectivity of the system.
5. The disappearance of reverberation after 17 DIV suggest that either i) there is substantial increase in noise or ii) there is a decrease in connectivity in the network.

Acknowledgement

This work was supported in part by the National Science Council under the Grants 99-2112-M-001-026-MY3.

References

[1] Segal, M., et al., *Determinants of spontaneous activity in networks of cultured hippocampus.* Brain Research, 2008. **1235**: p. 21-30.

[2] Bi, G.Q. and P.M. Lau, *Synaptic mechanisms of persistent reverberatory activity in neuronal networks.* Proceedings of the National Academy of Sciences of the United States of America, 2005. **102**(29): p. 10333-10338.

[3] Chan, C.K., et al., *Connectivities and synchronous firing in cortical neuronal networks.* Physical Review Letters, 2004. **93**(8).

Effect of electrical stimulation on neural network dynamics

Franz Hamilton[1*], Gretchen Knaack[2], Saugandhika Minnikanti[1], Timothy Sauer[3], Nathalia Peixoto[1]

1 Department of Electrical and Computer Engineering, George Mason University, Fairfax, VA USA
2 Department of Molecular Neuroscience, George Mason University, Fairfax, VA USA
3 Department of Mathematics, George Mason University, Fairfax, VA USA
* Corresponding author. E-mail address: fhamilto@masonlive.gmu.edu

Abstract
Understanding the dynamics of neural networks and how these dynamics can be manipulated is important for the study and treatment of various neurological disorders. Here we investigate the application of sinusoidal stimulation to networks of neurons. We investigate this stimulation in model using the Izhikevich neural network model and also *in vitro* through disassociated spinal cord and frontal cortex neural networks plated on microelectrode arrays. We observe the changes in network behavior.

1 Introduction

Endogenous fields are naturally generated electric fields within an organism. These fields, relatively small in terms of strength and frequency, can be found in the brain where they have a general oscillatory characteristic that is most frequently modeled as a sinusoidal wave. There is growing belief that endogenous fields in the brain carry important information about behavioral states and could provide insight into the dynamics of certain disorders of the brain [1-2].

Frohlich and McCormick looked at applying a variety of sine wave fields to an *in vitro* culture of coronal slices of ferret visual cortex. Wave frequencies between 0.075-0.375 Hz were shown to entrain the firings of the network to the oscillation of the stimulating wave [1]. Anastassiou et al. investigated a similar entrainment in slices taken from the primary somatosensory cortex of 14-18 day old rats. They observed a phase locking of spikes for stimulating sine waves with frequencies less than 8 Hz. Entrainment was most significant at 1 Hz, and although the effects were observed up to 8 Hz they became less noticeable as the frequency of the stimulating field increased. The authors hypothesize that the presence of this optimal 1 Hz frequency most likely results from the periodic polarization of the membrane leading to spike-phase preferences [2].

We would like to investigate this pattern manipulation further. By pattern we refer to a behavior state defined by some dynamic of the network. While these short term effects are interesting, it is unclear if such electrical stimulation can result in long term plasticity within the network. In particular, we would like to see if we can change the pattern of a network permanently by applying a specific characterized stimulation.

We examine *in vitro* low frequency sine wave stimulation in model and in developed 21 days *in vitro* (DIV) frontal cortex and spinal cord networks plated on microelectrode arrays (MEAs). Looking at pre and post stimulation recordings, we see if the applied stimulation alters network dynamics.

2 Methods

2.1 Cell Culturing

Frontal cortex and spinal cord was extracted from E17 ICR mice. After enzymatic and mechanical dissociation, cells were plated on a 64-channel MEA at a density of 150,000 for cortex and 300,000 for spinal cord. All cultures were incubated at 37 °C with 10% CO_2 and maintained in DMEM for cortex and MEM for spinal cord, both supplemented with horse serum, fetal bovine serum, B-27, and ascorbic acid for the first two days. At day 3, serum was removed and networks were maintained by a 50% media exchange twice a week.

2.2 Recording and Unit Identification

The MEA was connected to a recording system (64 channels at 40 kHz per channel, bandpass filter from 0.5 Hz to 8 kHz, 2000x gain) and temperature was adjusted to 37C through a heated base plate. Thresholds for spike detection were set to 6 standard deviations of the noise level of each electrode.

Individual unit sorting was done offline using a scanning K-means algorithm that clusters action potentials based on unit waveforms.

2.3 Stimulation

Stimulating sinusoidal waveforms were generated via an Agilent 33220A function generator. 1 Hz 20 mvPP sine wave stimulation was applied to an electrode with an active unit for 10 minutes. Recording

periods of 15 minutes occurred before and after stimulation.

3 Preliminary Results

3.1 Model Network Stimulation

We modeled sinusoidal wave stimulation of various frequencies using the Izhikevich neural network model [3]. The Izhikevich model is capable of reproducing biophysically accurate neural network behavior with a relatively low level of computational complexity compared to other more advanced models such as Hodgkin Huxley [3]. Fig. 1 shows the results on activity of a network of 20 simulated neurons when a multi-frequency sine wave is applied. There appears to be an entrainment of activity to the oscillations of the stimulating wave.

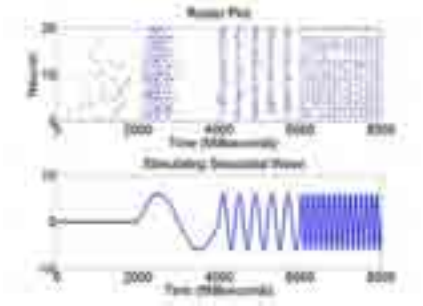

Fig. 1. Results of sinusoidal stimulation of various frequencies simulated using the Izhikevich model. Network activity entrains to the oscillation of the stimulating wave.

3.2 Network Stimulation

Given our results found in model, we apply the stimulation to neural networks plated on MEAs. Stimulation was applied after 21 DIV to disassociated networks of spinal cord and frontal cortex neurons. Application of stimulation shows an increase in network activity. Fig.2 shows the results for stimulation of a spinal cord network and Fig. 3 shows the results for stimulation of a frontal cortex network.

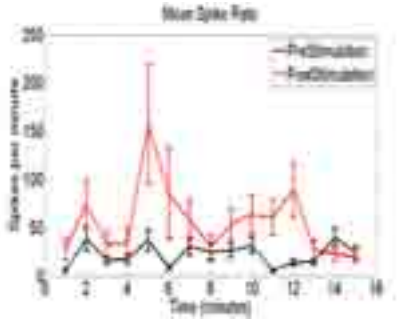

Fig. 2. Results of stimulation on firing rate of spinal cord network plated on MEA. Applied stimulation results in an increase in spike rate. Black curve represents pre stimulation and red curve represents post stimulation. Error bars reflect standard error amongst identified units within the network.

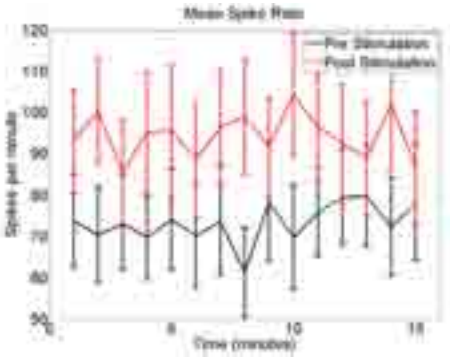

Fig. 3. Results of stimulation on firing rate of frontal cortex network plated on MEA. Applied stimulation results in an increase in spike rate. Black curve represents pre stimulation and red curve represents post stimulation. Error bars reflect standard error amongst identified units within the network.

One of the principal dynamics in frontal cortex networks is the occurrence of bursts. Examining changes in the bursting behavior of a network in response to stimulation is critical to identifying a change in network dynamics. Bursts were defined uniquely for each network using the methods described in [4]. Results of stimulation on bursting dynamics are being analysed currently.

4 Conclusion

The application of sinusoidal stimulation has shown an effect on network dynamics in model as well as *in vitro* in our cultured networks. We are currently working on applying stimulation throughout the developmental phase of neural networks (from plating to DIV 28) to see the effect on network behavior as compared to unstimulated networks.

Acknowledgement

This work was supported by National Science Foundation grant EFRI-1024713.

References

[1] F. Fröhlich and D. A. McCormick, “Endogenous Electric Fields May Guide Neocortical Network Activity,” *Neuron*, vol. 67, pp. 129-143, Jul. 2010.

[2] C. A. Anastassiou, R. Perin, H. Markram, and C. Koch, “Ephaptic coupling of cortical neurons,” *Nat Neurosci*, vol. 14, no. 2, pp. 217-223, Feb. 2011.

[3] E. M. Izhikevich, “Simple model of spiking neurons,” *IEEE Transactions on Neural Networks*, vol. 14, no. 6, pp. 1569-1572, Nov. 2003.

[4] J. V. Sellinger, N. V. Kulagina, T. J. O’Shaughnessy, W. Ma, J. J. Pancarazio, “Methods for characterizing interspike intervals and identifying bursts in neuronal activity,” *Journal of Neuroscience Methods*, vol. 162, pp. 64-71, May 2007.

Training hippocampal cultures using low-frequency stimulation: Towards Hebbian Learning.

Lorente Víctor[2]*, Ferrández Jose Manuel[1], de la Paz Felix[3], Fernández Eduardo[1]

1 Instituto de Bioingeniería, Universidad Miguel Hernández, Alicante, Spain
2 Departamento de Electrónica, Tecnología de Computadores y Proyectos, Universidad Politécnica de Cartagena, Spain
3 Departamento de Inteligencia Artificial, UNED, Madrid, Spain
* Corresponding author. E-mail address: victor.lorente@upct.es

Abstract
Electric stimulation has been widely used to induce changes in neuronal cultures coupled to microelectrode arrays (MEAs). In this paper we used low-frequency current stimulation on dissociated cultures of hippocampal cells to study how neuronal cultures could be trained with this kind of stimulation. We show that persistent and synchronous stimulation of adjacent electrodes may be used for creating adjacent physical or logical connections in the connectivity graph following Hebb's Law.

1 Introduction

Microelectrode Arrays have been designed for direct culturing neural cells over silicon or glass substrates, providing the capability to stimulate and record simultaneously populations of neural cells. Low-frequency stimulation have been used in the literature to enhance bursting activity in cortical cultures [1,2].

Hebbian learning describes a basic mechanism for synaptic plasticity wherein an increase in synaptic efficacy arises from the presynaptic cell's repeated and persistent stimulation of the postsynaptic cell. The theory is commonly evoked to explain some types of associative learning in which simultaneous activation of cells leads to pronounced increases in synaptic strength. Basically the efficiency of a synaptic connection is increased when presynaptic activity is synchronous with post-synaptic activity. In this work we use this kind of stimulation to create adjacent physical or logical connections in the connectivity graphs using Hebb's Law..

2 Methods

Cell culture preparation

Six dissociated cultures of hippocampal CA1-CA3 neurons (Fig 1) were prepared from E17.5 sibling embryos. During the extraction of the hippocampus a small amount of cortical tissue will have inevitably also been included. Tissue was kept in 2ml of HBSS. 10mg/ml of trypsin was added to the medium and placed in a 37° C water bath for 13 min for subsequent dissociation. The tissue was then transferred to a 15 ml falcon containing 4ml of NB/FBS and triturated using combination of fine pore fire polished Pasteur pipettes (Volac). Cells were then transferred onto 12 well plates (Corning Incorporated) containing glass coverslips (Thermo Scientific).

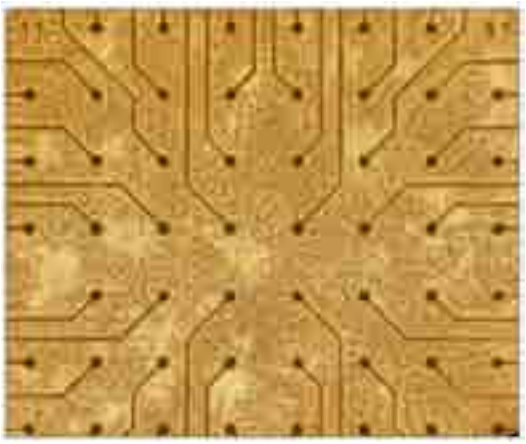

Fig. 1. Hyppocampal CA1-CA3 culture on a multielectrode array

The coverslips were pre-treated overnight with PDL (50mg/ml), a synthetic molecule used as a coating to enhance cell attachment. The PDL was then aspirated away and the coverslips washed twice with PBS. This was then followed by a final coating of laminin (50µg/ml), a protein found in the extracellular matrix, to further help anchor the dissociated hippocampal cells. The cells were maintained in a mixture of 500ml NB/B27 (promotes neural growth) and 500ml NB/FBS (promotes glial growth), each supplemented with Glutamax and Pen/Strep (dilution 1/100). Glutamax improves cells viability and growth while preventing build up of ammonia and Pen/Strep helps to prevent any infections. Cell density for each coverslip was roughly 200000 cells. Cells were kept in an incubator at 37˚ C in 6% CO2.

Experimental setup

Microelectrode arrays (Multichannel systems, MCS) consisted of 60 TiN/SiN planar round electrodes (200 μm electrode spacing, 30 μm electrode diameter) arrange in a 8x8 grid were used. Two pairs of electrodes were selected for creating connections in each pair. The activity of all cultures was recorded using a MEA60 System (MCS). After 1200X amplification, signals were sampled at 10kHz and acquired through the data acquisition card and MCRack software (MCS). Electrical stimuli were delivered through a two-channel stimulator (MCS STG1002) to each pair of electrodes.

Experimental protocol

Previously, two pairs of electrodes with no logical connections between them were selected using connectivity diagrams based on cross-correlation. In every stimulation session these steps were followed:

(1) Spontaneous activity was recorded for 2 min after a recovery period.

(2) Cultures were then stimulated through the two pairs of electrodes. A train of 5 biphasic pulses cathodic-first (50 μA peak, 100 μs phase, 50ms ISI) was delivered every 3s for 10 min.

(3) Spontaneous activity was recorded for 2 min after the stimulation.

Analysis performed

We observed the spontaneous activity of the cultures before and after the stimulation experiments, as well as their evoked response to the applied stimulus. Extensive burst analysis, post-stimulus time histograms and connectivity diagrams based on cross-correlation between electrodes were the main analysis performed to the registered data (Fig. 2). The physiological function of neural cells is modulated by the underlying mechanisms of adaptation and reconfiguration in response to neural activity.

Fig. 2. Connectivity graph based on cross-correlation between electrodes before stimulation. Electrodes 14,25, 83 and 84 were stimulated. No logical connections were observed before stimulation.

3 Results

The number of bursts and spikes per bursts increased in some electrodes after stimulation. Also, the responsiveness of the network was enhanced, reducing its response latency to the stimulus.

Connectivity diagrams based on cross-correlation between electrodes showed some kind of reorganization of connections after stimulations, concentrating them in a few electrodes. Furthermore, adjacent physical or logical connections in the connectivity graph following Hebb's law appeared in some pairs of stimulated electrodes (Fig.3). In some cases, the connection was intermittent, lasting one to several days. In others, a persistent connection was created. Finally, some cultures did not create any kind of connections. In this way, Hebbian tetanization created ad-hoc permanent or transient logical connections by modifying the efficiency of the paths between the selected electrodes. We speculate that the failed cultures may be caused by a not-homogenenous culture growth between the electrodes or by the neurobiological properties of the connections as will be confirmed using histological techniques in future works.

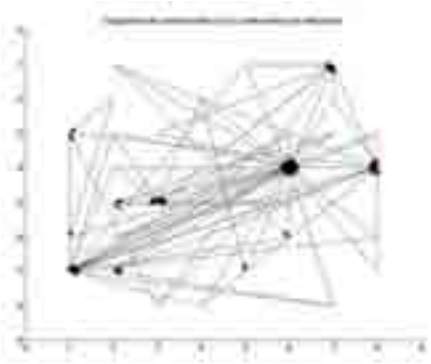

Fig. 3. Connectivity graph based on cross-correlation between electrodes. A connection (red arrow) between electrodes 83 and 84 has appeared.

4 Conclusions

Persistent and synchronous stimulation of relevant adjacent electrodes may be used for strengthen the efficiency of their connectivity graph. These processes may be used for imposing a desired behaviour over the network dynamics. In this work a stimulation procedure is described in order to achieved the desired plasticity over the neural cultures, and shaping in this way the functional connectivity of the neural culture

Acknowledgement

This work is being funded by grant 12361/FPI/09 from Séneca Foundation, from the region of Murcia and by the project 2010V/PUNED/0011 from UNED.

References

[1] Bologna LL, Nieus T, Tedesco M, Chiappalone M, Benfenati F, Martinoia S (**2010**). Low-frequency stimulation enhances burst activity in cortical cultures during development. Neuroscience 165:692-704.

[2] Ide, AN, Andruska, A, Boehler, MD, Wheeler, BC, and Brewer, GJ. (2010) Chronic Network Stimulation Enhances Evoked Action Potentials. J. Neural Eng. 7, 016008 (15 pp) doi: 10.1088/1741-2560/71/1/016008.

Optogenetic feedback control decouples network spiking from other forms of neural activity

Jonathan P. Newman, Ming-fai Fong[2], Nealen Laxpati[1,3], Riley Zeller-Townson[1], Ted French[1], Steve M. Potter[1*]

1 Dept. of Biomedical Engineering, Georgia Tech College of Engineering & Emory University School of Medicine, Atlanta, GA, USA, 30332/30322
2 Dept. of Physiology, Emory University School of Medicine, Atlanta, GA, USA, 30322
3 Dept. of Neurosurgery, Emory University School of Medicine, Atlanta, GA, USA, 30322
* Corresponding author. e-mail address: steve.potter@bme.gatech.edu

Abstract
We developed an optogenetic feedback controller that can clamp the firing rate of neuronal populations. This system can control network firing rate over a wide range of set points for short and long time periods. When used in conjunction with pharmacological agents, such as synaptic blockers, the system allows independent manipulation of network firing rate and other network dynamic to which it would be normally be causally intertwined.

1 Background

Neuronal and synaptic maturation is dependent on electrical activity patterns that occur during the development. Because many forms of neural activation are causally tied to somatic spiking, deducing the independent role of spiking in network development has been difficult [1]. Optogenetic techniques offer a powerful means for activating and/or inhibiting spiking activity in genetically specified neuronal populations using light [2]. Here, we sought to clamp multi-neuron spiking levels of dissociated cortical networks, as measured with microelectrode arrays (MEAs), to predefined setpoints using optical feedback control.

2 Methods

Dissociated cortical cultures of neurons and glia, derived from E18 rat cortical tissue, were plated onto planar MEAs and infected with AAV2-CaMKIIα::hChR2-mCherry at 1-5 days in vitro (DIV). We created an LED-based Köhler illumination system that extends our real-time electrophysiology platform, NeuroRighter [3] (NR; for optical stimulation applications. We used NR to test both PID and bang-bang control architectures in tracking target firing rates over long and short time periods.

3 Results

ChR2-mCherry expression appeared about 1 week following transfection and steadily increased for 2 weeks before levelling off (fig. 1). The reactivity of cortical networks to 460 nm light pulses also increased over the 20 days following transfection owing to the combined effect of increased ChR2 expression levels and network maturation. Throughout development, we found monotonic relationships between pulse width, frequency, and light intensity with evoked network firing rates. These parameters were collapsed into a single control variable, u(t) [0 1], using the following linear dependencies: *Pulse Frequency* = 10·u(t) + 10 [s^{-1}], *Pulse Width* = 5.0·u(t) [msec], *LED Current* = 1.5·u(t) [Amps]. The PID controller was defined as $u(t) = K\cdot[e(t) + 1/T_i \cdot\sum_t e(t) + T_d\, e'(t)]$ where, e(t) = F* - F(t), F* is the desired per-unit firing rate and F(t) is the measured per-unit firing rate, and K = 0.1, T_i =0.5 seconds, T_d = 0.1 seconds. Secondly, we defined the integral-based bang-bang controller: $u(t) = \text{ceil}\{\sum_t e(t)\}$. Each controller was implemented within a 10 millisecond real-time loop using NR.

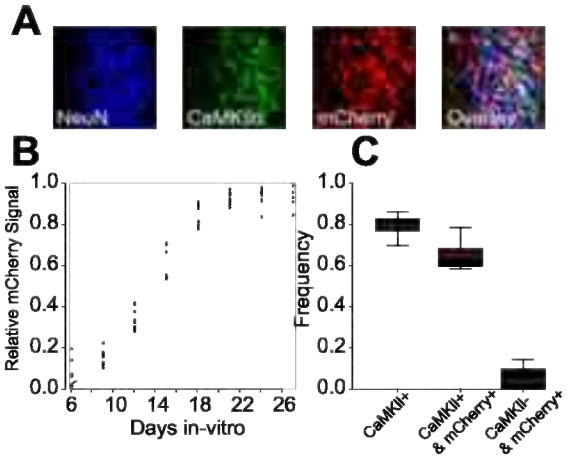

Fig. 1. Expression summary of AAV2-CaMKIIa-ChR2 in-vitro. (A) Confocal micrographs of Neuronal Nuclear protein (NeuN), CaMKIIα, and ChR2-mCherry. **(B)** The relative fluorescent signal of ChR2-mCherry from three cultures over 26 DIV. **(C)** Box plot showing the ratios of CaMKIIα+ cells, CaMKIIα+ cells that express

mCherry, and CaMKIIα- cells that express mCherry. Note the high true-positive and low false-negative expression rates.

We found that for short-term, fast-time-scale firing rate control, the PID architecture allowed rapid settling times and low-variance target tracking (fig. 2). For long-term target tracking, the bang-bang control architecture provided superior stability and dynamic range (fig. 3). This can likely be attributed to its maintenance of burst-like network activity throughout clamping, which is the primary activity state observed in dissociated cortical networks.

Finally, the bang-bang controller was capable of clamping firing activity even in the presence of bath-applied 20uM CNQX, decoupling AMPAergic neurotransmission and somatic spiking, over a 24 hour period.

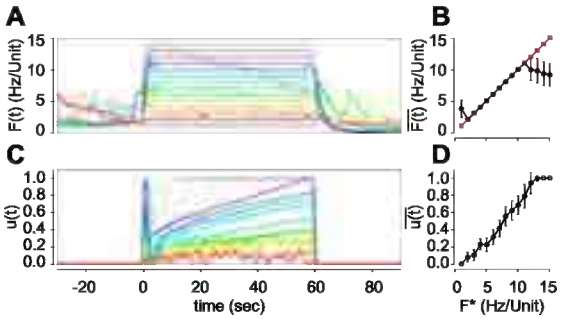

Fig. 2. Short-term, PID-based firing control. (A) Closed-loop step response of the unit normalized firing rate, F(t), and the corresponding control signal, u(t), as dictated by the PID controller for tracking various target rates, F*, which are displayed as black lines. Instances where the controller was unable to track the desired setpoint are shown in gray. **(B)** Time averaged unit normalized firing rates and corresponding control signals for the last 30 second of each trial. The red squares are F* plotted against itself. For an intermediate range of desired rates (2-11 Hz/Unit) the controller achieved perfect tracking. Error bars are ±SD.

4 Conclusion

Optogenetic feedback control is stable of over many hours, can exert control over a large range of firing rates, and provides a genetically specified input channel to complex, heterogeneous networks. Using optogenetic feedback, network firing rates can be decoupled from perturbations to AMPA-receptor-mediated glutamatergic neurotransmission, which would normally have a large effect on spiking activity. This technique can deconstruct neuronal networks into independently manipulable variables of network activation. This has significant implications for understanding activity-dependent developmental processes.

Acknowledgements

JPN conceived the system, designed and constructed the optical stimulation hardware, was lead developer on the real-time API for the NeuroRighter platform, designed and conducted experiments, and wrote the manuscript. MF created and maintained cell cultures and helped design and conduct experiments. NL created and amplified the viral vectors. RZT helped develop the real-time API. TF machined several parts for the optical rig. SMP oversaw experiments and edited the manuscript.

JPN and MF acknowledge the support of the NSF Graduate Research fellowship. Additionally, this work is supported by NIH Grant 1R01NS079759 - 01.

References

[1] Turrigiano, G. (2011). Too Many Cooks? Intrinsic and Synaptic Homeostatic Mechanisms in Cortical Circuit Refinement. *Annu. Rev. Neurosci, 34,89-103.*

[2] Mattis, J. et. al. (2011). Principles for applying optogenetic tools derived from direct comparative analysis of microbial opsins. *Nature Methods, 9:2,159-172.*

[3] Rolston, J.D. Gross, R.E., Potter, S.M. (2009). A low-cost multielectrode system for data acquisition enabling real-time closed-loop processing with rapid recovery from stimulation artifacts. *Frontiers in Neuroeng., 2,1-17.*

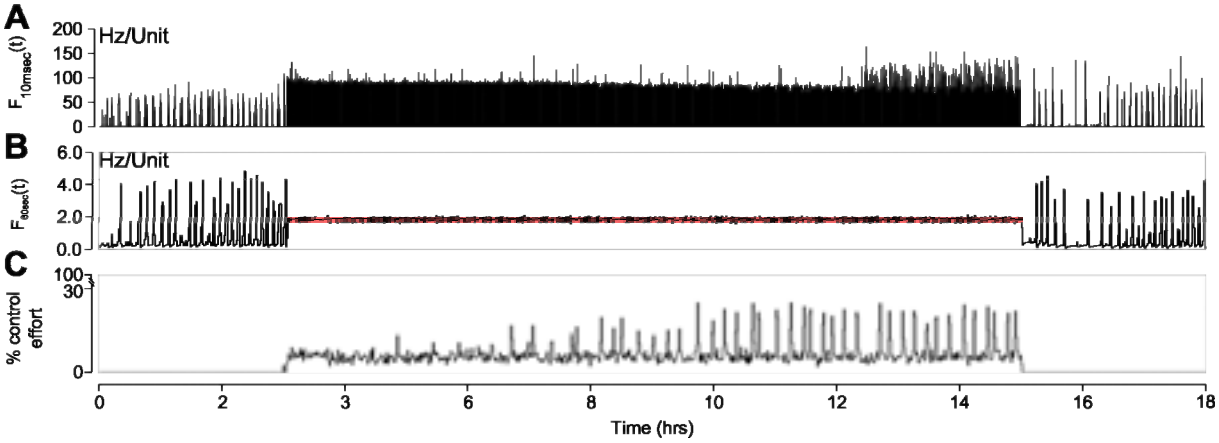

Figure 3: Long- term bang-bang firing control. (A) Unit-normalized firing rate calculated using 10 msec time bins. **(B)** Unit-normalized firing rate calculated using 60 second time bins. The target rate of 2 Hz/unit is shown as a thick red line. **(C)** Percent effort exerted by the bang-bang controller. Note that the controller is not close to saturation even during the 'down-states' that occur in the latter half of the 12 hour control session.

3D neuronal networks coupled to microelectrode arrays: An innovative in vitro experimental model to study network dynamics

Monica Frega[1], Mariateresa Tedesco[1], Paolo Massobrio[1], Mattia Pesce[2], Sergio Martinoia[1,2*]

1 Neuroengineering and Bio-nano Technology Group (NBT), Department of Informatics Bioengineering Robotics and System Engineering, University of Genova (DIBRIS), Genova, Italy
2 Department of Neuroscience and Brain Technologies, Italian Institute of Technology (IIT), Genova, Italy
* Corresponding author. E-mail address: sergio.martinoia@unige.it

Abstract
Large random networks of dissociated neurons developing *in vitro* and chronically coupled to Micro-Electrode Arrays (MEAs) represent a valid experimental model for studying the universal mechanisms governing the formation and conservation of neuronal cell assemblies. Up to now, *in vitro* studies have been limited to measurements of bi-dimensional neural networks (2DNs) activity. Given the intricate relationship between structure and dynamics, a great breakthrough is to understand the formation and the expressed dynamics of 3D neuronal networks (3DNs).

1 Introduction

In vitro electrophysiological studies on cultured neuron have been limited to measurements of bi-dimensional neural networks. Considering the relevance of the interplay between structure and dynamics, the establishment of three-dimensional cultured neurons would allow to better understand such interactions in a model system closer to the in-vivo situation. To this end, following what recently presented by Pautot et al [1], we developed a new experimental model that is constituted by hippocampal 3D neural networks coupled to Micro-Electrode Arrays (MEAs). We demonstrated that we constructed a physically connected 3D neural network that exhibits a rich repertoire of activity that cannot be found in conventional 2D neural networks and resembles the one detected in in-vivo measurements.

2 Methods

2.1 Cell culture

In this work we present a novel experimental model more realistic than the commonly used for studying the relationship between connectivity and dynamics: hippocampal 3DNs coupled to MEAs. Dissociated neuronal cultures were obtained from hippocampus of embryonic rats (E18). Neurons were plated onto 60-channel MEAs pre-coated with adhesion promoting factors (poly-D-lysine and laminin). Taking inspiration from the method presented by Pautot and coworkers [1], we developed 3DNs by forming different layers of micrometric silica beads (40 µm diameter) on which dissociated cultured neurons are able to grow. Cell suspension is dropped off single beads layers and then all the layers are assembled as shown in Fig. 1.

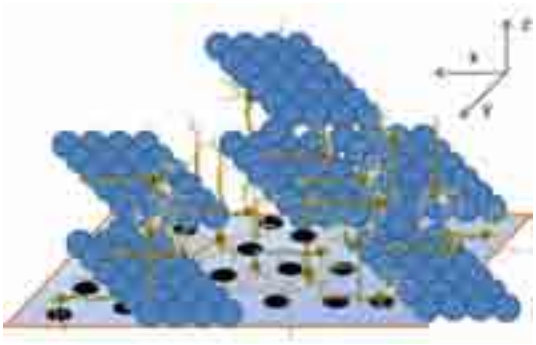

Fig. 1. Sketch of 3DNs structure.

Using this method, we constructed a physically connected. Fig. 2 shows images of 3DNs: on the left it is reported a particular of two beads on which neurons are able to grow and on the right a single layer of beads and dissociated cultured neurons (red) is depicted.

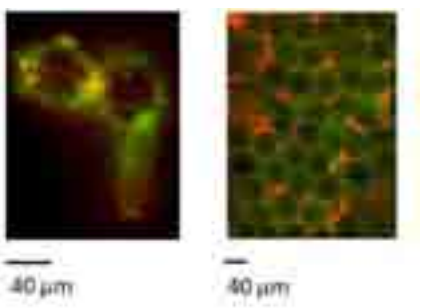

Fig. 2. Fluorescence microscopy images of 3D neural network.

2.2 Experimental protocol

We performed experiments considering both the spontaneous and stimulus-evoked activity; network activity was recorded for 30 min. We delivered electrical impulse both from the lowest and from the upmost 3DNs layers. Electrical stimuli were delivered from MEA electrodes or by using tungsten electrodes covered by glass (lowest or upmost layer stimulations). Test stimuli were sent sequentially at a frequency of 0.2 Hz for 5 min. Probe pulse amplitude was fixed at 1.5Vpp or 3Vpp (lowest or upmost layer stimulation). The stimulus pulse was biphasic (positive phase first) and lasted for 500 μs with a 50% duty cycle.

3 Results

3.1 Spontaneous activity

Activity patterns

2DNs and 3DNs exhibit different types of activity patterns (Fig. 3). 2DNs activity is synchronous and prevalently formed by network burst. The activity of 3DNs is more heterogeneous: there is synchronized activity, with the presence of network and super network burst and period of random spike activity, with almost no synchronization between channels.

(A)

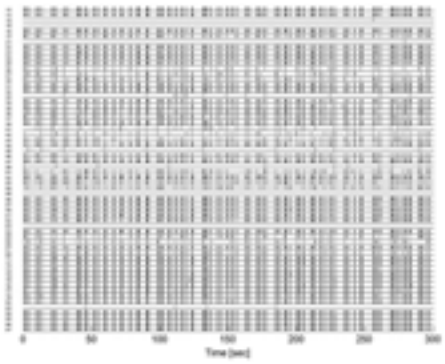

(B)

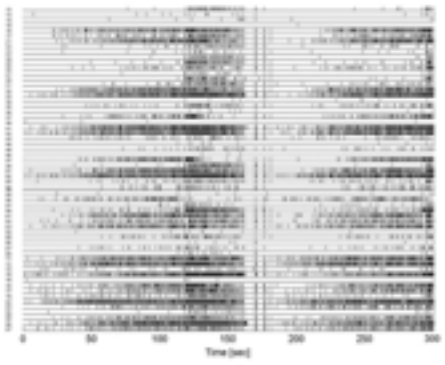

Fig. 3. (A) Raster plot of hippocampal cultures at 24 DIV in 2D configuration. (B) Raster plot of hippocampal cultures at 24 DIV in 3D configuration.

To quantify the different type of dynamics exhibited by 2DNs and 3DNs, we estimated the percentage of random spike value of all the experiments performed. 2DNs exhibit a strong synchronous activity: the percentage of random spike is very low. On the contrary, 3DNs dynamic is composed both by synchronous burst and random spikes activities: the percentage of random spike value is higher than the one estimated for 2DNs.

Activity synchronization

2DNs and 3DNs exhibit different level of activity synchronization among all the recording channels. 2DNs exhibit a very high correlation between channels; 3DNs show very low correlation between channels in the random spike activity period.

3.2 Stimulus-evoked activity

Electrical stimulation delivered by the lowest layer induce a fast and synchronized 2DNs response: it is generated by subsets of neurons in the 2D layer connected with other subsets of neurons in the some layer.

3DNs stimulated by the upmost layer exhibit a slow and synchronized response: it is generated by subsets of neurons in the 2D layer connected with subsets of neurons in the upper layers.

Electrical stimulation delivered by the lowest layer induce a slow and asynchronized 3DNs response. In this case there is both the response generated by subsets of neurons in the 2D layer connected with other subsets of neurons in the some layer, and the response generated by subsets of neurons in the 2D layer connected with subsets of neurons in the upper layers. Because of the different type of activated circuits described, the network response is no synchronized.

We also evaluate statistical analysis considering all the experiments performed. This analysis confirms that stimulation delivered by the lowest layer induce a fast 2DNs and slow 3DNs response; stimulation delivered by the upmost layer induce a slow 3DNs.

4 Conclusion

The obtained results demonstrated that we constructed a physically connected 3DN that exhibits a rich repertoire of activity that cannot be found in conventional 2DNs. This electrophysiological activity resembles the one detected in in vivo measurements far more than the classical 2DN cultures.

References

[1] Pautot S., Wyart C., Isacoff E. Y. (2008). Colloid-guided assembly of oriented 3D neuronal networks. Nature Methods, 5, 735-740, (2008).

Emergence of synchronized activity in confined neuronal populations cultured over microelectrode arrays

Marta Bisio[1], Alessandro Bosca[1], Michela Chiappalone[1*]

1 Neuroscience and Brain Technologies Dept, Fondazione Istituto Italiano di Tecnologia (IIT), Genova, Italy
* Corresponding author. E-mail address: michela.chiappalone@iit.it

Abstract
The development of in vitro models of patterned neuronal networks is of significant interest in the neuroscientific community and requires the convergence of electrophysiological studies with micro/nano-fabrication of adapted devices. Considering the multitude of connections arising in un-patterned neuronal cultures, the restraint of neurite outgrowth to specific pathways ensures a considerable control over network complexity. In this paper, towards the goal of facilitating reproducible and modular neuronal assemblies, we developed a technique to induce self-organization of networks into two clusters connected by one or two macro-channels (i.e. in the order of 50-100 µm width), on commercially available MEAs. We monitored the spontaneous activity during development of our engineered networks, from a few days up to eight weeks. Our results constitute important evidence that engineered neuronal networks are a powerful platform to systematically approach questions related to the dynamics of neuronal assemblies

1 Introduction

Cell assemblies, instead of single neuronal cells, can be considered the functional unit of the brain, being characterized by coordinate activity and interaction with other groups of cells [1]. This means brain architecture is inherently modular, being composed of local networks embedded in networks of networks, sparsely connected to each other [2]. Overall, these 'modules' activity plays a determinant role in any human thought or action. For this reason, an in vitro model has to have an intrinsic modularity, in order to provide a 'reduced' but plausible in vivo nervous system's representation.

In recent years, in vitro technologies supported by advanced substrate patterning methods have made it possible to force neural networks to develop a range of predefined modular structures [3]. While far from being 'real' brains, these in vitro designs have proved useful studies aimed at the characterization of activity dynamics in modular networks. Neuronal assemblies coupled to MEAs constitute a peculiar neurobiological model for investigating the strategies employed by the nervous system to represent and process information. Compartmentalization of cells and control over network connectivity may provide an ideal tool for further developing such in vitro neuronal systems.

In our previous work we demonstrated the possibility to functionally segregate a network in connected populations by integrating clustering microstructures on custom MEAs [4].

In this work, biocompatible masks have being coupled to MEAs' substrate in order to make the in vitro experimental culture more similar to the in vivo one. These confined networks have been tested, by the recording of their spontaneous activity during the in vitro development.

Fig. 1. A commercial MEA on which a PDMS mask has been placed. The two reservoirs can be noticed, used to load the cells into the designed compartments.

2 Methods

Hippocampal neurons extracted from rat embryos (E18) were cultured on planar arrays of 60 TiN/SiN electrodes (MultiChannel Systems, Reutlingen, Germany), pre-treated with adhesion factors (Poli-D-Lysine and Laminin).

A double layer PDMS structure was realized by replication form photostructured EPON SU-8 layers to define, once assembled on a MEA, two connected areas for distinct neuronal populations and two input reservoirs for loading neuronal cells. In Fig. 2 images of hippocampal cultures confined due to the PDMS structures can be observed.

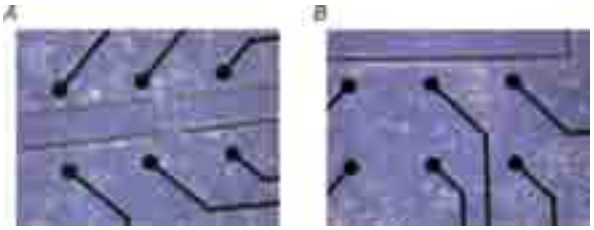

Fig. 2. Hippocampal cultures over MEA covered by a PDMS mask which confines the population into two connecting clusters. ***A.*** Detail of a channel connecting the two clusters (width of 50 μm). Hippocampal network at 13 DIV. **B.** Particular of a neuronal culture in one compartment. Hippocampal network at 13 DIV.

3 Results

We monitored a total of 25 cultures over their spontaneous development, from few days up to 60 DIVs. We found that the activity is partly confined to the two clusters, but still synchronized events occur at the level of the entire network, as shown in Fig. 3.

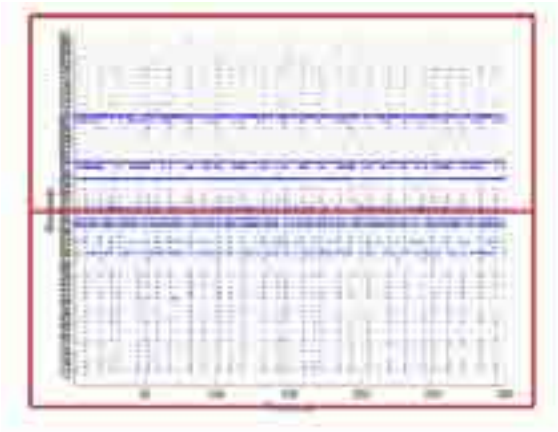

Fig. 3. Raster plot of the activity of a patterned neuronal network. The top compartment shows a desynchronized activity while the bottom compartment shows a strong synchronized activity.

On the later DIVs of the development, synchronized events occurring in the whole array increase in frequency.

Electrical stimulation delivered from specific sites of the network indicates that the evoked he activity is well confined, as shown in Fig. 4.

Fig. 4. Post Stimulus Time Histogram of the activity of a network when stimulated by an electrode of the top compartment.

4 Conclusions

We found that: i) activity is partly segregated in the two clusters, which are characterized by distinct patterns, but the two populations are not independent; ii) some phenomena (i.e. the network busts) are able to invade both the compartments; iii) during development the incidence of synchronized events increases; iv) one of the two compartments drives the network activity all along the development; v) electrical stimulation at specific DIV is strongly confined and it is dependent on the location of the stimulation.

Our results constitute important evidence that engineered neuronal networks are a powerful platform to systematically approach questions related to the dynamics of neuronal assemblies. Unlike networks in vivo, in which multiple activation pathways are impinging on any recorded region, these partially confined networks can be studied in a controlled environment [5]. Moreover, such a system can be easily interfaced to artificial artifacts in order to better investigate coding properties towards the final goal of integrating brains and machines.

References

[1] Hebb D. O. (1949). Organization of behavior. John Wiley & Sons New York 1949.

[2] Levy O., Ziv N. E. and Marom S. (2012). Enhancement of neural representation capacity by modular architecture in networks of cortical neurons. *European Journal of Neuroscience*, doi: 10.1111/j.1460-9568.2012.08094.x.,

[3] Jungblut M., Knoll W., Thielemann C. and Pottek M. (2009). Triangular neuronal networks on microelectrode arrays: an approach to improve the properties of low-density networks for extracellular recording. *Biomed Microdevices*, 11, 1269–1278.

[4] Berdondini L., Chiappalone M., van der Wal P. D., Imfeld K., de Rooij N. F., Koudelka-Hep M., Tedesco M., Martinoia S., van Pelt J., Le Masson G. and Garenne A. (2005). A microelectrode array (MEA) integrated with clustering structures for investigating in vitro neurodynamics in confined interconnected sub-populations of neurons. *Sensors and Actuators B: Chemical*, 114,1, 530-541.

[5] Shein M., Ben-Jacob E. and Hanein Y. (2010). Innate synchronous oscillations in freely-organized small neuronal circuits. *PloS One*, 5,12, e14443.

Spontaneous activity patterns of cortical *in vitro* networks depend on cellular network composition

Tom Reimer[1], Werner Baumann[1], Jan Gimsa[1*]

1 University of Rostock, Chair for Biophysics, Gertrudenstrasse 11a, 18057 Rostock, Germany
* corresponding author, jan.gimsa@uni-rostock.de

Abstract
We analyzed the relationship between the cellular composition (i.e. the ratios between interneurons (GABAergic as well as parvalbumin-positive) and pyramidal cells) and the spontaneous electric activity patterns of cortical networks which were cultivated on MEA glass-neurochips. Morphological data were correlated with the MEA recordings. Our results show a strong relationship between the number of interneurons in a certain network and characteristic features in its spontaneous activity pattern. While networks with numerous GABAergic or parvalbumin-positive interneurons were characterized by a relatively stable, synchronous bursting activity, the activity of networks with few or no interneurons was asynchronous or instable.

1 Background

Understanding native spontaneous activity of neuronal networks is one of the most important challenges in neuroscience. Cortical *in vitro* networks offer an enormous richness of patterns in their spontaneous electric activity. Our research aims at understanding the relationship of the underlying neuronal substrate and its activity pattern. The native cerebral cortex and our cortical *in vitro* networks are both composed of different pyramidal and non-pyramidal cells [1,2]. We focused on the role of GABAergic and parvalbumin-positive interneurons in the spontaneous activity of cortical networks on MEA glass-neurochips.

2 Methods

Cortices were prepared from embryonic mice (E13-16) followed by enzymatic dissociation. Cells were plated at a density of 1000-2000 cells/mm^2 on poly-D-lysine/laminin coated miniaturized (16x16mm²) glass – neurochips (developed at the Chair for Biophysics, University of Rostock, see [3]) with integrated 52-microelectrode arrays. The culture area was 20 mm^2. Cultures were incubated at 10% CO_2 and 37°C for four weeks. Cells were grown in Dulbecco's modified Eagle's medium (DMEM) with high glucose, stable glutamine and 10% horse serum. Half of the medium was replaced thrice a week. Recordings were performed with our modular glass chip system (MOGS) coupled to a preamplifier and data acquisition software (Plexon Inc., Dallas,TX,USA). For morphological characterization, networks were fixed with paraformaldehyd and immunohistochemically stained against parvalbumin (marker for chandelier and basket cells), GABA, MAP2 and neurofilament 200 kD before confocal laser scanning microscopy.

3 Results

Our *in vitro* networks showed a high variability in their cellular composition. 17 out of 20 networks contained numerous GABAergic or parvalbumin-positive interneurons (Fig.1, and 2) and 3 networks contained no or only very few (1-3/mm²) interneurons (Fig.3). Every network exhibited a unique electric activity pattern. The following differences in the spontaneous activity were observed: networks containing numerous interneurons exhibited relatively stable synchronous bursting or superbursting activity (Fig.1, and 2). Networks with no or few interneurons exhibited instable bursting and spiking or asynchronously spiking activity (Fig.3).

4 Conclusion

The cellular composition of cortical *in vitro* networks is critical for their spontaneous activity pattern. Our results suggest that interneurons are essential for a relatively stable synchronous bursting or superbursting activity. The patterns of spontaneous activity depend on the underlying neuronal substrate. The analysis of the relationship between the cellular network composition and spontaneous activity patterns will improve our understanding of the role of different neuron types in cortical processing.

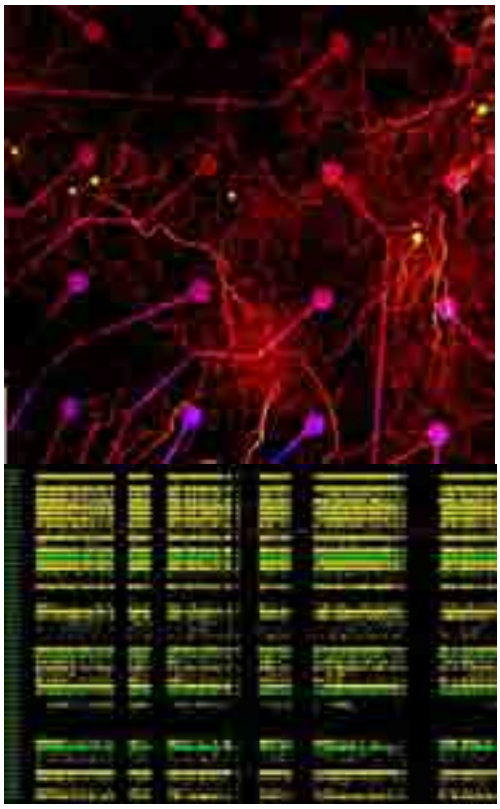

Fig.1. Network with parvalbumin-positive interneurons exhibiting superbursting activity. Above: microscopical image of the network growing on MEA. Green: parvalbumin; red: neurofilament 200; bar: 50 µm. Below: activity pattern over a time period of 30 sec.

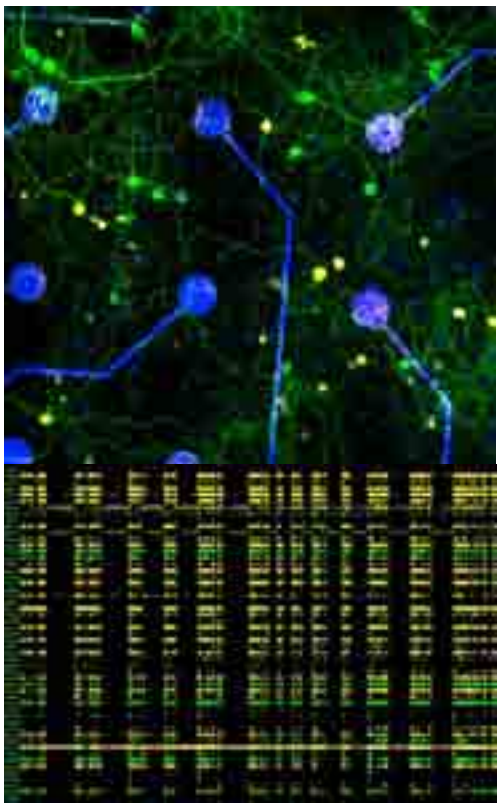

Fig.2. Network with numerous GABAergic interneurons that exhibited preliminary bursting activity. Above: microscopical image of the network growing on MEA. Green: MAP2; yellow (Alexa Fluor 488 superimposed with Alexa Fluor 594): GABA; bar: 50 µm. Below: activity pattern over a time period of 30 sec. The activity of unit 17b is suppressed during synchronous bursts (Reimer et al. Proceedings MEA Meeting 2010, 66-67)

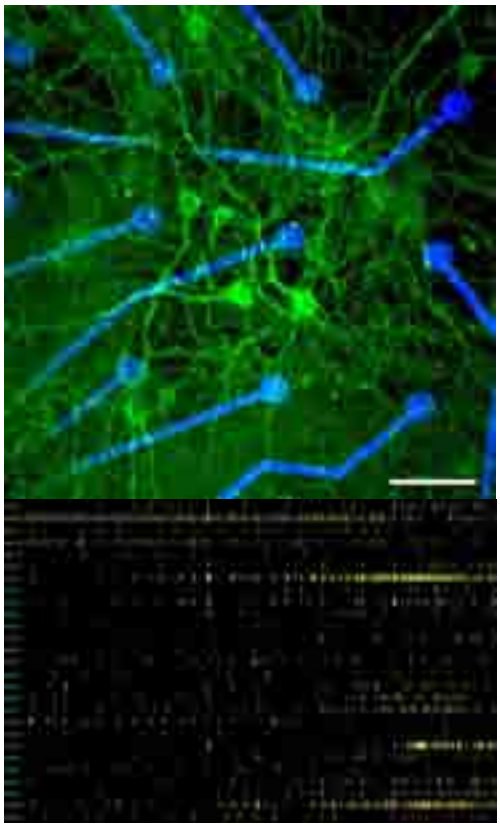

Fig.3. Network without GABAergic interneurons that exhibited asynchronous spiking activity. Above: microscopical image of the network growing on MEA. Green: MAP2; red: GABA; bar: 50 µm. Below: activity pattern over a time period of 30 sec.

Acknowledgements

This work was supported by the DFG-research training group *welisa* 1505/1.

References

[1] Gullo F., Mazzetti S., Maffezzoli A., Dossi E., Lecchi M., Amadeo A., Krajewski J. & Wanke E. (2010). Orchestration of "presto" and "largo" synchrony in up-down activity of cortical networks. *Frontiers in neural circuits*, 4, 1-16.

[2] Cajal S.R. (1988) Cajal on the cerebral cortex: an annotated translation of the complete writings. DeFilipe J., Jones E.G. (eds), Oxford University Press, NY.

[3] Koester P.J., Buehler S.M., Stubbe M., Tautorat C., Niendorf M., Baumann W. & Gimsa J. (2010) Modular glass chip system measuring the electric activity and adhesion of neuronal cells-application and drug testing with sodium valproic acid. *Lab-chip*, 10, 1579-86.

Extracellular multisite recording of synaptic potentials in human model neurons

Philipp Merling, Michael Peters, Lidia Bakota, Roland Brandt and Gunnar Jeserich*

Dept Neurobiology, University of Osnabrück, D-49069 Osnabrück, Germany
* Corresponding author. E-mail address: jeserich@biologie.uni-osnabrueck.de

Abstract
Extracellular recording of NT2N cells revealed spontaneous spiking activity initially in the third week after replating. Furthermore, biphasic voltage pulses above 500 µV evoked fEPSPs up to 3.7 mV. By combined application of the cholinergic antagonists tubocurarine (10 µM) and scopolamine (10 µM) a 15% reduction in fEPSP amplitudes was revealed while in the presence of the AMPA/kainate receptor blocker CNQX (10 µM) amplitudes were diminished by 33%. The high reproducibility of fEPSP amplitudes observed especially in astroycte-NT2N co-cultures renders this cell culture system a highly promising tool for future experimental studies on the effects of neuroactive substances in a human system.

1 Introduction

Human Model Neurons (NT2N) are neuronal cells obtained by in vitro differentiation of a human teratocarcinoma cell line [1]. They closely resemble human CNS neurons and offer a promising potential for therapeutic intervention in neurodegenerative diseases [2]. Furthermore, NT2N cells provide a suitable in vitro model to study the effect of neuroactive substances in a human system. In the present study we evaluated the electrophysiological properties of these cells in a long term approach using extracellular multichannel recording. Since glial cells are well known to provide important metabolic partnership with neurons and may support survival of neurons under pathological conditions we additionally tested an NT2N-astroycte co-culture system.

2 Methods

Cell cultures

Two different types of NTN2 cultures were tested for electophysiological recording (Fig. 1). In one case NT2N cells after differentiation with retinoic acid [1] were plated on a MEA surface that was previously coated with polylysine and laminin (Fig1A). Alternatively neurons were plated on a carpet of P3 mouse cortical astrocytes that had been seeded onto the bottom of the polylysine coated MEA biochip one week before (Fig 1B).

Electrophysiological recording

For multichannel recording of spontaneous spike activity and evoked fEPSPs the MEA60 device was used (Multi Channel Systems, Reutlingen, FRG). A MEA1060-Inv-BC pre-amplifier was combined with an FA60S-BC filter amplifier (gain 1100×) and run in parallel with the USB-ME64 data acquisition unit controlled by the MC_Rack software 4.0.0. Raw electrode

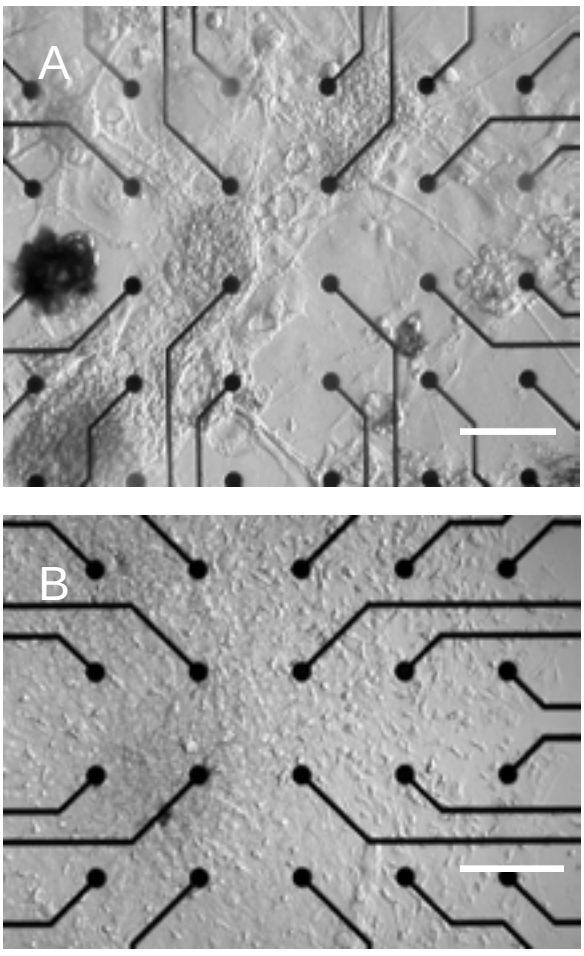

Fig.1: Hoffman modulation contrast photomicrographs of cultured human NT2N cells. A. Plating cells directly on a MEA surface yielded clusters of neurons connected by axon bundles. B. Plating cells on a layer of astrocytes elicited a uniform distribution of cells. Bars indicate 200 µm.

data were sampled at a rate of 25 kHz and recorded on a PC hard disc. Biphasic voltage pulses were applied via a STG 4002 stimulus generator.

3 Results

Three weeks after plating the cells exhibited spontaneous firing of action potentials. During the following period spontaneous activity gradually increased both in amplitude and frequency. In contrast with primary mouse cortical cultures NT2N cells mostly exhibited regular firing patterns without pronounced bursting activity (Fig. 2), similarly as was reported earlier [3]. By biphasic stimulation with 2V for 100 µs excitatory postsynaptic field potentials (fEPSPs) up to 3.7 mV could be elicited. In neuron-glia co-cultures generally lower but more uniform amplitude sizes up to 2.6 mV were revealed. Input-output curves in both cases revealed a linear relationship between voltage of stimulation and fEPSP amplitude with a threshold of 500 mV (Fig 3). In the presence of the AMPA/kainate receptor blocker CNQX (10µM) fEPSP amplitudes became reversibly reduced on average by 33%, suggesting a high proportion of glutamatergic synapses present in the cultures, while a combined application of the anticholinergic blockers tubocurarine (10µM) and scopolamine (10µM) caused a 15% reduction of fEPSP amplitudes. Taken together our pharmacological data are well consistent with recent immunohistochemical findings that documented quite similar proportions of cholinergic and glutamatergic neurons in NT2N cultures, respectively [4].

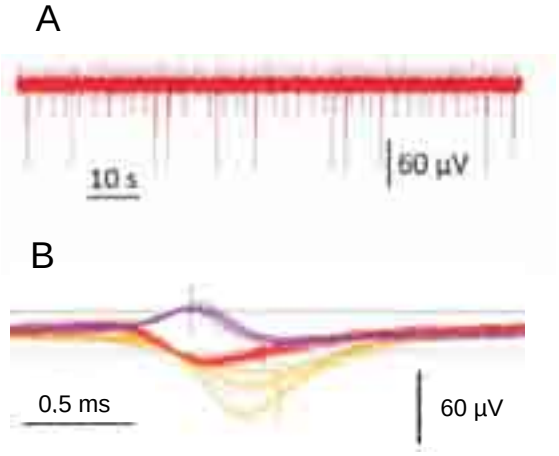

Fig.2: Extracellular recording of NT2N cells 28 days after replating shows a regular spiking pattern (A). Spike sorting reveals signals to originate from at least three different sources (B).

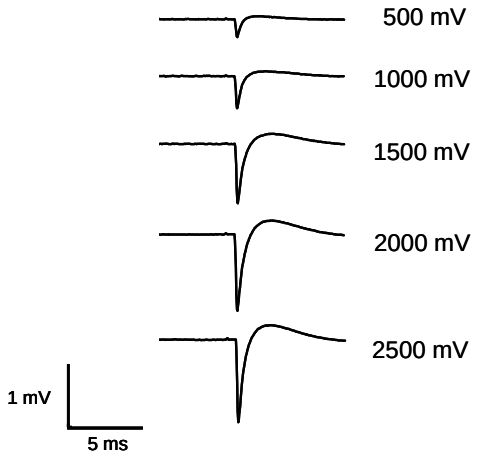

Fig.3: fEPSPs evoked in NT2N-astrocyte co-cultures (28 days after replating) by increasing biphasic voltage pulses as indicated on the right margin.

4 Conclusion

In particular when cultured in combination with astroytes NT2N cells proved as a most suitable system for experimental work with the MEA-system providing a uniform cellular distribution pattern (Fig. 1B) and a highly reproducible evoked synaptic activity**.** The data presented here can be considered as a framework for future *in vitro* studies on the neurophysiological effects of neuro-active substances potentially involved in the pathophysiology of neurodegenerative diseases.

Acknowledgement

The authors would like to thank Mrs. Bettina Flenker for expert technical assistance. This study was financially supported by the state of lower saxony.

References

[1] Pleasure S.J., Page C., Lee V.M. (1992). Pure postmitotic polarized human neurons derived from NTera 2 cells provide a system for expressing exogenous proteins in terminally differentiated neurons. *Journal of Neuroscience*, 12, 1802-1815.

[2] Kondziolka D., Wechsler L., Goldstein S., Meltzer C., Thulborn K.R., Gebel J., Jannetta P., DeCesare S., Elder E.M., McGrogan M., Reitman M.A., Bynum L. (2000). Transplantation of cultured human neuronal cells for patients with stroke. *Neurology*, 55, 565-569.

[3] Götz P., Fleischer W., Rosenbaum C., Otto F., Siebler M. (2004). Neuronal network properties of human teratocarcinoma cell line-derived neurons. *Brain Research*, 1018, 18-25.

[4] Podrygajlo G., Tegenge M.A., Gierse A., Paquet-Durand F., Tan S., Bicker, G., Stern M. (2009). Cellular phenotypes of human model neurons (NT2) after dissociation in aggregate culture. *Cell and Tissue Research*, 336, 439-452.

A neuro-robotic system to investigate the computational properties of neuronal assemblies

Jacopo Tessadori[1*], Marcello Mulas[1], Sergio Martinoia[1,2], Michela Chiappalone[1]

1 Neuroscience and Brain Technologies Dept, Fondazione Istituto Italiano di Tecnologia (IIT), Genova, Italy
2 Dept. of Informatics, Bioengineering, Robotics and System Engineering, University of Genova, Genova, Italy
* Corresponding author. E-mail address: jacopo.tessadori@iit.it

Abstract

Behaviours, from simple to most complex, require a two-way interaction with the environment and the contribution of different brain areas depending on the orchestrated activation of neuronal assemblies. We used cultured networks coupled to MEAs (i.e. Micro Electrode Arrays) as a simplified model system to investigate the computational properties of neuronal assemblies. The proposed neuro-robotic framework provides a suitable experimental environment for embodied electrophysiology as it allows long-term multisite recording and stimulation in a closed-loop configuration. Here we present what the main components of the experimental system are and how they can be conveniently used to study coding mechanisms in neuronal systems.

1 Background

Wiring of the brain is based on continuous interactions with the surrounding environment. The induction of neural plasticity is one of the primary processes leading to network modification and to reaction to the external world [1]. It is interesting to study how to 'extract' the essential information embedded in a biological system, while maintaining a satisfactory level of neuronal complexity capable to support simple behaviors. In order to reproduce a neural substrate for artificial applications, hybrid model systems (living neurons coupled with a robotic system) have been a possible choice in the recent past [2]. In this work we present a new hybrid system with added functionalities and oriented to study information coding mechanisms in neuronal systems.

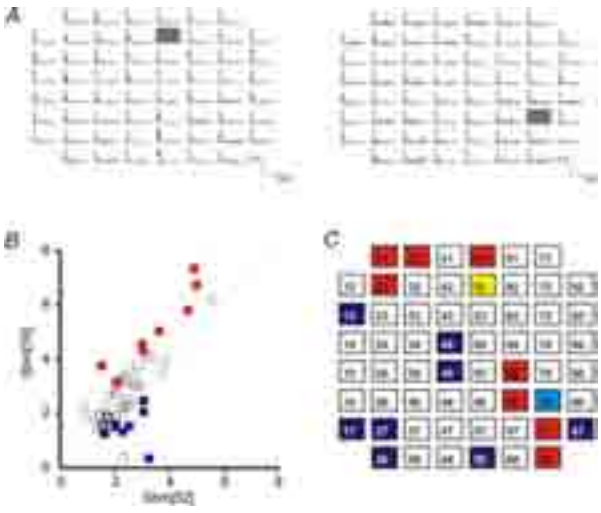

Fig. 1. A. Two PSTH plots depicting responses elicited by stimulation from one electrode (grayed out in the graph). B. Input-output combinations graph used for selection of best matches C. Example of selected sensory areas (yellow and cyan) and corresponding motor areas (red and blue).

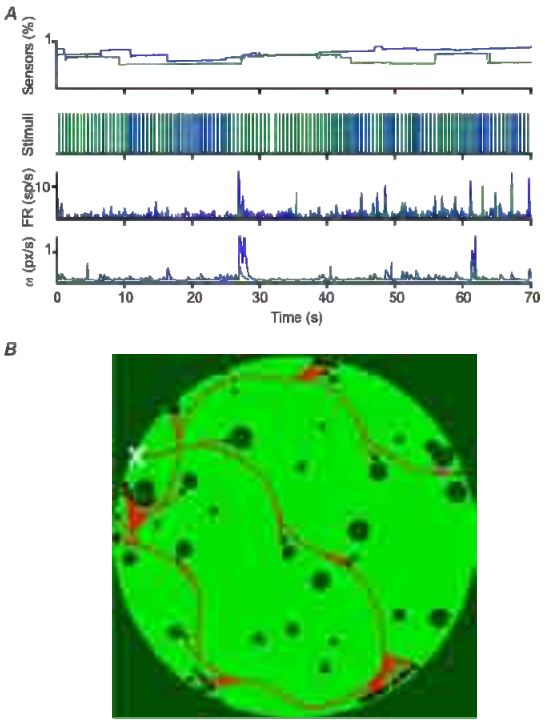

Fig. 2. A. 70s of robot run are shown here: top graph shows sensor readings, followed by stimulation rate in the corresponding sensory area, then spiking rate in the selected motor area and consequent wheel speed. B. An example of a 20min-long robot run experiment, with path followed and hits highlighted.

2 Methods

Since dissociated cultures lack predefined input and output sites, it is necessary to define 'sensory' and 'motor' areas of the network. Stimulation by delivery of 30 electrical stimuli (1.5 V peak to peak, biphasic pulses, 500 μs total duration) from 8-10 sites provides the information needed to obtain an effective connectivity map of the electrodes, necessary to define those I/O areas

Three different schemes implemented allow the exchange of data between biological and electronic modules: i) coding, ii) decoding and iii) learning. For coding, distance sensors relay information on obstacles to the network through the frequency of stimulation. In the decoding case, firing rate of the network in selected "motor areas" drives the robot wheels.

High frequency stimulation trains trigger the modification of connectivity to progress toward the desired behaviour: following each robot hit, a 2 second-long, 20 Hz stimulation is delivered to the corresponding sensory area [3].

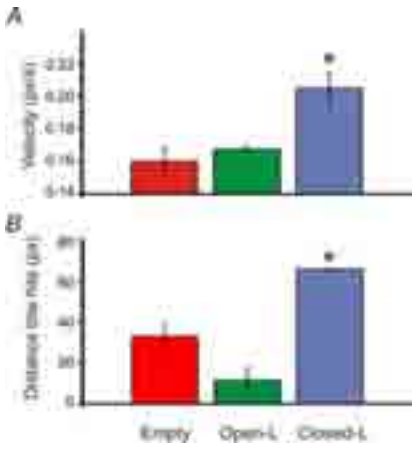

Fig. 3. Performance of the neuro-controlled robot during an obstacle-avoidance task. A. Mean velocity of the robot calculated in pixels/s. B. Mean distance between two consecutive collisions, calculated in pixels. The values are obtained in N=4 experiments for each case (red = emtpy MEA; green = open-loop MEA; blue = closed-loop MEA). The closed loop experiments give the best results for both parameters. Statistical analysis was carried out by using one-way ANOVA (*p<0.05) for normal distributions (Kolgomorov-Smirnov test of normality), while for mean comparison the Tukey-test was used.

3 Results

The PSTH area between each couple of stimulation-recording electrodes is computed (two examples are reported in fig. 1A). The best I/O combinations are selected on a graph like that in fig. 1B. Those specific pathways have been utilized for driving the robot and for implementing simple reactive behaviors (e.g., obstacle avoidance). Fig. 1C reports the selected sensory (i.e. input - stimulation) areas and the motor (i.e. output – recording) regions, characterized by 8 electrodes each.

While collisions are fairly frequent even in the case of a neuron-controlled robot, such as the case depicted in Fig. 2, the behaviour of the robot is still much closer to the desired one rather than in an open-loop configuration, or in the absence of a biological substrate. As can be observed from the graph in Fig. 3B, the average path travelled between hits is significantly higher in the case of a close loop. This finding is further reinforced by the fact that the average speed throughout the experiment is also higher in this case (Fig. 3A), a condition that should, all other being equal, make control harder to obtain

4 Conclusions

We presented our neuro-robotic architecture based on a neural controller bi-directionally connected to a virtual robot. The behavior of the robot during the closed-loop experiments resulted significantly better than that in open loop. Additionally it was significantly different from the performance of the 'empty' MEA, proving that the activity driving the robot is actually neurally-based.

Our results prove that a culture of dissociated neurons can be successfully interfaced in a bi-directional way with a robot with sensors and actuators. The presence of a robot bi-directionally connected to a simple neuro-controller based on living neurons allows to perform experiments in the context of the embodied electrophysiology paradigm, providing time-varying stimuli, testing learning schemes and managing sensory feedbacks in a more realistic environment. Our neuro-robotic framework can be exploited in order to study the mechanisms of neural coding and the computational properties of neuronal assemblies with the final goal to facilitate progress in understanding neural pathologies, designing neural prosthetics, and creating fundamentally different types of artificial intelligence.

References

[1] Chao Z. C., Bakkum D. J. and Potter S. M. (2008). Shaping Embodied Neural Networks for Adaptive Goal-directed Behavior. *PLOS Computational Biology*, 4,3

[2] Martinoia S., Sanguineti V., Cozzi L., Berdondini L., Van Pelt J., Tomas J., Le Masson G. and Davide F. A. (2004). Towards an embodied in-vitro electrophysiology: the NeuroBIT project. *Neurocomputing*, 58-60, 1065-1072.

[3] Chiappalone M., Massobrio P. and Martinoia S. (2008). Network plasticity in cortical assemblies. *European Journal of Neuroscience*, 28,1, 221-237.

Precisely timed spatiotemporal patterns in development of murine ES-derived neuronal networks

Stephan Theiss[1,2*], Fabian Marquardt[3], Felix Beyer[1], Georg Rose[3], Sebastian Illes[4], Alfons Schnitzler[1]

1 Institute of Clinical Neuroscience and Medical Psychology, Heinrich Heine University, Düsseldorf, Germany
2 RESULT Medical GmbH, Düsseldorf, Germany
3 Healthcare Telematics and Medical Engineering, Otto von Guericke University, Magdeburg, Germany
4 Institute of Molecular Regenerative Medicine, Paracelsus Medical University, Salzburg, Austria
* Corresponding author. E-mail address: theiss@hhu.de

Abstract

In vitro development of dissociated neuronal networks has been extensively studied on MEAs by analysis of spike and burst patterns. In this long-term study of murine ES-derived networks, precisely timed repetitive activity patterns on a 200 ms time scale have been regularly detected after 24 DIV, and occurred at highly increased frequency during distinct developmental phases with no substantial change in overall activity.

1 Background

Spontaneously recurring precisely timed neural activity patterns have been observed *in vivo*, in brain slices and even in dissociated neuronal networks lacking the intact brain's cytoarchitecture [1,2,4]. In accordance with large-scale computational models of neuronal networks equipped with spike time dependent plasticity (STDP), these patterns have been proposed as universal emergent feature in self-organizing neuronal networks, possibly related to Hebbian cell assemblies. In the present work, the emergence and development of such patterns has been examined for the first time in a long-term study of murine ES-derived neuronal networks on microelectrode arrays.

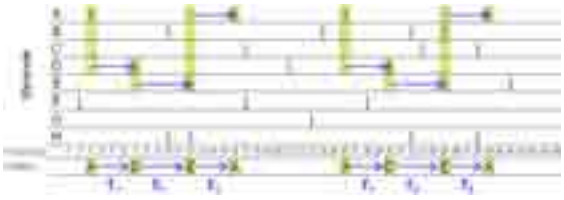

Fig. 1. Schematic spike raster plot representation displaying 45 milliseconds of an MEA recording with 8 electrodes (A—H). Yellow bars indicate spikes belonging to the pattern A—D—E—A with four spikes on three different electrodes (complexity). Blue arrows indicate time differences $T_{1,2,3}$ between pattern spikes identical in millisecond precision in both instances of this pattern.

2 Methods

Neural precursor cell enriched serum-free embryoid bodies (nSFEB) were derived from murine embryonic stem cells and subsequently cultured as aggregates on 200/30iR-Ti-gr MEAs as described in Illes et al. [3]. After a proliferation stage of 7—10 days, neuronal maturation was induced by withdrawal of FGF-2. Recordings were performed in culture medium at 39 different days between 10 DIV and 204 DIV after withdrawal of FGF-2. Fig. 1 shows a schematic representation of a precisely timed spike pattern. For the well-established "two tape" template matching algorithm [1,4], a novel matrix based implementation in MATLAB was developed. Spike time stamps were *ab initio* discretized in 1 ms wide bins, optimizing efficient template handling in sparse binary arrays. For pattern detection, a sliding template window of 200 ms was applied, and only patterns with a minimum complexity of 3 spikes occurring in at least 3 instances were retained. Statistical significance of pattern occurrence was assessed by comparison with surrogate data obtained by jittering all spike time stamps by ±2 ms.

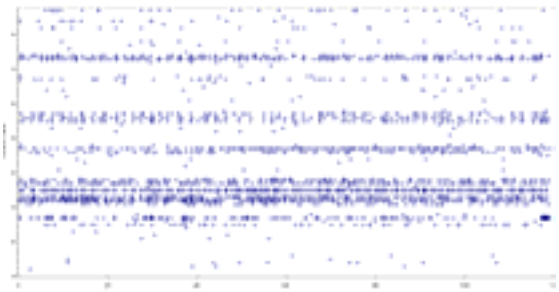

Fig. 2. Exemplary spike raster plot (120 sec) of an MEA recording (23 active electrodes with >10 spikes) in culture medium at 89 DIV. Most electrodes exhibited single spike activity rather than coordinated population bursting. 90% of all 2,876 spikes were detected on the 15 most frequently firing electrodes.

3 Results

MEA recordings in culture medium typically exhibited overall single spike activity rather than coordinated network bursting (see Fig. 2 for a typical spike raster plot at DIV 89). On the average, the overall number of spikes per minute increased 8.7-fold from ~300 at 10 DIV to ~2,600 at 45 DIV and remained between 40% and 60% of its maximum activity during the observation period (see Fig. 3). Pattern analysis was performed on 250 recordings obtained from 7 MEAs on 39 different DIV. No or only single electrode patterns caused by tonic firing were detected in 78 (16, resp.) recordings. Of the remaining 156 recordings, 84 (72) exhibited 1–30 (>30) different patterns on more than one electrode. A median number of 23 different patterns were detected that occurred more than 3 times and involved at least 3 spikes from 2 neurons.

Variable	Mean	SD
Max. complexity	4.0	2.0
Avg. complexity	3.1	0.3
Max. # instances	7.6	11.4
Avg. # instances	3.2	0.3
Max. # electrodes	3.1	1.4
Avg. # electrodes	1.9	0.6
Avg. pat. length [ms]	92.0	37.0

Table. Pattern characteristics (mean and standard deviation) of 156 recordings with multiple electrode patterns, obtained between 10 and 204 DIV.

Patterns were frequently detected from 24 DIV onward. Despite only slight changes in spike activity, pattern occurrence exhibited pronounced oscillatory behavior at 83—90 DIV, at 101—110 DIV and at 122—146 DIV, clearly separated by distinct patternless periods (see Fig. 3). For different MEAs, pattern incidence peaked at different DIV. Maximum and average pattern complexity, number of electrodes, number of instances and average length varied only slightly with DIV or with pattern frequency (see Fig. 2, Table).

4 Conclusions

Neuronal network development *in vitro* exhibits periodic phases of increased frequency of precisely timed spatiotemporal patterns in spontaneous activity. These patterns describe novel functional aspects of neuronal network development in ES-derived cultures beyond established spike- and burst analysis. Systematic evaluation of pattern occurrence after exposure to pharmacological agents may reveal chronic drug effects on synaptic modulation.

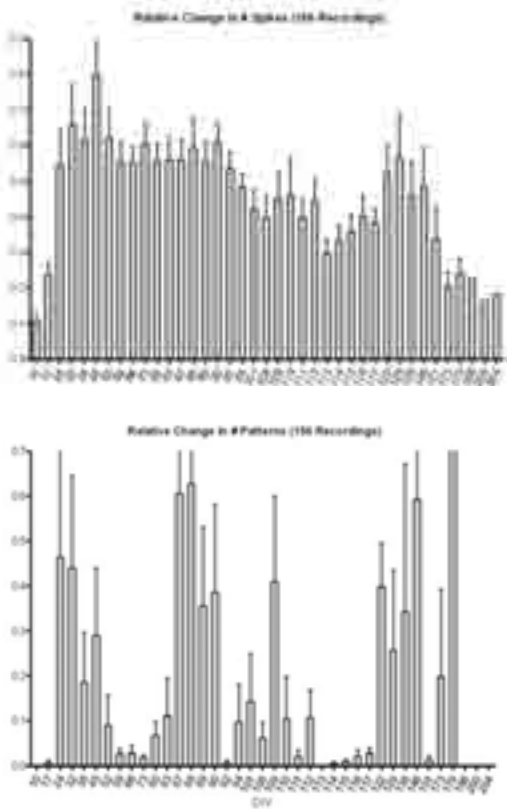

Fig. 3. Top: Average number of spikes between 10 and 204 DIV. Bottom: Average number of patterns (≥3 spikes, ≥2 electrodes, ≥3 instances). Both data are averaged across 156 recordings and normalized by the average of the largest three values for each MEA.

Acknowledgement

This work was supported by the German Ministry of Education and Research (BMBF: FKZ 0315641A) and the European Union (EURO-TRANS-BIO project ESSENCE).

References

[1] Abeles M., Gerstein GL. (1988). Detecting spatiotemporal firing patterns among simultaneously recorded single neurons. *J Neurophysiol* 60:909–924.

[2] Ikegaya Y. et al. (2004). Synfire chains and cortical songs: temporal modules of cortical activity. *Science* 304:559–564.

[3] Illes S. et al. (2009). Niche-dependent development of functional neuronal networks from embryonic stem cell-derived neural populations. *BMC Neuroscience* 10:93.

[4] Rolston JD. et al. (2007). Precisely timed spatiotemporal patterns of neuronal activity in dissociated cortical cultures. *Neuroscience* 148:294–303.

Two-dimensional analysis of the dorsal-root-ganglia neuron-electrode interface through time

Amanda Ferreira Neves[1*], Polyana Ferreira Nunes[1], Débora Vasconcelos[1], Celina Monteiro da Cruz Lotufo[2] e João-Batista Destro-Filho[1], Denise Cristina Da Silva[1]

1 School of Electrical Engineering, Federal University of Uberlandia, Uberlandia, Brazil
2 Institute of Biomedical Sciences, Division of Physiology, Federal University of Uberlandia, Uberlandia, Brazil
* Corresponding author. E-mail address: amanda.nvs@gmail.com

Abstract
Morphological monitoring of neural networks on micro-electrode array (MEA) permits to investigate the relation between cell and microelectrode, which is relevant for recording a good signal. Using images acquired at different *days-in-vitro*, we performed a quantitative study of the evolution of neural network topology on MEAs. This investigation presented a characterization of neuron-microelectrode interface, applied to dorsal root ganglia cultures, allowing further insights on electrical activity recordings.

1 Introduction

Nociceptors are primary sensory neurons with soma located at dorsal root ganglia (DRG) that are specialized in detection of painful stimulus. MEAs are probably a good means to detect changes in nociceptors excitability and a first step to test for this application is to monitor the cell culture topology by means of fluorescence confocal and scanning electron microscopy in order to evaluate the relation between cell and electrode, critical to recording a good-quality signal [1,2,3].

As well as MEA microelectrodes, rat-DRG neurons have diameters ranging from 10 to 40 μm [4]. In consequence, DRG neurons are more likely to cover MEA microelectrodes [5]. As discussed by [2], a substantial part of neuron soma must be in contact with the microelectrode surface to record a good signal, thus, the DRG culture on MEA devices represents an ideal system for monitoring neuron-microelectrode interface.

Here, our goal was to characterize the evolution of DRG neurons topology on MEA microelectrodes. It was performed a quantitative analysis in terms of cell distribution to compute a map of the distances between neurons and microelectrodes, using images acquired from the same cultures at different days *in vitro* (DIVs) using confocal microscopy.

2 Methods

2.1 Biological procedures

Dissociated cell cultures were prepared from *Wistar* rats (100 g), according to protocol described by [6], which was approved by the local Ethic Committee for Animal Experimentation. Dissociated cells were then plated on 60-channel MEAs (*Multichannel Systems*), precoated with *matrigel*. Fluorescent images of the culture stained with the voltage-sensitive dye Di-$BAC_4(3)$ were acquired daily, during three days, using a laser scanning confocal microscope (*Zeiss LSM 510*).

2.2 Quantitative Assessment

Neuronal distribution around microelectrodes was quantified manually using ImageJ software (*version 1.37c, National Institute of Health, USA*).

For each culture, the number of neurons on images was counted and, to assess if neurons belonged to a microelectrode area, it was enclosed a square area (200 μm side) whose center was placed exactly at the microelectrode, as shown in Fig.1. Since electrode-to-electrode distance is 200 μm, the entire surface of the array, divided into smaller microelectrode areas, was assessed.

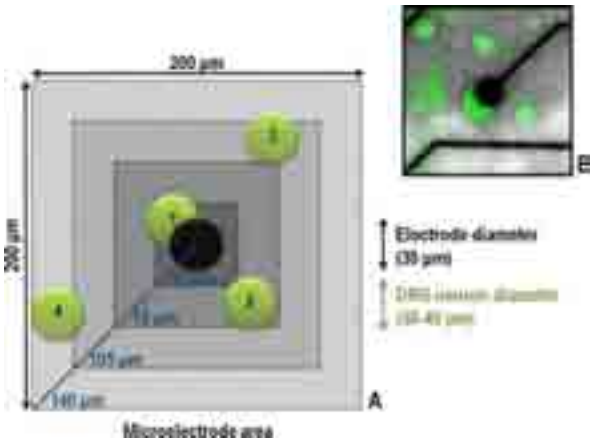

Fig.1. A- Diagram outlining an example of the proposed quantification, wherein four neurons (in green) round a microelectrode (in black); B- Real photograph of a DRG neuron and microelectrode interfacing in culture, taken by confocal fluorescent microscopy

Only neurons located at distances smaller than 140 μm from electrode center were considered. Neurons farther than 140 μm would be closer to the next microelectrode. For better understanding, see the example in Fig.1. As the microelectrode diameter (30 μm) is more or less the same dimension as the large DRG cells diameter (30-40 μm), neurons were classified according to their distance to microelectrode (*D*) as potentially connected ($D<35$ μm), for example neuron 1 in Fig.1; neighboring ($36<D<70$ μm), such as neuron 2 in Fig.1; distant ($71<D<105$ μm), as shown in neuron 3 of Fig.1; and remote ($106<D<140$ μm), such as neuron 4 in Fig.1.

3 Results and Discussion

Neuron counting and neuron-microelectrode distances (*D*) were assessed using the images from two cultures, which were compared to each other, and the results can be seen at Table 1 and summarized in Fig.2. Classifying neuron distances is important because their vicinity to microelectrodes establish the quality of signal recordings by the array, so that a substantial part of the neuronal soma need to be in contact with the microelectrode surface in order to obtain a good signal [2].

Table 1 - Results of Neuron Classification

DIV	Connected	Neighboring	Distant	Remote	*D* (μm)*
		MEA-1 CULTURE			
1st	12	38	71	26	79,96 ± 28,37
2nd	3	33	30	22	81,75 ± 28,21
3rd	5	28	24	4	71,30 ± 24,93
		MEA-2 CULTURE			
1st	4	35	59	14	81,28 ± 26,54
2nd	4	33	29	14	76,93 ± 28,71
3rd	10	22	26	8	61,42 ± 29,86

* Data are reported as mean ± standard deviation.

Both cultures presented a diffuse neuronal adhesion in which, at DIV 1, most part of neurons were found distant from microelectrodes; many were located neighboring; few were seen remote and in contact with microelectrodes. According to [5], this was expected since we did not use any technique to guide neuronal growth.

Considering culture time, at DIV 3, the number of cells reduced to 50% on average compared to DIV 1 (Fig.2). The most significant decrease occurred between DIV1 and DIV 2 in which neuronal loss was 40% on MEA-1 and 30% in MEA-2. For primary cultures, as in this case, it is expected that at least one third of the plated cells die under culture conditions [7].

Notice that neuronal death took place mainly to those cells located at larger distances, so that 94% of connected and 68% of neighboring neurons remained. Results point out that the recorded signal from MEA could remain throughout days without major interference on its amplitude, since there was not a significant loss in neighboring and connected neurons.

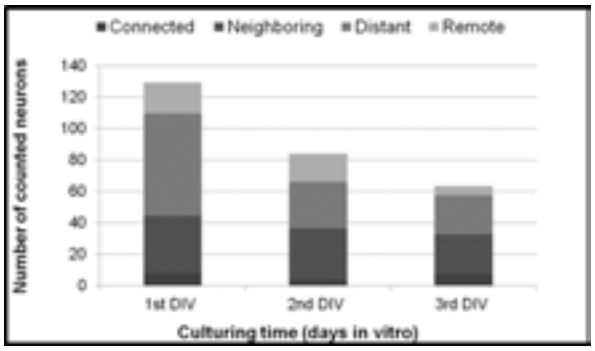

Fig.2. Amount of neurons estimated at different distances to the microelectrodes (D), regarding the time of culturing.

4 Conclusion

Results suggest that it is possible to improve neuronal activity recordings using MEA, considering only the evolution of the neural distribution topology. For long-term studies, recordings of electrical activity from DRG neurons with MEA are a possible new tool for the study of nociceptores sensitization and development of new analgesic drugs.

Acknowledgement

Authors financial support was provided by FAPEMIG (project TEC- APQ-02143-10), CNPq (grant 558114/2010-5) and UFU. We thank Prof. Martinoia from Genoa University and *Multichannel Systems Inc, Germanym.* for providing us with MEA devices; Mariani Silva and Prof. M.E. Beletti for their support at confocal microscopy imaging.

References

[1] Greve F., Frerker S., Bittermann A.G. (2007). Molecular design and characterization of the neuron-microelectrode array interface. *Biomaterials*, 28, 5246-5258.

[2] Van Pelt J., Wolters P.S., Corner M.A., Rutten W.L., Ramakers G.J. (2004). Long-term characterization of firing dynamics of spontaneous bursts in cultured neural networks. *IEEE Transactions on Biomedical Engineering*, 51(11), 2051-2062.

[3] Fromherz, P. (2003). Neuroelectronic interfacing: semiconductor chips with ion channels, nerve, cells, and brain. *In Nanoele-ctronics and Information Technology*, Wiley-VCH, 781-810.

[4] Harper A.A., Lawson S.N. (1985). Conduction velocity is related to morphological cell type in rat dorsal root ganglion neurons. *The Journal of Physiology*, 359, 31-46.

[5] Rutten W.L.C., Mouveroux J.M., Buitenweg J. (2001). Neuroelectronic interfacing with cultured multielectrode arrays toward a culture probe. *Proceeding of the IEEE*, 89(7), 1013-1029.

[6] Linhart O., Obreja O., Kress M. (2003). The inflammatory mediators serotonin, prostaglandin E2 and bradykinin evoke calcium influx in rat sensory neurons. *Neuroscience*, 118, 69-74.

[7] Potter S.M., De-Marse T.B. (2001). A new approach to neural cell culture for long-term studies. *Journal of Neuroscience Methods*, 110, 17-24.

A simple but plausible culture model recreates fast burst propagation and predicts their persistence

Sarah Jarvis[1,2,3], Steffen Kandler[1,2,3], Samora Okujeni[1,2,3], Stefan Rotter[1,2], Ulrich Egert[1,3]

1 Bernstein Center Freiburg, Univ Freiburg, Freiburg, Germany
2 Dept Biomicrotechnology, IMTEK, Univ Freiburg, Freiburg, Germany
3 Faculty of Biology, Univ Freiburg, Freiburg, Germany

Abstract
Present in the dynamics of cultured networks are periods of strongly synchronized spiking, termed 'bursting', whose role is not understood but dominates network dynamics and, due to their presence in cultures regardless of cell origin and their resistance to attempts to remove them, have been suggested to be an inherent feature in culture dynamics. Bursts have been demonstrated to contains distinct spatiotemporal motifs, repudiating the possibility that they are random or chaotic activity. However, the speeds of these propagating wavefronts has been measured as 5-100mm/s, and hence much faster than can be accounted for by local connectivity.
In attempting to represent cultured networks using 2D network models, typical connectivity models, such as random connectivity, prove to be insufficient for recreating some of the distinct phenomena associated with the dynamics of cultured networks, noticeably the fast propagation speeds.

1 Methods

Here, we introduce a simple but biologically plausible connectivity model that is able to reproduce phenomena. The relative simplicity of the connectivity scheme allows us to simulate a network of 12,500 neurons within a 1.5mm radius circular area on a 2D plane, resulting in a model that is comparable in density and size to experimental networks. We then extend this model to incorporate some of the subtle structural inhomogeneities observed experimentally, such as clustering of soma positions, to investigate their implications for network dynamics.

2 Results

We demonstrate that our simple but biologically plausible representation of network connectivity is able to emulate burst propagation with speeds comparable to those observed experimentally. Furthermore, the inclusion of structural inhomogeneities strongly facilitate burst propagation as well as form the emergence of distinct burst motifs. Importantly, our model confirms that bursts are indeed an inherent feature of such networks, as they are an inescapable by-product of network connectivity and structure.

Simulation of neuronal network without and with self-inhibition

Kerstin Lenk[1], Kay Barthold[1], Barbara Priwitzer[1], Olaf H.-U. Schröder[2]

1 Faculty of Engineering and Computer Science, Lausitz University of Applied Sciences, Senftenberg (Germany)
2 NeuroProof GmbH, Rostock (Germany)

Abstract
We developed a pulsing model called INEX which simulates neuronal activity as observed in neuronal networks cultivated on multielectrode array (MEA) neurochips. In an *in* vitro experiment approximately 500,000 cells of the frontal cortex of embryonic mice are cultivated on such a MEA neurochip (experiments are carried out by NeuroProof GmbH, Rostock, Germany). Circa 10,000 neurons and 90,000 glia cells of the total amount survive. Circa 20% of these neurons are interneurons (Brunel, 2000) which tend to self-inhibition (also known as recurrent or autaptic inhibition; Bacci et al., 2003). In this work we examine self-inhibition of neurons using the INEX model.

1 Methods

The INEX model is based on an inhomogeneous Poisson process (Heeger, 2000) to simulate neurons which are active without external input or stimulus as observed in neurochip experiments. It is accomplished using an Ising model with Glauber dynamics.

In a first step, the four parameter types for a network without self-inhibition were chosen in such a way that the resulting spike trains resemble spike trains of MEA neurochip experiments with respect to spike and burst rate. Five simulations were run with this constrains. In a second step, five simulations have been carried out after a parameter fit for a network with self-inhibition.

For validation we calculated five features for each of the simulated spike trains and compared them with the same features obtained from five multielectrode array neurochip experiments with cell cultures originated from frontal cortex of embryonic mice after 28 days in vitro. Furthermore, spike train statistics are applied to approve the resulting spike data (Kass et al., 2005). For this purpose the spike train data of one selected neuron were binned with a width of five seconds. A bar chart shows how many bins occur with a given number of spikes per bin. The binned INEX data were also plotted against the binned MEA data in a Q-Q plot.

2 Results

The simulated spike trains without self-inhibition show typical spike and burst patterns as known from experiments with MEA neurochips. Synchronous spiking and bursting is typical for frontal cortex neurons. The simulated spike trains with self-inhibition showed the typical spike and burst patterns again.

The validation of the spike trains with parameter fitting and without self-inhibition showed that all calculated averaged features of the INEX data are within the standard deviation of the MEA neurochip data. For the simulated spike trains with self-inhibition, except the burst rate all calculated averaged features of the INEX data are within the standard deviation of the MEA neurochip data. The plotted bar chart as well as the Q-Q plot of the simulated data and the MEA neurochip data exhibit similar behaviour.

3 Conclusion

Calculated features adapted from spikes and bursts as well as the spike train statistics show that the presented model without self-inhibition as well as with self-inhibition and parameter fitting can simulate neuronal activity similar to activity as observed on multielectrode array neurochips. We could show that our model is able to simulate the self-inhibition of interneurons.

Applications in Systems Neuroscience

Electrophysiological imaging of epileptic brain slices reveals pharmacologically confined functional changes

Ferrea E.[1*], Medrihan L.[1], Ghezzi D.[1],Nieus T[1]. Baldelli P.[1,2], Benfenati F.[1,2], Maccione A.[1]

1 Neuroscience and Brain Technology Department, Fondazione Istituto Italiano di Tecnologia (IIT), Genova, Italy.
2 Department of Experimental Medicine, University of Genova, Genova, Italy.
* Corresponding author. E-mail address: enrico.ferrea@iit.it

Abstract
Microelectrode arrays (MEAs) are employed to study extracellular electrical activity in neuronal tissues. Nevertheless, commercially available MEAs provide a limited number of recording sites and do not allow a precise identification of the spatio-temporal characterization of the recorded signal. To overcome this limitation, high density MEAs, based on CMOS technology, were recently developed and validated on dissociated preparations (Berdondini et al. 2009). We show the platform capability to record extracellular electrophysiological signal from 4096 electrodes arranged in a squared area of 2.7 mm x 2.7 mm with inter-electrode distance of 21 μm at a sampling rate of 7.7 kHz/electrode. Here, we demonstrate the performances of these platforms for the acquisition chemically evoked epileptiform activity from brain slices. Moreover the high spatial resolutions allow us to estimate the effect of drugs in spatially modulating Inter-Ictal ((I-IC) activity.

1 Introduction

Electrophysiological recording of neuronal activity in slices is a common experimental method for investigating complex brain processing circuits, brain plasticity or neuropharmacology. To this end, it is crucial to enable recordings of electrophysiological activity from large neuronal populations at sufficient spatial and temporal resolution, thus making possible to localize and track electrically or chemically evoked neuronal activity and to identify induced functional changes. Conventional electrophysiological include the use of electrodes and light-imaging methods to record action potentials from multiple single neurons as well as local field potentials generated by neuronal ensembles. Patch-clamp and field electrodes, approaches based on micro-positioned single glass pipettes, enable intracellular or extracellular recordings respectively, from single neurons or from neuronal populations surrounding the electrode respectively. Optical imaging based on fluorescent Ca2+ indicators [1] or voltage sensitive dyes (VSDs) [2, 3] are the current choice for spatially resolving electrical activity in the brain, but this approach suffers a modest temporal resolution due to sampling frequencies in the range of 1-3 kHz. Moreover, this approach does not offer a high signal to noise ratio and is not suited to record continuously for long periods of time (usually it can records for few seconds after a triggered electrical stimulus). Consequently, these recording performances are not sufficient to effectively track the electrical activity propagations over large areas of the brain tissue in real time, either due to insufficient spatial or temporal resolutions.

2 Materials and Methods

Horizontal cortico-hippocampal slices (400 μm of thickness) were placed on the active area of the chip (Fig.2). A platinum anchor of the same dimension was used to keep the slice in position for the whole recording. Epileptic-like discharges were induced in slices by treatment with the convulsant agents 4-aminopyridine (4AP) at a concentration of 100μM [4] and/or bicuculline (BIC) at a concentration of 30μM. Epileptiform activity was stable during recordings for at least two hours. Epileptiform activity in the form of I-IC was detected with a previously described Precision Timing Spike Detection algorithm (PTSD) [5] and represented in raster plots (see fig.1B). This algorithm, originally developed to detect spiking activity, has been re-adapted to detect Inter-Ictal (I-IC) events. To this aim, the threshold was set to 5 times the standard deviation of the noise while the refractory period and the peak lifetime period were set to 50 msec and 40 msec, respectively. Movie sequence frames as reported in Fig.1 were generated in *Matlab* after low pass filtering of single electrode traces.

3 Results

The large-scale high-density electrode array allow us to visually describe the involvement of cortical and hippocampal circuitries during propagation of epileptiform activity (Fig. 2). In this experiment the I-

IC was observed to originate in CA3 and propagating to CA2 (10 ms) and CA1 (30 ms). By litterally imaging the extracellular activity it is possible to study the spatial extention of the epileptic event which might be reflect different mechanisms of propagation through the network (e.g. synaptic versus non-synaptic propagation).

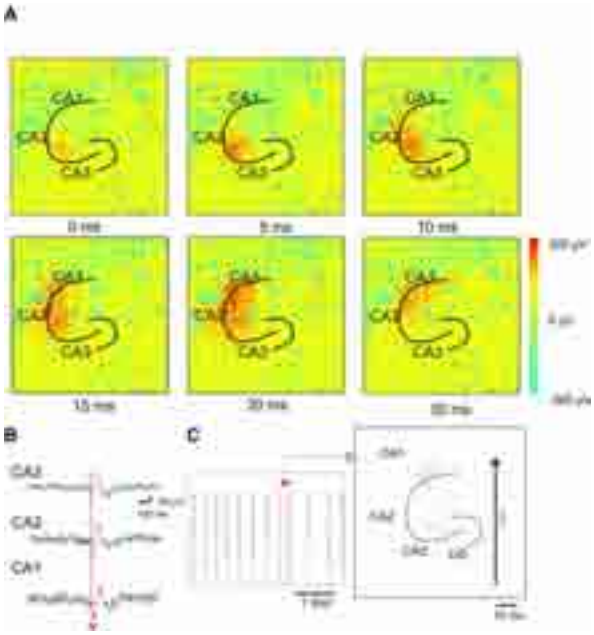

Fig. 1. Inter-Ictal like propagation. (A) Color-map coding voltages of extracellular activity. The map sequence is showing the consecutive activation of the distinct areas: CA3 first, then CA2 and finally CA1. (B) Inter-Ictal (I-IC) activity recorded in three representative electrodes in the hippocampus (CA3, CA2, CA1). Red vector is indicating the direction of propagation of the signal (C) Raster plot representation of detected I-IC events. (Left) On the large scale raster plot (10 minutes) the distribution of I-IC events seems to be synchronous on all the electrodes whereas on the close up (right) it is possible to note that different hippocampal regions are recruited at different times.

Moreover, our method enable to spatially depict the firing rate of different cortico-hippocampal regions over the active area of the chip (Fig. 2). In this experiment by adding BIC to the extracellular solution containing 4AP, the mean firing rate of I-IC events was found to spatially increase differently in different cortico-hippocampal regions (cfr. Fig. 2 middle and left)

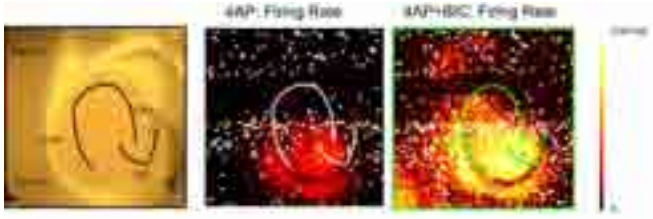

Fig. 2. (left) Cortico hippocampal slice over the active area. The mean firing rate has been calculated for every pixel in the slice under 4AP treatment (middle) and under 4AP+BIC treatment (right)

4 Discussion

Our system enables us to literally imaging the extracellular activity and to describe signal propagations over large areas. The spatial extention and propagation latencies of I-IC can be finely appreciated with the system. These are important aspects to evaluate the different types of synchronization mechanism which could play a role in the propagation of epileptic events (for review see[6]).

A part from propagation studies our system appears also to be a useful tool to assess the effect of chemical compounds in different regions in brain slices.

References

[1] Chang, W.P., et al., *Spatiotemporal organization and thalamic modulation of seizures in the mouse medial thalamic-anterior cingulate slice.* Epilepsia, 2011. **52**(12): p. 2344-55.

[2] Tominaga, Y., M. Ichikawa, and T. Tominaga, *Membrane potential response profiles of CA1 pyramidal cells probed with voltage-sensitive dye optical imaging in rat hippocampal slices reveal the impact of GABA(A)-mediated feed-forward inhibition in signal propagation.* Neurosci Res, 2009. **64**(2): p. 152-61.

[3] Carlson, G.C. and D.A. Coulter, *In vitro functional imaging in brain slices using fast voltage-sensitive dye imaging combined with whole-cell patch recording.* Nat Protoc, 2008. **3**(2): p. 249-55.

[4] Avoli, M., *Epileptiform discharges and a synchronous GABAergic potential induced by 4-aminopyridine in the rat immature hippocampus.* Neurosci Lett, 1990. **117**(1-2): p. 93-8.

[5] Maccione, A., et al., *A novel algorithm for precise identification of spikes in extracellularly recorded neuronal signals.* J Neurosci Methods, 2009. **177**(1): p. 241-9.

[6] Jefferys, J.G., *Nonsynaptic modulation of neuronal activity in the brain: electric currents and extracellular ions.* Physiol Rev, 1995. **75**(4): p. 689-723.

Targeting defined populations of retinal ganglion cells with CMOS microelectrode arrays

Michele Fiscella[1], Karl Farrow[2], Ian L. Jones[1], David Jäckel[1], Jan Müller[1], Urs Frey[3], Douglas J. Bakkum[1], Botond Roska[2] and Andreas Hierlemann[1],

1 ETH Zurich, Bio Engineering Laboratory, Basel, Switzerland.
2 Neural Circuits Laboratory, Friedrich Miescher Institute, Basel, Switzerland.
3 Riken Quantitative Biology Center, Kobe, Japan.

Abstract

Here we report on recording action potentials from a predefined neural population in the mouse retina by using a microelectronics-based high-density microelectrode array, containing 3,150 electrodes/mm^2. Single-cell action potentials are recorded constantly on multiple electrodes; thus, every action potential has a unique spatial distribution, which helps to improve the spike sorting process, and enables to distinguish the activity of densely packed retinal ganglion cells. Different physiological types of retinal cells can be distinguished, based on their light response. Finally, the variety of possible electrode configurations enables to target a specific population of retinal ganglion cells for extracellular recordings.

1 Background and Aims

The retina is a multilayered, light-sensitive sheet of neural tissue that encodes visual stimuli as complex spatio-temporal patterns of action potentials (Wassle, 2004). The final output of the retina is encoded in the ganglion cell layer, in which densely packed neurons, called retinal ganglion cells (RGCs), generate action potentials that proceed along the optic nerve to higher brain regions. The study of physiologically identified RGC types demonstrates that the synchronous activity of these neurons convey significant information about the visual stimulus (Pillow et al., 2008).

Here we used a high-density microelectrode array (MEA) (Frey et al., 2009; Frey et al., 2010) (Fig. 1), fabricated in standard microelectronics or CMOS (**C**omplementary **M**etal **O**xide **S**emiconductor) technology, to record the light-induced activity of mouse RGCs and to characterize the physiological type according to their response to light stimulation. We utilized the dynamic-configurability capabilities of the MEA to select defined populations of RGCs.

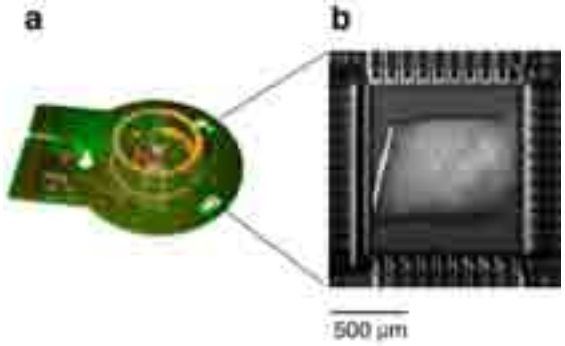

Fig. 1. (a) HD-CMOS MEA. (b) Mouse retina patch placed on the electrode area.

2 Methods

The high-density MEA features 11,011 platinum electrodes at an electrode density of 3,150 electrodes per mm^2. Amplification (0-80dB), filtering (high pass: 0.3-100 Hz, low pass: 3.5-14 kHz) and analog-to-digital conversion (8 bit, 20 kHz) are performed by on-chip circuitry. 126 channels can be simultaneously utilized for recording and/or stimulation.

Wild-type C57BL/6J mice (P30) were obtained from Charles River Laboratories (L'Arbresle Cedex, France). The retina was isolated under dim red light in Ringer's medium (in [mM]: 110 NaCl, 2.5 KCl, 1 $CaCl_2$, 1.6 $MgCl_2$, 10 D-glucose, 22 $NaHCO_3$), continuously bubbled with 5% CO_2 / 95% O_2. A section of the retina was placed such that the ganglion cell layer was in direct contact with the MEA surface. In order to stably secure the retina directly above the MEA, a permeable membrane (polyester, 10 µm thickness, 0.4 µm pore size) was lightly pressed against the tissue.

The light stimuli were designed using Psychtoolbox within the software application Matlab and were projected onto the electrode array by an LED projector with a refreshing rate of 60 Hz (Acer K10). The light stimulus was focused only on the electrode array area of the MEA chip by two camera lenses (Nikkor 60 mm 1:2.8 G ED, Nikon), a mirror (U-MBF3, Olympus) and a 5X objective (LMPLFLN5X Olympus). The light projection setup was assembled on an upright microscope (BX5IWI, Olympus).

The light-induced activity of RGCs was recorded at a time resolution of 50 µs and band-pass filtered (500 Hz-3 KHz). An independent-component analysis (ICA) (Hyvarinen, 1999)-based algorithm was used for online spike sorting during the experiment.

3 Results

Light was exclusively projected onto the electrode array area during the experiments. This way, it was possible to record light-evoked action potentials from RGCs in the absence of light-induced artifacts in the recorded signals (Fig. 2).

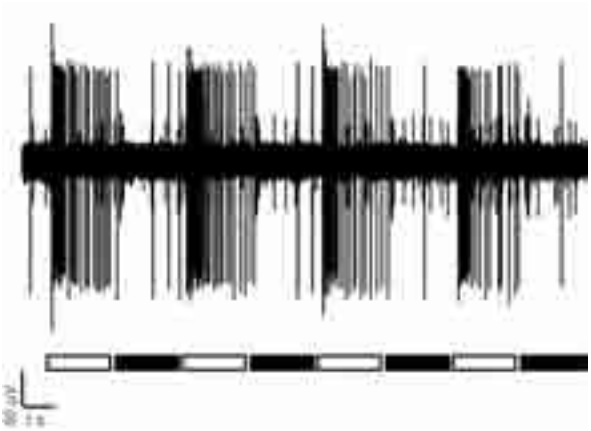

Fig. 2. An example of light-evoked responses from mouse RGCs, as recorded by the MEA. The white bar indicates the projection of a light stimulus brighter than the background light level ("light on"). The black bar indicates the projection of a light stimulus darker than the background light level ("light off"). The action potentials as recorded from one electrode are shown.

Single-cell action potentials were consistently detectable on multiple electrodes of the CMOS-based MEA chip (Fig. 3)

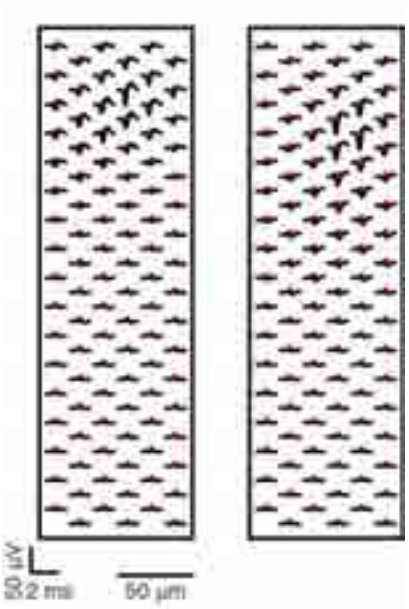

Fig. 3. Spatial distribution (footprint) of averaged signals of two neighboring RGCs over an area of 0.025 mm^2.

Furthermore, it was possible to target a population of RGCs by taking advantage of the high-density packing of the electrodes and the rapid dynamic configurability of the MEA system. We found the following process to be efficient: (i) Scanning the MEA for activity characteristic to the RGCs of interest, (ii) performing online spike sorting, and, finally, (iii) selecting a configuration of electrodes that could most effectively be used to stimulate and record from chosen RGCs (Fig. 4).

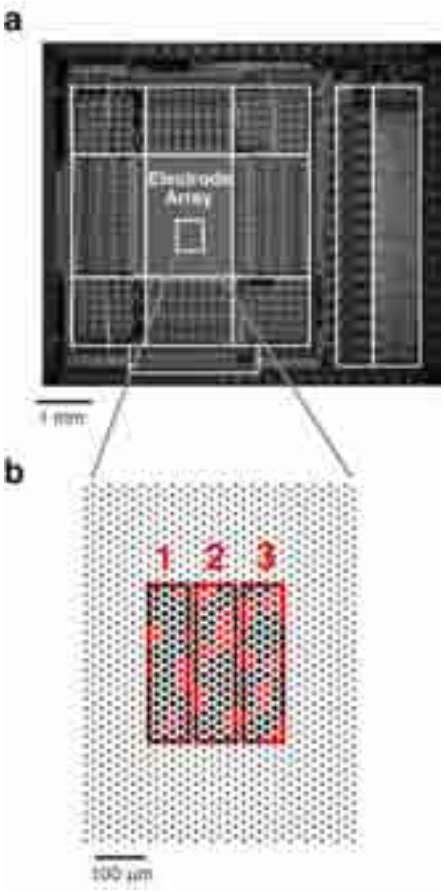

Fig. 4. (a) A region of interest within the piece of retina is stimulated with light and sequentially recorded from using high-density electrode blocks (indicated by rectangles 1, 2 and 3 in figure 4b). (b) A defined subset of electrodes can be selected at the location of a RGC of interest: These electrodes are selected so as to obtain the highest signals for each targeted RGC (indicated by red circles).

4 Conclusions

The ability to target specific populations of RGCs is a prerequisite for the design of experiments, aimed at understanding the population code of individual as well as combinations of visual channels.

In future studies, the method for cell identification and targeting system will be used to select defined physiological types of RGCs in an effort to decode further details of the retinal code.

Acknowledgement

Michele Fiscella acknowledges individual support through a Swiss SystemsX interdisciplinary PhD grant No. 2009_031.

This work was supported by the European Community through the ERC Advanced Grant 267351 “NeuroCMOS”.

References

[1] Frey U, Egert U, Heer F, Hafizovic S, Hierlemann A. Microelectronic system for high-resolution mapping of extracellular electric fields applied to brain slices. Biosens Bioelectron, 2009; 24: 2191-8.

[2] Frey U, Sedivy J, Heer F, Pedron R, Ballini M, Mueller J, Bakkum D, Hafizovic S, Faraci FD, Greve F, Kirstein K-U, Hierlemann A. Switch-Matrix-Based High-Density Microelectrode Array in CMOS Technology. IEEE Journal of Solid-State Circutis, 2010; 45

[3] Hyvarinen A. Fast and robust fixed-point algorithms for independent component analysis. IEEE Trans Neural Netw, 1999; 10: 626-34.

[4] Pillow JW, Shlens J, Paninski L, Sher A, Litke AM, Chichilnisky EJ, Simoncelli EP. Spatio-temporal correlations and visual signalling in a complete neuronal population. Nature, 2008; 454: 995-9.

[5] Wassle H. Parallel processing in the mammalian retina. Nat Rev Neurosci, 2004; 5: 747-57.

Following the assembly of functional circuitry: High resolution large-scale population neuronal dynamics in the neonatal mouse retina in health and disease

Evelyne Sernagor[1*], Matthias H. Hennig[2], Mauro Gandolfo[3], Matthew Down[1], Alyssa Jones[1], Stephen J. Eglen[4], Luca Berdondini[5]

1 Institute of Neuroscience, Newcastle University Medical School, Newcastle upon Tyne, UK
2 Institute for Adaptive and Neural Computation, School of Informatics, University of Edinburgh, Edinburgh, UK
3 Department of Biophysical and Electronic Engineering, University of Genova, Genova, Italy
4 Department of Applied Mathematics and Theoretical Physics, Cambridge University, Cambridge, UK
5 Department of Neuroscience and Brain Technologies, Italian Institute of Technology, Genova, Italy
* Corresponding author. E-mail address: evelyne.sernagor@ncl.ac.uk

Abstract

The developing retina exhibits spontaneous waves of activity spreading across the ganglion cell layer. These waves are present only during a limited perinatal period, and they are known to play important roles during the wiring of visual connections. Using the high density large scale (4,096 electrodes) Active Pixel Sensor (APS) MEA (BioCam 4096, 3Brain Gmbh), we have recorded retinal waves from the neonatal mouse retina at near cellular resolution (21x21µm electrodes, 42µm separation) (Berdondini et al., 2009). We found that the spatiotemporal patterns of the waves undergo profound developmental changes as retinal synaptic networks mature, switching from slow random events propagating over large retinal areas to faster, spatially more restricted events, following several clear repetitive, non-random propagation patterns. This novel pan-retinal perspective of wave dynamics provides new clues about the role played by retinal waves during visual map formation.

1 Introduction

During perinatal development, neighbouring retinal ganglion cells (RGCs) fire in correlated bursts of action potentials, resulting in propagating waves (for review see [1,2]). The spatiotemporal wave patterns are hypothesised to provide cues for the establishment of retinal receptive fields and for the binocular organisation and visual map formation in retinal targets. In mouse, retinal waves are present from late gestation until eye opening (postnatal day (P) 12). The earliest waves are mediated by gap junctions (Stage I), followed by lateral connections between cholinergic starburst amacrine cells (late gestation to P9; Stage II). Finally, once glutamatergic connections become functional and RGCs respond to light, waves switch to glutamatergic control (P10; Stage III). Despite such major developmental changes in network connectivity, there has been no clear report of parallel changes in wave dynamics, a problem we attribute to the use of recording approaches with relatively low spatiotemporal resolution. In this study, we have used the high density large scale APS MEA (BioCam 4096 from 3Brain Gmbh) [3], allowing us to investigate with unprecedented precision how the spatiotemporal properties of retinal waves change during development. The 64x64 APS MEA records at near cellular resolution (21x21µm electrodes, 21µm separation) and high temporal resolution (7.8 kHz/channel for full frame rate acquisition). The channels are integrated over an active area of 2.67x2.67 mm, which is large enough to cover most of the neonatal mouse retina. An example of pan-retinal propagation during a spontaneous episode of correlated activity is illustrated in Figure 1.

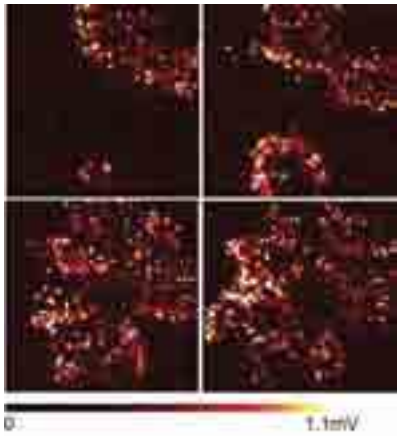

Fig. 1. Spontaneous activity propagating across a postnatal day 11 mouse retina, in presence of the $GABA_A$ antagonist bicuculline. Each dot (pixel) represents one electrode on the MEA. Propagating patterns are visualized in time lapse single frames (from left to right and top to bottom) of activity raw data acquired every 0.5 s. The extracellular signals are shown in a false colour map by computing the signal variance.

2 Materials and methods

All experiments were performed on retinal wholemounts isolated from wild type (C57bl6) mice or from the Cone rod homeobox (Crx) knockout mouse, a model of Leber congenital amaurosis [4]. Retinas were isolated between P1-14 and mounted on the APS MEA, RGC layer facing down onto the electrodes. All the analysis, from burst detection to the

computation of wave metrics was done using custom written codes in Matlab or in R.

3 Results

We found that Stage II cholinergic waves recruit relatively few cells, they are initiated at random locations and slowly propagate with a high degree of randomness, covering large retinal areas (Fig 2). They become larger, denser and faster up to P6. P8-9 Stage II waves become smaller and slower, a phenomenon reversed by blocking $GABA_A$ receptors with bicuculline.

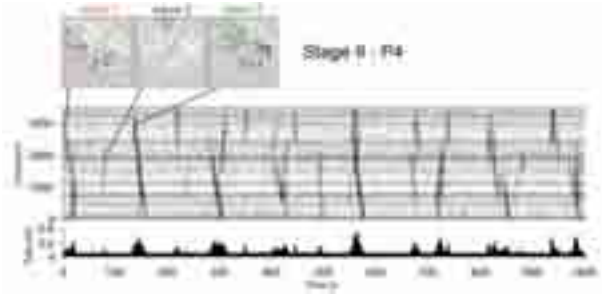

Fig. 2. Stage II waves (P4). Central panel: raster plot of consecutive waves recorded over 1000s. Top panel: 2-dimensional projections of the first 3 waves. Bottom panel: pan-retinal average firing rates over all electrodes.

Stage III glutamatergic waves are faster and denser, and they are more restricted spatially, following few repetitive, non-random propagation patterns (Fig 3).

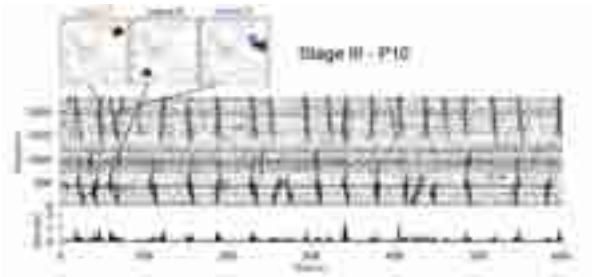

Fig. 3. Stage III waves (P10). Central panel: raster plot of consecutive waves recorded over 600s. Top panel: 2-dimensional projections of waves 7, 8 and 9. Bottom panel: pan-retinal average firing rates over all electrodes.

These findings are consistent with the hypothesis that the large and highly variable Stage II waves are important to guide the segregation of retinal projections into eye specific domains in the brain visual areas. The spatially more constrained late Stage II waves may be important to refine retinotopic projections. Stage III waves occur just before eye opening, after the central retinal projections have already matured. We propose that these late waves with characteristically small, dense and highly repetitive activity patterns may be important for strengthening retinal connections associated with the formation of RGC receptive fields.

To test this idea, we have looked at spontaneous activity patterns during the first few postnatal weeks in the Crx-/- mouse that carries a genetic mutation leading to photoreceptor degeneration between 1-6 months postnatal, resulting in complete blindness [4]. Because glutamatergic retinal connectivity is known to be abnormal from early developmental stages in inherited retinal dystrophies [5] (even before photoreceptor death), we postulated that Stage III waves may be abnormal in the Crx-/- retina. We found that Stage II waves were normal, whilst Stage III wave patterns were indeed completely disrupted (ranging from absence of correlated activity to very slow and prolonged episodes), demonstrating aberrant glutamatergic wiring before degeneration even starts in the outer retina. Glutamate-mediated slow oscillations (~10Hz) and strong bursting become apparent in the RGC layer during the third postnatal week and continue throughout the degeneration period.

4 Discussion and concluding remarks

In this study, we have demonstrated that the APS MEA is a powerful tool to investigate the spatiotemporal behaviour of developing retinal networks. Indeed, thanks to the unprecedented size and resolution of the system, we have achieved a novel pan-retinal perspective of early activity dynamics during retinal maturation, providing clues about the role played by early retinal activity during wiring of the visual system in health and disease.

Acknowledgement

This work was funded by BBSRC grant BB/H023569/1 (ES, MHH, SJE), EPSRC Grant EP/E002331/1 (CARMEN) (ES, SJE), MRC Grant G0900425 (MHH) and IDEA, FP6-NEST Grant 516432 (LB, MG).

References

[1] Sernagor E, Hennig MH (2012). Developmental Neuroscience: A Comprehensive Reference, Volume 1 doi:10.1016/B978-0-12-375711-1.00151-3 (Elsevier).

[2] Torborg CL, Feller MB (2005). Spontaneous patterned retinal activity and the refinement of retinal projections. *Prog Neurobiol*, 76, 213–235

[3] Berdondini L, Imfeld K, Maccione A, Tedesco M, Neukom S, Koudelka-Hep M, Martinoia S (2009). Active pixel sensor array for high spatio-temporal resolution electrophysiological recordings from single cell to large scale neuronal networks. *Lab Chip*, 9, 2644-2651.

[4] Furukawa, T, Morrow EM, Cepko CL (1997). Crx, a novel otx-like homeobox gene, shows photoreceptor-specific expression and regulates photoreceptor differentiation. *Cell*, 91, 531-541.

[5] Marc RE, Jones BW, Watt CB, Strettoi E (2003). Neural remodeling in retinal degeneration. *Prog Retin Eye Res*, 22, 607-655.

Investigation into the structural and functional changes in the gastrointestinal tract of transgenic mice with over-expressing amyloid precursor protein

C.W. Hui [1], C.K. Yeung [1], H. Wise [1], L. Baum [2], M.R. Fang [3], J.A. Rudd [1]

1 Neuro-degeneration, Development and Repair, School of Biomedical Sciences, Faculty of Medicine, The Chinese University of Hong Kong, Hong Kong SAR, China
2 School of Pharmacy, Faculty of Medicine, The Chinese University of Hong Kong, Hong Kong SAR, China
3 Institute of Anatomy and Cell Biology, Medical College, Zhejiang University, Hangzhou, China

Abstract

The interstitial cells of Cajal (ICCs) in the myenteric plexus interact with enteric nervous system (ENS) and generate slow waves to maintain phasic contractions of smooth muscles and the healthy peristalsis in the gastrointestinal (GI) tract [1]. In this study, both morphological and functional changes in the GI tract of an AD mouse model were identified and this provides a foundation for the investigation into degenerative diseases by studying the GI tract.

1 Introduction

Alzheimer's disease (AD) is associated with a deposition of amyloid plaques and a loss of cholinergic neurons in the central nervous system (CNS). Studies have shown that GI motility is always disturbed in Parkinson's disease but there is a dearth of information on the GI tract during AD. In the present study, the structural and functional changes in the GI tract of Alzheimer's transgenic mice (Tg2576) were investigated.

2 Methods and Materials

Six-month old Tg2576 mice (n = 8) and their wild type controls (n = 8) were used.

2.1 Morphological studies

Fluorescent immunohistochemistry was performed on whole mounts of the GI tract (antrum, duodenum, jejunum, ileum and colon). Morphologies of ICCs, enteric neurons and two types of enteric glial cells were observed using confocal microscopy, and cell areas were quantified using ImageJ software (National Institutes of Health). Statistical comparisons were made using Student's t-test (Prism Version 5, GraphPad Software Inc., U.S.A.).

Paraffin wax sections of antrum, duodenum, jejunum, ileum and colon were prepared and subjected to antigen retrieval using 80% formic acid. Sections were then incubated with antibodies against amyloid beta protein. After incubating with HRP-conjugated secondary antibodies, the presence of amyloid plaques was visualised using Zeiss Axioskop microscope.

2.2 Functional studies

Whole muscle layers of antrum and ileum containing myenteric plexuses were isolated and placed into the recording chamber of a microelectrode array (MEA) (Multichannel Systems, Germany, Figure 1). Baseline recordings (3 min) were obtained after 60 min perfusion in the presence of nifedipine (1 μM). Three minute recordings were then taken following the addition of 1 μM or 5 μM nicotine. The background noise was removed by 2.5 Hz low-pass and 0.1 Hz high-pass filtering. Power spectrums were generated using Spike2 (Version 7, Cambridge Electronic Design Limited, England). Statistical comparisons were made using One-way ANOVA.

Figure 1: Whole-muscle layer of ileum was placed directly on the electrodes in the recording chamber of the MEA system. Scale bar = 1 cm

3 Results

3.1 Morphological Studies

The fluorescent immunohistochemistry of whole mount tissues showed significant losses of neurons and glial cells in the ileum of Tg2576 and a significant loss of S100 positive glial cells in the antrum of Tg2576 ($P<0.05$). No morphological changes in enteric nervous system were observed in the duodenum, jejunum, and colon. However, the ratios of GFAP to S100 positive glial cells increased in the duodenum, jejunum and colon of Tg2576 and this reflects the occurrence of inflammation in these three GI regions. Also, there were no significant differences in the numbers of ICCs in all GI regions ($P>0.05$).

The ileal paraffin wax sections showed the presence of amyloid plaques in Tg2576 but not in the wild type controls. No amyloid plaques were identified in other GI regions and the brain of both Tg2576 and wild type controls.

The MEA study demonstrated that nicotine significantly increased electrical activity in the ileum and antrum of the wild type controls but not in Tg2576 ($P<0.05$). The effect of nicotine in Tg2576 mice compared with their wild-type control may be related to morphological differences in the GI tract.

4 Conclusion

These results support the hypothesis that the ENS is the gateway for the pathological changes, which occur initially in the gut and then spread to the CNS through autonomic/sensory nerves or circulation [2]. The present study also demonstrates that the biopsy of GI sections may provide a method for an early diagnosis for AD.

References

[1] Sean M. Ward and Kenton M. Sanders (2006). Involvement of intramuscular interstitial cells of Cajal in neuroeffector transmission in the gastrointestinal tract. J Physiol, 576:675-682.

[2] Natale G, Pasquali L, Paparelli A, Fornai F (2011). Parallel manifestations of neuropathologies in the enteric and central nervous systems. Neurogastroenterol Motil, 23, 1056-106

Electrically evoked responses of retinal ganglion cells in wild type and rd10 mouse retinas.

Archana Jalligampala [1,3,4], Daniel.L Rathbun [1,2,3], Eberhart Zrenner [1,2,3]

1 Institute for Ophthalmic Research, University of Tübingen, Tübingen, Germany
2 Bernstein Center for Computational Neuroscience Tübingen, Tübingen, Germany
3 Centre for Integrative Neuroscience, Tübingen, Germany
4 Graduate School of Neural and Behavioral Sciences, International Max Planck Research School, Tübingen, Germany

* Corresponding author. E-mail address: archana.jalligampala@biomed-engineering.de

Abstract

Over the years, retinal implants have been developed to restore limited functional vision in patients blinded by outer retinal diseases like retinitis pigmentosa (RP) and age–related macular degeneration through electrical stimulation of the surviving neurons. The most extensively characterized animal model is the *rd1* mouse. However, the recently identified *rd10* mouse, which has a relatively delayed onset and slower progression of degeneration may be a more appropriate model for human RP. To support ongoing efforts to optimize prosthetic retinal stimulation [1], optimal stimulation paradigms need to be established for this new mouse line. Here we investigate retinal ganglion cell (RGC) responses to different stimulation paradigms in adult *wt* and *rd10* mice.

1 Introduction

Retinitis pigmentosa (RP) and age-related macular degeneration (AMD) are two forms of outer retinal diseases which result in a substantial loss of photoreceptors. Although, the remaining inner retina undergoes some physiological and morphological changes, the characteristic cellular layering is still preserved, offering the opportunity to restore vision by electrical stimulation of the residual neurons via retinal implants. The most extensively characterized animal model is the rd1 mouse. However, the recently identified rd10 mouse, which has a relatively delayed onset and slower progression of degeneration, may be a more appropriate model for human RP. In order to support ongoing efforts to optimize prosthetic retinal stimulation, paradigms need to be established for this new mouse line. Here, we investigate retinal ganglion cell (RGC) responses to electrical stimulation in adult wt and rd10 mice.

2 Materials and Methods

RGC spiking responses were recorded in vitro from patches of wild-type and *rd10* retina using a planar multi-electrode (Multichannel Systems, Reutlingen, Germany). Prior to electrical stimulation, spontaneous activity was recorded. Stimuli were applied epiretinally via one of the 60 electrodes of a multielectrode array (MEA) while the remaining electrodes recorded electrically evoked responses (MC Rack, MC-Stim Multichannel Systems; **Fig 1A and B**). Stimuli consisted of square-wave, monophasic (either cathodic or anodic) constant-voltage pulses with varying voltages and durations. Stimulus randomization was employed to compensate for recording instability-induced biases that have been previously observed. The stored data were processed and analyzed offline (Offline Sorter, Plexon Inc, TX; Neuroexplorer, Nex Technologies; and Matlab) to generate rastergrams, peristimulus histograms, and stimulus-response curves.

(A)

(B)

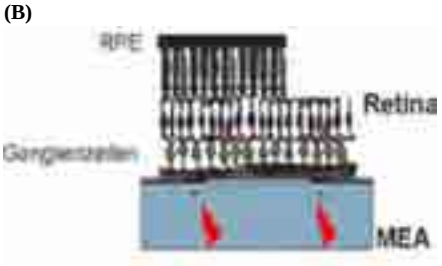

Fig1:(A) Standard planar MEA (30µm diameter electrodes, 200µm interelectrode distance, Multichannel systems, Reutlingen, Germany) . **(B)** Simultaneous epiretinal stimulation and recording from the retina (*image from Eckhorn et al,2001[2]*).

3 Results

In agreement with recent reports, spontaneous activity was higher and more oscillatory in *rd10* retina than in the wild-type [3]. For the *wt* retina, we found pulse voltage and duration requirements that are in agreement with previously published reports. In both *wt* and *rd10* cells, a dependence on duration was seen only for a few transitional voltages (near threshold; **Fig. 2**). Both above and below these voltages the influence of duration was not significant. A

subset of cells demonstrated an asymmetric preference for either negative or positive voltage pulses (**Fig. 3**). Additionally, ganglion cell responsiveness decreased with increased interelectrode distance out to around 800µm from the site of stimulation. Finally some cells in *rd10* retina showed an initial suppression of spontaneous activity upon epiretinal stimulation.

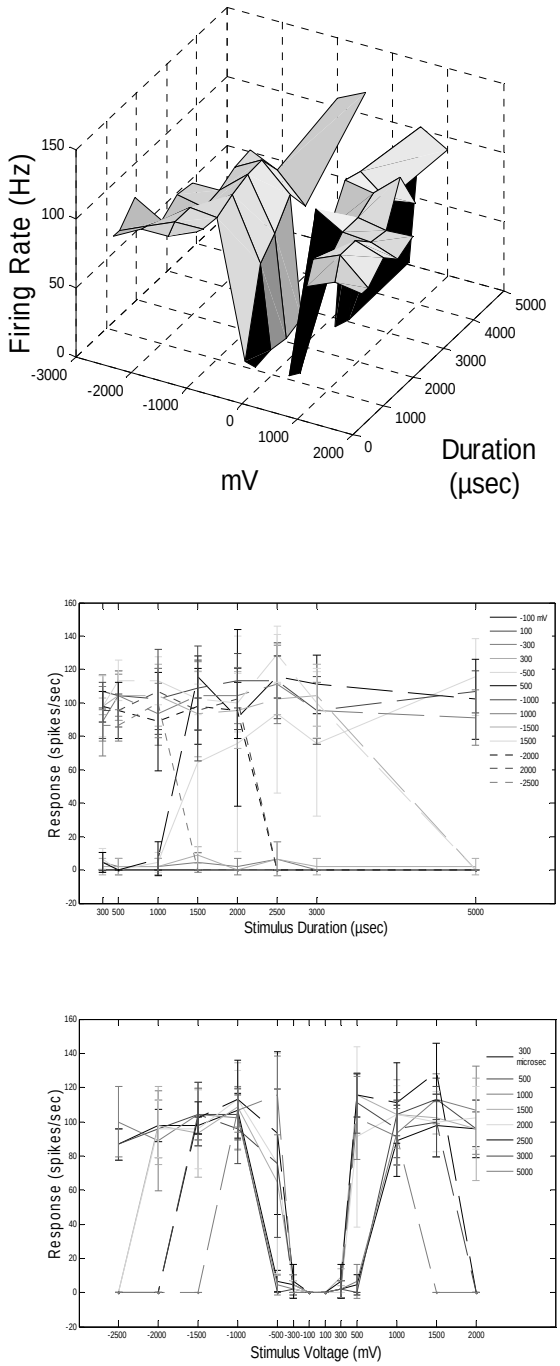

Fig. 2. Sample voltage-duration response functions for an *rd10* retinal ganglion cell.

4 Conclusion

Our preliminary findings present one of the first examinations of electrical stimulation in rd10 retina. Based on these findings, we propose tentative stimulation parameters appropriate for activation of rd10 retina. The relevance of our results to the continued development of efficient stimulation protocols for retinal prostheses is examined.

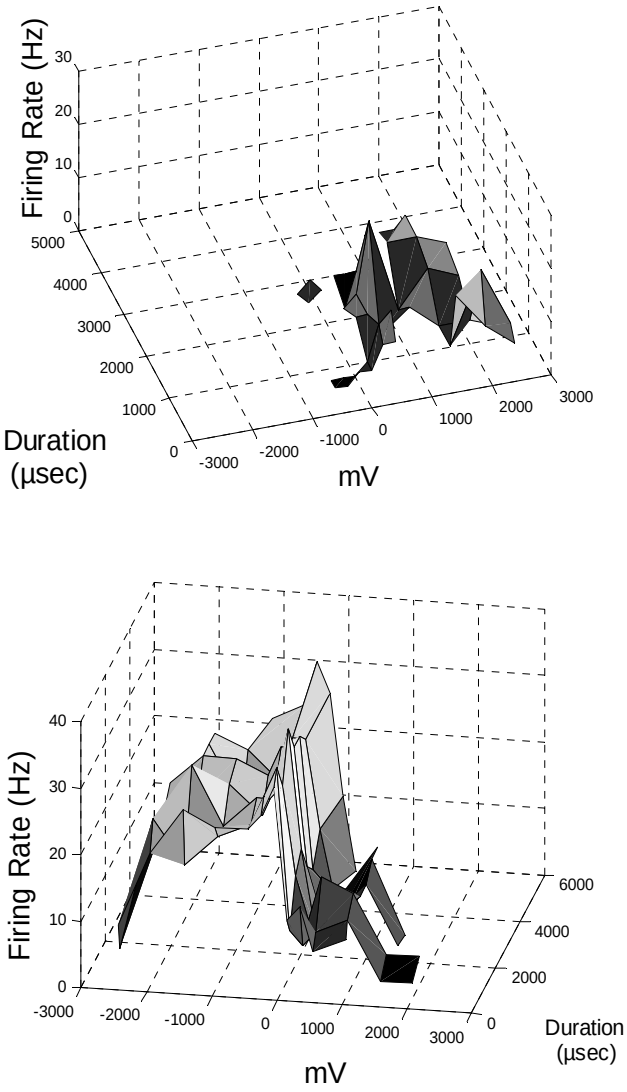

Fig. 3. Asymmetric voltage responses.3D plots showing asymmetric voltage responses to cathodic and anodic pulses in *rd10* retinal ganglion cells.

Acknowledgements

- BMBF;KFZ;01G1002
- Tistou and Charlotte Kerstan Foundation
- CIN(DFG EXC307,2011-07)

References

[1] Zrenner et al 2011 ''Subretinal electronic chips allow blind patients to read letters and combine then to words'' Proc.R.Soc.B

[2] Eckhorn R Stett A Schanze T Gekeler F Schwahn H Zrenner E Wilms M Eger M Hesse L Physiologische funktions Ophthalmologe 2001

[3] Goo et al.2011 Spontaneous Oscillatory rythm in retinal activities of two retinal degeneration (*rd1 and rd10*) mice

Population coding strategy during retinal adaptation

Xiao Lei[1], Wu Si[2], Liang Pei-Ji[1*]

1 Department of Biomedical Engineering, Shanghai Jiao Tong University, Shanghai, China
2 State Key Laboratory of Cognitive Neuroscience & Learning, Beijing Normal University, Beijing, China
* Corresponding author. E-mail address: pjliang@sjtu.edu.cn

Abstract
Neuronal responses to external stimuli attenuate over time when the stimuli remain invariant. Based on multi-electrode recording system, through simultaneously recording the activities of a subtype of bullfrog's retinal ganglion cells (dimming detectors) in response to sustained dark stimulations, we measured how the stimulus information encoded in firing rate and neural correlation changed over time, and found that there existed a transition in the coding strategy during the adaptation, i.e., at the early stage of the adaptation, the stimulus information was mainly encoded in the firing rate; whereas at the late stage of the adaptation, it was more encoded in the synchronized activities. Our results suggest that in encoding a sustained stimulation, the neural system can adaptively utlize concerted, but less active, neuronal responses to encode the information, a strategy which may be economically efficient.

1 Introduction

One of the principle goals in vision research is to elucidate how visual system encodes, decodes and transfers external information. It has been proposed that concerted activity among visual neurons is an important element of signal transmission [1]. On the other hand, adaptation is widely observed in visual activities in responses to sustained stimulations [2]. The mechanisms and properties of adaptation have both been intensively studied [2-4]. However, study about how the visual system encodes information during adaptation process is still lacking.

By using a multi-electrode recording system, we simultaneously recorded the activities of bullfrog retinal ganglion cells (RGCs) in response to sustained dark stimulations. We measured the time-dependent properties of information representation during the adaptation process and decomposed the stimulus information into parts carried by firing rates and correlation [5]. Our results suggest that concerted activities between RGCs are essential and effective for visual information encoding during adaptation. Although at the early stage of the adaptation, the stimulus information was mainly encoded in firing rates, at the late stage of the adaptation, it was more encoded in neuronal correlation.

2 Methods

Experiments were performed on isolated bullfrog retinas. Bullfrogs were dark adapted for about 40 min before experiments. We used a multi-electrode array (MEA, MMEP-4, CNNS UNT, USA) to record RGCs' firing activities in response to the stimulus protocol, which was 15-s flickering pseudo-random images followed by 15-s light-OFF stimulation and repeated 20 times. All procedures strictly conformed to the humane treatment and use of animals as prescribed by the Association for Research in Vision and Ophthalmology.

Based on the recorded data, we used an information theory approach to measure the amount of the stimulus information encoded in the neural activities [5,6]. Stimulus information was decomposed into portions carried the firing rates of neurons, and the pair-wise correlation between neurons.

3 Results

Dimming detector is a special type of bullfrog RGCs, which respond to a large darkening or dimming stimulation [7]. In our experiments, the adaptive response of dimming detector to sustained dark stimulation was analyzed.

To generate repeatable and reliable adaptive behaviors, the retina was exposed to 15-s flickering pseudo-random checker-board followed by 15-s dark stimulation (Fig. 1A). At the onset of the dark stimulation, the firing rate of the dimming detector first increased dramatically and then decreased gradually to a low level close to the background activity (Fig. 1B). The whole adaptation process lasted for about 5 seconds, then the firing of these cells ceased due to response characteristic of dimming detectors. In our study, we focused on this 5-s adaptation process.

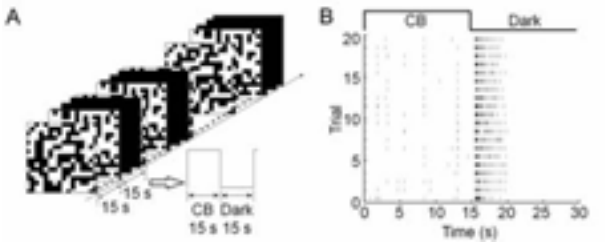

Fig. 1. Adaptation process of dimming detector. (A) The stimulation protocol. CB represents checker-board. (B) The raster plot of the activities of a dimming detector in 20 trials.

The information ratio contributed by the firing rate and synchronized correlation (SC) of 20 neuron pairs was compared during the adaptation. It is shown that the information ratio contributed by SC was less than 5% at the beginning (0 ~ 0.5 s) of neuronal response to dark stimulation, but was increased to more than 50% after about 2 s and remained high till the end of the adaptation (Fig. 2B).

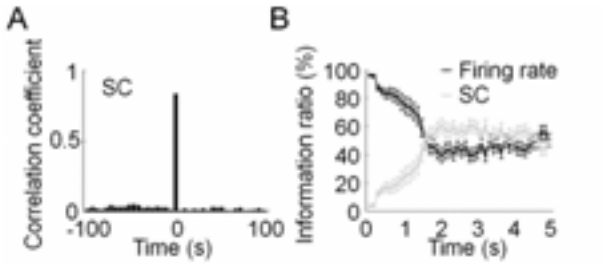

Fig. 2. Information encoding during adaptation. (A) An example of synchronized correlation between neurons (SC). (B) Information contained by firing rate and SC. Error-bars indicate ±SEM.

4 Conclusion

In summary, we investigated the dynamical nature of information representation during the retinal adaptation to a prolonged stimulation. Our results reveal that the attenuation of individual neurons' firing rates, a typical phenomenon associated with the luminance adaptation, is not a simple process of ignoring the sustained input, but rather indicates a dynamical transition from the independent firing rate coding to the correlated population coding. The latter encodes the stimulus information by using the concerted, low firing of neurons, and hence is economically more efficient.

Acknowledgement

We thank X.W. Gong and H.Q. Gong for important technical assitance. This work was supported by grants from National Fundation of Natural Science of China (No. 61075108, P.J.L.), The National Basic Reasearch Program of China (No. 2011CBA00406, S.W.) and Special Fund for Graduate Student Innovation Ability Training of Shanghai Jiao Tong University (L.X.).

References

[1] Shlens J, Rieke F, Chichilnisky EJ (2008) Synchronized firing in the retina. *Curr Opin Neurobiol 18:396-402.*

[2] Baccus SA, Meister M (2002) Fast and slow contrast adaptation in retinal circuitry. *Neuron 36:909-919.*

[3] Chander D, Chichilnisky EJ (2001) Adaptation to temporal contrast in primate and salamander retina. *J Neurosci 21:9904-9916.*

[4] Kim KJ, Rieke F (2003) Slow Na^+ inactivation and variance adaptation in salamander retinal ganglion cells. *J Neurosci 23:1506-1516.*

[5] Oizumi M, Ishii T, Ishibashi K, Hosoya T, Okada M (2010) Mismatch decoding in the brain. *J Neurosci 30:4815-4826.*

[6] Wu S, Nakahara H, Amari S (2001) Population coding with correlation and an unfaithful model. *Neural Comput 13:775-797.*

[7] Jing W, Liu WZ, Gong XW, Gong HQ, Liang PJ (2010) Influence of GABAergic inhibition on concerted activity between the ganglion cells. *Neuroreport 21:797-801.*

Characterization of retinal ganglion cell types in OPA-mice

Reinhard Katja[1,2], Gonzalez Menendez Irene[3], Wissinger Bernd[3], Münch Thomas[1,2*]

1 Centre for Integrative Neuroscience, Eberhard Karls Universität, Tübingen (Germany)
2 Bernstein Center for Computational Neuroscience, Tübingen (Germany)
3 Institute for Ophthalmic Research, Universitätsklinikum, Tübingen (Germany)
* Corresponding author. E-mail address: thomas.muench@cin.uni-tuebingen.de

1 Background/Aims

Autosomal dominant optic atrophy (adOA) is a progressive disease which leads to visual acuity loss, central and color vision defects, and optic disc pallor. The Opa1$^{enu/+}$ mouse is a model for adOA and carries a mutation in the optic atrophy gene 1 (OPA1) [1]. OPA1 is a ubiquitously expressed GTPase, which plays a major role in mitochondrial fusion. However, Opa1$^{enu/+}$ mice show mostly an ocular phenotype, characterized by slow, progressive loss of retinal ganglion cells (RGCs). A loss of >60% of RGCs in 1 year old mice was detected in histological studies [2]. However, except for electroretinography (ERG), no measurements of the effect of this mutation on retinal function have been performed.

The retina performs first processing steps of light stimuli. After activation of photoreceptors (rods and cones), the information is transmitted to intermediate neurons and eventually to RGCs, which transmit the processed visual stimulus to the brain. Many different RGC types exist and can be classified based on their functional properties such as response to light increment/decrement, transient/sustained activity, preferred direction and frequency of light stimuli etc.

The aim of this study is the functional characterization of RGC types in mutant (Opa1$^{enu/+}$) and wildtype (Opa1$^{+/+}$) mice in order to determine which RGC types are primarily affected by the mutation.

2 Methods

We used a perforated 60-electrode MEA (Multichannel Systems) with an electrode diameter of 30 µm and 200 µm spacing. 3-4 mutant and wildtype mice of each age group (1, 6, 12, 18 months) were dark-adapted. The retina was extracted from the eye bulb, placed ganglion cell-side down on the MEA, and the photoreceptors were stimulated with different light stimuli including full-field flashes of various intensities, bars moving in different directions or velocities, moving sine gratings, white noise flicker, and natural movies. This stimulus batch was repeated at different absolute brightness, starting with scotopic conditions (only rods active), and then switching to mesopic (rod and cones) and photopic (cones only) conditions. The RGC responses, i.e. the retinal output, were recorded, followed by semi-automated spike extraction and clustering (Offline Sorter, Plexon). Spike clustering based on amplitude and principal component analysis lead to "units" containing spike time-stamps originating from a single RGC. For each unit, we analyze the responses to each stimulus and extract one or several characteristic response parameters. Finally, we compare the units, i.e. the RGC types, found in mutant and wild type retinas.

3 Results

In our perforated-MEA recordings we obtain good signal-to-noise ratios for mouse retinas. Up to five different units can be detected on each active channel, of which we normally are able to extract one to two units. Recordings from mutant and wildtype mice are currently processed and analyzed.

4 Conclusion

About 25-30 clean units can be extracted from a single mouse retina with a 60-electrode MEA and about 20 additional multiunits can be separated from noise. With the described technique, we expect to successfully classify RGC types, and thereby to identify the types which are affected by the Opa1-mutation.

References

[1] Alavi M.V., Bette S., Schimpf S., Schuettauf F., Schraermeyer U., Wehrl H.F., Ruttiger L., Beck S.C., Tonagel F., Pichler B.J., Knipper M., Peters T., Laufs J., Wissinger B. (2007). A splice site mutation in the murine Opa1 gene features pathology of autosomal dominant optic atrophy. *Brain*, 130, 1029-42.

[2] Heiduschka P., Schnichels S., Fuhrmann N., Hofmeister S., Schraermeyer U., Wissinger B., Alavi M.V. (2010). Electrophysiological and Histologic Assessment of Retinal Ganglion Cell Fate in a Mouse Model for OPA1-Associated Autosomal Dominant Optic Atrophy. *Investigative Ophthalmology & Visual Science*, 51, 1424-31.

Light response patterns in silenced rd1 mouse retinal ganglion cells

Kosmas Deligkaris[1,2*], Jun Kaneko[3], Michele Fiscella[4], Jan Müller[4], Ian L. Jones[4], Andreas Hierlemann[4], Masayo Takahashi[3], Urs Frey[1,2]

1 RIKEN Quantitative Biology Center, Kobe, Japan
2 Osaka University, Graduate School of Frontier Biosciences, Osaka, Japan
3 RIKEN Center for Developmental Biology, Kobe, Japan
4 ETH Zurich, Department of Biosystems Science and Engineering, Basel, Switzerland
* Corresponding author. E-mail address: deligkaris@riken.jp

Abstract
Retinitis Pigmentosa, a retina disease, results in photoreceptor loss, retina circuitry remodelling and various electrophysiological alterations of retinal cells. In addition, the increased spontaneous activity of Retinitis Pigmentosa mouse-models (rd1) retinae hampers the assessment of preserved light stimulation responsivity. We aim at identifying ways of reducing the spontaneous activity of rd1 mouse retinae while preserving light stimulation responses.

1 Background

Retinitis Pigmentosa (RP) results in photoreceptor loss, retina circuitry remodelling and electrophysiological changes of cells [1]. To apply vision restoration techniques (e.g., stem-cell derived photoreceptor transplantation [2]) one needs to consider these changes, which requires a detailed understanding of the electrophysiological behaviour of degenerating retinae. However, increasing spontaneous activity hampers the detection and analysis of light responses in degenerating retinae. Using a high-density CMOS-based microelectrode array (HDMEA) [3], we investigated light responses from silenced rd1 mice retinae for the analysis of electrophysiological changes during degeneration.

2 Methods and Materials

2.1 Retina preparation

Three- and nine-week-old mice were sacrificed, and neural retinae were extracted. Animal procedures followed the RIKEN guidelines, and experiments were performed under dim red light.

2.2 Optical stimulation setup

A microscope (Olympus BX51), equipped with a projector set-up (Fig. 1), was used for optical stimulation. The retina on the HDMEA chip was perfused with recording solution containing (in mM); 120 NaCl, 3.1 KCl, 23 NaHCO3, 0.5 KH2PO4, 6 Glucose, 1 MgSO4 2 CaCl2 and 0.004% phenol red. A membrane held the retina in place, and a coverslip provided a suitable air/liquid interface, allowing for light projection.

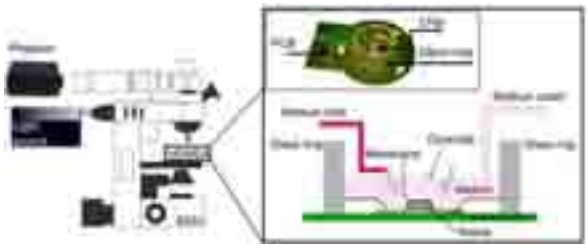

Fig. 1. Light stimulation set-up. A microscope was equipped with a projector, and the HDMEA chip (inset) was placed on the stage. A custom-built perfusion system was integrated. A membrane holds the retina on top of the electrodes, and a coverslip provides a suitable liquid/air interface.

2.3 Data analysis

Extracellular action potentials were recorded from retinal ganglion cells (RGC) with the HDMEA. All signals were bandpass-filtered within a range of 300-3000 Hz. Spike threshold was set to five times the rms noise. Mean firing rates (MFR, spikes/minute) were calculated from the total activity of 120 HDMEA channels. Raster plots were used to reveal activity patterns. Light responses were visually observed to identify ON-like and OFF-like responses.

2.4 Experiments

First, we increased inhibition in order to silence the RGC, while preserving light responses. We applied a GABA transaminase inhibitor to nine week-old rd1 mouse retinae, up to 16mM. Experiments included a baseline and a washout phase. Spontaneous activity was recorded for ten minutes, while the first five minutes were not used for data analysis.

In a next step, we tested the light responses of silenced three week-old rd1 mouse retinae. A uniform

blue light pattern (approximately 1.6 x 1.6 mm^2) was projected on the retinal sample for two seconds.

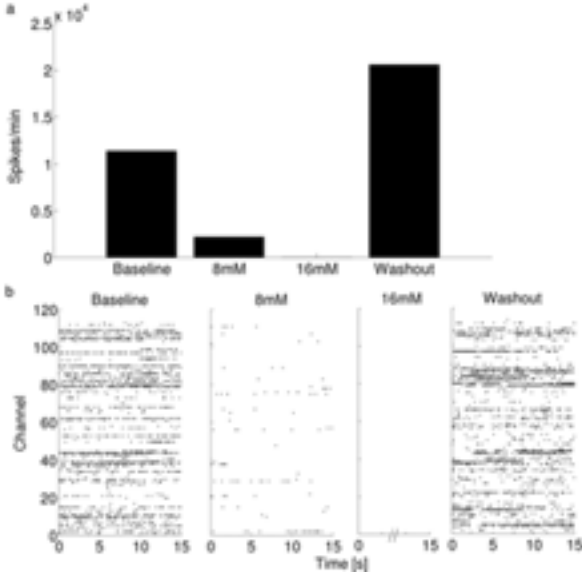

Fig. 2. Increasing inhibition by means of a GABA transaminase inhibitor eliminated spontaneous activity in nine week-old rd1 mouse retinae; (a): mean firing rates (spikes/min.) during the four experimental phases (baseline, 8mM, 16mM, and washout) during application of the GABA transaminase inhibitor; (b): raster plots of all phases. Fifteen seconds are shown for each phase. 120 channels of the HDMEA were used. Each phase lasted ten minutes; the first five minutes were not included in data analysis.

Manual inspection revealed ON-like and OFF-like responses. The repeatability of an ON-like light response was evaluated by projecting the same light pattern three times, with at least five-minute intervals in between to allow for opsin recovery.

3 Results

16mM of a GABA transaminase inhibitor eliminated the spontaneous activity of nine week-old rd1 mice retinae (Fig. 2). The silenced, degenerated retinae maintained partial light responsivity (Fig. 3 for three week-old retinae). ON-like responses featured increased latency (Fig. 3a). The first ON-like response to the same stimulus was faster than subsequent responses (Fig. 3b). Finally, all identified cells showed temporally sustained responses.

4 Conclusions/Summary

Light responses of silenced three-week-old rd1 mouse retinae revealed increased latency mainly for ON-like responses. Such disproportional degeneration was also seen by Stasheff [1], at P14-15, although no reliable light responses were observed after P21. We silenced the increasing aberrant spontaneous activity, while maintaining partial light responses in retinae of a mouse model of photoreceptor degeneration. The high resolution capabilities of the HDMEA will allow further quantitative analysis of electrophysiological properties during retina degeneration in early and late disease stages.

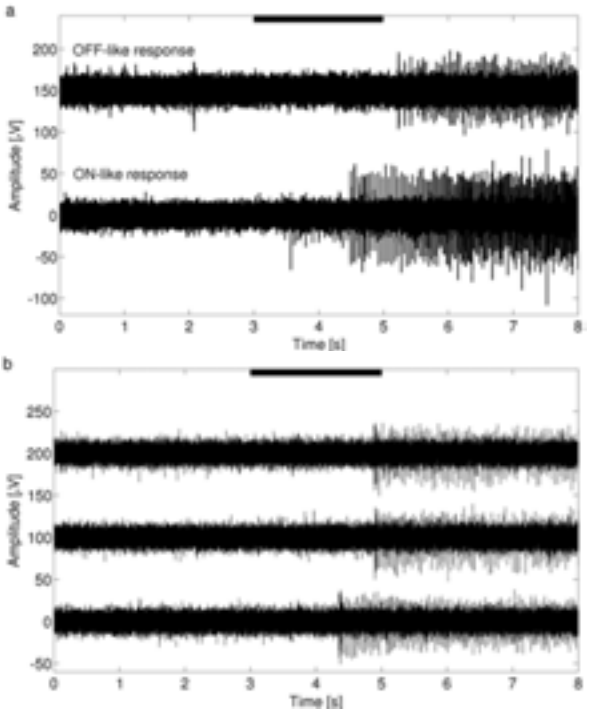

Fig. 3. Light stimulation: OFF-like and ON-like responses in silenced three week-old rd1 mouse retinal ganglion cells; the thick black lines at the top mark light exposure. (a): OFF-like (top) and ON-like (bottom) responses recorded from ganglion cells. (b): projection of the same stimulus three times reliably evoked ON-like responses at different response times. Data for each of the three trials are shifted by 100 µV.

References

[1] Stasheff S.F. (2008). Emergence of sustained spontaneous hyperactivity and temporary preservation of OFF responses in ganglion cells of the retinal degeneration (rd1) mouse. *Journal of Neurophysiology*, 99, 1408-1421.

[2] Osakada F., Ikeda H., Mandai M., Wataya T., Watanabe K., Yoshimura N., Akaike A., Sasai Y., Takahashi M. (2008). Toward the generation of rod and cone photoreceptors from mouse, monkey and human embryonic stem cells. *Nature Biotechnology*, 26, 215-224.

[3] Frey U., Sedivy J., Heer F., Pedron R., Ballini M., Mueller J., Bakkum D., Hafizovic S., Faraci F.D., Greve F., Kirstein K., Hierlemann A. (2010). Switch-matrix-based high-density microelectrode array in CMOS technology. *IEEE Journal of Solid-State Circuits*, 45 (2),467–482.

Versatile light stimulation of guinea pig retina with a laser system

Thoralf Herrmann[1] , Martin Schwarz[2], Gert Rapp[2] , Günther Zeck[1*]

1 NMI Natural and Medical Sciences Institute, Reutlingen, Germany
2 Rapp Optoelectronics GmbH, Hamburg, Germany
* Corresponding author. E-mail address: guenther.zeck@nmi.de

Abstract
Retina samples from guinea pigs were stimulated with light patterns presented by a laser system to identify different response types. Functional characterisation of the retinal ganglion cells showed sustained ON, transient ON and OFF behaviour. The activity of individual cells also depended on the size and the duration of the laser stimuli.

1 Background/Aims

The physiological characterization of electrical response properties in mammalian retina is aided by the use of microelectrode arrays and by versatile light-stimulation protocols [1]. Classical functional description of retinal ganglion cell responses is based on the increase or decrease of electrical activity upon incremental or decremental light stimuli (ON vs. OFF cells), on the response duration (transient vs. sustained) or the response latency (brisk vs. sluggish). However, these response properties are not mutually exclusive if different stimuli (small vs. full field, short vs. long) are presented to the same cell. Here we present first experiments that are aimed towards a complete mapping of ganglion cell responses to spatially, temporal and light-intensity modulated stimuli.

2 Methods

Ex vivo retinas from guinea pigs were prepared following the description given in [1]. A portion of the whole mount retina was interfaced ganglion cell side down on a Microelectrode Array (MEA 60, TiN electrodes, diameter 30µm, pitch 200µm, ITO lead). Light-induced ganglion cell action potentials were recorded extracellular with a MEA system (bandwidth 0.3 – 3.0 kHz, sampling rate 25 kHz). Voltage waveforms were analyzed offline and assigned to corresponding units using Offline Sorter (Plexon). Here, ganglion cell activity was assessed using raster plots and post-stimulus-time-histograms (PSTHs) of the action potential's timestamps. Light stimulation (diode laser, 473 nm) was performed using a digital mirror device (DMD) that was coupled through an optical fibre to the microscope fluorescence port (Zeiss Axiovert 200). Arbitrary stimuli could be selected by custom software. The stimulus intensity in the objective's (10x) focal plane ranged between 50 µW/mm2 – 1.5 mW/mm2.

3 Results

Stimulation of the whole mount retina with an ultrashort (1 millisecond) bright (1.5 mW/mm^2) light pulse elicited different light responses in the ganglion cell population. The majority of neurons displayed either an ON transient or ON sustained response (**Fig.1a**). However, the activity of a few ganglion cells was inhibited over more than 500 milliseconds (**Fig.1a,** right panel). Stimulation of the same retinal portion using a long (1 second) light pulse of the same intensity revealed that ON and OFF polarities were preserved (**Fig. 1b**) but some transient cells now displayed a sustained behaviour (**Fig. 1b**, middle panel). A switch from sustained to transient response was observed when light responses following small spots (10 micron diameter) or full field flashes were compared (data not shown).

4 Summary

The presented combination of light-stimulation by a laser-powered DMD and extracellular recording by a microelectrode array (MEA) allows for fast functional screening of electrical response properties in the retina.

References

[1] Zeck G , Masland RH (2007) Eur.J.Neurosci. vol. 26(2), page 367-80.

Supported by a BMBF grant (FKZ: 0312038) to TH and GZ.

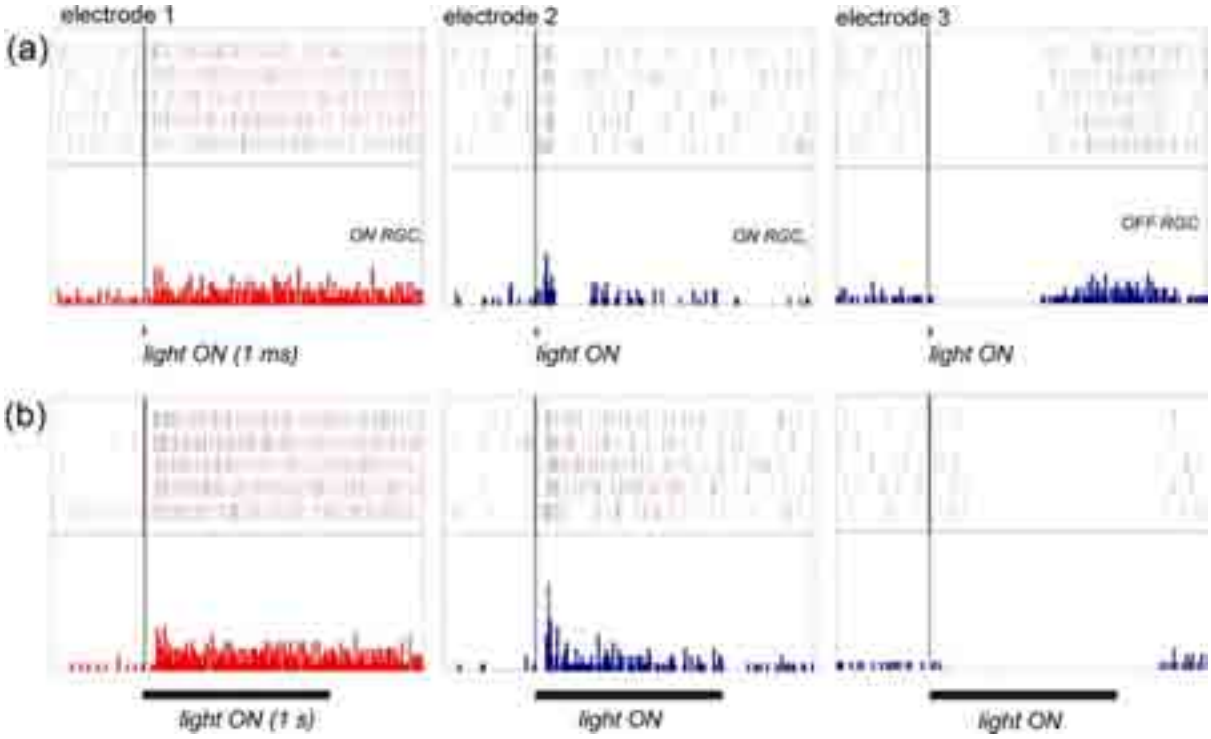

Fig. 1. Functional characterization of three retinal ganglion cells following light stimulation. Rasterplots (upper rows)/PSTHs (lower rows) of selected ganglion cells recorded on a 60 electrode microelectrode array (MEA).

(a) Light stimulation with a 1 millisecond full field incremental flash induces sustained ON (left panel), transient ON (middle) and OFF (right panel) behaviour in the selected cell. The vertical line marks the onset of the light stimulus. The stimulus was repeated five times. Red and blue ticks mark the occurrence of an action potential that is assigned to a ganglion cell recorded on the same electrode.
(b) Light stimulation with a 1 second long full field incremental flash induces sustained ON (left panel) and OFF (right panel) behaviour in the selected cells. The ON response (middle) becomes more sustained now. The presented ganglion cells were spatially separated by ~ 200 – 400 µm.

Effects of symmetric and asymmetric current stimuli on retinal ganglion cell (RGC) response modulation in retinal degeneration model (*rd1)* mice

Kun No Ahn[1,2], Wang Woo Lee[1,2], Yong Sook Goo[1,2,*]

1 Department of Physiology, Chungbuk National University School of Medicine, Cheongju, S. Korea
2 Nano Artificial Vision Research Center, Seoul National University Hospital, Seoul, S. Korea
* Corresponding author. E-mail address: ysgoo@chungbuk.ac.kr

Abstract

As a part of Korean retinal prosthesis project, we investigated effects of current stimuli on evoking RGC responses in degenerate retina for the long term goal of acquiring the optimal stimulation parameters for the upcoming prosthesis. Well-known animal model of RP, *rd1* mice were used for this study. In this study, we used both symmetric and asymmetric current pulses and compared the efficiency of both pulses on electrically-evoked RGC response modulation.

1 Introduction

Retinal prosthesis has been developed for the patients with retinitis pigmentosa (RP) and age related macular degeneration (AMD), and is regarded as the most feasible method to restore vision. Extracting optimal electrical stimulation parameters for the prosthesis is one of the most important elements. Previously, we compared voltage pulse and current pulse, and proposed preliminary optimal stimulation parameters [1]. Here, we used charge balanced biphasic current pulse and we tested polarity effect of evoking RGC responses by using anodic (or cathodic) phase-1st biphasic pulse and compared the efficiency of symmetric and asymmetric pulse on RGC response modulation.

2 Material and Methods

2.1 Recording of retinal ganglion cell activity

The well-known animal model for RP, *rd1 (Pde6b^{rd1})* mice at postnatal 9 to 10 weeks were used. From the e*x-vivo* retinal preparation (n=15), retinal patches were placed ganglion cell layer down onto 8 × 8 MEA and retinal waveforms were recorded.

2.2 Electrical stimulation & data analysis

8 X 8 grid layout MEA (electrode diameter: 30 μm, electrode spacing: 200 μm, and impedance: 50 kΩ at 1 kHz) was used for stimulation and recording the ganglion cell activity. The 50 identical pulses consisted of symmetric or asymmetric current pulses were applied. For symmetric pulse, the amplitude (*a*) and duration (*d*) of pulse were the same, while for asymmetric pulse, a current pulse of amplitude *a* and duration *d*, followed immediately by a pulse of amplitude *a'* and duration *d'* (Fig. 1). Stimulation frequency was 1 Hz. For amplitude modulation, duration of the 1st pulse was fixed to 500 μs and the amplitudes of the 1st pulse (*a*) were modulated from 2 to 60 μA, while those of 2nd pulse (*a'*) were modulated from 2 to 10 μA. For duration modulation, amplitude of the 1st pulse (*a*) was fixed to 30 μA and the durations of the pulse (*d*) were modulated from 60 to 1000 μs. The amplitude of 2nd pulse (*a'*) was fixed to 10 μA, to avoid evoking substantial RGC responses and the durations of the 2nd pulse were modulated from 180 to 3000 μs (*d'*). The electrically-evoked retinal ganglion cell (RGC) spikes was defined as positive when the number of RGC spikes for 400 ms after stimulus was 1.3 times higher than that for 400 ms before stimulus in post-stimulus time histogram. By this definition, we included both short and long latency spikes. We fitted the amplitude modulation curve and duration modulation curve with sigmoidal function (y=(a-d)/(1+[(x/c)]^b), y=a/(1+[(x/b)]^c), respectively).

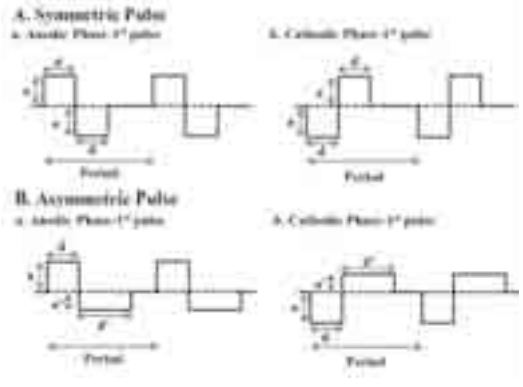

Fig. 1. Symmetric and Asymmetric biphasic pulse used in this study. (a) anodic phase-1st pulse, (b) cathodic phase-1st pulse.

3 Results

RGC responses were well modulated both with symmetric and asymmetric biphasic pulses. But the response patterns of amplitude modulation and duration modulation are different; in duration modulation curve (Fig. 2A), with cathodic phase-1st pulse, the modulation range is broader regardless of symmetric or asymmetric pulse. In amplitude modulation curve (Fig. 2B), cathodic phase-1st pulse shows better modulation curve with symmetric pulse not with asymmetric pulse.

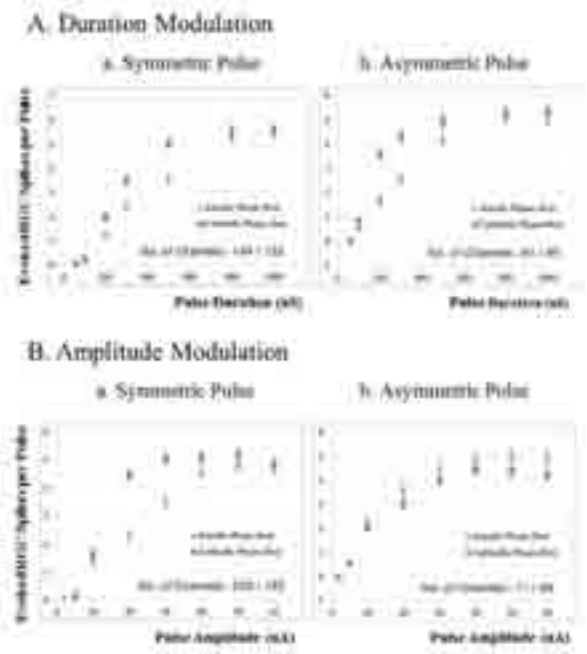

Fig. 2. Electrically-evoked RGC response curves (A) Duration modulation curve, (B) Amplitude modulation curve obtained with application of biphasic current pulses shown in Fig. 1.

4 Summary & Conclusion

The result showed that the RGC responses were well modulated both with symmetric and asymmetric pulse. In general, cathodic phase-1st pulse seems to be more effective in modulating RGC responses except amplitude modulation with asymmetric pulse.

Acknowledgement

This study was supported by grants from the Ministry of Health and Welfare (grant No. A050251), MEST (2009-0065444), and happy tech program of MEST (2010-0020852).

References

[1] Goo Y.S., Ye J.H., Lee S., Nam Y., Ryu S.B., Kim K.H. (2011). Retinal ganglion cell responses to voltage and current stimulation in wild-type and *rd1* mouse retinas. *J. Neural Eng.*, 8, 035003(12pp).

Stimulus discrimination of retinal ganglion cells influenced by firing synchronization

Hao Li, Pei-Ji Liang*

Department of Biomedical Engineering, Shanghai Jiao Tong University, Shanghai, China
* Corresponding author. E-mail address: pjliang@sjtu.edu.cn

Abstract

Our perception of visual environment relies on the capacity of neural population to encode and transmit the information in incoming stimuli. Studying how neural population activity influences the visual information processing is essential for understanding the sensory coding mechanisms. In the present study, by using multi-electrode array system (MEA), we simultaneously recorded spike discharges from a group of bullfrog's RGCs. To examine how synchronous activity between RGCs influenced stimulus discrimination, we evaluated the visual pattern discrimination performance via single neuron activity and synchronized sequence of multiple neurons. It was found that the enhancement in synchronous activity decreased the discrimination performance. Our result suggests that population activity exhibits distinct patterns in response to different stimuli, and the gap junctional connections contribute to the modulation of the neural network performance during visual process.

1 Introduction

Perception of the environment relies on the ability of neurons to transmit neuronal signals effectively and encode/decode environmental stimuli efficiently. Population activity of neurons is implicated in improving the transmitting and coding processes [1]. In the retina, correlated firing plays an important role in visual signal transmission from retina to the central visual part [2], and correlated activity among a large group of population can be reflected by the correlated activity between pair-wise neurons [3].

It is now clear that gap junctional connectivity between RGCs are highly plastic, which is effectively adjusted by the neuromodulator dopamine (DA) [4], resulting in the changes of gap junctional conductance, as well as the strength of synchronous activity [5]. One intriguing question comes from a consideration of how DA-induced changes in the gap-junctionally-coupled network affect the performance of neuron population in discriminating different spatial patterns.

The present study aimed to examine the role of synchronous activity of RGCs in stimuli discrimination and the DA-induced effects on the discrimination performance. It was found that the performance of single neuron activity did not exhibit obvious changes with and without exogenous DA application. The performance of multi-neuronal activity was related to the synchronization strength and the size of the synchronized network.

2 Methods

Bullfrogs were dark adapted for 30 minutes prior to the experiments. Isolated retinas were used for electrophysiological experiments in accordance with guidelines for the care and use of animals as prescribed by the Association for Research in Vision and Ophthalmology. We used a multi-electrode array (MEA60, MCS GmbH, Germany) to record RGCs' firing activities in response to the stimulus patterns. A trial of stimulus consisted of 3 different spatial patterns presented in random order: checkerboard (CB), horizontal gratings (GT) and full-field illumination (FF) (Fig 1). Each pattern was presented for 0.5 s with 1-s intervals. Totally 100 trials were displayed continuously with 1-s inter-trial-interval. The same stimulus was applied both in control experiment and with dopamine application.

To estimate the contribution of single neurons and neuron population to patterns discrimination, we performed the classification analysis using support vector machines method (SVMs) on single and synchronized sequences.

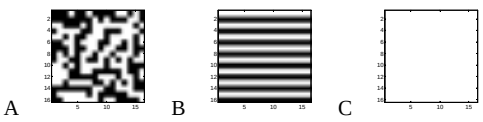

Figure 1. Three stimuli patterns used in the present study. A: Checkerboard (CB). B: Gratings (GT). C: Full-field illumination (FF).

3 Results

We presented bullfrog retina a series of repeated stimuli while multiple RGCs' responses were recorded with multi-electrode array system. Only those cells showed good stability and

ON-OFF transient responses were further investigated (Fig 2).

There was no obvious change in correct rate of stimulus discrimination during control and DA application, and the mean correct rate exhibited a slight but not significant decrease with DA application (0.683 ± 0.006 vs 0.673 ± 0.006, p = 0.118), suggesting that DA exerted no noticeable effect on single neurons in stimulus discrimination.

DA enhanced gap junctional connection between RGCs, and the synchronization strength of neuron pair was significantly increased by DA. The DA-induced increase in synchronization resulted in a decreasing tendency of correct rate (0.750 ± 0.007 vs 0.704 ± 0.007, **p < 0.001).

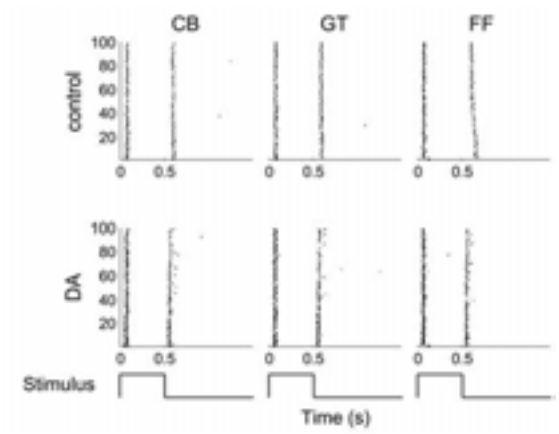

Figure 2. Typical responses of RGC to stimuli ON-OFF. Responses of a RGC evoked by checkerboard (CB), grating (GT) and full-field white (FW) in control and DA application (1 μM) respectively, with stimulus presented as 0.5s-ON and 1s-OFF and repeated 100 times. Each dot denotes a spike firing. (Bottom) Stimulus protocol.

4 Conclusion

The application of DA induced increase in synchronization strength between ganglion cells, but decreased the stimulus discrimination ability, which may be considered as a blurring-like effect in stimulus discrimination. These results suggested that the ability of neuron population in discriminating stimuli is influenced by the synchronized activity of RGCs, and DA probably contributes to the modulation in population coding.

Acknowledgement

We thank X.W. Gong and H.Q. Gong for important technical assitance. This work was supported by grants from National Fundation of Natural Science of China (No. 61075108).

References

[1] Brivanlou, I.H., D.K. Warland, and M. Meister, *Mechanisms of concerted firing among retinal ganglion cells.* Neuron, 1998. **20**(3): p. 527-39.

[2] Schnitzer, M.J. and M. Meister, *Multineuronal firing patterns in the signal from eye to brain.* Neuron, 2003. **37**(3): p. 499-511.

[3] Nirenberg, S. and P.E. Latham, *Decoding neuronal spike trains: How important are correlations?* Proceedings of the National Academy of Sciences of the United States of America, 2003. **100**(12): p. 7348-7353.

[4] Bloomfield, S.A. and B. Volgyi, The diverse functional roles and regulation of neuronal gap junctions in the retina. Nature Reviews Neuroscience, 2009. **10**(7): p. 495-506.

[5] Li, H., W.-Z. Liu, and P.-J. Liang, Adaptation-Dependent Synchronous Activity Contributes to Receptive Field Size Change of Bullfrog Retinal Ganglion Cell. PLoS ONE, 2012. **7**(3): p. e34336.

Measuring enteric neuronal activity with microelectrode arrays

Lisa Würner, Martin Diener*

Institute for Veterinary Physiology and Biochemistry, University Giessen, Germany
* Corresponding author. E-mail address: Martin.Diener@vetmed.uni-giessen.de

Abstract
The microelectrode array is a successfully established method to investigate electrophysiological properties of neurons. We adapted this technique for enteric neurons and measured the effect of the inflammatory mediator bradykinin.
Bradykinin leads to a triphasic change of excitability. The stimulation is mediated by B1-, as well as B2-receptors. It is likely that the expression of B1-receptors is driven by the procedure of cell culture. Prostaglandins are involved in the mediation of the effect of bradykinin.

1 Introduction

The enteric nervous system plays a crucial role in the regulation of intestinal functions such as epithelial ion transport, barrier function of the epithelium, blood flow in the mucosa or gastrointestinal motility [1]. Since microelectrode arrays (MEAs) have been successfully used to investigate the electrical properties of neurons of different origins, we wanted to apply this technique to enteric neurons, in particular myenteric neurons which control the motility of the gut.

Our interest is focused on the cross-talk between the immune system and the enteric nervous system, so we performed experiments with the potent inflammatory mediator bradykinin, which plays an important role in the genesis of inflammatory bowel diseases [2] .

2 Methods

Myenteric neurons were enzymatically isolated from newborn rats and plated on poly-L-lysin/laminin coated 200/30iR-Ti-MEAs (Fig.1). After an incubation period of one to three days action potentials were recorded. The administration of bradykinin and bradykinin-receptor agonists and antagonists was performed with a pipette. The measurement took place over a period of 12 minutes after the administration of the substance and the frequency of action potential was expressed as spikes per 30 seconds.

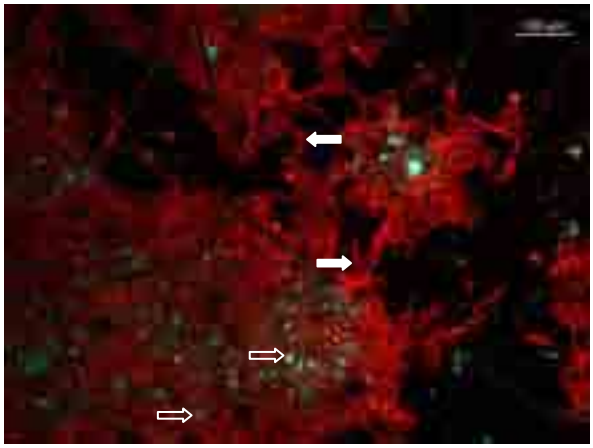

Figure 1: Myenteric ganglionic cells cultured on a MEA. Neurons are marked against MAP2 (green, open arrows) and glial cells against S-100 (red, filled arrows). Cell nuclei staining was performed with DAPI (blue). For better orientation, the immunohistochemical photo was merged with a light microscopical photograph of the same MEA depicting the positions of the electrodes relative to the cells.

3 Results

The myenteric neurons displayed a spontaneous activity which could be reversibly inhibited by tetrodotoxin (TTX) (Fig.2).

The addition of bradykinin led to a triphasic change of excitability, which consisted in a biphasic stimulation interrupted by an inhibitory phase (Fig.3).

Experiments with agonist and antagonists of bradykinin receptors showed that the constitutively expressed B2-receptor as well as the inducible B1-receptor is involved in this effect. Real-time PCR and immunohistochemistry confirmed this hypothesis.

In the presence of a cyclooxygenase inhibitor the effect of bradykinin was reduced.

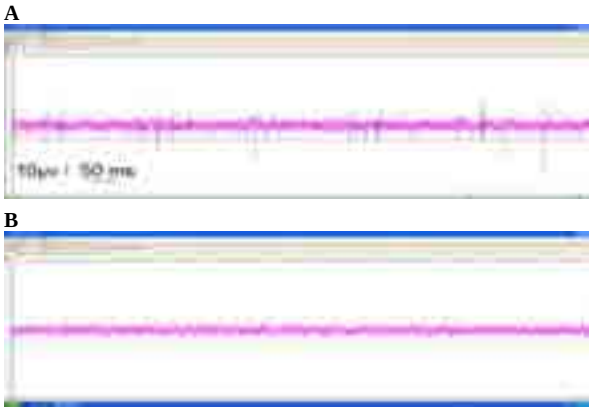

Figure 2 A+B: Original tracing of MEA-measurement of myenteric neurons with (B) and without (A) tetrodotoxin as blocker of voltage-dependent Na^+-channels.

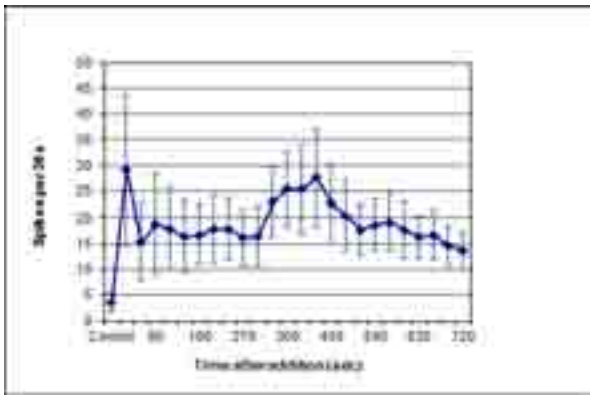

Figure 3: Influence of bradykinin on the electrical activity of myenteric neurons.
After measuring the baseline ("Control") bradykinin was added to the buffer solution and the frequency of action potentials in "spikes per 30 seconds" was detected for 720 seconds.
The graph shows the means ± SEM of 34 electrodes.

4 Conclusions

MEAs have been successfully established in different fields of neurosciences. In this study we show that MEAs are promising tools to investigate enteric neurons, too.

We examined the effect of the inflammatory mediator bradykinin on myenteric neurons.

Bradykinin leads to an excitation of myenteric neurons. This effect is mediated by B1- as well as B2-receptors, which allows the assumption that the inducible B1-receptor is upregulated during cell culture on the MEAs.

Due to the inhibition of the effect of bradykinin in the presence of a COX inhibitor it seems most likely that the effect of bradykinin is at least partly mediated by prostaglandins.

In future experiments the effect of bradykinin on inflamed tissue will be investigated.

Acknowledgement

We thank Bayer Health Care for the fellowship funding this project.

References

[1] Wood, J.D. (1999) : Fundamentals of neurogastroenterology. *Gut, 45 Suppl 2, II6-II16*

[2] Stadnicki, A. (2005) : Immunolocalization and expression of kinin B1R and B2R receptors in human inflammatory bowel disease. *Am. J. Physiol. Gastrointest. Liver Physiol., 289, G361-366*

Post stroke plasticity impairment and its dependence on interhemispheric interactions

Jan A. Jablonka

Warsaw University, Institute of Zoology, Animal Physiology Department
E-mail address: j.jablonka@nencki.gov.pl

Abstract
Brain activity desynchronisations after a focal cortical stroke are widely known. In rats the general activity level in both hemispheres is changed for at least one month. The unilateral stimulation of row B on the deprived side of the snout results in the visualized representation of the non-deprived row B widening. After focal cortical stroke the widening was no more observed. The results presented here show the bilateral widening of the homotopic areas of the rows B representations in the animals deprived for one month just after the stroke. This confirms our suspicion that the cortical plasticity impairment after stroke depends on the destabilization of interhemispheric interactions.

1 Introduction

Brain activity desynchronisations after a focal cortical stroke are widely known [1]. In rats the general activity level in both hemispheres is changed for at least one month [2]. The ischemic hemisphere suffers from diaschisis and in the same time the contralateral hemisphere activity is strongly up-regulated.

Rodent whisker representation in the somatosensory cortex has a highly somatotopic organization. Each whisker has its sensory representation in the area of the barrel field (BF) of the contralateral hemisphere (Fig. 1).

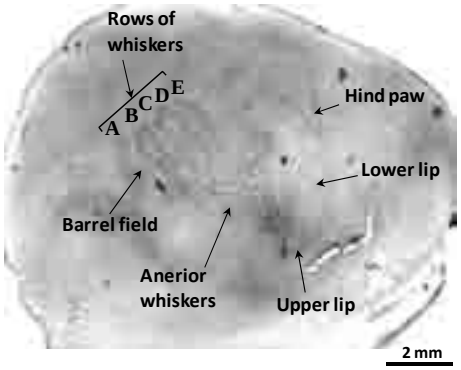

.

Fig. 1. Tangential section of the rat's brain stained for cytochrome oxidase (CO) activity.

Fig. 2. Row B representation visualised by the autoradiography of the [^{14}C]2DG incorporation on tangential sections.

One month unilateral, partial whiskers deprivation results in the row representation widening. The widening can be visualized by [^{14}C]-2 deoxyglucose (2DG) brain mapping (Fig. 2).

As we previously presented the widening extend depends on whether the unilateral or bilateral whiskers stimulation during brain mapping was performed [3]. When the deprivation starts just after the stroke the widening is no longer visible in the 2DG brain mapping with bilateral rows B whiskers stimulation [4].

This time I present the effect of unilateral whiskers stimulation during 2DG brain mapping in deprived rats after the focal cortical stroke.

2 Materials & Methods

2.1 Unilateral partial hiskers deprivation

Sensory deprivation was performed by trimming all the whiskers contralateral to the stroke except for the row B. The trimming was repeated every second day for one month.

2.2 Unilateral photothrombotic focal stroke in the cortex

Rats were anasthetised by 3% isoflurane/air mixture. The body temperature was controlled and sustained at the 36.5ºC ± 0.5˚C. A catheter (0.75 mm) was inserted into the rat's femoral vein. An incision was made down the midline of the head and the skull surface exposed and cleaned. An fibre-optic bundle mounted on a cold light source was placed stereotaxically on the exposed skull bone, with its light centre (Ø = 1.5 mm) 4.5 mm posterior to bregma, and 4 mm lateral to, the midline (aperture E/2; 2750K, KL 1500 LCD, Schott, Germany). The Rose Bengal (0.4 ml, 10 mg/ml; Aldrich 330000) was injected intravenously through a catheter implanted into the femoral vein and the skull surface was illuminated for 20 minutes.

2.3 The functional brain mapping

Brain mapping

After a month of vibrissae deprivation, the 2DG functional brain mapping were performed. The animals were put in a restrainer and the whiskers of the non-deprived side were cut close to the skin apart from row B. [^{14}C] – 2DG (7 µCi/100 g, American Radiolabeled Chemical, spec. act. 55 mCi/mmol; St.Louis, MO, USA) was injected intramuscularly. The whiskers of rows B were stroked unilaterally in rostro-caudal direction with frequency of 2Hz. After 30 minutes of stimulation, the rats were killed by i.p. Vetbutal (0.4 ml/100 g; Biovet, Pulawy, Poland) injection and perfused with 4% paraformaldehyde (Sigma-Aldrich; St.Louis, MO, USA). Then the brain was removed and the cortex of both hemispheres flattened between glass slides, frozen in heptane at -70°C. Hemispheres were cut on a cryostat at -20°C into 40 µm tangential sections, which were collected alternately on specimen slides and cover slips. The sections on cover slips were immediately dried and exposed on Kodak Mammography film for 2 weeks with a set of [^{14}C] standards (American Radiolabeled Chemicals; St.Louis, MO, USA). The remaining sections were stained for cytochrome oxidase (CO) activity to identify the barrel field.

Image analisis

The autoradiograms were analyzed by a computer image analysis program (MCID, Res Inc., Ontario, Canada). The software allows displaying an image of a stained section (from which the autoradiogram was obtained) and an adjacent cytochrome oxidase stained section which was superimposed on the autoradiogram so that the relations of the barrel field and the position of the stroke could be accurately determined (Fig. 1). The width of the 2DG labeled cortical representation of row B whiskers was measured on every section at three locations across the row. Pixels with 2DG-uptake intensity exceeding the mean of the surrounding cortex by more than 15 % were considered as labeled representations. Results tested first for the relatively equal widening within layers were averaged for all sections (layers II to VI) of one hemisphere.

3 Results and discussion

Results

The unilateral stimulation of row B on the deprived side of the snout (in contrast to bilateral whiskers stimulation) results in the visualized representation of the non-deprived row B widening by 25% (1156µm (unilateral) vs. 918µm (bilateral); $p<0.05$). However, the unilateral stimulation of the non deprived row B on the intact side of the snout results also in its representation widening when compared to the healthy deprived animals (1142µm vs 845µm; $p<0.05$) and the uni- vs. bilateral whiskers stimulation is pronounced (31%, 1142µm vs. 846µm; $p<0.05$).

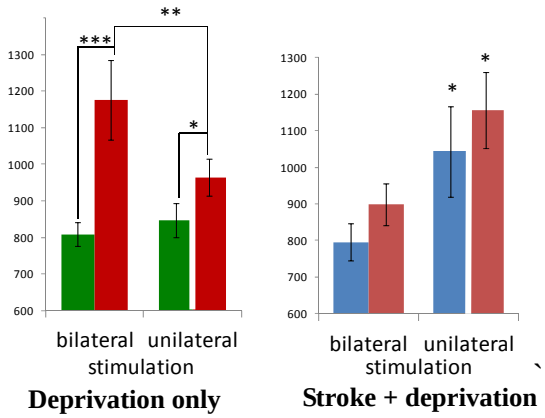

Fig. 3. The width of the 2DG incorporation in the rows B representations of the deprived and non-deprived hemispheares and its dependence on uni- vs. bilateral whiskers stimulation in the healthy and post stroke animals. * Mean ± SD; * P < 0.05

As the whiskers–barrel cortex connectivity is supposed to be completely crossed we may expect that the callosal connections interact with basic plasticity rearrangements and that the post stroke cortical activity remodelling and the interhemisferic activity balance results with abnormal experience-dependent plasticity mechanisms.

4 Conclusion/Summary

The results confirm our suspicion that the cortical plasticity impairment after stroke depends on the destabilization of interhemispheric interactions. The local field potential recording and the current source density analysis with simultaneous 2DG brain mapping will allow us to follow more precisely the signal transmission within the cortex during brain plasticity changes.

Acknowledgement

The research was supported by Polish Ministry of Science and Higher Education grant
0133/P01/2010/70

References

[1] Dijkhuizen R.M., Ren J, Mandeville J.B., Wu O., Ozdag F.M., Moskowitz M.A., Rosen BR, Finklestein SP. (2001): Functional magnetic resonance imaging of reorganization in rat brain after stroke. Proc Natl Acad Sci U S A. 98:12766-71.

[2] Jablonka, J.A., Burnat, K., Witte, O.W., and Kossut, M. (2010): Remapping of the somatosensory cortex after a photothrombotic stroke: dynamics of the compensatory reorganization. Neuroscience, 165, 90-100.

[3] Jablonka, J.A., Kazmierczak M., Olkowicz S., Rokosz K. (2011): Interhemispheric contribution in experience dependent plasticity. Society for Neuroscience 41th Annual Meeting, Washington, 12-16 Nov., Prog. 181.16/PP21.

[4] Jablonka, J.A., Witte, O.W., and Kossut, M. (2007). Photothrombotic infarct impairs experience-dependent plasticity in neighboring cortex. Neuroreport, 18, 165-169.

Modulation of neuronal network activities using magnetic force-based astrocytic network integration

Atsushi Saito[1], Lui Yoshida[1], Kenta Shimba[1], Aki Saito[1], Yuzo Takayama[2], Hiroyuki Moriguchi[1], Kiyoshi Kotani[1], Yasuhiko Jimbo[1*]

1 Graduate School of Frontier Sciences, University of Tokyo, Chiba, Japan
2 Graduate School of Information Science and Technology, University of Tokyo, Tokyo, Japan
* Corresponding author. E-mail address: jimbo@k.u-tokyo.ac.jp

Abstract
In order to establish widespread neuronal and glial cell interaction in culture, we attempted the magnetic nanoparticles (MNPs)-based 3-Dimensional neuronal and astrocytic network construction. Here, the monolayer neuronal networks were covered with MNPs-injected astrocytes by using external magnetic force, and evaluated the modulation of spontaneous activities by using microelectrode arrays (MEAs). As a result, we observed the time-dependent modulation of synchronized periodic bursting activities during 48 hours culture. Therefore, the results suggested the spontaneous activities of neuronal networks were modulated by astrocytic networks.

1 Introduction

To reveal the complex brain function, the investigation of neuron-glia interaction is one of the important themes. Actually, it is known that synaptic transmission is modulated by an astrocyte in the pre- and postsynaptic terminal [1, 2], and its phenomenon is related with the synaptic activity and plasticity [3, 4]. However, until now, the modulation of network-wide neuronal activities depending on neuronal and glial cell interaction was not understood. Furthermore, an astrocyte makes an activation spread to the surrounding astrocytes through gap junctions [5], and these activations interact with the wide scale neuronal network activity [6]. Therefore, it is necessary to evaluate functional connections between neuronal networks and astrocytic networks. Here, in this study, we discussed the 3-Dimensional co-culture method for network-wide interaction of neurons and astrocytes by using the magnetic nanoparticles (MNPs)-injected astrocytes (MNPs-AS) and the external magnetic force. In addition, we evaluated the time-dependent modulation of spontaneous activities of MNPs-AS integrated neuronal networks by using MEAs during stable stage of neuronal network activities.

2 Materials and Methods

The schematic view of the methods of 3-Dimensional astrocytic network integration on the monolayer neuronal network is shown in Fig.1. Briefly, the methods described below. The neuronal and glial cells were dissociated from E18-19 rat cortical tissue by using trypsin-EDTA, and some of these cells cultured on the MEAs or the polystyrene dishes. Here, to separate the neuronal cells and astrocytes during MNPs injection, neuronal cells cultured on polystyrene dishes were killed by cold medium stimulation (4℃, 10 min) and subculture. Next, magnetically-collected MNPs-AS were re-plated on the cultured monolayer neuronal networks by using the magnetic-hold device which was set up under the MEAs dish. After MNPs-AS integration on the monolayer neuronal networks, the spatiotemporal patterns of spontaneous electrical activities were evaluated by the extracellular recording using MEAs during network reconstruction.

Fig. 1. Schematic view of 3-Dimensional integration of astrocytes on the monolayer neuronal networks by using MNPs-As and external magnetic force.

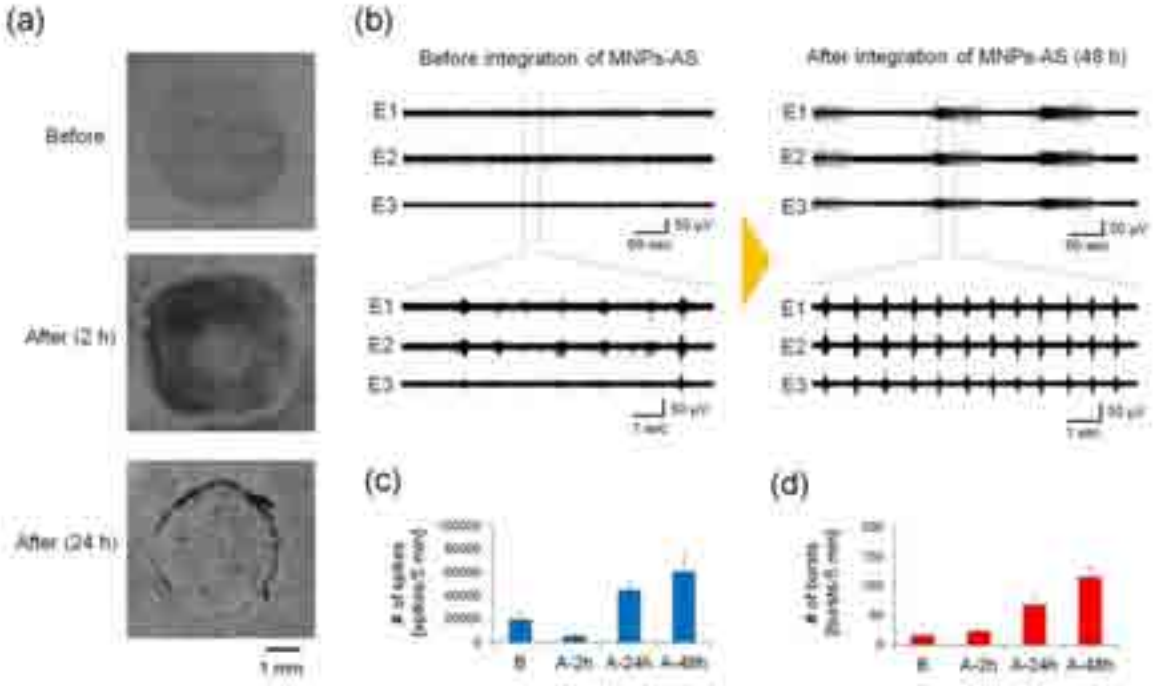

Fig. 2. Morphological changes of neuronal networks and modulation of neuronal network activities by MNPs-AS integration. Time-dependent changes of (a) morphologies (0, 2, 24 h) and (b) spontaneous activities (0 and 48 h). Number of (c) spikes and (d) synchronized periodic bursting activities during MNPs-AS integration. (N=4, ±SD).

3 Results and Discussion

The time-dependent (0, 2, 24 hours) morphological changes of 3-Dimensional neuronal networks which applied MNPs-AS integration were shown in Fig. 2 (a). These images showed the astrocytes were able to integrate on the monolayer neuronal networks with high-density by external magnetic force after 2 hours culture. And the obvious morphological changes of integrated MNPs-AS were observed during 24 hours culture. Here, the time-dependent changes of the wave forms of spontaneous electrical activities after MNPs-AS integration were shown in Fig.2 (b). These results indicated the spatiotemporal patterns of spontaneous activities were widely modulated during 48 hours culture. In particular, the spontaneous synchronized bursting activities were organized to the periodic bursting activities in the whole of MNPs-AS integrated area. And the quantitative results of time-dependent changes of spontaneous activities were shown in Fig. 2 (c) and (d). In these results, the decrease of spike frequencies observed at 2 hours culture. However, the synchronized bursting activities were highly increased at 2 to 48 hours culture. In addition, the number of bursting activities was increased during culture period.

Therefore, these results suggested the monolayer neuronal network activities were modulated by MNPs-AS integration. And the spontaneous activities were activated and organized by high-frequency synchronized bursting activities during MNPs-AS integration.

4 Conclusion

In this study, we observed network-wide modulation of spontaneous activities by using MNPs-injected astrocytes and magnetic force-based 3-Dimensional co-culture method. These results revealed the astrocytic networks were interacted with the neuronal networks related with its spontaneous activities.

Acknowledgement

This study was supported by Japan society for the promotion of science (JSPS).

References

[1] Newman E. A. (2003). New roles for astrocytes : Regulation of synaptic transmission. *Trends Neurosci*, 26, 536-542.
[2] Eroglu C., and Barres B. A. (2010). Regulation of synaptic connectivity by glia. *Nature*, 468, 223-231.
[3] Koizumi S., Fujishita K., Tsuda M., Shigemoto-Mogami Y., and Inoue K. (2003). Dynamic inhibition of excitatory synaptic transmission by astrocyte-derived ATP in hippocampal cultures. *Proc Natl Acad Sci USA*, 100, 11023-11028.
[4] Pannash U., Vargova L., Ezan P., Holcman D., Giaume C., Sykova E., and Rouach N. (2011). Astroglial networks scale synaptic activity and plasticity. *Proc Natl Acad Sci USA*, 108, 8467-8472.
[5] Scemes E., and Giaume C. (2006). Astrocyte calcium waves: what they are and what they do. *Glia*, 54, 716-725.
[6] Fellin T. (2009). Communication between neurons and astrocytes: relevance to the modulation of synaptic and network activity. *J Neurochem*, 108, 533-544.

A network of weakly coupled oscillators in the ventral tegmental area

Luuk van der Velden*, Martin Vinck, Taco R. Werkman and Wytse J. Wadman

SILS-CNS at Science Park, University of Amsterdam, Amsterdam (The Netherlands)
* Corresponding author. E-mail address: l.j.j.vandervelden@uva.nl

Abstract

The ventral tegmental area (VTA) is implicated in a synchronizing loop with the prefrontal cortex and the hippocampus [1]. In-vivo, but also in-vitro, the VTA is characterized by spontaneously firing dopaminergic neurons (frequency 1-4 Hz). It is not clear whether these neurons operate in isolation or whether they form a large (partly) synchronized network. Recording simultaneously from a large population of VTA neurons using 3D MEAs allows investigation of this question. Here we describe analysis techniques aimed at quantifying the level of coupling and synchronization of multiple (>20) dopaminergic neurons in the local VTA network.

1 In vitro ensemble recordings

In acute brain slices the substantia nigra and VTA can be readily identified by colour and shape. When positioned on 3D MEA60 chips more than 20 spontaneously active dopaminergic neurons can be stably recorded for several hours (Fig. 1). Interneurons (recognized by higher firing rates and lack of dopamine receptors) are rarely picked up, probably due to their small soma size, which leads to low amplitude spikes with a small signal to noise ratio. The spikes of the principle cells can be transformed to point processes and an analysis of the relationship between these spike trains allows us to determine the coupling state in the network.

2 Methods

2.1 Preparation and recording

Acute brain slices (300 μm), that contained the VTA, were prepared from male Wistar rats [2] and positioned on a 3D MEA-60 chip (Qwane inc.) under slight magnification. The slice was submerged at all times in artificial cerebral spinal fluid (composition in mM: NaCl 120; KCl 3.5; $MgSO_4$ 1.3; NaH_2PO_4 1.25; $CaCl_2$ 2.5; D-glucose 10; $NaHCO_3$ 25), perfused at 2 ml/s and kept at 32 °C (bubbled with 95% O_2 / 5% CO_2). The recording of the spontaneous baseline activity in the network lasted up to 1 hour to ensure acclimatization of the slice to the recording conditions. The D_2-receptor agonist quinpirole (1 μM) was used to identify dopaminergic neurons as the induced hyper-polarization quickly and completely silenced them. The 60 electrode signals were sampled at 20 kHz and were further analysed using software written in the Python language.

2.2 Network analysis

The synchronization between a given pair of dopaminergic VTA neurons was analysed using the PPC (Paired Phase Consistency) [3]. Briefly, the two spike trains were converted to point processes (resolution 1 ms) and divided into time segments. For each segment the phase of the binary signal was computed using the Fourier transform. From these the relative phase (from in-phase to anti-phase) between the two spike trains was computed for each time segment separately. Finally the PPC, which is an unbiased form of the classic phase-locking-value (PLV), measures the similarity / consistency of these relative phases over all time segments. The PPC measures the strength of the synchronization between two neurons from 0 (random phase relationship) to 1 (fully synchronized spike timing) and can be negative to remain unbiased. To obtain an overall measure of synchronization of spontaneous activity in the VTA network, we computed the PPC across all stationary pairs (214 pairs from five separate recordings) during baseline conditions. Additionally an identical analysis was performed on shuffled data, where for each neuronal pair the time segments of one neuron were randomized.

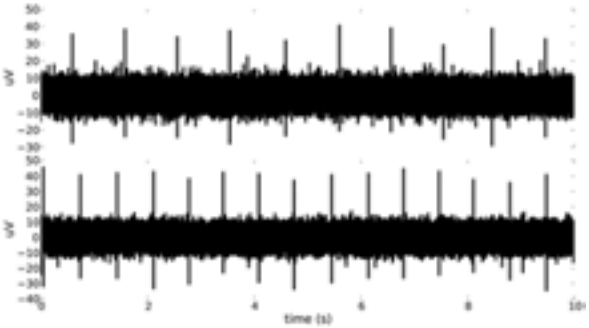

Fig. 1. Spontaneous activity of two dopaminergic neurons (traces were high-pass filtered at 200 Hz).

3 Results

The spontaneous firing rates of the dopaminergic VTA neurons were observed to be around 1-2 Hz (Fig. 1). The autocorrelation functions show that the dopaminergic neurons have a dominant oscillatory frequency, which was extracted by calculating the intervals between the peaks in the autocorrelation function (Fig 2). The oscillation frequency was used to focus the PPC analysis on the relevant frequency domain.

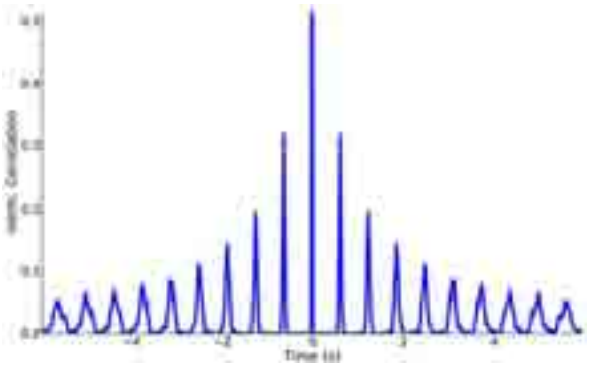

Fig. 2. Auto-correlation function of the binary spiketrain of a typical dopaminergic VTA neuron, showing regularly oscillating side lobes (normalized to lag-0).

The average PPC, which measures the strength of the network synchronization, was significantly higher than zero (t-test, $p<0.0001$, mean=0.0042, SEM=0.0003, blue bars Fig. 3). Although it has been proven that the mean PPC is an unbiased estimate of phase coupling [3], we also determined the PPC distribution for the same spike trains after random shuffling (red bars Fig. 3). The shuffled PPC values are tightly distributed around zero confirming the significance of the measured baseline phase coupling.

.

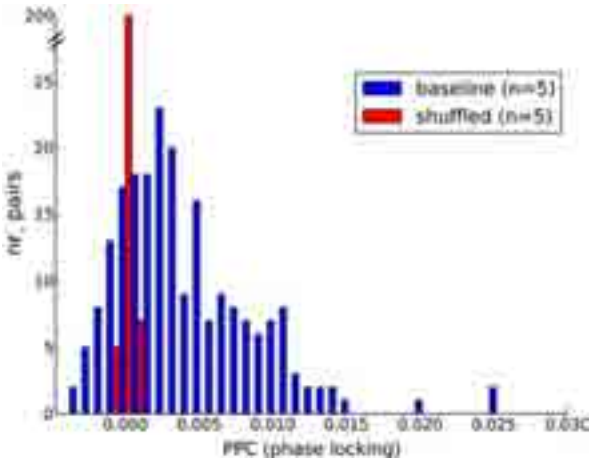

Fig. 3. PPC distribution of the spontaneously active VTA network (blue bars) has a higher than zero average and shows higher network strength than the randomized network (shuffled, red bars)

The PPC estimates the square of the classic PLV therefore the values found here (0.001-0.015) represent weak to moderately strong phase coupling.

4 Conclusions and discussions

Our in vitro MEA experiments were able to record ensembles of dopaminergic neurons in the VTA. These neurons fire in a highly rhythmical fashion and have one dominant oscillation frequency. Together these auto-oscillators form a weakly coupled network, in which there is a significant amount of phase locking between the spike activity of the neurons.

Acknowledgement

We thank the Python Foundation for their software, with which we build our object-oriented analysis environment. This project was partly funded by PAD 114000091.

References

[1] Fujisawa S., Buzsaki G. (2011): A 4 Hz oscillation adaptively synchronizes prefrontal, VTA and hippocampal activities. *Neuron, 72, 153-165*

[2] Werkman T.R. et al. (2001): In vitro modulation of the firing rate of dopamine neurons in the rat substantia nigra pars compacta and the ventral tegmental area by antipsychotic drugs. *Neuropharmacology, 40, 927-936*

[3] Vinck M. et al. (2010): The pairwise phase consistency: A bias-free measure of rhythmic neuronal synchronization. *NeuroImage, 51, 112-122*

Gating of hippocampal output by beta-adrenergic receptor activation

S Grosser[1,2], KE Gilling[1,2], J.-O. Hollnagel[1] and J Behr[1,2]

1 Department of Neurophysiology, Charite Berlin, Germany
2 Department of Psychatry and Psychotherapy, Charite Berlin, Germany

Abstract
The subiculum is the principal target of CA1 pyramidal cells and thus serves as the major relay station for the outgoing information of the hippocampus. Subicular pyramidal cells are classified as regular- and burstspiking cells. In regular firing cells, induction of long-term potentiation (LTP) relies on the activation of postsynaptic NMDA receptors. In contrast, in burst-spiking cells, LTP is induced by presynaptic NMDA receptor-mediated Ca2+-influx that results in the activation of the cAMP-PKA cascade (Wozny et al., 2008 a,b). Activation of beta-adrenergic receptors at CA1-subiculum synapses induces a cell-type-specific form of chemical LTP in burst-spiking but not in regular-spiking cells (Wojtowicz et al., 2010).

1 Methods/Statistics

Using a multi-channel electrode system, we simultaneously recorded field-EPSPs in acute rodent brain slices from 59 electrodes located in the subiculum, presubiculum, parasubiculum and the medial and lateral EC to assess if beta-adrenergic receptor activation changes the information transfer from the hippocampus to its parahippocampal target structures.

2 Results

We demonstrate that beta-adrenergic receptor activation modulates trafficking of hippocampal output and therefore may play an important role in the facilitation of interaction between the hippocampus and distinct parahippocampal target structures..

3 Conclusion

Activation of beta-adrenergic receptors in the subiculumgates hippocampal output information to specific target regions in the parahippocampal cortex.

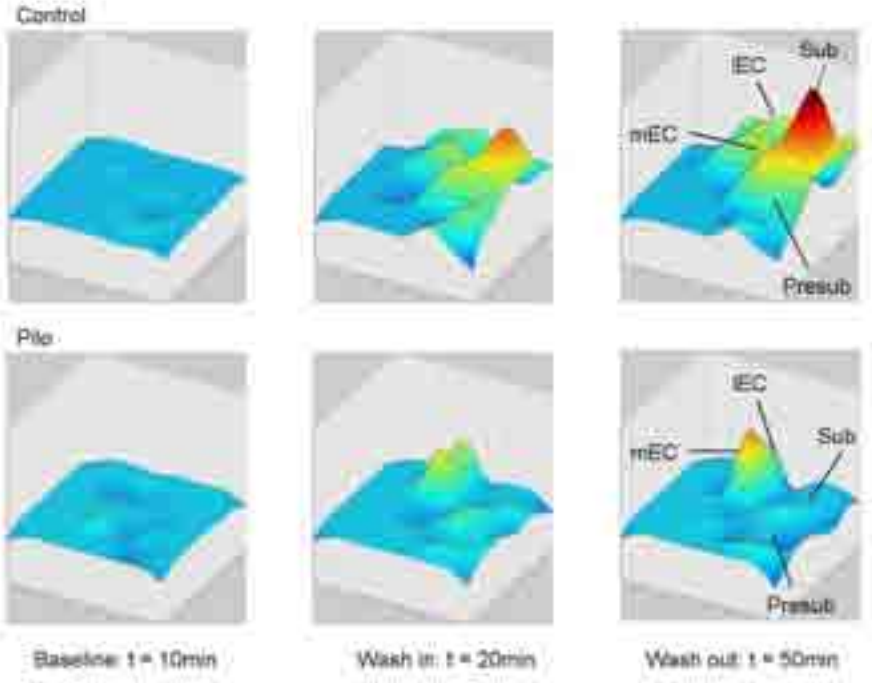

Fig. 1. Relative rise of amplitudes over time in control and pilocarpine treated rats after β-adrenergig receptor activation by Isoproterenol.

On the relationships between morphology and electrical activity recorded based on a MEA platform

Rodolfo dos Santos Ribeiro[1*], Lívia Alves de Oliveira[1], Denise Cristina da Silva[1], Aurélia Aparecida Rodrigues[2], Lúcio Araújo[2]

1 School of Electrical Engineering, Federal University of Uberlandia, Uberlandia, Brazil
2 School of Mathematics, Federal University of Uberlandia, Uberlandia, Brazil
* Corresponding author. E-mail address: rodolfosant@gmail.com

Abstract
Neuronal signalling in cell cultures is strictly tied to the topology of the biological network. This paper develops quantitative assessments to relate parameters characterizing the culture morphology with both classical and new quantifications of electrical activity.

1 Introduction

Electrical activity profile of a cell culture is quite dependent on the morphology and connections among neurons [1]. In fact, several computational methods exist for estimating neural connectivity based on electrical recordings [2,3], which are closely related to neurocomputational models of cultures [4]. Few works in the literature consider imaging information tied to electrical activity [4,5]. In this paper, our goal is to build simple statistical models to investigate the relationships existant among electrical activity variables and some parameters tied to cell morphology, the last ones estimated from imaging performed on the culture plated on a planar MEA.

2 Methods and Matherials

2.1 Laboratory procedures

Primary cultures of cortical neurons of rat hyppocampus were performed by extracting the tissue of embryos at 18 days of development, considering all procedures requested by Ethics Committee of University of Genoa. The cultures were grown on planar MEAs containing 60 microelectrodes, with 30 μm diameter and 200 μm spacing between them (*Multichannel Systems, Reutlingen, Germany*). Data was monitored and recorded by the commercial software *MCRack* (*Multichannel Systems, Reutingen, Germany*).

The spontaneous activity of a mature culture of 39 days in vitro (DIVs) was recorded during 20 minutes just one time, which was immediately followed by imaging at a *Olympus* microscope, including the magnification of 10 X. A complete set of pictures of all electrodes was taken, by using a *Samsun*g device of 3.1 Megapixels of resolution,

Electrical activity was analysed by two different techniques. The first one was classical spike analysis [3], leading to the following quantities that characterize spike and burst profiles: average interburst intervals (abbreviated by IBI [s]) and average mean time elapsed between two consecutive spikes (MISI [ms]). The second technique involves a nonlinear-dynamical-system approach [3], so that to estimate the following average parameters on the raw MEA signal (i.e., considering the pure amplitudes of the signal before performing burst analysis): kurtosis (CURT), skewness (OBL), standard deviation (DP) and Hurst coefficient (HURST), all of them adimensional. For both techniques, “average” considers average taken over all channels and during all the recording time.

Images were analysed by an expert biologist that could identify neurons and circle them, so that to generate another set of images (abbreviated S1) composed of just traces highlighting neuronal borders as a result of visual analysis. In the following, by means of image processing, the microelectrode tracks were separated in another set of data, and then computationnally added to S1. The resulting images were then processed by means of the *ImageJ* platform, so that to estimate the following parameters: the average distance between one cell and all the other ones in the image (DM [micrometers]), where “average” consider all identified cells by the biologist. The fractal dimension tied to the image (DF) and its entropy (ENT) were also estimated, based on [4]. These quantities characterize the randomness of cell distribution throughout the MEA surface, but also considering the microelectrodes.

2.2 Statistical methods

Regression analysis is a technique to model and investigate the relationship between variables. In a multiple linear regression, there is an expected value of Y for each value of X_i with $i=1...n$ [6]. In this case, the expected value of Y is given by (1)

$$Y = \beta_0 + \beta_1 X_1 + \beta_2 X_2 + ... + \beta_n X_n + e \quad (1)$$

Where β_0 corresponds to a linear coefficient; β_i is the coefficients of variable X_i (with *i=1...n); e* is a random error supposing normal distribution, zero-mean and variance σ^2.

Linear correlation between variables is measured by Pearson's linear correlation coefficient, represented by letter R, which can vary between -1 and 1. The extreme values concern to perfect correlation, and 0 means no correlation at all.

P-values should be considered in linear regression studies. Considering α = 0,05 and the hypothesis to test the relevance of coefficients β_i: H_0: β_i =0; H_1: $\beta_i \neq 0$. If p-value is less than or equal to α, reject H_0 and the respective variable contributes to the model [6].

The difference between the estimation of the fitted model ($\hat{Y}$) and the actual value of the dependent variable (Y) corresponds to the residue, that should be random and present normal distribution to validate the model. There is also the possibility of model adjustment for the models that could not be validated [6].

Only data of 33 channels were considered, since after preliminary analysis some of them were considered possible outliers.

3 Results

The two most significant models obtained from this database are presented in this section.

3.1 Model 1

$$HURST = 0.3 - 0.008 * OBL + 0.1237 * DF - 0.021 * DP \quad (2)$$

Pearson's coefficient value is R = 0.8294 and P-value is P = 0.00001.

The first model presents HURST as dependent variable. It was used the step-by-step technique to disclose the most significant independent variables, that are skewness of electrical activity signal, fractal dimension of images and standard deviation of electrical activity signal amplitude.

3.2 Model 2

$$DM = 86.469 + 0.0205 * CURT + 0.0819 * ENT + 0.0595 * IBI + 0.1281 * MISI \quad (3)$$

Pearson's coefficient value is R = 0.5871 and P-value is P = 0.0156.

The second model presemts DM as dependent variable. The same technique of model 1 was used to derive model 2. The independent variables are CURT, ENT, MISI and IBI. The second model was not validated because its residuals are not random.

4 Discussion and conclusions

For the first model, considering the very high value of its Pearson coefficient and the low p-value, a quite interesting result arises. It states that the nonlinear characteristics of the raw signal (HURST) may be derived or estimated based on both signal high-order statistics (OBL, DP) and the randomness of the cell distribution (DF), which is closely related to the culture morphology.

For the second model, one may conclude that the distance between cells (DM) may be derived from both spike (MISI) and burst (IBI) characteristics, but also considering the nonlinearities of the electrical activity tied to its kurtosis (CURT), as well as the randomness of cell distribution in terms of its entropy (ENT). However, considering the low value of the Pearson coefficient, this may be considered a poor result.

In brief, it is interesting to put forward that Model 1 attests the mutual relationship between electrical signaling and morphology, whereas Model 2 highlights that classical spike/burst analysis may not provide the best results. On the other hand, as the raw MEA signal is analysed, including also the biological noise (as in parameters CURT, OBL), we can derive a better relationship .

Acknowledgements

Authors are indebted to IBRO, UFU, Fapemig for finantial support, University of Genoa (UniGe) for providing the laboratory that led to the database, Danilo R. Campos (UFMG) for performing experimentations at UniGe, B.Tedesco for helping with imaging; Mauro Guzo and Mona Shinba (USP-RP) for data analysis, Amanda F Neves (UFU) for visual analysis of images and Prof. Joao Destro (UFU) for technical support.

References

[1] Kandel, E.C.; Schwartz, J.H., Jessel, T.M.(2000). *Principles of neural sciences*. New York: Mc-Graw Hill Inc.

[2] Glaser, E.M; Ruchkin, D.S.(1976). *Principles Of Neurobiological Signal Analysis*. Academic Press: N York, USA.

[3] Taketani, M.; Baudry, M., editors. (2006). *Advances in Network Electrophysiology - Using Multi Electrode Arrays*. New York: Springer Press, 478 p.

[4] Makki-Martunen, T., Acimovic, J., et alli.(2011). Information diversity in structure and dynamics of simulated neuronal networks. *Frontiers in Computational Neuroscience*. Vol.5, Article 26, pp.1-17.

[5] Takahashi, N., et al.. (2007). Watching neuronal circuit dynamics through functional multineuron calcium imaging (fMCI). *Neuroscience Research*, 58, 219-225.

[6] Montgomery, D.C.; Peck, E.A.; Vinning, G. *Introduction to linear regression analysis*. 4th ed. Ed. Wiley Interscience, 2007.

Heart

Mesenchymal stem cells improve functional and morphological integration of induced pluripotent stem-cell derived cardiomyocytes into ventricular tissue

Martin Rubach[1], Roland Adelmann[1], Florian Drey[2], Sven Baumgartner[1], Tomo Saric[4], Yeong Choi[2], Klaus Neef[2], Azra Fatima[4], Anette Köster[1], Moritz Haustein[1], Marcel Halbach[3], Juergen Hescheler[4], Konrad Brockmeier[1], Markus Khalil[1]

1 Department of Pediatric Cardiology, University of Cologne
2 Department of Thoracic Surgery, University of Cologne
3 Department of Cardiology, University of Cologne
4 Institute for Neurophysiology, University of Cologne

Abstract

Introduction: Transplantation of induced pluripotent stem cell-derived cardiomyocytes (iPS-CMs) into damaged myocardium might become a therapy to improve cardiac function. There is cumulating evidence reporting beneficial effects of cell transplantation strategies combining a source for CMs with other cell types. From these observations we hypothesized that non-myocytes might be necessary for an improved functional integration.

Aim: To investigate whether *murine* mesenchymal stem cells (MSCs) improve electrical and morphological integration of *murine* iPS-CMs into vital cardiac tissue

Methods: *Murine* ventricular slices (thickness 300 µm) were co-cultured with iPS-CMs and MSCs for 4 days. Integration was evaluated by visual methods, field potential (FP) recordings and propagation maps via multi-electrode array (MEA) measurements. To determine the origin shift of pacemaking activity, we programmed the "LabVIEW" based mapping software "Mapview RuBo".

Results: IPS-CM clusters had an average beating frequency of 333 ± 140 (n=32). Vital slices with (n=28; 78 ± 55 bpm) or without (n=29; 78 ± 44 bpm) iPS-CM clusters served as controls and displayed similar average frequencies after 4 days of co-culture. Co-cultures of vital slices with iPS-CMs and MSCs (n=16; 238 ± 133 bpm) showed a significant increase in beating rates compared to the controls indicating an improved electrical integration of the iPS-CMs. Propagation map analysis exhibit a shift of pacemaking region towards iPS-CM cluster.

Summary/Conclusion: Improved integration of rapidly beating iPS-CM cluster induces a raised frequency of the slice, meaning that the iPS-CM cluster serves as a pacemaker for the cardiac slice. We conclude that non-cardiac cells like MSCs support morphological and electrical integration of iPS-CMs. MSCs are an easy accessible cell source and could be used in future as mediator cells for a successful transplantation of iPS-CMs.

1 Introduction

A worldwide persisting donor organ shortage requires the development of alternative cell replacement strategies to regenerate damaged myocardium (1). Application of embryonic stem cells and their differentiated derivates are often immune-rejected (1-3). Cardiomyocytes derived from *murine* induced pluripotent stem cells (iPS-CM) offer a promising ethical acceptable cell source. Unfortunately, the resulting purified differentiated cardiomyocytes offer insufficient engraftment and integration which reduces the functional improvement of damaged myocardium (4). Therefore, we tested different non-myocyte cell lines like mesenchymal stem cells (MSCs) to enhance morphological, electrical and functional integration of iPS-CM in vitro (5). Mesenchymal stem cells can be easily isolated from adults and are already often used for transplantation trials and tissue engineering (6). Beside structural advantages, positive immunomodulatory paracrine effects and conduction enhancement by Cx43 are described (7, 8).

2 Methods

2.1 Generation of ventricular Slices

Vital contracting slices were generated as described earlier (11). Briefly, embryonic myocardial ventricles (day 17,5 post coitum) were prepared and embedded in 4% low melt agarose (Carl Roth GmbH Co. KG, Karlsruhe, Germany). Preparation and slicing was

performed in ice cold (~4°C), pre-oxygenated calcium-free Tyrode's solution with a vibratom VT1000s (Leica, Wetzlar, Germany).

2.2 Generation of avital cardiac tissue by oxygen and glucose deprivation

An ischemia mimicking slice model was produced by elimination of oxygen and glucose for 45h as previously described (11). Accordingly, slices were transferred into a custom made hypoxia chamber, fumigated with nitrogen and retained in Tyrode solution with deoxy-glucose instead of glucose.

2.3 Investigation of electrical coupling by multi electrode measurement

Vital slices were co-cultured with a single contracting iPS-CM cluster either with or without MSCs on multi electrode arrays (12). Field potential (FP) recordings were performed using the MEA System (sampling rate 20 kHz) with an MEA amplifier 1060 (Multi Channel Systems). Frequency was analyzed by MC^Rack (Multi Channel Systems, Reutlingen, Germany). Origin shift of pacemaking area was determined by an selfmade programmed mapping software based on "LabVIEW" (NI, Houston, Texas; "Mapview RuBo"). The FPs of iPS-CM clusters were distinguished from FPs of ventricular slices by their different morphology and smaller amplitude. Data are represented as mean ± standard deviation, level of significance is set to $p<0.05$.

2.4 Investigation of morphological Integration and force measurement

Avital slices were co-cultured with iPS-CM clusters in a custom made dish with a funnel shaped cavity to ensure close contact up to 7 days (12, 13). Integration into avital tissue was judged by a scoring system (scores: 1-3).

3 Results

3.1 Electrical integration of iPS-CM cluster into vital cardiac tissue

Successful electrical integration resulted in a significantly raised contraction frequency of the slice and a shift of conduction offspring to the clusters area. On the first day after co-culture procedure, the beating rate of the vital slice was significantly higher in co-cultures containing MSCs and iPS-CM cluster compared to either vital slices or vital slices with iPS-CM clusters alone ([iPS-CM MSC Vital] n=16; 87 ±102 bpm vs. [iPS-CM Vital] n=29; 33 ± 39 bpm; $p<0.05$ and vs. [vital] slices n=25; 31 ± 52 bpm; $p<0.05$). During 4 days of co-culture the beating rate increased subsequently. Due to its peaks with low amplitude and their initial higher beating rate, the iPS-CM cluster FPs could be detected correspondingly to the cluster location and were further distinguishable from the slice FPs. Appearance of interfering cluster signals continued in almost all vital slices containing only iPS-CMs over all 4 days. Whereas discrimination between iPS-CM cluster and slice signal was often not possible in MSC supported co-cultures accompanied by a raised beating rate, indicating a 1:1 coupling.

3.2 Morphological integration of iPS-CM cluster into avital cardiac tissue

During 7 days of co-culture, slices with purified iPS-CM cluster alone failed to obtain the highest score of integration (n=11/13; score 1/3). In only 2 of 13 slices, an intermediate integration score (score 2/3) could be observed whereas all co-cultures containing MSCs achieved the highest integration score (n=13; score 3/3) on day 3.

4 Conclusion

The advantages of differentiated purified iPS-CM are that they can be produced from relevant patients in a high number with a lower teratogenic potential in comparison to embryonic stem cells (14, 15). Our results indicate that they integrate poorly in vital and avital cardiac tissue. MSCs support the integration. Additionally, a significant raise of the beating rate as well as a shift of the dominant offspring of field potential to the clusters area indicate improved electrical integration. MSCs are an easy accessible cell source and could be used in future as mediator cells for a successful transplantation of iPS-CMs.

References

[1] Sian Pincott E, Burch M. Indications for heart transplantation in congenital heart disease. Curr Cardiol Rev. 2011;7(2):51-8.

[2] Deuse T, Seifert M, Phillips N, Fire A, Tyan D, Kay M, et al. Human leukocyte antigen I knockdown human embryonic stem cells induce host ignorance and achieve prolonged xenogeneic survival. Circulation. 2011;124(11 Suppl):S3-9.

[3] Kahan B, Magliocca J, Merriam F, Treff N, Budde M, Nelson J, et al. Elimination of tumorigenic stem cells from differentiated progeny and selection of definitive endoderm reveals a Pdx1+ foregut endoderm stem cell lineage. Stem Cell Res. 2011;6(2):143-57.

[4] Hattori F, Fukuda K. Strategies for replacing myocytes with induced pluripotent stem in clinical protocols. Transplant Rev (Orlando).

[5] Xi J, Khalil M, Spitkovsky D, Hannes T, Pfannkuche K, Bloch W, et al. Fibroblasts support functional integration of purified embryonic stem cell-derived cardiomyocytes into avital myocardial tissue. Stem Cells Dev.20(5):821-30.

[6] P M, S H, R M, M G, W SK. Adult mesenchymal stem cells and cell surface characterization - a systematic review of the literature. Open Orthop J.5(Suppl 2):253-60.
[7] Boomsma RA, Geenen DL. Mesenchymal stem cells secrete multiple cytokines that promote angiogenesis and have contrasting effects on chemotaxis and apoptosis. PLoS One.7(4):e35685.
[8] Pijnappels DA, Schalij MJ, van Tuyn J, Ypey DL, de Vries AA, van der Wall EE, et al. Progressive increase in conduction velocity across human mesenchymal stem cells is mediated by enhanced electrical coupling. Cardiovasc Res. 2006;72(2):282-91.
[9] Cappellesso-Fleury S, Puissant-Lubrano B, Apoil PA, Titeux M, Winterton P, Casteilla L, et al. Human fibroblasts share immunosuppressive properties with bone marrow mesenchymal stem cells. J Clin Immunol. 2010;30(4):607-19.
[10] Jang S, Park JS, Won YH, Yun SJ, Kim SJ. The Expression of Toll-Like Receptors (TLRs) in Cultured Human Skin Fibroblast is Modulated by Histamine. Chonnam Med J. 2012;48(1):7-14.
[11] Pillekamp F, Reppel M, Dinkelacker V, Duan Y, Jazmati N, Bloch W, et al. Establishment and characterization of a mouse embryonic heart slice preparation. Cell Physiol Biochem. 2005;16(1-3):127-32.
[12] Hannes T, Halbach M, Nazzal R, Frenzel L, Saric T, Khalil M, et al. Biological pacemakers: characterization in an in vitro coculture model. J Electrocardiol. 2008;41(6):562-6.
[13] Pillekamp F, Reppel M, Rubenchyk O, Pfannkuche K, Matzkies M, Bloch W, et al. Force measurements of human embryonic stem cell-derived cardiomyocytes in an in vitro transplantation model. Stem Cells. 2007;25(1):174-80.
[14] Yoshida Y, Yamanaka S. iPS cells: a source of cardiac regeneration. Journal of molecular and cellular cardiology. 2011;50(2):327-32. Epub 2010/11/03.
[15] Oh Y, Wei H, Ma D, Sun X, Liew R. Clinical applications of patient-specific induced pluripotent stem cells in cardiovascular medicine. Heart (British Cardiac Society). 2012;98(6):443-9. Epub 2012/01/31.

Measurement of electrophysiological changes during catheter cryoablation in the heart of domestic pig: A proof of concept study

Roland Kienast[1*], Michael Handler[1], Markus Stöger[2], Friedrich Hanser[1], Florian Hintringer[2], Gerald Fischer[1], Christian Baumgartner[1]

1 UMIT, Institute of Electrical and Biomedical Engineering, Hall in Tyrol, Austria
2 Medical University of Innsbruck, Department of Cardiology, Innsbruck, Austria
* Corresponding author. E-mail address: roland.kienast@umit.at

Abstract
Catheter cryoablation (CCA) is an alternative minimal-invasive surgical method to radio frequency catheter ablation in order to tread cardiac arrhythmias by ablating arrhythmic cardiac tissue using shock-freezing. In relation to mechanical changes, electrophysiological mechanisms in cardiac tissue are largely unknown during selective cooling which are, however, crucial to obtain a better understanding of cell death during cryoablation. The aim was to detect hypothermia-induced effects in registered signals in vivo such as abnormalities in the T wave formation or an elevated J-point, termed J- or Osborne wave. For this purpose, a pilot study with domestic pigs was carried out to demonstrate the feasibility of measuring the epicardial electrograms in the ablation area during CCA. For registering ECG a mobile measurement equipment (Multi Channel Systems, MCS GmbH, Reutlingen) with a flexible high-resolution multi-electrode array was used. Typical induced hypothermia effects, such as J waves or prolonged QT intervals could be detected. Our preliminary results demonstrate the feasibility of measuring electrophysiological changes in cardiac tissue in-vivo during selective cooling with a high-resolution electrode array.

1 Introduction

Catheter cryoablation (CCA) is an alternative minimal invasive surgical method to radio frequency (RF) catheter ablation in order to tread cardiac arrhythmias. In comparison to a RF heating system CCA permanently ablates arrhythmic cardiac tissue by shock-freezing [1]. This freezing process induces mechanical changes in form of intra- and extracellular ice formation which leads to cell death [2]. In relation to mechanical changes, electrophysiological mechanisms in cardiac tissue are largely unknown during selective cooling which are, however, crucial to obtain a better understanding of cell death during cryoablation. In particular, the measurement and assessment of electrical signals during ablation may help to further advance knowledge on cooling-induced cell death mechanisms. For this purpose, a pilot study with domestic pigs was carried out to demonstrate the feasibility of measuring the epicardial electrograms during CCA with a high resolution multi-electrode array (MEA). The aim was to detect hypothermia-induced effects in registered signals in vivo, anticipating morphological changes in action potentials of epi-, M- and endocardial cells [3]. These may lead to abnormalities in the T wave formation, an elevated J-point, termed J wave or Osborne wave [3] and a prolonged action potential duration [4], which are characteristic indicators of hypothermia.

2 Methods

To study the electrophysiological changes on the beating open heart during CCA two domestic pigs, weighing about 50 kg, were anesthetized with Propofol und Dipidolor and mechanically ventilated. Additional application of 7.5 mg Dipidolor every 30 minutes and a continuous administration of 40 ml Propofol per hour ensured the maintenance of deep anesthesia. To enable epicardial ECG recordings using a MEA, the chest was opened to expose the heart. The study protocol was approved by the ethical review committee of the Medical University of Innsbruck, Austria.

Time [s]	Condition
0 – 100	before the first ablation
100 – 340	first ablation
340 – 470	thaw phase
470 – 710	second ablation

Tab. 1: Timing of the experiment

Briefly, the cryo-tip catheter was positioned by a cardiologist proximally in the right ventricle and multiple ECG signals were recorded over a period of approximately 12 minutes. During this procedure the catheter was cooled two times over a period of four minutes each with a thaw phase of approximately two minutes in between. The ablation protocol is shown in Table 1.

2.1 Epicardial recordings

For recording unipolar epicardial electrograms, a mobile ECG measurement equipment (Multi Channel Systems, MCS GmbH, Reutlingen) was used. The system comprises a flexible multi-electrode sensor array (EcoFlexMEA) which is directly connected to a miniature 32-channel preamplifier, a 32-channel programmable gain amplifier and a data acquisition system. The purpose-built EcoFlexMEA sensor consists of 32 gold electrodes with a diameter of 50 microns, two reference and two ground electrodes, which are applied to a flexible substrate made of polyimide (Kapton). The recording electrodes are arranged in a grid pattern over an area of 7.8 x 7.8 mm with an interelectrode distance (center to center) of 1300 microns. The reference electrodes were connected with the ground of the measuring setup. All signals were recorded using a 1-5 kHz bandwidth and amplified with a gain of 100. The sampling rate for the digitization was 10 kHz.

For positioning the electrode array as accurately as possible in the ablation area, both the catheter and the array were aligned using an X-ray based positioning system. The array was positioned using a portable measuring arm. It was not fixed onto the epicardium by e.g. sewing or gluing. This, however, resulted in a breathing cycle induced movement of the array during ECG registration (see figure 1).

Fig. 1. Multi-electrode array positioned onto the epicardium. The contraction of the heart, the respiratory movement of the thorax as well as lack of fixation of the array caused a slight movement of the array during measurement.

2.2 Data analysis

The breathing-cycle-induced movement of the array resulted in artifact-afflicted signals of single electrodes due to poor contact and motion. To minimize alteration in ECG signals four virtual electrodes were defined by median averaging of five electrodes each (see figure 2(a)) to detect putative J waves and QT intervals of the averaged signals. Figure 2(b) shows an example of one averaged QT interval including the detected Q- ,R-, J- and T waves.

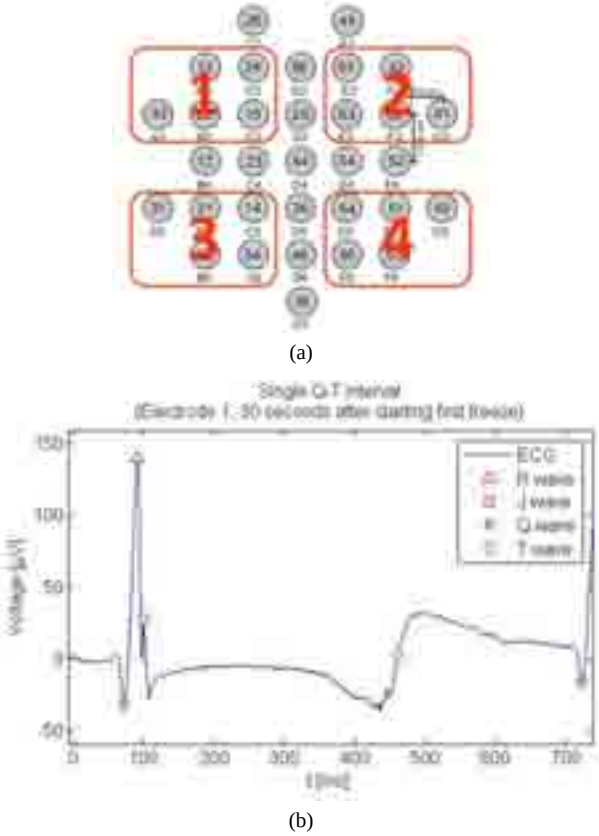

(a)

(b)

Fig. 2. Four virtual electrodes (adjacent epicardial areas) were defined (a) to improve signal to noise ratio by averaging signals of five electrodes each for detecting Q-,R-, J wave (peak) and T wave (maximal slope) automatically in the registered ECG (b).

2.3 Q-, R- and J wave detection

A computer algorithm optimized for the recorded signals was developed to detect Q-, R- and J waves by combining a threshold- and slope-based detection method. Additionally, a wavelet-based algorithm was applied [5] to increase the detection rate of the R waves. To examine effects of hypothermia by analyzing the height of the J wave, a baseline drift independent measure, as described in equation 1, was applied.

$$\textit{relative Amplitude of the J wave} = \frac{R_{\textit{peak value}} - Q_{\textit{peak value}}}{R_{\textit{peak value}} - J_{\textit{peak value}}}$$

Eq. 1 calculates a baseline drift independent measure to examine effects of hypothermia by analyzing the relative height of the J wave compared to the height of the R wave.

2.4 QT interval detection

The experimental registered ECG signals comprise biphasic T waves where the negative phases are always followed by positive phases. To estimate activation recovery intervals the QT time was defined as the time between the absolute minimum of the Q wave and the point of maximum slope of voltage (maximum dV/dt) in the ascending phase of the biphasic T wave (see figure 2(b)). This baseline

independent method relies on a correlation between action potential duration and activation recovery intervals by determining the maximum voltage slope in the T wave of unipolar electrograms which is described by Millar et al. [6] and Haws et al. [7].

3 Results

3.1 RR interval

Global effects of hypothermia on the heart lead to a decrease of heart rate and, thus, to a prolonged RR interval [8] [9] [10]. In our experiments, the heart was not cooled as a whole, but locally in a single spot using a cryocatheter. As expected the heart rates during the interventions remain almost equal (see table 2).

Condition	RR interval [ms]	heart rate [bpm]
before the first ablation	667 ± 8,5	89,9 ± 1,1
first ablation	652 ± 6,3	92,0 ± 0,9
thaw phase	686 ± 5,0	87,4 ± 0,6
second ablation	670 ± 5,3	89,5 ± 0,7

Tab. 2: RR interval and heart rate within the respective states of the ablation protocol.

3.2 J waves

As known from literature J waves as pathophysiological indicators of ECG abnormality appear with decreasing heart temperature [8]. This process is reversible with rewarming [3]. Therefore, the number of J waves is expected to rise with increasing expansion of the cooled tissue.

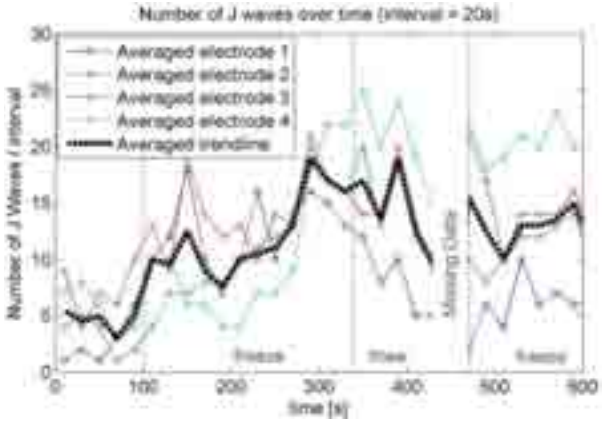

Fig. 3. Number of J waves during experiment for the four clustered electrodes. Each data point represents the number of detected J waves within a time interval of 20 seconds. During freezing phase a temperature gradient of approx. -35°C/s (target temperature: -60°C), and during thawing phase a gradient of 8°C/s at the top of the catheter was applied. The black dotted line indicates the averaged trendline.

To reproduce this, the number of J waves was counted at different temperature levels.

Figure 3 demonstrates the frequency of J waves during freeze and thaw cycles for the clustered electrodes where each data point represents the number of detected J waves within a time interval of 20 seconds. This suggests a correlation of increasing numbers of J waves and decreasing temperature. Amplitudes of hypothermia-induced J waves yield a reciprocal characteristic to temperature changes [11].

Because the array position is slightly changing the occurrence of this effect can only be verified for individual time points. Figure 4(a) shows the spatial distribution of J waves amplitudes for a single time step 30 seconds after start of the first freezing phase, indicating a temperature-dependent distribution of J waves amplitudes. This means, in turn, that the distribution of J waves amplitudes represents the spatial distribution of tissue temperatures during cooling.

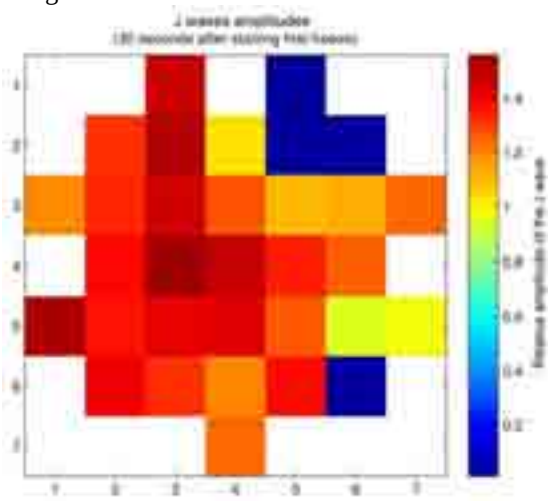

(a)

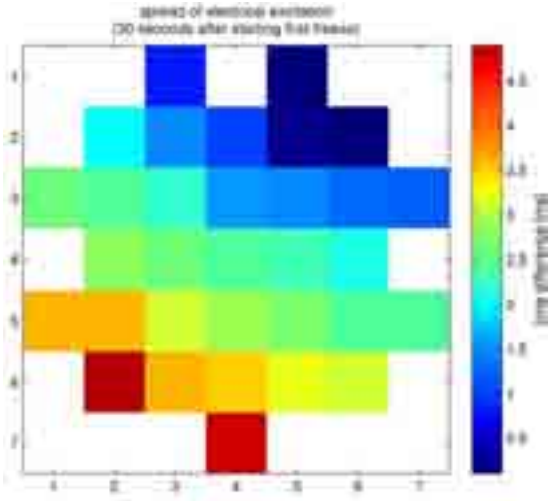

(b)

Fig. 4. Spatial distribution of J waves amplitudes (4(a)) and excitation propagation (4(b)) for a single time step 30 seconds after starting the first freezing phase (32 electrode EcoFlexMEA array). The lower left corner represents the lowest temperature.

Figure 4(b) depicts the excitation propagation across the array for the same time point coded in pseudo colour. A spread from top right to bottom left is apparent.

3.3 QT interval

It is known that a prolonged action potential duration caused by hypothermia results in a prolonged QT interval [8] [12]. For each virtual electrode QT times were determined in successive 30-second time intervals. For each time interval the median of measured QT times was calculated. Figure 5 illustrates the results of both experiments where the black line shows the averaged trendline over all electrodes. As expected the QT time increases during the first freezing process, begins to normalize in the thaw phase and rises again during the second ablation. Thus, it could be confirmed that prolonged QT intervals correlate to decreasing temperature levels.

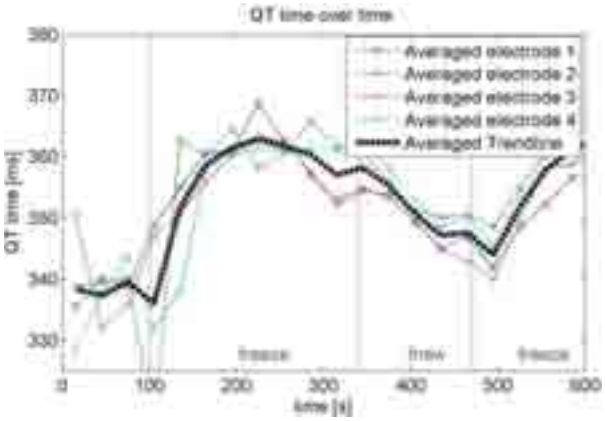

Fig. 5. Estimated QT interval over a freeze-thaw-freeze cycle. QT intervals increase during the first freezing (ablation) phase, begin to normalize in the thawing phase and rise again during the second freezing phase. The black dotted line indicates the averaged trendline.

4 Discussion

Our preliminary results demonstrate the feasibility of measuring electrophysiological changes in cardiac tissue in vivo during selective cooling with a high-resolution electrode array. Typical induced hypothermia effects, such as J waves or prolonged QT intervals could be detected. The problem of a periodic local dislocation of the array mainly caused by the respiratory movement of the thorax is still evident. In our experiments, the respiratory rate was estimated to be 15 breaths per minute at a heart rate of about 90 beats per minute. Thus, only one within six recorded QT intervals represented the local ablation site. To overcome movement of the array a fixation of the sensor array is planned for the next experiments. Note that the objective of cryoablation is to create a permanent conduction block in the myocardium. To achieve this, a lesion which is caused by a hypothermia-induced necrosis of the myocardium is created. The area of lesion is subsequently almost totally replaced by fibrosis [2].

The aim of our ongoing work is to derive a focused understanding at cardiac muscle cell death during the lesion formation within the cryoablation process, which allows us to develop a computer model for simulating and assessing the abnormal electrophysiological mechanisms and morphological changes during the intervention. These findings are expected to contribute to reduction of duration of treatment and to increase the clinical acceptance using this ablation method.

Acknowledgement

This project was funded by the *Standortagentur Tirol*, Austria within the program *"K-regio"*.

References

[1] Skanes A., Klein G., Krahn A., Yee R. (2004). Cryoablation. *Journal of cardiovascular electrophysiology,* 15, 28-34.
[2] Schwagten B., Belle Y. V., Jordaens L. (2010). Cryoablation: how to improve results in atrioventricular nodal reentrant tachycardia ablation?. *Europae.,* 12, 1522-1525.
[3] Antzelevitch C. (2006). Cellular Basis for the Repolarization Waves of the ECG. *Annals of the New York Academy of Sciences,* 1080, 268-281.
[4] Kiyosue T., Arita M., Muramatsu H., Spindler A., Noble D. (1993). Ionic mechanisms of action potential prolongation at low temperature in guinea-pig ventricular myocytes. *The Journal of physiology,* 468, 85-106.
[5] Pal S., Mitra M. (2010). Detection of ECG characteristic points using multiresolution wavelet analysis based selective coefficient method. *Measurement,*43, 255-261.
[6] Millar C., Kralios F., Lux R. and others. (1985). Correlation between refractory periods and activation-recovery intervals from electrograms: effects of rate and adrenergic interventions. *Circulation,* 72, 1372-1379.
[7] Haws C., Lux R. (1990). Correlation between in vivo transmembrane action potential durations and activation-recovery intervals from electrograms. Effects of interventions that alter repolarization time. *Circulation,* 81, 281-288.
[8] Aslam A.F., Aslam A.K., Vasavada B., Khan I. (2006). Hypothermia: evaluation, electrocardiographic manifestations, and management. *The American journal of medicine,* 119, 297-301.
[9] Wang H., Hollingsworth J., Mahler S., Arnold T. (2010). Diffuse ST segment depression from hypothermia. *International Journal of Emergency Medicine,* 3, 451-454.
[10] Mustafa S., Shaikh N., Gowda R., Khan I. and others. (2005). Electrocardiographic features of hypothermia. *Cardiology,* 103, 118-119.
[11] Yan G., Antzelevitch C. (1996). Cellular basis for the electrocardiographic J wave. *Circulation,* 93, 372-379.
[12] Slovis C., Jenkins R. (2002). Conditions not primarily affecting the heart. *Bmj,* 324, 1320-1323

Analysis of electrophysiological characteristics of cardiomyocytes following radiation exposure

Frederik Steger[1] Johannes Frieß[1], Andreas W. Daus[1], Sylvia Ritter[2] and Christiane Thielemann[1]

1 biomems lab, Faculty of Engineering, University of Applied Sciences Aschaffenburg, Germany
2 Biophysics division, GSI Helmholtz Centre for Heavy Ion Research Darmstadt, Germany

Abstract
Several studies have shown an increased risk of heart disease and stroke in patients after radiotherapy for cancer [1; 2]. More recently, epidemiological studies point to an increased risk of adverse cardiovascular effects at low and moderate doses (< 5 Gy) of ionising radiation, typically developing with a long latency [3]. With the increasing use of heavy ions in cancer therapy, an assessment of their possible cardiovascular late effects is important, in particular when young patients are treated. Essentially no information is available on the potential cardiovascular risks associated with the exposure to heavy ions. To address this issue we studied the induction of cellular late effects in primary beating cardiac myocytes after particle beam exposure. As endpoints with relevance to cardiovascular disease physiological and cellular parameters such as the electrical activity of cardiac myocytes, cell death and proliferation of cardiac myocytes are investigated

1 Motivation

There is increasing evidence that exposure to low doses of ionising radiation can have adverse effects on the cardiovascular system [4; 5]. These effects usually occur many years after the exposure. Especially for the radiation treatment of young patients, an assessment of the possible late effects is important. It also carries an unknown risk for the planning of manned space missions [6]. To address the question if and to what extent radiation affects cardiac function, exposure of avian cardiomyocytes to heavy ions and x-rays was performed and the electrophysiological functionality of the cardiac cells was measured with microelectrode array (MEA) chips.. The comparative evaluation of these parameters will help to clarify the role of high LET radiation in the etiology of radiation induced cardiovascular disease.

Fig. 1. Radiation therapy treatment with x-ray. Heidelberger Ionenstrahl Therapiezentrum, Germany.

2 Methods

To assess the effects of ionising radiation on cardiac functionality, the electrical properties of cardiac myocytes have been measured by use of a microelectrode array system. For this purpose an in vitro model system based on avian cardiac myocytes isolated from embryonic chicken has been established. Tissue from chick embryonic heart (E8) was chopped and enzymatically dissociated. Subsequently the cells were plated on fibronectin coated MEAs [7].

Irradiation experiments were performed at the GSI Helmholtz Centre for Heavy Ion Research in Darmstadt. The samples received various doses of carbon ions (25-mm extended Bragg peak, LET = 75keV/um) and x-rays after two days in vitro. Effects were examined up to one week after exposure. For high LET radiation with C-ions, MEA containers were covered tightly and adjusted upright into the ion beam at the heavy ion synchrotron SIS18 GSI Darmstadt, see Figure 2. Relevant investigated electrophysiological parameters were changes in the shape of the field action potentials, signal propagation and beat rate.

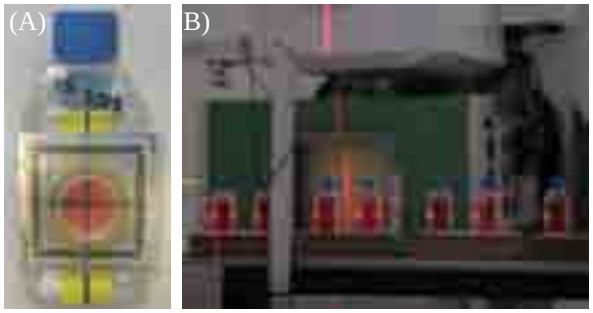

Fig. 2. (A) Covered MEA container with cell medium. The MEA is attached to a water filled cell culture flask to enable irradiation in an upright position. The markers allowed an easy tracking by the Ion-Beam. (B) Culture flasks on the conveyer belt inside the irradiation chamber at GSI, photo courtesy by GSI.

3 Results

The experiments revealed a high resistance of the cells to radiation damage. The cellular networks remained active and uniformly contractile even after an exposure to high doses above 20 Gy of x-rays and up to 30 Gy of heavy ions, respectively. Whereas the commonly applied dose in order to kill tumour cells is up to 60 Gy. Also no influence on signal amplitude and shape could be verified. However, slight changes in beat rate and signal propagation were detected at higher doses.

4 Conclusion

In summary, the data obtained so far indicate that the exposure to high LET particles has only minor effects on the electrophysiological functionality of cardiomyocytes. However, further experiments are conducted to statistically verify these data. Additionally, the impact of heavy ions on cardiac cells under pre-stressed, arrhythmic conditions will be investigated. The comparison of data obtained for normal and pre-stressed cells will provide information on possible combined effects of ionising radiation and other stressors. Furthermore, immunohistochemical staining and cell sorting methods will permit further insight into proliferation, differentiation and cell death of the cultures. Lastly, expanding the cell culture model from a two dimensional monolayer to a three dimensional spheroid culture will increase the comparability of the in vitro culture to cardiac myocytes in vivo [8].

Acknowledgement

This work is supported by the DLR in the frame of the ESA IBER-10 program. We gratefully thank the Association for the Promotion of Tumor Therapy with Heavy Ions for supporting the project.

References

[1] Cutter, D. J., Darby, S. C., Yusuf, S. W. (2011). Risks of Heart Disease after Radiotherapy , *Tex Heart Inst J.*, 38(3): 257–258

[2] Baker, J. E., Moulder, J. E., Hopewell, J. W. (2011). Radiation as a Risk Factor for Cardiovascular Disease. *Antioxid Redox Signal,. 15(7):* 1945–1956.

[3] Little, M. P., Tawn, E. J., Tzoulaki, I., Wakeford, R., Hildebrandt, G., Paris, F., Tapio, S., Elliott, P. (2010). Review and meta-analysis of epidemiological associations between low/moderate doses of ionising radiation and circulatory disease risks, and their possible mechanisms. *Radiat Environ Biophys.*, 49(2):139–53

[4] Roychoudhuri, R., Robinson, D., Putcha, V., Cuzick, J., Darby, S., Møller, H. (2007). Increased cardiovascular mortality more than fifteen years after radiotherapy for breast cancer: a population-based study, *BMC Cancer*, 15;7:9

[5] Hooning, M. J., Botma, A., Aleman, B. M. P., Baaijens, M. H. A., Bartelink, H., Klijn, J. G. M., Taylor, C. W., van Leeuwen, F. E. (2007). Long-term risk of cardiovascular disease in 10-year survivors of breast cancer, *J Natl CancerInst.*, 7;99 (5):365–75.

[6] Durante, M., Cucinotta, F. A.,Heavy ion carcinogenesis and human space exploration, Nat. Rev. Cancer, 8(6):465-72

[7] Daus, A. W., Goldhammer, M., Layer, P. G., Thielemann, C. (2011), Electromagnetic exposure of scaffold-free three-dimensional cell culture systems. *Bioelectromagnetics*, 32: 351–359

[8] Daus, A. W., Layer, P. G., Thielemann, C. (2012), A spheroid-based biosensor for the label-free detection of drug-induced field potential alterations, Sensors and Actuators B: Chemical, 165(1): 53–58

Effect of electrical stimulation on beat rate of pluripotent cell-derived cardiomyocytes innervated by sympathetic neurons

Akimasa Takeuchi[1*], Kenta Shimba[1], Yuzo Takayama[2], Kiyoshi Kotahi[1], Jong-Kook Lee[3], Yasuhiko Jimbo[1]

1 Graduate School of Frontier Sciences, The University of Tokyo, Chiba, Japan
2 Graduate School of Information Science and Technology, The University of Tokyo, Tokyo, Japan
3 Graduate School of Medicine, Osaka University, Osaka, Japan
* Corresponding author. E-mail address: takeuchi@bmpe.k.u-tokyo.ac.jp

Abstract
Rat sympathetic superior cervical ganglion (SCG), one of autonomic ganglia, neurons were co-cultured with pluripotent (P19.CL6) cell-derived cardiomyocytes (P19CMs) in compartmentalized co-culture device, which was fabricated using photolithographic microfabrication techniques. Synapses was formed between sympathetic neurons and P19CMs, as confirmed by immunostaining for beta-3 tubulin, synapsin I and cardiac troponin-I. Changes in the beat rate of P19CMs were triggered after electrical stimulation of the co-cultured SCG neurons, and were affected by the pulse frequency of the electrical stimulation. These results suggest that the beat rate of differentiated cardiomyocytes can be modulated by electrical stimulation of connected sympathetic neurons.

1 Introduction

Stem cell transplantation has great therapeutic value for heart failure such as ischemic heart disease, congestive heart failure and myocardial infarction[1,2]. However, little is known whether the sympathetic nervous system (SNS), a component of the autonomic nervous system, innervates the stem cell-derived cardiomyocytes in the same manner as the SNS controls the non-damaged cardiac tissue. In this study, device for co-culture of sympathetic superior cervical ganglion (SCG) neurons and plripotent (P19.CL6) cell-derived cardiomyocytes had been developed using microfabrication. Then, the functional relationship of the two components was evaluated in terms of changes in the beat rate of the derived cardiomyocytes after applying electrical stimulation to SCG neurons.

2 Materials and Methods

We developed a device to achieve compartmentalized co-culture of SCG neurons and cardiac-differentiated P19.CL6 cells (P19CMs). This device contained a microelectrode-array (MEA) substrate [3] and a co-culture chamber (Fig. 1A), both of which were fabricated using photolithography techniques. The co-culture chamber, fabricated using polydimethylsiloxane, were designed to separate the SCG neurons from P19CMs, and consisted of two culture compartments connected with 16 microchannels (Fig. 1B). The co-culture chamber was fabricated based on our previous study [4]. These microchannels had pockets, which assisted neurite outgrowth from the sympathetic neurons. One of the culture compartments acted as a flow channel when the SCG neurons were seeded into the chamber. Suspension containing SCG neurons, obtained from 1- to 2-day-old Wistar rats, flowed into one of the culture chambers, and SCG neurons were trapped in each microchannel. An embrioid body, cluster of P19CMs induced by dimethylsulfoxide, was dropped in the other chamber. The SCG neurons trapped outgrew their neurites toward the culture chamber in which the P19CMs were cultured.

3 Results

SCG neurons and P19CMs were successfully conpartmentalized in the culture devise. SCG neurons were adhered to the microchannels, P19CMs to the chamber (Fig. 2A). According to immunostaining for bet3-tubuline (Fig. 2B), Cell bodies of the neurons were retained in a pocket, and the neurites were retained near the electrode. The SCG neurons extended their neurites along the microchannels, and the neurites reached compartment B, in which the P19CMs were cultured. Then, synapses of the SCG neurons were formed on the P19CMs, as comfirmed by using double immunostaining for synapsin I and caveoline-3. Spontaneous electrical activities of the P19CMs were observed in synchronization with the beating of them (Fig. 3). Constant-voltage stimulations, biphasic square pulses, were applied to the SCG neurons in each microchannel. Evoked responses were observed in several electrodes after electrical stimulation was applied to the SCG neurons. Beat rate of the P19CMs

increased after applying electrical stimulation of co-cultured SCG neurons. Two-way ANOVA revealed that frequency of electrical stimulation affected on the changes in beat rate of the P19CMs (Fig.4).

4 Conclusion

A compartmentalized co-culture method employing a MEA substrate was developed to examine the functional connections between sympathetic neurons and differentiated cardiomyocytes. First, the formation of synapses between sympathetic neurons and differentiated cardiomyocytes was confirmed by immunostaining with antibodies against -3 tubulin, synapsin I and cardiac troponin-I. Second, the observed spontaneous electrical activities were associated with synchronous beating of differentiated cardiomyocytes. Finally, changes in the beat rate of the differentiated cardiomyocytes triggered by electrical stimulation of the co-cultured sympathetic neurons were shown to be affected by the pulse frequency of the stimulation.

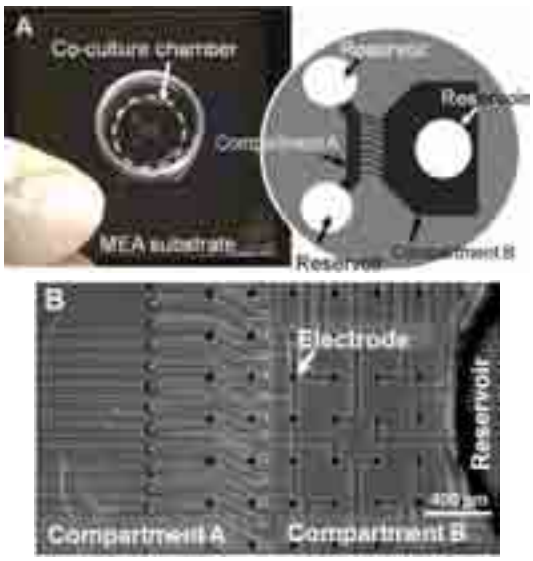

Fig. 1. Device for compartmentalized co-culture. (A) The culture device consisted of an MEA substrate with 64 electrodes embedded and a co-culture chamber. Schema of the co-culture chamber. The chamber consisted of compartments A and B, which were connected via 16 microchannels. Compartments B and A had one and two reservoirs, respectively. (B) Close-up of the middle part of co-culture chamber. Compartments A and B were 70 μm in height. Each pocket included an electrode for electrical stimulation of, and extracellular recording from, the SCG neurons cultured in the pocket. The pocket also assisted neurite outgrowth from the sympathetic neurons. The pockets were 50 μm in width and 70 μm in height.

Acknowledgement

We gratefully acknowledge the partial financial support provided by the Japan Society for the Promotion of Science (JSPS) via a Grant-in-Aid for JSPS Fellows (22-6118) and a Grant-in-Aid for Scientific Research A (23240065).

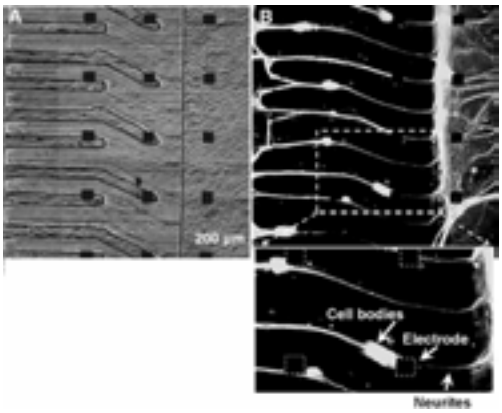

Fig. 2. Compartmentalized co-culture of SCG neurons and P19CMs on the microfabricated culture device. (A) Co-culture was maintained for more than 10 days after the start of co-culture. (B) Fluorescence immunostaining for β-3 tubulin (green), a specific marker of neurons. Cell bodies of the neurons were retained in a pocket (see the arrow in the figure), and the neurites were retained near the electrode. The SCG neurons extended their neurites along the microchannels, and the neurites reached compartment B, in which the P19CMs were cultured. 5.8±2.4 somata of SCG neurons were confined in one pocket (n = 11).

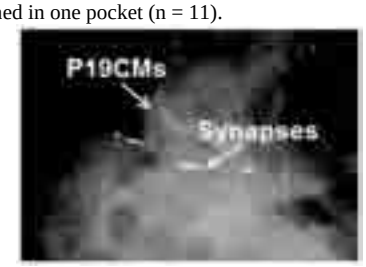

Fig. 3. Fluorescence immunostaining for synapsin I and cardiac troponin-I. P19CMs were stained with the anti-cardiac troponin-I antibody, and the SCG neurons with the anti-synapsin I antibody. Synapses of the SCG neurons were formed on P19CMs.

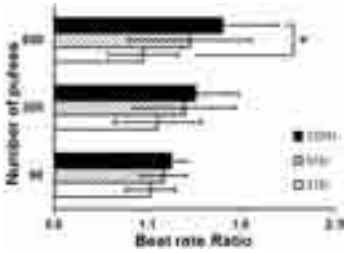

Fig. 4. Changes in beat rate of P19CMs after electrical stimulation to co-cultured SCG neurons (n = 5). Bonferroni's multiple comparison *post hoc* test revealed that the change in the beat rate after stimulation with 600 pulses at 1 Hz was significantly different from that after stimulation with 600 pulses at 10 Hz (*P <0.05).

References

[1] Orlic D., Hill J.M., Arai A.E., (2002). Stem cells for myocardial regeneration. *Circulation Research*, 91, 12, 1092-1102.

[2] Orlic D., (2005). BM stem cells and cardiac repair: where do we stand in 2004? Cytotherapy, 7, 3-15.

[3] Stett A., Egert U., Guenther E., Hofmann F., Meyer T., Nisch W., Haemmerle, H. (2003). Biological application of microelectrode arrays in drug discovery and basic research. Analytical and Bioanalytical Chemistry, 377, 486-495.

[4] Takeuchi A., Nakafutami S., Tani H., Mori M., Takayama Y., Moriguchi H., Kotani K., Miwa K., Lee J.K., Noshiro M., Jimbo Y., (2011). Device for co-culture of sympathetic neurons and cardiomyocytes using microfabrication", Lab Chip, 11, 13, 2268-2275.

Pharmacology, Toxicology, and Drug Screening

Speed-up of CNS drug development processes on MEA-based assays

Esther Steidl*, Mélanie Gleyzes, Fabien Maddalena, Benoit Quentin, Hélène Savinel, Romain Teyssié, Bruno Buisson.

Neuroservice, Aix-En-Provence, France
* Corresponding author. E-mail address: esther.steidl@neuroservice.com

Abstract

Multi-Electrode Array recordings in acute brain slices provides an exceptional macroscopic view of neuronal networks function but also provide mid-throughput, highly-sensitive, high-quality, robust and standardized assays.
MEA based-assay can answer to most of the questions arising along Central Nervous System (CNS) drug development processes:
1- To select and optimize hit and lead compounds. 2- To investigate or to confirm compounds Mechanism Of Action (MOA), thanks to a wide panel of protocols, within a fully physiological context. 3- To phenotype Transgenic (Tg) rodents over a wide range of neurophysiological properties and with a minimal number of animals. 4- To clarify compounds' safety with rapid turnaround and with a small quantity of compounds.
The power of MEA recordings is illustrated here with a few protocols performed in rodent cortex, hippocampus or cerebellum slices.
In conclusion, MEA recordings, performed in industrial processes, are perfectly suited to address pharmacological, toxicological and drug screening issues.

1 Introduction

While the investment in Research and Development (R&D) of pharmaceutical companies increases exponentially since 25 years, the emergence of New Chemical Entities (NCE) is not proportional to the increase of R&D budget. Developing a NCE becomes more and more expensive each year and takes more time than in the past [1, 2]. The development and marketing of new drugs is obviously more difficult than in the past years: on one hand compounds have to be more effective than the panel of compounds already approved, and on the other hand some current R&D programs focus on diseases of great complexity. Another reason of the cost increase of new drugs is the higher stringency of regulatory agencies to deliver marketing authorizations. Because of many drugs withdrawal after marketing, regulatory agencies want to have maximal guarantees in the new drugs safety and effectiveness.

For every 5,000-10,000 compounds that enter into R&D programs, ultimately only one will receive an approval. In clinical phases, the average attrition rate reaches 89%, and is even higher for CNS area. One major reason for such high attrition rate in the CNS area is a lack of predictibilty of existing CNS pathological models [3]. Paradoxically, the huge advances in genomics and proteomics over the end of the 20th century have concentrated a large part of the budget and research work of pharmaceutical companies, to the detriment of physiological approaches.

The CNS is much more complex than any other organ. Recording directly into brain slices provides the most effective way to integrate CNS neuronal networks complexity, and to use the most relevant models for compounds evaluation in true physiological conditions. MEA recording is an ideal technique to reach this aim, since it allows non-invasive - and multi-points - extracellular recordings. By providing high-content information at any step of drug development, MEA-based assay allows to speed-up R&D processes and maximize the probability of final drug approval. The added values of the MEA technique along drug development are summarized in Figure 1 and discussed hereinafter.

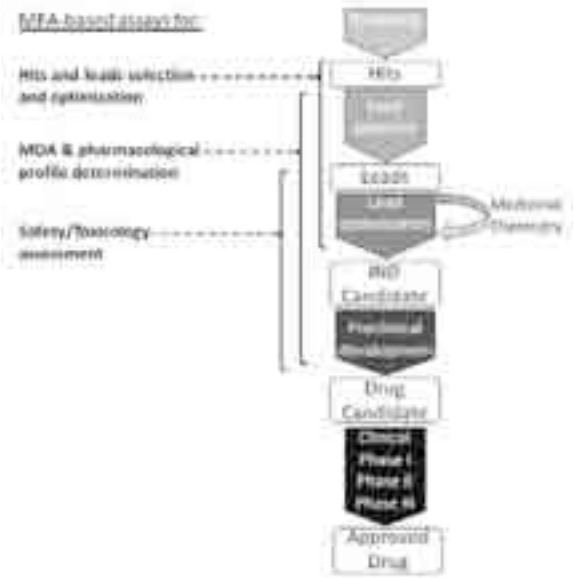

Fig. 1. Uses of MEA-based assays along drug development process.

2 Materials and Methods

Brain slices preparation

Brain slices are prepared from 3-5 week-old Sprague Dawley rats or 7-10 week-old C57black/6 mice. Hippocampus, cerebellum or cortex slices (350 to 400 µm thickness) are prepared alternatively with a MacIlwain tissue-chopper or a Leica VT1200S vibratome, and let to recover at 18 – 22 °C for at least 1 h in oxygenated Artificial Cerebro-Spinal Fluid (ACSF) of the following composition: (in mM; NaCl, 126, KCl 3.5, NaH_2PO_4 1.2, $MgCl_2$ 1.3, $CaCl_2$ 2, $NaHCO_3$ 25, D-glucose 11).

Multi-electrode array set-up

All data are recorded with a MEA set-up from Multi-Channel Systems (MCS). All of the experiments are carried out with 60 electrodes MEA (Qwane or MCS) spaced by 100 or 200 µm. During recordings, slices are continuously perfused with oxygenated (95% O_2-5% CO_2) ACSF at 37°C at a rate of 3 $ml.min^{-1}$.

Recording/stimulation protocols

fEPSP and PS recording: The brain slice is placed on the MEA and one electrode is chosen to stimulate the afferent pathway. The stimulus consists of a monopolar biphasic current pulse of 120 µs applied at a frequency of 0.03 Hz. An Input/Output curve is performed to adjust a stimulus intensity evoking 40% of maximal amplitude responses.

Interictal-like Epileptiform Discharges (ED): The hippocampal slices is placed on the MEA, so that MEA electrodes square the largest slice area.

CA1 or Purkinje neurons firing: MEA electrodes are positioned in order to record spontaneous firing of a maximal number of neurons.

Data analysis

fEPSP and PS amplitude: The amplitude values are normalized to the control period. Normalized fEPSP and PS values are averaged for experiments carried out in same conditions. The fEPSP and PS mean values (± SEM) are expressed as a function of time.

Interictal-like ED: The ED number by 30 s sweep is averaged for each slice and presented cumulated (± SEM) as function of time.

CA1 or Purkinje neurons firing: The neurons firing rate is normalized to the control period, and data from slices in the same conditions are averaged and expressed (± SEM) as a function of time.

3 Uses of MEA-based assays along CNS drug development processes

3.1 Hit and lead selection and optimization

The most obvious interest of MEA-based assays along drug development consists in selecting compounds of interest among a series of hits or leads in an environment as close as possible to the *in vivo* situation. Neuroservice have a wide panel of tests available, allowing to screen numerous targets under physiological conditions. The added value, while compared to cell based assays, is that compounds' target(s) is(are) the native one(s), in a true neuronal network, with all metabolic, signalling and regulating pathways functional.

Another advantage of MEA recordings for functional series of compound testing is it is much faster than electrophysiological testing with classical glass electrode. Neuroservice current screening capability is over 100 slices/week. Such throughput is then well suited for screening small chemical libraries, for hit or lead selection and lead optimization. In addition, the rapid turnaround of MEA-based assays allows a very dynamic interaction between Chemist and Biologist, to investigate Stucture-Activity Relationship and achieve an efficient chemical optimization. An illustration of screening of a few compounds targeting Long-Term Potentiation (LTP) mechanism in the temporal cortex is presented in Figure 2.

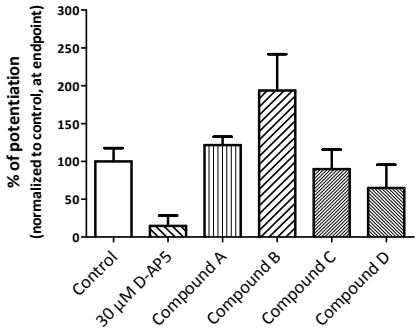

Fig. 2. Evaluation of a series of compounds on LTP recorded in the layer II/III of adult mice temporal cortex slices (stimulation in the cortical layer IV). Compounds A, B, C and D modify synaptic plasticity with different potencies, the compound B being the more effective to enhance LTP. LTP is strongly inhibited by 30 µM D-AP5, thereby confirming that LTP is NMDA-dependent.

MEA-based assay have been standardized and are performed as industrial processes. The reproducibility of such assays allows to compare data performed over months or years of interval with a remarkable confidence. Well-known pharmacological compounds are used to validate MEA-based electrophysiological measurements and to provide a reference activity; very consistent and reliable results are observed over years. As an illustration, 30 µM D-AP5 effect on LTP amplitude varied within a window of only 8% over 4 years of testing (in hippocampal rat slices it decreased LTP amplitude by 96 ± 2% in average). The reliability of the data, and their subsequent statistical processing, is also increased by the ability to record multiple evoked-responses within a single slice (in parallel at different electrodes and within the same region of interest).

3.2 MOA investigation or confirmation

MEA-based assays can be used to investigate and/or to confirm the MOA of compounds within a

fully physiological context. In addition they allow to identify off-target effect(s) which cannot be observed while performing target-restricted measurements. Then, MEA-based assays performed with acute CNS slices constitute the better approach and the more reliable strategy to develop Investigational New Drug (IND) candidates for CNS diseases with the optimal information on MOA and "off-target" possible activities.

Target-oriented screenings have largely evolved over the past decades, and cell-based and functional assays have replaced simple binding screenings. However, some compounds identified as receptors potent agonists, in recombinant systems for instance, have been demonstrated to be devoid of agonist properties within a brain slice as well as *in vivo*. For example, the compound AMN082 was initially identified as a mGluR7 selective agonist from experiments on transfected cells. Subsequent researches have proven that AMN082 activity or absence of activity depends on the recombinant system used (according the nature on the G-protein coupling) and that AMN082 is unable to activate mGluR7 receptors in rat hippocampal slices [4].

MEA-based assays, assessing compounds effect(s) at the overall neuronal network level, are an especially suitable technique to elucidate compounds MOA. MEA recordings can provide insightful information about a compound effect on overall synaptic transmission and plasticity processes. Thanks to a wide panel of tests available, MEA-based assays allow to progress step by step until elucidating the compound MOA. Once identified, agonist, antagonist or allosteric modulators properties can be documented in a very physiological context. Complete dose-response or dose-inhibition curves can be determined for compounds, yielding EC_{50} or IC_{50} as well as Hill coefficient. Figure 3 illustrates the dose-effect of a compound A targeting M1 mAChR, in the presence or in the absence of a sub-maximal concentration of the M1 mAChR antagonist Pirenzepine.

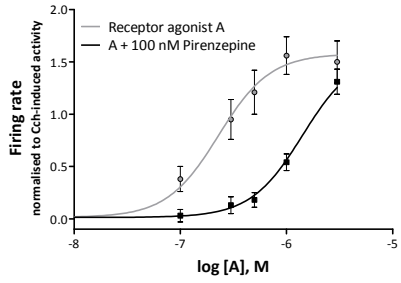

Fig. 3. Dose-response of compound A (a M1 mAChR agonist) on CA1 neurons firing, in the absence (grey circles) or in the presence (black squares) of 100 nM Pirenzepine. Note that the agonist dose-response curve is right-shifted in the presence of Pirenzepine, thereby indicating a competitive inhibition mechanism.

Thus, functional pharmacological data, together with the Blood Brain Barrier (BBB) crossing and Adsorption Distribution Metabolism Excretion (ADME) profile, provide a very good forecast of the *in vivo* behaviour of compounds.

Another advantage of MEA recordings relies on their capacity to evaluate Drug-Drug interaction. Phase III clinical development consists in evaluating the drug candidate on volunteer patients. When a drug for the targeted disease already exists, it is most of the time co-administered with the potential new drug under investigation. It is then crucial to determine as soon as possible along the drug development process what could be the interaction between the potential new drug and the already existing one(s). Potential adverse side-effects of drugs co-administration could thus be anticipated.

3.3 Tg rodent phenotyping

One of the most underestimated benefits of MEA-based assays is as a tool to investigate Tg rodent neuronal properties. MEA-based assays are perfectly suited to characterize rapidly a CNS deficit (or a CNS gain of function) of engineered rodents, from a few as 5 animals per genotype. When Tg animals are engineered to mimic a human CNS disease, the ability to evaluate the drug candidate both on WT and Tg brain slices constitute a very elegant manner to confirm both target(s) and compounds' activities in a pathophysiological context.

The Figure 4 below presents the large LTP deficit observed in a Tg mice model for Huntington's Disease (HD).

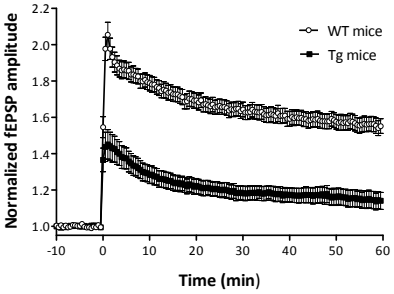

Fig. 4. LTP in hippocampal slices from WT (white circles) or Tg mice model of HD (black squares). Tg mice display a strong synaptic plasticity deficit while compared to WT mice.

Knowing physiological differences between WT and Tg neuronal properties, it is possible to determine a compound (or a series of compounds) efficacy to reverse the observed deficit. Compounds can be tested directly on brain slices, allowing to reach a mid-throughput, thus providing a robust screening assay. Further investigations can be undertaken on Tg animals, that can be treated with a validated compound, and compared with vehicle-treated ones.

3.4 Safety/toxicology assessment

The MEA technique has not the patch-clamp technique resolution but could be compared with a "wide angle objective" to observe compound effect(s) on the entirety of a neuronal network. Then, it is a

technique of choice to investigate the safety of new chemicals entities towards CNS network properties.

In addition MEA-based assays represent an interesting *in vitro* alternative to behavioural or toxicological tests performed on animals. Only a few milligrams of compound are required to determine its safety profile, which is compatible with compound's availability at early development stages. In addition, these *in vitro* measurements (based on electrophysiological precised quantifications) require lesser animals than *in vivo* behavioural tests and are more ethics.

Neuroservice provides a set of assays for compounds safety determination that consists in evaluating the compound acute or chronic toxicity on main neurons and neuronal network properties: genesis and propagation of action potentials, synaptic transmission and synaptic short- and long-term plasticity properties. Determination of the acute toxicity of compounds has a rapid turnaround and can be performed within one week for a single compound. In addition, compounds' chronic toxicity could be investigated in slices prepared from treated rodents versus slices from vehicle-treated ones.

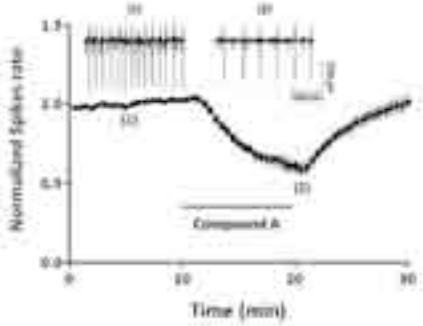

Fig. 5. Compound A acute effect on cerebellar Purkinje neurons spontaneous firing. Illustrations of neurons firing in control conditions or after a 10-minute exposure to the compound A are shown in inset 1 and 2, respectively.

A toxicological issue often encountered along drug development is the discovery of pro-convulsive side-effects [5]. It is then crucial to identify possible seizure liabilities early in the drug development process. Neuroservice provides an innovative screening platform utilizing MEA-based assays to detect the pro-convulsive properties of compounds. As illustrated in Figure 6, compounds displaying pro-convulsive properties are susceptible to modify the Population Spikes (PS) shape, or to trigger Epileptiform Discharges (ED) synchronous over the whole hippocampal area or to increase the CA1 neurons excitability. Compounds displaying weak pro-convulsive properties can be characterized by testing them in association with sub-threshold concentrations of a reference pro-convulsive compound (as it is done for Pentylenetetrazole (PTZ) test *in vivo*).

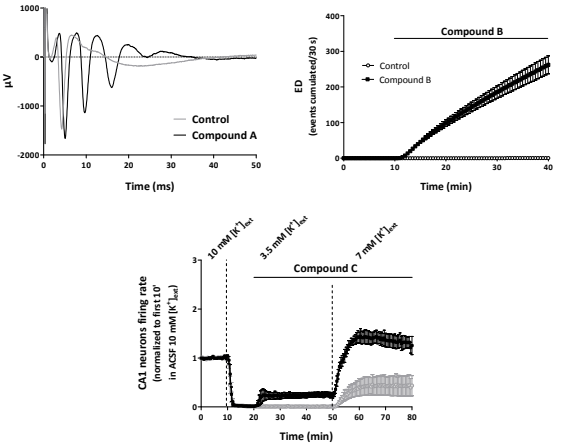

Fig. 6 Evaluation of compounds A, B and C pro-convulsive properties. PS display multiple spikes after exposure to the compound A (black trace) whereas they display a single spike in control conditions (grey trace). Compound B triggers ED (black squares) whereas the neuronal network remains "silent" in control conditions (white circles). The compound C (black squares) largely increases the CA1 neurons excitability in physiological conditions (3.5 mM $[K^+]_{ext}$) or in conditions of enhanced excitability (7 mM $[K^+]_{ext}$) while compared to control conditions (grey circles).

4 Summary

Acute brain slice recordings with MEA can provide answers to most of the questions arising along CNS drug development:

- Select and optimize hits or lead compounds; MEA recordings can facilitate the screening of a series of compounds in parallel, with a remarkably quick turnaround.
- Investigate or confirm compounds' targets and/or MOA, thanks to a wide panel of tests within a fully physiological context. Very precise pharmacological effects and profiles can thus be determined.
- Phenotype transgenic mice or rats for a wide range of neuronal properties and with a minimal number of animals and subsequently determine compound's target or drug candidate efficacy in these transgenic models.
- Clarify compounds' safety with rapid turnaround and a small quantity of compounds.

References

[1] DiMasi JA, Hansen RW, Grabowski HG (2003). The price of innovation: new estimates of drug development costs. J Health Econ. 22(2):151-85.

[2] Adams CP, Brantner VV (2010). Spending on new drug development. Health Econ. 19(2):130-41.

[3] Kola I, Landis J (2004). Can the pharmaceutical industry reduce attrition rates? Nat Rev Drug Discov. 3(8):711-5.

[4] Ayala JE, Niswender CM, Luo Q, Banko JL, Conn PJ (2008). Group III mGluR regulation of synaptic transmission at the SC-CA1 synapse is developmentally regulated. Neuropharmacology. 54(5):804-14.

[5] Easter A, Bell ME, Damewood JR Jr, Redfern WS, Valentin JP, Winter MJ, Fonck C, Bialecki RA (2009). Approaches to seizure risk assessment in preclinical drug discovery. Drug Discov Today. 14(17-18):876-84.

Functional cerebrospinal fluid diagnostics on micro-electrode arrays - ready for the clinic?

Marcel Dihné

Abteilung Neurologie mit Schwerpunkt Epileptologie
Hertie Institut für Klinische Hirnforschung
Universität Tübingen
Hoppe-Seyler-Straße 3
72076 Tübingen

In the last years, we described that human cerebrospinal fluid (CSF) specimens of healthy controls support in vitro-neuronal network activity (ivNNA) generated from primary rat or murine embryonic stem cell-derived populations. The basis for these experiments is the fact that the composition of the CSF influences brain development, neurogenesis, and behavior [1]. The bi-directional exchange of CSF and interstitial fluid (ISF) across the ependymal and pia-glial membranes is required for these phenomena to occur. As ivNNA represent an integration of the fundamental aspects of brain activity that are exhibited by functionally important collections of receptors, excitatory and inhibitory neurons of neurotransmitter-specific phenotypes, supporting astrocytes, and extracellular matrix molecules, ivNNA might serve as a reductionist model of global brain activiy. In succession we investigated the impact of CSF taken from patients suffering from traumatic brain injury [2] or anti-NMDA receptor encephalitis (submitted) on ivNNA. Additionally, we showed that the key player in hepatic encephalopathy disturbs ivNNA on microelectrode arrays and serves as a platform to discover counteracting or therapeutic strategies[3]. The overall goal is to identify functionally relevant substances in pathologically altered CSF and to recover ivNNA by pharmacological intervention. If, additionally, human ivNNA is applied generated from human induced pluripotent stem cells, our strategy could pave the way to identify new therapeutic options and towards individualized medicine.

Acknowledgement

This work was supported by the German Ministry of Education and Research (BMBF: FKZ 0315641A) and the European Union (EURO-TRANS-BIO project ESSSENCE)

References

[1] Dihné M, Hartung HP, Volume transmission-mediated encephalopathies: a possible new concept? , Arch Neurol. 2012 Mar;69(3):315-21.

[2] Otto F, Illes S, Opatz J, Laryea M, Hartung HP, Schnitzler A, Siebler M, Dihné M. Cerebrospinal fluid of brain trauma patients inhibits neuronal network function.. Ann Neurol. 2009 Oct;66(4):546-55.

[3] Schwarz C, Ferrea S, Quasthoff K, Walter J, Görg B, Häussinger D, Schnitzler A, Hartung H, Dihné M. Ammonium chloride influences in vitro-neuronal network activity. Exp Neurol. 2012 May;235(1):368-73.

Oscillatory activity in murine islets of Langerhans evaluated by extracellular recordings

Sven Schönecker[1-2], Martina Düfer[2], Peter Krippeit-Drews[2], Gisela Drews[2], Elke Guenther[1], Udo Kraushaar[1*]

1 Department of Electrophysiology, NMI, Reutlingen, Germany
2 Institute of Pharmacy, University of Tübingen, Tübingen, Germany
* Corresponding author. E-mail address: udo.kraushaar@nmi.de

Abstract
Insulin secretion of beta-cells within islets of Langerhans is mediated by electrical activity characterized by oscillations of depolarising bursts of action potentials and silent phases that are modulated by extracellular glucose concentration. Electrical activity thus directly combines blood glucose levels to insulin release, and therefore it is not only an indirect measure of insulin release but also an ideal parameter to assess beta-cell function. Here we show a non-invasive approach to record oscillatory activity of intact islets of Langerhans on a MEA based system that will allow to easily monitor alterations in beta-cell function in vitro.

1 Introduction

The proteohormone insulin is one of the key players for the maintenance of blood glucose homeostasis in humans. Pancreatic beta-cells are responsible for production and release of insulin after nutrient uptake. Elevated blood glucose concentration is directly sensed by the beta-cells, resulting in an instantaneous release of insulin finely adjusted to the glucose concentration. Dysfunction of beta-cells leads to a pathological change of the blood glucose level.

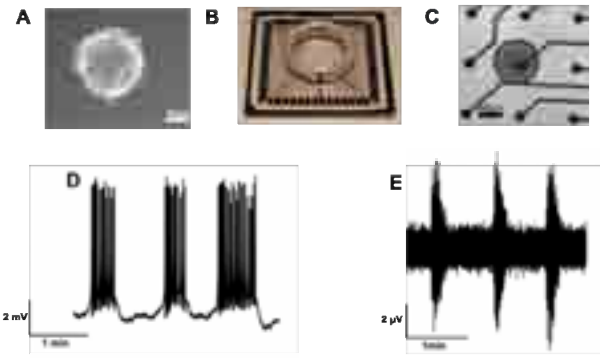

Fig. 1: A Microscopic view of a single murine islet of Langerhans. **B** Microelectrode array (MEA, Multi Channel Systems). **C** Islet of Langerhans placed on top of a MEA electrode **D** Membrane potential recording with an intracellular microelectrode from a beta-cell in an intact islet. Upward voltage deflections are Ca^{2+} action potentials on top of the so-called plateau phase. **E** Field potential recording on MEA electrode. The recording is qualitatively comparable to intracellular measurements. D and E in 10 mM glucose.

Modern sedentary life style and malnutrition are among the factors that can leads to chronically increased insulin secretion and a subsequent progressive degeneration of beta-cells triggered by oxidative stress and low-grade inflammation. As a result the beta-cells cannot compensate for the increased insulin demand of the body. Consequently, blood glucose level rises, culminating in type 2 diabetes mellitus (T2DM). Within the next 20 years a dramatic increase of T2DM patients worldwide is predicted, rising from 171 million in the year 2000 to estimated 366 million in 2030 [1]. The increasing prevalence and the fact that T2DM is still not curable demonstrates the importance to better understand the underlying cellular mechanisms of this disease.

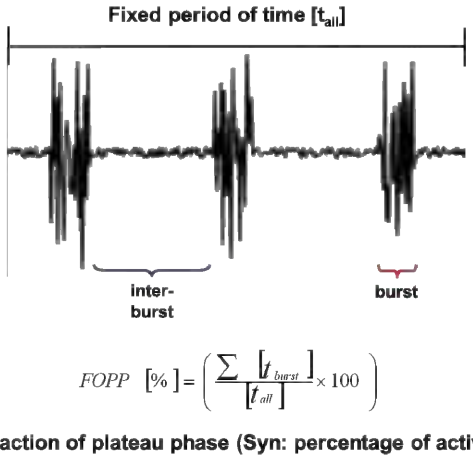

Fig. 2: Sketch of the fraction of plateau phase [%] (FOPP) for the quantification of beta-cell activity.

The secretion of insulin is mediated by a characteristic oszillatory electrical activity within the beta-cells that is modulated by blood glucose concentration. This direct linkage between glucose level, electrical activity and insulin secretion is called stimulus-secretion-coupling (SSC). In brief, glucose enters the beta-cells via glucose transporters, resulting

in an acceleration of metabolism and ATP production. This closes ATP-sensitive K^+ channels (K_{ATP}-channels), resulting in depolarisation of the membrane potential (V_m) followed by the opening of voltage-dependent Ca^{2+} channels. The subsequent rise of the cytosolic Ca^{2+} concentration ($[Ca^{2+}]_c$) is the trigger for the exocytosis of insulin containing vesicles. The effect of repolarisation occurs due to the activation of voltage- and Ca^{2+}-dependent K^+ channels, respectively.

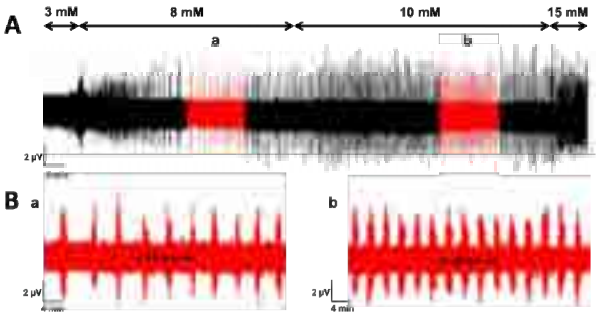

Fig. 3.: Increasing extracellular glucose concentration results in higher FOPP. **A** Long term recording at different glucose concentrations. **B** Magnification of recordings in 8 and 10 mM glucose.

Long-lasting glucose stimulation above a threshold (~ 6 mM glucose) initiates electrical activity. Thus, electrical activity in beta-cells appears as characteristic oscillations of depolarising Ca^{2+} action potential bursts and hyperpolarised interburst phases. The length of the bursts is modulated by the extracellular glucose concentration.

The oscillatory pattern can be analysed by calculating the ratio of burst to interburst phases, specified as fraction of plateau phase (FOPP ~ percentage of time with spike activity) (Fig. 2). The FOPP increases in dependence of the glucose concentration between ~ 6 - 25 mM.

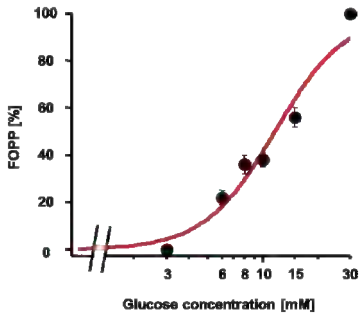

Fig. 4: Glucose concentration response curve (CRC) plotted as FOPP against glucose concentration [mM]. In 3 mM glucose no activity was detected while 30 mM led to continuous activity. The obtained glucose CRC is in good agreement with findings of other studies using intracellular methods.

The classical electrophysiological tools to measure the FOPP like the sharp microelectrode or patch-clamp technique require high technical skills and/or interfere with beta-cell function. Here we present a new tool to overcome these limitations, by using microelectode arrays (MEA) to non-invasively record beta-cell activity from islets of Langerhans [2]. The advantages of this approach include its simplicity and high throughput compared to classical methods. In the following extracellular recordings of beta-cell oscillations and their modulation by substances are shown not only to demonstrate the validity of the method to access beta-cell function but also to illustrate its suitability as pharmacological test platform.

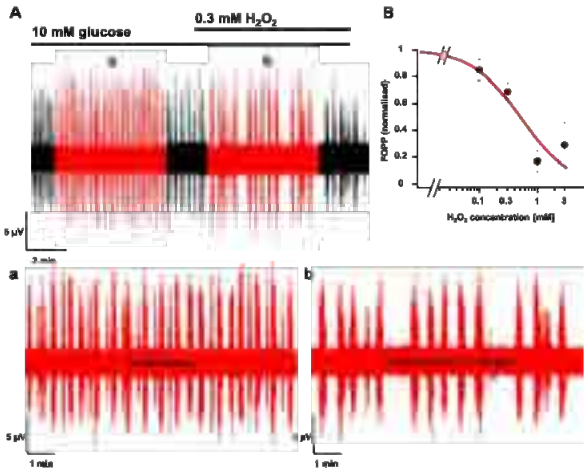

Fig. 5: A Application of H_2O_2 induces oxidative stress. 0.3 mM H_2O_2 decreased the FOPP by 31 ± 3 % (n=14) in 10 mM glucose. **a** and **b** magnification of recordings in 10 mM glucose (left trace) and 10 mM glucose + 0.3 mM H_2O_2 (right trace). **B** H_2O_2 concentration-response-curve. Data are normalized to control in 10 mM glucose and plotted as ΔFOPP against the H_2O_2 concentration.

2 Material and Methods

Islet preparation

Intact islets of Langerhans were isolated from adult C57Bl/6 N or NMRI mice (Janvier, France) by collagenase digestion and subsequently cultured up to 3 days in RPMI 1640 medium supplemented with 10% fetal calf serum, 100 U/ml penicillin and 100 µg/ml streptomycin.

Solution and chemicals

Extracellular recordings of V_m by MEA were achieved in a solution containing (in mM) : 140 NaCl, 5 KCl, 1.2 $MgCl_2$, 2.5 $CaCl_2$, 10 HEPES, pH 7.4, and glucose as indicated. The culture medium RPMI 1640, fetal calf serum, penicillin/streptomycin and the Ca^{2+} binding fluorescent dye fura2-AM were provided by Invitrogen (Karlsruhe, Germany).

MEA Setup

MEA recordings were obtained using a MEA1060-inv amplifier with MC-Rack software (Multi Channel System, Reutlingen, Germany). Data were filtered online (10 Hz - 3 kHz), sampled at 5-25 kHz and low pass filtered offline at 25 Hz. Mouse islets were arranged on a MEA and substances were either applied by bath perfusion or added directly into the bath. All experiments were performed at 37°C whereby $[Ca^{2+}]_c$ was determined by imaging technique.

Electrophysiological recordings

Whole islets of Langerhans with a diameter of 100 to 300 µm were incubated for 10 min in 3 mM glucose and then placed on top of a MEA electrode (Fig. 1 C). The overall procedure for islet handling took less than 20 min. The MEA bath chamber was continuously perfused throughout the recordings. The measurements typically started in 3 mM glucose that is below the threshold to trigger electrical activity. Oscillatory activity was observed at extracellular glucose concentrations between 6 and 25 mM. Analysis of the oscillatory activity was obtained by determining the alterations of FOPP.

3 Results

Elevation of the extracellular glucose concentration from initial 3 mM to 10 mM led to a transient electrical activity followed by rhythmic alterations between bursts and silent phases. This oscillatory pattern was stably detectable over extended time periods (more than 2h). The success rate to detect these signals was in the order of 75 % (Fig. 3).

The MEA-based non-invasive extracellular recordings were qualitatively comparable to conventional intracellular recordings (Fig. 1 D and E). Length of bursts and interbursts are dependent on the extracellular glucose level. At 3 mM glucose no activity was recorded (n=10). Concentrations of 6, 8, 10 and 15 mM resulted in dose-dependent oscillations with FOPPs of 22 ± 3 % (n = 5), 36 ± 4 % (n = 5), 38 ± 3 % (n = 8), and 56 ± 4 % (n = 11), respectively. A further increase to 30 mM led to a transition into continuous activity (n = 5). The obtained concentration-response curve revealed a half-maximal stimulation at 12 ± 2 mM (Fig. 4), in line with previous data recorded intracellularly [3].

The electrical activity of the islets was influenced by ion channel modulators known to have an impact on beta-cell activity. Application of the K_{ATP} channel opener diazoxide (100 µM) resulted in a silencing of the oscillatory pattern, most likely due to hyperpolarization of V_m. Subsequent application of the K_{ATP} channel blocker tolbutamide (150 µM) on the other hand, partially restored the electrical activity, probably by depolarization of the cells beyond the threshold for L-type Ca^{2+} channels (Fig. 7 B). Furthermore the application of 10 µM nifedipine, a specific Ca^{2+} channel antagonist, completely diminished the oscillatory activity (Fig. 7 A). Next we investigated the link between V_m and the cytosolic Ca^{2+} concentration. Therefore MEA recordings were combined with simultaneous Ca^{2+} imaging, using fura2-AM as Ca^{2+} sensitive dye. In 10 mM glucose it could be shown that burst phases and transient increases of $[Ca^{2+}]_c$ were highly correlated (Fig. 6). Taken together these findings confirmed that the burst activity recorded by the MEA technology is Ca^{2+} driven as shown previously by intracellular recordings [4].

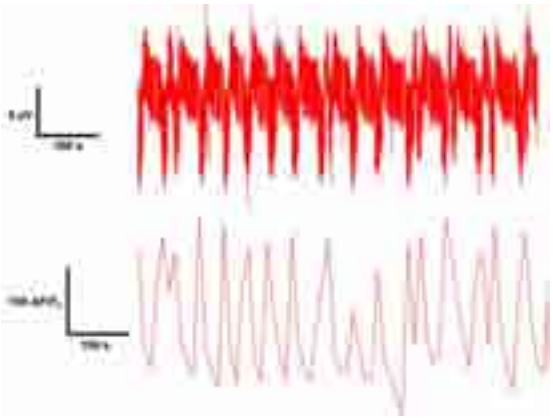

Fig. 6: Simultaneous recordings of electrical activity and $[Ca^{2+}]_c$. The upper trace display glucose-induced electrical activity. The lower trace show measurements of $[Ca^{2+}]_c$. Each burst of APs is accompanied by a peak in $[Ca^{2+}]_c$. Glucose concentration was 10 mM.

It is well known that oxidative stress progressively leads to the impairment of beta-cell function and is crucial for the development of T2DM. Oxidative stress can be induced experimentally by confronting the cells with low concentrations of H_2O_2, a well described donor of free radicals. Application of H_2O_2 in 10 mM glucose led to a concentration-dependent decrease of the FOPP. At 0.3 mM H_2O_2 the FOPP decreased from 44 ± 4 % to 31 ± 4 % which equals a reduction of 30 ± 3 % (n=14). Overall the half maximal inhibition of the FOPP was 0.49 ± 0.2 mM (Fig. 5). The high sensitivity of the system to record even small changes of electrical activity as shown in the H_2O_2 experiments will enable us to test for the effects of beta-cell modulators precisely.

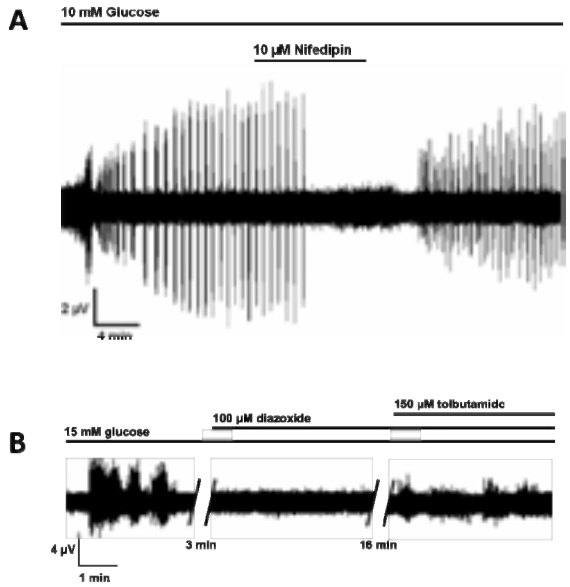

Fig. 7: A Application of 10 µM nifedipin to a oscillating islet of Langerhans. The specific Ca^{2+} channel antagonist completely inhibits the oscillatory activity. The effect of nifedipin is reversible. **B** The application of the K_{ATP} channel opener diazoxide (100 µM; middle trace) results in a silencing of the oscillatory activity. An additional application of the K_{ATP} channel blocker tolbutamide (150 µM; right trace), on the other hand, restored the electrical activity.

4 Discussion

Here we demonstrate a novel tool to non-invasively record physiological electrical activity of beta-cells in intact islets of Langerhans. The signals most likely reflect the summation of potential changes from several beta-cells rather than discrete field action potentials. The validity of this novel approach was demonstrated by using modulators with known effects of beta-cell activity recorded by classical electrophysiological methodologies such as intracellular recordings. In comparison to the classical methods, however, the MEA based technology has several advantages. First, recordings are easy to obtain and with higher success rate in comparison to conventional methods. Second, the non-invasiveness of the method conserves the natural behaviour of the cells. This enables detection of even small modulatory FOPP changes as shown by the effect of oxidative stress on oscillatory activity.

To summarise, MEA-based recordings of beta-cell oscillatory activity can be a useful platform to e.g. better understand the mechanism of T2DM and the beta-cell physiology in general.

Several further applications are imaginable, such as addressing both acute and chronic effects of metabolites or to study transgenic animal models. In addition the simplicity and high throughput potential of the method makes it suitable as a screening tool in diabetes drug development.

References

[1] Genuth S, Alberti KG, Bennett P, Buse J, Defronzo R, Kahn R, Kitzmiller J, Knowler WC, Lebovitz H, Lernmark A, Nathan D, Palmer J, Rizza R, Saudek C, Shaw J, Steffes M, Stern M, Tuomilehto J, Zimmet P. Expert Committee on the Diagnosis and Classification of Diabetes Mellitus. Follow-up report on the diagnosis of diabetes mellitus. Diabetes Care. 2003 Nov;26(11):3160-7.

[2] Kraushaar U. et al. (2010) Oscillatory activity in murine Langerhans islets. Conference Proceedings of the7th International Meeting onSubstrate-Integrated MicroelectrodeArrays; BIOPRO Baden-Wurttemberg GmbH, Stuttgart

[3] Henquin JC. (2009) Regulation of insulin secretion: a matter of phase control and amplitude modulation. Diabetologia 52:739–51

[4] Santos, R. M., L. M. Rosario, et al. (1991). "Widespread synchronous $[Ca^{2+}]_i$ oscillations due to bursting electrical activity in single pancreatic islets." Pflugers Arch 418(4): 417-22.

Impact of ammonium chloride on neuronal network activity

Clara-Sophie Schwarz[1], Stephan Theiss[2], Marcel Dihné[3*]

1 Department of Neurology, Heinrich Heine University Düsseldorf, Germany
2 Institute of Clinical Neuroscience and Medical Psychology, Heinrich Heine University, Düsseldorf, Germany
3 Department of Neurology & Epileptology, Hertie Institute for Clinical Brain Research, Tübingen University, Tübingen, Germany
* Corresponding author. E-mail address: Marcel.Dihne@uni-tuebingen.de

Abstract
In this work, a novel *in vitro* model of ammonia toxicity is introduced as a tool for studying hepatic encephalopathy (HE). Electrically active rat neuronal networks on microelectrode arrays (MEAs) were exposed to ammonium chloride solution, and their responses to glutamine synthetase inhibition and N-methyl-D-aspartic-acid (NMDA) receptor antagonists were examined. Blocking NMDA receptors turned out to be sufficient to prevent ammonium chloride effects. Our model of ammonia toxicity could be helpful to deepen the understanding of HE and to evaluate potential pharmacological targets.

1 Background/Aims

HE is a neuropsychiatric syndrome in patients with liver disease mediated mainly by ammonia. Ammonia neurotoxicity is associated with enzymatic glutamine formation in astrocytes and excessive activation of NMDA receptors [1]. The present work introduces an *in vitro* model of HE using co-cultures appropriate to study the disturbance of astrocytic-neuronal interaction on a functional level, representing complex *in vivo* conditions while profiting by the advantages of an *in vitro* model.

2 Material and Methods

Synchronous bursting behaviour of rat cortical cells was recorded on MEAs after 24 hours of ammonium chloride exposure (5 mmol/l) as described elsewhere [2]. Additionally, the glutamine synthetase inhibitor methionine sulfoximine and the NMDA receptor antagonists DL-2-Amino-5-phosphono-pentanoic acid [2] and Memantine hydrochloride (n=5 MEAs) were applied both individually and in combination with ammonium chloride.

As a statistic measuring firing synchrony, Cohen's kappa (range ±1) was averaged across all active pairs of electrodes. Numbers of bursts per minute and kappa are given relative to medium baseline. For statistical analysis, the Wilcoxon signed-rank test (medium set to 1) was performed.

3 Results

Ammonium chloride increased bursting activity (Fig.1) but suppressed firing synchrony (Fig. 2). Inhibition of glutamine synthetase, which prevents ammonia fixation in astrocytes, caused qualitatively similar changes, although not statistically significant (Fig. 1, 2). Methionine sulfoximine pretreatment neutralized ammonium chloride induced excitation (Fig. 1), but could not prevent ammonium chloride induced desynchronization (Fig. 2).

While NMDA receptor antagonists did not influence burst rates after 24 hours (Fig.1), they increased kappa (Fig.2). Furthermore, NMDA receptor antagonists prevented ammonium chloride induced changes in both burst rate and synchrony (Fig. 1, 2).

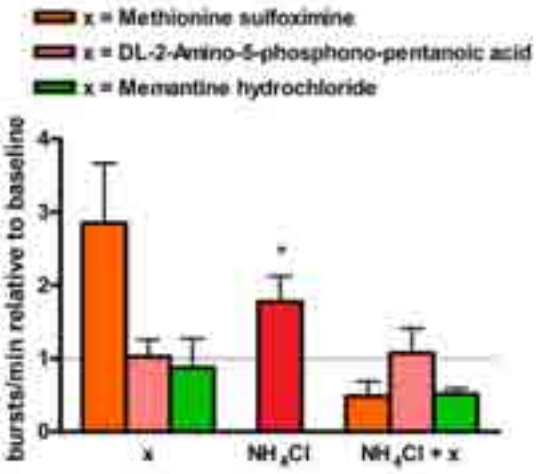

Fig. 1: Bursts/min 24 hours after application of test substances. Data concerning Ammonium chloride, Methionine sulfoximine and DL-2-Amino-5-pentanoic acid adopted from [2].

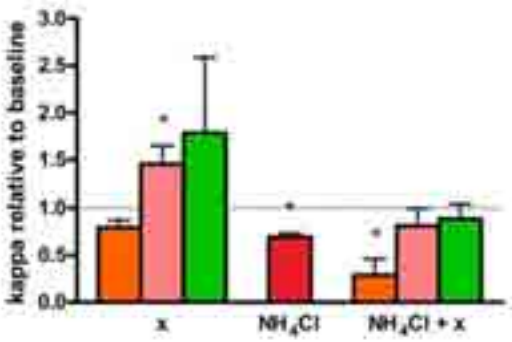

Fig. 2: Kappa 24 hours after application of test substances. Data concerning Ammonium chloride, Methionine sulfoximine and DL-2-Amino-5-pentanoic acid adopted from [2].

4 Conclusions

Ammonium chloride induced desynchronization of *in vitro* neuronal networks may appropriately represent neuronal network dysfunction in HE. This suggests MEA technology to be a valuable tool for studying protective measures against ammonia toxicity. The results of the present work support the assumption that NMDA receptor activation is the principal mechanism mediating ammonia toxicity to the brain.

Acknowledgement

This work was supported by the German Ministry of Education and Research (BMBF: FKZ 0315641A) and the European Union (EURO-TRANS-BIO project ESSSENCE).

References

[1] Häussinger F., Schließ F. (2008): Pathogenetic mechanisms of hepatic encephalopathy. *Gut*, 57 (8), 1156-1165.

[2] Schwarz C.-S., Ferrea S., Quasthoff K., Walter J., Görg B., Häussinger D., Schnitzler A., Hartung H.-P., Dihné M. (2012): Ammonium chloride influences in vitro neuronal network activity. *Experimental Neurology*, 235 (1), 368-373.

Assay for drugs to treat tinnitus

Ernest J. Moore[1,3], Calvin Wu[1,2,3], Kamakshi Gopal[1,3*], Thomas J. Lukas[4], Guenter W. Gross[2,3]

1 Department of Speech and Hearing Sciences, University of North Texas, Denton, TX USA
2 Department of Biological Sciences, University of North Texas, Denton, TX USA
3 Center for Network Neuroscience, University of North Texas, Denton, TX USA
4 Department of Molecular Pharmacology & Biological Chemistry, Feinberg School of Medicine, Northwestern University, Chcago, IL USA
* Corresponding author. E-mail address: gopal@unt.edu

Abstract

Tinnitus ("ringing in the ears") affects approximately 50 million people worldwide, with 10 million being highly debilitated. Pharmacotherapy for tinnitus is still in emerging stages due to time consuming clinical trials and/or animal experiments. We tested a new cellular model where induced rapid neuronal firing or spiking was used as a mimic for the presumed type of aberrant activity that may occur in tinnitus. Spontaneously active auditory cortical networks growing on microelectrode arrays were exposed to 1.0 mM Pentylenetetrazole (PTZ) and showed increases in spike rate by 139.6 ± 27 percent and burst rate of 129.7 ± 28 percent. Reductions of increased activity were observed; the potency of the drugs was linopirdine > L-carnitine > pregabalin > gabapentin. These studies provide proof of principle for the use of auditory cortical networks on microelectrode arrays as a workable platform for semi-high throughput application for screening of drugs that might be used for the treatment of tinnitus.

1 Introduction

Tinnitus is a highly debilitating otological condition that has defied medical and rehabilitative treatment. The sounds perceived as tinnitus are usually high-pitched whistles, but some individuals report hearing other noises such as hissing, buzzing, chirping, clicking, or other internally generated annoying sounds [1]. The condition affects approximately 50 million people worldwide. Contemporary approaches to treatment consist of behavioral modification techniques and so-called tinnitus maskers. Pharmacological agents to treat tinnitus have not been readily forthcoming due to unconvincing clinical trials and a lack of well-established animal models [2]. Previous *in vivo* animal models for testing drugs that may alleviate tinnitus have also not proven effective [3]. Furthermore, drug companies that are involved in bringing new drugs to market have not developed an interest in tinnitus. Given the number of people who are suffering from tinnitus, the condition cannot be classified for the development of orphan products. Therefore, the basic mechanisms underlying tinnitus that would lead to better treatment regimens are not well understood and therefore needs further clarification.

2 Method

We induced a tinnitus-like excitatory activity *in vitro* in spontaneously active mouse auditory cortical networks growing on microelectrode arrays (MEA). We exposed the cultures to Pentylenetetrazole (PTZ), a pro-convulsant $GABA_A$ antagonist, that up-regulated electrical firing. We surmised that $GABA_A$ receptors are perhaps involved in the initiation and maintenance of tinnitus. Auditory cortical networks were then treated with four experimental "tinnitus drugs", Linopirdine (a potassium channel blocker), L-Carnitine (an antioxidant), and the selective Ca2+ channel blockers Pregabalin (Lyrica) and Gabapentin (Neurontin).

3 Results

PTZ significantly increased spike rate and burst rate activity of auditory cortical networks (Table 1). We interpreted the increased neuronal activity to be presumably mimicking tinnitus, with phenotypic high firing of over-excited neurons. We saw a reduction of the increased network activity that was brought on by PTZ when the experimental tinnitus drugs were applied. The potency of the drugs was Linopirdine > L-Carnitine > Pregabalin > Gabapentin (Fig. 1).

Table 1. Percent increase in spike rate and burst rate under 1.0 mM PTZ (n = 39)

	% Spike	% Burst
Average	139.6	129.7
SEM	27.2	27.7

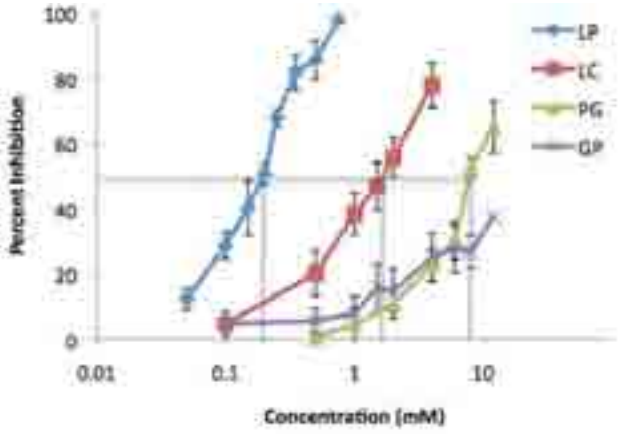

Fig. 1. Concentration-response curves for auditory cortical networks pre-treated with 1.0 mM PTZ followed by application of linopirdine (LP; n = 3), L-carnitine (LC; n = 3), pregabalin (PG; n = 3), and gabapentin (GP; n = 3). EC50 are shown by 50% reduction with solid line. Note: GP does not reach 100% inhibition.

4 Conclusions

The *in vitro* auditory cortical networks growing on MEAs served as an effective platform for semi-high throughput application for screening of drugs that might be used for the treatment of tinnitus. Our purpose, therefore, was to test the efficacy of several drugs already available on the market (repurposed drugs) that might attenuate increased ongoing electrical activity of mouse auditory cortical neurons. We conclude that the MEA platform served as an efficient vehicle for initially screening drugs that may (or may not) prove efficacious for reducing the percept of tinnitus [4].

Acknowledgement

This research was supported in part by a Faculty Research Grant (GA9289) from UNT awarded to EJM, and the Charles Bowen Endowment to the Center for Network Neuroscience. This paper is a modification of [4].

References

[1] Littler, T.S. (1965). The Physics of the Ear. Oxford, UK: Pergamon Press.

[2] Baguley, D.M. (2002). Mechanisms of tinnitus. *Br. Med. Bull*, 63, 195-212.

[3] Turner, J.G. (2007). Behavioral measures of tinnitus in laboratory animals. *Prog Brain Res*, 166, 147-156

[4] Wu, C., Gopal, K., Gross, G.W., Lukas, T.J., Moore, E.J. (2011). (2011). An in vitro model for testing drugs to treat tinnitus. *European J Pharmacol*, 667, 188-194.

Multiphasic concentration-response curve fitting for examining activity changes when applying the cancer pain drug Dynorphine A to an *in vitro* neuronal network

Kerstin Lenk[1*], Jan Engelmann[1], Olaf H.-U. Schröder[2]

1 Faculty of Engineering and Computer Science, Lausitz University of Applied Sciences, Senftenberg, Germany
2 NeuroProof GmbH, Rostock, Germany
* Corresponding author. E-mail address: kerstin.lenk@hs-lausitz.de

Abstract

In *in vitro* experiments, the concentration-response curve of Dynorphine A shows for some features a triphasic shape. These concentration-response curves can exhibit non sigmoid shape, then indicating that different mechanisms affect the neuronal activity. So far, there is no tool available which can cover sufficiently triphasic (i.e. the curve has two local extremes) concentration-response curves.

1 Background/Aims

Concentration-response curves of MEA-neurochip experiments can be very often multiphasic. Considering that, it is a great need to have robust and reliably concentration-response curve fits especially for high-throughput needs and to identify certainly multiphasic behaviour.

In *in vitro* experiments, the concentration-response curve of Dynorphine A shows for some features a triphasic shape. The aim is to provide a satisfying fit of such a curve.

For the experiments frontal cortex neurons extracted from embryonic mice are cultivated on multielectrode array (MEA) neurochips [1]. The activity of single neurons in such networks is recorded especially the change of network activity caused by long-term application of neuroactive substances, such as Dynorphine A. Dynorphine A is used in cancer pain treatment [2]. Based on the data, different features [3] are calculated adapted from spikes and bursts and separately displayed in concentration-response curves [4]. These concentration-response curves can exhibit non sigmoid shape, then indicating that different mechanisms affect the neuronal activity. So far, there is no tool available which can cover triphasic (i.e. the curve has two local extremes) concentration-response curves.

2 Methods

2.1 Data

We applied both curve fitting approaches described below to respectively data from nine different experiments which are derived by adding Dynorphine A with concentrations between 1E-16 and 1E-04 Mol.

The concentration-response curve is given as one of twelve chosen features depending on the logarithm of concentration (Table 1). The features are calculated as means of nine experiments with Dynorphine A.

2.2 Curve Fitting

We present two methods to calculate multiphasic concentration-response curves: A fitting algorithm, extending the method described in Motulsky and Christopoulos (2003) [4], is developed to fit multiphasic, biologically reasonable concentration-response curves. To fit triphasic concentration-response curves the datasets have to have at least 10 data points. For a triphasic curve a sigmoid curve is calculated for each of the three phases (see Figure 1(a)). The three sigmoid curves are added up in their corresponding range. We call this method multiphasic concentration-response relationship (MCRR). Secondly, an asymmetric Gaussian function is applied to the MEA neurochip data (data by courtesy from NeuroProof GmbH, Rostock, Germany). The lower and upper boundaries as well as the starting values are chosen according to the datasets. Because our models are non-linear, the fitting method 'non-linear least squares' was chosen. As fitting algorithm the trust region method was used.

2.3 Validation

Firstly, the validation was done visually. Secondly, the adjusted *R*-squared was calculated.

3 Results and Discussions

We have calculated the concentration-response curves for twelve features and nine experiments, i.e. 108 graphs are plotted respectively for each method.

Twenty-two of these 108 graphs are triphasic (one example is shown in Figure 1) based on the definition that the data points possess two local extremes.

For the MCRR method the visual validation exhibits that 16 of 22 fits follow the data points well. The visual validation of the asymmetric Gaussian function showed that 20 of 22 fits are sufficient. The curves appear “edgy” and have to be smoothened.

Table 2 shows the sufficient and insufficient fits of the triphasic concentration-response curves for the MCRR method and the asymmetric Gaussian function. One of the two insufficient fits with the asymmetric Gaussian function was satisfactorily fitted with the MCRR method.

The methods described above lead to new features, e.g. area under the curve and curvature. We aim to use these features for classification with machine learning algorithms like neuronal networks or support vector machines to identify unknown substances.

4 Conclusions

Both methods, MCRR and asymmetric Gaussian function, deliver good fits of triphasic concentration-response curves. The methods do not require interaction by the user, e.g. for the choice of parameters; therefore both methods are suited for high-throughput evaluation.

Table 1: Twelve chosen features; each depending on the concentration of the added neuroactive substance.

Representation	Feature
General activity	Mean spike rate (spikes per minute)
	Mean burst duration
	Mean per cent of spikes in burst
Synchronisation	Simplex (number of highly synchronized spike events)
	Event of summarized integrated approximation curve
	SynShare (fraction of highly synchronized neurons)
Oscillation properties	Standard deviation of the burst plateau
	Standard deviation of burst rate (bursts per minute)
	Standard deviation of burst period (burst duration and the following duration to the next burst)
Burst structure	Mean burst plateau
	Mean burst amplitude
	Mean plateau position

Table 2: Fitting results of the triphasic concentration-response curves. The table shows the number of sufficient and insufficient fits for the MCRR method and the asymmetric Gaussian function.

Method	MCRR	Asymmetric Gaussian function
adjusted *R*-squared ≥ 0.8	9	20
adjusted *R*-squared < 0.8	13	2

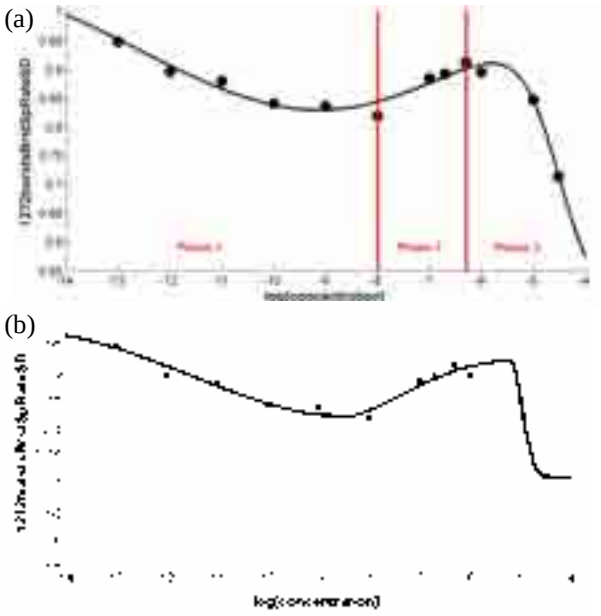

Fig. 1. Fit of a triphasic concentration-response curve for the feature standard deviation of the burst rate. (a) The graph shows the three phases which depend on the two local extremes. The MCRR method was used to fit the concentrations-response curve. In this case, the adjusted *R*-squared is 0.90. (b) The asymmetric Gaussian function was used. In this case, the adjusted *R*-squared is 0.96.

Acknowledgement

We thank Matthias Reuter (Clausthal University of Technology, Germany) and Barbara Priwitzer (Lausitz University of Applied Sciences, Germany) for their continuous support.

References

[1] Johnstone, A., Gross, G.W., Weiss, D., Schroeder, O.H.-U., Gramowski, A., Shafer, T. (2010): Microelectrode arrays. A physiologically based neurotoxicity testing platform for the 21st century. *Neurotoxicology*, 31(4), 331-350.

[2] Gramowski, A., Jügelt, K., Weiss, D.G., Gross, G.W. (2004): Substance identification by quantitative characterization of oscillatory activity in murine spinal cord networks on microelectrode arrays. *Eur. J. Neurosci*.,19, 2815-2825.

[3] Schroeder, O. H.-U., Gramowski, A., Jügelt, K., Teichmann, C., Weiss, D.G. (2008): Spike train data analysis of substance-specific network activity: Application to functional screening in preclinical drug development. *Proceedings of the 6th Int. Meeting on Substrate-Integrated Microelectrodes*, 113-116.

[4] Motulsky, H., Christopoulos, A. (2003): Fitting Models to Biological Data Using Linear and Nonlinear Regression: A Practical Guide to Curve Fitting. *http://www.graphpad.com/manuals/prism4/RegressionBook.pdf*. Accessed 2 Sept 2009.

Modulation of neuronal network activity with ghrelin

Stoyanova II[1*], Rutten WLC[1], le Feber J[1]

1 Neurotechnology Group, Faculty of Electrical Engineering, Mathematics and Computer Sciences, University of Twente, Enschede, the Netherlands
* Corresponding author. E-mail address: stoyanovai@yahoo.co.uk

Abstract
Ghrelin is a neuropeptide regulating multiple physiological processes, including high brain functions such as learning and memory formation. However, the effect of ghrelin on network activity patterns and developments has not been studied yet. Therefore, we used dissociated cortical neurons plated on multi electrode arrays (MEAs) to investigate *in vitro* how acute and chronic exposure to ghrelin affects neuronal activity. We found that ghrelin application has a strong stimulatory effect on neuronal activity, and causes a switch from synchronous to more dispersed asynchronous network firing. When chronically applied, ghrelin leads to earlier generation of "mature" activity patterns, including neuronal bursts.

1 Introduction

The neuropeptide ghrelin plays a role in multiple physiological processes regulating energy metabolism, it has an excitatory effect on neuronal activity and stimulates synaptic plasticity. Recently it was related to dendritic spine architecture, long-term potentiation and cognition. However, the effect of ghrelin on neuronal networks activity patterns and development has not been studied yet. Since this data is difficult to acquire *in vivo*, and dissociated neuronal cultures plated on multi electrode arrays (MEA) are useful model for brain inquiry, we aimed at investigating *in vitro* how the acute or chronic exposure to ghrelin affects neuronal activity patterns.

2 Material and Methods

Dissociated cortical neurons were cultured on MEAs. In the acute experiments, cultures were moved to the measurement set up and we recorded baseline activity for 1 hour. Then we replaced 300 µl of the medium with additional ghrelin to obtain a final concentration of 1 µM and recorded activity for 1 hour. In the chronic experiments (n=12), neurons were cultured for a period of 4 weeks in a medium supplemented with ghrelin at 1 µM concentration. As a control we used 12 cultures from the same plating incubated in plain medium. Their activity was recorded for at least one hour on different days *in vitro* (DIV).

3 Results

When applied acutely, ghrelin significantly raised the level of network activity (t-test: $p<0.001$), by 40% on average. Furthermore, ghrelin induced much lower synchronicity in the firing patterns compared with the controls. Cultures usually had an initial pattern consisting of periods of dispersed firing, alternated with periods of intense firing at most or all electrodes (Fig. 1a). Ghrelin largely reduced these periods of synchronized firing, leaving a more dispersed firing pattern in 90% of the experiments (Fig. 1b). In the chronic experiments, all cultures exhibited highly variable patterns of spontaneous activity during their maturation. In the controls, at 7 DIV usually only random spikes were generated and there was no clear evidence of

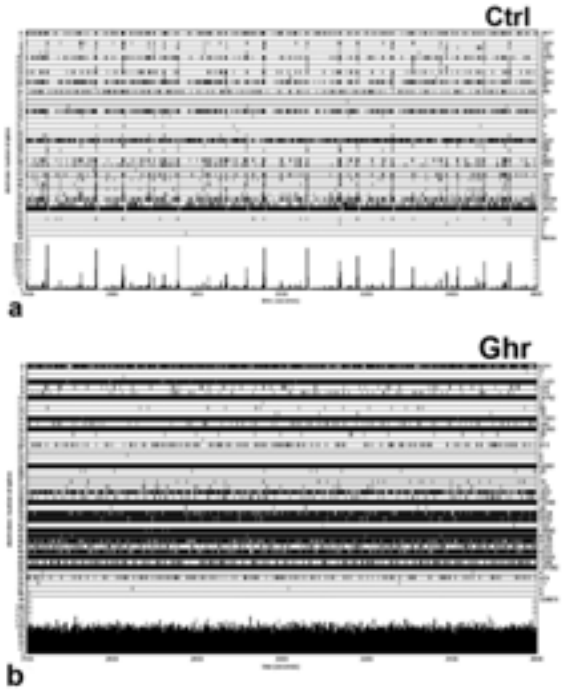

Fig. 1. Effects of acute ghrelin application on activity patterns, culture at age 10 DIV. The figure shows 20 minutes of activity before (a), and after ghrelin application (b). The top rows of the panels depict the 60 electrodes, each tick represents a recorded action potential. The bottom rows of both panels represent summed network activity.

collective bursts. However, ghrelin led to earlier formation and activation of the networks. At young age,

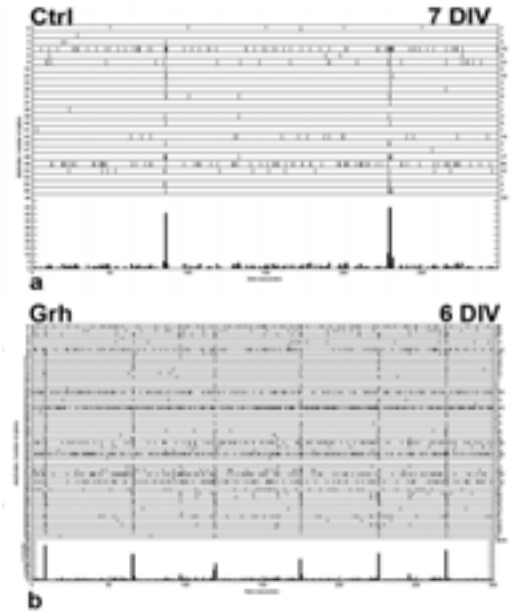

Fig. 2. Raster plots of the neuronal activity recordings in a control, 7 DIV (a), and in culture incubated with ghrelin, 6 DIV (b). In the control culture at 6 DIV we did not measure any activity. The bottom rows of both panels represent summed network activity.

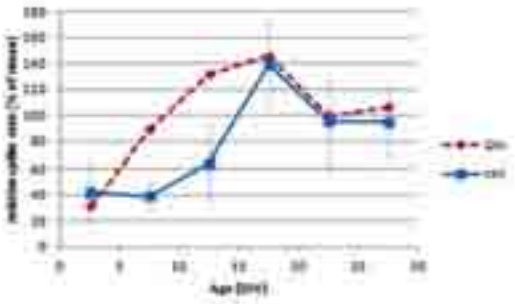

Fig. 3. Development of mean firing rates (normalized) of cultures incubated with ghrelin (n=6, ■) and under control conditions (n=5, ♦). All activity levels in individual cultures are expressed as a fraction of the mean level of that culture throughout development, and pooled into 5 day bins. The activity levels are averaged across cultures for each bin. Both curves show an initial increase, followed by a plateau. Ghrelin (Ghr) cultures show higher activity levels in the first two weeks of development, and consequently reach their plateau earlier than controls (CTRL).

the activity of ghrelin cultures was substantially higher than that of the controls, and was exhibited as early as 3 DIV (Fig. 2). The activity pattern we observed at 6 DIV in ghrelin cultures normally did not appear before 11-12 DIV in control cultures. In ghrelin cultures the mean firing rate reached a plateau around day 10-12, which is also considerably earlier than the controls (17-18 DIV) (Fig. 3).

3 Conclusion/Summary

Ghrelin has a stimulatory effect on the network activity levels, and changes the burst patterns *in vitro*. These probably result from increased synaptogenesis in ghrelin treated cultures, as it was shown recently about orexin A [3]. Our results also provide clear evidence that chronic application of ghrelin has a strong stimulating effect on functional network formation and leads to earlier generation of ”mature” activity patterns. Therefore, it could provide a molecular target for novel therapeutics for disorders related to neurodegeneration and impaired synaptic plasticity.

Acknowledgement

We thank Karin Groot Jebbink and Bettie Klomphaar for their assistance in cell culturing. This study is part of the EU research project NEURoVERS-it (MRTN-CT-2005-019247).

References

[1] Nakazato M., Murakami N., Date Y., Kojima M., Matsuo H., Kangawa K., Matsukura S. (2001). A role for ghrelin in the central regulation of feeding. *Nature*, 409(6817), 194-198.

[2] Diano S., Farr S.A., Benoit S.C., McNay E.C., da Silva I., Horvath B., Gaskin F.S., Nonaka N., Jaeger L.B., Banks W.A., Morley J.E., Pinto S., Sherwin R.S., Xu L., Yamada K.A., Sleeman M.W., Tschöp M.H., Horvath T.L. (2006). Ghrelin controls hippocampal spine synapse density and memory performance. *Nature Neurosci*, 9(3), 381-388.

[3] Stoyanova I.I., Rutten W.C.L., le Feber J. (2012). Orexin A in cortical cultures: expression and effect on synaptogenesis during development. *Cell Mol Neurobiol*, 32(1), 49-57.

Pharmacological studies of connections in human pluripotent stem cells derived neuronal networks

Mäkinen Meeri[1,2], Mäkelä Hanna[1,2], Penkki Sanna[1,2], Heikkilä Juha[1,2], Narkilahti Susanna[1,2*]

1 Institute of Biomedical Technology, University of Tampere, Tampere, Finland
2 BioMediTech, Tampere, Finland
* Corresponding author. E-mail address: susanna.narkilahti@uta.fi

Abstract
The cellular subpopulations and connections of the circuits forming spontaneously during the neural differentiation of human pluripotent stem cells are not well characterized. We experimented with several pharmacological protocols to find a protocol suitable for dissecting cellular subpopulations of the spontaneously forming networks.

1 Background

Several methods for differentiating neural cells from human pluripotent stem cells (hPSCs) have been published [1]. However, the cellular subpopulations and connections of the circuits spontaneously forming from these neurons remain unclear. The analysis of functional cellular subpopulations and connections requires activity measurements. Neural cell cultures are commonly measured with microelectrode arrays (MEAs) [2]. MEA measurements can be combined with pharmacological studies utilizing substances targeting specific connections. Here, we tested several different pharmacological methods to study the subpopulations underlying the activity of hPSC-derived neuronal networks. Particularly, we were interested in the participation of gap junctions, glutamatergic and GABAergic signalling in the network activity.

2 Methods

Obtaining neuronal networks

The neural differentiation of hPSCs has been described earlier [1]. Briefly, stem cell colonies were cut and allowed to from aggregates in a neural differentiation medium. For final maturation, the cells were seeded as pieces of aggregates onto MEA dishes or cover slips.

MEA measurements

The maturation of the network was followed by performing MEA measurements at least once a week. The baseline was measured 2 hours after medium change. The pharmacological substance applications were performed by adding 1-2µl of the substance to the MEA dish. Carbenoxolone (CBX, 25µM) and glycyrrhizic acid (GZA, 25µM) were applied for 15 minutes or 1 hour while CNQX (50µM), D-AP5 (35µM), glutamate (0.5, 1.5, 6.5, 11.5, 31.5, 51.5µM), bicuculline (Bic, 10µM) and GABA (0.5, 1.5, 6.5, 11.5, 31.5, 51.5µM) were applied for 5 minutes before MEA measurement. Washout was measured after changing the whole medium to fresh culture medium and allowing the culture to stabilize for 2 hours.

Calcium imaging

Fura-2 AM (4µM) was incubated on cover slips in room temperature (+22°C) for 30 minutes. Ringer solution (44µM KH_2PO_4, 20mM HEPES, 4.2mM $NaHCO_3$, 5mM glucose, 1mM $CaCl_2$, 1.2mM $MgCl_2$, 137mM NaCl, 5mM KCl, pH adjusted to 7.4 with NaOH) was used for perfusion. $GABA_A$ receptor blocker Bic (10µM) was applied to induce intracellular calcium rises [3]. CBX (25µM) was used to block gap junctions.

3 Results

Gap junction studies

Gap junction blocker CBX is known to have unspecific effects. The specificity of CBX was studied by comparing its effects to the effects of a known analogue GZA. GZA is not known to block gap junctions. The gap junction blocker CBX seemed to have more clear activity diminishing effect than its non-specific analogue GZA in a young (9 days) network. In a more mature network (45 days), the effect of CBX was even clearer. This stronger effect of the same CBX application could reflect a change in the gap junction content of the neuronal network during maturation. The effect of CBX was reversible by washout to some extent.

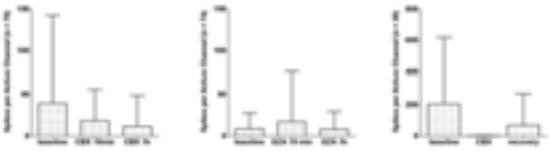

Fig. 1. Gap junction pharmacology on MEA. Error bars represent standard deviation.

The gap junction content of maturing networks was studied with calcium imaging. The network was first applied with Bic, then Bic + CBX and finally with Bic. The Bic application produced a calcium level increase in cells. Cells which produced a calcium level increase in response to both Bic applications were considered as Bic responsive cells. The amount of Bic responsive changed gradually during network maturation. This possibly reflects change in the GABAergic signalling. During the simultaneous application of Bic and CBX some cells produced a response to Bic while the rest were not affected. The amount of affected cells was thought to reflect the amount of cells with gap junction mediated activity. The amount of these cells decreased rapidly during network maturation.

Studying glutamatergic and GABAergic subpopulations

Glutamatergic and GABAergic signalling were studied with MEAs by applying a competitive antagonist (CNQX+D-AP5 or bicuculline) and an increasing concentration of the agonist (glutamate or GABA). Three different groups of hPSC -derived neuronal networks were applied with this protocol. Two of these groups were produced from the same hESC -line but were differentiated towards neural progenitors for different periods (8 or 12 weeks). The third group was produced from hIPSC -line and was differentiated for 8 weeks. All groups were allowed to mature for 34 days. The activity of all of these groups was reduced by the application of CNQX and D-AP5. The activity of all of the cultures was recovered to some extent with subsequential glutamate concentration increases. However, the networks of different origin recovered differently. Thus, possibly reflecting a difference in cellular subpopulations and connections formed.

After washout, a similar pharmacological protocol was used to study the GABAergic signalling differences. The application of Bic decreased the activity in the two of the groups (12 weeks differentiated hESC -line and 8 weeks differentiated hIPSC -line) and increased the activity slightly in one of the group (8 weeks differentiated hESC -line). The trend of this change seemed to continue in all groups during the application of the lowest concentration of GABA. Hence, it is possible that the time point for Bic effect measurement should be later or the incubation time should be longer. The application of Bic and an increasing GABA concentration had very little effect on the hIPSC –line derived network. However, 31.5 and 51.5µM GABA concentrations had a clear and uniform effect on the networks derived from the same hESC –line. Thus, it could be possible that this kind of protocol reflects the difference in cellular subpopulations and connections formed.

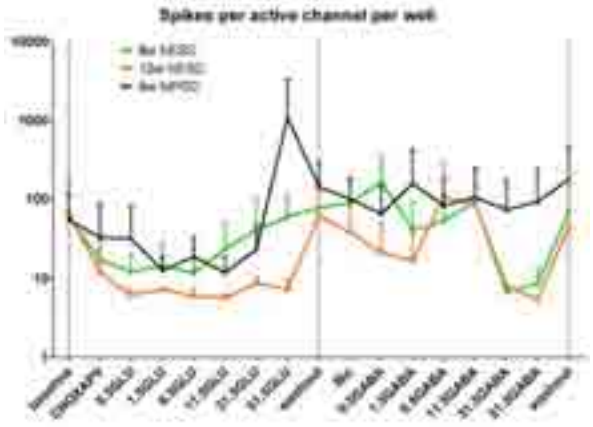

Fig. 2. Glutamatergic and GABAergic pharmacology on MEA. Error bars represent standard deviation.

4 Conclusions

Early activity of the hPSC-derived neuronal networks was found to be mediated by gap junctions as well as by glutamatergic and GABAergic signalling. These mechanisms are known to participate in the network activity occurring during the early brain development. The amount of gap junction and GABAergically mediated signalling seemed to change during network maturation. The described pharmacological protocols seemed promising for studying differences in cellular composition and functional connections. However, these results should be in the future cross checked with immunocytochemistry.

Acknowledgement

This work was financially supported by TEKES, The Finnish Funding Agency for Technology and Innovation.

References

[1] Lappalainen R., Suuronen R., Skottman H., Narkilahti, S. (2010). Similarly derived and cultured hESC lines show variation in their developmental potential towards neuronal cells in long-term culture. *Regenerative Medicine*, 5, 749-762.

[2] Heikkilä T., Ylä-Outinen L., Tanskanen J., Lappalainen R., Skottman H., Suuronen R., Mikkonen J., Hyttinen J., Narkilahti, S. Human embryonic stem cell-derived neuronal cells form spontaneously active neuronal networks in vitro. *Experimental neurology*, 218, 109-16.

[3] Arumugam H., Denisova J., Neve R., Corriveau R., Belousov, A. (2008) Use of calcium imaging for analysis of neuronal gap junction coupling. *Neuroscience Letters*, 445, 26-30.

Unit specific responses to ω-Agatoxin in a cultured neuronal network

Knaack Gretchen[1*], Hamilton Franz[2], Charkhkar Hamid[2], Peixoto Nathalia[2], Pancrazio Joseph[2,3]

1 Psychology Department, George Mason University, Fairfax, VA, USA
2 Electrical and Computer Engineering Department, George Mason University, Fairfax, VA, USA
3 Bioengineering Department, George Mason University, Fairfax, VA, USA
* Corresponding author. E-mail address: gknaack@masonlive.gmu.edu

Abstract
ω-Agatoxin has been previously researched in single cells using patch clamps. These data have determined that this toxin blocks P/Q type calcium channels and inhibits neurotransmitter release. Although this information is pertinent to understanding the brain, it is also imperative to comprehend how ω-Agatoxin changes network activity. Frontal cortex networks plated on micro electrode arrays were utilized to record changes in spontaneous action potentials in response to increasing concentrations of ω-Agatoxin. Results illustrate that there are actually two separate populations of neurons, which have differing responses. Further examination by isolating glutamatergic synapses suggests that these populations represent excitatory and inhibitory synapses.

1 Introduction

ω-Agatoxin is a P/Q type calcium (Ca^{2+}) channel blocker in vertebrates [1]. These Ca^{2+} channels are presysnatptic and highly involved in the release of neurotransmitters into the cleft [2, 3]. As such, blocking them will reduce the amount of neurotransmitter released. It is therefore believed that administration of ω-Agatoxin will have a similar effect, which has been demonstrated in single cell patch clamp studies [1, 3].

However, neurons do not function solely as individual cells, but as a functionally connected network. Therefore, we investigated the effect of ω-agatoxin on the spontaneous action potentials of cultured frontal cortex networks using microelectrode arrays (MEA).

2 Methods/Statistics

2.1 Cell Culture

Frontal cortex was extracted from timed pregnant E17 ICR mice. The tissue was enzymatically and mechanically dissociated. The cells were then plated on 64-channel MEAs at a denisty of 150,000 cells. Cultures were contained in DMEM supplemented with B27, acorbic acid, fetal bovine, and horse serum for the first two days, at which time serum was removed. Dishes were maintained in an incubator at 37 °C with 10% CO_2 and 50% media changes twice a week.

2.2 Extracellular Recordings

After three to four weeks *in-vitro* pharmacological experiments were performed by measuring extracellular action potentials. Cultures were kept at 37 °C and perfused constantly at 1mL/min with DMEM enhanced with HEPES, Sodium Bicarbonate, and glucose. After a 90 minute baseline was established, ω-Agatoxin was adminstered to the perfusion media for 30 minutes each at the following concentrations: 10nM, 50nM, 100nM, and 200nM. To examine if the observed changes were reversible, fresh media was perfused for 60 minutes.

Frontal cortex contains both excitatory and inhibitory neurotransmitters and blocking them presynaptically may have differing effects on the postsynaptic firing. To investigate this possibility, additional networks underwent the same procedure, but had 5μM Bicuculline, a GABA receptor blocker, added to the perfusion media. This permitted the recording of excitatory synapses only.

2.3 Data Analysis

Mean spike rates were determined for each unit and normalized to its baseline. Rates were then averaged within a network. Outliers were removed if they were 2 standard deviations from the mean on at least half of the time points examined. Results were analyzed with a repeated measures ANOVA proceeded by planned contrasts to compare each concentration to baseline. Data represent responses from 168 units over six networks. Since networks are heterogeneous, a two-step cluster analysis was conducted to assess whether or not differential effects of ω-agatoxin exposure on spike rate could be distinguished. Resulting clusters were analyzed separately.

3 Results

Cluster analysis concluded that there were two types of responses to ω-agatoxin (Table 1).

Cluster	Number of Units	Percent (%)
1	79	47
2	89	53
Total	168	100

Table. 1. Two-step cluster analysis of mean spike rate of frontal cortex neurons

A repeated measures ANOVA of cluster 1 revealed a significant main effect across doses of ω-Agatoxin on spike rate, $F(5, 25) = 21.51$, $p < .01$ (Fig. 1). Planned contrasts indicated that, compared to baseline, the spontaneous firing rate decreased in a concentration dependent manner. Although this reduction was partially reversed during wash, spike rate was still significantly less $p < .01$.

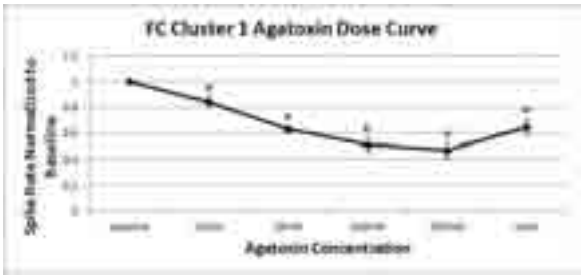

Fig. 1. Spike rate of cluster 1 frontal cortex neurons in response to increasing concentrations of Agatoxin. Mean spike rate was determined for each unit and normalized to its baseline and then averaged across a network. Values represent mean ± SEM.

A repeated measures ANOVA of cluster 2, indicated that there was no statistically significant change in the spontaneous firing rate with exposure to ω-Agatoxin, $p > .05$ (Fig. 2)

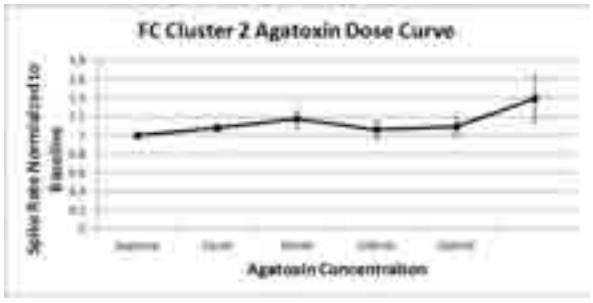

Fig. 2. Spike rate of cluster 2 frontal cortex neurons in response to increasing concentrations of Agatoxin. Mean spike rate was determined for each unit and normalized to its baseline and then averaged across a network. Values represent mean ± SEM.

To determine if the two effects detected in frontal cortex cultures were from GABAergic vs. Glutamatergic populations, Bicuculline was added (Fig. 3). Examination of the dose curve illustrates a pattern which parallels cluster one.

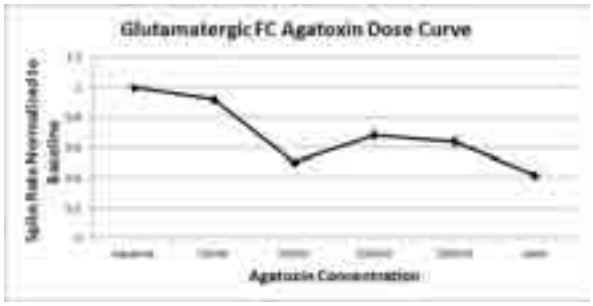

Fig. 3. Spike rate of glutamatergic frontal cortex neurons in response to increasing concentrations of Agatoxin. Mean spike rate was determined for each unit and normalized to its baseline and then averaged across a network. Values represent mean ± SEM.

4 Conclusions

Inspection of the data suggests that there were different reactions to ω-agatoxin depending on the unit. Two-step cluster analysis of spike rate modulation revealed two sub-populations. Cluster one displayed a significant decrease in activity compared to baseline and this reduction was only partially remediated with a wash (Fig. 1). Decline of action potentials to 50% of baseline occurred at 100 nM, with the maximum drop of 47% at 200 nM. Cluster two demonstrated an increase in firing, although this change was not significant compared to baseline (Fig. 2).

Since P-type Ca2+ channels have a significant role in both excitatory and inhibitory neurotransmission, it is possible that the clusters identified are associated with these two different classes of neurons. To ascertain this theory, the GABA receptors were blocked with Bicuculline. These networks also exhibited a decline in spike rate (Fig. 3). Moreover, this response was most similar to that observed in neurons classified as cluster 1.

This preliminary data supports the theory that the individual clusters detected in frontal cortex networks represents excitatory and inhibitory populations. These results further suggests that ω-agatoxin affects these groups differently such that it decreases activity by blocking Glutamate release, but increases activity by blocking GABA release.

References

[1] Mintz IM ; Venema VJ ; Swiderek KM ; Lee TD ; Bean BP ; Adams ME. (1992) : P-type calcium channels blocked by the spide toxin ω-Aga_IVA. Nature, 355, 827-829

[2] Bean BP. (1989) Classes of calcium channels in vertebrate cells. *Annu. Rev. Physiol., 51, 367-384*

[3] Takahashi T ; Momiyama A. (1993) : Different types of calcium channels mediate central synaptic transmission. *Nature, 366, 156-158*

Acute quantification of cisplatin toxicity and protection by D-Methionine

Kamakshi V. Gopal[1,3*], Calvin Wu[1,2,3], Bibesh Shrestha[1,3], Ernest J. Moore[1,3], Guenter W. Gross[2,3]

1 Department of Speech and Hearing Sciences, University of North Texas, Denton, TX USA
2 Department of Biological Sciences, University of North Texas, Denton, TX USA
3 Center for Network Neuroscience, University of North Texas, Denton, TX USA
* Corresponding author. E-mail address: gopal@unt.edu

Abstract
Cisplatin is a platinum-based chemotherapy drug which is widely used to successfully treat various types of cancers. However, patients undergoing cisplatin treatment often suffer from numerous side effects including ototoxicity, tinnitus, nephrotoxicity, peripheral neuropathy and seizures. D-Methionine (D-Met), a sulfur-containing nucleophilic antioxidant, has been shown to prevent cisplatin-induced side effects in animals without antitumor interference. Herein, we have used an *in vitro* model of cortical networks (CNs), enriched in auditory cortex cells, to quantify cisplatin neurotoxicity and the protective effects of D-Met. Results show that 1.0 mM D-Met effectively protected against excitation induced by lower concentration of cisplatin and irreversible activity loss by higher concentration. Lower concentration (0.5 mM) of D-Met showed less protective effect.

1 Introduction

1.1 Background

Cisplatin Toxicity

The widely used anticancer drug cisplatin [cis-diamminedichloroplatinum(II) (CDDP)] has serious side effects including neurotoxicity, ototoxicity and chemo brain [1-2]. To date, there are no chemoprotective agents in clinical use to combat these side effects.

Neuroprotection of D-Methionine

D-Methionine (D-Met) is an antioxidant that has shown to prevent cisplatin-induced ototoxicity in animals without antitumor interference [3-4]. However, D-Met has never been evaluated for its neuroprotective effects.

1.2 Aim

The aim of this study was to evaluate acute neurotoxic effects of cisplatin and assess the protective effects of D-Met using an *in vitro* model of cortical networks (CNs), growing on microelectrode arrays (MEA).

2 Method

Dissociated neurons from auditory cortices of mouse embryos (E 16-17) were grown on MEAs with 64 transparent indium-tin oxide (ITO) electrodes that enabled electrophysiological recording of neuronal activity. In addition, the glass carrier plate of the MEA and transparent ITO electrode conductors enabled maximum optical access during recording for morphological evaluations. CNs that were at least 21 days in vitro (div), were place in sterile stainless steel recording chambers and mounted on an inverted microscope stage. The networks were maintained at a temperature of 37^0 C, pH of 7.3 and an osmolarity of 320 mOsm/kg. The network activity (reference) was recorded continuously using a two-stage, 64-channel amplifier system (Plexon, Dallas, TX), and digitized simultaneously using digital signal processors. Various concentrations of cisplatin were added to the bath and continuous recordings were made.

3 Result

3.1 Cisplatin dose-response on CNs

Cisplatin concentrations of 0.10 and 0.25 mM increased the spiking activity up to 200% over a period of seven hours. Cisplatin concentrations at or above 0.5 mM caused irreversible loss of neuronal activity within two to three hours. (Fig.1). The loss of activity was accompanied by cell death, which is shown in Fig.2. The left top panel depicts neurons in the reference condition (yellow arrows), and the right top panel shows extensive neuronal death following exposure to 0.5 mM cisplatin for seven hours.

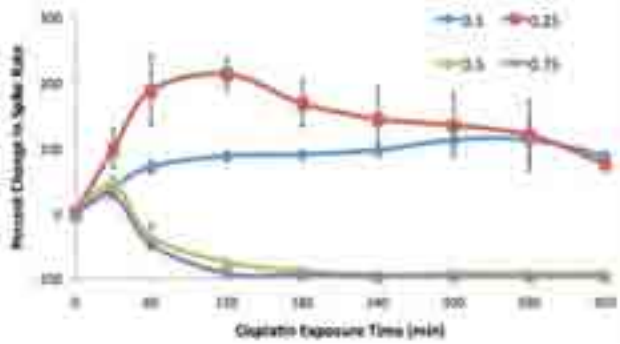

Fig. 1. Dose response of cisplatin at 0.1 (n = 2), 0.25 (n = 3), 0.5 (n = 3), or 0.75 mM (n = 2) measured by percent change in spike rate monitored for 7 hours.

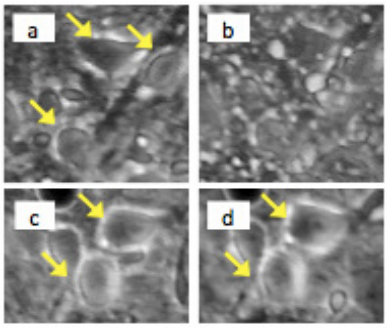

Fig. 2. Phase-contrast image of selected neurons under reference (a), 0.5 mM cisplatin (b), reference under 1.0 mM D-Met (c) and 1.0 mM D-Met + 0.5 mM cisplatin (d).

3.2 Protective effect of D-Met at 1.0 mM

Pretreatment of CNs with 1.0 mM D-Met for one hour, prevented the cisplatin-induced excitation at 0.10 and 0.25 mM (Fig.3), caused sustained excitation at 0.5 mM and delayed cessation of neural activity at 0.75 mM cisplatin. Protection from D-Met pretreatment was also evident in the morphological analysis. In Fig.2, the left bottom panel depicts neurons (arrows) that are pretreated with 1.0 mM D-Met. The right bottom panel depicts the same set of neurons that are morphologically intact (arrows) despite application of 0.5 mM cisplatin application.

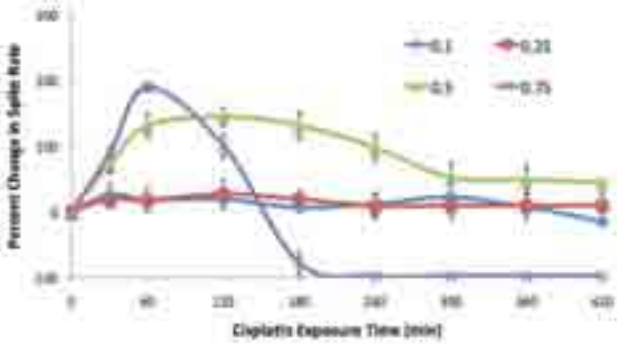

Fig. 3. Dose response of cisplatin at 0.1 (n = 2), 0.25 (n = 2), 0.5 (n = 5), or 0.75 mM (n = 2) under 1.0 mM D-Met pretreatment for 1 hour.

3.3 The effect of pretreatment concentration

In order to identify if lower concentrations of D-Met was equally protective, we pretreated the CNs with 0.5 mM of D-Met prior to application of 0.5 mM cisplatin. Fig.3 shows that the lower D-Met concentration did not prevent cessation of neural activity, thus exhibiting lesser protection (Fig.4).

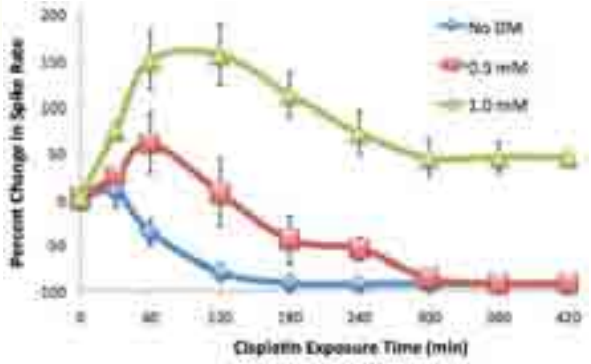

Fig. 4. Effect of pretreatment concentration of D-Met at 0 (n = 3) 0.5 (n = 2), or 1.0 mM (n = 5) for 1 hour under 0.5 mM cisplatin exposure for 7 hours.

4 Conclusion

Pretreatment of CNs with 1.0 mM D-Met one hour prior to application of cisplatin provides effective protection against cytotoxicity induced by cisplatin up to concentrations of 0.5 mM. Lower D-Met concentration of 0.5 mM showed less protective effects. Acute studies at high concentrations of cisplatin represent an efficient approach to establishing D-Met protection and justify a second phase of more laborious chronic studies in vitro.

Acknowledgement

The authors thank Nga Nguyen for unfailing assistance with cell culture. EJM is supported in part by internal start-up funds from UNT. This research was also supported by The Charles and Josephine Bowen memorial endowment to the CNNS.

References

[1] McWhinney S.R., Goldberg R.M., McLeod H.L. (2009). Platinum neurotoxicity pharmacogenetics. *Mol Cancer Ther*, 8, 10-16.

[2] Rybak L.P., Whitworth C.A., Mukherjea D., Ramkumar V. (2007). Mechanisms of cisplatin-induced ototoxicity and prevention. *Hear Res*, 226, 157-167.

[3] Campbell K.C., Meech R.P., Rybak L.P., Hughes L.F. (1999). D-Methionine protects against cisplatin damage to the stria vascularis. *Hear Res*, 138, 13-28.

[4] Campbell K.C., Rybak L.P., Meech R.P., Hughes L. (1996) D-methionine provides excellent protection from cisplatin ototoxicity in the rat. *Hear Res*, 102, 90-98.

Antioxidants D-Methionine and L-Carnitine modulate neuronal activity through GABAergic inhibition

Calvin Wu[1,2,3], Kamakshi Gopal[2,3*], Ernest J. Moore[2,3], Guenter W. Gross[1,3]

1 Department of Biological Sciences, University of North Texas, Denton, TX USA
2 Department of Speech and Hearing Sciences, University of North Texas, Denton, TX USA
3 Center for Network Neuroscience, University of North Texas, Denton, TX USA

* Corresponding author. E-mail address: gopal@unt.edu

Abstract

D-methionine (D-Met) and L-Carnitine (L-Car) are potential neuroprotective compounds against reactive oxygen species- (ROS) induced toxicity. The exact mechanism, however, remains unknown. In this study, we used *in vitro* cortical networks growing on microelectrode arrays to study the mechanism of D-Met and L-Car neuronal modulation. Results indicated that both compounds activate $GABA_A$ receptors, which may offer an alternative pathway to their neuroprotective properties.

.

1 Introduction

D-methionine (D-Met) and L-Carnitine (L-Car) are known for their neuroprotective properties against reactive oxygen species- (ROS) induced cellular degenerations of cortical neurons and auditory cells [1-3]. However, their effects on electrophysiological activity modulation and their underlying mechanism of protection are less understood. Herein, we investigated the effect of D-Met and L-Car on neuronal networks and have proposed an alternative pathway for cellular protection other than their known antioxidant properties.

2 Method

Neurons dissociated from auditory cortex of mouse embryos (E 16-17) were grown on monolayer MEAs consisting of 64 substrate-integrated indium-tin oxide microelectrodes spaced to a 1mm x 1mm matrix. D-Met and L-Car were applied to network cultures maintained at physiological conditions and spike production was used for quantification. The concentration response was normalized to percent decrease from the reference activity, recorded independently for each experiment.

3 Result

D-Met and L-Car both reduced spike activity with 100% efficacy. However, this was readily reversible by a complete medium change (wash). The EC_{50} values for D-Met and L-Car were 1.08 ± 0.05 mM and 0.22 ± 0.01 mM, respectively. In the presence of 1.0 to 40 µM $GABA_A$ antagonist bicuculline, the sigmoidal dose curves of both compounds exhibited up to 10-fold step-wise shifts toward higher EC50, without change in efficacy. The EC_{50} values increased to 11.2 ± 1.0 mM for D-Met and 3.6 ± 0.3 for L-Car under a maximal bicuculline concentration of 40 µM (Fig.1 and 2). Nonlinear regression analysis of receptor binding kinetics revealed that the agonist action of D-Met and L-Car are not directly competitive with bicuculline (Fig.3).

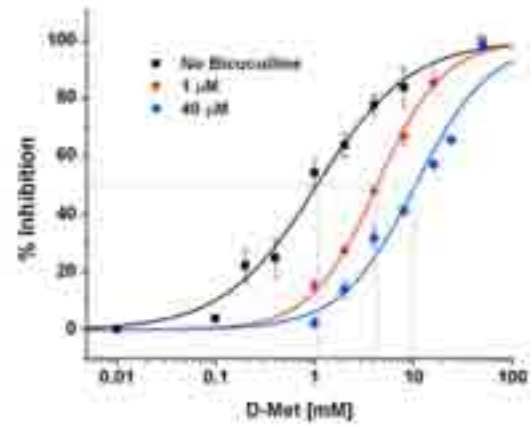

Fig. 1. Concentration-response curves of D-Met in the presence of 0 ("No Bicuculline"; n = 3), 1 (n = 3), or 40 µM (n = 3) bicuculline.

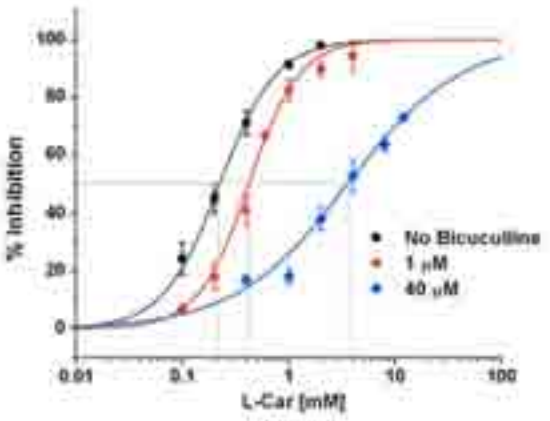

Fig. 2. Concentration-response curves of L-Met in the presence of 0 (n = 3), 1 (n = 3), or 40 μM (n = 3) bicuculline.

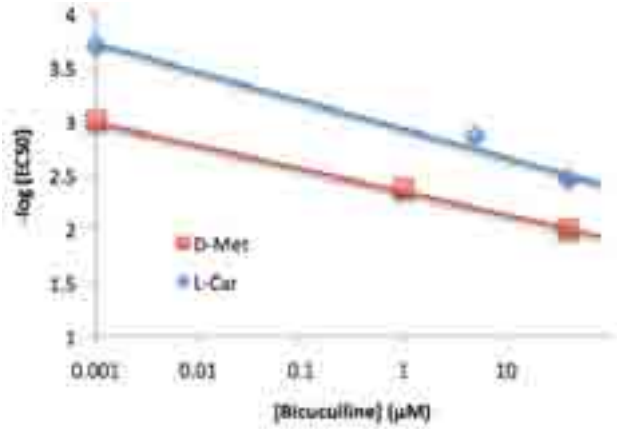

Fig. 3. Non-linear (semi-log) regression curve fit for pEC50 (-log EC50) funtions (y-axis) of bicuculline concentration (x-axis). Non-standard slope (logarithmic slope ≠ 1) indicates a mechanism of receptor antagonism other than competitive binding.

4 Conclusion

The results indicate that the antioxidants D-Met and L-Car both modulate neuronal activity through reversible $GABA_A$ receptor binding. Though the exact binding kinetics is yet to be investigated, the involvement of GABAergic mechanism may contribute to the protective actions of these compounds against neuronal excitotoxicity and degeneration.

Acknowledgement

This research was supported by a Faculty Research Grant from UNT awarded to EJM, and the Charles Bowen Endowment to the Center for Network Neuroscience.

References

[1] Gülçin, I. (2006). Antioxidant and antiradical activities of L-carnitine. *Life Sci*, 78, 803-811.

[2] Rybak, L.P. (2005). Neurochemistry of the peripheral and central auditory system after ototoxic drug exposure: implications for tinnitus. *Int Tinnitus J*, 11, 23-30.

[3] Campbell, K.C., Meech, R.P., Klemens, J.J., Gerberi, M.T., Dyrstad, S.S., Larsen, D.L., Mitchell, D.L., El-Azizi, M., Verhulst, S.J., Hughes, L.F. (2007). Prevention of noise- and drug-induced hearing loss with D-methionine. *Hear Res*, 226, 92-103.

Cerebrospinal fluid of anti-NMDA receptor encephalitis patients modulates *in vitro* neural network activity

K. Quasthoff[1*], S. Theiss[1], M. Dihné[2] and N. Goebels[1]

1 Dept. Neurology, University Hospital Düsseldorf, Germany
2 Dept. Neurology & Epileptology & Hertie Institute for Clinical Brain Research, University Tübingen, Germany

* Corresponding author. E-mail address: kim.quasthoff@uni-duesseldorf.de

Abstract

Anti-NMDA receptor encephalitis is presumably caused in a direct way by antibodies against the N-methyl-D-aspartate receptor (NMDAR). The clinical picture predominantly comprises subacute psychosis and epileptic seizures. In first experiments, we tested if antibody-positive cerebrospinal fluids (CSF) of patients suffering from this disease modulate in vitro neuronal network activity which was recorded by microelectrode array.

1 Introduction

1.1 Anti-NMDA-R encephalitis

This kind of autoimmune disease belongs to a newly identified group of paraneoplastic syndromes.. Most patients are young females with a median age of 23 and an ovarian teratoma [1]. Tumor removal often leads to an excellent clinicalrecovery. The disease entity was first described by Dalmau et al in 2007 [2]. It was shown that antibody binding to the NR1 subunit of the NMDA-R leads to internalization of the receptor and therefore to a complete loss of function [3]. In pilot experiments we tried to recapitulate these findings on microelectrode arrays (MEA) to get an idea about the electrophysiological changes in network activity that may lead to various neurological symptoms.

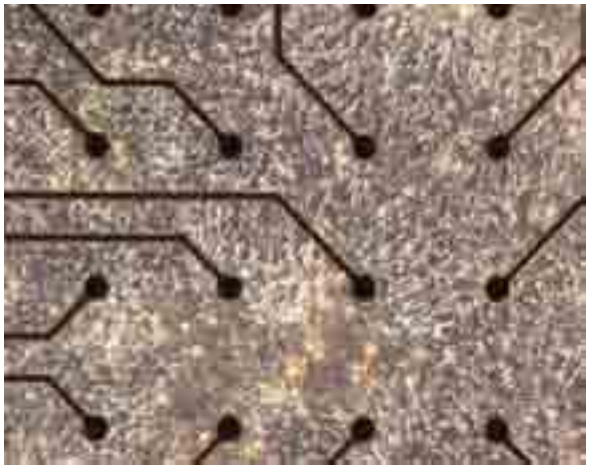

Fig. 1. E18 rat cortical cells plated on MEA chip form a dense neuronal network after 23 DIV.

2 Material and methods

2.1 Cell culture

Cultures were prepared from cortical hemispheres of E18 Wistar rats. Tissue was digested enzymatically and seeded in a density of 150,000 cells/MEA in an 80µl drop on PDL and laminin coated MEAs. 24h after seeding the MEAs were flooded with 1ml of cell culture medium. These cells begin to spike spontaneously after 2 weeks of culture, synchronized activity can be detected a few days later..

2.2 CSF recordings

CSF samples from patients with anti-NMDA-R encephalitis were kindly provided by Dr. Malter (Dept. of Epileptology, University Hospital Bonn). We took different patient CSF samples to verify the effects of anti-NMDA-R antibodies on neuronal network activity. As control, CSF from patients without neurological diseases was used. From all patients informed consent was obtained according to institutional guidelines. CSF. Samples were centrifuged and pH was adjusted to 7.4 with 1mM HEPES prior to measurement. As an additional control we used an artificial CSF (131) consisting of 150mM NaCl, 1mM $CaCl_2$, 3mM KCl and 1mM $MgCl_2$. For each experiment, the array activity in “131” averaged from triplicate recordings was taken as baseline. All recordings were done for 3 min with 2 min interruptions und an adaptation phase of 3-5 min after change of medium. Recordings were analysed using the “SPANNER” software (Result GmbH, Düsseldorf). As readout parameters we choose the spike- and burst-ratio as well as Cohens kappa.

Our first experiments indicate that CSF from patients with anti-NMDA-R encephalitis blocks network activity.

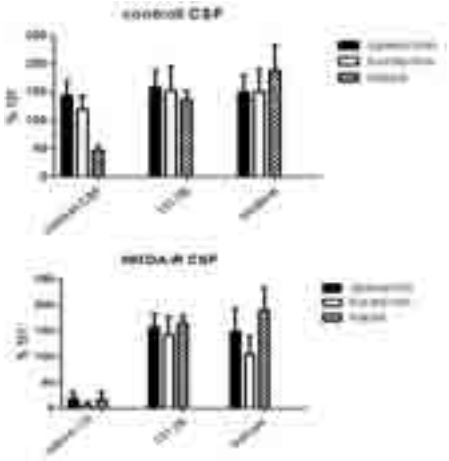

Fig. 2. Treatment with control CSF leads to increased network activity whereas NMDA-R CSF almost completely blocks the network activity.

Acknowledgement

We thank Dr. Wiebke Fleischer for her technical support and Dr. Malter (Bonn) for kindly sending us NMDAR CSF samples.

References

[1] Dalmau J, Gleichman AJ, Hughes EG, Rossi JE, Peng X, Lai M, Dessain SK, Rosenfeld MR, Balice-Gordon R, Lynch DR (2008) Anti-NMDA-receptor encephalitis: case series and analysis of the effects of antibodies. *Lancet Neurol 7:1091-1098*

[2] Dalmau J, Tuzun E, Wu HY, Masjuan J, Rossi JE, Voloschin A, Baehring JM, Shimazaki H, Koide R, King D, Mason W, Sansing LH, Dichter MA, Rosenfeld MR, Lynch DR (2007) Paraneoplastic anti-N-methyl-D-aspartate receptor encephalitis associated with ovarian teratoma. *Ann Neurol 61:25-36*

[3] Hughes EG, Peng X, Gleichman AJ, Lai M, Zhou L, Tsou R, Parsons TD, Lynch DR, Dalmau J, Balice-Gordon RJ (2010) Cellular and synaptic mechanisms of anti-NMDA receptor encephalitis. *J Neurosci 30:5866-5875*

Functional impact of the human epileptogenic Nav1.1 channel mutation R1648H on the activity of murine neuronal networks

Daniel Kirschenbaum, Snezana Maljevic, Holger Lerche, Marcel Dihné

University of Tuebingen, Neurology

Abstract

Mutations in the SCN1A gene, encoding the Nav1.1 voltage-gated sodium channel have been associated with different forms of inherited epilepsy. The R1648H mutation, affecting the voltage sensor of the domain IV of these channels, was detected in a family with generalised epilepsy with febrile seizures plus (GEFS+). To examine its functional consequences, a knock-in mouse model carrying human Nav1.1-R1648H mutation was generated (Martin et al., 2010). The aim of this study was to analyze possible differences of in- vitro neuronal network activity (ivNNA) generated in dissociated hippocampal cell cultures obtained either from mice carrying epileptogenic SCNA1 mutation (R1648H) or the wildtype mice. Functional neuronal network activity was recorded with Multielectrode Arrays (MEAs). We recorded baseline network activity, as well as the activity under the influence of different concentrations of the GABA antagonist bicuculline. Our preliminary data indicate significant differences of several parameters of ivNNA under all experimental conditions predominantly 3 weeks after dissociated cells were plated. This indicates that functional consequences of a clinically important human mutation affecting a sodium channel gene can be visualized in dissociated murine cultures on MEAs, which now offers possibilities to perform pharmacological studies to clarify mechanisms of disturbances of functional neuronal network activity and investigate counteracting strategies in a reductionist but still complex system.

Electrical Stimulation

Repetitive capacitive stimulation of the retina in a stack-configuration

Max Eickenscheidt[1], Günther Zeck[1]

1 Neurochip Research, Natural and Medical Sciences Institute at the University of Tübingen, Reutlingen (Germany)

Abstract

Electric stimulation of the retina aims for partial restoration of visual function in blind patients. It appears highly attractive to understand the response pattern of Retinal Ganglion Cells (RGC) to any given electrical stimulus. A CMOS based stimulation chip was used to excite different retinal neurons [1]. Based on these results we combined the stimulation chip with a flexible MEA to detect multiple cells in the same retinal portion. Sinusoidal stimuli of appropriate frequency have been suggested to excite bipolar cells, which are preserved in blind patients. Here we investigate the ganglion cell response to such sinusoidal stimulation

1 Methods

The CMOS based stimulation-chip comprised a multi capacitor array of 400 stimulation sites (each 50x50 µm2 each, stimulation area: 1mm^2). The chip surface is covered by a thin layer of TiO2/ZrO2 with a capacitance of 3 µF/cm^2 [1]. Voltage detection was preformed by 14 metal electrodes (300 µm spacing) embedded in a polyimide substrate (FlexMEA14, Multi Channel Systems) (**Fig. 1A**).

We studied the stimulation and detection of neuronal activity from adult guinea pig retina in a stack configuration comprising a stimulation chip, whole-mount retina and MEA (**Fig. 1B**). Here the photoreceptors are in close contact with the stimulation chip while the FlexMEA is interfaced to the retinal ganglion cell layer. Sinusoidal stimuli were applied to a subset of the stimulation sites. The detected voltage was a superposition of the stimulus artefact (passive response) and cell activity. By subtracting the mean response of several repeats from each single trace the passive response disappeared while cell activity became visible (**Fig. 2A**).

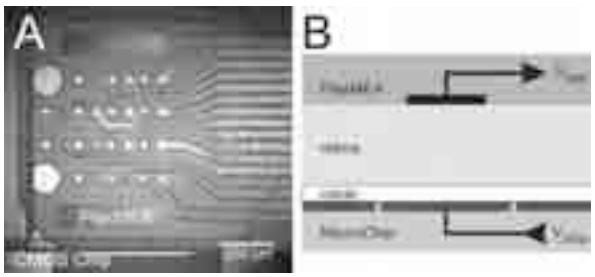

Fig. 1. (A) Top view of stack configuration of a CMOS based Neurochip, retina (not shown) and polyimide based FlexMEA. **(B)** Schematic cross-section of the experimental setup. Vchip indicates the stimulation voltage and Vraw the voltage measured at the tissue surface.

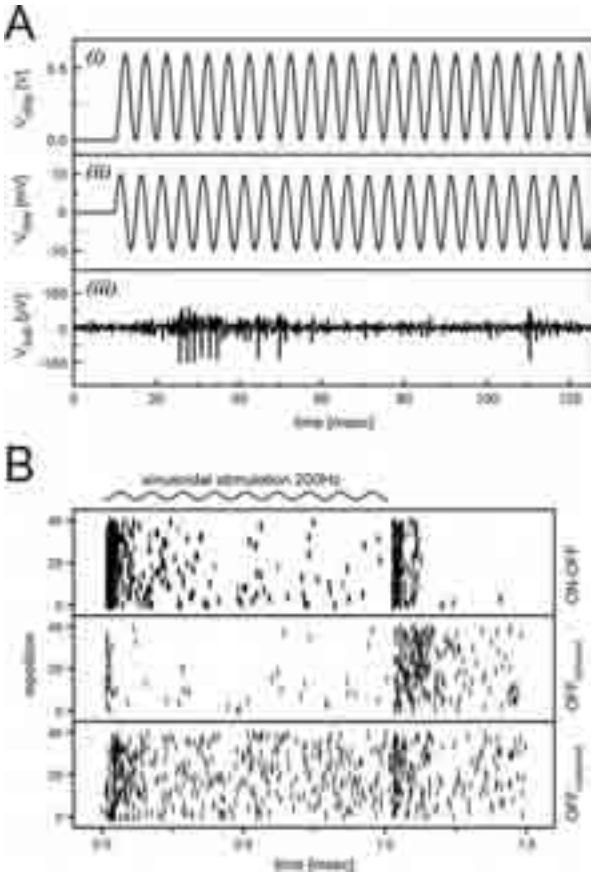

Fig. 2. RGC activity during and after a repetitive stimulation. **(A, *i)*** Sinusoidal voltage applied to the centre chip area (500x500 µm2). ***(A, ii)*** Extracellular voltage Vraw measured at the retinal surface. ***(A,iii)*** The RGC signals are revealed after "artefact subtraction" **(B)** Three different cell responses during and after the stimulation and corresponding cell classification based on light stimuli (right label)

2 Results

The stack configuration allowed for stable recordings (up to 5 h) and RGC light activation (Fig. 1A). Prior to each electrical stimulation protocol, RGCs were classified using standard light stimuli.

Stimulated cell activity could be identified in high frequency electrical stimuli even though the passive tissue responses were 100 x larger than the active responses (Fig. 2A). The “artefact subtraction” was possible because of stable stimulus waveforms, low amplification and no hardware filtering.

Here we studied the RGC response pattern during and after sinusoidal stimulation (variable frequency, stimulus duration and amplitude). Preliminary experiments indicate a cell type specific spiking pattern, which is compared to the light-induced spiking pattern. For some cells the electrically stimulated response is similar to the light-induced activity (Fig. 2B, first and second row). However, other RGCs differed in their electrical and light-induced response property. The different response patterns will be discussed assuming bipolar cell stimulation [2].

3 Conclusion

The stack configuration represents a useful tool for simultaneous detection of multiple cells during capacitive subretinal stimulation. Arbitrary stimulus waveforms may allow for a better understanding of near-physiological retinal stimulation.

References

[1] Eickenscheidt, M., Jenkner, M., Thewes, R., Fromherz P., Zeck, G. (2012). Electrical Stimulation of Retinal Neurons in Epiretinal and Subretinal Configuration using a Multi-Capacitor-Array. *J. Neurophysiol.* 107: 2742-2755

[2] Freeman, D., Eddington, D., Rizzo, J., Fried, SI. (2010). Selective Activation of Neuronal Targets With Sinusoidal Electric Stimulation. *J. Neurophysiol* 104: 2778-2791

Supported by a BMBF grant (FKZ:0312038) to ME and GZ.

Highly non-localized retinal activation verified with MEA and Ca imaging techniques

Giora Beit-Yaakov, Dorit Raz-Prag, Yael Hanein

School of Electrical Engineering, Tel-Aviv University, Tel-Aviv 69978, Israel

Abstract

Retinal photoreceptors instigate a cascade of neuronal responses triggered by light perception. Accordingly, their degeneration is a major cause of blindness. An artificial approach to offset the adverse effects of such degeneration is through localized electrical stimulation using a multi-electrodes array (MEA) implanted on the retina. Despite extensive investigation over the last two decades, there is still a lack of *ex-vivo* quantitative and functional characterization of retinal activation. Such mapping is critically needed for the development of effective neuronal electrode technology. Using complementary methods of optical (calcium imaging) and multi-unit electrical recordings, the spatial activity patterns in response to electrical stimulation was quantified. Using chick retina as a model system for epi-retina stimulation we demonstrate that while indirect activation of the retinal ganglion cells (RGC) through pre-synaptic cells appears to be spatially confined to the stimulation site, direct activation of the RGC axons near the stimulation site does not preserve the retinotopic information, therefore is spatially unconfined to the stimulation site. The combined MEA-calcium imaging technique reported here helps to unravel the limitation of MEA recordings in mapping direct neuronal activation.

1 Introduction

The capacity of retinal implants to mimic natural stimulation in a degenerated retina strongly depends on their ability to trigger RGC to send retinotopic-like information to the brain. Primarily, the stimulated RGC activity must be spatially confined to the stimulation site. Despite extensive investigation over the last several years, most characterization methods aimed to explore the efficacy of retinal implants dealt with single cell responses to electrical stimulation, and therefore provide only limited information about the spatial characterization of the stimulated activity.

Progress in mapping the elicited electrical neuronal responses is commonly hampered by various limitations. Primarily, extra cellular electrical recordings from neuronal tissue directly after electrical stimulation is challenging owing to strong coupling between the stimulating event and the recording amplifiers. Accordingly, significant information, associated with short latency events, is often difficult to obtain. Extra-cellular recording also suffers from significant cross-talk making source identification cumbersome. Therefore, an additional method is needed to allow a more reliable mapping while avoiding the challenges mentioned above.

The study presented here focuses on developing experimental and analytical tools for multi-unit recording of electrically stimulated activity for retinal implant characterization. In particular, we suggest and demonstrate the use of complementary methods of optical and electrical recording for the detection of various responses to different stimulation patterns. The combine approach allows mapping at different spatial and temporal scales which cannot be achieved with by the use of a single technique.

2 Methods

2.1 Retinal model, preparation and handling

In this study we used embryonic chick retinas (embryonic days 13-17), which show spontaneous neural activity [1], as do degenerated retinas [2]. Conveniently, the cell composition of chick retinas during the different developmental stages is well known [3]. All animal procedures were conducted under the institutional animal care standards. The retinas were dissected and the isolated retina was then transferred to the experimental chamber and placed, RGC layer facing down (as in epi-retinal implant), onto highly-dense MEAs consisting of 60 titanium nitride (TiN) electrodes (10 μm diameter, 30 or 40 μm spacing) on indium tin oxide substrate (MultiChannel Systems, Reutlingen, Germany). Better coupling between the tissue and the electrodes was achieved by placing a small piece of polyester membrane filter (5 μm pores) (Sterlitech, Kent, WA, USA) on the retina followed by a slice anchor holder. Retinas were kept at physiological conditions, mentioned elsewhere [4]. To validate the viability of the retina, spontaneous activity was electrically recorded.

2.2 Electrical recording

Signals were amplified (gain ×1,200), acquired and digitized using a 128-channel analogue to digital converter (MultiChannel Systems MC_Card, Reut-

lingen, Germany). The spontaneous activity was digitized at 10 kHz and the spikes were detected and recorded using the software MC_Rack (MultiChannel Systems MC_Card, Reutlingen, Germany) by thresholding according to their signal to noise ratio (SNR>5). All additional signal analysis was done using Matlab (MathWorks). The electrically stimulated activity was digitized at 20 kHz and the raw data during the post-stimulus 400 ms were recorded. Due to the artifact of electrical charging of the electrodes at the first post-stimulus 20 ms, this period was ignored. Spikes from the subsequent raw data were detected by threshold (SNR>4, related to the pre-stimulus noise level). Recording at the stimulating electrode was ignored due to a high noise level. The responsivity of the retinal site to electrical stimulation was defined as the number of detected spikes at the sites sampled by the electrodes and interpolated to get a continuous response image.

2.3 Optical recording

To be able to record activity right after the stimulation, in a 20 ms window, we developed an optical recording approach based on calcium imaging. Calcium ion dynamics has a strong correlation to initiation of action potentials and can be imaged by calcium indicators (Oregon Green 488 Bapta-1AM Hexapotassium salt, Invitrogen) loaded into the cells. Unlike calcium imaging (CI) of neuronal cultures that can be easily achieved in parallel to MEA recording and stimulation using AM ester dye loading [5], a similar method in the retina leads to massive non-specific loading of the dye that masks the RGC layer. More selective retrograde loading of this dye into the retinal RGC through the axons was introduced by Behrend et al. [6, 7], but this method demands a long diffusion time for massive labeling, which is possible only in retinas of cold-blooded animals. We used bulk electroporation as introduced by Briggman et al. [8] for selective and widespread loading of RGC cells and axons, and imaged the calcium ions dynamics during epi-retinal electrical stimulation. Briefly, we used a commercial electroporation dish / electrode pair (CUY700P3E/L; Nepagene/Xceltis, Meckesheim, Germany); an isolated retina was mounted photoreceptor side down on a filter paper. The well of the electroporation dish, containing the lower electrode, was filled with 7 µL of saline. The retina was then centered over the lower electrode, and excess saline was wicked away from the filter paper with a Kimwipe. A 5 µL drop of the Ca indicator dissolved in saline was applied to the underside of the upper electrode. The upper electrode, mounted on a micromanipulator, was lowered until the drop was in contact with the retina. The retina was then electroporated (10 pulses of 10V, 0.1Hz pulse rate and 100 ms pulse width), the upper electrode was raised, and the filter paper with the attached retina transferred to the recording chamber. Time lapse data were taken with an Olympus upright microscope (BX51WI) fitted with an EMCCD camera (Andor Ixon-885) and a ×40 water immersion objective (Olympus, LUMPLFL NA 0.8). This setup allows the visualization of cells residing on top of nontransparent electrodes, with a field of 0.4 mm^2. Fluorescent excitation was provided via a 120 W mercury lamp (EXFO x-cite 120PC) coupled to a dichroic mirror with a filter to match the dye spectrum (Chroma T495LP). Camera control utilized Andor propriety SOLIS software. Time lapse recordings were performed at 2×2 binning mode for resolution of 500×502 and 50 fps. Time lapse sequences were collected via a dedicated 12-bit Andor data acquisition card installed on a personal computer, spooled to a high capacity hard drive (typically >1 TB) and stored as uncompressed multi-page tiff file libraries. To compensate for the fast photo-bleaching of the dye, bi-exponential curve was fitted to the pre-stimulus fluorescence values for estimation of the fluorescence base line [9], and the fluorescence change ($\Delta F/F$) was calculated.

2.4 Electrical stimulation

Retinas were electrically stimulated using a dedicated stimulator (STG-1008, MultiChannel Systems, Reutlingen, Germany) through one electrode (versus an external reference) each time, with charge-balanced bi-phasic current stimulation at the safety range of these electrodes (pulse width: 1ms, pulse amplitude: 1-10µA). Each stimulation session included stimulations at the whole intensity range (increased by 1µA every 10 seconds) and was repeated 5 times.

3 Results

3.1 Spontaneous activity

Spontaneous spike trains were electrically recorded and their statistics was analyzed. These recorded spikes are characteristic for a developing system, and a comparison between E13 and E17 reveals marked differences between spontaneous activity patterns (Fig. 1). Each graph presents the spikes rate recorded from 60 electrodes (time bin size: 100 ms) during 25 minutes. While in early developmental stage (E13) the activity is periodic and synchronized (known also as “retinal waves”), in late stages (E17) the activity is unsynchronized.

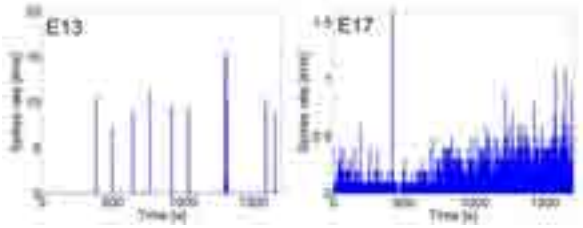

Fig. 1. Comparison between the spontaneous activity of check retinas recorded during different developmental stages (E13-left and E17-right). Different ranges of spikes rate are clearly apparent.

3.2 Indirect electrical activation

Spike trains were electrically recorded in response to stimulation (Fig. 2A). The activity patterns indicate indirect activation of RGCs typified by electrical activation of pre-synaptic cells, which in turn activate synaptically the RGCs. This hypothesis was validated using excitatory synaptic blockers: application of APV and CNQX (400 µM and 75 µM respectively, Sigma) totally abolished the response (Fig. 2B).

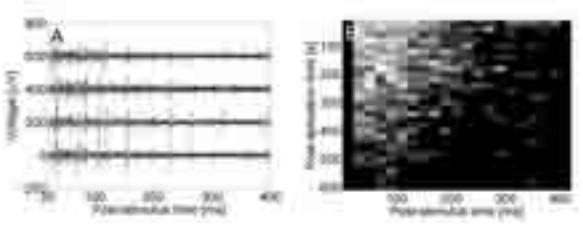

Fig. 2. A: Retinal response to electrical stimulation, recorded electrically by adjacent electrodes (the voltage scale is shifted for clarity). B: A raster plot of retinal responses to repetitive electrical stimulation following application of synaptic blockers. The data show a gradual decrease in the response intensity with time (the firing rate is color coded, between 0 to 250 Hz).

We next mapped the response around each of the stimulating electrodes. For each electrode a color coded map was plotted showing the intensity response (Fig. 3A). Examination of the spatial distribution of the responses revealed a longitudinal configuration of the electrodes in which retinal function was detected. Accumulated data from other electrodes reveals the same pattern. This result suggests that recorded responses are recorded from RGC axons rather than from somas. This was verified by focusing on the response recorded from adjacent electrodes of highly-dense MEA with 30µm inter-electrode intervals (data not shown); one can see clearly the same spike train with a phase difference of 0.1ms, consistent with RGC axon conduction velocity of 0.3 m/sec, similar to the conduction velocities recorded in healthy retinas in response to visual stimuli [10].

To study the functional topology of the retina, we used stimulation at different electrodes equally distributed over the recorded area. We found that the recorded response is consistently longitudinal, parallel, and uni-directional, i.e. stimulation at one side of the retina evoked response in one direction, but not vice versa. To demonstrate this, responses from responding zones over different stimulations (>60% of the maximal responsivity) were summed (Fig. 3B).

To find the real effective stimulation distance of the pre-synaptic cells, regardless of axon location, we plotted the responsivity recorded by each electrode in response to each stimulating electrode versus the perpendicular component of the Euclidian electrode-electrode distance, according to the inner axis coordinate system imposed by the axonal topology (Fig. 3C). The obtained effective distance is around 60 µm. In Figure 3D we plot a simplified model, depicting the effects described above: An electrode stimulates a small number of nearby bi-polar cells. These cells activate a small group of nearby RGCs (red drops). Upstream electrodes (green disks) record the activity in nearby RGC axons.

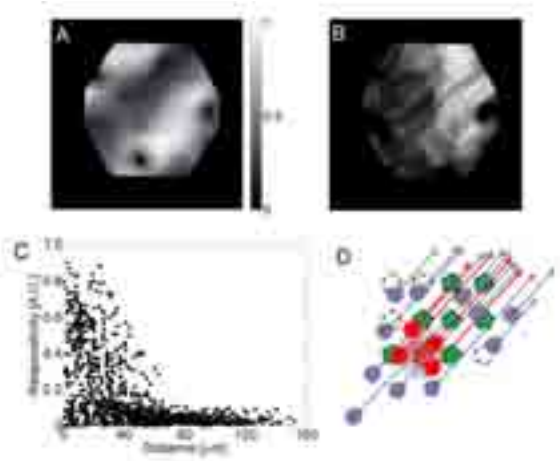

Fig. 3. Mapping the stimulation range using MEA recording. A: Retinal response to electrical stimulation. Two representative stimulation sites are marked by black filled circles; recording sites are marked by open circles. Inter-electrode distance: 40µm, color codes interpolated post-stimulus spikes number. B: Summed response to stimulation recorded from 20 electrodes equally distributed over the retina. C: Responsivity vs. perpendicular component of the distance to stimulation site. D: Indirect activation and recording model of RGCs (drops) by MEA (circles): RGC at the stimulation site (red circle) vicinity are activated indirectly (red-filled), and their axons (arrows) are recorded by the MEA (green-filled).

3.3 Direct electrical activation

Owing to the fact that electrical recording is blinded during the several milliseconds after stimulation, it is clear that the data and the model presented above provide only partial view of the actual response to electrical stimulation. To reveal the true stimulated response at the vicinity of the stimulation site, in particular to map the activity within a narrow time window after the stimulation, we simultaneously recorded optical and electrical responses to electrical stimulation (Fig. 4A). A chick retina (E14) was used after electroporation and selective dye introduction. The retina was placed on a high density MEA and its spontaneous activity was recorded. Normal spontaneous activity was recorded validating the viability of the retina. Next, electrical stimulation was performed and the response was recorded electrically and optically. Although no electrical response was detected, the optical recording shows RGC axons response to the stimulus (Fig. 4B). All the axons at the vicinity of the

electrode responded, regardless of the position of the original somas. This is apparent from the fact that the response range was found to depend on the stimulus intensity, while the cell bodies are not necessarily close to each other. These findings indicate direct electrical activation of the RGC axons regardless of their somas.

To map the effective stimulation distance of RGC axons, we plotted the fluorescence change recorded across the axons in response to the stimulation versus the distance to the stimulation site (Fig. 4C). The obtained effective distance is around 60 µm, in agreement with the electrical recording results presented above. In Figure 4D we plot a simplified model, depicting the effects described above: An electrode stimulates a small number of nearby bi-polar cells. These cells activate a small group of nearby RGCs (red drops). In addition, the electrode activates axons from other RGC cells (yellow drops). Overall, the true activation map is highly non-local and completely unrevealed by MEA recording.

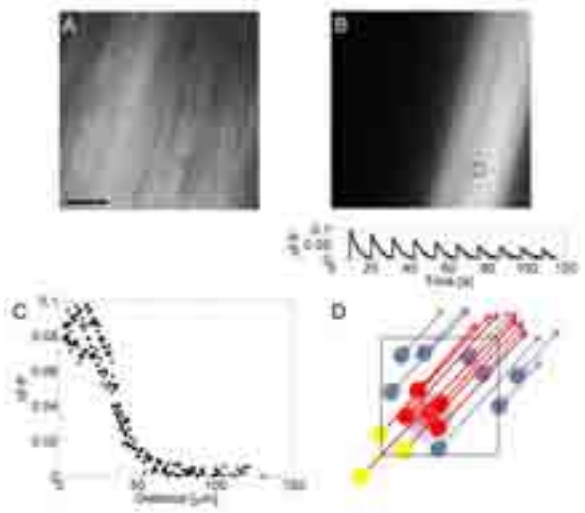

Fig. 4. Mapping the stimulation range using Ca imaging. A: RGC axon layer loaded with Ca indicator, faced toward MEA (scale bar: 40µm, exposure time: 1 second). B: Fluorescence change during stimulation (stimulation intensity: 10nC, color code range: 0-10%, stimulating electrode at the bottom-right corner is marked by a black circle, exposure time: 20 ms, smoothed over 0.64 μm^2). C: Fluorescence change across the axons vs. distance to stimulation site. D: Direct activation model of RGC (drops) by CI (square): RGC axons (arrows) at the stimulation site vicinity are activated directly (red-filled), regardless of their somas (yellow-filled).

4 Summary

As reported before [11], two mechanisms govern the RGC response to electrical stimulation: direct activation of the somas and axons, and indirect activation through pre-synaptic cells. Here we presented a tool set for measuring the effective stimulation distance for both of these processes, enabling improved *ex-vivo* characterization of epi-retinal implants. Consistent with previous report our data suggests that direct axonal activation is a dominant effect in epi-retina stimulation, rendering the stimulation to be highly delocalized. Moreover, our data also indicate that the full nature of the stimulation pattern is best revealed by the combined electrical-Ca mapping.

References

[1] Wong W. T., Sanes J. R., Wong R. O. L. (1998). Developmentally Regulated Spontaneous Activity in the Embryonic Chick Retina. *The Journal of Neuroscience*, 18(21):8839–8852

[2] Menzler J. and Zeck G. (2011). Network Oscillations in Rod-Degenerated Mouse Retinas. *The Journal of Neuroscience*, 31(6):2280 –2291.

[3] Doh,Hao S. T., H., Loh S. C., Patel T., Tawil H. Y., Chen D. K., Pashkova A., Shen A., Wang H., Cai L. (2010). Analysis of retinal cell development in chick embryo by immunohistochemistry and in ovo electroporation techniques. *BMC Developmental Biology*, 10:8.

[4] Hammerle H., Egert U., Mohr A., Nisch W. (1994). Extracellular recording in neuronal networks with substrate integrated microelectrode arrays. *Biosensors & Bioelectronics* 9, 691-696.

[5] Herzog N, Shein-Idelson M, Hanein Y (2011). Optical validation of in vitro extra-cellular neuronal recordings. *Journal of Neural Engineering*, 8 056008.

[6] Behrend M. R., Ahuja A. K., Humayun M. S., Weiland J. D., Chow R. H. (2009). Selective labeling of retinal ganglion cells with calcium indicators by retrograde loading in vitro. *Journal of Neuroscience Methods* 179 166–172

[7] Behrend M. R., Ahuja A. K., Humayun M. S. (2011). Resolution of the Epiretinal Prosthesis is not Limited by Electrode Size. *IEEE Transactions on Neural Systems and Rehabilitation Engineering*, 19, 4

[8] Briggman K. L., Euler T. (2011). Bulk electroporation and population calcium imaging in the adult mammalian retina. *The Journal of Neurophysiology* 105:2601-2609

[9] Rodrigues I., Sanches J. (2010). Photoblinking/photobleaching differential equation model for intensity decay of fluorescence microscopy images. *ISBI'10 Proceedings*

[10] Zeck G, Lambacher A, Fromherz P (2011) Axonal Transmission in the Retina Introduces a Small Dispersion of Relative Timing in the Ganglion Cell Population Response. *PLoS ONE* 6(6): e20810.

[11] Freeman D. K., Rizzo J. F., Fried S. I. (2011) Encoding visual information in retinal ganglion cells with prosthetic stimulation. *Journal of Neural Engineering* 8 035005 (18pp)

Photonic stimulation of neurons in vitro at 337.1 nm

Ryan A. Bennett[1,3], Jose Perez[1,3], Guenter W. Gross[2,3]

1 Department of Physics, University of North Texas, Denton, TX, USA
2 Department of Biology, University of North Texas, Denton, TX, USA
3 Center for Network Neuroscience, University of North Texas, Denton, TX, USA

Abstract

Spontaneously active nerve cell networks, derived from embryonic mouse cortical tissue and grown on microelectrode arrays (MEAs) were used to investigate neuronal responses to low energy near UV laser pulses. Twelve nanosecond pulses at a wavelength of 337.1 nm, focused through a microscope on the cell body outside the nucleus, allowed repetitive stimulation of nerve cells. Responses often occurred after a single laser pulse at approximately 0.8 J/cm^2 radiant exposures. Shortest delay times from the first pulse were approximately 30 ms, which implies the involvement of biochemical mechanisms, most likely Ca++ release from mitochondria and smooth endoplasmic reticulum. However, secondary transynaptic responses have not been ruled out. Responses were generated in the form of multi-action potential bursts with a large range of burst durations and spike frequencies. This reflects the stimulus intensity, influences of the spontaneous activity in the network, laser focus and subcellular location, and other photonic phenomena not yet understood. Laser pulse trains applied at 6.8 Hz revealed neuronal stimulation triggered by pulse numbers ranging from 1 to 19. Multiple exposures to 150 - 300 pulses at 6.8 Hz did not appear to cause neuronal death as evidenced by continual 48 hrs of recording of activity with wave shape identification.

1 Introduction

Photonic stimulation of neural tissue has the potential to add new dimensions to present stimulation methods and may, in the future, dominate the neurostimulation domain. The method is artifact-free, contact-free, immune to electromagnetic interference (EMI), has high spatial specificity, and may allow rapid multiplexing of stimulation signals at different wavelengths [1-3]. Future prosthetic devices as well as deep brain stimulation require sophisticated interfaces. Photonic supplementation of electrical stimulation or replacement of metal electrodes will greatly expand the capabilities of such interfaces and allow for more precise stimulation. Theoretical network research would also benefit. Cultured neuronal networks grown in vitro on microelectrode arrays (MEAs) provide extensive simultaneous action potential (AP) readout. Although electrical stimulation is possible through thin film electrodes, cell-electrode coupling is not uniform due to random interactions of neuronal and non-neuronal cells with MEA recording sites. The ability to stimulate optically any neuronal compartment (axon, dendrite, cell body) would open new dimensions of communicating with neural tissue. However, despite lucrative applications, direct photonic stimulation, devoid of genetic or chemical tissue manipulations, has only recently been explored systematically, primarily in the infrared spectrum [4].

One of the earliest investigations of UV effects on neural tissue was that of Audiat et al. [5] who irradiated a whole frog sciatic nerve in Ringer's solution. This led to changes in the electrical excitation threshold and eventual loss of the compound action potential (CAP). Filtering out wavelengths below 310 nm prevented this deterioration. Hutton-Rudolph [6] extended these investigations to differential sensitivities of nerve fibers at the nodes of Ranvier and in internodal regions. Again, filters that blocked radiation below 300 nm prevented damage. Booth et al. [7] followed up with a nerve-muscle preparation by quantifying electrical threshold changes during exposure to a mercury vapor lamp coupled to a prism monochromator able to produce wavelengths from 370 to less than 200 nm. Only UV light below 320 nm had photochemical effects (threshold increases and conduction blocks) on the nodes. Stimulation was not mentioned in these early papers working with UV. Stimulation in the UV was finally reported by Allegre et al. [8] where bundles of central nervous system fibers were stimulated with an excimer laser (λ:308 nm, pd:40 ns) resulting in CAPs at a radiant exposure of 0.9 J/cm^2.

We have used a pulsed nitrogen laser emitting light at 337.1 nm with pulse durations of only 12 ns and radiant exposures of approximately 0.8 J/cm^2 to stimulate action potentials from nerve cells in networks growing on MEAs. With focal diameters of 4.5 µm (x10 Zeiss Ultrafluar quartz objective), exposure of subcellular compartments is possible. We have found that such irradiation of somal cytoplasm triggers cellular as well as network activity.

2 Methods

2.1 Cell Culture

Frontal cortex tissues were dissociated from embryos of IRC, mice (Harlan Spraque, Dawley) at age E15-16. Cortices were minced mechanically, enzymatically digested with papain, triturated, combined with Dulbecco's Modified Minimal Essential Medium (DMEM), supplemented with 5% fetal bovine serum and 5% horse serum, and seeded at 600K cells per ml on MEAs in volumes of 100 µl to 3 mm diameter adhesion islands. After 2 hours, the cultures were transitioned to medium containing 6% horse serum with a 1% B-27 supplement, maintained at 37 °C in a 10% CO_2 atmosphere, and given half medium changes biweekly. This procedure yielded networks with 300 to 500 neurons per mm^2 over the electrode array and approximately 2,000 neurons in the entire network. Neurons grown under such condition developed shallow, three-dimensional networks with neuronal cell bodies generally situated on top and neural processes situated both above and below the glial carpet. Minimum culture age for experiments was limited to three weeks after seeding.

2.2 Laser Exposure Technique

A laser microbeam system (Fig. 1) was used for photonic stimulation of cells in a closed chamber assembly. The UV nitrogen work laser and HeNe target laser were collinearly aligned. Both beams were reflected into a Leitz Orthoplan microscope fitted with quartz objectives, a quartz interphase optics lens, and appropriate front surface mirrors. The sys-tem was used effectively for laser cell surgery investigations that were designed to simulate neuronal trauma via laser lesions, describe the subcellular damage, and explore neurite resealing dynamics [9-10]. UV stimulation was not considered at those early times. Network activity was recorded and processed with a Plexon Inc. (Dallas) multichannel data acqui-sition system. For coordination of stimulation with network activity (resolution of 25 µs), laser pulses were displayed and recorded on one of the 32 digital signal processors. Neurons were identified optically and selected for stimulation by positioning under the HeNe target laser. Manually controlled laser pulse trains at 6.8 Hz and approximately 0.8 J/cm^2 radiant exposures were applied to the target cells. Responses were detected visually from overt changes in the Plexon raster display (Fig. 2).

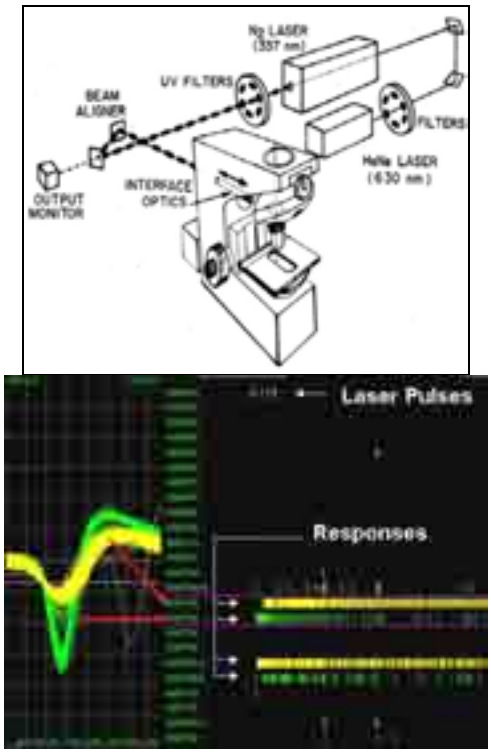

Fig. 2. Plexon raster display of a 4 neuron reponse to 5 UV laser pulses recorded by the top dsp (window: 7.5 s). AP time stamps are shown in the raster display under „responses." The waveshape templates generating the top 2 AP rasters are shown to the left.

3 Results

Fig. 3 shows laser pulses (top row) and network responses in terms of AP time stamps from four different neurons. The three successive stimulation episodes shown (S1 – S3) were separated by 4-5 min. At 6.8 Hz the pulse period was about 148 ms. Fig. 3B shows a segment of the MEA and the location of the irradiated cell near channel 14 (arrow). Responses were seen on that channel and on the neighboring channel (16). It is evident that very few laser pulses are required to elicit strong bursting. The responses are not immediate, as is usually seen with electrical stimulation, but reveal delay times ranging from 30 to 350 ms. It is not yet clear which are primary (direct) or secondary (synaptically triggered) responses. How-ever, if it is assumed that the shortest delay times represent the irradiated neuron, these times range from 30 to 147 ms (Table 1). Also, the neural spike production varies substantially. Table 1 summarizes extracted short response times from the first responder (second neuron response row in Fig. 3A) for four stimulation episodes.

In order to determine whether neurons were adversely affected by the laser pulses at 0.8 J/cm^2, we applied over 300 pulses at 8 Hz. The stimulation and recording sites were separated by 750 µm, indica-ting that cell electrode coupling is random and does not necessarily favor nearest neighbor electrodes. Although only 2 response episodes are shown in Fig. 4D, the neuron was stimulated four consecutive times in 12 minutes with long laser pulse trains and also six

times 4 hours later in the same time period. Activity on electrode 2,8 (second row, 8th column) was monitored for two days in a closed chamber showing no activity loss and no overt changes in waveshape (Fig.4B).

Fig. 1. Laser microbeam system. BTG GmbH, Munich

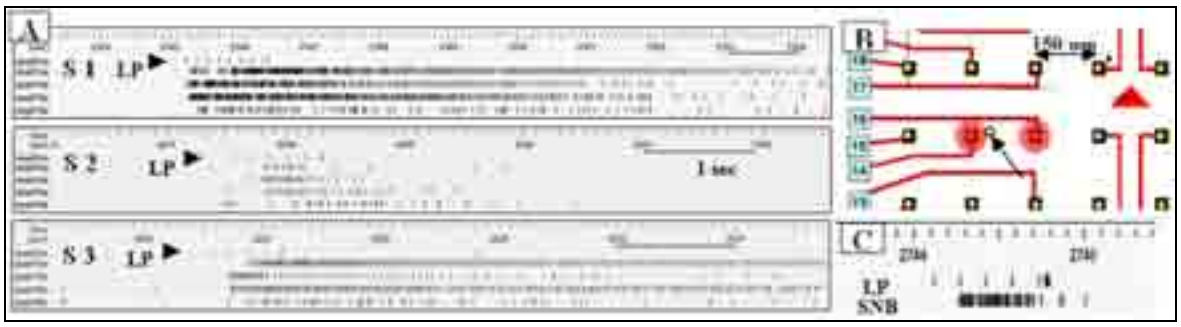

Fig. 3.. Response of four units to short laser pulse trains. (A) Three successive trials (S1 – S3) spaced by approximately 4 min showing variable responses to laser pulse trains of 9, 6, and 5 pulses. All laser pulses were given to the same neuron and at the same subcellular location. Bars represent 1 sec. Top row (arrow head): laser pulses; rows below are action potential time stamps from 2 units on channel 14, and 2 units on channel 16, shown in (B). The stimulation site is represented by the small circle (arrow) in (B). (C) Short burst in response to the second laser pulse from stimulation trial S 6 (not shown in A). LP: laser pulse time stamps (spaced at 148 ms); SNB: single neuron burst; burst duration is ~0.5 sec.

	Laser Parameters				Neural Response Data		
Trial	1st Pulse Time (sec)	Approx. Radiant Exposure (J/cm²)	Pulse Train Duration (sec)	Total # of Pulses	Response Time (sec)	Effective pulse number	Delay After Effective Pulse (ms)
S1	2145.2253	~0.6	1.12	8	2145.2515	1	26.15
S2	2437.5661	~0.8	0.75	6	2437.7013	1	135.15
S3	2626.5657	~0.6	0.46	4	2626.7128	1	147.05
S4	2825.7391	~0.8	0.46	4	2825.7984	1	59.35

Table 1. Laser parameters and neural response data from first responder of Fig. 3A (second row of the 4-row neural response.)

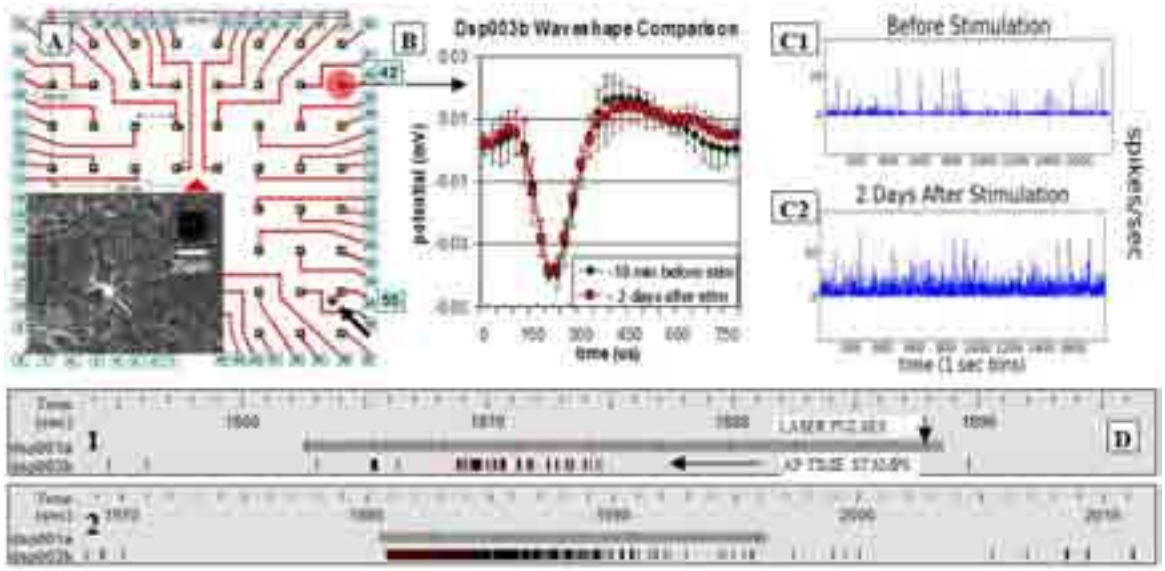

Fig. 4. Neuronal responses to long pulse trains. (**A)** Electrode arrangement of a CNNS M-4 array. 8 µm wide transparent ITO conductors terminate in an equidistant 8 x 8 pattern with 150 µm separation between electrodes. Laser-deinsulated, recessed recording craters are electrolytically gold plated resulting in impedances of 0.8 to 1 MΩ. The dot at the tip of the arrow is the stimulation area (near E-55). This electrode is also shown in the insert, which depicts the target cell and HeNe laser on the stimulation site. The circle over channel 42 shows the response area. **(B)** Waveshapes logged 10 min before stimulation and from the same electrode 2 days after stimulation. No overt shape changes are evident (800 µs window, 32 data points per AP, n: 7 waveshapes. **(C1 and C2)** Spike rates before and 2 days after stimulation on E 42. The increase in spike production on day 2 is network related and is not considered a consequence of laser irradiation. **(D)** Examples of two long laser pulse trains (top trace) and time stamp responses of the same neuron (bottom trace). Train duration D1 and D2: 26 and 17 sec; number of laser pulses: 172 and 112, respectively. The interval between the D1 and D2 stimulation was 92 sec.

Stimulation episode D2 has a minimal delay (after pulse 1) of 363.5 ms. If this neuronal response represents a direct stimulation, the delay time is the sum of conduction delay, processing delay due to network influences, and "ignition delay", where the latter represents photochemical processes. If we assume that the axon in question is a C-fiber with a conduction velocity of 1 m/sec (1 mm/ms), then the straight line distance of 750 µm is covered in less than one ms. Assuming no network inhibition delay for this

particular stimulation episode, about 360 ms are required to trigger the action potential burst. This delay time is possibly a function of photon density and the concomitant calcium ion release from mitochond-ria and/or the endoplasmic reticulum. In this case the response was triggered after the 3rd laser pulse.

4 Discussion

This report is based on simple pilot experiments that showed robust reponses to 12 ns pulses at 337.1 nm and demonstrated that repetitive stimulation was possible. We can also state that cells do not die even after several episodes of long pulse train exposure (Fig. 4), supporting expectations that safe stimulation envelopes may be established. The responses logged so far ranged from relatively long bursts of action potentials to short population bursts after only one or two laser pulses, suggesting that a broad dynamic stimulation range may be routinely achieved. A weakess of the present methodology is the manual control of the laser output and lack of programs allowing real-time identification of very short reponses. As bursts become shorter the native spontaneous activity interferes with a clear identification of reponses to laser pulses. Hence, we do not yet have a good understanding of response refractory periods associated with near UV pulsed laser stimulation. Finally, it is still difficult to distinguish between direct and indirect (or secondary) responses that are synaptically coupled.

Usually, only 10 to 20% of thin film, substrate integrated electrodes allow effective electrical network stimulation and the (normally) 64 recording sites can see only about 10% of the cells in the network. Although electrode yield can be improved by higher densities and higher numbers of electrodes, the limits of electrical stimulation are removed by photonic stimulation through the microscope. Every neuron that can be visualized can potentially be stimulated. Photonic stimulation is also completely selective for the targeted neurons, which is not achievable with electrical stimulation where all axons crossing an electrode or neuronal compartments on the electrode are usually triggered. Further, it is important to realize that the same microbeam system can transition from safe stimulation to process transection or cell elimination with no system manipulation except for the increase of the laser output and number of pulses. This ability expands substantially our level of communication with - and manipulation of- nerve cell networks in vitro. The cell surgery mode allows targeted or random network alterations during multichannel recording of action potentials.

Although it is premature to present a detailed mechanism, action potentials are likely triggered by a Ca++ release from mitochondria and endoplasmic reticulum. Not many types of biochemical molecules absorb at 337 nm. However, the reduced forms of nicotinamide adenine dinucleotide (NADH) as well as NADPH have absorption maxima at 340 nm [11]. NADH, which is a ubiquitous metabolic coenzyme shuttling electrons to mitochondria, has a 0,3 mM cytosol concentration and is found in high concentrations in mitochondria where local heating can induce the release of calcium ions. However, we also anticipate that the short 12 ns pulse duration at low energy density allows rapid local recovery and repetitive stimulation.

These experiments set the stage for a systematic evaluation of stimulation and damage thresholds. Clearly, this method cannot be applied unless a safe stimulation envelope can be defined. Neuronal refractory periods as a function of energy density and number of laser pulses must also be established. Protocols to determine direct and indirect, synaptically coupled responses also have to be generated. Finally, comparative experiments at different wavelengths should be initiated. The MEA provides a highly effect test bed for such comparative studies.

Acknowledgement

The laser microbeam system was designed by BTG, GmbH of Munich, Germany in 1977 and donated to Prof. Gross by the Sandoz Corp., Basel Switzerland in 1982. This research was supported in part by a neurophotonics DARPA grant (CIPHER) to GWG..

References

[1] Zhang F., Wang L-P., Brauner M., Liewald J.F., Kay K., Wtzke N., Wood P.G., Bamberg E., Nagel G., Gottschalk A., Deisseroth K. (2007). Multimodal fast optical interrogation of neural circuitry. *Nature,* 466, 633-639.

[2] Shoham ZS, Deisseroth K. (2010). Special issue on optical neural engineering: advances in optical stimulation technology. *J. Neural Eng.*, 7, 1-3.

[3] Izzo A. D., Joseph J., Walsh T., Jansen E.D., Bendett M., Webb J., Ralph H., and Richter C.P. (2007). Optical parameter variability in laser nerve stimulation: a study of pulse duration, repetition rate, and wavelength. *IEEE Trans. Biomed. Eng.*,54, 1108–1114.

[4] Richter, C-P., Matic A., Wells J., Jansen E., and Walsh, J. (2011). Neural stimulation with optical radiation. *Laser & Photonics Reviews*, 5, 68–80.

[5] Audiat J. (1935). Action des rayonnements ultraviolet et X sur les proprietes electrophysiologiques du nerf isole. These Sciences, Faculte des Sciences de Paris, Paris, France.

[6] Hutton-Rudolph. (1944). Photchemische Versuche an einzelnen Nervenfasern. Dissertation, University Bern.

[7] Booth J., von Muralt A., Staempfli R. (1950). The photochemical action of ultra-violet light on isolated single nerve fibres. *Helv. Physiol. Acta*, 8,110-127.

[8] Allegre G., Avrillier S., Albe-Fessard D. (1994). Stimulation in the rat of a nerve fiber bundle by a short UV pulse from an excimer laser. *Neurosci. Lett.*, 180(2), 261–264.

[9] Lucas J.H., Gross G.W., Emery,D.G. , Gardner C.R. (l985). Neuronal survival after dendrite transaction close to the perikaryon. *Central Nervous System Trauma,* 2, 231-255.

[10] Kirkpatrick J.B., Higgins M.L., Lucas J.H., Gross G.W. (1985). Neural trauma simulation by laser in vitro. *J. Neuropath and Exp. Neurol.*, 44, 268-284.

[11] Lehninger AL (1972) Biochemistry, 6th edition. *Worth Publishers, N.Y.*, pg 370.

MEA electrodes record and stimulate distinctly different neuronal populations

Nitzan Herzog[1*], Gilad Wallach[1], Mark Shein-Idelson[1], Yael Hanein[1]

1 School of Electrical Engineering, Faculty of Engineering, Tel Aviv University, Tel Aviv, Israel
* Corresponding author. E-mail address: nitzan.herzog@gmail.com

Abstract
To better understand the efficacy of extra-cellular electrical stimulation we have combined conventional multi electrode array (MEA) recording with upright calcium imaging microscopy, to obtain detailed activation maps. The maps reveal neuronal activation around and between stimulating electrodes with single cell resolution indicating a highly non-localized spatial distribution of responding neurons. Additionally, every electrode appears to activate only a specific subset of neurons with almost no overlap between the populations activated by different electrodes. Moreover, soma position relative to the stimulating electrode plays only a minor role in determining the identity of activated neurons. Our results indicate that, for a given electrode, stimulated neuronal population differs substantially from the recorded population which is restricted to a very close proximity to the electrode.

1 Background

Extra cellular (EC) electrical stimulation is commonly used to directly interface with neural tissue. It has r pathways(3, 4) of uniform neuronal cultures. This technique has allowed researchers to induce plasticity by affecting the spontaneous activity patterns (3, 4) or the network's response to stimulation (5). Electrical stimulation thus serves as an important tool to study basic principles underlying learning and memory. Proper utilization of electrical stimulation has been hampered by limited knowledge of activation location (i.e., soma or neurites) and of the spatial distribution

cortical neuronal cultures as described before (6). Electrical stimulation patterns consisted of either voltage or current trains of 5 pulses at 20 Hz. Bi-phasic pulses, positive followed by negative, with each phase lasting 400 µs were used. Consecutive trains were

been utilized in the realm of multi-electrode-arrays (MEAs) to activate single neurons(1, 2) o

of activated cells around the stimulating electrodes. To probe the effect MEA stimulation we have combined a conventional MEA recording apparatus with upright calcium imaging microscopy. For the first time, we can directly map the efficacy of MEA stimulation and compare it with that of MEA recording [6].

2 Methods

Calcium imaging was performed on dissociated typically 4 seconds apart. Voltage or current levels were changed between consecutive trains, cycling through a variable number of values. Recordings were performed with excitatory synapse blockers (APV, CNQX).

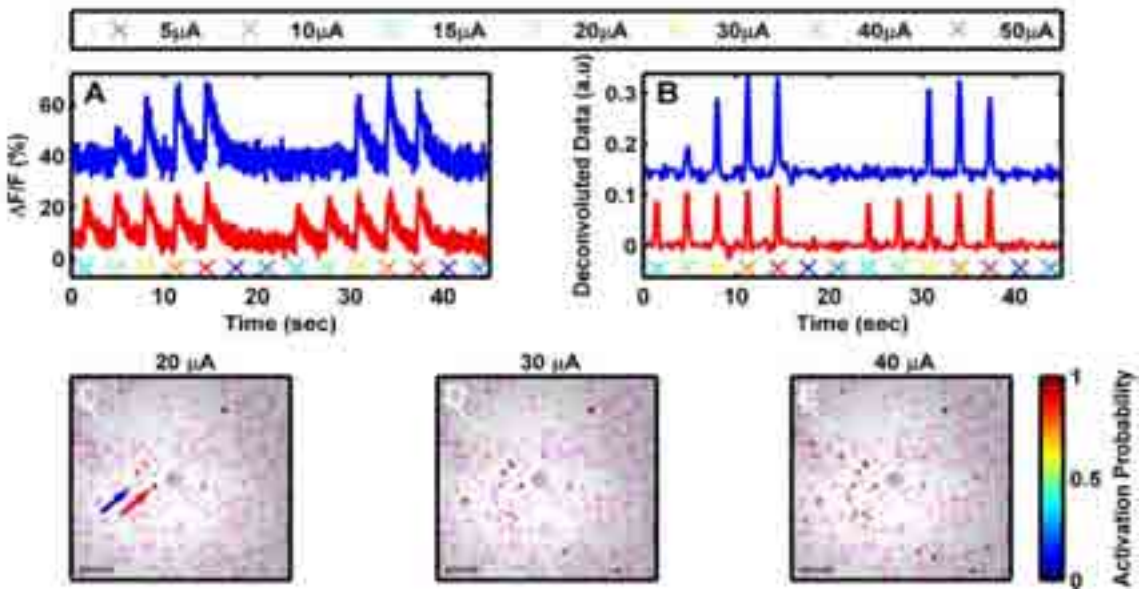

Figure 1: (A) Calcium imaging data from two neurons (indicated by blue and red arrows in C). Electrical stimulation timing is indicated as crosses, colour coded as described for different current amplitudes. (B) Traces from (A) after de-convolution. (C-E) Activation maps for specific stimulation amplitudes as indicated (current driven). Stimulation parameters are described under Methods. Scale bars are 50 µm.

3 Results

To identifiy neuronal activation during stimulation sessions, calcium imaging flurescence traces were collected from all cells in the viewfield. Typical traces exhibited neuronal activation spiking events in correlation with the stimulation trains. (Figure 1A). Next, fluorescence traces were deconvoluted to precisely delineate the timing of spiking activity (6) (Figure 1B). Next, calcium events in the deconvoluted traces were identified via simple threshold crossing detection. Events occuring in conjunction with stimulation trains were classified as “activations”. Finally, activation maps were produced for each stimulation amplitude (Figure 1C-E). Activation maps show soma location around a stimulating electrode with color coding indicating the proportion of activations out of all stimulation events at the relevant amplitude. Activation maps show that, in a 400×400 μm^2 window around the electrode, only a small fraction of the cells responded to stimulations. Moreover, activation appears not to be restricted to somatas near the electrode but extends to remote cells positioned hundreds of microns away.

Figure 2 shows two activation maps for stimulation from two nearby electrodes positioned in two opposite sides of the recording view field. Evidently, each electrode activates a unique set of neurons with a very small neuronal population that responds to both.

4 Conclusions

Using a unique setup of MEA and calcium imaging we can directly map neuronal response to electrical stimulation. Our results show that each electrode stimulates only a specific subset of neurons. This electrode-neuron association is only partially determined by the distance between the electrode and the soma. These findings suggest that electrical stimulation is dominated by process rather than by soma activation. Also, in a previous study we demonstrated that recording is limited to neurons with somas in almost physical contact with the electrode. Therefore, these two findings explicitly demonstrate for the first time that neuronal recording and stimulations apply to substantially different neuronal populations.

References

[1] Wagenaar D, Pine J, Potter S. Effective parameters for stimulation of dissociated cultures using multi-electrode arrays. *Journal of Neuroscience Methods*. 2004;138(1-2):27-37.

[2] Gal A, Eytan D, Wallach A, Sandler M, Schiller J, Marom S. Dynamics of excitability over extended timescales in cultured cortical neurons. *The Journal of Neuroscience*. 2010;30(48):16332-42.

[3] Jimbo Y, Tateno T, Robinson H. Simultaneous induction of pathway-specific potentiation and depression in networks of cortical neurons. *Biophysical Journal*. 1999;76(2):670-8.

[4] Bakkum DJ, Chao ZC, Potter SM. Spatio-temporal electrical stimuli shape behavior of an embodied cortical network in a goal-directed learning task. *Journal of neural engineering*. 2008;5:310.

[5] Shahaf G, Marom S. Learning in networks of cortical neurons. *The Journal of Neuroscience*. 2001;21(22):8782-8.

[6] Herzog N, Shein-Idelson M, Hanein Y. Optical validation of in vitro extra-cellular neuronal recordings. *Journal of neural engineering*. 2011;8:056008.

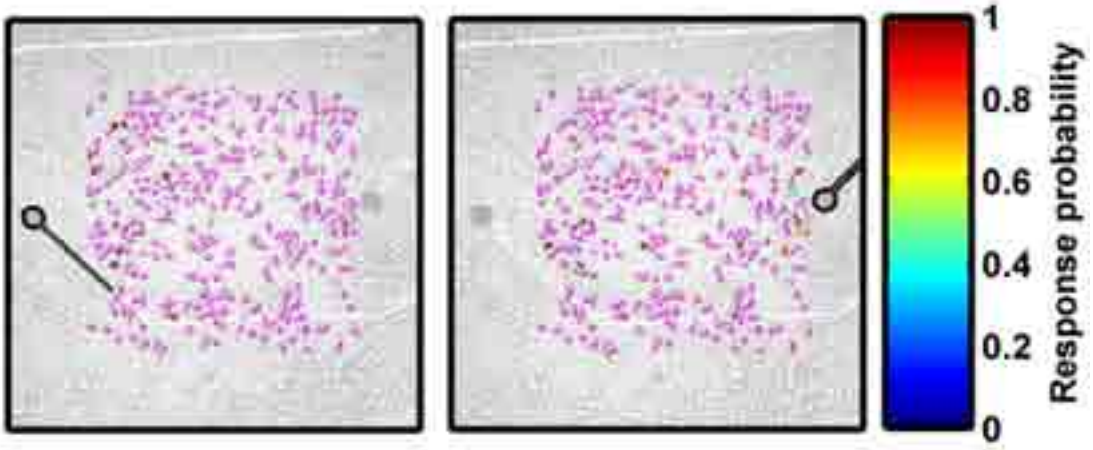

Figure 2: Activation maps describing the response to stimulation from two different electrodes (highlighted in black). All stimulations consisted of 500 mV pulses (voltage driven). Electrodes were 30 µm in diameter.

Replicating light-evoked activity in a population of retinal ganglion cells with MEA-based electrical stimulation

Paweł Hottowy[1,2*], Andrzej Skoczeń[1], Deborah E. Gunning[3], Sergei Kachiguine[2], Keith Mathieson[3], Alexander Sher[2], Piotr Wiącek[1], Alan M. Litke[2,**], Władysław Dąbrowski[1,**]

1 AGH University of Science and Technology, Faculty of Physics and Applied Computer Science, al. Mickiewicza 30, 30-059 Krakow, Poland
2 Santa Cruz Institute for Particle Physics, University of California, Santa Cruz, 1156 High Street, Santa Cruz, CA 95064, USA
3 Institute of Photonics, University of Strathclyde, Glasgow G4 0NW, Scotland
* Corresponding author. E-mail address: hottowy@agh.edu.pl
** A.M.L and W.D. contributed equally

Abstract
Using a custom-designed 61-electrode system for simultaneous low-artifact electrical stimulation and recording, we replicated the light-evoked activity in a population of retinal ganglion cells (RGCs) by application of a spatio-temporal pattern of stimulation pulses to an isolated rat retina.

1 Methods

We used a custom designed MEA system based on 61-electrode array with 60 µm interelectrode spacing and two 64-channel integrated circuits for electrical stimulation and recording. The details of the system design were described in [1].

For classification of the RGC types, we recorded the retinal output spiking activity under visual white-noise stimulation and classified the 28 identified RGCs as described in [2]. We targeted a single RGC type (the OFF cells with large receptive fields – the 'OFF-1' cells) for the electrical stimulation.

We always used triphasic current pulses (positive-negative-positive sequence with relative amplitudes of 2:-3:1 and duration of 100 µm per phase - see [1]) to stimulate the cells. To find the stimulation threshold currents for individual RGCs, we applied stimulation pulses to all the 61 electrodes with amplitudes (defined as the current value for the negative pulse phase) ranging from 0.15 to 1.5 µA and with 10% amplitude increments. We always stimulated one electrode at a time, with 15 ms delay between pulses on consecutive electrodes. By repeating this procedure 100 times for each amplitude, in ~45 minutes we recorded the responses of a population of RGCs as a function of the stimulating electrode location (61 electrodes) and current amplitude (26 values).

We found online the stimulation thresholds for 10 out of 13 'OFF -1' RGCs identified in this preparation. For each of these cells, we identified the electrode that activated the given cell with the lowest current amplitude (the so-called primary electrode) and the threshold current for stimulation of this cell with >98% efficacy. To replicate the spiking activity of a single RGC, we defined a 1-second long sequence of stimulation pulses that matched the time series of the visually-evoked action potentials recorded previously from this RGC. To replicate the activity of a population of RGCs, we combined the pulse sequences for the 10 cells into one spatio-temporal pattern of stimulation pulses. The pulses were finally generated with an additional amplitude scaling. The 10 threshold current values were multiplied by the same factor, incremented from 0.8 to 2.0 with 10% steps, and for each scaling factor value, we applied the complete pattern of stimulation pulses 20 times with a repetition period of 3 seconds.

2 Results

The best matching between the electrical stimulation-evoked activity and the light-evoked activity was obtained for the scaling factor value of 1.56. For seven of the stimulated cells we found the desired responses: each of these cells was reliably stimulated by its primary electrode and showed no activity synchronized with the stimulation pulses applied to any of the other electrodes. One cell was activated by both its primary electrode and one of the other electrodes. The responses of these 8 neurons to the applied stimulus are shown in figure 1. For the two other cells, the large stimulation artifact made the neuronal responses to some of the stimulation pulses unclear and we excluded these cells from further analysis.

3 Conclusion/Summary

In this proof-of-principle study, we replicated with high fidelity the light-evoked activity in a selected population of rat RGCs. However, we were not able to stimulate independently 100% of the targeted

cells, and it is clear that independent stimulation of RGCs of different types will be even more challenging. This is an area of ongoing study, including application of multielectrode stimulation to target individual RGCs (in collaboration with EJ Chichilnisky at the Salk Institute).

Acknowledgement

This work was supported by the Polish Ministry of Science and Higher Education grants for scientific research in the years 2009-2012 (W.D.), National Institutes of Health Grant 5R21EB004410, National Science Foundation Grant PHY-0750525 and the McKnight Foundation (A.M.L.) and Burroughs Wellcome Fund Career Award at the Scientific Interface (A.S.). D.E.G. was funded through EPSRC LSI and RAEng fellowships. K.M. was funded through fellowships from the Royal Society of Edinburgh and the SU2P, an RCUK Science Bridges programme.

References

[1] Hottowy P, Dąbrowski W, Kachiguine S, Skoczeń A, Fiutowski T, Sher A, Rydygier P, Grillo AA, Litke AM (2008): An MEA-based System for Multichannel Low-Artifact Stimulation and Recording of Neural Activity. *Proc. of the 6th MEA Meeting (Reutlingen)*, 259-262.

[2] Litke AM, Bezayiff N, Chichilnisky EJ, Cunningham W, Dąbrowski W, Grillo AA, Grivich M, Gryboś P, Hottowy P, Kachiguine S, Kalmar RS, Mathieson K, Petrusca D, Rahman M & Sher A (2004). What Does the Eye Tell the Brain?: Development of a System for the Large-Scale Recording of Retinal Output Activity. *IEEE Transactions on Nuclear Science*, 51, 1434-1440.

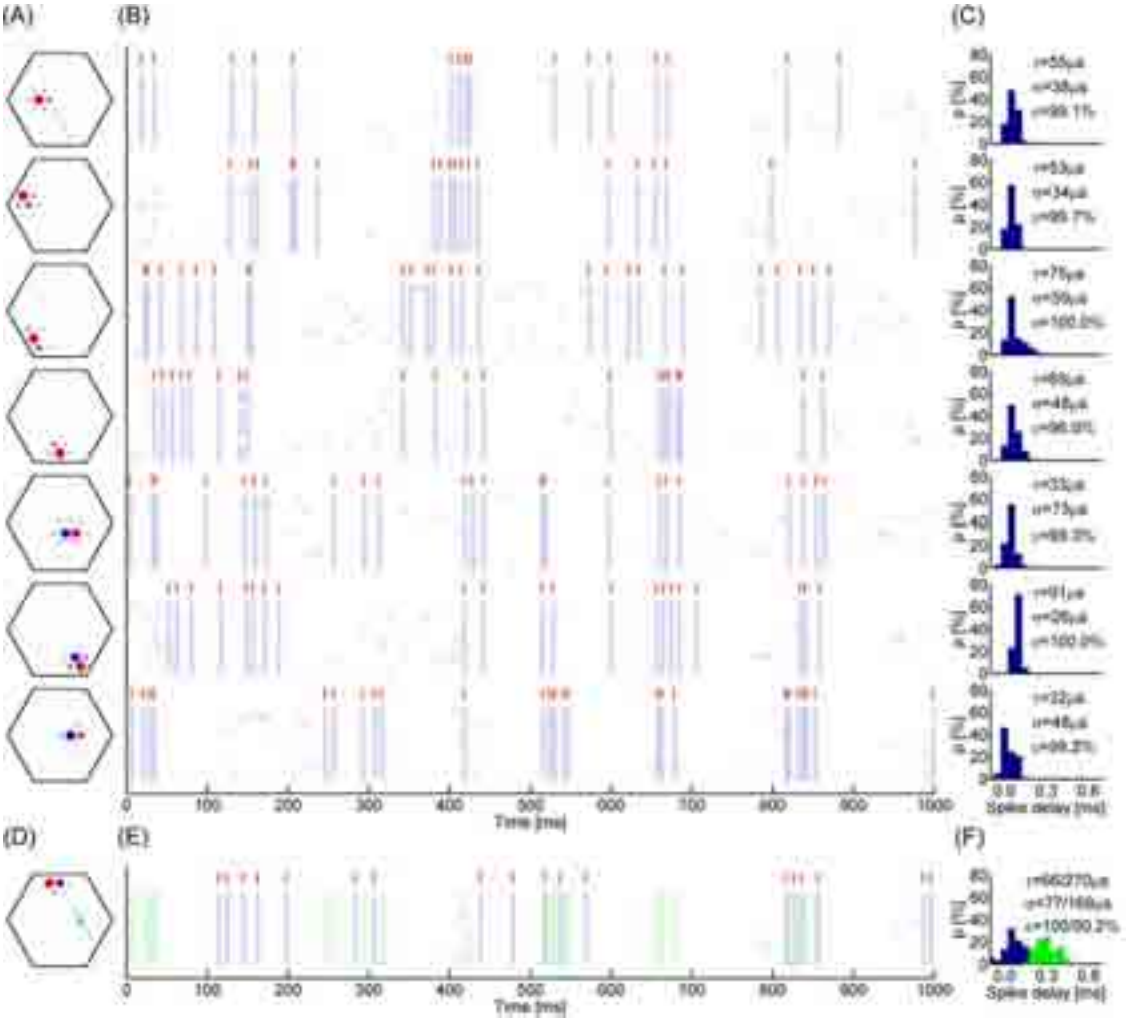

Fig. 1. Replication, in an isolated rat retina, of the visual stimulus-evoked spiking activity of a retinal ganglion cell (RGC) population with patterned electrical stimulation. (A) Averaged recorded visually-evoked spiking signal amplitudes (Electrophysiological Image - EI) of 7 'OFF-1' RGCs, shown on all 61 electrodes. The circle diameter is proportional to the average amplitude and the circle center corresponds to the position of the given recording electrode. The red circle marks the electrode that was used for the electrical stimulation of the given cell. (B) RGC responses to the patterned electrical stimulation. For each cell, the red lines mark the stimulation pulse times and the blue diamonds mark the spike times. The spike times are presented in 20 rows that correspond to 20 repetitions of the stimulation pattern. The stimulation amplitude was adjusted for each cell independently. (C) Distributions of spike delays relative to the end of the stimulation pulse; τ – average delay; σ – variability (SD) of neuron response delay; ε – stimulation efficacy; p – probability of response within 2 ms after the stimulation pulse. (D,E,F) EI, stimulation response and spike delay distribution for one RGC that was stimulated by both its primary electrode and another electrode (most likely by antidromic axonal stimulation). The electrode causing the crosstalk (D), the spikes resulting from the crosstalk (E) and the distribution of these spike delays (F) are marked with green color.

Microdevices for adherent mammalian cells electroporation by means of electrolyte oxide semiconductor capacitors

Alessandra Brocca[1], Marta Maschietto[1], Stefano Girardi[1], Stefano Vassanelli[1*]

1 University of Padova, Dept. Biomedical Sciences, Padova, Italy
* Corresponding author. E-mail address: stefano.vassanelli@unipd.it

Abstract
Electroporation is one of the most widely used approaches for the delivery of molecules in cultured cells, like plasmids to express exogenous genes. In the last years, several types of microsystems have been developed to electroporate groups of few cells or single cells growing in adhesion to the chip substrate. Most devices are based on metal multi-electrodes arrays. Here we show the use of two generations of Si/SiO_2 and Si/TiO_2 Electrolyte Oxide Semiconductor Capacitors (EOSCs) to perform efficient and selective electroporations of mammalian cells. Applying low-voltage pulses, Chinese Hamster Ovary cells (CHO-K1) were efficiently electroporated for the delivery of intracellular actin markers. EOSCs based microchips are then presented as efficient tools for the delivery of DNA to induce the production of fluorescent proteins, suggesting their possible general use in exogenous genes expression experiments and in large-scale production of stable cell lines.

1 Background/Aims

Many chemical and physical approaches are used to transfect cells with molecules of interest, allowing them to pass through the plasmatic membrane that protects cells from undesired transport. Among physical methods, electroporation is one of the most widely used, and a recent development is the use of microsystems to electroporate cells either in suspension [1] or in adhesion to a substrate. For what concerns the latter, most of the microdevices are based on multi-electrodes arrays: electrical stimuli are delivered by means of small metal electrodes, inducing transient pores in the membrane of cells growing on them. Transfections with different molecules can be obtained, including nucleic acids for exogenous genes expression. The major advantage respect to standard electroporation is the independence of each stimulation site and, as a consequence, the possibility to choose which cell [2] or group of few cells to stimulate, thus carrying out spatially and/or temporally-controlled electroporations. Moreover, reduced voltage amplitudes are required, thus cells undergo a reduced electrical and thermal stress [3]. In the present work, Si/SiO_2 and Si/TiO_2 EOSCs integrated in microchips were used in the electroporation of CHO-K1 cells. Modifying the protocols previously used for the stimulation of nerve cells from *Lymnaea stagnalis* [4], both markers for intracellular proteins and plasmids for exogenous genes expression were successfully delivered into the cells. The results demonstrate the reliability of EOSC-mediated transfection, suggesting them as a new mean for the generation of cell lines stably expressing proteins of interest.

2 Methods

The basic unit is an Electrolyte Oxide Semiconductor Capacitor (EOSC): 64 Si/SiO_2 EOSCs with 10 nm thick oxide and 30 to 50 μm width are organized in two linear arrays [5]. A plastic chamber is mounted on the chip for cell culture. To provide the stimulus, each EOSC was selected through its connector on the board. Si/TiO_2 chips, mounted on a petri dish, are based on a single round capacitor with 10 nm TiO_2 thickness and a diameter from 0.125 to 2 mm (Fig. 1).

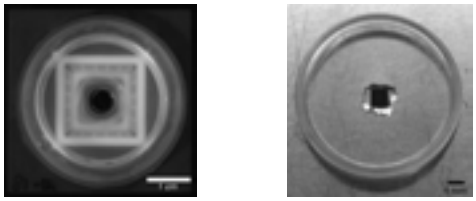

Fig. 1. First (*left*) and second (*right*) generation chips with SiO_2 and TiO_2 coating, respectively. The plastic chambers for the cell culture are visible. Scale bars: 1 cm and 4 mm.

Epithelial CHO-K1 cells were maintained at 37°C and 5% (v/v) CO_2. Two days before the electroporations, 10^4 and 4 x 10^3 cells/cm^2 were seeded on sterilized Si/SiO_2 and Si/TiO_2 chips, respectively. Fast-slope and high-frequency stimuli were delivered through the waveform generator Agilent 33250A 80 MHz. All the electroporation trials were carried out in a high ionic strength buffer [2]. 2 μg of ECFP/EGFP fluorescent proteins DNAs, cloned into pcDNA3.1(-) plasmid, were used in each electroporation experiment. Actin was marked with Alexa568-conjugated Phalloidin or Alexa488-conjugated anti-actin antibody (Life Technologies). Nuclear staining was obtained with DAPI (Life Technologies).

3 Results

3.1 EOSC with SiO_2

Figure 2 shows an example of CHO-K1 cells that produce the fluorescent protein EGFP 24 hours after the electroporation with the corresponding plasmid by Si/SiO_2 EOSCs. On most of the capacitors cells succeeded in producing the exogenous protein, becoming fluorescent. As previously shown [6], these results confirmed the reliability of the device in transient gene expression experiments.

The same chip has been used for live-imaging experiments: in Fig. 3 an example of actin double staining with fluorescent Phalloidin and specific antibody is shown. Respect to standard immunofluorescence protocols, this technique has the advantage of using non-fixed cells, thus allowing to monitor changes in the protein turnover.

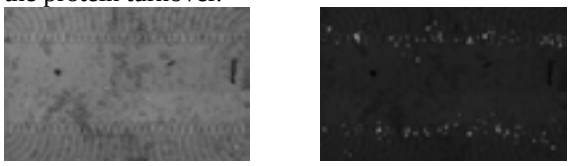

Fig. 2. Gene expression with the SiO_2-based EOSC. *Left*: central area of the microchip with the two linear arrays of 32 EOSCs. *Right*: EGFP expression in CHO-K1 cells after electroporation: superimposition of visible and UV light image. Scale bars: 20 μm.

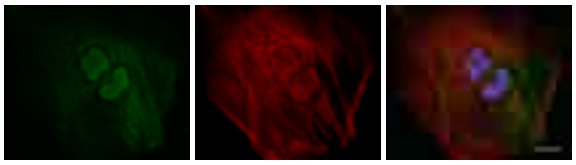

Fig. 3. Live-imaging with the SiO_2-based EOSC. Electroporation of CHO-K1 with fluorescent anti-actin antibody (*left*), Phalloidin (*middle*) and merge with DAPI for nuclear staining (*right*). Scale bar: 20 μm.

3.2 EOSC with TiO_2

Figure 4 shows EGFP expression in CHO-K1 cells after electroporation by a single-spot EOSC with TiO_2 as dielectric. Most part of cells on the capacitors expressed the exogenous protein, thus showing that also microchips based on Si/TiO_2 technology can be used for transient gene expression experiments.

To test whether the same device could be used to transfect cells with more than one plasmid at the same time, CHO-K1 were electroporated with 2 plasmids coding for ECFP and EGFP. Figure 5 shows that many cells expressed both fluorescent proteins, thus demonstrating the possibility to perform double expression experiments.

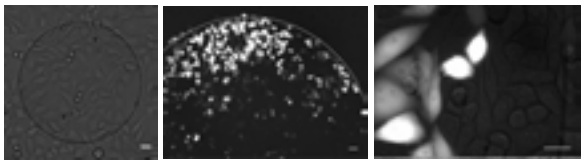

Fig. 4. Gene expression with the TiO_2-based EOSC. *Left:* single TiO_2 insulated EOSC (270 μm diameter). Cells are growing on the entire chip surface. *Middle, Right:* EGFP expression in CHO-K1 cells after electroporation on a EOSC with a larger diameter. Superimposition of visible and UV light images. The capacitor on the middle picture is marked by a dotted line. Scale bars: 40 μm (*middle*); 20 μm (*left, right*).

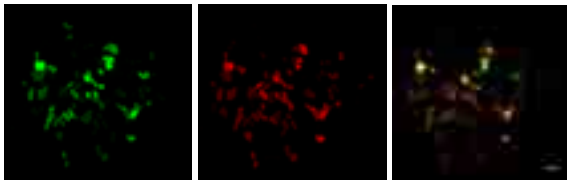

Fig. 5. Multiple gene expression with the TiO_2-based EOSC. Example of cells transfected with two plasmids, ECFP (*left*) and EGFP (*middle*). *Right:* merge of two fluorescent signals. Scale bar: 40 μm. Picture are in false colours.

4 Conclusions

The present work proposed the use of SiO_2 and TiO_2-based EOSCs to perform electroporations of mammalian cells growing in adhesion. The results demonstrate the reliability of the devices: transfections with different molecules, like plasmids coding for exogenous proteins or intracellular markers for live imaging experiments, can be obtained.

Acknowledgement

We thank Prof. Peter Fromherz for providing us with the chips.

References

[1] Geng T., Zhan Y., Wang H.Y., Witting S.R., Cornetta K.G., Lu C. (2010) Flow-through electroporation based on constant voltage for large-volume transfection of cells. *Journal of Controlled Release*,144, 91-100.

[2] Vassanelli S., Bandiera L., Borgo M., Cellere G., Santoni L., Bersani C., Salamon M., Zaccolo M., Lorenzelli L., Girardi S., Maschietto M., Dal Maschio M., Paccagnella A. (2008) Space and time-resolved gene expression experiments on cultured mammalian cells by a single-cell electroporation microarray. *New Biotechnology*, 25, 55-67.

[3] Pucihar G., Kotnik T., Teissié J., Miklavcic D. (2007) Electropermeabilization of dense cell suspensions. *European Biophysics Journal*, 36, 173-185.

[4] Schoen I., Fromherz P. (2007) The mechanism of extracellular stimulation of nerve cells on an electrolyte-oxide-semiconductor capacitor. *Biophysical Journal*, 92, 1096-1111.

[5] Schmidtner M., Fromherz P. (2006) Functional Na+ channels in cell adhesion probed by transistor recording. *Biophysical Journal*, 90, 183-189.

[6] M. Maschietto, S. Girardi, M. Dal Maschio, S. Vassanelli (2009) Microchip-Integrated EOSCs (Electrolyte Oxide Semiconductor Capacitors) as Devices for High Efficiency and Selective Electroporation of Mammalian Cells. *WC 2009 IFMBE Proceedings*, 25/VIII, 321–324.

Effects of DC electric field on synaptic plasticity and seizure activities in thalamocingulate circuitry

Wei Pang Chang[1], Bai Chuang Shyu[2]

1 Graduate Institute of Life Sciences, National Defense Medical Center, Taipei, Taiwan, Republic of China
2 Institute of Biomedical Sciences, Academia Sinica, Taipei, Taiwan, Republic of China

Abstract

Seizure affects 1 % of population, and 30 % among them suffered from drug-resistant epilepsy. Clinical application of transcranial magnetic stimulation, transcranial current stimulation and direct current (DC) electric field stimulation provide non-invasive approaches for the treatment of drug-resistant seizures. Previous studies showed that field stimulation could modulate synaptic plasticity as well as influence epileptiform activities in various brain regions, such as in motor cortex and hippocampus. However, seldom research focus on the field effect on synaptic transmission within thalamocortical system, which is an important circuitry in sensory processing and in generating epileptiform activities. The medial dorsal (MD) thalamic nucleus is heavily connected to anterior cingulate cortex (ACC) and medial prefrontal cortex (mPFC) and could regulate seizure activities in cortical regions. Seizures generated in mPFC and ACC are often drug-resistant and alternative treatment such as field stimulation needs to be evaluated in this brain region. Therefore, the current study is aimed to investigate the effect of DC field stimulation on the changes of thalamocingulate synaptic plasticity and seizure-like activities generated within this circuitry.

1 Methods/Statistics

Male C57BL/6J mice were used in study. Previously developed brain slice cutting method preserve the pathway between MD and ACC was used in this study. The local field potentials were recorded with multielectrode array (MEA, Multi Channel Systems, Reutlingen, Germany). Data were acquired by the PC based data software MC_Rack at a sampling rate of 10 kHz and analyzed with MATLAB 7.5. Uniform electric fields were generated by passing constant current between two parallel AgCl-coated silver wires placed inside the MEA chamber. Currents were generated by a stimulator (A-M Systems, Inc. Carlsborg, USA) under the control of a pulse generator (STG 1002, Multi Channel Systems, Reutlingen, Germany)

2 Results

Application of 10 minutes of anodal DC field stimulation could potentiate the synaptic transmission in the MD-ACC pathway. The potentiation effect could last 20 minutes after ceasing application of DC stimulation (Fig.1). The potentiation effect was mediated by the volume changes of extracellular space, which will in turn increase the concentration of neurotransmitter. The potentiation was prevented by the application of furosemide which was used to stabilize the extracellular space (Fig.2) The effect of DC field stimulation on synaptic potentiation was also blocked by the application of APV, the NMDA receptor antagonist (Fig.3). Drug resistant seizure was induced by perfusion brain slice with 4-amino pyridine (250 μM) and bicuculline (5 μM), application of anodal DC enhanced the seizure-like activities while cathodal DC suppressed them (Fig.4). Furosemide also abolished the effect of DC field on seizure-like activities, which indicated that DC field also influence the seizure-like activities by the modulation of extracellular space (Fig.5).

3 Conclusion/Summary

DC mediated potentiation is caused by increasing concentration of neurotransmitter because application of furosemide and APV could prevent potentiation. Cathodal DC could suppress spontaneous and thalamic-evoked seizure-like activities, while anodal DC application has opposite effects. Field effect on seizure-like activities is caused by the alterations of extracellular potassium concentration which is mediated by NKCC cotransporter.

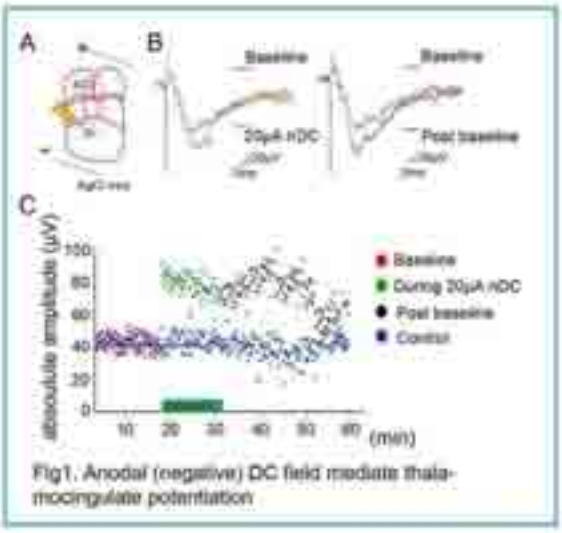

Fig1. Anodal (negative) DC field mediate thalamocingulate potentiation

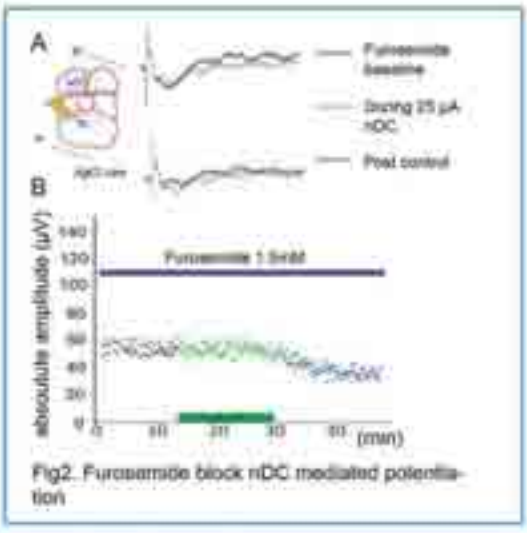

Fig2. Furosemide block nDC mediated potentiation

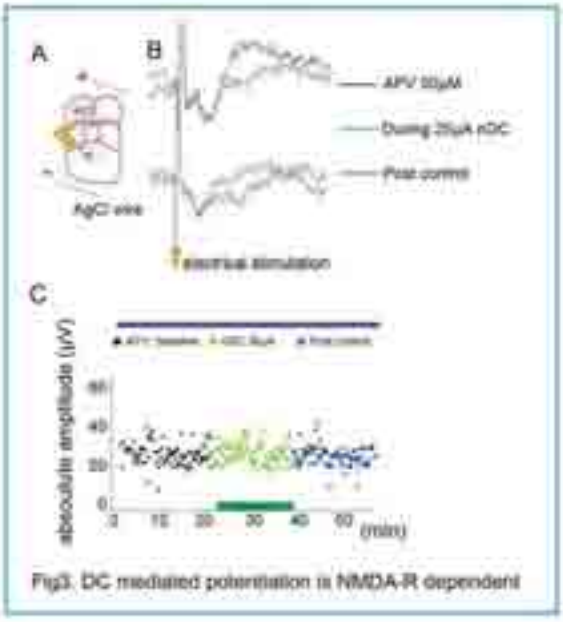

Fig3. DC mediated potentiation is NMDA-R dependent

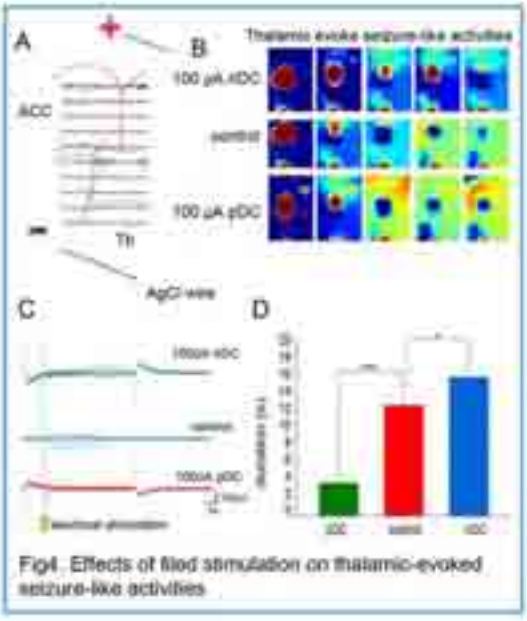

Fig4. Effects of filed stimulation on thalamic-evoked seizure-like activities

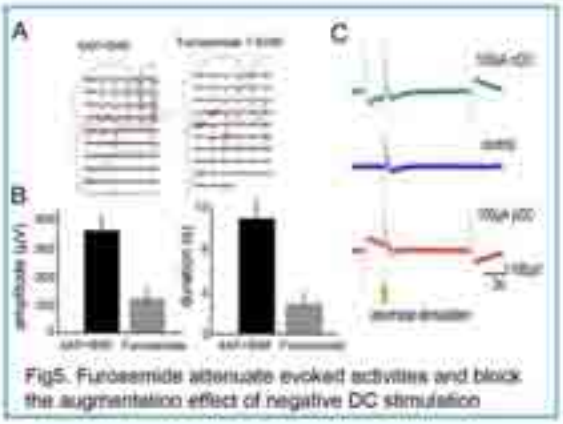

Fig5. Furosemide attenuate evoked activities and block the augmentation effect of negative DC stimulation

Capabilities of a high-density CMOS microelectrode array to identify, record, and stimulate individual neurons in cultured networks

Douglas J Bakkum[1*], Urs Frey[2], Jan Mueller[1], Michele Fiscella[1], Branka Roscic[1], Hirokazu Takahashi[3], Andreas Hierlemann[1]

1 ETH Zurich, Department of Biosystems Science and Engineering (D-BSSE), Basel, Switzerland
2 RIKEN Quantitative Biology Center, Kobe, Japan
3 Research Center for Advanced Science and Technology (RCAST), The University of Tokyo, Japan
* Corresponding author. E-mail address: douglas.bakkum@bsse.ethz.ch

Abstract
Complementary Metal Oxide Semiconductor (CMOS) technology is an emerging tool in neuroscience that is being used to create next-generation multi-electrode arrays having large numbers of closely-spaced electrodes. Consequently, these arrays produce large amounts of novel data. Here, we report preliminary data using one such array to identify, record, and stimulate individual neurons.

1 Introduction

Complementary Metal Oxide Semiconductor (CMOS) technology is an emerging tool in neuroscience that is being used to create next-generation multi-electrode arrays [1]. The technology gives the ability to create arrays having large numbers of closely spaced electrodes along with on-chip circuitry for amplifying neuronal signals and providing electrical stimulation. Consequently, experiments produce novel and large amounts of data. A preliminary step in adopting the technology is to characterize the type of data produced and the array's capabilities as a neural interface.

2 Methods

2.1 Cell culture

Cells from E18 rat cortices, dissociated in trypsin, were grown in DMEM with 10% horse serum on top of the CMOS arrays. A thin layer of PEI and a 15 µL drop of laminin were used for cell adhesion. Experiments were conducted inside an incubator to control environmental conditions.

2.2 CMOS array

The microsystem chip was fabricated in 0.6 µm CMOS technology, is 7.5x6.1mm^2 in size, and features 11,011 metal electrodes, as well as 126 bidirectional circuitry channels capable of recording and stimulation. All 7-µm-diameter platinum (Pt) electrodes are placed within a 2.0x1.75mm^2 area (3,150 electrodes per mm^2), and were realized during a 3-mask post-CMOS processing step. Flexibility in the electrode selection (126 can be selected at the same time) is attained through an analog switch matrix, integrated underneath the electrode array, consisting of 13k SRAM cells and analog switches that define the routing from the electrodes to the amplifiers of the channel units. The SRAM cells store information about the traversed switches between connected electrodes and readout/stimulation channels. Dedicated algorithms optimize the routing for a defined configuration. See [2] for more details.

3 Results

Action potentials could be assigned to individual somata if they were relatively isolated from other somata. On average, somatic action potentials of a given neuron could be recorded over an 85 µm diameter area. The extracellular signals of each soma had its own unique temporal dynamics and spatial distribution (Fig. 1). Most participated in network bursts, typical in such cultures, by producing their own individual burst, frequently composed of a set of action potentials having different amplitudes.

Spike-sorting algorithms are needed in order to assign signals to non-isolated somata, but the combination of overlapping signals from nearby neurons and their varying amplitudes showed that conventional spike-sorting techniques, based on the analysis of signal waveforms, are inadequate (Fig. 2 right). Alternatively, stimulation served as a reliable means to identify somata. This was because action potentials evoked in axons antidromically propagated and produced somatic action potentials at distant sites that were isolated and had consistent waveforms (Fig. 2 left).

4 Conclusion

CMOS microelectrode arrays allow high spatial and temporal resolution two-way experimentation without limitations on experiment duration. Novel results are emerging, as their advantages are beginning to be explored in more detail, and further studies are expected to provide a wealth of additional data that will in turn advance our basic understanding of the brain's capabilities.

Acknowledgement

We thank members of the Bio Engineering Lab for support and ideas. Funding includes: Swiss National Science Foundation Ambizione grant; Japanese Society for the Promotion of Science Post-doctoral grant; FP7 of the European Community through the ERC Advanced Grant 267351 “NeuroCMOS”; the TEPCO Research Foundation; and an RCAST internal grant.

References

[1] A. Hierlemann, U. Frey, S. Hafizovic, F. Heer (2011): Growing Cells atop Microelectronic Chips: Interfacing Electrogenic Cells in Vitro with CMOS-based Microelectrode Arrays. *Proceedings of the IEEE*, Vol. 99, No. 2, pp. 252-284.

[2] Frey U, Sedivy J, Heer F, Pedron R, Ballini M, Mueller J, Bakkum D, Hafizovic S, Faraci FD, Greve F, Kirstein KU, Hierlemann A (2010): Switch-Matrix-Based High-Density Micro-electrode Array in CMOS Technology. *IEEE Journal of Solid-State Circuits*, 45(2)

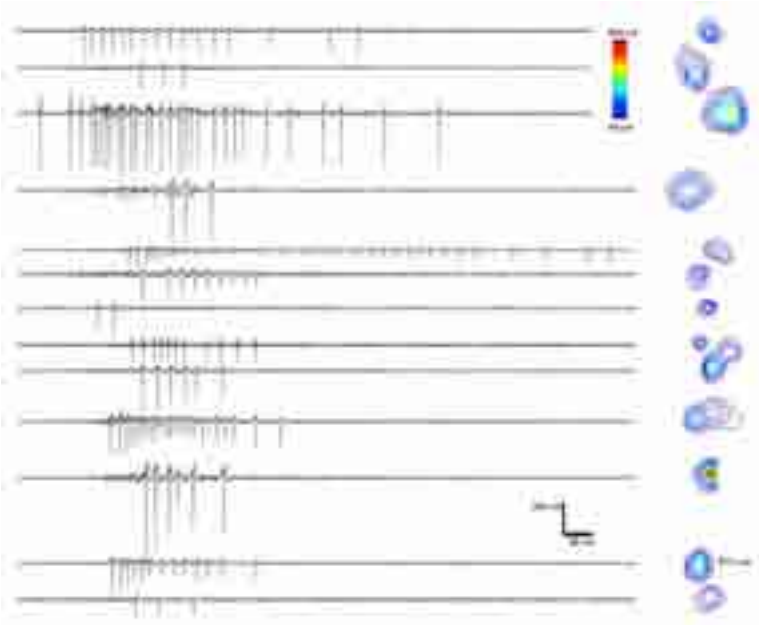

Fig. 1. Somata produced unique spatiotemporal signatures. Footprints (right, showing the spatial extent of the peak amplitude) and traces (left) from extracellular recordings of relatively isolated somata are plotted. The traces were similar in different network bursts, and examples during a given network burst are plotted. Footprints were averaged from the 10 largest individual spikes found from 10 network bursts. This produces the maximum sized footprint and also further minimizes contamination from nearby cells (see the small spikes in the fourth trace from the top).

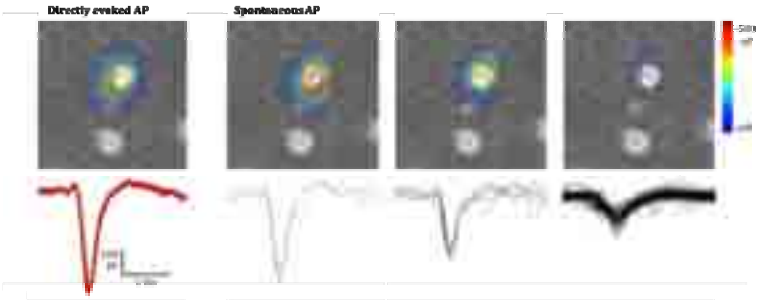

Fig. 2. Directly evoked action potentials produced large and consistent spike waveforms, while spontaneous action potentials could be mistaken as originating from different neurons. Footprints (top) and overlaid traces (bottom; the same recording electrode was used for each panel) from extracellular recordings are presented. In this case, common spike-sorting techniques assign the spontaneous waveforms as originating from three separate cells. However the underlying images of somata (MAP2 immunostaining) show that the traces originate from a single cell.

Using Braitenberg's principles for stimulate and record simultaneously populations of hippocampal cells: a biorobotic approach

Lorente Víctor[2]*, Ferrández Jose Manuel[1], de la Paz Felix[3], Fernández Eduardo[1]

1 Instituto de Bioingeniería, Universidad Miguel Hernández, Alicante, Spain
2 Departamento de Electrónica, Tecnología de Computadores y Proyectos, Universidad Politécnica de Cartagena, Spain
3 Departamento de Inteligencia Artificial, UNED, Madrid, Spain
* Corresponding author. E-mail address: victor.lorente@upct.es

Abstract
Multielectrode Arrays Setups have been designed for direct culturing neural cells over silicon or glass substrates, providing the capability to stimulate and record simultaneously populations of neural cells. The main objective of this work will be to control a robot using this biological neuroprocessor and a new simple Braitenberg's behaviour scheme.

1 Introduction

Valentino Braitenberg in his book "Vehicles: experiments in synthetic psychology" [1] proposed some theoretical experiments demonstrating that very simple connections between sensors and motor circuits in a robot may develop complex behaviours. These simple connectivity topologies can easily be implemented in our proposal using living tissue to connect sensors and motor circuits in a robot. In order to carry out with these experiments we must first identify valid circuits in the living tissue and connect them as Braitenberg explains. In Fig.1 two of the simplest topologies can be seen, known as vehicles 2a and 2b. In our experiment we will use range sensors instead of light sensor and the microrobot e-puck will be used.

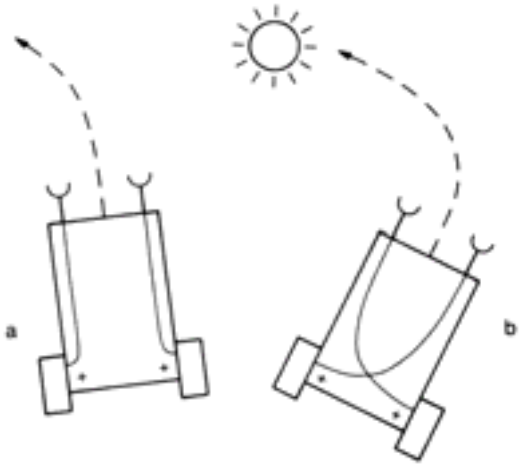

Fig. 1. Simple Braitenberg's vehicles

2 Methods

Stimulation

A tetanic stimulation consists of a high-frequency sequence of individual stimulations of a neuron. It is associated with long-term potentiation, which is the objective of this work. High-frequency stimulation causes an increase in transmitter release called post-tetanic potentiation. This presynaptic event is caused by calcium influx. Calcium-protein interactions then produce a change in vesicle exocytosis. Some studies use repetitive stimulation for training neural cultures, achieving activity potentiation.

In all the experimentation performed, tetanic stimulation was applied as a training method. The electrophysiological properties of the hippocampal culture change during tetanization, getting a potentiation effect on the spontaneous firing, modulating in this way the culture neural activity.

We apply some basic Braitenberg's principles, cross-connectivity versus parallel connectivity to the system in order to study the biological neural network behaviour induced by the biological network topology over a robotic system (Fig. 1).

Robotic system

We use a mobile robot called e-puck, which was developed for educational and research purposes [2]. It has a circular body of approximately 7.5 cm diameter, and weighs approximately 150g. The e-puck is a differential- wheeled robot, having an inter-wheel distance of 5.1 cm. The e-puck has two step motors, eight infrared sensors measuring ambient light and proximity of obstacles in a range of 4 cm, color camera with a maximal resolution of 640x480, 3 omni-

directional microphones for sound localization, 3D accelerometer along the X, Y and Z axis, 8 red LEDs on the ring and one green LED in the body and on-board speaker capable of playing WAV or tone sounds. The e-puck is open hardware and its on-board software is open source, and is built and sold by several companies.

Fig. 2. Microrobot e-puck

3 Results

As explained in our previous work [3], cultures were stimulated through the two pairs of electrodes where no previous logical connection existed. A train of 5 biphasic pulses cathodic-first (50 μA peak, 100 μs phase, 50ms ISI) was delivered every 3s for 10 min for creating ad hoc induced connections (Fig. 3).

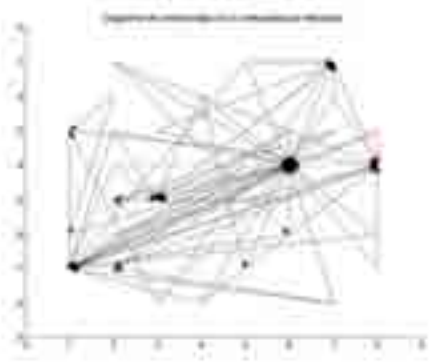

Fig. 3. Connectivity graph based on cross-correlation between electrodes. A connection (red arrow) between electrodes 83 and 84 has been created.

We use only two proximity sensors, left and right, for detecting the obstacles. The distance to the obstacle is coded for stimulating two pairs of induced connections. The final electrode of the two induced links is used for controlling the two step-motors that drive the epuck wheels. The motors are connected in parallel or with cross-connectivity with the corresponding culture induced input for analysing the robotic behaviour.

The results illustrate the existence of qualitatively different responses to the culture structure. If the wheels are connected to the same lateral sensor, that is in a parallel connection, the robot directs to the obstacle, where if the induced links are fixed with cross laterality the robot tries to avoid the obstacle. Our results indicate the existence of a clear facilitation mechanism in response to the coded stimuli at different stages of cell development. The emergent robotic complex behaviour is coded in the biological culture structure with its input/output represented electrodes. The same behaviour is used in [1] for directing or avoiding a light source.

4 Conclusions

In this work a stimulation procedure is described in order to control robot behaviour. First, the neural physiology is analysed for identifying the relevant and practical electrodes. Tetanization is performed in order to obtain a desired ad-hoc connectivity graph. The robot sensor and robot wheels are connected to the induced culture links in parallel or cross-connectivity. The sensors of the robot stimulate specific electrodes while the information in specific connected ones is used for control the robot motors keeping the laterality or inverting it. The robot directs or avoids obstacles depending on the type of linking structure.

Induced neural connections may be used for driving motor elements in a robotic system following Braitenberg's principles and getting a characteristic complex emergent behaviour with very simple connectivity paths.

Acknowledgement

This work is being funded by grant 12361/FPI/09 from Séneca Foundation, Science and Technology Agency from the region of Murcia and by the project 2010V/PUNED/0011 from Universidad Nacional de Educación a Distancia.

References

[1] Braitenberg, V.: Vehicles: Experiments in Synthetic Psichology. MIT Press, Cam- bridge (1984).

[2] F. Mondada, M. Bonani, X. Raemy, J. Pugh, C. Cianci, A. Klaptocz, S. Magnenat, J.-C. Zufferey, D. Floreano, and A. Martinoli. The e-puck, a robot designed for education in engineering. In Proc. of the 9th Conf. on Autonomous Robot Systems and Competitions, volume 1, pages 59–65. IPCB: Instituto Politécnico de Castelo Branco, 2009.

[3] Lorente Víctor, Ferrández Jose Manuel, de la Paz Felix, Fernández Eduardo. Training hippocampal cultures using low-frequency stimulation: Towards Hebbian Learning. MEA Meeting 2012, Reutlingen, in press.

Multichannel real-time feedback system with mili-second precision for STDP experiments

Seokyoung Lee[1], Sunghoon Joo[1], Yoonkey Nam[1*]

1 Neural Engineering Laboratory, Department of Bio and Brain Engineering, Korea Advanced Institute of Science and Technology (KAIST), Daejeon, Republic of Korea
* Corresponding author. E-mail address: ynam@kaist.ac.kr

Abstract
A real-time feedback system can be used for various purposes such as BCI(Brain Computer Interface) study, neural activity modulation, goal-directed task, and also for synaptic plasticity study. Beyond discovery of LTP(Long-Term Potentiation) phenomenon, STDP(Spike-Timing-Dependent Plasticity) has been regarded as a general synaptic plasticity theory. According to the STDP theory, activation timing between pre-synaptic neuron and post-synaptic neuron is a key parameter to enhance or reduce the synaptic transmission efficacy. And the effective time scale is known as below 40 ms. Thus, a real-time feedback system that has very low feedback latency time is required to perform such STDP-related experiments. In this work, we developed a microcontroller-based low-cost, PC-free, multichannel real-time feedback system that has sub-ms feedback latency time, and this system was tested with dissociated hippocampal neural culture on an MEA. This system will be widely applicable for *in vitro* or *in vivo* STDP experiments for the study of neural plasticity.

1 Introduction

Though MEA has been regarded as a convenient tool for the neuroscience studies, the lack of reproducibility on dissociated neural culture should be solved in the case of synaptic plasticity study[1].

As a recent synaptic plasticity theory, STDP theory[2] can explain both LTP and LTD phenomenon, thus STDP is regarded as a general synaptic plasticity theory. But, its application to neural culture on MEA is uncommon due to difficulty to implement STDP experiment that is configured with real-time feedback system. Therefore, most previous neural plasticity studies on MEA were usually done with tetanic stimulation for the LTP induction, but, dissociated neural culture cannot guarantee the reproducible results, and this suggests alternative induction method with closed-loop system will be needed to change their network more effectively[3-5].

In this study, development of multi-channel real-time feedback system based-on dual-microcontroller for MEA is introduced, and experimental results on dissociated neural culture are also discussed as its application. This system is ultra-low cost, simple and PC-free comparing to commercial real-time system.

2 Methods

The entire system consists of real-time feedback system (RTFS) core board, switch board, Head-stage amplifier, break-out box, and MEA (figure 1(a)).

Two general purpose microcontrollers (AVR ATxmega128A1, Atmel) were connected via SPI (Serial Peripheral Interface) for RTFS core board, and operated independently as figure 1(b). And 60-channel switch board was designed with latches (8 X 74HC574) and switches (15 X 74HC4316). The maximum number of input channels was 8, and a break-out box (Multichannel systems, Germany) connected with a head-stage amplifier (custom-built) was used for selecting input channels manually.

In MCU#1, the following processes were continuously performed: 8-ch analog-to-digital conversion with dual-buffer (f_s = 16.4kHz, ADC resolution: 12-bit, input voltage range: -1V ~ +1V, single buffer frame size: 305μs); Baseline noise estimation; Spike detection with thresholding; Transmission of time-stamp (time resolution: 30.5μs) and channel information to MCU#2 via SPI.

In MCU#2, stimulation channel and timing was determined from received timestamp from MCU#1, and voltage stimuli was generated with two DACs; Stimulation channels were selected by controlling a switch board. In addition, each real-time counter (RTC) was synchronized every 1-min, and operation parameters can be changed from PC connected with MCU#2 via UART communication.

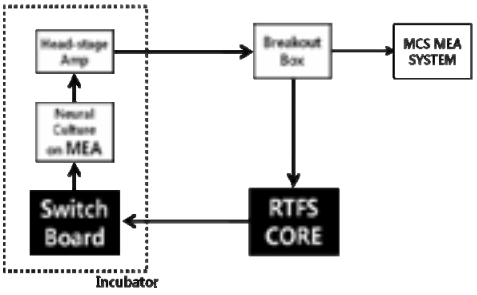

Fig. 1. (a) Block diagram of the entire system

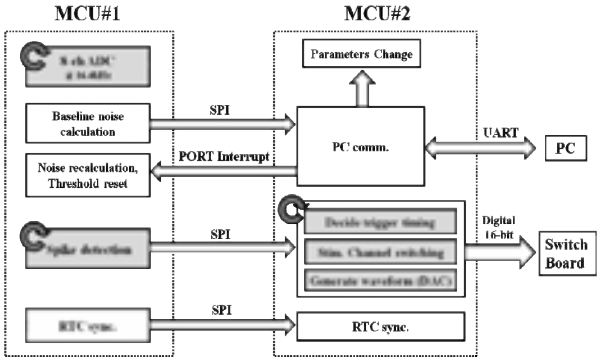

Fig. 1. (b) Operation of dual-microcontroller for RTFS Core

3 Results

The mean feedback latency time was 218 μs (s.d.: 5.6 μs, n=100), thus sub-ms feedback latency time was achieved.

The system was tested for STDP operation using dissociated hippocampal cultures (Fig. 2). Feedback stimulation (positive-first-biphasic pulse, ± 400mV, 200μs/phase) was applied to 8 different target channels 9 ms after the detection of action potential on source channels. After 3 hours of closed-loop stimulation (in an incubator), there were significant increases in firing rates, burst rates, and number of spikes per bursts in source and target channels (Fig.3).

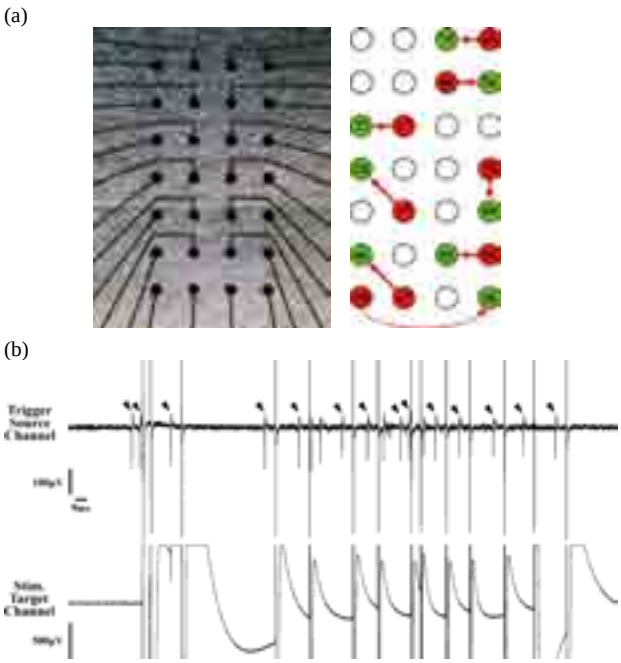

Fig. 2. (a) Assignment of source (red) and target (green) channels. (b) Real-time feedback operation during a burst from a source channel (top) to target channel (bottom). Spikes (arrowheads) triggered stimuli at target channels recorded as stimulation artifacts.

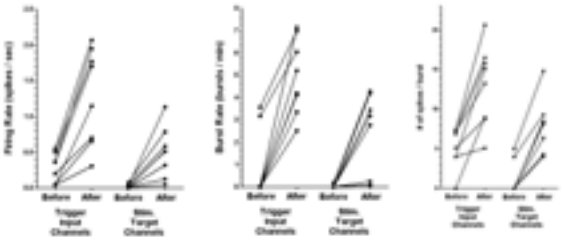

Fig. 3. Changes of spontaneous activities after 3-hour experiment (firing rate, burst rate, # of spikes / burst)

4 Conclusion

Low-cost, stand-alone, dual-general purpose microcontroller-based multi-channel real-time feedback system that has sub-ms feedback latency time was developed, and fully tested on dissociated hippocampal culture on MEA with STDP feedback mode.

Acknowledgement

This work was supported by Mid-career Researcher Program through National Research Foundation grant (No. 2009-0080081, 2012007327) and the Brain Research Center of the 21st Century Frontier Research Program funded by the Ministry of Education, Science and Technology.

References

[1] D. A. Wagenaar, J. Pine, and S. M. Potter, "Searching for plasticity in dissociated cortical cultures on multi-electrode arrays," *J Negat Results Biomed*, vol. 5, p. 16, 2006.

[2] G. Q. Bi and M. M. Poo, "Synaptic modifications in cultured hippocampal neurons: dependence on spike timing, synaptic strength, and postsynaptic cell type," *J Neurosci*, vol. 18, pp. 10464-72, Dec 15 1998.

[3] A. Jackson, J. Mavoori, and E. E. Fetz, "Long-term motor cortex plasticity induced by an electronic neural implant," *Nature*, vol. 444, pp. 56-60, Nov 2 2006.

[4] G. Shahaf and S. Marom, "Learning in networks of cortical neurons," *J Neurosci*, vol. 21, pp. 8782-8, Nov 15 2001.

[5] J. Mavoori, A. Jackson, C. Diorio, and E. Fetz, "An autonomous implantable computer for neural recording and stimulation in unrestrained primates," *J Neurosci Methods*, vol. 148, pp. 71-7, Oct 15 2005.

Highly ordered large-scale neuronal networks of individual cells

Moria Kwiat[1], Roey Elnathan[1], Alexander Pevzner[1], Asher Peretz[2], Boaz Barak[3], Hagit Peretz[1], Tamir Ducobni[1], Leonid Mittelman[2], Uri Ashery[3] and Fernando Patolsky[1]*

1 School of Chemistry, The Raymond and Beverly Sackler Faculty of Exact Sciences, Tel Aviv University, Tel Aviv 69978, Israel
2 Department of Physiology, Sackler Medical School, Tel Aviv University, Tel Aviv 69978, Israel
3 Department of Neurobiology, The George S. Wise Faculty of Life Sciences, School of Neuroscience, Tel Aviv University, Tel Aviv 69978, Israel
* Corresponding author. E-mail address: Fernando@post.tau.ac.il

Abstract
The use of artificial, pre-patterned neuronal networks in vitro is a promising approach to study the development and dynamics of small neural systems. The present work describes a high fidelity and robust procedure for controlling neuronal growth, enabling us to obtain mature and durable neural networks of individual cells at designed geometries. It includes a number of advantages compare to other related techniques mainly due to its high yield and reproducibility. Its main achievements are assessed on creating a large scale neuronal network of individual cells without any glia-supportive cells straight from the plating stage, with relatively long term survival up to 4 weeks. An important application of the method is its use on nano-pillars and nanowire-device arrays, enabling not just the cell bodies but also their neurites to be positioned directly on the electrical devices and grow with registration to the recording elements underneath.

1 Introduction

The culturing of cells on pre-patterned surfaces compared to a natural environment enables to fabricate more simple networks, which might be better suited to study the basic interactions between neurons [1]. Specifically for purposes of extracellular recording from MEAs, patterning is important due to the low signal to noise ratio that is partially because of the imprecise positioning of electrodes relative to the cell [2], and glia cells that often occlude electrodes from detecting neuronal activity [3]. We have, therefore, established a simple and yet robust protocol to confine the growth of cortical and hippocmpal neuronal cells alongside their axons and dendrites into ordered and defined architectures. It fulfills essential and non trivial requirements such as low cell density without any glia cells straight from the plating stage, and persistent survival on the growth pattern until mature and functional synapses are formed. It is applied on silicon wafers and polished glasses, as well as on nanopillars and Si nanowires (NWs) field effect transistor (FET)-devices.

2 Methods

2.1 Patterning by surface chemistry

The substrates surface is coated with hydrophobic fluorosilane self assembled monolayer (SAM), and then, followed by a photolithography step that defines the micro-pattern and a plasma treatment that peels the flouorosilane layer from the pattern-region, polylysine is added, rendering the pattern to hydrophilic (Fig.1). A pattern that confines the cellular bodies to prescribed 30-50 µm width squares and the neuritic growth to thin 2 µm width lines on different substrates is eventually obtained (Fig.2). Critical to the success of our approach is tuning the hydrophobicity surface coverage of the flouorosilane layer. E18 primary cortical or hippocampal cells from Sprague/Dawley rat brain (99.9% glia-free, Genlantis comp.) are immediately plated. We were able to overcome the low survival rate that naturally is accompanied to low cell densities and the absence of glia by using a sandwich configuration for the cells growth with a glass slide on top of the cells, by that reducing the oxygen concentration to physiological levels [4].

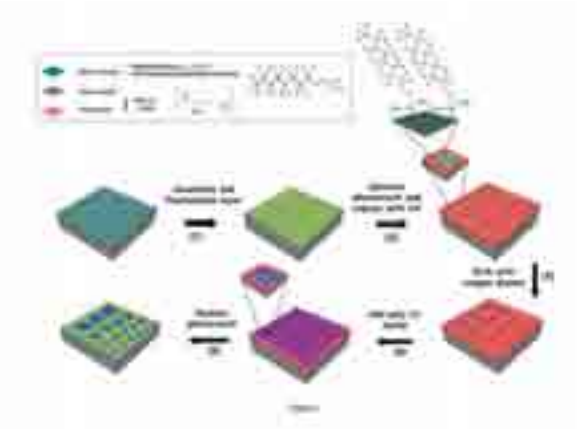

Fig. 1. Schematic of the chemical surface modification

3 Results

Although there have been previous demonstrations of related methods for the creation of individual neuronal networks [5], our method exhibits significantly improved fidelity and reproducibility with persistent neurites growth according to the pattern. Cortical and hippocampal rat neurons, 99.9% glia-free, have been successfully cultured and developed with intact neuronal physiology up to 4 weeks in defined and highly ordered large-scale networks. In average, about 1-3 cells were settled in each square and developed their neurites according to the interconnecting lines. Immunocytochemistry with typical common markers such as Tau and MAP2 for axons and dendrites, and Synaptophysin for synapses revealed that the network exhibit normal morphology and neurite extension. In addition, electrophysiology studies of the network using the whole-cell configuration of the patch-clamp technique exhibited evoked and spontaneous electrical activity.

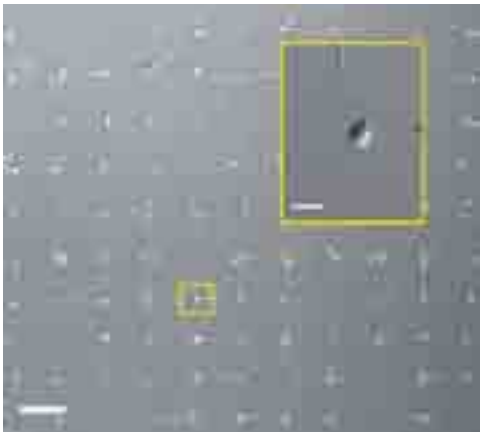

Fig.2. Optical image of cortical neuronal network glia-free cultured on chemically pre-patterned Si wafer designed as linear network. Inset shows a magnification of the boxed cell. Scales bar are 100 and 10 μm, respectively.

The procedure was also applied on vertical Si nanopillars, exhibiting tight contact not only with the cell body, but with the neurite projections as well. Cells survived for at least 10 days presenting intact neuronal physiology and mature synapses (Fig.3).

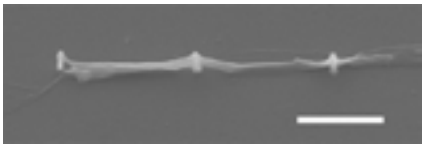

Fig.3. SEM image of a neurite growing along the pillars, tightly wrapping them. Scale bar is 2.5 μm.

Lastly, our procedure was implemented on SiNW field effect transistor (FET) devices in an attempt to improve the effective electrical coupling between the cell and the recording element, allowing us to obtain controlled neurons growth with individual cells crossing the NWs, and in the same time, connected to each other, forming a controlled network (Fig.4).

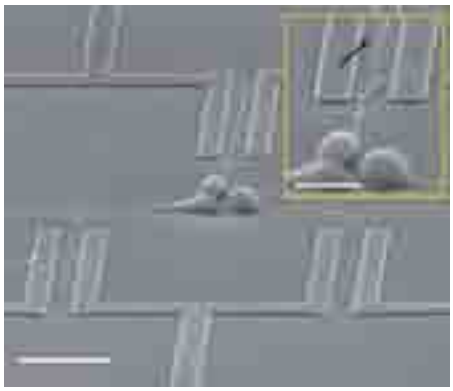

Fig.4. SEM image of controlled neurons growth, glia free, on SiNWs-FET according to chemical pattern. Inset shows zoom in on a neurite crossing a NW (indicated by arrow). Scale bars are 20 μm and 10 μm, respectively.

4 Conclusions

The primary purpose of the protocol described here is to produce highly ordered, mature and functional artificial mammalian neuronal networks that are maintained at low densities down to single cells. we have deliberately excluded glia cells from our system as glia would potentially compromise the stated goal to grow solely electrically-active neuronal networks. Hence, this protocol fulfills core requirement for variety of possible applications that will assist to provide new and important insights to the field of neurobiology.

Acknowledgements

This work was in part financially supported by the Legacy Fund-Israel Science Foundation (ISF) and the German-Israel Foundation (GIF).

References

[1] Stenger D. A., McKena T. M. (1994). Enabling technologies for cultured neural networks; *Academic press, San Diego*.

[2] Li N., Tourovskaia A., Folch A. (2003). Biology on a chip: microfabrication for studying the behavior of culture cells. *Critical Reviews in Biomedical Engineering, 31* 423.

[3] Chang J., Wheeler C. (2000). MEA recordings of patterned hippocampal neurons for weeks. *Biomedical Microdevices, 2*, 245.

[4] Brewer G. J., Cotman C. W. (1989) Survival and Growth of Hippocampal-Neurons in Defined Medium at Low-Density - Advantages of a Sandwich Culture Technique or Low Oxygen. *Brain Research, 494* (1), 65-74.

[5] Wyart, C., Ybert C., Bourdieu L., Herr C., Prinz C., Chatenay D. (2002). Constrained synaptic connectivity in functional mammalian neuronal networks grown on patterned surfaces. *Journal of Neuroscience Methods, 117* (2), 123-131.

Silicon-based microelectrode arrays for spike stimulation and signal recording of neurons assembles

Xiao-Ying Lü[1], Zhi-Gong Wang[2*], Tian-Ling Ren[3], Jie Zhang[1], Haixian Pan[1], Tao Fang[1], Shuai An[1], Feng Yuan[2], Xian Li[1], Chang-Jian Zhou[3]

1 State Key Laboratory of Bioelectronics, Southeast University, Nanjing 210096, China
2 Institute of RF- & OE-ICs, Southeast University, Nanjing 210096, China
3 Institute of Microelectronics, Tsinghua University, Beijing 100084, China
* Corresponding author. E-mail address: zgwang@seu.edu.cn

Abstract

Micro-electrode arrays (MEA) for spike stimulation and signal recording of *in vitro* cultured neuron assemble are presented. A series of PC12 cells culture experiments validates the effectiveness of the modification. Following experiments have been carried out already: 1) signal recording under stimulation of Ach (acetylcholine) of different concentrations, 2) signal recording under stimulation of different voltages, 3) signal recording under stimulation of combined Ach concentration and voltage. Both the thresholds of the Ach-concentration and the voltage have been obtained, and the relationship of two stimuli which act on cells simultaneous has been found. It is demonstrated that silicon-based MEAs are feasible for study of the performance of neuron assembles cultured *in vitro*.

1 Introduction

It is the most significant natural science topic to explore the structure of the nervous system and the mechanism of information processing and revealing the essence of higher nervous activity. Now it reaches an agreement that all advanced functions of the nervous systems are inseparable from the information transmission, processing and storage [1]. In this researching field microelectrode arrays (MEA) are powerful tools.

In this paper the relationships among the spike bursting of cell assemble and two kinds of stimuli, Ach (acetylcholine) and voltage are studies by using silicon-based MEAs. Both the thresholds of the Ach-concentration and the voltage have been obtained. It is demonstrated that silicon-based MEAs are feasible for study of the performance of neuron assembles cultured *in vitro*.

2 Materials and Methods

Silicon-based MEAs we developed [2] were used for cell culture and signal stimulating and detecting. The MEA is composed of 30 pairs of electrode sites and the site area is 15μm×25μm. For the experiment, we have used high differentiated PC12 cells from Rattus norvegicus adrenal medullary pheochromocytoma (a sympathetic nervous system tumors), which have neuronal traits.

The test instruments include: 1) MEA bracket (Germany Multichannel System); 2) Cerebus 64 channels neural signal detector (USA Cyberkinetics); 3) Master8 signal generator(Israel AMPI); 4) DSO6014A oscillograph (USA Agilent); 5) BX51 upright microscope (Japan Olympus), and so on.

According to the stimulating types, there are 3 kinds of experiments as follows:

2.1 Ach Stimulation

Beginning with 150-μl 5-μg/ml, more Ach (acetylcholine) was added slowly into the MEA cultivation cavity, using the concentration cumulative method. The response signals of PC12 cells under the stimulation at concentrations of 5, 7.5, 10, 20, 40 and 80 μg/ml were studied. For each Ach concentration the recording duration is about 50s.

2.2 Electrical Signal Stimulation

Two or more electrode sites among which a connection made of cell structures was formed were selected to study the signal generating and transferring characteristics of cells. One site along with a reference site was used as the port of the stimulation and other form the detecting ports, where a specially-designed large-area electrode site is used as reference (ground). The bipolar pulse as shown in Fig. 1 was designed as stimulating signal waveform. Its amplitude is adjustable.

Fig. 1 Waveform of the stimulating signal

2.3 Concurrent Stimulation of Ach and Electrical Signal

The spikes evoked by voltage pulse of different amplitudes were recorded at the Ach concentrations of 1, 2, 3, 4, 5, 6, 7 and 8 μg/ml. Thus, the threshold values of the voltage were obtained versus different concentration of Ach.

3 Experimental Result and Discussion

Observing the MEA under the microscope after 72 h PC12 cell culture, it was found that the PC12 cells grew on silicon based MEA surface normally, and formed the initial network as shown in Fig. 2. It can be seen that a recognizable cell network has been formed,

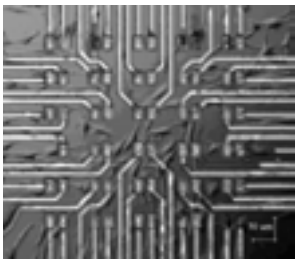

Fig. 2 Microphotograph of PC12 cells cultured on MEA for 72 h

Fig. 3 is a record of the response signal and the expansion of two peak potential waveforms under 20-μg/ml Ach stimulation.

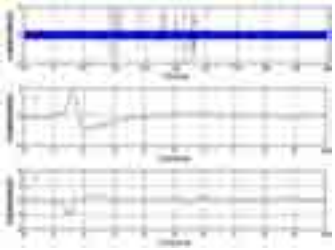

Fig. 3 The long term signal waveform (upper) and two expanded waveforms of typical spike recorded under 20-μg/ml Ach stimulation.

Fig. 4 shows the curve of the highest values of the spikes evoked in PC12 cells versus the Ach concentration. The threshold of the Ach concentration for the spontaneous burst of spikes is 7.5 μg/ml.

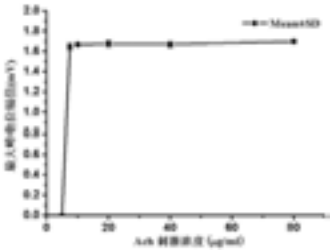

Fig. 4 The highest values of the spikes evoked in PC12 cells versus the Ach concentration

Fig. 5 shows the curve which describes the relationship of the signal amplitude of detected spikes versus the amplitude of the stimulating voltage pulse. It can be seen that the threshold of the stimulating voltage pulse for the evoked spikes is 35 mV.

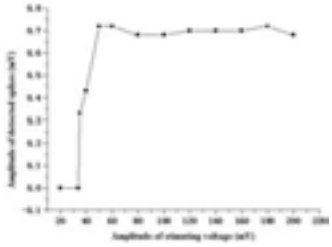

Fig. 5 The curve which describes the relationship of the signal amplitude of detected spikes versus the amplitude of the stimulating voltage pulse

Fig. 6 shows the threshold values of the stimulating voltage under different Ach concentrations. We can see that the threshold voltage of stimulating pulse reduces from 35 mV to 0 mV when the Ach concentration increases from 0 to 7.5 μg/ml. In the range of 1~6 μg/ml, the equivalent value of Ach concentration and stimulating voltage amplitude is about 4 μg/ml to 1 mV.

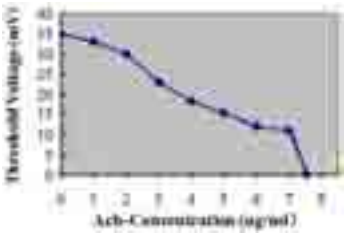

Fig. 6 Threshold curve of the stimulating voltage versus the Ach concentrations.

4 Conclusion

PC12 cells have been cultured on the silicon-based MEAs we realized. The threshold of the Ach concentration for spontaneous spike burst is about 7.5 μg/ml and that of the stimulating voltage pulse is 35 mV. Under the threshold, the equivalent value of Ach concentration and stimulating voltage amplitude is about 4 μg/ml to 1 mV

Acknowledgement

Thanks to the National Natural Science Foundation of China for the support under No. 61076118, 90307013 and 90707005, and the Open Subjects of Southeast University State Key Lab of Bioelectronics and Key Lab. of Child Development and Learning Science (Southeast University), Ministry of Education.

References

[1] Luo Xuegang, Neural Science foundation [M]. Central South University Press: 2002

[2] Haixian Pan, Xiaoying Lü, Zhigong Wang, et al. Silicon-based Microelectrode Arrays for Stimulation and Signal Recording of in Vitro Cultured Neurons. Sci China Ser F-Info Sci, 2011, 54(10): 2199-2208

Signal Analysis and Statistics

High performance spike sorting for high-density multielectrode arrays

Felix Franke[1,*], David Jäckel[1], Andreas Hierlemann[1]

1 ETH Zürich, Department of Biosystems Science and Engineering, 4058 Basel, Switzerland
* Corresponding author. E-mail address: felix.franke@bsse.ethz.ch

Abstract
The analysis of high-density multielectrode arrays requires powerful algorithms to make use of the large number of recording electrodes. Here we present the evaluation of a template matching technique that can be used to compute single neuronal spike trains from the recordings. The algorithm constructs one linear filter for every template and resolves overlapping, i.e. near synchronous, action potentials in the filter outputs. We show that if the templates are known, near error-free spike sorting is possible.

1 Introduction

High-density multielectrode arrays (HDMEAs) are a powerful tool to measure the activity of large numbers of neurons simultaneously, but they also pose a serious challenge to data analysis. How can we efficiently analyse the massive amount of redundant data? The dense spacing of the recording positions underneath a neuronal population yields highly redundant recordings of individual action potentials. Every neuron is recorded by many electrodes and every electrode records potentially the activity of many neurons. This makes it necessary to efficiently combine the information of many electrodes in order to reconstruct single neuronal activity, a process referred to as spike sorting.

MEA recordings impose special demands on the employed spike sorting algorithms: Firstly, simultaneous recordings from many neurons increase the chance to find synchronous firing of more than one neuron. This causes the recorded extracellular waveforms – the spikes – to overlap in time. Secondly, spatially redundant recordings of an action potential of the same neuron provide a distinct amplitude distribution of this neuronal signal across the different electrodes – its "footprint or template". In principle this will increase the signal-to-noise ratio in comparison to single channel recordings, but the information from different channels must be combined efficiently.

2 Methods

Since most available spike sorting algorithms are only capable of analyzing a single recording channel, or a very limited number of recording channels, they do not make use of the multi-channel information and are not applicable to HDMEA recordings. Here, we present the application of a previously developed Bayes optimal template matching (BOTM) procedure [1] for HDMEA recordings that can be efficiently implemented by a set of matched finite impulse response (FIR) filters and that optimally combines information from different channels. FIR filters are especially suited for this task, since they can be efficiently implemented in hardware.

3 Results

We evaluated the performance of the algorithm on simulated retinal ganglion cell recordings with 90 high-density electrodes using spike waveform templates, estimated from real recordings of mouse retinal preparations (Fig.1). Neurons were spaced on a grid at varying inter-neuron distance (between 20 and 40μm), and their position was randomly jittered. Therefore, some of the neurons were placed outside of the electrode array. Each simulation was 30 seconds long and contained, on average, between 32 to 111 neurons with firing rates between 5 and 50Hz. Fig. 2 shows the percentage of those neurons that could be sorted without a single spike sorting error. Neurons that were on the electrode array and were not perfectly sorted had an average error rate of 9.5%. One reason for the low error rates is the ability of the algorithm to successfully resolve overlapping spikes.

4 Conclusion

We showed that BOTM on HDMEA recordings provides, in principle, the possibility for error-free spike sorting of a large fraction of the neurons, if multichannel neuronal template waveforms are known. However, the question of how to find the templates in a reliable and automatic way has still to be answered.

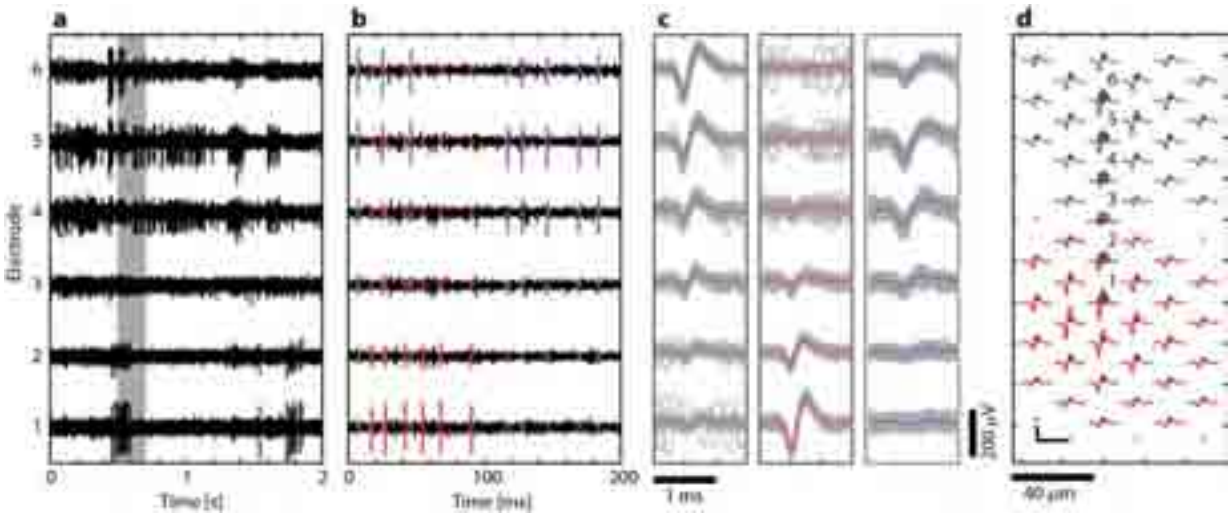

Fig. 1. Recorded data used to create the simulations. **(a)** 2 seconds of 6 selected electrodes (labelled in (d)); **(b)** close up of (a) with spikes from 3 chosen neurons indicated by colour; **(c)** cut and peak-aligned spikes of the 3 neurons; **(d)** footprints of 2 of the 3 neurons on the electrode array (grey dots).

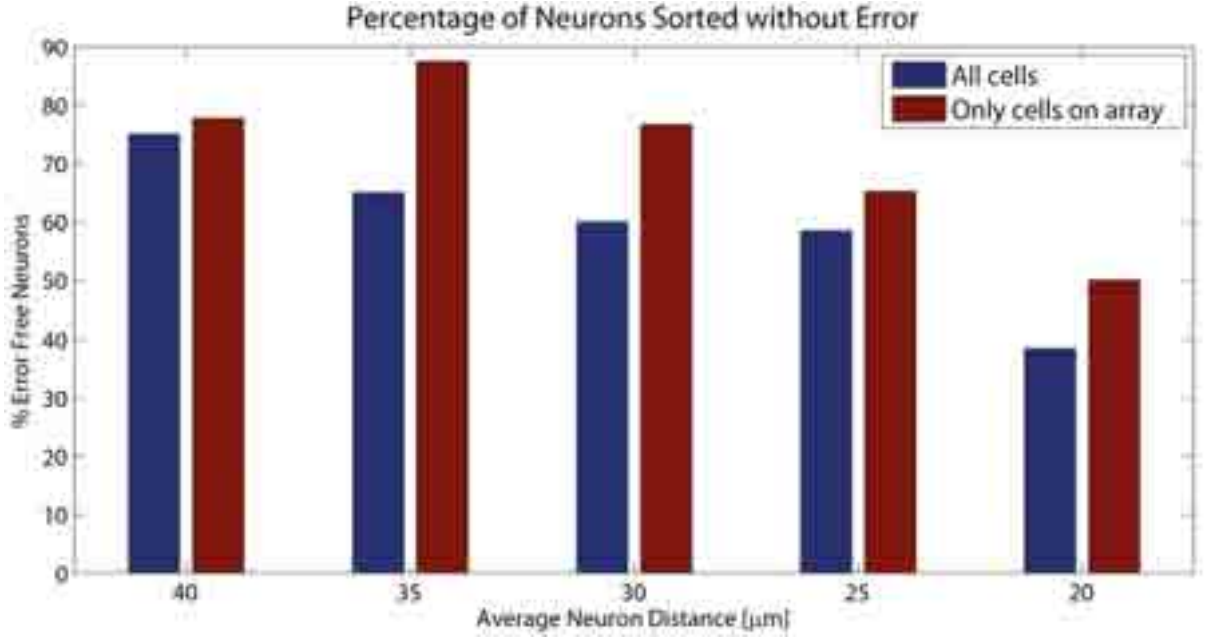

Fig. 2. Recorded data used to create the simulations. **(a)** 2 seconds of 6 selected electrodes (labelled in (d)); **(b)** close up of (a) with spikes from 3 chosen neurons indicated by colour; **(c)** cut and peak-aligned spikes of the 3 neurons; **(d)** footprints of 2 of the 3 neurons on the electrode array (grey dots).

Acknowledgement

We thank Michele Fiscella for the recordings of mouse retinal ganglion cells that were used to construct realistic templates for the simulations.

References

[1] F. Franke, *Real-Time Analysis of Extracellular Multielectrode Recordings*. Berlin: PhD Thesis, Technische Universität Berlin, 2011.

Biomedical-ASIC with reconfigurable data path for *in vivo* multi/micro-electrode recordings of bio-potentials

Janpeter Hoeffmann[1*], Jonas Pistor[1], Dagmar Peters-Drolshagen[1], Elena Tolstosheeva[2], Walter Lang[2] and Steffen Paul[1]

1 University of Bremen/Faculty 01/NW 1, Institute of Electrodynamics and Microelectronics, Bremen (Germany)
2 University of Bremen/Faculty 01/NW 1, Institute for Microsensors, -Actuators and -Systems, Bremen (Germany)
* Corresponding author. E-mail address: hoeffmann@me.uni-bremen.de

Abstract
This paper presents a Biomedical-ASIC for a fully implantable Neural Measurement System (NMS), able to record bio-potentials from the cortex of a subject in research applications and medical diagnostics. The ASIC (**A**pplication **S**pecific **I**ntegrated **C**ircuit) as a key component in the presented measurement system is able to truncate and preprocess neural raw data to be transmitted to an external base station. The ASIC itself can be considered as the consequent advancement of the FPGA-based NMS presented in [1]. The digital ASIC is capable of real time processing up to 128 channels with a maximum resolution of 16 Bit and a sample rate up to 10 kS/s/channel. The whole design covers a chip area of 1.8x1.8 mm^2 in a standard 150 nm CMOS process (LF150), consuming a core power of 900 µW@1.8 V at an operating frequency of 4 MHz.

1 Introduction

Neural engineering has brought up a variety of different measurement systems [2] to serve in the field of diagnostics and neural prostheses. Some of them use ASICs (e.g. [3]) which are mostly equipped with a fixed data path. This paper presents a digital Biomedical-ASIC with a reconfigurable data path for a fully implantable **N**eural **M**easurement **S**ystem (NMS). The ASIC is designed for the acquisition of biopotentials provided by up to eight *RHA2116* amplifier arrays [4], each containing 16 low-noise amplifiers for 16 input channels and an integrated 16-bit SAR ADC based on the charge redistribution principle.

Fig. 1 shows a block diagram of the overall NMS. After the measurement data is collected using a novel flex-rigid ECoG (Electrocorticogram) array with 128 electrodes [5], neural data is amplified, filtered and digitized by the eight amplifier arrays. Subsequently, data runs in the reconfigurable digital ASIC where the high amount of incoming raw data (~20 Mbit/s) is reduced in a user defined way to fit the maximum transmission rate of 4 Mbit/s or less, according to the connected output device (e.g. a wireless transceiver as depicted in Fig. 1). Regardless of configuration one receives a serial close-packed bit stream, containing only relevant (user-intended) data at the output of the ASIC. The configuration is obtained using the same interface and allows runtime reconfiguration.

Due to the reconfigurable data path, one can stream out *Local Field Potentials* (LFPs), as well as *Action Potentials* (APs) or *Spikes*, depending on the type of measurement task one would like to perform. The ability of measuring different signal types comes along with the highly flexible way of data handling in the design. In a previous work [1] the system was implemented on a FPGA-based prototype for pre-silicon validation and initial measurements.

The system concept in its final realization is shown in Fig. 1. It is planned to power the NMS wirelessly over an inductive link through the skin and skull. All electrical devices will be assembled on a flexible substrate in order to align them to the surface of the subjects brain. The final NMS will be programmable through the wirelessly coupled Base Station.

This work concentrates on the signal acquisition of *Local Field Potentials* (LFPs) from the Multielectrode ECoG Array over the amplifier stage and propagation in the reconfigurable Biomedical-ASIC (Fig. 1).

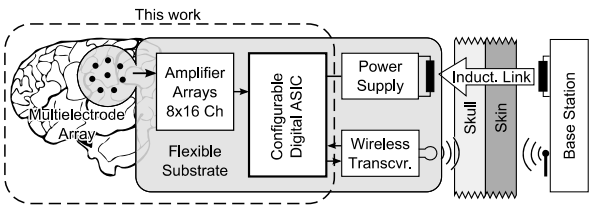

Fig. 1. Block diagram of the Neural Measurement System (NMS).

2 Architecture of the Digital ASIC

The architecture of the digital ASIC is strictly serial and works with only one system clock of 4 MHz.

The serial approach was chosen for two different reasons:

1. The input data (from each of the eight amplifier arrays) and the output data of the ASIC as well are serial.

2. The output data rate of the system will be limited by the Zarlink transceiver IC to approximately 500 kbit/s [6], which is much less than the 20.5 Mbit/s input rate of the 128 measurement channels. In a serial data stream, the resolution can efficiently be reduced from 16 bits to 1 bit in bitwise steps. This allows the user to have a fine adjustment of the data rate, together with the number of transmitted channels and the sample rate. As long as the configuration makes use of the maximum average data rate of 4 Mbit/s, especially the reduction of the sample rate (combined with high resolution and channel count) results in high peak data rates. Because the output rate is limited to 4 Mbit/s, each input channel has its own 16 bit buffer to store the data between two consecutive samples. The 4 Mbit/s output rate fits the maximum input rate of the Zarlink Transceiver, which will be attached in the next step. Since there were no SRAM modules available in the LF150 process, a lot of chip area is occupied by registers to provide the necessary buffer memory (compare Fig. 4).

Fig. 2 shows a block diagram of the architecture.

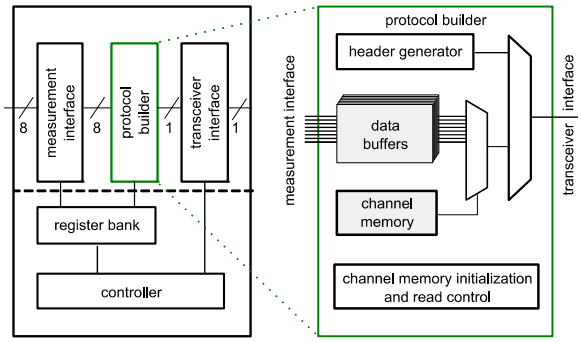

Fig. 2. Architecture of the digital ASIC.

The measurement data arrives on 8 serial lines, each carrying 16 channels with a resolution of 16 bits and a sample rate of 10 kS/s/channel. The measurement interface reduces the data rate in a flexible combination of sample rate, resolution and number of active channels, according to the settings of the operator.

The protocol builder buffers the filtered data of the last sample point, adds a header with timestamp and configuration data and combines the 8 serial lines to one single close-packed serial data line containing all selected channels in the desired resolution and sample rate.

This truncated data is fed into the transceivers interface, which makes an adoption to the transceiver or any other interface to a certain base station. It also manages the transfer of incoming commands to the controller, which basically sets the system to the configuration given by the operator (see Section 2.1).

The modularity of this architecture allows exchanging the analog data acquisition ICs as well as the transceiver, or it allows varying the amount of measurement ICs and transceiver ICs.

2.1 Commands

The user may influence the NMS with the following set of commands:

- *enable/disable*: Activation of the data transfer.
- *samplerate*: Adjustable between 39 S/s/channel and 10 kS/s/channel for the digital sample rate.
- *resolution*: Selectable between 1 and 16 Bits of resolution for all active measurement channels.
- *channelmask*: Masks out a user defined subset of all available channels to be transmitted.
- *filter*: controls four output pins of the digital ASIC, which could be used to setup a analog bandpass filter for the amplifiers (0.02 Hz – 1 kHz for the lower bandwidth, 10 Hz – 20 kHz for the upper bandwidth).

2.2 Data Frames

For the command inputs, the controller interprets byte sequences which encode the commands and parameters. The byte sequences start with a unique pattern and also contains a device specific ID in case the transceiver does not manage the channel access in an environment with multiple independent measurement units.

The measurement data is combined to a packet for each single sample point in time. The packet consists of a header and the measurement data. The header contains 4 bits for the type of packet, 8 bits for the device ID, 128 bits for the identification of the appended measurement channels, 4 bits for the filter settings, a 16 bits time stamp for synchronicity, 8 bits for the sample rate and 4 bits for the resolution. The segmentation of measurement data depends on the resolution and number of activated channels and has a maximum length of 2048 bits.

3 Measurement Setup

In this application the sensor frontend of the NMS is a novel microelectrode ECoG array with 128 gold electrodes. It is composed of a flexible recording area, a flexible flat ribbon cable and a rigid soldering field for the *OMNETICS* connectors. The free-standing polyimide membrane is depicted in Fig. 3. The array is flanked by two land patterns from two additional identical ECoG arrays on the same wafer. Each land pattern contains pads for four *OMNETICS* SMD-connectors with 32 pins each.

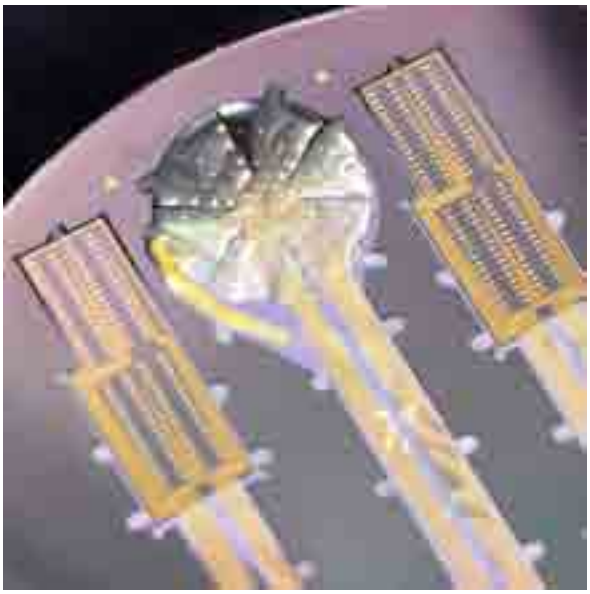

Fig. 3. Flexible ECoG array with 128 gold electrodes (300 nm thick), sandwiched between two 5 µm polyimide thin-films.

The membrane is attached to its carrier substrate only by several polyimide straps. By cutting the straps the array can be released from its substrate. This construction allows a high level of control during soldering, characterization of the electrodes and during soft release of the electrode array off its carrier right before chronic implantation on a subject's cortex.

The electrodes of the array are situated on the edges of concentric hexagons and have three distinct diameters – 100, 300 and 500 µm [5]. This spatial arrangement allows grouping of equidistant electrodes for spatial spectrum analysis. The measuring array is a hexagon with a side length of 7.2 mm.

The ECoG array is designed for chronic implantation on the primary visual cortex of a Rhesus monkey. The hexagonal outline ensures symmetry and conforms to the intended region of implantation. One array is already implanted and allows *in Vivo* Multi/Micro-Electrode recordings of biopotentials.

A chip photo of the digital biomedical-ASIC with a floor plan overlay is shown in Fig. 4. The core area has a size of 1 mm² with a utilization of 34%. The power consumption of the core is 900µW.

The floor plan shows a large area for the 2048 bit *data buffer*. Since no SRAM was available in the standard design kit, the memory was built from ca. 7000 standard cells. The 384 bit *channel memory* which controls the sequence of the activated channels is much smaller and uses ca. 900 gates. The remaining 1200 gates in the *Ctrl* area represent the actual functionality of the design.

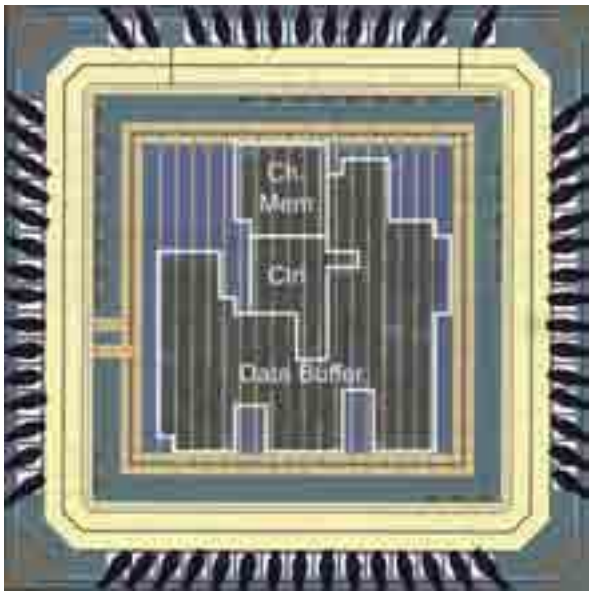

Fig. 4. Photo of bonded digital ASIC

The ASIC incorporates 58 pads from which 27 pads are output pads and 31 input pads. On the upper edge of the padring one can see two spacers, separating 10 pads from the rest of the chip. From these pads there are 8 output pads and one dedicated pair of supply and GND for the stimulation circuit, which is currently under development.

In Fig. 5 the *In Vitro* test setup is illustrated. In the lower left there is a basin filled with saline solution in which the ECoG array is placed. Over an *OMNETICS* cable the array is connected to our amplifier test board (lower center) carrying one *RHA2216*. From this board data runs into the ASIC test board shown in the upper right. The whole system is battery-powered in order to reduce noise coupling from any external power source. From the ASIC test board data is fed over a VHDCI connector into a *PXI*-measurement system from *National Instruments* with an integrated *NI-FlexRio-FPGA* module. The *PXI*-system runs a *LabView* program which captures the measurement data and performes a visualization of the electrode signals.

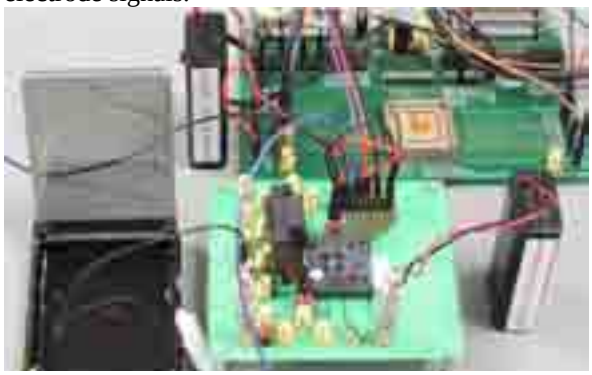

Fig. 5. *In Vitro* test setup with the ECoG array placed in saline solution (lower left). In the lower center the test board for the amplifier array is depicted. The upper right shows the ASIC test board.

4 Results

First measurements using an arbitrary waveform generator as electrode input served as successful functional test for the system, consisting of the amplifier ICs, filters, ECoG-Array, digital ASIC and software.

For the examination of the system in a realistic measurement environment we used the test setup shown in Fig. 5. Measurements were conducted using a Petri dish with a size similar to the brain of the monkey filled with saline solution in order to rebuild the impedance parameters of a real monkey in a most realistic way. Additional shielding is used to reduce environmental noise. For the test, the analog filter was chosen to 1Hz for the high pass and 1 kHz for the low pass and no stimuli were applied to measure the system noise as depicted in Fig. 6. The spectrum of the noise shows a lot of energy above 100 Hz and peaks at multiples of 100 Hz which could be filtered, so that the resulting noise level stays in the range of approximately 20 µV. According to [2] the amplitude of LFPs lies in the range between 0.5-5 mVpp, so the noise can be considered as not severe enough to influence the upcoming *in Vivo* measurements in a sustainable way. In addition to that, one expects that the remaining environmental noise is further reduced at the time the NMS is really implanted on to the subject's cortex.

Fig. 6. Measurement of the noise floor from the NMS [7] over a period of 1 second.

5 Conclusion and Outlook

This work presents a Biomedical-ASIC as a key component of a NMS. Due to the reconfigurable data path incorporated in the ASIC, it can be used for many applications in brain research, medical diagnostics or neural prostheses. Based on the high degree of flexibility, one can easily shrink or expand the systems performance in order to fit the functional constraints defined by the application. Depending on the sensor frontend one is able to measure LFPs as well as APs.

In the current application the presented new developed flex-rigid soft release ECoG array serves as sensor frontend for 128 channels providing LFPs. This array has already been successfully implanted onto the cortex of a primate. Measurement results are presented using the electrode array and placing it into saline solution as a model for the brain of the monkey and measuring the noise floor. It is expected that the noise further decreases, once that the NMS (as shown in Fig. 1) is connected wirelessly in terms of energy- and data transfer due to the decoupling of the connected measurement system.

At the moment there is a new version of the presented Biomedical-ASIC in fabrication. It incorporates a transceiver interface for the *ZL70102* [6] and a power gating feature for the 8 amplifier arrays. So if the transmitted power is not high enough or a group of 16 channels belonging to the same measurement frontend are out of interest, the measurement ICs could be switched off in a controlled manner. Thus, there is an increase in system stability of the overall NMS under critical conditions in terms of power supply, as well as a low-power operation to reduce heating of the surrounding tissue.

Acknowledgement

The authors would like to thank the German Federal Ministry of Education and Research (*BMBF*) for subsidizing this work within the *KALOMED*-project.

References

[1] J. Pistor, J. Hoeffmann, D. Peters-Drolshagen, und S. Paul, „A programmable neural measurement system for spikes and local field potentials“, in 2011 Symposium on Design, Test, Integration and Packaging of MEMS/MOEMS (DTIP), 2011, S. 200–205.

[2] B. Gosselin, „Recent Advances in Neural Recording Microsystems“, Sensors, Bd. 11, Nr. 5, S. 4572–4597, Apr. 2011.

[3] H. Gao, R. M. Walker, P. Nuyujukian, K. A. A. Makinwa, K. V. Shenoy, B. Murmann, und T. H. Meng, „HermesE: A 96-Channel Full Data Rate Direct Neural Interface in 0.13 µm CMOS“, IEEE Journal of Solid-State Circuits, Bd. PP, Nr. 99, S. 1–13, 2012.

[4] Intan Technologies, „RHA2116 - Fully Integrated 16-Channel Biopotential Amplifier Array“. 19-Mai-2010.

[5] E. Tolstosheeva, V. Gordillo-Gonzalez, T. Hertzberg, L. Kempen, I. Michels, A. Kreiter, und W. Lang, „A novel flex-rigid and soft-release ECoG array“, in 2011 Annual International Conference of the IEEE Engineering in Medicine and Biology Society,EMBC, 2011, S. 2973–2976.

[6] Zarlink Semiconductor (now Microsemi), “ZL70102 –Third Generation Medical Implantable RF Transceiver”. Chip Revision: 04, Jan. 2011.

[7] Generated with the assistance of LabView 2010 from National Instruments©.

Computational methods for large-scale MEA studies of functional connectivity in brain slice preparations in-vitro

Przemysław Rydygier[1*], Shinya Ito[2,3], Fang-Chin Yeh[2,3], Paweł Hottowy[1], John M. Beggs[3], Władysław Dąbrowski[1], Deborah E. Gunning[4], Alexander Sher[2], Alan M. Litke[2]

1 Faculty of Physics and Applied Computer Science, AGH University of Science and Technology, Kraków, Poland
2 Santa Cruz Institute for Particle Physics, University of California, Santa Cruz, USA
3 Department of Physics, Indiana University, Bloomington, Indiana, USA
4 Institute of Photonics, University of Strathclyde, Glasgow, Scotland, UK
* Corresponding author. E-mail address: rydygier@agh.edu.pl

Abstract
In this paper we present computational methods for determining functional connectivity in brain slice preparations in-vitro using a 512-electrode MEA recording system [1]. Our methods are based on Cross-Correlation analysis of neuron spiking and allow us to obtain information about excitatory and inhibitory neural connections and their statistical significance. A widely used spike jittering method [2] has been substituted with digital filtering, drastically reducing the computational power requirements.

1 Introduction

Large-scale multielectrode array (MEA) recording systems can simultaneously record the spiking activity of hundreds of neurons in brain slice preparations in vitro [3]. This technological advance opens up the possibility of studying the functional connectivity of a neural system at fine spatial and temporal resolution, at hundreds of recording sites, over a large area. Here we report on preliminary measurement of functional connections in the hippocampal region of an organotypic cultured wildtype mouse brain slice preparation.

2 Materials and methods

Organotypic cultures were prepared from wildtype mouse pup (of strain Black-6) brain slices, 400 µm thick, at postnatal day 6-7, incubated for 2-3 weeks. The cultures were then placed on a 512-electrode MEA, arranged in a 32×16 rectangular configuration, with 5 µm diameter electrodes, 60 µm interelectrode separation, and an active area of 1.9×0.9 mm^2. We aimed to place the tissue so that the hippocampal CA1 region covers the active recording area (Fig. 1).

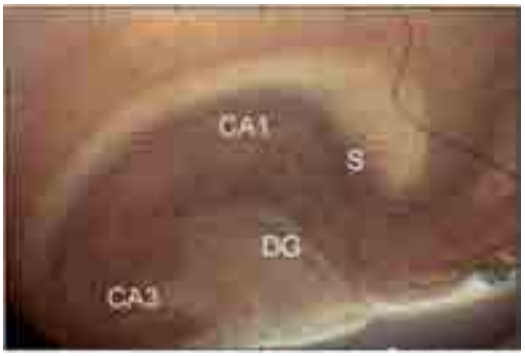

Fig. 1 Day In Vitro 1 (DIV1) photo aligned on photo of the tissue on the array immediately after recording to show the hippocampal region on the array; DG-dentate gyrus, S-subiculum

The spiking waveforms from the cultures were recorded on each of the 512 electrodes at a sampling rate of 20 kHz. Spike sorting was carried out as described in [4]. Typically, 100-200 neurons are identified in a single preparation.

3 Statistics

To determine the functional connectivity for the neural network, we calculate the cross-correlogram (CC) for every neuron pair. Three example CCs are shown in Fig. 2. Fig. 2 A, B and C show, respectively, examples of excitatory, inhibitory and combined excitatory/inhibitory bi-neuron connections.

To extract statistically significant functional connections, we start with the original CC (black lines in Fig. 2), convoluted with a low-pass box filter of 20 ms width to obtain the filtered CC (red lines with diamonds in Fig. 2). The background noise level (SD) is then calculated as the standard deviation of the mean of the sideband regions of the CC for lag times of -80 to -10 ms and +10 to +80 ms. Next the maximum and minimum local limits (green lines in Fig. 2) are calculated as the filtered CC offset by ±3×SD. Finally, to be consistent with the procedure presented in [2], the global limits are calculated as max/min values of the filtered CC ±0.99×3×SD over a lag time range from -30ms to +30ms (blue dashed lines in Fig. 2). If the original CC lies above (below) the maximum (minimum) global limit for at least 1 ms it is classified as an excitatory (inhibitory) connection. CCs that pass both

the excitatory and inhibitory criteria are classified as combined excitatory/inhibitory connections. This method of extracting significant connections is much less demanding computationally than the widely-used method based on spike jittering [2]. A mathematical proof of the equivalence of the low-pass box filter and time jittering methods can be found in [5]. This is of particular importance when dealing with the thousands of CCs derived from preparations with hundreds of identified neurons.

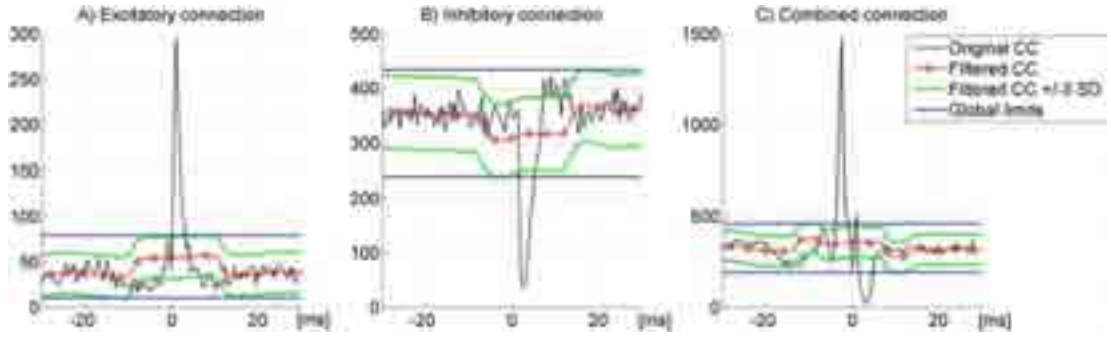

Fig. 2 Examples of excitatory, inhibitory, and combined excitatory-inhibitory CCs. The vertical axis shows the number of entries per 0.5ms. The horizontal axis specifies the time interval between a spike from one neuron and a spike from the second neuron.

4 Results

We present pilot results of functional connectivity maps obtained as described above. Fig. 3 shows the connectivity maps for the excitatory and inhibitory connections, in a preparation with 79 identified neurons. For the results presented in Fig. 3, with 6162 potential bi-neuron connections (using a 2.8GHz CPU, 3GB RAM computer), the extraction of statistically significant connections took 112 hours with the time jittering method but only 86 minutes with the filter method, which gave reduction by a factor of 78.

5 Summary

We have developed methods of finding functional connections in mouse brain organotypic cultures using a 512-electrode MEA recording system and cross-correlation analysis. Our method of assessing statistically significant connections requires approximately 1.3% of the computational time to obtain the same results compared to the spike jittering method.

Acknowledgements

This work was supported by NSF CRCNS grants IIS-0904413 (AML) and IIS-0904912 (JMB), NSF PoLS grant 1058291 (JMB), Polish Ministry of Science and Higher Education grants for scientific research in the years 2009-2012 (WD), a Burroughs Welcome Fund Career Award at the Scientific Interface (AS), and a scholarship from the Polish-American Fulbright Commission (PR). The authors thank Keith Mathieson and Sergei Kachiguine for technical contributions, and PR thanks the UC, Santa Cruz for hosting him.

References

[1] Hottowy P., et al. (2010): 512-electrode MEA System for Spatio-Temporal Distributed Stimulation and Recording of Neural Activity. *Proc. of the 7th Int.MEA Meeting*, 327-330

[2] Fujisawa S., et al. (2008): Behavior-dependent short-term assembly dynamics in the medial prefrontal cortex. *Nature Neuroscience*, Vol.11, No. 7, 823-833

[3] Tang A., et al. (2008): A maximum entropy model applied to spatial and temporal correlations from cortical networks in vitro. *J. Neurosci.*, 28, 505-518

[4] Litke A.M., et al. (2004): What does the eye tell the brain ? Development of a system for the large scale recording of retinal output activity. *IEEE Trans. Nucl. Sci.*, 51, 1434-1440

[5] Rompelman O., Ros H.H. (1986): Coherent Averaging Technique: A Tutorial Review. Part 2. *Journal of Biomedical Engineering*, 8, 30-35.

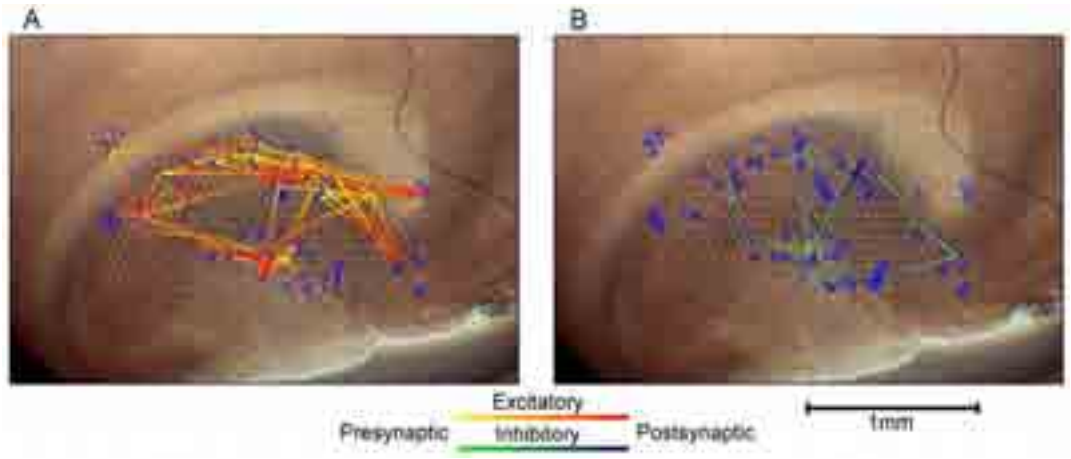

Fig. 3 Connectivity map: A) single excitatory connections, B) single inhibitory connections. Blue triangles indicate neuron positions.

Detection of multiple spike transmission pathways in neuronal networks based on multichannel recordings

Prokin Ilya[1*], Gladkov Arsenii[1], Mukhina Irina[1,3], Kazantsev Victor[1,2]

1 Lobachevsky State University of Nizhny Novgorod, Nizhny Novgorod, Russia
2 Institute of Applied Physics of RAS, Nizhny Novgorod, Russia
3 Nizhny Novgorod State Medical Academy, Nizhny Novgorod, Russia

* Corresponding author. E-mail address: isprokin@gmail.com

Abstract
The problem of classification of neuronal network bursting activity monitored by multielectrode arrays is one of important computational tasks in the studies of neuronal culture dynamics. We propose a novel method to analyze spiking patterns capable to identify multiple statistically significant functional connections between cells/electrodes characterized by different spike transmission timings.

1 Method

1.1 Similarity measure

The detection method is based on the estimate of functional connectivity [1] between pairs of channel in the multichannel binary data of spikes detected. We introduce a new similarity measure [2] in the following way. Let

$$K_j^{[t_1,t_2]} = \sum_{t=t_1}^{t_2} X_j(t)$$

be the number of spikes at j-th channel recorded within $[t_1,t_2]$ time interval, $X_j(t)$ is the discrete time binary vector representing spike train in j-th channel. Next we define spike transmission operator as

$$X(t_1)\,\&\,Y(t_2) = \max_{t\in[t_2-\delta,t_2+\delta]}\left(X(t_1)Y(t)\exp(-\frac{2|t-t_2|}{\delta})\right)$$

where $\delta << (t_2-t_1)$ is a parameter controlling the width of coincidence detection window. Then, we define the similarity measure:

$$\sigma_{ij}(\tau) = \sqrt{\sigma_{ij}^{-}(\tau)\sigma_{ij}^{+}(\tau)},$$

$$\sigma_{ij}^{-}(\tau) = \frac{1}{\mathrm{K}_i^{[\tau+\delta,T]}}\sum_{t=\tau+\delta}^{T} X_i(t)\,\&\,X_j(t-\tau),$$

$$\sigma_{ij}^{+}(\tau) = \frac{1}{\mathrm{K}_j^{[0,T-\tau-\delta]}}\sum_{t=0}^{T-\tau-\delta} X_j(t)\,\&\,X_i(t+\tau).$$

$\sigma_{ij}(\tau)$ estimates the fraction of spikes successfully transmitted from channel j to channel i with the time lag τ. Note that $\sigma_{ij}(\tau)$ accounts for the geometric mean between forward and backward spike transmission factors.

1.2 Significance testing

For each peaks $\sigma_{ij}(\tau)$ we perform significance test using surrogate data [3]. The surrogates are created from the original data by random shifts of whole spike trains, hence, destroying temporal cross-dependences but keeping the temporal statistics. Next we build surrogate sigma distribution $P(\sigma)$ for each peak. The peak is considered as significant if the probability to get sigma value greater than the peak value by chance is lower than a significance level.

In the result we obtain collections of significant peaks σ_{ij} and corresponding lags τ_{ij}. Each significant peak associated with connection $j\rightarrow i$ and σ_{ij} is considered as a spike transmission probability estimator and τ_{ij} is considered as time delay estimator.

2 Results

2.1 Applying method to modelled data

To verify the method the similarity test was applied first to model data generated by random network of integrate-and-fire neurons with plastic connections [4]. It was found that the method can identify significant direct and indirect functional connections between net elements.

2.2 Applying method to experimental data

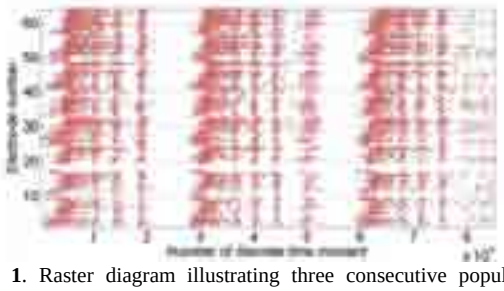

Fig. 1. Raster diagram illustrating three consecutive population burst discharges.

Next we applied the method to experimental data generated by neuronal network in primary hippocampal cultures and recorded by multi-electrode array sensor (MED64, Alpha MED Sciences and USB-MEA120, MultiChannel Systems). We analyzed raster diagrams of binary events corresponding to spikes detected by a threshold algorithm. The activity displays a sequence of population burst discharges (Fig.1).

Figure 2 shows corresponding multigraph (isolated nodes excluded) with edges weighted by estimated transmission delay in milliseconds.

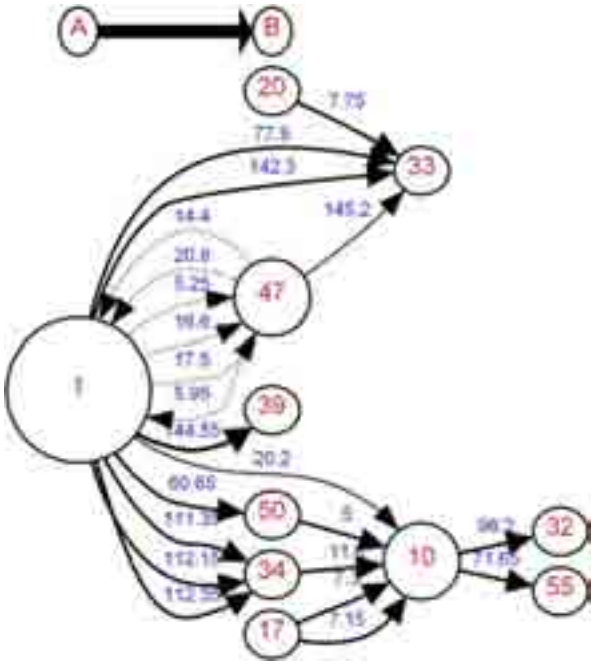

Fig. 2. Multigraph corresponding to population bursts (Fig. 1). The width of *A*→*B* edge corresponds to maximum sigma-value which is 1.

The size of node is proportional to node degree. The multigraph apparently detects network hubs (nodes with higher degrees) with functional connection pathways. Note, that there may be multiple spike transmission paths between particular nodes illustrating the presence of different direct/indirect connectivity modes. Next, the graph can be characterized the summary input/output connections per electrode. One can note “sinks” (electrodes 10, 33, 34 and 47) and “sources” (electrode 1 and 47) in the spike transmission.

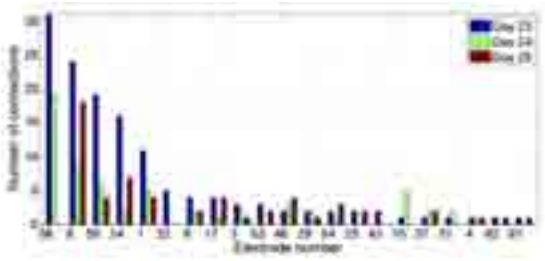

Fig. 3. Connectivity diagram illustrating changes in connectivity during three days.

Figure 3 shows changes in the node degrees in development during three days. Typically, active electrodes preserve higher number of connections indicating that the signalling pathways evolve in some continuous manner. Thus, the culture networks demonstrate a stable (robust) functional organization at certain stage of development. Connectivity changes detected by the graph illustrate general trends in development of network architecture (see, for example, electrodes 55 and 1 reducing the number of connections).

3 Conclusion

In conclusion we summarize key points of the method. Its key advantage that it is applicable to non-stationary multichannel data typically recorded by MEA sensors from neuronal culture networks generating population bursts. The method estimates multiple connections corresponding to many different signal transmission pathways activated in the network within particular burst or sequence of bursts. Each connection is supplied with direction (incoming or outgoing) and values of time delay corresponding to effective time of spike transmission from one electrode to the other.

Finally, the method provides directed graph of signal transmission pathways. Characteristics of the graph (e.g. number of active nodes, number of input/output connections, source/sink distributions) may be used to identify functional states of the culture network in spontaneous development and its changes after stimulation.

Acknowledgement

This work is supported by the Russian Foundation for Basic Research (Grant No 11-04-12144), by Russian Federal Program (No 16.512.11.2136), by MCB RAS Program and by the Russian President grant MD-5096.2011.2.

References

[1] le Feber, J., Rutten, W. L. C., Stegenga, J., Wolters, P. S., Ramakers, G. J. a, & van Pelt, J. (2007). Conditional firing probabilities in cultured neuronal networks: a stable underlying structure in widely varying spontaneous activity patterns. *Journal of neural engineering*, 4(2), 54-67. doi:10.1088/1741-2560/4/2/006

[2] Chao, A., Chazdon, R. L., Colwell, R. K., & Shen, T.-J. (2006). Abundance-based similarity indices and their estimation when there are unseen species in samples. *Biometrics*, 62(2), 361-71. doi:10.1111/j.1541-0420.2005.00489.x

[3] Pipa, G., Wheeler, D. W., Singer, W., & Nikolić, D. (2008). NeuroXidence : reliable and efficient analysis of an excess or deficiency of joint-spike events. *Journal of Computational Neuroscience*, 64-88. doi:10.1007/s10827-007-0065-3

[4] Prokin, I. S., & Kazantsev, V. B. (2012). Analysis of pulsed-signal transmission in a system of interacting neural oscillators with frequency-dependent connections. *Radiophysics and Quantum Electronics*, 54(11), 763-772. doi:10.1007/s11141-012-9338-4

Reconstructing current sources from multielectrode potential recordings using kernel methods (kCSD)

Wójcik Daniel K[1*], Potworowski Jan[1], Jakuczun Wit[2], Łęski Szymon[1]

1 Nencki Institute of Experimental Biology, Polish Academy of Sciences
2 WLOG Solutions, Warsaw, 02-389, Poland
* Corresponding author. E-mail address: d.wojcik@nencki.gov.pl

Abstract
Long range of electric potential brings about significant correlations between simultaneous recordings from contacts separated millimetres away in the tissue. To maximize relevant information from data it is useful to reconstruct the volume density of net transmembrane currents, called the Current Source Density (CSD), which generates the recorded potentials. We present here Kernel Current Source Density method (kCSD) as a convenient way to estimate sources from arbitrary distribution of contacts in different dimensions, and robust against noise.

1 Introduction

Long range of electric potential brings about significant correlations between simultaneous recordings from contacts separated millimetres away in the tissue. To maximize relevant information from data it is useful to reconstruct the volume density of net transmembrane currents, called the Current Source Density (CSD), which generates the recorded potentials. Since the CSD in homogeneous and uniform tissue is given by the Laplacian of the potential, numerical second derivative of the recordings from regularly spaced microelectrodes has been commonly used as an estimate of CSD at least since Nicholson and Freeman [1]. Recently, a number of deficiencies of this approach has been identified and inverse CSD and kernel CSD methods were proposed to circumvent them [2,3,4,5]. We propose here Kernel Current Source Density method (kCSD) [5] as a convenient way to estimate sources from arbitrary distribution of contacts in different dimensions, and robust against noise.

2 Kernel Current Source Density method

The idea behind kCSD is to first estimate the potential using kernel estimation, then replace the kernels in the potential space by corresponding kernels in the space of sources. One can define the kernel explicitly (direct kCSD) or in terms of the basis elements of a finite dimensional space (kCSD). While the first approach conceptually seems simpler, our tests so far indicate superiority of the approach described by Potworowski et al. [5].

We look for sources in the space span by densely distributed elementary sources, each representing small neuron populations. The potential generated by each source is calculated by forward modeling in a way dependent on dimensionality of the setup and the necessary assumptions about the symmetry. For example, for 2D grids we assume the properties of the sources in the directions normal to the plane of the grid (e.g. step or Gaussian profile) [3]. If the anatomy and physiology of the studied systems are better known, their properties can be included in the kCSD method by adapting the basis, improving the results further. To avoid over-fitting to noise we use ridge-regression and cross-validation is used to adaptively tune the parameters of the method for optimal results.

3 Results

We show that kCSD is a general non-parametric framework for CSD estimation including all the previous variants of iCSD methods as special cases. The method is robust against noise and adaptive. A MATLAB implementation of the method for reconstruction of 1D and 2D problems is available online at http://software.incf.org/software/kcsd. 3D code is available per request.

4 Conclusion/Summary

We propose kernel Current Source Density method as a convenient way to reconstruct current sources from arbitrary distribution of contacts in different dimensions in the presence of noise.

Acknowledgement

Supported by an infrastructural grant from the Polish Ministry of Regional Development, POIG.02.03.00-00-003/09.

References

[1] Nicholson C., Freeman J. A. (1975). Theory of current source-density analysis and determination of conductivity tensor for anuran cerebellum. *J. Neurophysiol.*, 38(2), 356–368.

[2] Pettersen K.H., Devor A., Ulbert I., Dale A.M., Einevoll G.T. (2006). Current-source density estimation based on inversion of electrostatic forward solution: Effects of finite extent of neuronal activity and conductivity discontinuities. *J.Neurosci. Methods*, 154(1–2), 116–133.

[3] Łęski S., Pettersen K.H., Tunstall B., Einevoll G., Gigg J., Wójcik D.K. (2011). Inverse current source density method in two dimensions: Inferring neural activation from multielectrode recordings. *Neuroinformatics* 9 (2011) 401-425

[4] Łęski S, Wójcik D.K., Tereszczuk J, Świejkowski D.A., Kublik E, Wróbel A (2007). Inverse current-source density method in 3D: Reconstruction fidelity, boundary effects, and influence of distant sources. *Neuroinformatics*, 5(4), 207–222.

[5] Potworowski J., Jakuczun W., Łęski S., Wójcik D.K. (2012) Kernel Current Source Density Method. Neural Computation 24, 541-575

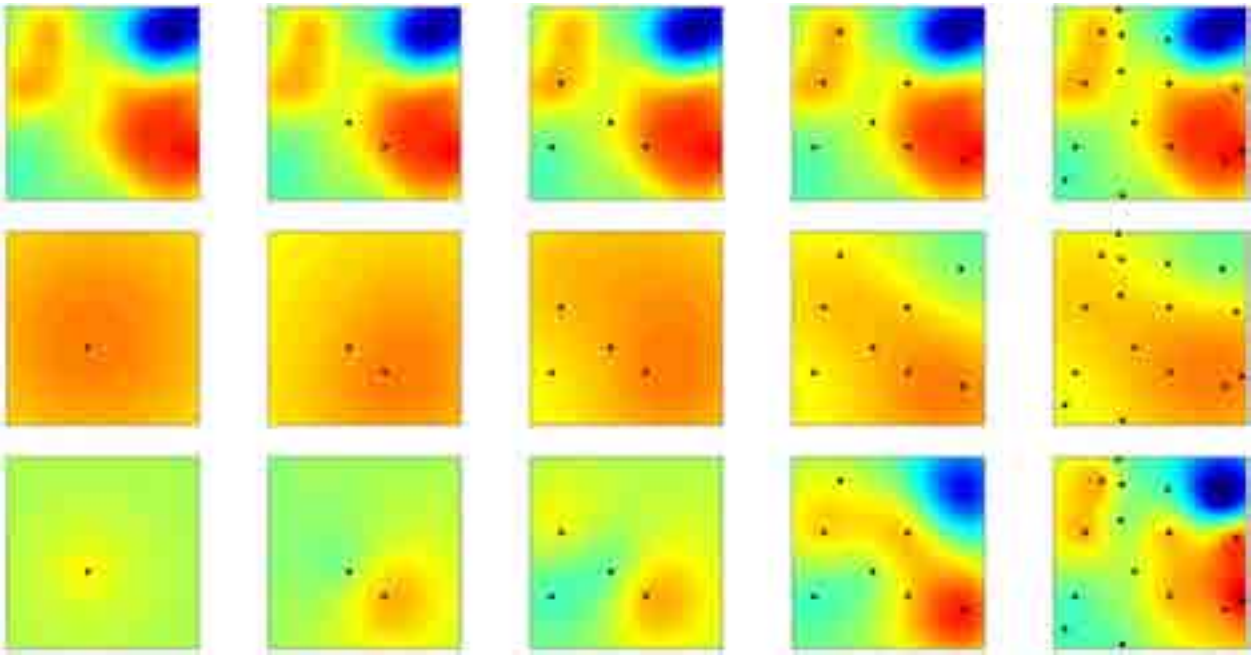

Fig. 1 Reconstruction of current sources from randomly distributed contacts. The number of contacts is A) 1, B) 2, C) 4, D) 8 E) 16. Top panel – test sources. Middle panel – potential reconstructed from measurements. Bottom panel – CSD reconstructed from measurements. Black dots show localization of contacts. Observe a) significant differences between reconstructed potential and the sources, b) fast improvement of reconstruction quality with the increasing number of the electrodes.

Photoelectric effect in multielectrode arrays

Bröking, Kai[1,4,5,*], Elhady, Ahmed[1,2,3,4],Fleischmann, Ragnar[1], Geisel, Theo[1,3,4,5],Wolf, Fred[1,3,4,5]

1 Max-Planck-Institut für Dynamik und Selbstorganisation, Göttingen
2 Max-Planck-Institut für experimentelle Medizin, Göttingen
3 Bernstein Center for Computational Neuroscience Göttingen
4 Bernstein Focus for Neurotechnology, Göttingen
5 Fakultät für Physik, Georg-August-Universität Göttingen
* Corresponding author. E-mail address: kai@nld.ds.mpg.de

Abstract
Recently, optogenetic tools have been widely used in neuroscientific research, opening the opportunity to stimulate neurons with high spatial and temporal resolution. Using optogenetic tools for photostimulation and combining it with extracellular measurements on a multielectrode array brings with it the problem that the photostimulus may lead to unwanted voltage signals which may be so large, that the signal intended to be measured is completely overshadowed by the photostimulus. In order to rule out the possibility of such artifacts in a given photostimulation setup, we examine the effect strong light signals derived from laser diodes of different wavelengths have on the noise recorded from a multielectrode array filled with an electrolyte solution. No photoelectric effect was found for the irradiances derived from a high power LED array.

1 The Problem

Photostimulation of biological tissues using optogenetics is emerging as a viable alternative to electrical stimulation. Since for different optogenetic tools, photostimulation in different wavelengths may be employed [2], it is crucial for signal analysis to quantify artefacts deriving from the photoelectric effect at the electrode surface. Although the photoelectric properties of most materials commonly used in multielectrode array electrodes (TiN or ITO), are well-known for an interface with a vacuum [3], the photoelectric effect for metal surfaces immersed in an electrolyte solution leads to a greater sensitivity to incident light on the electrode by means of lowering the work function of the interface [4].

While the physics of the photoelectric effect is complicated by the presence of an electrolyte solution [4], the most basic principle of the effect still holds true, namely that the mere presence of a photoelectric signal only depends on the incident wavelength [1], the net current derived form the effect depends on the number of incident photons.

1.1 Photoelectric effect of Titanium Nitride

At the interface of a metallic compound and a a vacuum, the energy balance of a photon of frequency ν absorbed by an electron at this surface can be expressed by $h \cdot \nu = \Phi + E_{kin}$, wherein h is Planck's constant, Φ the work function of the compound, and E_{kin} the kinetic energy of the electron after the absorption of the photon. It is easily seen that for photon energies smaller than the work function, no photoelectric effect can occur. Due to the quantized nature of light, above this energy, the current derived from the effect is proportional to the number of incident photons, and thus to the irradiance.

The work functions for most materials in technical usage are well-known and have been studied intensely as far as the junction with a vacuum or with other solids are concerned [3,5]. The vacuum work function is also easily accessible to direct measurement via a Kelvin probe [5]. If the material in question is immersed into an electrolyte solution, a lowering of the work function occurs. This effect is strongly dependant on the material in question, its surface properties, and the interaction of the surface with the electrolyte solution it is contact with [4,5]. However, a survey of work functions of metals immersed in electrolyte solution shows that the work function of the metal in question is lowered considerably by the presence of the electrolyte solution at the surface [4].

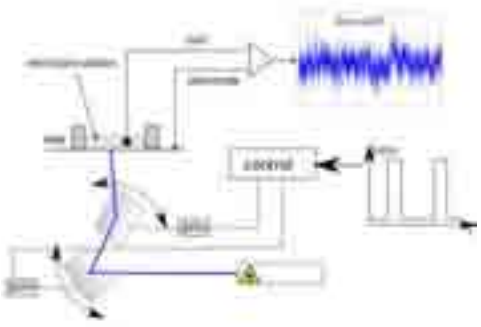

Fig.1. The experimental setup (schematically).

2 Experimental Setup

The MEA is placed on an inverted microscope to the epifluorescence port of which a commercial galvanometer (galvo) setup (Rapp OptoElectronic) is coupled (cf. Fig. 1). With a programmable controller and control software, it is possible to move the image of the terminal of an optical fibre over the MEA.
The chamber of this MEA is filled with buffer solution as employed in experiments with cell cultures. Different stabilized laser diodes are subsequently coupled to the galvo-setup, and a laser spot of (20 +/-2) μm diameter is projected onto the MEA and can be moved freely in the object plane of the microscope.

Measurement

Four electrodes of the MEA are selected, and the control software for the galvos is programmed to move the laser spot from electrode to electrode in a given sequence. Each jump is triggered by a TTL pulse form a signal generator. After a jump, the spot stays on the next electrode for 10 ms, and after four such jumps, the spot returns to the initial electrode (cf. Fig.2, d). During this process, the voltage signals as picked up by the individual electrodes are measured. The laser intensity of the diode can be adjusted continuously from 0 to 100 %, so that the process can be repeated for several irradiances, which are derived from light power measurements with a photodiode, and a measurement of the cross section of the laser spot with an object micrometer. The spot diameters are found to be (20 +/- 2) μm.
These measurements are carried out before each run. Control runs are made using Ringer's solution. The results of these measurements do not differ from the ones made with the buffer solution.

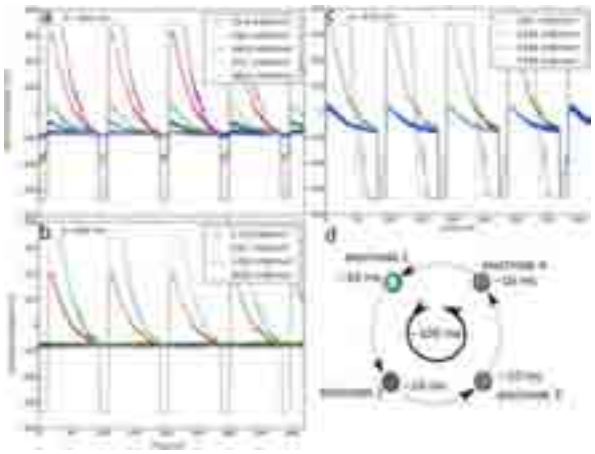

Fig. 2. Signals picked up by a single TiN electrode for different wavelengths (a: 405 nm, b: 450 nm, c: 473 nm) and irradiances. d: movement of the laser spot.

3 Results

Photoelectric signals were measured at photon energies E_{hv} = 3.06 eV (λ = 405nm), E_{hv} = 2.76 eV (λ = 450 nm), and at E_{hv} = 2.62 eV (λ = 473nm). The vacuum work function of TiN is $\Phi_{vac} = 3.2$ eV [6], which would allow for a photoelectric effect only for incident wavelengths $\lambda < 388$ nm. However, since the work function is lowered due to the immersion in a liquid dielectric, a photoelectric effect can be measured even at photon energies as low 2.6 eV, albeit only at very high irradiances (several hundred mW/mm^2).
Also, for the method of illumination chosen in our experiments, namely high power LEDs (λ = 480 nm) yielding irradiances in the order of 10 mW/mm^2, no photoelectric effect has been measured with this technique.

Acknowledgement

We thank Rapp OptoElectronics, Hamburg, for providing the galvo system, the laser diodes, and Kristin Klotz of Rapp OptoElectronics for assistance with the laser setup. We also thank Frank Killich of KiwiTechnik, Göttingen, for helpful discussions.

References

[1] Albert Einstein, Über einen die Erzeugung und Verwandlung des Lichts betreffenden heuristischen Gesichtspunkt. *Annalen der Physik 322, Nr. 6, (1905)*
[2] F. Zhang &al., Optogenetic interrogation of neural circiuts: technology for probing mammalian brain structures. *Nat. Protoc 5, 439-456 (2010)*
[3] Charles Kittel, Solid State Physics, Table 17.1
[4] Zolotovitskii, Ya. M., Korshunov, L. I., and Benderskii, V.A., Electron work function from metals in a liquid dielectric. *Russian Chemical Bulletin, Volume 21, Number 4, 760-763*
[5] Ashcroft, N., Mermin, D. (1976): Solid State Physics. *Harcourt College Publishers, ch.18.*
[6] Nakamoto, M., and Moon, J., Suitability of low work function titanium nitride coated transfer mold field-emitter arrays for harsh environment applications. *J. Vac. Sci. Technol. B 29, 02B112 (2011)*

Hardware implementation, optimisation and performance analysis of a real-time spike sorter for high-density microelectrode recordings

Jelena Dragas[1*], David Jäckel[1], Felix Franke[1], Andreas Hierlemann[1]

1 ETH Zurich, Department of Biosystems Science and Engineering, Basel, Switzerland
* Corresponding author. E-mail address: jelena.dragas@bsse.ethz.ch

Abstract
Analysis of the electrically active cell networks asks, in some cases, for tightly constrained time intervals between the occurrence of an electrical activity inside the network and reliable information about the origin of this activity. A High Density Microelectrode Array (HDMEA) - based system can provide high-resolution recordings of network activity, increasing the reliability of the decoded information, but at the same time, implies handling large amounts of data needed to be processed in real-time. This work describes the implementation and optimisation of a real-time spike-sorting algorithm on a Field-Programmable Gate Array (FPGA) targeting HDMEA-based systems. The achieved data processing latency ensures a real-time analysis of electrically active cell networks, making close-loop experiments possible. In addition, it offers an option of data throughput and data storage reduction by removing the redundant information from the recorded data.

1 Introduction

HDMEAs provide a way to simultaneously record the electrical activity of a large population of cells in neuronal cultures, retinal preparations or cortical slices. The complementary capability of cell stimulation enables, in principle, the stimulation to be triggered by the recorded cell activity. So-called “closed-loop” stimulation bears the potential of being able to selectively change the neuronal wiring diagram in a controlled manner.

In order to generate a specific stimulation, it is necessary to correctly detect and classify the electrical activity of a potentially large number of neurons - a problem known as “spike-sorting” - and to do this in a very short time. However, the large number of recording electrodes, and the large number of recorded neurons result in high data throughput and high data flow complexity, which, in turn, may lead to high latency between spike recording and stimulus generation. Moreover, the high data throughput entails a rapid growth of data storage memory requirements.

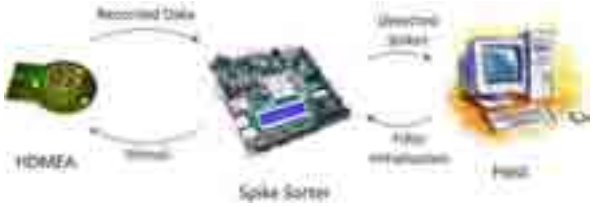

Fig. 1. HDMA-based closed-loop system.

Here we present a system that can overcome these difficulties using an optimised spike-sorting algorithm implemented in hardware.

2 System description

The system consists of an HDMEA device that performs data recording, a spike sorter implemented on an FPGA running a custom-designed algorithm, and a general purpose host machine used for algorithm initialisation and, optionally, for further data analysis and data storage, as shown in Figure 1.

The algorithm relies on optimal linear filters [1], matched to the prototypical multichannel spike waveforms (“footprints”), where every neuron has exactly one associated multichannel filter. Filter coefficients are the result of a pre-processing step, performed off-line on a host, and can be loaded in the FPGA memory periodically in order to adapt the filters to changing cell footprints, caused by the cell drift.

3 Performance assessment

Limited hardware resources of an FPGA call for a trade-off between the number of channels per filter and the sorting performance. The performance has been assessed by simulations of mouse retinal ganglion cell recordings [2]. Figure 2 shows the total number of spike sorting errors, normalised to the actual number of spikes as a function of channels per filter. The result shows that the number of channels per filter can be drastically reduced while still maintaining a high sorting quality. An example system has

been implemented, capable of performing a real-time sorting of data from 200 neurons, recorded on 1024 electrodes, considering 6 channels for each filter; it requires approximately 13k Virtex 6 logic slices and instantiates 3Mb of block RAM, used for storing the filter coefficients.

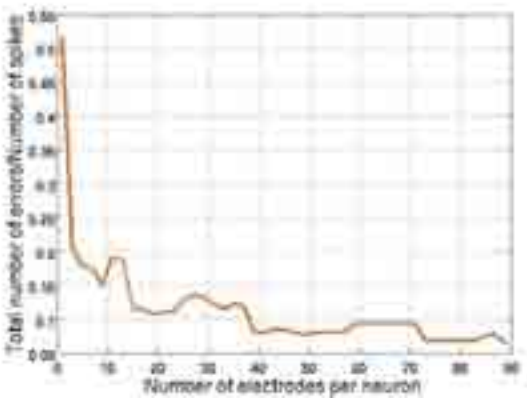

Fig. 2. Spike-sorting performance versus the number of channels per filter.

Latency of the spike detection and classification is data dependent and corresponds to half of the single channel footprint length in addition to the overhead of the algorithm. In the above-mentioned data set, single channel footprints were 3ms long (60 samples at 20kHz sampling rate), and the algorithmic overhead was 15 sampling clock cycles, resulting in a total latency of 2.25ms.

4 Conclusion

The achieved low latency between the spike occurrence and the stimulus generation allows for performing real-time closed-loop stimulations. In addition, high data throughput can be decreased by streaming out only relevant information from the MEA chip. However, the presented spike sorter is not a stand-alone module, and pre-processing needs to be done in order to obtain the filter coefficients.

Acknowledgement

This work was financially supported by the European Community through the ERC Advanced Grant 267351, NeuroCMOS.

References

[1] Franke F. (2011). Real-time analysis of extracellular multielectrode recordings. *PhD Thesis, Technische Universität Berlin.*

[2] Jäeckel D, Frey U., Fiscella M., Franke F, Hierlemann A. (2012). Applicability of independent component analysis on high-density microelectrode array recordings. *Journal of Neurophysiology, in press.*

Modeling extracellular spikes and local field potentials recorded in MEAs

Torbjørn B. Ness[1*], Espen Hagen[1], Moritz Negwer[2], Rembrandt Bakker[3,4], Dirk Schubert[2], Gaute T. Einevoll[1]

1 Dept. of Mathematical Sciences and Technology, Norwegian University of Life Sciences, Ås, Norway
2 Donders Inst. for Brain, Cognition & Behaviour, Radboud University Medical Centre Nijmegen, The Netherlands
3 Donders Inst. for Brain, Cognition & Behaviour, Radboud University Nijmegen, The Netherlands
4 Juelich Research Institute, Germany
* Corresponding author. E-mail address: torbjorn.ness@umb.no

Abstract
Multielectrode array (MEA) measurements of neuronal activity in brain slice preparations have become an important research tool. However, to take full advantage of this technology, accurate and reliable tools for quantitative modeling and analysis of the recorded data are required. In particular, the “measurement physics”, i.e., the link between the potentials recorded at the electrode contacts and the underlying neural activity, must be properly established. We here present and demonstrate the use of a physics-based modeling scheme based on the Finite Element Method (FEM), addressing this issue.

1 Background

Multielectrode array (MEA) measurements offer the possibility to record neuronal activity *in vitro* at a high spatial and temporal resolution. However, the interpretation of the recorded data is not always straightforward. Biophysically detailed modeling studies emulating both (i) the underlying neural activity and (ii) the measurement physics, i.e., the link between intrinsic neural activity and the potentials recorded in the MEA set-up, will be a necessary component in quantitatively accurate and reliable analysis of such data. The power of modern computers, combined with the recent establishment of freely accessible databases containing hundreds of reconstructed neuronal dendritic morphologies (e.g., NeuroMorpho.org), a key ingredient in such modeling [1, 2], now places such modeling within reach for all scientists in the field.

2 Methods

We employ LFPy [3], a new Python module developed in our group, running on top of the NEURON simulator [4], to obtain the compartmental transmembrane neuronal currents setting up the recorded potentials. Until now most biophysical forward modeling of extracellular potentials assume an infinite homogeneous extracellular electrical medium [1, 2]. This allows for a simple analytical solution of the electrostatic forward problem in terms of treating compartments as point-sources or line-sources [1, 2]. While applicable for the modeling of *in vivo* multielectrode recordings, this assumption is in general not valid in *in vitro* slice recordings, because the electrical conductivities in the electrode array, neural tissue and saline covering the slices are widely different. Spatial inhomogeneities and anisotropies of the electrical conductivity can be handled by using the Finite Element Method (FEM, Fig. 1) to solve the forward modeling problem. Using FEM we can in principle mathematically model the link between any neural activity and the corresponding recorded MEA potentials, both the high-frequency (spikes) and low-frequency (local field potential) components. The approach will be applicable to any number of neurons, kind of neuronal morphologies, ionic membrane channels and synaptic input.

Fig. 1. Illustration of a FEM forward modeling scheme for calculating recorded activity on a MEA, from activity in a layer V pyramidal neuron in a cortical slice. The green and orange arch represents grey matter in a 300 µm thick slice of cortical tissue in a MEA set-up, and the grid of dots directly below the layer V pyramidal neuron represent the set of MEA contacts.

3 Results

Here, results from two projects will be presented:

In the first project the modeling tool is used for generation of spike-sorting test data to validate automated spike-sorting algorithms, where the simulation framework is used to generate extracellular spikes in high-density MEA recordings [5]. This project is part of an international coordinated effort where such test data will be collected and made available at a website hosted by the German node of the International Neuroinformatics Coordinating Facility (INCF) (www.g-node.org/spike), allowing for a systematic benchmarking of spike-sorting algorithms.

In the second project the tool is used to study how individual neurons contribute to the local field potential (LFP) as measured by MEAs in an acute brain slice setting [6]. The model output is compared to corresponding experimental data, which includes the detailed reconstruction of the excited neuron.

Acknowledgement

This work is supported by the Research Council of Norway (NevroNor, eScience, Notur), and the Norwegian node of the International Neuroinformatics Coordinating Facility (INCF).

References

[1] Holt G. R., Koch C. (1999). Electrical Interactions via the Extracellular Potential Near Cell Bodies. *J Comp Neurosci* 6:169-184.

[2] Pettersen K. H., Einevoll G. T., (2008). Amplitude Variability and Extracellular Low-Pass Filtering of Neuronal Spikes. *Biophys J*, 94:784-802.

[3] LFPy [http://compneuro.umb.no/LFPy]

[4] Hines M. L., Davison A. P., Muller E., (2009). NEURON and Python. *Front Neuroinformatics*, 3:1-12.

[5] Einevoll G. T. , Franke F., Hagen E., Pouzat C., Harris K. D., (2012). Towards reliable spike-train recordings from thousands of neurons with multielectrodes. *Curr Opin Neurobiol*, 22:11-17.

[6] Bakker R., Schubert D., Levels K., Bezgin G., Bojak I., Kötter R., (2009). Classification of cortical microcircuits based on micro-electrode-array data from slices of rat barrel cortex. *Neural Networks*, 22:1159-1168.

Are spike waveforms distinct enough to separate adjacent neurons?

Christian Leibig[1,2,3 *], Armin Lambacher[4], Thomas Wachtler[2], Günther Zeck[1]

1 Neurochip Research, Natural and Medical Sciences Institute at the University of Tübingen, Reutlingen (Germany)
2 Department Biology II, Ludwig-Maximilians-Universität München, Martinsried (Germany)
3 Graduate School of Neural Information Processing, University of Tübingen, Tübingen (Germany)
4 Membrane- and Neurophysics, Max-Planck-Institute of Biochemistry, Martinsried (Germany)

* Corresponding author. E-mail address: christian.leibig@g-node.org

1 Background / Aims

In order to understand the functionality of neural networks, reliable parallel spike trains must be recorded from neuronal ensembles [1, 2]. Silicon-based multi-transistor arrays ('Neurochips') are large enough to map the activity of hundreds to thousands of neurons within an area of 1 mm^2.

In order to retrieve reliable parallel spike trains, action potentials (APs) have to be properly assigned to their corresponding units. The signal separation of adjacent neurons in neural tissue or cell culture represents a serious challenge, as their electrical coupling areas on the sensor array overlap. In this work we aim to determine whether this problem can be solved based on extracellular action potential waveforms together with their positional information.

2 Methods

A potential algorithm for assigning APs to corresponding units was presented in [3]. Here, we test its capabilities by using synthetic data with known positions, signal shapes and amplitudes of the extracellular signal. The synthetic data were generated from recordings of four retinal ganglion cells (RGCs). Measurements were done with a multi-transistor array (size 1mm^2, pitch 7.4µm, sampling rate 78kHz). For each RGC several hundred threshold crossings were averaged and down sampled to either 11.5 or 23 kHz respectively (Fig.1). Gaussian noise was added with appropriate amplitude to obtain a signal-to-noise ratio of 11 [4]. Thus a template was obtained for each RGC. Finally, synthetic data sets were generated by combining template pairs at different distances from each other (7.4, 14.8 or 22.2 µm) and fed to the algorithm described in [3]. The quality of spike sorting was quantified by an error rate defined as the sum of false positive and false negative assignments with respect to the known ground truth. This procedure was carried out for two sampling rates (11.5 and 23 kHz).

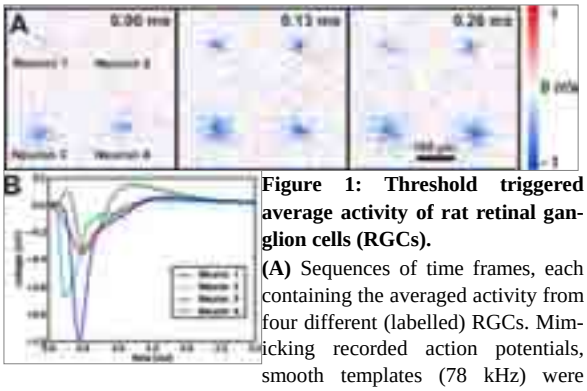

Figure 1: Threshold triggered average activity of rat retinal ganglion cells (RGCs).
(A) Sequences of time frames, each containing the averaged activity from four different (labelled) RGCs. Mimicking recorded action potentials, smooth templates (78 kHz) were down sampled to 23 kHz and rescaled (to S/N = 11; S/N = absolute maximum / rms(Noise)). Every third frame is shown. For purposes of illustration, templates are temporally aligned in (A), so that the signal maxima in the different templates occur at the same time. **(B)** Transients of those pixels that contain the signal maximum of the corresponding neuron template (78 kHz, original S/N).

3 Results

We compared spikes from pairs of different neuronal templates with centres of electrical coupling areas separated by multiples of 7.4 µm. At a sampling rate of 23 kHz, spikes could be reliably separated down to the smallest separation distance (7.4 µm).

However, for waveforms sampled at 11.5 kHz, units with similar waveforms were not separated at this distance. By increasing the distance to 14.8 µm a full separation could be obtained.

4 Conclusion / Summary

For given conditions (signal-to-noise ratio and noise distribution) our results provide parameter settings for which spiking activity can be reliably assigned to the corresponding source. By spatially interpolating the values between pixels the separation can be varied continuously, which allows further refinement of the results.

References

[1] Buzsáki, G. (2004). Large-scale recording of neuronal ensembles. *Nature Neuroscience*, 7(5), 446-451.

[2] Einevoll, G. T., Franke, F., Hagen, E., Pouzat, C., & Harris, K. D. (2011). Towards reliable spike-train recordings from thousands of neurons with multielectrodes. *Current Opinion in Neurobiology*, 22, 1-7.

[3] Lambacher, A., Vitzthum, V., Zeitler, R., Eickenscheidt, M., Eversmann, B., Thewes, R., & Fromherz, P. (2011). Identifying firing mammalian neurons in networks with high-resolution multi-transistor array (MTA). *Applied Physics A*, 102(1), 1-11.

[4] Leibig, C., Wachtler, T., and Zeck, G., (2011). Resolution Limit of Neurochip Data. *Front. Comput. Neurosci. Conference Abstract: BC11 : Computational Neuroscience & Neurotechnology Bernstein Conference & Neurex Annual Meeting 2011*. doi: 10.3389/conf.fncom.2011.53.00069

Supported by a BMBF grant (FKZ: 0312038) to CL and GZ.

Comparison of MEA signals derived from peritoneal mast cells and RBL-2H3 cells

Jessica Ka-Yan Law[1], Tobias Oberbillig[1], Chi-Kong Yeung[2], John Anthony Rudd[2], Mansun Chan[3], Sven Ingebrandt[1*]

1 Dept. of Informatics and Microsystem Technology, University of Applied Science Kaiserslautern, Zweibrücken, Germany
2 School of Biomedical Sciences, The Chinese University of Hong Kong, Shatin, New Territories, Hong Kong
3 Dept. of Electronic and Computer Engineering, Hong Kong University of Science and Technology, Clear Water Bay, Hong Kong
* Corresponding author. E-mail address: sven.ingebrandt@fh-kl.de

Abstract
In the present study, the activation of different immunological cells was studied using the microelectrode array. Events of spike activities were observed when calcium ionophore A23187 was added to the mast cell culture, while no activities were observed with the leukocyte culture. The distinct difference between the primary mast cells and the leukocytes might be explained by the amount of histamine released upon activations. We are now applying a standard test for the amount of histamine released from these cells to further investigate the signal origin. The present MEA system provides a platform for studying the activation of different immunological cells.

1 Introduction

The microelectrode array (MEA) has been used extensively as a tool in the field of excitatory cell research for several decades [1, 2]. There is increasing evidence that shows biological signals from activated non-excitatory cells can also be detected by the MEA [3, 4]. In our previous studies, signals from activated rat peritoneal mast cells were detected using our custom-made MEA system. Different signal shapes were observed upon stimulation by different mast cell secretagogues [3, 5]. The differences in signal shapes, however, are not fully understood. An experimental setup that combines patch-clamp and MEA recording may thus provide us with more real-time information regarding the measured MEA signals upon immune cells activation.

RBL-2H3 is an adherent rat leukocyte cell line, which has similar properties as the rat peritoneal mast cells in terms of the activation mechanism. A calcium oscillatory mechanism is activated upon stimulation. Secretory vesicles, including histamine and other inflammatory mediators, are then released as a result [6]. Compared to the previously used peritoneal mast cells, the adherent property of the RBL-2H3 cells offers an ideal immune cell type for simultaneous patch-clamp and MEA recordings.

2 Methods

In the present study, both peritoneal mast cells and RBL-2H3 were cultured on our custom-made MEA devices and stimulated using calcium ionophore A23187 (Fig. 1). We aimed to study the signal shapes generated by the primary mast cells and compared them with the signals by the leukocytes. Our combined patch-clamp and MEA recording system offers the possibility of studying the origin of the signals generated in simultaneous recordings.

Fig. 1. Microscopy images showing cultures of the primary peritoneal mast cells (a) and RBL-2H3 cells on the MEA devices (b). Scale bars 10 and 50 µm, respectively.

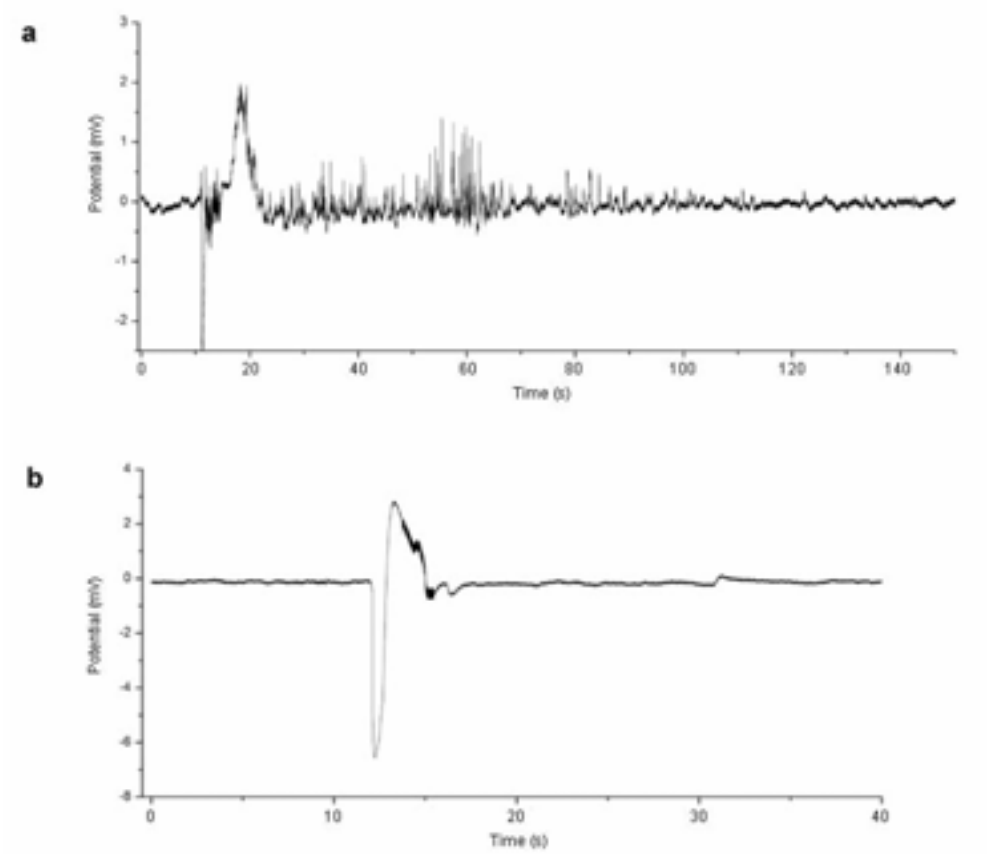

Fig. 2. MEA signals recorded in the presence of 10 μM A23187 with or without primary mast cells on the MEA chip. Events of spikes are observed after the introduction of A23187 and the spike activities continue for the next 2 minutes (a). Spike activities are not observed when the same concentration of A23187 is applied to the mast cell-free MEA chip (b).

3 Results

A response was elicited shortly after the addition of A23187 (10 μM) to the primary mast cells and events of spikes were observed 2 minutes after the introduction of the chemical (Fig. 2a). A negative control was carried out on a blank MEA without any mast cells on it to demonstrate the signals recorded were the results of interactions between the cells and A23187 (Fig. 2b). But no signals were observed when the same experimental protocol was applied to the RBL-2H3 cells. At the moment, we are trying to explain the signal origin with the amount of histamine released upon activation.

4 Conclusion

The detection of immuno-responsive cells with the MEA system opens up a novel and promising application in cell biology. There are few studies that have so far looked into the origin of these signals, and the interpretations of which are necessary for the understanding of any pharmacological studies. The present study provides additional information for explaining the possible biological signals recorded by the present MEA setup.

Acknowledgement

This work was supported by BMBF/AIF 17042X11 and BMBF/AIF 17N2110.

References

[1] Yeung C.K., Sommerhage F., Wrobel G., Offenhausser A., Chan M., Ingebrandt S. (2007). Drug profiling using planar microelectrode arrays. *Analytical and Bioanalytical Chemistry*, 387, 2673-2680.

[2] Stett A., Egert U., Guenther E., Hofmann F., Meyer T., Nisch W., Haemmerle H. (2003). Biological application of microelectrode arrays in drug discovery and basic research. *Analytical and Bioanalytical Chemistry*, 377, 486-495.

[3] Yeung C.K., Law J.K., Sam S.W., Ingebrandt S., Lau H.Y., Rudd J.A., Chan M. (2008). The use of microelectrode array (MEA) to study rat peritoneal mast cell activation. *Journal of Pharmacological Sciences*, 107, 201-212.

[4] Pfeiffer T., Kraushaar U., Dufer M., Schonecker S., Haspel D., Gunther E., Drews G., Drews P.K. (2011). Rapid functional evaluation of beta-cells by extracellular recording of membrane potential oscillations with microelectrode arrays. *Pflugers Archiv-European Journal of Physiology*, 462, 835-840.

[5] Law J.K., Yeung C.K., Wan S.P., Ingebrandt S., Lau H.Y., Rudd J.A., Chan M. (2011). The significance of chloride in the inhibitory action of disodium cromoglycate on immunologically-stimulated rat peritoneal mast cells. *Biochimica et Biophyisca Acta*, 1810, 867-874.

[6] Hide M., Beaven M.A. (1991). Calcium influx in a rat mast cell (RBL-2H3) line. Use of multivalent metal ions to define its characteristics and role in exocytosis. *Journal of Biological Chemistry*, 266, 15221-15229.

Burst analysis methods for analyzing maturing neuronal networks with variable firing statistics

Kapucu Fikret Emre[1,4*], Tanskanen Jarno M A[1,4], Mikkonen Jarno E[2], Ylä-Outinen Laura[3,4], Narkilahti S[3,4], Hyttinen Jari A K[1,4]

1 Department of Biomedical Engineering, Tampere University of Technology, Finland
2 Department of Psychology, University of Jyväskylä, Jyväskylä, Finland
3 NeuroGroup, Institute of Biomedical Technology, University of Tampere and Tampere University Hospital, Tampere, Finland
4 Institute of Biosciences and Medical Technology, Tampere, Finland
* Corresponding author. E-mail address: emre.kapucu@tut.fi

Abstract
Maturing neuronal networks, such as human embryonic stem cell (hESC) derived networks, exhibit highly time-varying action potential dynamics. To analyze the developing burst/spike activities of such networks, we propose a burst analysis algorithm which utilises firing statistics based on inter spike interval (ISI) histograms. Algorithm calculates ISI thresholds for burst spikes as well as pre-burst spikes and burst tails (burst related spikes) based on the cumulative moving average (CMA) and skewness of ISI histogram. The proposed method is a potential tool for analyzing hESC-derived neuronal cell networks and can be utilized to understand the development and functioning of human neuronal networks and as an analysis tool for in vitro drug screening and neurotoxicity assays.

1 Introduction

Neuronal activity is generally described by single cell firing called spikes or actual network activity manifested by short episodes of intense firing called bursts [1, 2]. Bursting is an activity during which neurons are interacting and firing in an orchestrated manner. It is suggested that bursts reflect and influence the plasticity mechanisms and for that reason could be used for assessment of network activity [3].

Although bursting is a commonly accepted feature of a neuronal network, the definitions of bursts and burst detection methods differ between studies. Among those definitions, some define bursts according to inter spike interval ISI thresholds and the numbers of spikes in bursts which are set by visual inspection [4]. Others utilize calculated average ISIs of the measurements [5], average firing rates and alternatively a fixed ISI threshold [6], or logarithmic histogram of ISIs to calculate an ISI threshold for detecting bursts [7, 8].

Most of the earlier suggested methods focused on rodent primary cultures which are widely studied *in vitro* neuronal networks [4, 5, 6, 7, 8]. In comparison to these cultures, networking mechanisms of hESC-derived neurons exhibits more variable statistics from individual spikes to bursts [9]. In fact, beside the frequent occurrence of "primitive" bursts which are formed by a few spikes, we also observed bursts with tens of spikes and bursts lasting from milliseconds to seconds while studying maturing hESC-derived neuronal networks [9]. However, the previously mentioned burst detection methods ignore the primitive and "unstable" spike train and burst activity of hESC-derived neuronal networks.

We have previously suggested a burst detection method without any a priori fixed burst criteria [10] and in this paper we demonstrated its applicability on a data collected from maturing hESC-derived neuronal networks and further studied how spiking statistics differ during maturation by means of ISI histogram skewness.

2 Materials and Methods

2.1 Cell Cultures and Electrophysiological Recordings

hESCs were differentiated into neuronal cells using the previously published method [11] and plated on MEAs as described in [9].

Recordings were done on MEAs with square arrays of 59 substrate-embedded titanium nitride microelectrodes (model: 200/30iR-Ti-gr, MCS) and internal embedded reference electrodes.

Measurements were obtained from eight different days during eight weeks. Each measurement day had two to six measurements, each of which lasts approximately two minutes.

2.1 Cumulative Moving Average for Detecting Bursts

Bursts were detected using CMA algorithm [10]. Shortly, from inter spike interval (ISI) histogram we calculated the cumulative moving average where ISI threshold for burst was defined for each analysed data

independently. Algorithm utilizes CMA and skewness of the ISI histogram to calculate burst threshold. Fig. 1 presents how CMA was obtained from ISI histograms. Spike trains with at least three spikes in a row with ISIs below the CMA calculated ISI threshold were defined as bursts. A second threshold was calculated similarly for the detection of burst related spikes (burst tails and pre-burst spikes) and these burst related spikes were included in their neighbouring bursts. Finally, the bursts which were closer to each other than the second threshold calculated were merged together. In this paper we further utilize the skewness to demonstrate how the ISI-histogram itself shows important information regarding the development of the network.

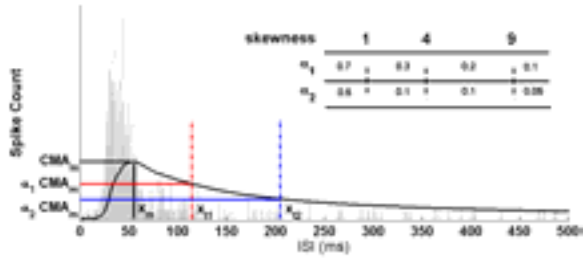

Fig. 1. Calculation of burst threshold (red vertical line) and burst related spikes threshold (blue vertical line) via CMA curve (black line) of the ISI histogram (grey bars). α coefficients used for corresponding skewness values.

3 Results

ISI histograms of single channels were obtained from eight different measurement days. The skewnesses of these ISI histograms are demonstrated in Fig. 2. Spike count from each measurement has also been presented to show the correlation between skewness values and channel activity.

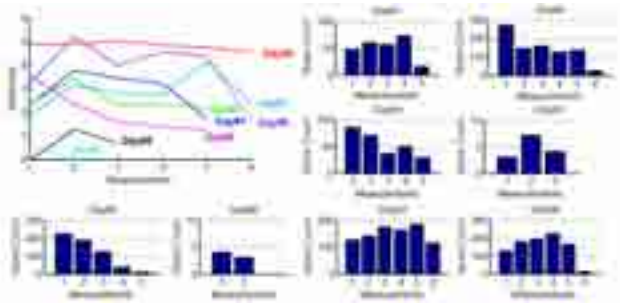

Fig. 2. Skewness of ISI histograms from different measurements of each measurement day are shown on top left. Spike counts for eight different days are shown with bars.

Recordings with detected bursts are shown in Fig. 3 Fig. 3a demonstrates higher activity where bursts include more spikes and the ISI histogram has a greater skewness value. On the other hand, Fig. 3b presents a rarely spiking channel with shorter bursts which are formed by a few spikes. Skewness values of these measurements can be seen in Fig. 2.

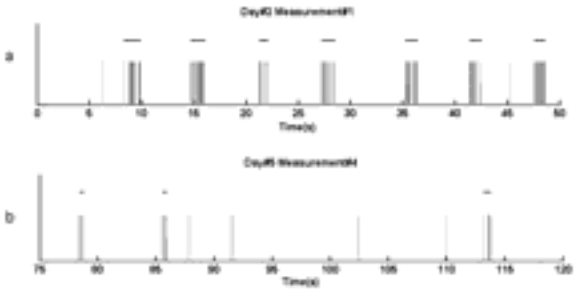

Fig. 3. Detected bursts by CMA method. (a) 50 s window of the recording from first measurement of Day 1 (b) 45 s window of the recording from fourth measurement of day 5.

4 Conclusions

Our CMA algorithm provides a new network adaptable burst detection method [10]. Further, skewness of the ISI histogram provides network information and could offer a promising tool to assess neuronal network behaviours. Together with CMA burst detection method utilizing the concept of network activity adaptable analysis, they can be used as a metric to enhance the present network analysis methods.

References

[1] Connors, B. W., Gutnick, M. J., and Prince, D. A. (1982). Electrophysiological properties of neocortical neurons in vitro. *J. Neurophysiol.*, 48, 1302-1320.

[2] Kandel, E. R., and Spencer, W. A. (1961). Electrophysiology of hippocampal neurons. II. After-potentials and repetitive firing. *J. Neurophysiol.*, 24, 243-259.

[3] Lisman, J. E. (1997). Bursts as a unit of neural information: making unreliable synapses reliable. *Trends Neurosci.*20,38-43

[4] Chiappalone, M., Novellino, A., Vajda, I., Vato, A., Martinoia, S., and van Pelt, J. (2005). Burst detection algorithms for the analysis of spatio-temporal patterns in cortical networks of neurons. *Neurocomputing* , 65-66, 653-662.

[5] Mazzoni, A., Broccard, F. D., Garcia-Perez, E., Bonifazi, P., Ruaro, M. E., and Torre, V. (2007). On the dynamics of the spontaneous activity in neuronal networks. *PLoS One*, 2, e439.

[6] Wagenaar, D. A., Pine, J., and Potter, S. M. (2006). An extremely rich repertoire of bursting patterns during the development of cortical cultures. *BMC Neurosci.*, 7:11.

[7] Selinger, J. V., Kulagina, N. V., O'Shaughnessy, T. J., Ma, W., and Pancrazio, J. J. (2007). Methods for characterizing interspike intervals and identifying bursts in neural activity. *J. Neurosci. Methods*, 162, 64-71.

[8] Pasquale, V., Martinoia, S., and Chiappalone, M. (2010). A self-adapting approach for the detection of bursts and network bursts in neuronal cultures. *J. Comput. Neurosci.*, 29, 219-229.

[9] Heikkilä, T., Ylä-Outinen, L., Tanskanen, J. M. A., Lappalainen, R. S., Skottman, H., Suuronen, R., Mikkonen, J. E., Hyttinen, J. A. and Narkilahti, S. (2009).Human embryonic stem cell-derived neuronal cells form spontaneously active neuronal networks in vitro. *Exp. Neurol,* . 218, 109-116.

[10] Kapucu, F. E., Tanskanen, J. M. A., Mikkonen, J. E., Ylä-Outinen, L., Narkilahti, S., and Hyttinen, J. A. K., "Burst analysis tool for developing neuronal networks exhibiting highly varying action potential dynamics", *Frontiers in Computational Neuroscience* (in review).

[11] Lappalainen, R. S., Salomäki, M., Ylä-Outinen, L., Heikkilä, T. J., Hyttinen, J. A., Pihlajamäki, H., Suuronen, R., Skottman, H., and Narkilahti, S. (2010). Similarly derived and cultured hESC lines show variation in their developmental potential towards neuronal cells in long-term culture. *Regen. Med.*, 5, 749-762.

Unified spike sorting framework using multi scale-space principle component analysis

Asim Bhatti[1*], Saeid Nahavandi[1], Steve Potter[2], Hamid Garmestani[2]

1 Deakin University, Pigdons Rd, Waurn Ponds 3217, Australia
2 Georgia Institute of Technology, Atlanta, Georgia 30332, US
* Corresponding author. E-mail address: asim.bhatti@deakin.edu.au

Abstract
In vitro multichannel recordings from neurons have been used as important evidence in neuroscientific studies to understand the fundamentals of neural network mechanisms in the brain. Consequently, accurate detection and sorting of neural activity waveforms becomes a key requirement for creating meaningful machine brain interfaces and to understand the working principles of neural networks. In this work we propose a unified framework for unsupervised neural spike clustering. Proposed framework exploits the features of wavelets scale-space representation and time-frequency localisation as well as multiscale principle component analysis to minimise the dimensionality of the raw data at different scales prior to clustering.

1 Introduction

In vitro multichannel recordings from neurons have been used as important evidence in neuroscientific studies to understand the fundamentals of neural network mechanisms in the brain. Consequently, accurate detection and sorting of neural activity waveforms becomes a key requirement for creating meaningful machine brain interfaces and to understand the working principles of neural networks. Number of spikes detection and sorting algorithms are proposed based on the variance maximisation of the sum of distances between the waveform clusters. Wavelet coefficients are also employed to exploit the time-frequency localisation and scale-space representation of the waveforms [1, 2] however in a very simple way.

2 Unified spike sorting framework

To exploit the maximum potential of wavelet transform and available statistical technique, we propose a unified framework for unsupervised neural spike clustering. Proposed framework exploits the features of wavelets scale-space representation and time-frequency localisation through the use of wavelet transform modulus maxima (WTMM). WTMM are translation invariant high profile multiscale wavelet coefficients that remain unaltered by the shifted versions of the same action potential spike. Multiscale principle component analysis minimises the dimensionality of the raw data at different scales prior to clustering. Principle component analysis provides variance-distribution of the waveforms at different scales and spaces, generated by wavelets transform, and help in estimating the optimised number of clusters. Number of clusters are automatically selected based on the percentage of accumulative variance distribution of the waveforms and is usually set to within the range of 90% to 98%. Percentage of accumulative variance implies; the number of possible clusters that would accumulate the desired percentage of variances of all waveforms with total sum of distances between the clusters below set threshold, normally set to 5×10^{-6}. An example of accumulative variance distribution is presented in Figure 1.

Fig1. Accumulative variance distributions of original, WTMM and MPCA waveforms shown in Fig3 A, B and C respectively

2.1 Methods/Statistic

The block diagram of the proposed framework is presented in Figure 2. As is obvious from the diagram; algorithm has three distinct branches to perform clustering utilising original waveforms, wavelet transform modulus maxima coefficients and multiscale principle component analysis of wavelets coefficients.

Original Waveform
stream employs raw data and perform principle component analysis to estimate optimised numbers of clusters based on the variance distribution and then performs hierarchical and k-mean clustering to cluster data into different bins as shown in Figure 3A.

WTMM coefficients
stream employs translation invariant wavelet transform modulus maxima coefficients that represent high value features of the original waveforms in scale-

space representation. Due to the inherent time frequency separation characteristic of the wavelets transforms, neural waveforms can be separated into higher number of clusters by amplifying even smaller variations as is shown in Figure 3B.

MPCA coefficients

Stream uses the wavelets transform coefficients and perform principle component analysis on each scale to estimate and extract high variance coefficients to perform clustering as shown in Figure 3C.

All clusters, shown in Figure 3, fulfil the separation criteria of total sum of distances between the clusters, set to 5×10^{-6}.

An example of the proposed framework highlighting three streams of clustering and respective outcomes is shown in Figure 3.

3 Conclusion

In this work we presented a unified spike sorting framework employing multi scale-space principle component analysis. The proposed framework exploits well-known features of principle component analysis, wavelets transform, hierarchical and K-means clustering to perform optimised separation of waveforms automatically.

References

[1] R. Quian Quiroga, Z. Nadasdy and Y. Ben-Shaul, Unsupervised Spike Detection and Sorting with Wavelets and Superparamagnetic Clustering, Neural Computation 16, 1661–1687, 2004

[2] Chenhui Yang, Byron Olson and Jennie Si, A Multiscale Correlation of Wavelet Coefficients Approach to Spike Detection, Neural Computation 23, 215–250, 2011

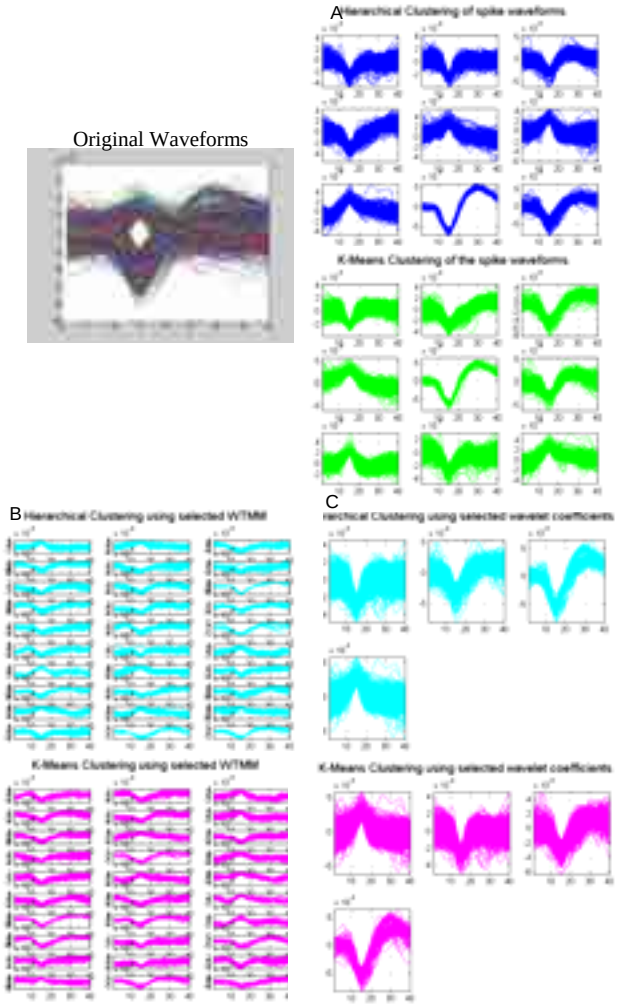

Fig3. Hierarchical and K-means clustering using proposed framework and 98% variance

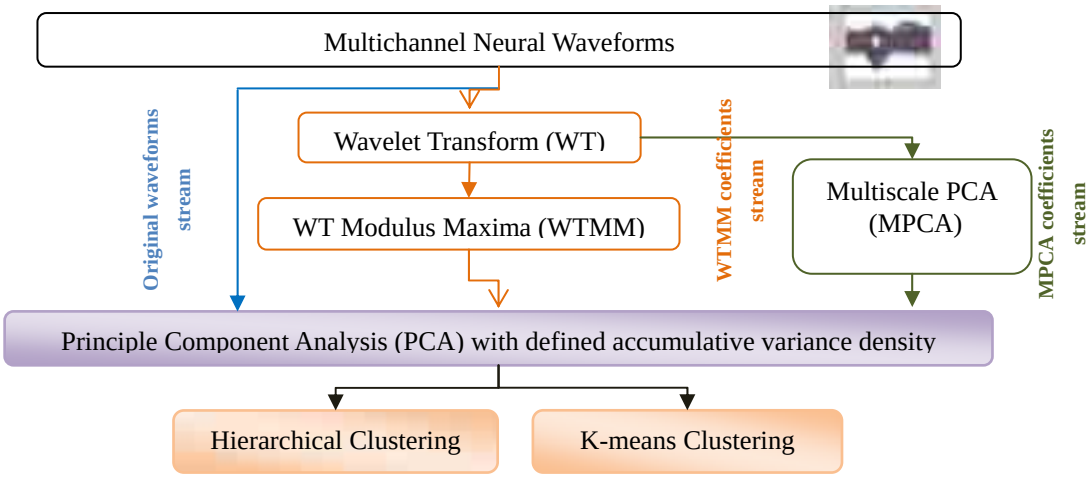

Fig2. Block diagram of multiscale spike sorting framework

Effect of structural connectivity on spatial distribution of functional connectivity in patterned neuronal networks

Sankaraleengam Alagapan[1], Eric Franca[1], Liangbin Pan[1], Thomas DeMarse[1], Bruce Wheeler[1*]

1 J Crayton Pruitt Family Department of Biomedical Engineering, University of Florida, Gainesville, FL, USA
* Corresponding author. E-mail address: bwheeler@ufl.edu

Abstract
Understanding the correlation between anatomical connections and the functional activity observed in a particular brain structure has been a challenge in neuroscience. In vitro patterned neuronal networks provide a novel approach to study these correlations and overcome shortcomings of traditional approaches like numerical modelling and simulations. These are networks in which biological neurons are constrained to grow in a predefined structure whose activity is then measured using a multielectrode array. The degrees of convergence and divergence can be manipulated with this technology. This report is a summary of our investigation of correlation between functional connectivity ascertained from Granger Causality and structural properties of patterned neuronal networks.

1 Introduction

Traditional approaches to understand the effect structure of a neuronal network has on its functions typically involve mathematical models and simulations. The main disadvantage of simulations is that the number of assumptions that underlie a mathematical model severely limits the model behaviour with a consequent loss of generalization. A model system of the brain comprising living neurons where the connections can be controlled and activity can be sufficiently sampled from the network would enable overcoming some of the limitations of mathematical models. In vitro patterned neuronal networks constitute such a model system that partially meets the needs for known network topology (Nam et al. 2004; Chang, Brewer, and Wheeler 2001; Branch et al. 1998). In this study we created patterned neuronal networks whose degree of convergence was predefined and we studied how this affects the functional connectivity of the network. We hypothesized that as the degree of convergence increases, the mean strength of functional connections should increase and also be less affected by increasing distance.

2 Methods

2.1 Patterned Network Cultures

Polydimethysiloxane (PDMS) stamps of different patterns were fabricated from SU-8 molds on silicon substrates. The patterns consisted of a grid of circular nodes with the difference between patterns being the number of nearest neighbours each node is connected to. Accordingly, the patterns were termed 2-connect, 4-connect, 8-connect (Connected to two, four and eight nearest neighbors respectively). These stamps were then immersed in Poly – D – Lysine and stamped on Multi Electrode Arrays pre-treated with 3-glycidoxypropyl-trimethoxysilane. This procedure created a cytophilic (PDL) pattern on a cytophobic (3-GPS) background restricting neural growth to the cytophilic pattern (Boehler et al. 2011).

Primary neuronal cultures were created by dissociating embryonic day 18 cortical tissue (BrainBits LLC) in medium made of NBActiv4 and plated on MEAs treated as mentioned in the previous step. The plating density was maintained at 700 cells/mm^2 . Apart from the patterned networks, random networks were also cultured as a case where the connectivity is not constrained in any manner.

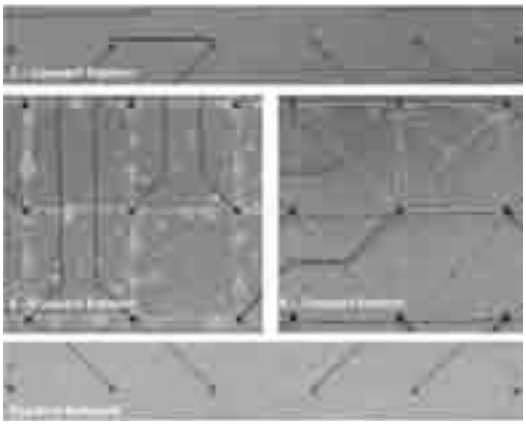

Fig 1. The different patterned networks studied in this report

2.2 Data Analysis

Extracellular signal were collected from the patterned networks at around 2 - 3 weeks after plating. A typical recording was 5 minutes long and action potentials were detected from each channel, binned in 5ms bins and smoothed to produce a continuous

waveform. Conditional Granger Causality (CGC) was computed from the continuous waveform using the GCCA Toolbox(Seth 2010). CGC values were then grouped according to distance between channels from which the values were computed.

3 Results

Mean Firing Rates

The first functional property to be compared across the different networks was the mean firing rate. We hypothesized that networks with higher levels of convergence should have higher firing rates as each node receives more input from other nodes. However, we could not find evidence to support the hypothesis as there was no significant differences between the firing rates.

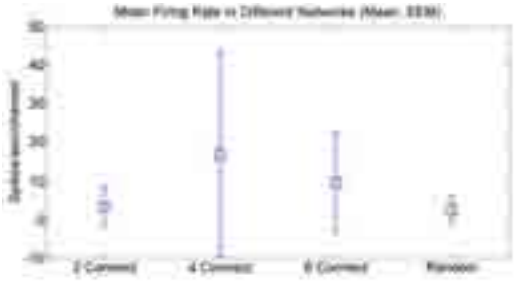

Fig 2. Mean Firing Rate of Different Networks

Mean CGC Values

The next property we tested was the mean connection strength between nodes in different networks. CGC values give an estimate of how correlated the activity in the network is. Again, here we hypothesized that higher levels of convergence will yield higher mean CGC values. However, as was the case with firing rates, we could not find evidence to support this hypothesis. The patterned networks had similar mean CGC values while the random networks had slightly higher mean CGC values.

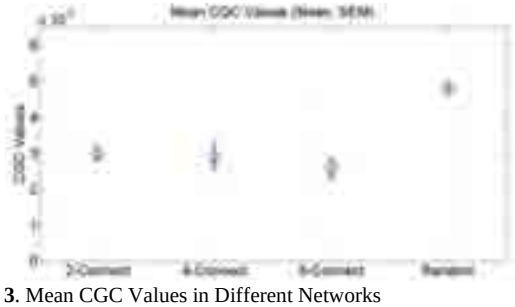

Fig 3. Mean CGC Values in Different Networks

Spatial Distribution of CGC Values

To understand how the constraint in convergence affected the CGC values, we compared the CGC values from different networks at different distances. The hypothesis was that for networks with higher levels of convergence, the rate of decrease in connection strength with increasing distance should be lower as there is a higher probability of connecting to farther nodes compared to those in network with lower levels of convergence. We observed a similar trend in the CGC values from the different networks. The CGC values from 2-connect networks decreased with distance significantly quicker in comparison to the CGC values from random networks. This can be seen in Fig 4 where the slopes of the lines fitted to the CGC values over distance decrease with increasing levels of convergence.

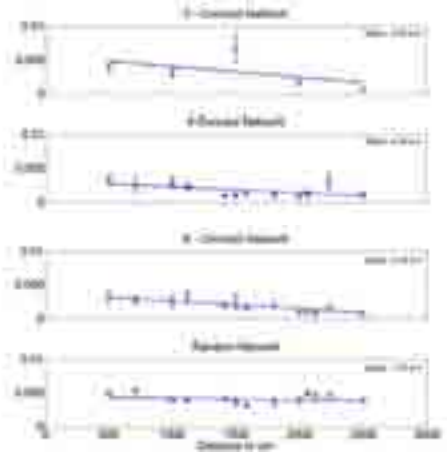

Fig 4. Falloff of CGC Values with distance

4 Conclusion

Patterning technologies allow us to construct neuronal networks with different levels of convergence and the functional properties of these networks are affected by the constraints we impose on the network. The strategy we followed in this work was not effective in altering certain functional properties like firing rate and connection strength while it affected others like the spatial distribution of connection strengths.

Acknowledgement

This work was partly supported by NIH grant NS052233-05

References

[1] Boehler, M. D., S. S. Leondopulos, B. C. Wheeler, and G. J. Brewer. 2011. “Hippocampal networks on reliable patterned substrates.” *Journal of Neuroscience Methods*.

[2] Branch, DW, JM Corey, JA Weyhenmeyer, GJ Brewer, and BC Wheeler. 1998. “Microstamp patterns of biomolecules for high-resolution neuronal networks.” *Medical and Biological Engineering and Computing* 36 (1): 135-141.

[3] Chang, J. C., G. J. Brewer, and B. C. Wheeler. 2001. “Modulation of neural network activity by patterning.” *Biosensors and Bioelectronics* 16 (7-8): 527-533.

[4] Nam, Y., J. Chang, D. Khatami, GJ Brewer, and BC Wheeler. 2004. “Patterning to enhance activity of cultured neuronal networks.” *Nanobiotechnology, IEE Proceedings*- 151 (3): 109-115.

[5] Seth, A. K. 2010. “A MATLAB toolbox for Granger causal connectivity analysis.” *Journal of neuroscience methods* 186 (2): 262-273.

Investigating electrical network dynamics in plant root cells by means of a high-density CMOS-based microelectrode array

Elisa Masi[1*], Michele Fiscella[2], Jan Müller[2], Urs Frey[3], Stefano Mancuso[1], Andreas Hierlemann[2]

1 Department of Plant, Soil and Environmental Science, University of Florence, Italy
2 ETH Zurich, Bio Engineering Laboratory, Basel, Switzerland
3 RIKEN Quantitative Biology Center, Kobe, Japan
* Corresponding author E-mail address: elisa.masi@unifi.it

Abstract
A complementary metal-oxide-semiconductor (CMOS)-based MEA approach is described to characterize the spatio-temporal electrical activity in root apex of maize. Many electrically active units have been found, covering different numbers of electrodes; these units, especially the bigger ones, are supposed to include a certain number of root cells. We also observed that spikes belonging to different units had different amplitudes and shapes. The explanation of these phenomena will advance our understanding of how electrical signals are generated and how they propagate in plants.

1 Background and Aims

The spatio-temporal characteristics of electrical network activity in plants have been recently studied in root apex slices by using a circuitless 60-channel microelectrode array (MEA) [1]. In order to confirm and better understand the nature of plant electrical network dynamics, we now used a complementary metal-oxide-semiconductor (CMOS)-based MEA [2] (Fig.1).

2 Methods

Measurements have been performed on the root apex of maize (*Zea mays* L.). Longitudinal slices of 400 µm thickness have been cut with a vibratome (Leica VD 1200S) and placed on the MEA chip. The CMOS-based MEA provides high spatio-temporal resolution (electrode diameter 7 µm, center-to-center distance 17 µm, sampling rate 20 kHz) and high signal-to-noise ratio (~7 µV rms under experimental conditions). It features 3150 electrodes per mm^2 and allows for simultaneous recording from 126 channels.

The flexibility of the system enables to record extracellular electrical activity at cellular and subcellular resolution.

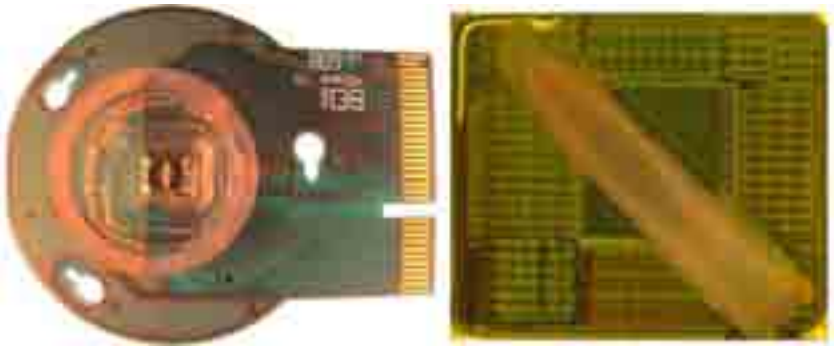

Fig. 1. HD-CMOS device and magnification of the electrode area with a root slice on top.

The recording procedure included a preliminary scanning phase, where a relatively low spatial resolution was used to find the active regions of the root section. Subsequently, a relatively long recording at higher spatial resolution was started (~ 60 min). Voltage traces were recorded at a time resolution of 50 µs and band-pass filtered (30 Hz-3 KHz). Spike waveforms were then extracted using a threshold of 4.5 standard deviations of the noise level.

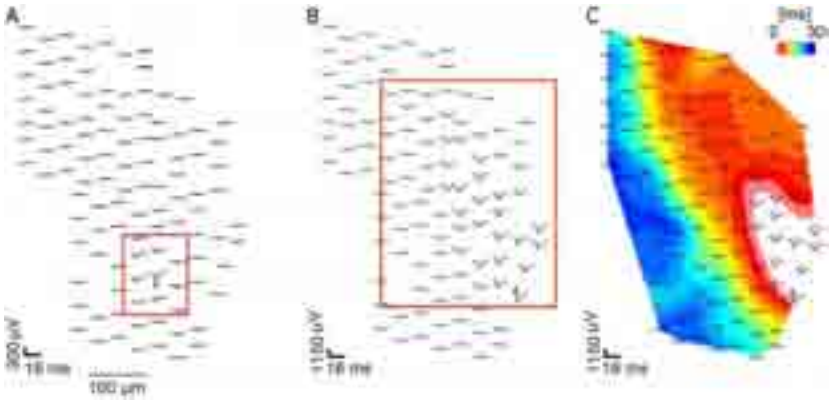

Fig. 2. (A and B) Spatial distribution of signals of two units of different size in the same root section (footprints). (C) Signal propagation within a single large unit: the signal rapidly spreads from the origin (white region) to neighboring areas.

3 Results

Extracellular activity was detected in different regions of the same root. Electrically active units were recorded that covered different areas, i.e., numbers of electrodes (Fig. 2A, Fig. 2B). In certain cases, extracellular activity was detected simultaneously over a relatively large area (~300*300 µm^2) (Fig. 2B). Furthermore, due to the high spatial resolution recordings, it was possible to follow the signal propagation across these units (Fig. 2C). Considering their extension, it is reasonable to assume that a unit may include groups of cells.

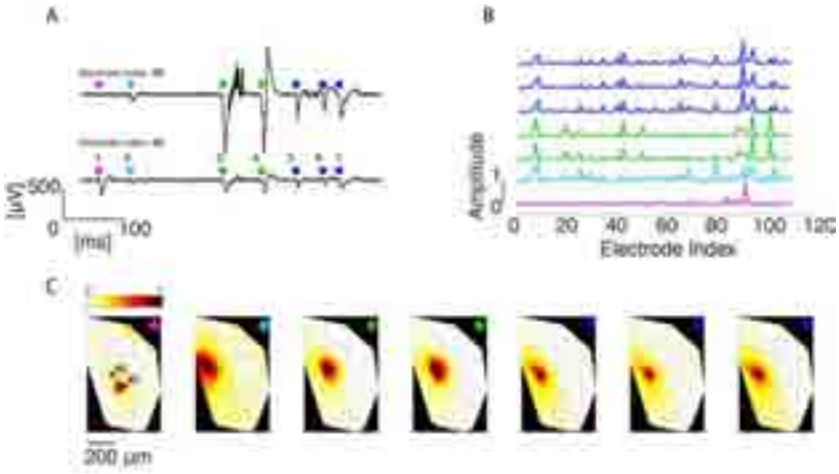

Fig. 3. (A) Seven types of spikes recorded on two different electrodes (see Fig. 3C for the electrode locations indicated by arrows) from four different units (spikes of different units are marked with dots of different colors). (B) Normalized (with regard to maximum amplitude) spike amplitudes of the units shown in A: Every line shows how the spike amplitude changes across 110 recording electrodes. (C) Spatial arrangement and extension of the four units; note that, the spatial profile of a certain unit does not vary a lot although spike shape and amplitudes are different (scale bar above first image refers to the spike amplitude, which has been normalized to the largest observed signal). The 2 black arrows represent indices and locations of the 2 electrodes shown in Fig. 3A.

Spike waveforms were recorded with different amplitudes, shapes and spatial distributions (Fig. 3). Several kinds of spikes, belonging to different units, have been consistently recorded on multiple electrodes (Fig. 3A). Although the amplitudes and shapes of the spikes are different, the spatial profile of a unit does not vary (Fig. 3B, Fig. 3C).

4 Conclusions

The analysis of the single spikes showed that defined spatial patterns of activity can be generated by either the same cell, or by ensembles of cells. Plant cells contain one or more big vacuoles. As a consequence, there are two membranes, the outer plasmalemma and the inner tonoplast. The contributions from these two membranes and the variation of ion concentration in both cytoplasmic and vacuolar compartments could be the reasons for the variable characteristics, i.e., shape and amplitude of the observed plant electrical signals. A better understanding of this phenomenon will require the elucidation of the ionic transport mechanism and, consequently, of the ion channels that are involved in the generation of electrical signals in plants.

References

[1] Masi E, Ciszak M, Stefano G, Renna L, Azzarello E, Pandolfi C, Mugnai S, Baluška F, Arecchi FT, Mancuso S (2009) Spatio-temporal dynamics of the electrical network activity in the root apex. *PNAS*, 106:4048-4053.

[2] Frey U, Egert U, Heer F, Hafizovic S, Hierlemann A (2009) Microelectronic system for high-resolution mapping of extracellular electric fields applied to brain slices. *Biosensors and Bioelectronics* 24: 2191–2198.

Identifying neuronal assemblies generating spontaneous synchronous network bursts *in vitro*

Stephan Theiss[1,2*], Johannes Slotta[1,2], Marcel Dihné[3], Alfons Schnitzler[1]

1 Institute of Clinical Neuroscience and Medical Psychology, Heinrich Heine University, Düsseldorf, Germany
2 RESULT Medical GmbH, Düsseldorf, Germany
3 Department of Neurology and Epileptology, Hertie Institute for Clinical Brain Research, Tübingen, Germany
* Corresponding author. E-mail address: theiss@hhu.de

Abstract
In dissociated neuronal networks, synchronous bursting is generated by pools of neurons firing in coordinated fashion. In the present work, such neuronal assemblies have been reliably identified in real and surrogate data by non-linear dimension reduction algorithms and subsequent clustering. Changes in network dynamics induced by pharmacological stimulation were reflected in the 2-dimensional cluster structure of population bursts.

1 Background

Synchronous bursting is a generic and stable pattern of spontaneous *in vitro* electrophysiological activity in mature neuronal networks cultured on microelectrode arrays (MEA) [1,2]. Network bursts are generated by spatially distributed pools of neurons firing in coordinated fashion. Recently, such neuronal assemblies have been identified in calcium imaging recordings by means of dimension reduction algorithms, and have been used to characterize network dynamics and its pharmacological modulation [3,4,5]. In the present study, neuronal subpopulations ("pools") participating in synchronous network bursts have been reliably identified and modulated in microelectrode array data.

2 Methods

Network bursts were identified by a standard heuristic algorithm using a minimum of 3 spikes per active electrode and 25 ms bin and a maximum interspike-interval of 100 ms within a burst [2,6]. For each network burst, a sixty-dimensional burst vector was computed from intra-burst firing rates normalized separately on all electrodes. The i^{th} component of this vector for a given network burst corresponded to the percentage of all spikes on electrode i within this burst. In the next step, the set of all 60-dimensional (network burst) vectors was analyzed using five established dimension reduction algorithms: Principal Component Analysis (PCA), Multi-Dimensional Scaling (MDS), Locally-Linear Embedding (LLE), ISOMAP and Diffusion Map (DM) [7]. Applying these algorithms, each network burst was mapped to a point in the resulting two-dimensional projection plane. Finally, this two-dimensional set of points was subjected to fuzzy *c*-means clustering (100 random initial conditions), and the optimal number of clusters—types of network bursts—was determined from the maximum of Dunn's index.

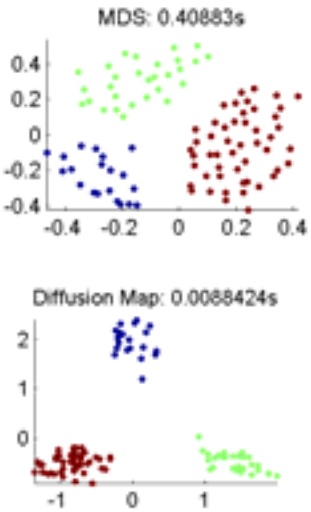

Fig.1 Two-dimensional projections of three network burst types: 100 surrogate data burst vectors with 30 common electrodes and three individual electrodes specific for each type, each with signal-to-noise ratio of 4. Top: Multi-dimensional scaling. Center: Diffusion map. Clusters corresponding to the three burst types are clearly separated. The corresponding plot (not shown) for locally linear embedding (LLE) maps each burst type exactly into one of the corners of a rectangle.

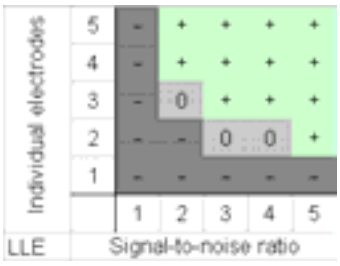

Fig.2 Phase diagram: overview of LLE classification accuracy for 1 to 5 individual electrodes and SNR varying between 1 and 5. "+" corresponds to 100% accurate burst type classification.

3 Results

The performance of five different dimension reduction algorithms was comparatively evaluated on 100 surrogate data sets containing three network burst types differing in up to 5 of 35 participating electrodes, superimposed on a Poissonian background with a mean firing rate of 1.3 spikes per second and electrode. Individual intra-burst firing rate, burst duration and onset jitter were adapted to experimental recordings of bursting dissociated networks of cortical neurons at ~28 DIV. Each 300 second long recording contained 20+30+50 bursts of type 1, 2, 3, respectively. All network bursts had 30 active electrodes in common and between 1 and 5 individual electrodes with their signal-to-noise (SNR, burst-to-background spikes) ratio varying between 1 and 5.

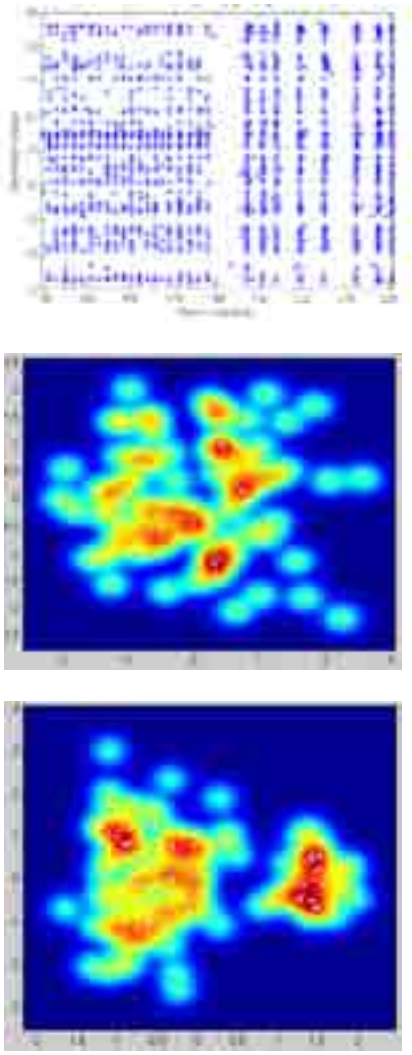

Fig.3 Transition zone (140—220 sec) from human CSF exposure (0—180 sec) to aCSF washout (180—360 sec). Top: Spike raster plot Center/bottom: Diffusion map plots of two recordings of dissociated cortical networks (31 DIV) after application of human CSF (center, 90 bursts) and in artificial cerebrospinal fluid (right, 90+37 bursts). Changes in network burst frequency are visible in the SRP, while DM plots reveal alterations in neuronal pools.

In contrast to linear PCA and MDS, the nonlinear algorithms LLE and DM performed well at obtaining clearly separated clusters (see Fig. 1). In the phase diagram (Fig. 2), the accuracy of burst type identification is indicated by +, 0 and – for independent combinations of number of burst type-individual electrodes and signal-to-noise ratio. LLE permitted excellent separation of the burst generating "neuronal pools" for as few as three characteristic electrodes and SNR of 2.5. In cortical networks exposed to artificial or human cerebrospinal fluid (CSF), LLE and DM plots clearly differentiated between different network dynamics and underlying structure of neuronal pools (see Fig. 3).

Conclusions

Neuronal assemblies—groups of neurons generating network bursts—can be reliably identified from MEA recordings by nonlinear dimension reduction algorithms like LLE. Pharmacological effects on the network dynamics are reflected in the two-dimensional signature of neuronal pools.

Acknowledgement

This work was supported by the German Ministry of Education and Research (BMBF: FKZ 0315641A) and the European Union (EURO-TRANS-BIO project ESSENCE). The authors thank Dr. Luis Carrillo-Reid and Prof. Gordon Arbuthnott for valuable discussions.

References

[1] Wagenaar D. et al. (2006). An extremely rich repertoire of bursting patterns during the development of cortical cultures. *BMC Neuroscience* 7:11.

[2] Van Pelt J. et al. (2004). Longterm stability and developmental changes in spontaneous network burst firing patterns in dissociated rat cerebral cortex cell cultures on multi-electrode arrays. *Neurosci Lett* 361:86–89.

[3] Carrillo-Reid L. et al. (2008). Encoding network states by striatal cell assemblies. *J Neurophysiol* 99:1435–1450.

[4] Jaidar O. et al. (2010). Dynamics of the Parkinsonian striatal microcircuit: entrainment into a dominant network state. *J Neurosci* 30(34):11326 –11336.

[5] Carrillo-Reid L. et al. (2011). Dopaminergic modulation of the striatal microcircuit: receptor-specific configuration of cell assemblies. *J Neurosci* 31(42):14972–14983.

[6] Chiappalone M. et al. (2005). Burst detection algorithms for the analysis of spatio-temporal patterns in cortical networks of neurons. *Neurocomp* 65–66:653–662.

[7] Van der Maaten LJP. et al. (2009). Dimensionality Reduction: A Comparative Review. *Tilburg University Technical Report*, TiCC-TR 2009-005.

Frequency analysis of developmental experiments

Ricardo Camargos Lopes[1], Suelen Moreira Marques[1], Joao Batista Destro-Filho[1]

1 School of Electrical Engineering, Federal University of Uberlandia, Uberlandia, Brazil
* Corresponding author. E-mail address: r_camargos@hotmail.com

Abstract
In this work frequency analysis of biological recordings of neuronal cultures, based on multielectrode arrays (MEAs), is presented. Using statistical tools, the main frequencies associated to the raw data and separated segments of spikes, bursts and noise are estimated, as well as the electrical behaviour of these cultures along its life.

1 Introduction

Several tools have been used to analyze signals acquired from the electrical activity of excitable cells, such as heart cells or neural signals, and their relationship with biological phenomena. Among these tools, we can put forward the signal processing of medical exams, such as electrocardiograms and electroencephalograms, and signals from relatively new technologies, such as multi-electrode array (MEA) [1][2][3]. Most approaches of data analysis uses a representation of signal as a function of time, but in designing of systems, is frequently used the domain of frequency, since the main characteristics of the signal are more easily expressed in this domain. While in domain of time there are variations of signal amplitudes over the time, the domain of frequency shows the variations of intensity over the frequency axis.

2 Materials and Methods

Primary cultures of neurons of *Wistar* rats were performed extracting the tissue of embryos at 18 days of gestation. The cultures were plated on a planar microelectrode array consisted of 60 TiN/SiN electrodes, each one with diameter of 30 μm and spacing of 200 μm, distributed in a square array of 8x8 electrodes, excluding corners (*Multichannel Systems, MCS, Reutlingen, Germany*). The signals were amplified in 1200x and sampled with a rate of 10 kHz. The experiment was conducted in a temperature controlled environment, under 37ºC and without administration of drugs, collecting only basal activity, from the 8th day in vitro (DIV) to 88th DIV.

Data analysis was performed using custom software developed in MATLAB© (The Mathworks, Natick, MA, USA). The data were imported in MATLAB from .mcd files (MCD format) and spike detection was performed using the PTSD (Precise Timing Spike Detection) algorithm [4], and the software *Spike Manager* [5], developed in University of Genoa, Italy.

An algorithm was developed to separate segments of spikes, bursts and biological noise (Fig. 1). For this purpose, the user establishes the number of samples before and after each peak (distinguishing one spike), the minimal number of spikes inside a burst and the minimal distance between them, allowing to perform an analysis of these separated components.

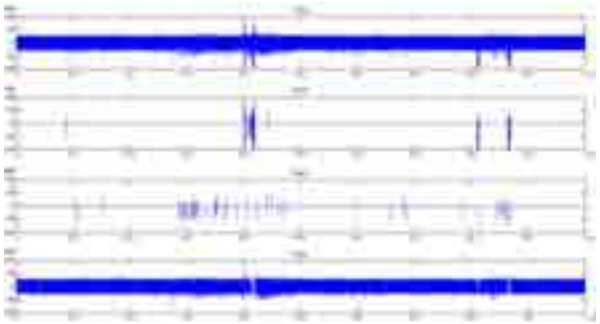

Fig. 1. Separation of raw data (first row) in segments of spikes (third row), bursts (second row) and biological noise (fourth row).

Afterwards, each one of these separated signals, as shown in Fig. 1, are segmented in stationary records by a rectangular window of 0.5 ms and processed by spectral analysis techniques, leading to spectral parameters [1] such as peak frequency [Hz] (the frequency tied to the maximum amplitude of the modulus of the average Fourier transform), median frequency [Hz] (the frequency tied to the average spectral contribution, considering the amplitude of all modules of the Fourier transform) and spectral power [W] (total variance tied to the average Fourier transform). Here “average” considers all the recording time (20 min) and all sixty channels.

3 Results

For each parameter calculated in the 60 channels, averages and standard deviations were estimated, considering the oscillations along the days *in vitro*. Table 1 depicts results on the average values of peak frequencies, which are very similar amongst themselves, within a frequency band of 0 - 0.002 Hz, suggesting that the highest peaks occurs at very low frequencies. In consequence, this parameter is not useful, since it does not enable to make difference be-

tween signals. In addition, the values of median frequencies in raw signal and in segments of noise are very similar. The same remark may be stated in terms of spectral power. Consequently, the signal is composed mainly by noise. Median frequencies of spikes and bursts lie within the range 75 – 110 Hz, respectively. One may conclude that summing up the particular signal power of spikes, bursts and noise lead to the global value of the spectral power in the raw signal.

Parameter	Peak Frequency [Hz]		Median Frequency [Hz]		Spectral Power [W]	
	Mean	Std Dev	Mean	Std Dev	Mean	Std Dev
Raw Signal	0,0012	0,0013	279,15	11,12	44,56	7,43
Spikes	0,00001	0,000065	75,16	14,56	0,05	0,26
Bursts	0,00025	0,0019	109,99	20,07	0,10	0,54
Noise	0,0454	0,0019	280,85	11,01	43,37	9,51

Table 1. Mean and standard deviation values of the peak frequeny, median frequency and spectral power calculated for raw signal, segments of spikes, bursts and noise at DIV 8.

In terms of standard deviations, Table 1 points out that spikes and bursts present the highest frequency variations in terms of median frequency, whereas power variations are much more intensive at segments of biological noise.

During the whole life of this culture, the median frequencies concentrates arount 250 and 350 Hz, with small oscillations, including a standard deviation between 50 and 150 Hz (See Fig.2 and Table 1).

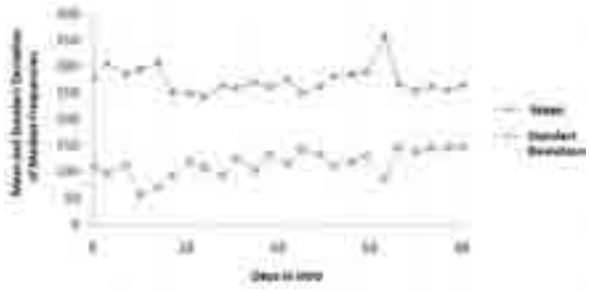

Fig. 2. Average median frequency changements at the raw signal through time.

From Fig. 2, there is a progressive increase of values, attaining its highest amplitude around the 29th day in vitro. As the culture becomes older, its spectral power tends to decrease, reaching in the last day of collected data (DIV88) the spectral power observed in the first day (DIV8).

In (Fig.3) it is shown the average amount of spikes, burst and segments of noise for each day *in vitro*. Notice that the more intensive electrical activity amplitude takes place at DIV29, based in the mean number of spikes and bursts. At DIV67, there was a great reduction of the number of segments, outlining the degeneration process of the culture.

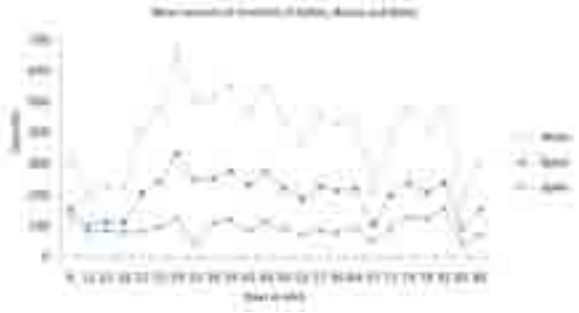

Fig. 3. Mean amount of segments, classified as spikes, bursts and biological noise.

4 Conclusion

In terms of results tied to the median frequency and quantity of segments, it is remarkable that during the first days of life of neuron cultures, these parameters grow progressively, presenting a peak at 29 DIV, attaining their maturation, so that to decrease in the next DIVs. It is also very important to put forward that biological noise plays an important role, since it establishes the median frequency and the spectral power of the raw signal. Moreover, time variations in median frequency are much more intensive at spikes, whereas in terms of spectral power, time variations are more relevant for noise segments.

For future work, we suggest using the tools developed in this work, in particular the separation of qualitative signs MEA signals containing spikes, noise and bursts to perform a more detailed analysis about the behavior of each one of these signals. Concurrently, it is desirable to carry out a detailed study on the physiological processes involved in the activity of these cultures in order to obtain a better understanding of the behavior of these cultures and their relation to neuronal activities.

Acknowledgements

Authors would like to thank CNPq (Brazilian National Research Council) for funding this work, as well as Prof Sergio Martinoia for enabling signal recording at Genoa University, as well as to Danilo R Campos (UFMG) for performing all experimentations.

References

[1] Akay, M (1997). *Time Frequency and Wavelets in Biomedical Signal Processing*. New York, USA, 739 pp.

[2] Akay, M (2003). Nonlinear biomedical signal processing. Prentice-Hall Inc, USA, 356 pp.

[3] Rangayyan, R. M. (2001) Biomedical Signal Analysis. Piscataway, NJ. 325 pp.

[4] Maccione A, Gandolfo M, Massobrio P, Novellino A, Martinoia S, Chiappalone M. A. (2009) novel algorithm for precise identification of spikes in extracellularly recorded neuronal signals. J Neurosci Methods;177:241–9.

[5] Vato A, Bonzano L, Chiappalone M, Cicero S, Morabito F, Novellino A, and Stillo G. (2004) Spike Manager: a new tool for spontaneous and evoked neuronal networks activity characterization. *Neurocomputing* 58-60: 1153-1161.

SONAR: Framework for sharing MEA analysis tools and recordings

Marijn Martens1* , Dirk Schubert2, Paul Tiesinga1

1 Neuroinformatics, Donders Institute for Neuroscience, Radboud University Nijmegen, Nijmegen, The Netherlands
2 Cognitive Neuroscience, Donders Institute for Neuroscience Radboud University Nijmegen, The Netherlands
* Corresponding author. E-mail address: marijn.martens@science.ru.nl

Abstract
To improve transparency and reproducibility of data analysis of multi electrode recordings, we developed the SONAR (Sharing Of Neuronal Analysis Routines) framework. The aim of this framework is to facilitate sharing of data analysis tools. SONAR is a hybrid framework that uses scripted routines for fast and robust data processing, combined with a graphical user interface (GUI) to assess the quality and structure of the data. It consists of four Matlab® modules: (1) scripted electrode selection and stimulation, producing a configuration file that aids the structuring of the data set, (2) scripted data loading and analysis, (3) GUI data visualization, and (4) data simulation module, which simulates neuronal culture data in a format identical to the recorded data, allowing application of the same analysis routines.
Eventually SONAR aims to include complex functions to perform non-linear analysis of multivariate time series, and to further stimulate theoretical researchers to share their routines with experimentalists, and give experimentalists an easy way to share data with theoretical groups.

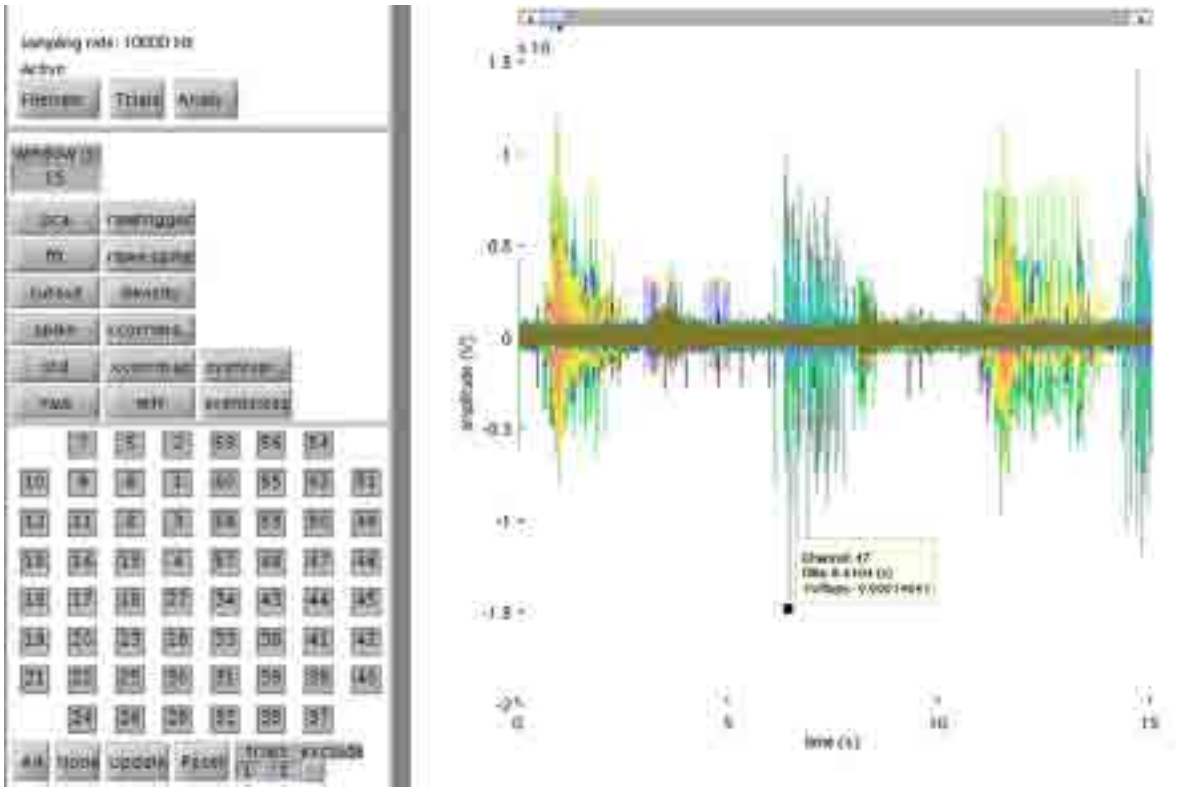

Figure. 1. The SONAR GUI allows for easy assessment of the quality and structure of the data

1 Introduction

Multidimensional electrophysiological data requires a robust (pre)processing as well as flexible routines to extract details specific to each experiment. Although commercially available data analysis tools (e.g. MC_Rack from Multi Channel Systems) are sufficient for basic analysis, they are not easily extended. There are powerful analysis software packages available (GUI based SPYCODE [1], open-source toolbox FIND [2], as well as unix based MEABench [3]). The advantage of GUI-based analysis packages is that they are generally easy to comprehend. However, to exchange (processed) data between labs, it is often difficult to reproduce the analysis steps. Inspired by Fieldtrip [4], SONAR is developed with five basic ideas in mind: (1) scripted analysis which is easily extendible, (2) any analysis function should be easily replaceable or incorporated in a analysis pipeline, (3) analysis configuration options are stored within the data structure, (4) a GUI should be used to browse through the data, but not perform any data processing, (5) the configuration file from the experimental recordings could assist the data analysis and structuring.

Diagram 1. The four modules SONAR modules.

SONAR consists of four modules (diagram 1). The first module can be used for scripted electrode selection and stimulation. Through MATLAB the analog and sync outputs of the Multi Channel Systems Stimulus generator can be controlled. The configuration file from the first module can be used to assist the structuring of the data, which is then processed in module two.

Module two contains processing functions in a scripted way (Figure 2). The resulting data structure can be browsed through in module three. This module allows for easy addition of new visualization functions. The last module simulates data in a format used by the analysis modules.

```
cfg.channels     = 1:60;
cfg.trial        = 1;
cfg.layout       = 'MEA60_200_30';
data             = sonar_mcd2matlab(filename);
data             = sonar_matlab2sonar(cfg,data);
data             = sonar_triggerdataext(cfg,data);

cfg.filtertype   = 'highpass';
cfg.filterdesign = 'butterworth';
cfg.filterfreq   = 300;
data             = sonar_filter(cfg,data);
data             = sonar_fft(cfg,data);
data             = sonar_spikedetect(cfg,data);

cfg.sigmagauss   = 0.010;
data             = sonar_spikedensity(cfg,data);
data             = sonar_princcomp(cfg,data);

cfg.eventthrshld = 3;
data             = sonar_spikesinevent(cfg,data);

cfg.xcorrdelay   = 0.002;
cfg.xcorrwindow  = 0.005;
data             = sonar_xcorr(cfg,data);
```

Figure 2. Example scripted data analysis in SONAR.

2 Results

SONAR is a hybrid analysis framework that combines the flexibility of scripted analysis with the accessibility of a GUI interface. SONAR works cross-platform (Linux, MAC, Windows), uses only SI unit (seconds, volts, etc.), loads all available MEA chip configurations, and uses a standard format for the function calls. This hybrid approach allows for high volume data throughput as well as flexibility in sharing data analysis routines.

Acknowledgement

We would like to thank Michela Chiappalone for hosting us and valuable data-analysis discussions.

References

[1] Bologna LL, Pasquale V, Garofalo M, Gandolfo M, Baljon PL, Maccione A, Martinoia S, Chiappalone M. *Investigating neuronal activity by SPYCODE multi-channel data analyzer.* Neural Netw. 2010 23(6):685-97.

[2] Meier R, Egert U, Aertsen A, Nawrot MP (2008) *FIND--a unified framework for neural data analysis.* Neural Netw. 21(8):1085-93.

[3] Wagenaar DA, DeMarse TB, POTTER SM (2005) *MEABench: A Toolset for Multi-electrode Data Acquisition and Online Analysis.* Proc. 2nd Int. IEEE EMBS Conf. Neural Eng. 518–521

[4] Oostenveld R, Fries P, Maris E, Schoffelen JM (2011) *FieldTrip: Open Source Software for Advanced Analysis of MEG, EEG, and Invasive Electrophysiological Data.* Computational Intelligence and Neuroscience.

New Materials and MEA Design

Nanomembrane electronics enable minimally-invasive cardiac electrophysiological mapping

Roozbeh Ghaffari[1], Dae Hyeong Kim[2,3], Nanshu Lu[4], Stephen Lee[1], Yung-Yu Hsu[1], Clifford Liu[1], John Rogers[2]

1 MC10 Inc., Cambridge, MA. USA
2 Department of Materials Science, University of Illinois Urbana Champaign, Urbana, IL. USA
3 Department of Chemistry and Bioengineering, Seoul National University, Seoul, South Korea
4 Department of Aerospace Engineering and Engineering Mechanics, University of Texas at Austin, Austin, TX. USA

1 Background/Aims

Critical biological processes operate at the nano- and microscale levels, whereas most present-day medical instruments are limited to interactions with biological structures in the millimeter regime. This spatial mismatch (>10^3) is pervasive in many areas of medicine. In cardiology, electrophysiological instruments, such as pacemakers and ablation catheters contain many orders of magnitude fewer stimulating electrodes than there are addressable cardiomyocytes in the heart (10^1 electrode channels vs 10^9 cells). The current generation of cardiac medical devices is largely limited to electrical sensing, with no feedback on mechanical or physicochemical properties. In addition to density and modality mismatches, there is a significant incompatibility in mechanical properties between devices and soft, deformable tissues of the heart. Development of devices capable of intimate, conformal integration with biological structures for applications ranging from basic measurements of electrophysiological signals to delivery of advanced therapy thus requires new classes of medical instruments (1, 2).

2 Methods

2.1 Balloon catheter sensor fabrication

Fabrication of stretchable electrode arrays on balloons (7) starts with spin coating of thin polyimide film (PI, ~1.2 μm) after coating a sacrificial layer of poly(methylmethacrylate) (PMMA, 100 nm), on a handling wafer. Metal evaporation for adhesion layer and electrode (Cr/Au, 5 nm/150 nm) and following photolithography and wet etching define metal electrodes with serpentine-shaped interconnection. Top insulation layer is formed by additional PI spin coating. The stretchable shape is formed by oxygen reactive ion etching (RIE). After transfer printing to the 3D surface of a balloon catheter, anisotropic conductive film (ACF) is connected for external wiring to the data acquisition system.

2.2 Cardiac sheet sensor fabrication

The fabrication of sensor sheets starts with spin coating of polyimide (PI, ~1.2 μm, Sigma Aldrich, USA) onto a film of poly(methylmethacrylate) (PMMA, 100 nm, MicroChem, USA) cast on a silicon wafer. Electron beam evaporation forms an adhesion layer and metallization for electrodes and interconnects (Cr/Au, 5 nm/150 nm), defined into appropriate patterns by photolithography and etching. A second, top layer of PI (~1.2 m) insulates the system and places the metal near the neutral mechanical plane in the PI/metal/PI stack. The open web design results from etching through the entire thickness of this trilayer with oxygen reactive ion etching (RIE) in a patterned defined by photolithography. Dissolving the PDMS releases a free-standing web that is transfer printed to a silk substrate, and then connected to an anisotropic conductive film (ACF) for interfacing to a data acquisition system, thereby completing the fabrication.

2.3 Fabrication of temperature sensor and strain gauge webs

The designs and fabrication procedures are similar to those described above. The temperature sensing web uses platinum resistors at the locations of the islands. Here, thin layers of Ti/Pt (5 nm/50 nm) deposited by electron beam evaporation and patterned by photolithography and lift-off define the sensors. Surface treatment of the PI with UV/Ozone or deposition of a thin silicon dioxide (SiO_2) layer (~50 nm) on top of PI improves the adhesion of the Ti/Pt. Fabrication of strain gauge rosettes relies on transfer printing of boron-doped (doping concentration ~ 5×10^{18} /cm^3), 340nm-thick silicon resistors onto the island regions. Both sensors use serpentine interconnects of Cr/Au. Additional encapsulation with PI prevents electrical leakage currents, and places the components near the neutral mechanical plane. Transfer printing the mesh to silk and establishing ACF connections completes the process.

The fabrication process for strain, temperature and pressure sensors is identical to the stretchable

electrode array processing with one important exception. Flexible printed circuit boards were connected to the sensor arrays using anisotropic conductive epoxy through the application of heat (175° C) and pressure. The ribbons and wires were then insulated with thin-walled heat shrink to provide water-proof encapsulation.

2.4 Data acquisition systems

The data acquisition system consists of an electrophysiological mapping module and a temperature/strain/pressure sensing module. A MMBT4403 PNP transistor is placed in the feedback path of the AD8671 operational amplifier to create a voltage-controlled current source. The excitation current from the current source passes through tissue to generate a voltage, which is then measured with a National Instruments PXI-6289 data acquisition card. Custom LabView software was written to control the output current and frequency of the excitation current. For the experiment, the excitation current is set at 10 µA and measurements were taken at 1 kHz and 10 kHz.

3 Results

Mapping electrical activity of the heart is critical for diagnosing and treating complex arrhythmias. Existing approaches use single-point electrical mapping catheters while newer systems exploit arrays of electrodes integrated on catheter-type delivery systems (Fig. 1a-d) and balloon-based substrates that emit ablative energy (Fig. 1e-g) (7). The devices in Fig. 1a-d contain electrodes that are millimetre-scale in size and spaced a few millimetres apart. In all cases, clinical procedures involve the measurement of electrical potentials in a point-by-point, manual fashion, from locations within the ostium of the pulmonary veins and within the atria. Positioning these catheters within the cardiac chambers requires significant time and dexterity, often leading to inconsistent outcomes across patients (1-3). Furthermore, several sequential therapeutic procedures, such as ablation, followed by cycles of electrical mapping are required to produce a representation of electrical activity over a large region of interest.

Advances in stretchable electronics enable integration of conformal sensors on balloon substrates deployable on a single, multi-functional instrumented catheter platform (7). A representative example of a device of this type is shown in Fig. 2. Electrodes for electrical mapping integrate on the balloon surface with the types of serpentine interconnects described previously (5-8) (Fig. 2a,b). Fig. 2c shows temperature sensors and stretchable arrays of micro-light emitting diodes (LEDs) with the balloon in deflated and inflated states. Electrogram recordings from an inflated balloon substrate positioned in direct mechanical contact with a live porcine heart are presented in Fig. 2d. This mode of operation is particularly useful for balloon ablation catheters, where assessment of ablation can be achieved quickly, without the need for separate diagnostic devices. In addition to electrical and temperature sensors, contact sensors and stimulation electrodes (Fig. 2e) are also supported on this platform. Contact sensors can report the moment when the balloon skin and endocardial tissue touch, thereby providing important feedback (without x-ray imaging or contrast dye injection) on how to adjust and manoeuver inflated balloons to achieve optimal occlusion of the pulmonary veins during ablation procedures.

More advanced bio-integrated mapping systems have been demonstrated (1,2,4,9) to allow conformal contact with the anterior surface of the heart. Here, high-density electrodes enable electrophysiological mapping with both high spatial and temporal resolution. Figure 3a,b shows images of a stretchable mapping array with electrodes that can adhere to anterior ventricular sections of the heart through surface tension forces alone, without penetrating pins or separate adhesives. In addition to electrical mapping (Fig. 4a,b), strain gauges (Fig. 4c-e) and temperature sensors (Fig. 4f-i) with similar designs can be used to map thermal activity and mechanical deformations during ablation and surgical procedures. Key demonstrated advantages of the sheet-based sensors include: (i) heterogeneous integration of sensors for measuring electrograms, strain and temperature data; (ii) high density arrays for microscale mapping of complex arrhythmias like persistent atrial fibrillation; and (iii) ultrathin profiles to allow soft, conformal interfaces with biological tissue in the heart.

4 Conclusion/Summary

The materials and mechanics concepts introduced here represent a technology foundation for advanced, minimally invasive surgical and diagnostic tools, with demonstrated examples in diagnosing and resolving complex arrhythmogenic disease states of the heart. These devices constitute significant advances over existing balloon and multielectrode catheters in mechanical properties, the number of sensing modalities and the spatial density of sensors. Use of such 'instrumented' catheters in live animal models illustrates their specific utility in cardiac ablation therapy.

References

[1] Calkins H, *et al* (2007) HRS/EHRA/ECAS expert consensus statement on catheter and surgical ablation of atrial fibrillation: Recommendations for personnel, policy, procedures and follow-up. *Europace* 9: 335-379.

[2] Calkins H, *et al* (2012) HRS/EHRA/ECAS expert consensus statement on catheter and surgical ablation of atrial fibrillation: Recommendations for patient selection, procedural techniques, patient management and follow-up,

definitions, endpoints, and research trial design. *Heart Rhythm Society* 9: 632-718.
[3] Dewire J & Calkins H (2010) State-of-the-art and emerging technologies for atrial fibrillation ablation. *Nat Rev Cardiol* 7: 129-138.
[4] Friedman P (2002) Novel mapping techniques for cardiac electrophysiology. *Heart* 87: 575-582.
[5] Kim D, *et al* (2008) Stretchable and foldable silicon integrated circuits. *Science* 320: 507-511.
[6] Kim D, *et al* (2010) Dissolvable films of silk fibroin for ultrathin conformal bio-integrated electronics. *Nat Mater* 9: 511-517.
[7] Kim D, *et al* (2011) Materials for multifunctional balloon catheters with capabilities in cardiac electrophysiological mapping and ablation therapy. *Nat Mater* 10: 316-323.
[8] Kim D, *et al* (2011) Epidermal electronics. *Science* 333: 838-843.
[9] Packer D (2004) Evolution of mapping and anatomic imaging of cardiac arrhythmias. *J Cardiovasc Electrophysiol* 15: 839-854.
[10] Viventi J, *et al* (2010) A conformal, bio-interfaced class of silicon electronics for mapping cardiac electrophysiology. *Science Translational Medicine* 2: 24ra22.
[11] Viventi J, *et al* (2011) Flexible, foldable, actively multiplexed, high-density electrode array for mapping brain activity in vivo. *Nat Neurosci* 14: 1599-U138.

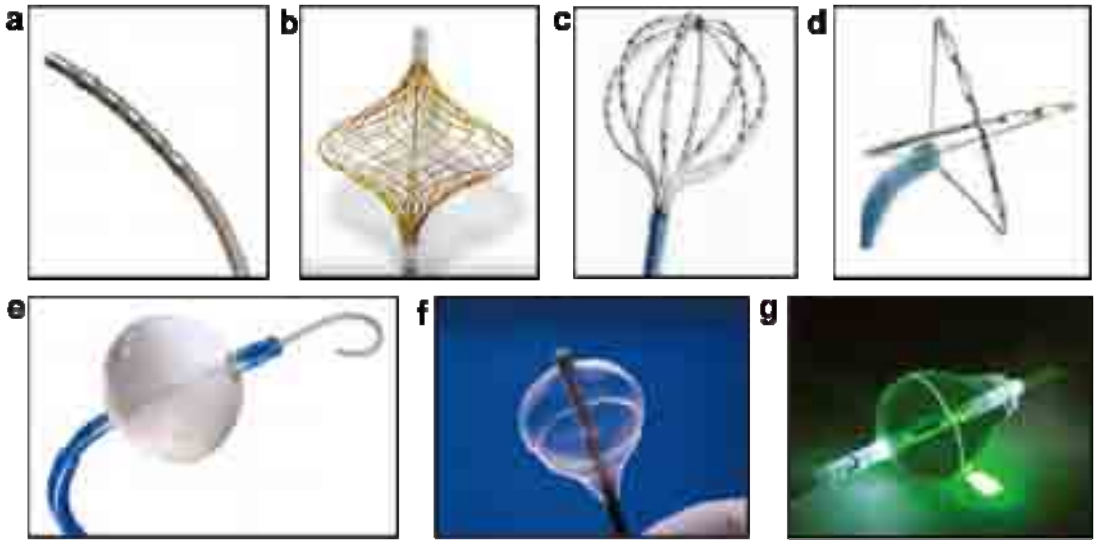

Figure 1. Existing classes of electrode-based (a-d) and balloon-based (e-g) cardiac ablation devices.

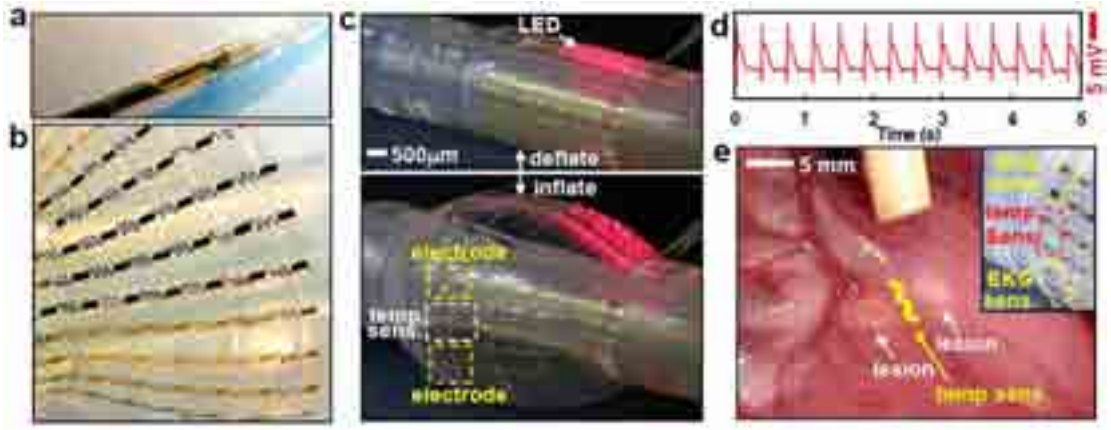

Figure 2. Multifunctional balloon catheter.

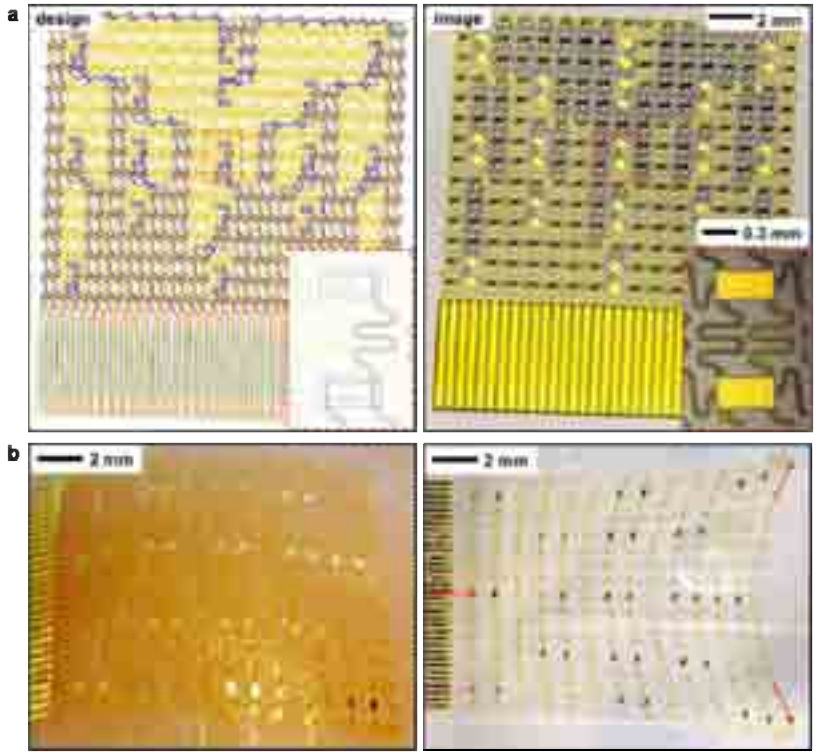

Figure 3. Sheet based sensors for mapping electrical activity in live heart

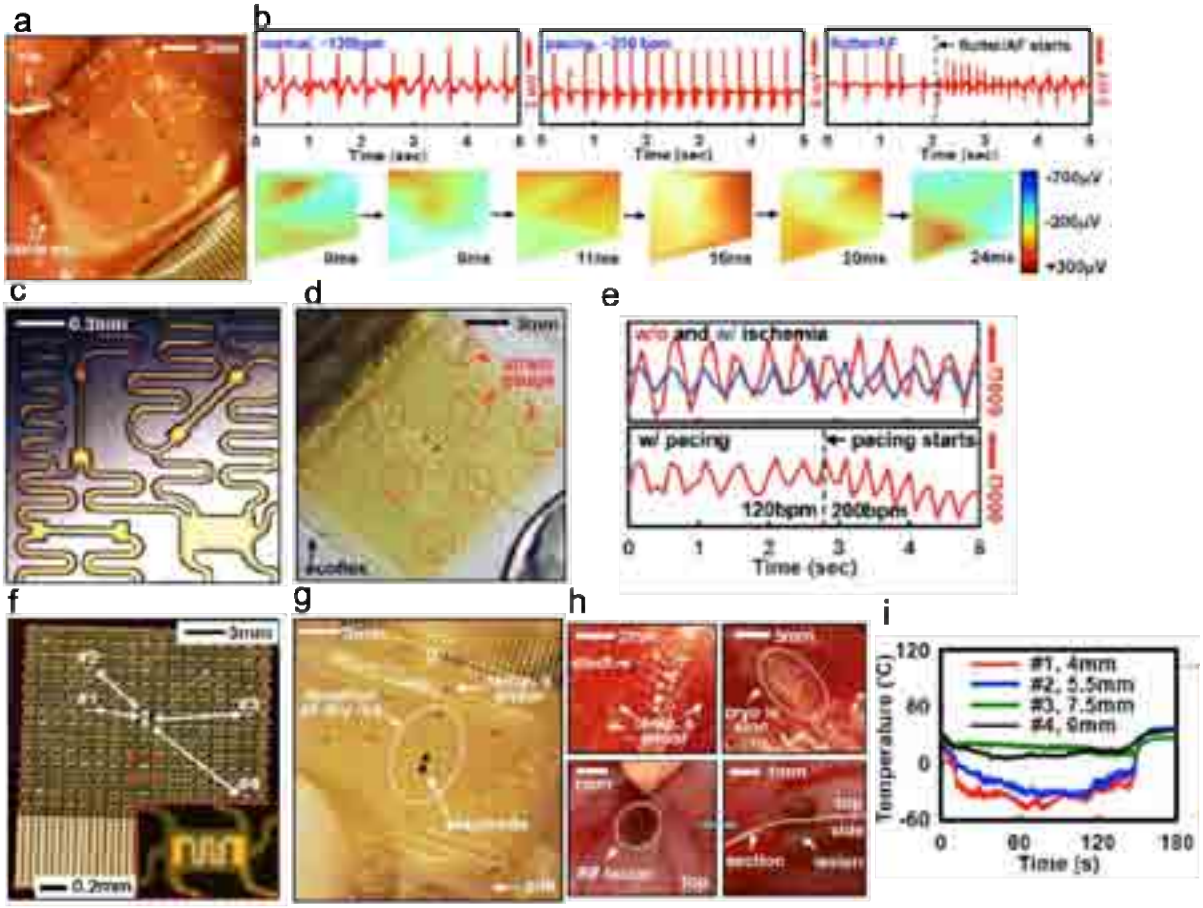

Figure 4. Epicardial web sensor electrogram, strain and temperature results collected in live rabbit models.

Using Conductive-PDMS to produce stretchable multi-electrode array for epidural electrical stimulation of paralyzed rats

Alexandre Larmagnac[1,2], Niko Wenger[2], Pavel Musienko[2], Janos Voeroes[1], Grégoire Courtine[2]

1 Laboratory of Biosensors and Bioelectronics, ETH Zurich, Switzerland
2 UPCOURTINE, Brain Mind Institute, EPFL, Switzerland

Abstract
Individuals who remain permanently paralyzed after a SCI represent 50% of the total human disabled population. Consequently, there is a critical need to improve rehabilitative strategies to help these patients to regain the ability to stand or step. We recently demonstrated the impressive capacity of pharmacological and electrical spinal cord stimulations to promote full weight bearing walking in paralyzed rats when combined with rehabilitation [1]. Specifically, we showed that epidural electrical stimulation (EES) applied at S1, L4, or L2 spinal segments could each promote unique patterns of locomotion, which were biased toward flexion when stimulating upper lumbar segments and toward extension when stimulating the sacral level. Next, we revealed that the combination of two, and even more efficiently three, sites of EES promoted clear synergistic facilitation of stepping in paralyzed rats [2]. Together, these results suggest that multi-site EES strategies would enable a finer control of locomotion after a SCI than currently possible with existing stimulation paradigms. However, no systematic studies on the potential benefit of multi-site EES have been conducted so far, largely because of the lack of interfaces for the concurrent stimulation of multiple spinal cord locations. Here, we present a novel neuroprosthetic multi-electrode array (MEA) for multi-site EES in vivo.

1 Methods

Our MEAs have been designed to be implanted epidurally and act as a second biocompatible skin that bends with the spinal cord. They have to survive large mechanical stresses caused by the relative movements between the spine and the back muscles or soft connective tissues (Figure 1). These mechanical deformations should be reduced by designing the MEAs andimplanting them adequately (Figure 2). It is also necessary that the electrodes positions remain stable over time to stimulate in a controlled manner. The stimulating platinum electrodes should be capable of delivering sufficient electrical charges to recruit neural structures while avoiding tissue damage. The MEAs are made of conductive PDMS tracks embedded in PDMS and connected to an external stimulator via medical fine wires and connector. A custom-made fatigue test machine is used to evaluate the performances of the MEAs prior to implantation. The effects of different stresses on the electrical properties of the MEAs were also investigated.

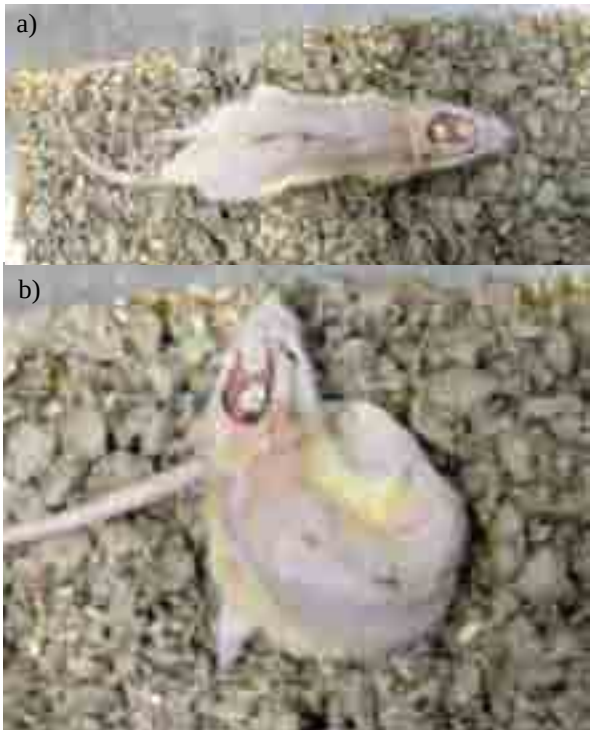

Figure 1: Pictures of a freely behaving rat implanted with our stretchable MEA in a a) normal position and b) bending position with the spine forming a closed circle.

Figure 2: CT scans of an implanted device. The S-loop that corresponds to the part of the MEA entering the spinal canal is visible on the left. We believe this is damaging the MEA.

2 Results

The elastic properties of conductive silver-PDMS promote stretchability to the implant. Such MEAs can be deformed to high strain while maintaining electrical conductivity. They also resist well to fatigue and recover their initial properties whenever the applied stress is removed (Figure 3).

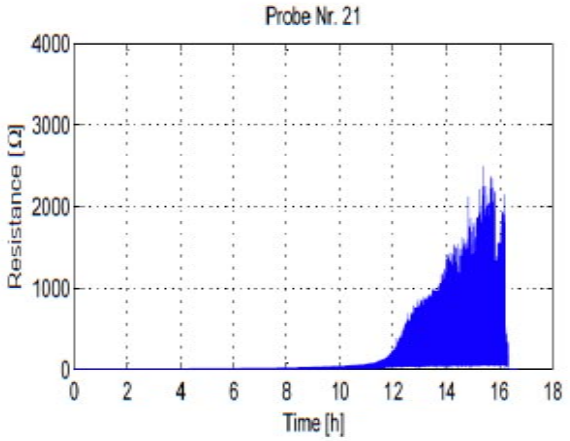

Figure 3: Fatigue test of a 50mm x 4mm x 80 m conductive PDMS probe stretched 25% at a speed of 1mm/s. The value of the resistance was initially around 10Ω and remains stable after 10 hours (~2000cycles). The increase of the resistance after 10 hours may be due to the clamps that are slowly damaging the probe.

Preliminary testing in rats with chronically implanted MEA over lumbosacral segments showed no sign of inflammation and preserved implant integrity up to 8 weeks after surgery. As early as 1 week after a complete spinal cord transection, EES applied at the various electrodes of the MEA could encourage continuous locomotion on the treadmill. CT scans and post-explantation measurements suggest that the part of the MEA entering the spinal canal is damaged by some sharp aspects of vertebrae and should be more resistant. Moreover, we found how to parameter pulsed currents in order to avoid tissue damage in vitro [3].

3 Conclusion

Using the results in vivo and the electromechanical properties of the conductive PDMS, we are now optimizing the surgical technique and the design of the MEAs. We will investigate the potential of multi-site EES to encourage weight bearing locomotion in paralyzed spinal rats, and to improve the functional outcomes of neurorehabilitative locomotor training.

Acknowledgements

This project was financed by the ETH Zurich, the NCCR Neural Plasticity and Repair and the "NEU-Walk" project of the European Union FP7 program.

References

[1] Courtine et al. (2009). Transformation of nonfunctional spinal circuits into functional states after the loss of brain input. *Nature Neuroscience*, 12, 10, 1333-U167.

[2] Musienko et al. (2009). Combinatory Electrical and Pharmacological Neuroprosthetic Interfaces to Regain Motor Function After Spinal Cord Injury. *IEEE Transactions on Biomedical Engineering*, 56, 11, 2707-2711.

[3] Gabi et al. (2009). Influence of applied currents on the viability of cells close to microelectrodes. *Integrative Biology*, 1, 1, 108-115.

Neural electrical activity measurements of isolated axons using multi-electrode arrays

Johann Mika[1], Andreas Amon[1], Karin Schwarz[2], Maximilian Stanger[2], Jianqiu Kou[2], Heinz D. Wanzenboeck[1*], Sigismund Huck[2] and Emmerich Bertagnolli[1]

1 Institute for Solid State Electronics, Vienna University of Technology, Vienna, Austria
2 Center for Brain Research, Medical University of Vienna, Vienna, Austria
* Corresponding author. E-mail address: heinz.wanzenboeck@tuwien.ac.at

Abstract
Extracellular recording of neural activities is a powerful tool in neuroscience to investigate the communication within neural cell cultures. The extensive and complex wiring in cell cultures makes it very difficult to observe and analyze neural electrical behavior of individual neurons. We present a versatile platform that allows direct electrical measurement of extracellular potentials originating not from neuronal networks but from isolated axons from dissociated neural cell cultures. The platform consists of a microstructured axon isolation device (AID) aligned and mounted atop of a microelectrode array (MEA). This setup facilitates specific electrical recording of neural activity of well-identifiable axons. The proof of isolated axon growth was performed with sympathetic neurons from the superior cervical ganglion of P5 WT mice [3] grown on the AID-MEA platform. Due to the transparent structure of the device, electrical recordings could be correlated with the optical observations. The benefit of the presented approach is the capability to design the whole platform to the requirements of the experiment. The presented platform will facilitate neurological studies where axons and somata can be treated independently of each other.

1 Introduction

Extracellular recordings are powerful tools to monitor the wiring of populations of neurons. The propagation of action potentials in single neurons can be recorded using the patch clamp technique which measures the intracellular potential [1] [2] whereas measuring the extracellular potential using CMOS based [3] [4] and planar [5] [6] [7] [8] microelectrode arrays allows the enhancement of the point of view to the whole network. A disadvantage of the CMOS technique is the non-transparent behaviour for optical light. Hence, transmitted-light microscopy is not possible with CMOS sensors [9].

To investigate the behaviour of neural cell cultures, it is necessary to reduce the complexity of neural wiring. The controlled growth of neural cell cultures can be performed by microcontact printing [10] [11] and by the use of microfluidic structures [12] [13] [14]. Microfluidic structures in contrast to microcontact printing allow a specific treatment of a cell culture.

The combination of microelectronic and microfluidic concepts enables to specifically record neural activities of neurons and neural networks. Furthermore, this combination allows for precise control and for manipulation of the cellular environment. Takeuchi et al developed a microfluidic platform positioned atop a microelectrode which allows the recording of action potentials of dissociated neural cell cultures and ventricular myocytes [15]. The detection of action potentials in axons was shown by Dworak et al, with the disadvantage, that the electrodes were conducted to all microchannels [16].

In this work we present a culture platform, the "Axon Isolation Microelectrode System" (AIMS) which allows the isolation of axons from the soma (axon isolation device, AID) positioned on top of a microelectrode array (MEA). The MEA was tailored to the design of the AID to enable the specific recording of action potentials in the axons. The goals of AIMS are (1) the development and fabrication of a platform combining the guiding structure (AID) and the measurement structure (MEA); and (2) perform the proof of concept with neurons from the superior cervical ganglion, which are innervating target organs.

2 Methods

2.1 Fabrication of Axon Isolation Device (AID)

The design of the upper part follows the design of Taylor et al [13]. It consisted of four reservoirs which acted as buffer for the culture medium (Figure 1). Each two of the reservoirs were connected by macrochannels. One macrochannel was used to seed the dissociated neurons onto the platform. The second macrochannel was connected to the first one by 35 microchannels. These microchannels acted as physical barriers for the soma and enabled only axons to pass through into the second macrochannel.

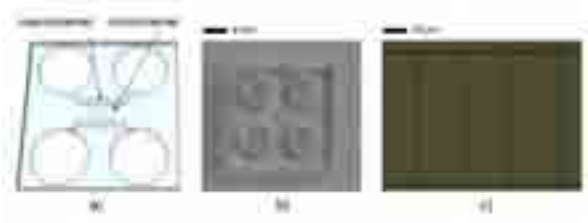

Fig. 1. Axon Isolation Device (AID). a) Concept of the AID, consisting of 4 reservoirs linked on the bottom side by 2 macrochannels, which are connected with the microchannels. b) Image of the final device fabricated in PDMS with the 4 reservoirs. c) Microscopic image of microchannels connecting the two macrochannel.

2.2 Fabrication of Microelectrode Array (MEA)

The lower part of the AIMS is made on a glass substrate which fits the recording setup. The MEA consists of 60 gold electrodes (Figure 2). Each microchannel was equipped with a microelectrode (35 µm x 35 µm) and the residual 25 electrodes (diameter 100 µm) were placed in one macrochannel.

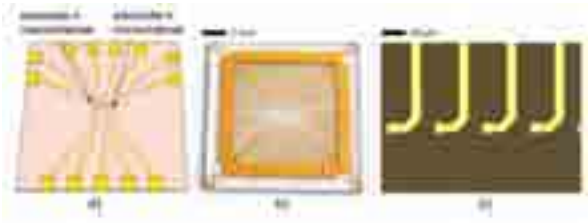

Fig. 2. Multielectrode Array (MEA). a) Concept of the MEA, consisting of 35 microchannel electrodes and 25 macrochannel electrodes. b) Image of the MEA with 60 gold electrodes. c) Microscopic image of microchannels electrodes.

2.3 Fabrication of culture platform

The culture platform (AIMS) was formed out of the two components, the AID and the MEA. The microchannels were positioned accurately on top of the microelectrodes to allow the recording of neural signals from axons (Figure 3). A tight seal between the AID and the MEA was obtained by an oxygen plasma treatment.

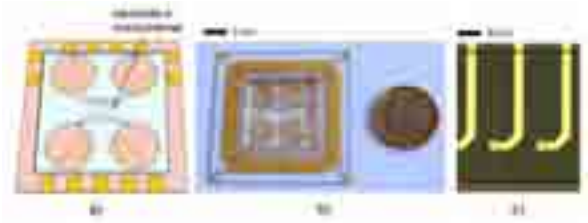

Fig. 3. Multielectrode Array (MEA). a) Concept of the MEA, consisting of 35 microchannel electrodes and 25 macrochannel electrodes. b) Image of the MEA with 60 gold electrodes. c) Microscopic image of microchannels electrodes.

2.4 Preparation of cell culture

Superior cervical ganglia were dissected from 5-day-old mouse pups. The ganglia were dispersed to single cells, and plated as previously described [17] [18].

2.5 Preparation of culture platform and cell seeding

The culture platform was coated with poly-D-lysine, followed by laminin. Approximately 10.000 cells were seeded into one reservoir. For recording the extracellular potential, cells were cultured in an incubator for 3 days. After 2 days, the culture medium was removed from each reservoir and replaced with fresh culture medium.

2.6 Preparation for extracellular recording

The culture medium in the reservoirs was exchanged by a bathing solution. Further, two solutions containing bathing solution and nicotine to initiate neural cell activities as well as buffer solution and tetrodotoxin were prepared inhibit neural cell activities.

The detected neural signals were recorded and analyzed using a MEA1060-Up amplifier with the software MC_RACK (Multichannel Systems, Germany).

3 Results

3.1 Optical investigation

The transparent characteristic of the device enables optical investigations of cell cultures by both conventional light and fluorescence microscopy. With the AIMS it is possible to link the monitored nerve cells in culture with the electrical behaviour of the neural network. Figure 4 shows neurons from the superior cervical ganglion of P5 rats that were cultured for 5 days. Note the neurites invading the microchannels.

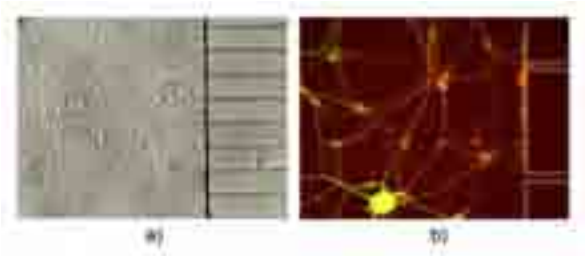

Fig. 4. AIMS with cultured neurons, macrochannels (left) and microchannels (right) a) Bright field microscopy of cultured neurons. The cell bodies adhere in the macrochannel of the fabricated platform. b) Fluorescence microscopy of cultured neurons (SMI31 and MAP2). Only neurites can enter the microchannels.

3.2 Electrical Characterization

Electrical signals originating from neurons were recorded using the AIMS. The signals were detected by the electrodes and then amplified and filtered by the Multichannel Systems measurement setup. The signals were investigated with the analysis software

provided. With the developed platform it was possible to successfully detect spike signals.

Fig. 5. Electrical recordings were performed three days after plating the cells onto the device. The AIMS was connected to a MCS measurement setup for recordings of neural electrical activities. Action potentials originating from neurites in a microchannel with amplitudes in the range of 100 µV and a duration of approximately 4 ms were detected.

4 Conclusions & Discussion

The developed platform allows for the separation of axons from the cell body utilizing artificial microchannels. The presented approach enables the simultaneous detection of action potentials with a high spatial and temporal resolution. The geometry of the axon isolating device facilitates biochemical and neurological studies where axons and cell bodies can be treated independently of each other. The used techniques provide further potential to develop and fabricate highly diverse channel geometries.

References

[1] Fertig N., Blick R.H., Behrends J.C. (2002). Whole Cell Patch Clamp Recording Performed on a Planar Glass Chip. *Biophysical Journal*, 6, 3056-3062.

[2] Stett A., Burkhardt C., Weber U., van Stiphout P., Knott T. (2003). Cytocentering - a novel technique enabling automated cell-by-cell patch clamping with the Cytopatch chip. *Receptors and Channels*, 9, 59-66.

[3] Frey U., Egert U., Heer F., Hafizovic S., Hierlemann A. (2009). Microelectronic system for high-resolution mapping of extracellular electric fields applied to brain slices. *Biosensors and Bioelectronics*, 24, 2191-2198.

[4] Eversmann B., Lambacher A., Gerling T., Kunze A., Fromherz P., Thewes R. (2011). A neural tissue interfacing chip for in-vitro applications with 32k recording / stimulation channels on an active area of 2.6mm² *European Solid-State Circuits Conference*, 211-214.

[5] Charvet G., Rousseau L., Billoint O., Gharbi S., Rostaing J.-P., Joucla S., Trevisiol M., Bourgerette A., Chauvet P., Moulin C., Goy F., Mercier B., Colin M., Spirkovitch S., Fanet H., Meyrand P., Guillemaud R., Yvert B. (2010). BioMEA - A versatile high density 3D microelectrode array system using integrated electronics. *Biosensors and Bioelectronics*, 25, 1889-1896.

[6] Kim J.H., Kang G., Nam Y., Choi Y.-K. (2010). Surface-modified microelectrode array with flake nanostructure for neural recording and stimulation. *Nanotechnology*, 21.

[7] Hofmann B., Kätelhön E., Schottdorf M., Offenhäusser A., Wolfrum B. (2011). Nanocavity electrode array for recording from electrogenic cells. *Lab on a Chip*, 11, 1054-1058.

[8] Gabriel G., Gómez R., Bongard M., Benito N., Fernández E., Villa R. (2009). Easily made single-walled carbon nanotube surface microelectrodes for neuronal applications. *Biosensors and Bioelectronics*, 24, 1941-1948.

[9] Hierlemann A., Frey U., Hafizovic S., Heer F. (2011). Growing Cells Atop Microelectronic Chips: Interfacing electrogenic cells in vitro with CMOS-based microelectrode arrays . *Proceedings of the IEEE, 99*, 252-284.

[10] James C.D., Davis R., Meyer M., Turner A., Turner S., Withers G., Kam L., Banker G., Craighead H., Isaacson M., Turner J., Shain W. (2000). Aligned microcontact printing of micrometer-scale poly-L-lysine structures for controlled growth of cultured neurons on planar microelectrode arrays. *IEEE Transactions on Biomedical Engineering*, 47, 17-21.

[11] James C.D., Spence A.J.H., Dowell-Mesfin N.M., Hussain R.J., Smith K.L., Craighead H.G., Isaacson M.S., Shain W., Turner J.N. (2004). Extracellular recordings from patterned neuronal networks using planar microelectrode arrays. *IEEE Transactions on Biomedical Engineering*, 51, 1640-1648.

[12] Taylor A.M., Blurton-Jones M., Rhee S.W., Cribbs D.H., Cotman C.W., Jeon N.L. (2005). A microfluidic culture platform for CNS axonal injury, regeneration and transport. *Nature Methods*, 2, 599-605.

[13] Millet L.J., Stewart M.E., Nuzzo R.G., Gillette M.U. (2010). Guiding neuron development with planar surface gradients of substrate cues deposited using microfluidic devices. *Lab on a Chip*, 10, 1525-1535.

[14] Hosmane S., Yang I.H., Ruffin A., Thakor N., Venkatesan A. (2010). Circular compartmentalized microfluidic platform: Study of axon-glia interactions. *Lab on a Chip*, 10, 741-747.

[15] Takeuchi A., Nakafutami S., Tani H., Mori M., Takayama Y., Moriguchi H., Kotani K., Miwa K., Lee J.-K., Noshiro M., Jimbo Y. (2011). Device for co-culture of sympathetic neurons and cardiomyocytes using microfabrication. *Lab on a Chip*, 11, 2268-2275.

[16] Dworak B.J., Wheeler B.C. (2009). Novel MEA platform with PDMS microtunnels enables the detection of action potential propagation from isolated axons in culture. *Lab on a Chip*, 9, 404-410.

[17] Boehm S., Huck S. (1995). α_2-Adrenoreceptor-mediated inhibition of acetylcholine-induced noradrenaline release from rat sympathetic neurons: An action at voltage- gated Ca^{2+} channels *Neuroscience, 69*, 221-231.

[18] Fischer H., Orr-Urtreger A., Role L.W., Huck S. (2005). Selection deletion of the α5 subunit differentially affects somatic-dendritic versus axonally targeted nicotinic ACh receptors in mouse. *Journal of Physiology*, 563, 119-137.

Advanced cardiac and neuronal recording using PEDOT-CNT MEA

Ramona Gerwig[1*], Paolo Cesare[1], Udo Kraushaar[1], Alfred Stett[1] and Martin Stelzle[1]

1 Natural and Medical Sciences Institute at the University of Tuebingen, Markwiesenstrasse 55, 72770 Reutlingen
* Corresponding author. E-mail address: ramona.gerwig@nmi.de

Abstract
PEDOT-CNT electrodes show highly promising properties for recording from and stimulation of excitable tissue. PEDOT and PEDOT-CNT show significant lower impedance and higher charge transfer capacitance as compared to state-of-the art neuronal electrodes. *In vitro* testing with cardiomyocytes reveals improved cultivation duration and recording signal quality. Recordings from primary sensory neurons also indicate superior signal quality with a significant noise reduction of more than 30%. Electrochemical sensing of dopamine in buffer solution shows the feasibility of using the recording and stimulation electrode also as a sensor for neurotransmitters.

1 Background and aims

Recording from excitable tissue is applied in cardiac as well as in neurological research to gain an understanding of physiological functions and disorders. Using microelectrode arrays (MEA) provides for precise measurements of small signals in high spatial resolution [1-3]. Typically, the electrodes of these arrays are fabricated using metal based materials [2, 4]. In order to improve signal to noise ratio, cell viability and sensing properties, efforts have been made in the modification of the electrode surface using conducting polymers like poly(3,4-ethylene-dioxythiophene) (PEDOT) and carbon nanotubes (CNTs). PEDOT has shown to be one of the most stable conducting polymers. Previous reports have demonstrated its suitability as a material for micro-neural interfaces [5]. Furthermore, exceptional viability of cells and their efficient integration with layers composed of CNTs has been observed [6-8]. CNTs are biocompatible and biostable and have been used to form layers that exhibit large effective porosity and surface area. This results in favorable charge transfer capabilities and low impedance [6]. These properties enable the precise measurement of very small signals and changes thereof which can be advantageous in cardiac and neuronal research.

Moreover, CNTs modified electrodes provide for enhanced sensing properties towards neurotransmitters such as dopamine [9]. This technology enables the assessment of the “brain chemistry” and thus could improve diagnosis of neuronal diseases ultimately leading to new and advanced therapeutic approaches.

PEDOT-CNT composite materials are therefore considered attractive candidates for the fabrication of electrodes in neuroprostheses as well as for *in vitro* cardiac and neuronal research.

The ultimate goal of this project is to establish robust technologies to fabricate mechanically stable PEDOT-CNT electrodes and to integrate them into MEAs. Recordings from cardiomyocytes and primary neurons as well as electrochemical detection of dopamine show the suitability in these applications.

2 Materials and methods

2.1 Fabrication and characterization

To generate the PEDOT-CNT composite material electropolymerization was carried out in suspensions of ethylenediethoxythiophene (EDOT, 0.02 M), poly(sodium-p-styrenesulfonate) (PSS, $M_w \approx 70{,}000$ g mol^{-1}; 1 %) and carbon nanotubes (0.03 %). Pure PEDOT coatings were electropolymerized with the same concentrations in the absence of CNTs. The electrochemical deposition on gold electrodes with a diameter of 30 µm of a MEA (NMI-TT GmbH) was performed under ambient conditions in a three electrode system with galvanodynamic control applying a final current density of 2 mA/cm^2 and potentials of ca. 0.7 V vs. Ag/AgCl. Charge densities of 30-110 mC/cm^2 were passed during deposition in order to control the amount of deposited material on the electrodes. Employing an 8-channel potentiostat/galvanostat it is also possible to coat all 59 electrodes of a standard MEA in a fast and reproducible way. This method is highly promising allowing integration into commercial production processes.

2.2 Applications

Substrates were autoclaved and coated with nitrocellulose. Primary ventricular cardiomyocytes from embryonic chicken (E12-13) were cultured on MEAs for up to 10 days. The medium was changed every 2-3 days. Recordings were performed using amplifiers (MEA1060-USB, 1200x and MEA1060-BC, 1100x, Multi Channel Systems).

Primary sensory neurons isolated from neonatal rat dorsal root ganglia (DRG) were seeded on TiN and

on PEDOT-CNT MEAs, respectively, and cultivated for 48 h. Spontaneous activity and activity after stimulation with 1 µM capsaicin were recorded using an MEA1060-BC, 1100x amplifier (Multi Channel Systems).

Different concentrations (0.5-100 µM) of dopamine in phosphate buffered saline (PBS) were measured using square wave voltammetry. The parameters were optimized to 25 mV amplitude, 4 mV step size and 100 ms pulse width. After preconditioning for 1 min, the potential was scanned from -200 to 500 mV.

3 Results and discussion

PEDOT and PEDOT-CNT electrodes show extraordinary low impedances below 20 kΩ at 1 kHz (Ø = 30 µm) and very high charge storage capacitances between 4 and 10 mF/cm^2 depending on the film thickness. They withstand rinsing with solvents, autoclaving and plasma cleaning and can be used repeatedly in cell culture experiments. Delamination was not observed.

Primary cardiomyocytes from embryonic chicken were seeded on Au, TiN, PEDOT and PEDOT-CNT MEAs and cultivated for up to ten days. After two days in vitro, visible autorhythmic activity could be detected. Cell viability and activity recorded from cells on PEDOT and PEDOT-CNT MEA was still excellent after ten days. Recordings of field action potentials show high signal amplitude and excellent signal-to-noise ratio, indicating good cell adhesion on both PEDOT and PEDOT-CNT electrodes (Figure 1. Note that the recordings from TiN and Au were taken on day 4. On day 10 no qualitatively satisfying signals could be detected on these reference MEAs). Three improvements compared to the reference system where seen: the cultivation duration could be increased to at least ten days, the signal amplitude of the voltage deflections was increased strongly and the shape of the T-wave was well-defined. All three advantages are of compelling importance for applications envisaged in cardiac drug research.

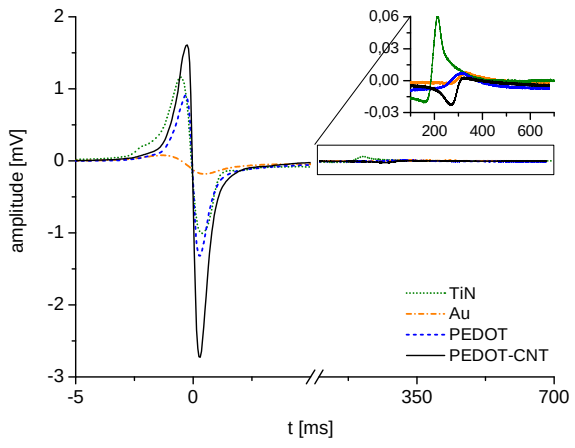

Fig.1. Recordings of autorhythmic action from cardiomyocytes after 10 days of culture (PEDOT and PEDOT-CNT) and 4 days of culture (TiN and Au).

Preliminary results also demonstrate feasibility of reliable electrical stimulation of cardiomyocyte cultures on PEDOT-CNT MEA whereas no reliable repetitive stimulation has been possible using standard Au or TiN electrodes. Through biphasic stimulation with ± 1.5-2.0 V, the intrinsic cellular pacemaker rhythm could be overwritten within a broad range of pacing frequencies. The length of the cardiomyocyte field action potential pattern showed adaptions accordingly, reflecting physiological compensatory mechanisms. If these results can be confirmed in future experiments, this would be most useful in safety pharmacological assays.

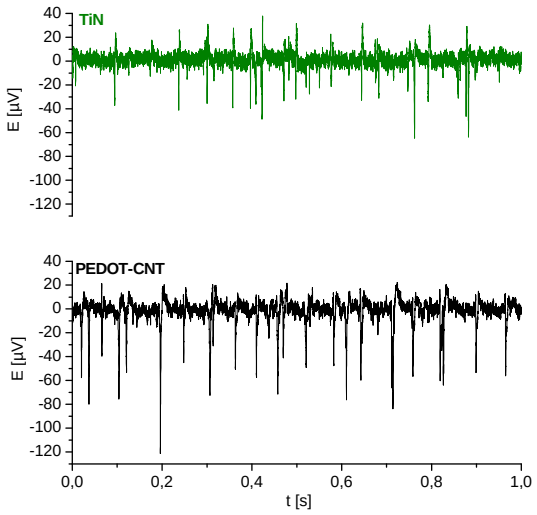

Fig. 2. Recordings from primary sensory neurons after stimulation with capsaicin.

Primary sensory neurons isolated from neonatal rat dorsal root ganglia (DRG) were seeded on TiN and PEDOT-CNT MEAs and cultivated for 24 h. Cell viability was similar on PEDOT-CNT as well as reference MEAs. Preliminary results show increased signal amplitudes and reduced noise (Figure 2). The noise could be reduced by more than 30% as compared to TiN MEAs. As a result, it is possible to identify even very small action potentials, making these electrodes suitable for *in vivo* applications.

Electrochemical measurements of dopamine were performed proving the applicability of PEDOT and PEDOT-CNT electrodes in neurotransmitter sensing. As compared to pure PEDOT, PEDOT-CNT shows higher peak currents for the same concentration of dopamine (Figure 3). A detection limit of 500 nM and a sensitivity of 37 pA/µM (7.6 µA/µMcm^2) and 70 pA/µM (14.3 µA/µMcm^2) for PEDOT and PEDOT-CNT respectively could be obtained. Previous work [10] demonstrates that PEDOT provides for selectivity when dopamine is to be detected in the presence

of interference such as ascorbic acid. This has yet to be confirmed in ongoing work.

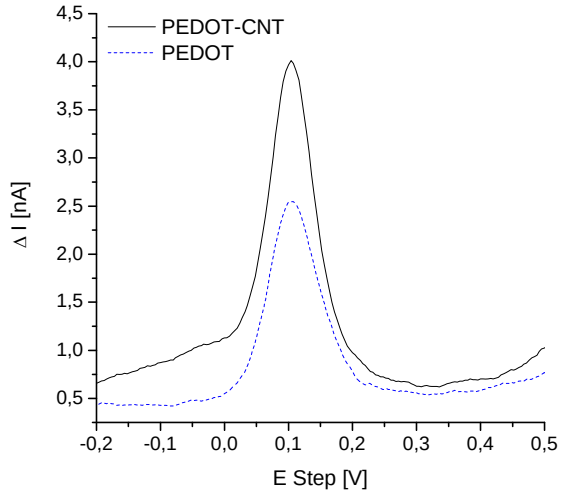

Fig. 3. Representative square wave voltammograms of 50 µM dopamine in PBS recorded with a PEDOT (blue, dashed) and a PEDOT-CNT (black, solid) microelectrode (Ø = 30 µm).

PEDOT and PEDOT-CNT electrodes show highly promising properties for recording from and stimulation of excitable tissue. When comparing with Au or TiN electrodes, PEDOT and PEDOT-CNT show significant lower impedance and higher charge transfer capacitance. *In vitro* experiments with cardiomyocytes reveal improved cultivation duration and recording signal quality. *In vitro* recordings from neurons also indicate superior signal quality due to significantly lower noise. Electrochemical sensing of dopamine in buffer solution shows the possibility to use the recording and stimulation electrode also as a sensor for neurotransmitters.

Reproducibility and stability make these electrodes usable in real world applications [11] (see also the extended abstract and poster: Gerwig et al.: "Towards real world applications: reproducible and stable PEDOT-CNT microelectrodes").

Acknowledgement

The support of Ilona Matiychyn, Lydia Kiesel and Sebastian Epple and helpful discussion with Kai Fuchsberger are kindly acknowledged. Funding: BMBF Grant no. 01GQ0834 and Multi Channel Systems GmbH.

References

[1] M. D. Johnson, R. K. Franklin, M. D. Gibson, R. B. Brown, D. R. Kipke, *Journal of Neuroscience Methods* **2008**, *174*, 62-70.
[2] D. R. Kipke, W. Shain, G. Buzsaki, E. Fetz, J. M. Henderson, J. F. Hetke, G. Schalk, *Journal of Neuroscience* **2008**, *28*, 11830.
[3] S. F. Cogan, *Biomedical engineering* **2008**, *10*, 275.
[4] K. D. Wise, D. J. Anderson, J. F. Hetke, D. R. Kipke, K. Najafi, *Proceedings of the IEEE* **2004**, *92*, 76-97.
[5] S. J. Wilks, S. M. Richardson-Burns, J. L. Hendricks, D. C. Martin, K. J. Otto, *Frontiers in Neuroengineering* **2009**, *2*.
[6] E. W. Keefer, B. R. Botterman, M. I. Romero, A. F. Rossi, G. W. Gross, *Nature Nanotechnology* **2008**, *3*, 434-439.
[7] V. Lovat, D. Pantarotto, L. Lagostena, B. Cacciari, M. Grandolfo, M. Righi, G. Spalluto, M. Prato, L. Ballerini, *Nano Letters* **2005**, *5*, 1107-1110.
[8] A. Mazzatenta, M. Giugliano, S. Campidelli, L. Gambazzi, L. Businaro, H. Markram, M. Prato, L. Ballerini, *Journal of Neuroscience* **2007**, *27*, 6931-6936.
[9] P.-Y. Chen, R. Vittal, P.-C. Nien, K.-C. Ho, *Biosens. Bioelectron.* **2009**, *24*, 3504-3509.
[10] S. Kumar, J. Mathiyarasu, K. Phani, V. Yegnaraman, *J. Solid State Electrochem.* **2006**, *10*, 905-913.
[11] R. Gerwig, K. Fuchsberger, B. Schroeppel, G. S. Link, G. Heusel, U. Kraushaar, W. Schuhmann, A. Stett, M. Stelzle, *Frontiers in Neuroengineering* **2012**, *5*, 1-11.

Towards the development of carbon nanotube-based retinal implant technology: Electrophysiological and ultrastructural evidence of coupling at the biohybrid interface

Cyril G. Eleftheriou[1], Jonas Zimmermann[1], Henrik Kjeldsen[1], Moshe David Pur[2], Yael Hanein[2], Evelyne Sernagor[1*]

1 Institute of Neuroscience, Newcastle University Medical School, Newcastle Upon Tyne, United Kingdom
2 School of Electrical Engineering and Physical Electronics, Tel-Aviv University, Tel-Aviv, Israel
* Corresponding author. E-mail address: evelyne.sernagor@ncl.ac.uk

Abstract

One of the many challenges in the development of neural prosthetic devices is the choice of electrode material. Electrodes must be biocompatible, and at the same time, they must be able to sustain repetitive current injections in highly corrosive physiological environment. We investigated the suitability of carbon nanotube (CNT - an advanced material with high biocompatibility and superior electrical properties) electrodes for prolonged repetitive stimulation of retinal ganglion cells (RGCs). In our experiments, retinas were maintained alive on multielectrode arrays (MEA) for two days to establish whether the bioelectrical properties of the system change over time. CNT electrodes were compared to commercially available titanium nitride (TiN) electrodes. When using CNT electrodes, larger spikes were observed on Day 2. Moreover, stimulation of the same electrodes using the same stimulation parameters on Day 2 yielded significantly lower thresholds and recruited more RGCs, suggesting that coupling between the tissue and the CNT electrodes becomes stronger with time. At the same time, transmission electron microscopy (TEM) revealed the formation of intimate contacts over time between CNTs and the tissue, including engulfment of CNT islands by the retina and CNT penetration towards the RGC layer. These results demonstrate that the retina grows towards CNTs with time, resulting in better coupling at the interface. We conclude that CNTs are a promising material for inclusion in retinal prosthetic devices.

1 Introduction

Epi-retinal stimulation of RGCs as a means for the purpose of restoring sight in blind patients is a challenge which has been an active focus of research in the past few years [1], and more recently it has been implemented by industrial groups [2]. In an attempt to mimick the anatomical and physiological conditions characterising human retinal dystrophic disorders, our group uses the Cone rod homebox (Crx) knockout mouse, a model of Leber congenital amaurosis [3]. The Crx gene is responsible for the development of photoreceptor outer segments. Crx -/- mice undergo a gradual loss of photoreceptors and remodelling of the neural retina, resulting in complete blindness by the fifth post-natal month. We investigated the use of CNT electrodes for recording [4] and stimulation of retinal neurons. Their large geometric surface area not only confers them superior electrical properties (lower impedance, higher capacitance and higher charge injection limit) than conventional electrodes [5], but also porosity which promotes cellular adhesion and migration [6]. The mechanical properties of CNTs (large tensile strength, Young's modulus and hardness) make them biocompatible. These characteristics are ideal for designing chronic retinal implants where low charge stimulation is imperative to stimulate individual RGCs and to reduce the amount of energy required to fire these cells. In this study, we investigated the dynamics of electrophysiological and structural interactions occuring between isolated retinal tissue and CNT electrode assemblies over two days *in vitro*.

2 Methods

Electrophysiology

Retinas were isolated and mounted onto MEAs with the RGC layer facing down onto the electrodes and the optic disc to the side (not in contact with electrodes) as this part of the retina has no RGC somata.

Electrophysiological signals were recorded at 25 kHz sampling frequency using 60-channel MEAs interfaced with a computer running the proprietary software MC_Rack using a MEA1060-INV (Multi Channel Systems, Reutlingen, Germany) amplifier. To preserve physiological conditions, the tissue was

perfused with oxygenated artificial cerebro-spinal fluid (aCSF, in mM: 118 NaCl, 25 $NaHCO_3$, 1 NaH_2PO_4, 3 KCl, 1 $MgCl_2$, 2 $CaCl_2$, 10 glucose) at 0.9 ml/minute and maintained at 32˚C.

CNT MEAs were fabricated as in [5] with 30µm diameter electrodes, 200 µm pitch. Control MEAs were commercial TiN devices (200/30-Ti-Gr, Multi Channel Systems, Reutlingen, Germany). For each experiment, we used four different stimulating electrodes on the MEA. Stimuli consisted of charge-balanced biphasic current pulses of various amplitudes and durations delivered using the stimulator STG 2008 (Multi Channel Systems, Reutlingen, Germany). Each stimulus was applied 30 times, and different stimuli were presented in random order. The same stimuli applied to the same electrodes were used on both experimental days. Intervals between individual stimuli were varied randomly from 1 to 2 s, averaging 0.67 Hz to avoid artefacts such as low frequency potentiation or resonance with intrinsic oscillations of the RGC as seen by Margolis et al. [7].

Raw MCD data files were imported into Matlab (The MathWorks, USA) using the FIND toolbox [8] and the artefact introduced by applying electrical stimulation was removed using the SALPA algorithm [9]. Spikes were extracted and sorted by supra-paramagnetic clustering and wavelet analysis using Wave_clus [10].

Anatomy

Isolated Crx -/- retinas were flat-mounted, RGC layer facing down over large (100 µm diameter) CNT islands loosely attached to a SiO_2 substrate glued to the bottom of a petri dish with Cyanoacrylate (Lyreco, UK). Weighed down onto the islands with polyester membrane filters topped with a sterile stainless steel ring, the tissue was perfused with oxygenated aCSF at a rate of 0.9 ml/min over the course of 4, 12, 24, 48 or 72 hours.

The retinas were subsequently lifted off from the SiO_2 substrate with a nitrocellulose membrane and fixed in 2% Glutaraldehyde, postfixed in osmium tetroxide, dehydrated in acetone, and embedded in epoxy resin. Semi-thin (1 µm thick) and ultrathin (70-90 nm thick) sections were cut perpendicular to the plane of the retina, stained with toluidine blue or Uranyl acetate and lead citrate, respectively.

CNT islands adhering to the retinal tissue were observed under a Philips CM100 Compustage transmission electron microscope (TEM).

3 Electrophysiological evidence of increased coupling

3.1 Signal amplitudes increase with time

Crx -/- retinas display a considerable amount of spontaneous activity consisting of local field potential oscillations and vigorous bursting. The size of the action potentials is an indication of the quality of the coupling between the retinal tissue and the recording electrode, as the propagation of such signals through resistive biological tissue is attenuated with increasing distance between the two. When comparing the size of single units over time, we noted (for CNT electrodes, but not for TiN electrodes) a significant increase after the tissue had been in contact with the electrode for several hours.

Average spike amplitudes were calculated from 8 min long recordings for each clustered spike waveform recorded on each channel for a particular experiment. Figure 1 illustrates the distribution of spike amplitudes recorded on a CNT electrode on Day 1 (blue) and Day 2 (red) for one RGC. There is a clear shift towards larger amplitudes on Day 2. Such time dependent increase in signal amplitude was not observed on TiN electrodes.

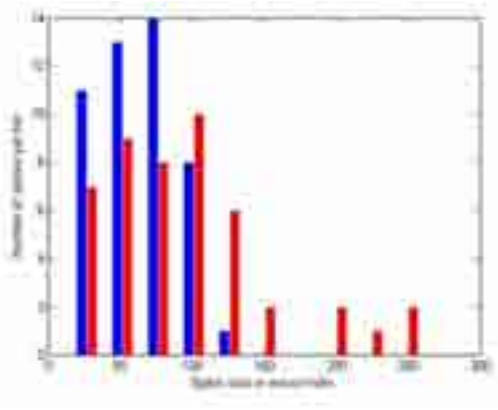

Fig. 1. Distributions of spike amplitudes for one RGC recorded on a CNT electrode over two days (Day 1, blue; Day 2, red).

3.2 Stimulation thresholds decrease with time

The charge delivered by each pulse was modulated by altering either the current intensity (10-100 µA per phase) or phase duration (10-100 µs). Evoked responses were identified by their time-locked appearance on raster plots after repetitive trials of the same stimulus condition and by their disappearance below a given amount of charge delivered, determining the firing threshold (fig.2).

When stimulating with CNT electrodes, the average threshold values were lower on Day 2 than on Day 1(fig.2). The effect was significantly less pronounced when using TiN electrodes. These results indicate that smaller amount of current are required to depolarise RGCs past their firing threshold as the resistivity of the retina-CNT electrode interface decreases with time, suggesting that the retina becomes gradually more intimately coupled to the CNTs.

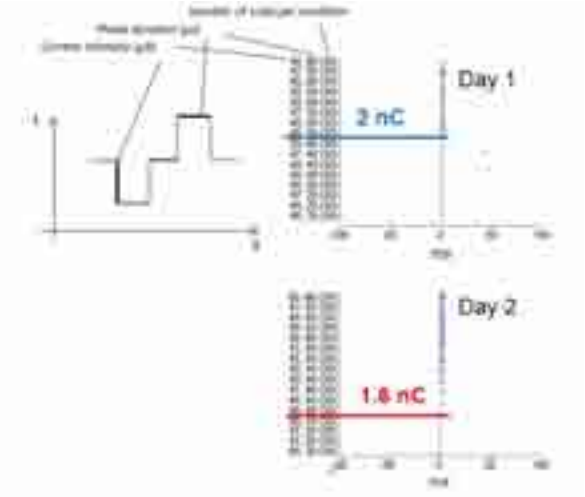

Fig. 2. Raster plots of responses evoked by charge balanced biphasic pulses in one RGC on Day 1 and Day 2.

3.3 Cellular recruitment increases with time

Stimulation pulses delivered at a particular electrode location evoked responses which were recorded on neighbouring electrodes and sometimes even as far as 1 mm away. The numbers of evoked responses and responding channels were significantly higher on Day 2 when using CNT electrode MEAs. Figure 3 illustrates an example of this phenomenon with the pulses delivered by the stimulating electrode (green) evoking responses on 9 electrodes on Day 1 (blue), and on 15 electrodes on Day 2 (red). This activity map also reveals that the stimulation of a certain area does not necessarily yield a concentric field of activation.

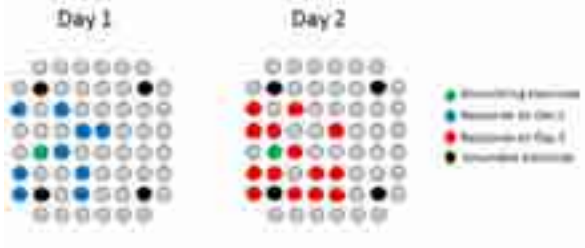

Fig. 3. Electrical stimulation activity field on two consecutive days for the same stimulating electrode (green disk). Stimulation of the same area leads to responses on more electrodes on Day 2 (red disks) than Day 1 (blue disks).

4 Ultrastructural evidence of increased coupling

4.1 The gap between the retina and CNT-assemblies decreases with time

Semi-thin sections (1 µm) revealed that coupling at the interface between the retinal inner limiting membrane (ILM) and the CNT assemblies becomes more intimate with time (fig.4). Indeed, the distance between the ILM and CNT islands decreases with the amount of time the retina is maintained alive in contact with the CNT assemblies. After 4 hours, the assemblies are on average 200 µm away from the ILM, and the distance decreases to 50 µm after 12 hours. After 24 hours, the CNT islands make direct contact with the retina and after 48 hours, the islands appear to be physically integrated within the ILM.

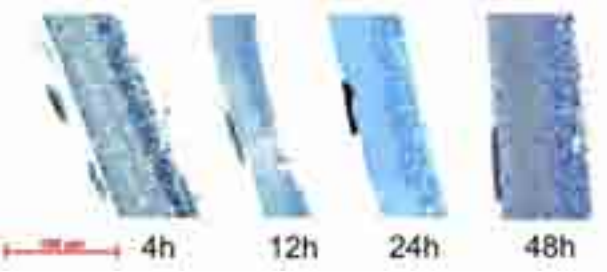

Fig. 4. Transverse retinal sections through CNT islands at increasing incubation times. With time, CNTs become more intimately coupled to the retina.

4.2 Penetration of the ILM by individual CNTs

Ultrastructural studies [11] show that the RGC layer is separated from the vitreous by the nerve fibre layer (RGC axons), retinal glia (Muller cells end feet and astrocytes) and the ILM. This membrane is 70-400 nm thick and composed of a basement membrane of collagen fibrils and hyaluronic acid encompassing a juxtaposition of the Muller cell plasma membrane and the vitreous itself [12]. We have used TEM to visualise interactions between CNTs and this complex structure.

TEM micrographs reveal that individual CNTs penetrate the retina through the ILM and that they establish close contacts with organelles (fig.5). No sign of rejection by the tissue is observed. In addition, between 24 and 48 hours, it could clearly be seen that the retina starts engulfing CNT islands.

5 Conclusions

Electrophysiological data from our experiments indicate that CNT electrodes are more effective than TiN electrodes at recording and stimulating RGCs after time spent *in vitro*. This is characteristic of a decrease in the resistivity between the electrode and its biological target and may be due to gradual narrowing of the gap at the biohybrid interface. Our anatomical observations confirm this possibility and further indicate that CNTs do not trigger tissue rejection when maintained *in vitro*, suggesting biocompatibility of this type of material.

6 Discussion

Some of the major issues faced by epi-retinal prosthetic devices are selective activation of RGCs and attachement of electrodes to the retina. The electrical properties of CNT electrodes allow the use of very small electrodes delivering dense current pulses strong enough to activate RGCs without

causing damage at the tissue-electrode interface. Advances in nano-fabrication techniques and bio-fuctionalisation of CNTs open the possibilities of intracellular stimulation by future electrode generations. Commercial epi-retinal devices use surgical tacks to fix their devices to the retinal tissue [2] resulting in spacing between the electrode and the target neurones. The use of CNT stimulating electrodes could potentially resolve this problem by ensuring functional adhesion point at each stimulating electrode location.

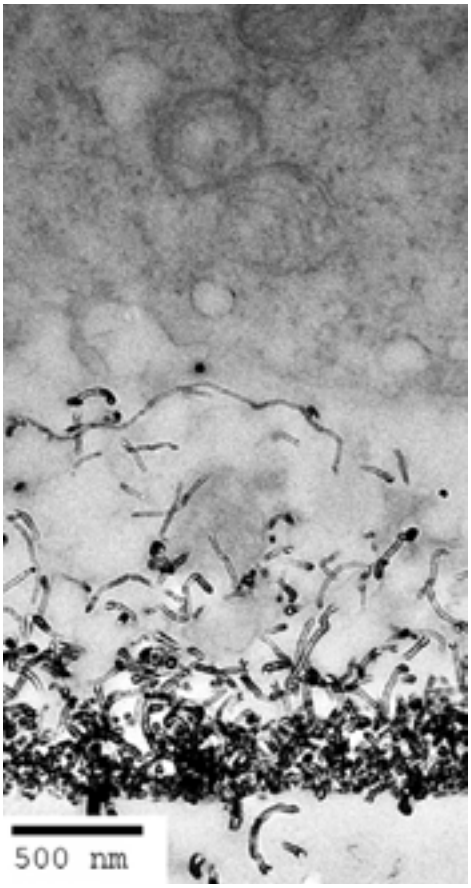

Fig. 5. TEM micrograph showing infiltration of CNTs in the retina through the ILM.

Acknowledgement

We thank Dr Kath White, Tracey Davey and Vivian Thompson from Newcastle University EM research services for the training, help and support they provided during the course of this study.

References

[1] Rizzo, J.F., 3rd, et al., *Retinal prosthesis: an encouraging first decade with major challenges ahead.* Ophthalmology, 2001. **108**(1): p. 13-4.

[2] Humayun, M.S., et al., *Preliminary 6 month results from the Argus II epiretinal prosthesis feasibility study.* Conf Proc IEEE Eng Med Biol Soc, 2009. **2009**: p. 4566-8.

[3] Furukawa, T., E.M. Morrow, and C.L. Cepko, *Crx, a novel otx-like homeobox gene, shows photoreceptor-specific expression and regulates photoreceptor differentiation.* Cell, 1997. **91**(4): p. 531-41.

[4] Shoval, A., et al., *Carbon nanotube electrodes for effective interfacing with retinal tissue.* Front Neuroeng, 2009. **2**: p. 4.

[5] Gabay, T., et al., *Electro-chemical and biological properties of carbon nanotube based multi-electrode arrays.* Nanotechnology, 2007. **18**(3): p. 035201.

[6] Sorkin, R., et al., *Process entanglement as a neuronal anchorage mechanism to rough surfaces.* Nanotechnology, 2009. **20**(1): p. 15101.

[7] Margolis, D.J., et al., *Functional stability of retinal ganglion cells after degeneration-induced changes in synaptic input.* J Neurosci, 2008. **28**(25): p. 6526-36.

[8] Meier, R., et al., *FIND--a unified framework for neural data analysis.* Neural Netw, 2008. **21**(8): p. 1085-93.

[9] Wagenaar, D.A. and S.M. Potter, *Real-time multi-channel stimulus artifact suppression by local curve fitting.* J Neurosci Methods, 2002. **120**(2): p. 113-20.

[10] Quiroga, R.Q., Z. Nadasdy, and Y. Ben-Shaul, *Unsupervised spike detection and sorting with wavelets and superparamagnetic clustering.* Neural Comput, 2004. **16**(8): p. 1661-87.

[11] Bussow, H., *The astrocytes in the retina and optic nerve head of mammals: a special glia for the ganglion cell axons.* Cell Tissue Res, 1980. **206**(3): p. 367-78.

[12] Heegaard, S., O.A. Jensen, and J.U. Prause, *Structure and composition of the inner limiting membrane of the retina. SEM on frozen resin-cracked and enzyme-digested retinas of Macaca mulatta.* Graefes Arch Clin Exp Ophthalmol, 1986. **224**(4): p. 355-60.

A 1024-channel 26k-electrode, low-noise, CMOS microelectrode array for *in-vitro* recording and stimulation of electrogenic cells at high hesolution

Marco Ballini[1*], Jan Müller[1], Paolo Livi[1], Yihui Chen[1], Urs Frey[2], Flavio Heer[1], Alexander Stettler[1], Andreas Hierlemann[1]

1 ETH Zurich, Department of Biosystems Science and Engineering, Basle, Switzerland
2 now at RIKEN, Quantitative Biology Center, Kobe, Japan
* Corresponding author. E-mail address: marco.ballini@bsse.ethz.ch

Abstract
We report on a CMOS Microelectrode Array chip, featuring 26400 electrodes in a large sensing area (3.85 mm x 2.10 mm), and capable of recording and stimulation at high spatial and temporal resolution (17.5 µm pitch, 20 kHz sampling rate) with very low noise levels. The chip was fabricated in 0.35-µm technology, and preliminary experiments show proper functionality.

1 Background

Complementary Metal-Oxide-Semiconductor (CMOS)-based Microelectrode Arrays (MEAs) have been demonstrated [1-4] to feature, on the same substrate, a very large number of electrodes with high density, and low-noise circuits for signal acquisition and processing.

2 System Design

Here, we report on a new CMOS-based MEA, implemented in 0.35-µm technology (2P4M). A block diagram of the chip is shown in Fig. 1. The chip features: (1) an active area of 3.85 mm × 2.10 mm, carrying 26400 platinum electrodes, arranged in a square grid with a center-to-center pitch of 17.5 µm; (2) 1024 low-noise fully-differential readout channels, each including three stages of amplification, as well as band-pass filtering with configurable gain and adjustable high-pass and low-pass cut-off frequencies; (3) 1024 parallel single-slope analog-to-digital converters (ADCs) for on-chip digitization of the data (20 kSamples/s, 10 bits resolution); (4) 32 configurable stimulation buffers, providing both, voltage and current stimulation capabilities; (5) a switching matrix underneath the electrode array, enabling an arbitrary subset of electrodes to be flexibly and reconfigurably connected to the readout channels and to the stimulation buffers.

3 Results

A micrograph of the fabricated chip is shown in Fig. 2. The frequency response of the readout channels has been measured: The high-pass cut-off frequency can be set as low as 120 mHz. The input-referred noise in the action-potential band of 300 Hz ÷ 10 kHz is 2.4 µV rms. The total power consumption of the chip is approximately 75 mW. Further electrical characterization and measurements of biological preparations are ongoing.

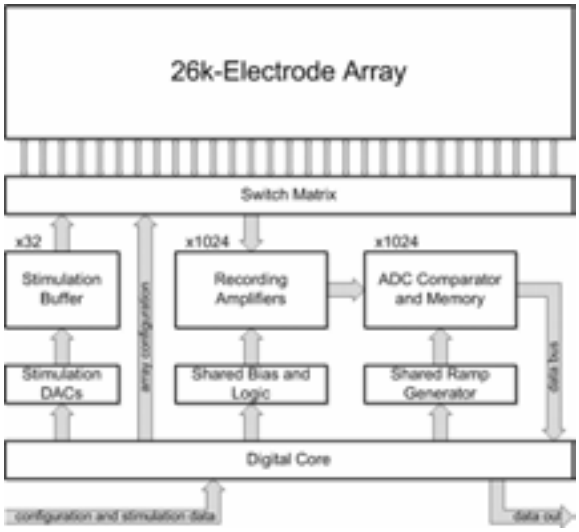

Fig. 1. Block diagram of the CMOS MEA chip.

4 Conclusion

A new CMOS MEA in 0.35-µm technology has been designed and fabricated, which provides a large readout-channel count for neural recording and stimulation at high spatial and temporal resolution.

Acknowledgement

This work was financially supported by the FP7 of the European Community through the ERC Advanced Grant 267351 “NeuroCMOS”. Marco Ballini acknowledges individual support through the EU

Marie Curie RTN “CellCheck” (MRTN-CT-2006-035854).

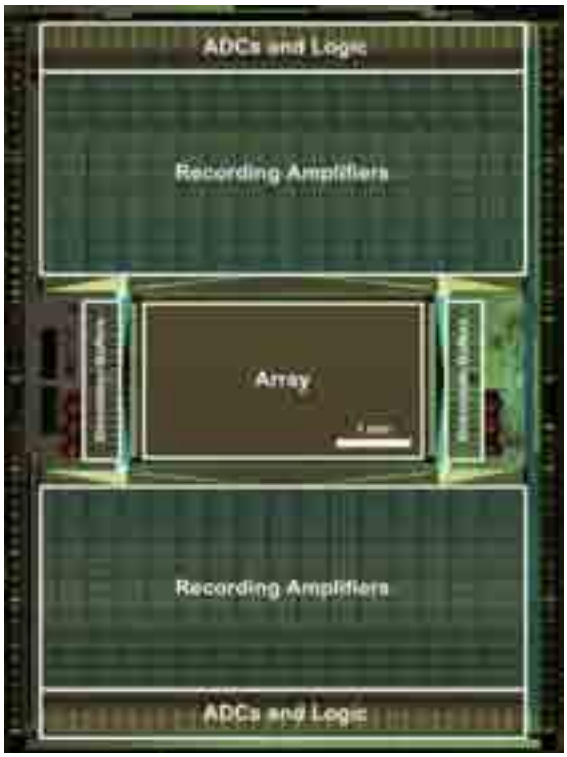

Fig. 2. Chip Micrograph. The size of the electrode array is 3.85 mm × 2.10 mm.

References

[1] Heer F., Hafizovic S., Franks W., Blau A., Ziegler C., Hierlemann A. (2006). CMOS microelectrode array for bidirectional interaction with neuronal networks. *IEEE Journal of Solid-State Circuits*, Vol. 41, No. 7, 1620-1629.

[2] Berdondini L., Imfeld K., Maccione A., Tedesco M., Neukom S., Koudelka-Hep M., Martinoia S. (2009). Active pixel sensor array for high spatio-temporal resolution electrophysiological recordings from single cell to large scale neuronal networks. *Lab on a Chip*, Vol. 9, No. 18, 2644-2651.

[3] Frey U., Sedivy J., Heer F., Pedron R., Ballini M., Mueller J., Bakkum D., Hafizovic S., Faraci F. D., Greve F., Kirstein K.-U., Hierlemann A. (2010). Switch-matrix-based high-density microelectrode array in CMOS technology. *IEEE Journal of Solid-State Circuits*, Vol. 45, No. 2, 467-482.

[4] Eversmann B., Lambacher A., Gerling T., Kunze A., Fromherz P., Thewes R. (2011). A neural tissue interfacing chip for in-vitro applications with 32k recording / stimulation channels on an active area of 2.6 mm^2. *2011 Proceedings of the ESSCIRC*, 211-214.

A novel multi-electrode array chip for neurotransmitter mesurement

Ikuro Suzuki[1*], Mao Fukuda[1], Aoi Odawara[1], Amani Alhebshi[1], Masao Gotoh[1]

1 Department of Bionics, Graduate school of bionics, computer and media science, Tokyo University of Technology, Tokyo, JAPAN
* Corresponding author. E-mail address: isuzuki@bs.teu.ac.jp

Abstract
We have developed the carbon nanotube (CNT) microelectrode array. Using this CNT microelectrode array, we successfully detected their response to 10nM dopamine, serotonin and glutamic acid. This demonstrated the potential for real-time recording method of the neurotransmitter released from neurons.

1 Introduction

Dynamic detection of neurotransmitter release from living neurons has always been an area of great interest in neuroscience field and medical science. Since multi-electrode arrays was developed for use in recording from cultured cells 40 years ago(1), many scientists has been used by the advantages of multi-site measurement and long-term measurements. However, the cell functions detected from multi-electrode arrays remain virtually unchanged such as action potentials and filed synaptic potentials.

In our present study, to measure neurotransmitter in real time using multi-electrode arrays, we developed carbon nano tube coated 64ch multi-electrode arrays. We successfully detected 10nM neurotransmitter using their CNT micro electrodes by electrochemical measurement.

2 Methods

Multi-electrode arrays (MEAs) were formed on the glass slide comprised 64 20x20-μm ITO electrodes. Single wall carbon nano tube (SWCNT) and multi wall carbon nano tube (MWCNT) were dispersed through ultrasonic agitation in phosphate buffer saline (pH7.4). Each CNT electrodeposition onto ITO electrode was carried out under 1.5V conditions. To confirm sensitivity for neurotransmitter, dopamine, glutamate acetylcholine and noradrenaline were prepared by diluting 10nM solutions in phosphate buffer saline (pH7.4). Electrochemical measurements were carried out using a CHI electrochemical workstation. CNTs-ITO acted as the working electrode, Ag/AgCl as the reference electrode, and the platinum wire as the counter electrode.

3 Results

Fig. 1 shows the 64ch SWCNT modified ITO electrode arrays developed through the direct current electrodeposition. MWCNT modified ITO electrode arrays have been also developed as well as SWCNT.

We found that the detection of neurotransmitter at a high sensitivity depended on the electrode surface structure. Fig. 2A shows the surface of electrodeposited MWCNT onto ITO electrode successfully detecting 10nM neurotransmitter. It can be seen that electrode surface was composed of small CNT particles (0.020±0.018 m^2), and that CNT particles were separated by a gap. We found that a number of gap play a key role in high sensitive neurotransmitter detection as well as SWCNT electrode.

Fig. 3 shows the cyclic voltammograms of 10nM glutamate at the CNTs modified ITO electrode and conventional pt/pt-black electrode. Comparing the results, it can be seen that in the former the glutamate shows a redox peak and there was an increase in peak current. The results also show that the sensitivity of glutamate at the conventional pt/pt-black electrode is low, whereas the CNT modified ITO electrode exhibits good electrochemical behaviours which improve the sensitivity. Also CNT modified ITO electrode specifically exhibits high sensitivity as well as 10nM dopamine, acetylcholine and noradrenaline.

4 Summary

In this work we have developed CNTs modified ITO electrode arrays and detected 10nM neurotransmitter. These results suggest that CNTs multi-electrode arrays have the potential to measure the neurotransmitter released from neurons. The results also show a novel measurement method using multi electrode arrays other than action potentials and filed synaptic potentials, and suggest this technique will be useful for investigating the mechanism of neural dynamics and neurological disorder and for applying a drug screening instrument.

References

[1] Thomas, C.A. et.al, (1972) *Exp Cell Res.*, 74(1), 61-66.

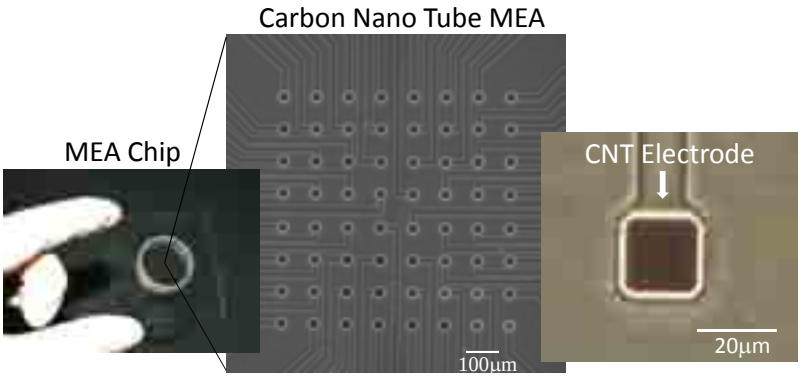

Fig.1 Carbon nano tube Multi electrode arrays.
64ch multi electrode arrays comprised of electrodeposited SWCNT onto 20x20-μm ITO electrode.

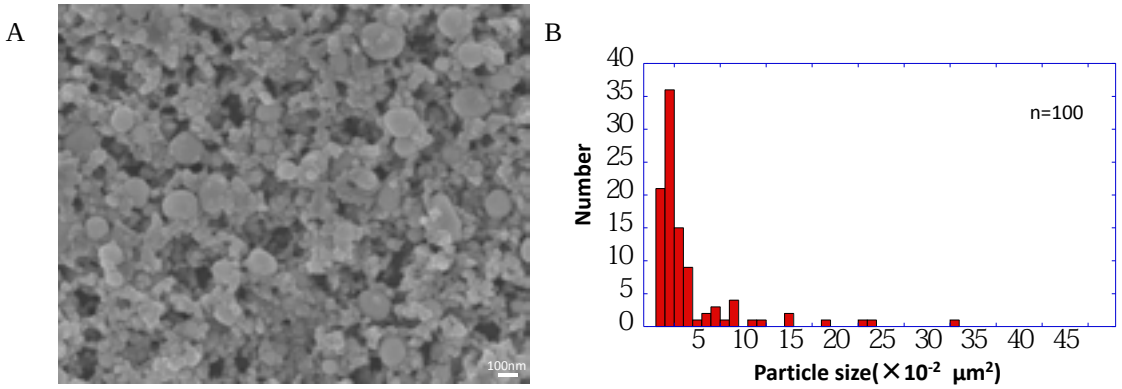

Fig.2 SEM image of CNT micro electrode and particle size distribution. (A) SEM image of MWCNT electrode surface. (B) Size distribution of agglomerated MWCNT(n=100). Particle size was randomly analyzed by means of image J software.

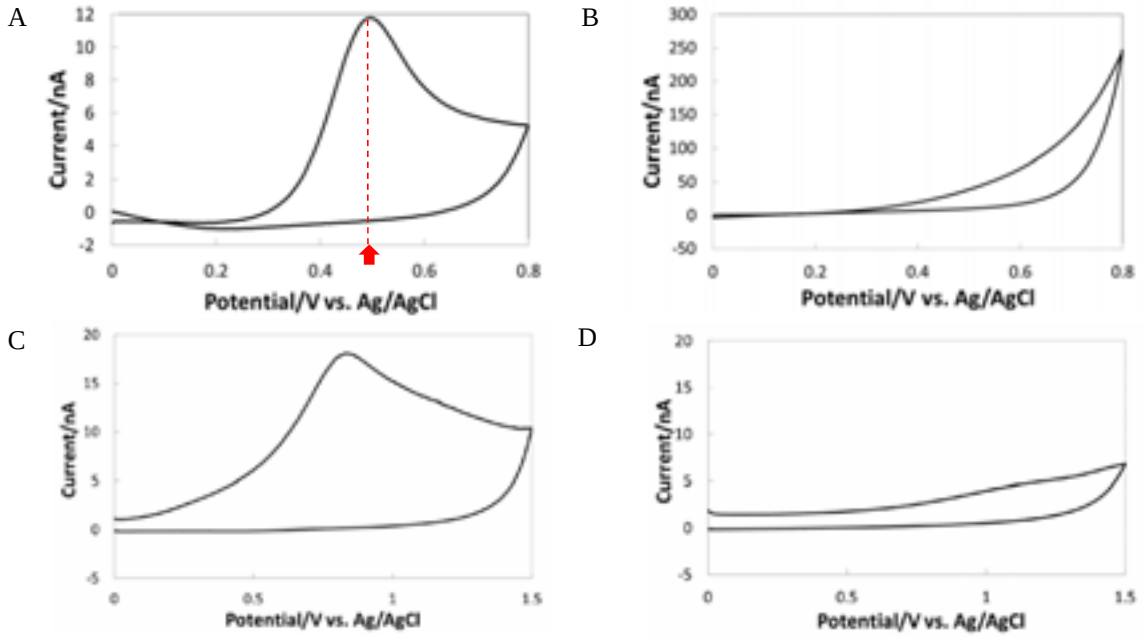

Fig. 3. Cyclic voltammograms of 10nM neurotransmitter.(A) 10nM glutamate at the CNT modified ITO electrode supported by phosphate buffer solution (pH=7.4). (B) 10nM glutamate at conventional pt/pt-black modified ITO electrode. (C) 10nM dopamine at the CNT electrode. (D) Phosphate buffer solution at the CNT electrode.

Silicon nanowire field effect transistors to probe organized neurons networks

Cecile Delacour[1*], Raphael Marchand[1], Thierry Crozes[1], Thomas Ernst[2], Julien Buckley[2], Ghislain Bugnicourt[1], Guillaume Bres[1], Jean Luc Mocelin[1], Catherine Villard[1]

1 Institut Néel, CNRS, Grenoble, France
2 CEA Léti, Grenoble, France
* Corresponding author. cecile.delacour@grenoble.cnrs.fr

Abstract
We present the fabrication and characterization of silicon nanowire field effect transistors (SiNW-FETs). Electrical behaviour of the devices are compared with 2D simulations that estimate the expected conductance modulation assisted by electrical field effect for operation in liquid environment. Then, we demonstrate the neurons growth and differentiation in vitro and their efficient coupling to the SiNW-FETs arrays.

1 Introduction

Neurons are excitable cells and electrical recording offers a privileged access to neuronal activity. To analyze the overall activity of neuronal networks it is crucial to record from many points of the network at once. Several methods have been developed to enable such multisite recording. They are either based on voltage sensitive or calcium sensitive dyes, extracellular micro electrode arrays or CMOS technologies for field potential recording. Silicon nanowire field effect transistor is the only configuration that has recently offered the sensitivity, length scale and timescale required to monitor neuronal activity at a sub-cellular level. Top-down technologies using Silicon-On-Insulator substrates have in parallel demonstrated their ability to detect some biological signals like DNA hybridization and pH variations, suggesting their potential use for cellular signal detection.

We present electrical characterization of field effect transistors made from SOI substrates. The overall nanoFET array has been designed to record and stimulate neuron networks of controlled architectures grown on top of the silicon chip. One example of such network will be presented.

2 Methods

Field effect transistors are fabricated by etching the 50 nm-thick silicon top layer of a SOI substrate oriented (100). The doping concentration of the top Si layer is 10^{21} at./cm^3 (Boron implantation) at the metal-silicon junction and a10 µm width ribbon in which the nanowire is etched remains non-implanted.

Contacts lines are made to address each nanowire by deposition of titanium (20 nm) and gold (60 nm) on a resist-patterned surface, followed by the lift-off of the resist. An aluminum hard mask hides the nanowire during the etching process. This hard mask is made by aluminum deposition and the lift-off of an electron beam lithography patterned resist. The following structure was been obtained by reactive ion etching of the uncovered silicon (figure 1).

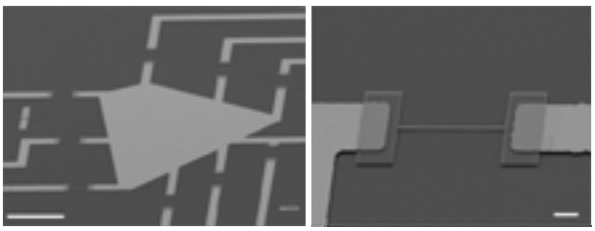

Fig. 1. Electron beam micrographs of 100 nm wide Si-NWFETs (right) integrated in a triangular array (left). The design is chosen to follow the spike propagation along a closed triangular neurons network (Fig.5). Scale bars are 40 µm (left) and 1µm (right).

Then a thick oxide (typ. 200 nm-thick-parylen-C or Silica) is deposited to electrically isolate the contact lines during liquid operations. Oxide is then removed above silicon nanowires by RIE etching while the rest of the chip is protected with a DUV resist pattern (figure 2, left). The resist is then removed and a thin gate oxide (typ. 5-20 nm thick HfO_2 or Al_2O_3) is deposited by atomic layer deposition to cover and isolate the nanowires (Figure 2, right).

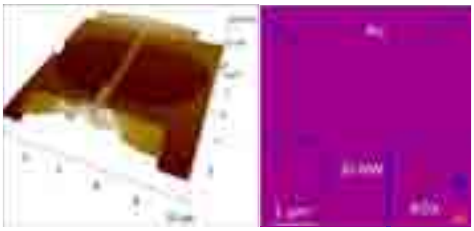

Fig. 2. Left. Atomic force micrograph of the final SI-NW device. Source and drain are covered by a thick oxide (Parylen or SiO_2) that is removed on the top of the Si-NW. Right. Tunneling atomic force micrograph of a connected Si-NW covered with a thin front gate oxide (5nm, alumina). Color scale is 1V, current-voltage converter gain is 10mV/pA.

A rapid thermal annealing at 500°C is performed before oxide deposition in an inert Ag/H atmosphere without oxygen-gases. The annealing induced a titanium silicide alloy on top of the contacts [1,2] that forms a conductive layer with a low Schottky barrier height. Before annealing, nanowires exhibit a resistance higher than 10MΩ, while it is reduced to 300kΩ after the annealing. The resistance has been reduced by almost 30 times.

3 Results and discussion

The drain source current-voltage (I_{DS}-V_{DS}) characteristic curves are measured by changing the voltage bias of the nanowires while the drain to source current is recorded.

First, modulation of the nanowire conductance is measured as function of a back gate voltage (fig.3) applied on the Si-substrate forcing charge accumulation at the Si/buried oxide (200nm thick) interfaces. The leakage current through the buried oxide is controlled with a picoampermeter (typically few pA).

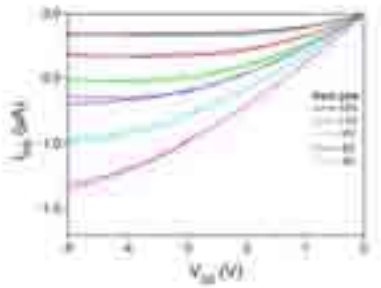

Fig. 3. Drain source current I_{DS} as function of the applied drain source voltage V_{DS} for several back gate voltage applied on the Si substrate.

Then, we investigate the response of the SiNW-FETs to voltage spikes applied in a front side physiological environment. An accurate control of the solution potential could be achieved with a three-probes potentiostat experiments. For these applications the nanowires conductance are measured with a home-made electronics card of 12 parallel acquisition inputs with a 200µs average measurement time allowing stable long time recordings [3].

These experiments are compared with 2D numerical experiments performed with commercial software (Silvaco). These allow rapid estimations of the expected conductance modulation with a liquid front gate, for several parameters such as doping concentration and device geometry. Figure 4 shows the expected conductance of a 30 nm thick, 10^{19} at./cm^3 boron doped Si-ribbon as a function of the front gate voltage, and the corresponding carriers distributions in the depletion regime.

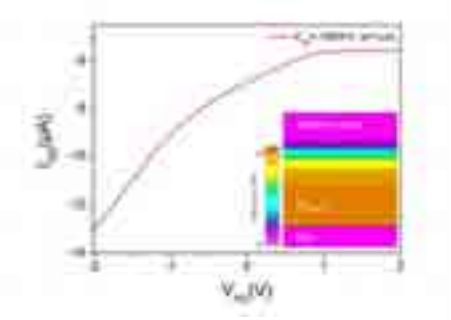

Fig. 4. 2D simulation of the drain source current as function of a front gate applied voltage. A dielectric layer (e_r~78.5) of same dielectric constant than water replaces the front side solution. Inset shows the layers stack and the hole concentration distribution in the depletion regime.

Finally, in vitro neurons networks are achieved with poly-lysine polymer patterns made on the SiNW-FETs with conventional lift-off process. The PLL polymers allow neurons adhesion and growth, while the PLL pattern geometry generates mechanical forces on the neurites that control the axonal differentiation (fig.5) [4]. Accurate localization of the axons in the network is essential for an efficient SiNW-neurons arrays alignment aimed to follow spikes propagation.

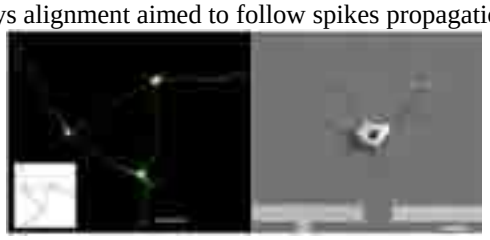

Fig. 5. Left. Fluorescent micrograph of a three-neurons network (6DIV). Axons are marked with a red fluorofore. The growth guidance was achieved through the use of adhesion PLL micropatterns shown with the inset. Scale bar is 50µm. Right. Scanning electron micrograph showing the efficient neurite-nanowire coupling. Scale bar is 10µm.

4 Conclusion

We have shown fabrication and characterization of SiNW-FETs arrays and their coupling to neurons networks that should be useful for in vitro neuronal signals detection. This method appears suitable to investigate signal transmission and synaptic plasticity in several network architectures.

Acknowledgement

We thank I. Ioanina, V. Bouchiat, L.Leroy, A. Bernand-Mantel for experimental supports and discussions. RTB “Neurowire” funding is thanks for partial support.

References

[1] Jaim Nulma, US Patent 5 043 300, 1991.
[2 Yi Cui et al. Nano Lett., Vol. 3, No. 2, 2003.
[3] C. Delacour et al. MRS Proceedings 1350:mrss11-1350-ee11-01, 2011.
[4] S. Roth et al. Small, doi: 10.1002/smll.201102325, 2012.

Coupling force-controlled nanopipettes with micro-electro arrays: A new approach for studying neuronal network response to single cell chemical stimulation

Jose F. Saenz Cogollo[1], Harald Dermutz[1], Tomaso Zambelli[1], Janos Vörös[1*]

1 Laboratory of Biosensors and Bioelectronics, Institute for Biomedical Engineering, University and ETH Zurich, Switzerland
* Corresponding author. E-mail address: janos.voros@biomed.ee.ethz.ch

Abstract
In this work we present a novel experimental platform based on the combination of MEAs with force-controlled nanopipettes. This new approach allows not only to perform atomic force microscopy (AFM) studies of neurons cultured onto MEAs, but also to chemically modulate the activity of single cells while recording the induced electrical response from the entire neuronal network.

1 Introduction

The complexity and scale of neuronal interconnections drive the demand for more specific and more spatially precise physiology research tools. Despite the great advantage of using micro-electrode arrays (MEAs) in recording in vitro neural activity, its applicability to cell stimulation presents some important limits, related to the presence of large stimulus artifacts and the poorly controlled spread of electrical stimuli in medium. One solution is to interact with individual neural cells by mimicking the neurons' own combination of electrical and chemical signaling. Such approach, intended to achieve a kind of "artificial synapse", consists in reproducing a critical behavior of real synapses: the local release of neurotransmitters. Recent developments of systems for precise neurotransmitter release include the use of micropipettes systems [1], microfluidic substrates [2], organic electronics [3] and optical release of caged compounds [4]. However, none of those methods have demonstrated spatially controlled single cell stimulation. Here we propose to combine the MEA technology with the recently developed FluidFM technology [5] which is based on the use of hollow- atomic force microscopy (AFM) cantilevers as force-controlled nanopipettes thus making it possible to have localized neurotransmitter release on the cell membrane with very precise control over force and spatial position.

2 Methods

In FluidFM a nanofluidic channel in the AFM cantilever allows soluble molecules to be dispensed through a sub-micrometer aperture in the tip. Force feedback is ensured by a standard AFM laser detection system that measures the deflection of the cantilever and thus the force applied by the tip to the cells during approach and delivering (see Fig. 1).

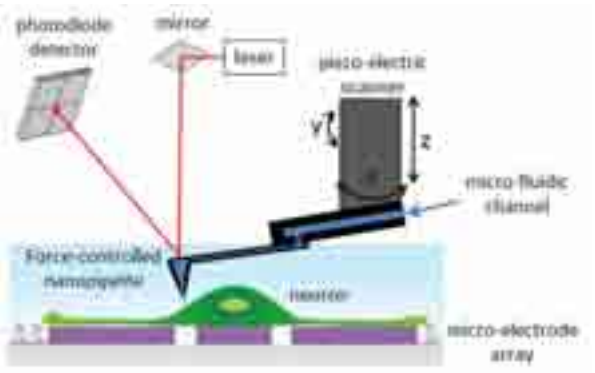

Fig. 1. Schematic drawing of the combination of MEA and FluidFM technologies.

For the construction of the experimental setup we started from existing commercial solutions: a MEA2100 system from Multi Channel Systems (Reutlingen, Germany) and a FluidFM system from Cytosurge (Zurich, Switzerland). Then we designed a specific mechanical stage for coupling both instrumentations and integrate them with a state of the art optical microscope. Custom-made glass-based MEAs with ITO electrodes make it possible to have optical access from bellow, enabling the implementation of functional optical evaluation techniques, like calcium imaging, for complementing the monitoring of the network activity.

For the experiments shown here, we used FluidFM cantilevers with blunt tip and 2 µm openings. The micro-fluidic channel was filled with physiological solution (NaCl 150 mM, KCl 2.8mM, MgCl 0.7mM, CaCl 1.3mM, Glucose 10mM, HEPES 10 mM) containing 200 µM of glutamate.

Dissociated E18 rat hippocampal neurons were cultured for up to 3 weeks. Neurobasal medium supplemented with B27 was used without serum. Cell plating density was 70.000 – 100.000 cells/cm2. Experiments were conducted after two weeks in vitro.

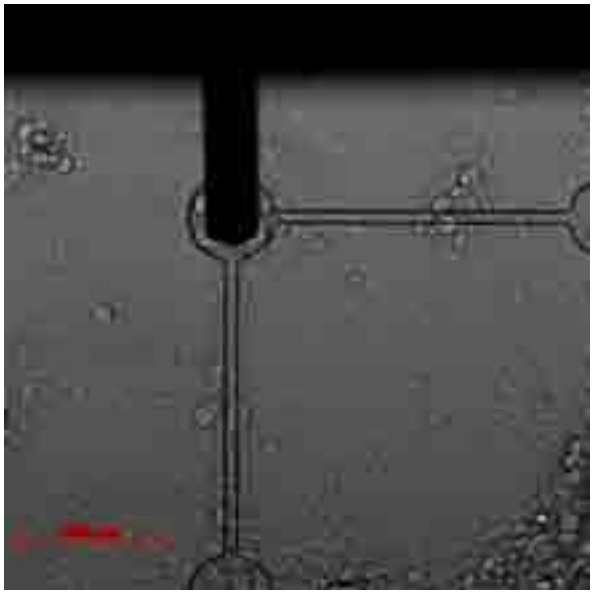

Fig. 2. Bright field image of a FluidFM tip delivering the neurotransmitter glutamate to a single neuron over an ITO electrode.

3 Results

Preliminary results have shown that the combined MEA-FluidFM set-up does not compromise the capability neither of the FluidFM to perform chemical delivering with a high spatial and force resolution, nor the capability of the MEA to record small extracellular potentials.

In order to chemically induce a local electrical response in a culture we first brought the FluidFM cantilever in contact to the cell membrane and then we applied pulses of pressure between 50 mbar and 300 mbar with 300 ms duration. In the fig. 3B a typical chemically induced local response is shown and compared with the more spread spontaneous activity (fig. 3A).

4 Conclusion/Summary

We have presented a new experimental platform that put together the MEA and FluidFM instrumentation for measuring and modulating the behavior of neuronal networks *in vitro*. The localized chemical delivering capability of the FluidFM allows us to precisely control the stimulation, sized down to single neuron, and the MEA multi-point electrical recording make it possible to record the changes in the electrical activity of the entire network, thus potentially enabling the study of the role of single cell activity in network computation.

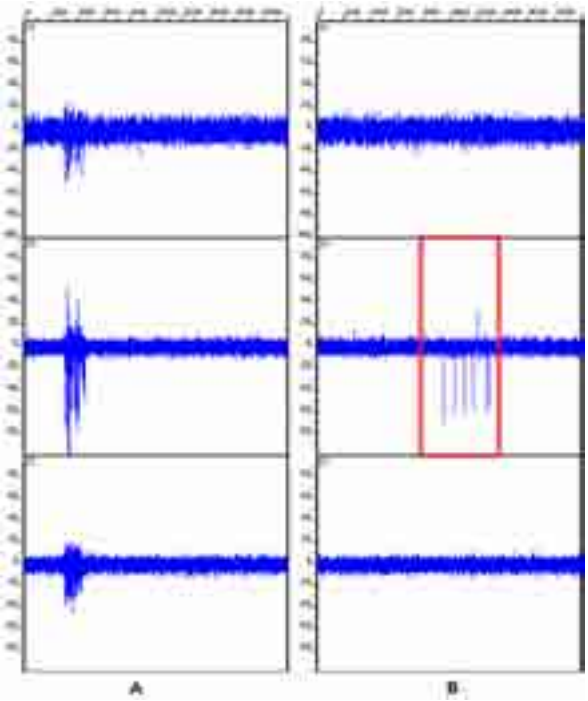

Fig. 3. Spontaneous electrical activity recorded from three nearby electrodes (A) and local electrical response induced by the release of glutamate over a cell in the middle electrode during the time indicated by the red square (B).

Acknowledgement

We thank Multi Channel System GmbH for their support in the designing process of the experimental setup. We would also like to thank the Institute of Pharmacology and Toxicology – Morphological and Behavioral Neuroscience, which kindly provided us the hippocampal neurons.

References

[1] O. Feinerman, “A picoliter ‘fountain-pen’ using co-axial dual pipettes,” *Journal of Neuroscience Methods*, vol. 127, no. 1, pp. 75-84, Jul. 2003.

[2] M. C. Peterman, J. Noolandi, M. S. Blumenkranz, and H. a Fishman, “Localized chemical release from an artificial synapse chip.,” *Proceedings of the National Academy of Sciences of the United States of America*, vol. 101, no. 27, pp. 9951-4, Jul. 2004.

[3] D. T. Simon et al., “Organic electronics for precise delivery of neurotransmitters to modulate mammalian sensory function.,” *Nature materials*, vol. 8, no. 9, pp. 742-6, Sep. 2009.

[4] D. Ghezzi, A. Menegon, A. Pedrocchi, F. Valtorta, and G. Ferrigno, “A Micro-Electrode Array device coupled to a laser-based system for the local stimulation of neurons by optical release of glutamate,” *Journal of Neuroscience Methods*, vol. 175, no. 1, pp. 70-78, 2008.

[5] A. Meister et al., “FluidFM: combining atomic force microscopy and nanofluidics in a universal liquid delivery system for single cell applications and beyond.,” *Nano letters*, vol. 9, no. 6, pp. 2501-7, Jun. 2009.

Carbon nanotube electrodes for neuronal recording and stimulation

Boris Stamm[1*], Kerstin Schneider[2], Thoralf Herrmann[1], Monika Fleischer[2], Claus Burkhardt[1], Wilfried Nisch[1], Dieter P. Kern[2], and Alfred Stett[1]

1 NMI Natural and Medical Sciences Institute at the University of Tuebingen, Reutlingen, Germany
2 Institute for Applied Physics, University of Tuebingen, Germany
* Corresponding author. E-mail address: boris.stamm@nmi.de

Abstract
Carbon Nanotube (CNT) microelectrodes are deemed to have enhanced properties compared to conventional metal electrodes. This holds in particular for electrochemical properties and the ability of CNTs to act as a good substrate for neuronal cells. The aim of our research was to synthesize structured CNT microelectrodes and compare them with established titanium nitride (TiN) microelectrodes.

1 Introduction

In order to record or stimulate electrical cell activity, e. g. of neuronal cells, microelectrode arrays (MEAs) comprising several independent electrodes are a well established in vitro test system [1]. MEAs are e. g. used in basic research in order to investigate neuronal network formation or in applied research in order to investigate the effects of new pharmaceutical agents on cells or cell tissue.

Beyond biocompatibility and biostability for long term applications of the MEA and their substrate (usually an insulating layer deposited on glass slides) important properties are the impedance and charge transfer capability of the electrodes. Desirable are a low electrode impedance to gain the electrical spike activity of cells as loss-free as possible while recording and a high charge transfer while electrically stimulating cells with voltage pulses.

Due to their chemical inertness, high charge transfer capability, low impedance [2] and good substrate properties for neuronal cells the integration and characterisation of carbon nanotubes as micro electrodes has become of interest. Here we present the approach and results of synthesizing structured CNT electrodes via a chemical vapor deposition (CVD) process directly on MEA substrates.

2 Materials and Methods

For all experiments the MCS MEA design 200iR 30 [3] was used in order to achive comparable test systems. This design consists of 59 working electrodes each 30 microns in diameter and 200 microns apart plus one internal reference electrode. For the synthesis of structured CNT microelectrodes on MEA substrates a thermal CVD process at a temperature of 520 °C was applied. Because of this high temperature and the thermal instability of the established MEA system, which resulted in first experiments in a cracked insulating layer, a new material combination was developed, now consisting of TiN circuitry and silicon oxide (SiO_x) insulating layer instead of titanium circuitry and silicon nitride (Si_3N_4) insulating layer. This circuitry-insulating layer system is high temperature stable, meaning that neither any layer cracking nor decreased insulating properties occur after CNT synthesis.

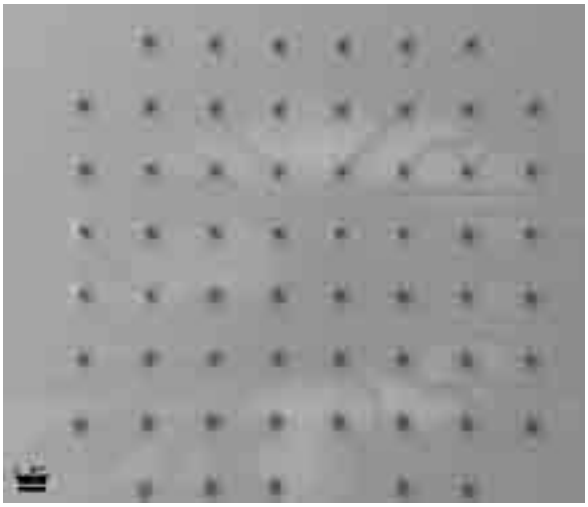

Fig. 1. SEM image of a CNT-MEA (array design according to MCS MEA 200iR 30 [3]). The scale bar represents 100 micrometers.

The CNT synthesis on a substrate is structured by patterning its enabling catalyst layer, which is usually a thin film of Fe or Ni. Here, a 10 nm Fe catalyst layer was sputter-deposited and afterwards patterned via lift-off technique to cover just the electrodes. For the CNT synthesis itself a NH_3-C_2H_2 gas atmosphere with a ratio of 1:1 for a time period of 30 min at 5 mbar (3,76 Torr) recipient pressure was applied. SEM images of CNT microelectrodes are shown in Fig. 1 and Fig. 2.

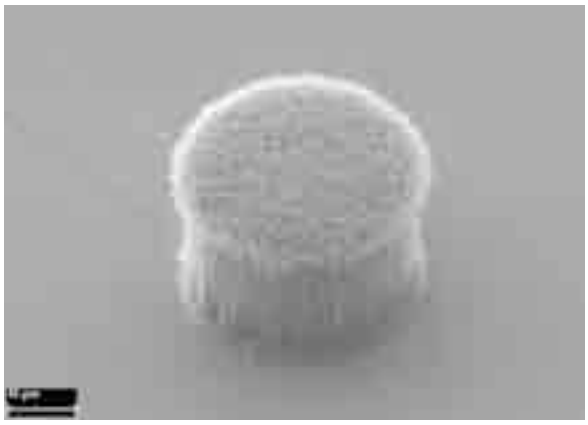

Fig. 2. SEM image of a single CNT microelectrode. The scale bar represents 10 micrometers.

After the CNT synthesis the CNT microelectrodes were briefly exposed to an O_2-plasma in order to remove residual amorphous carbon which surrounds the CNTs. This plasma treatment reduces the impedance of the electrodes.

3 Results

The CNT-MEAs were electrochemically characterized in phosphate buffered saline (PBS) by measuring the impedance at 1 kHz and the charge transfer with monophasic voltage pulses with amplitudes ranging from -1 V to +1 V and pulse duration 500 µs [4]. The measured impedance of CNT microelectrodes was 20 kΩ at the mentioned frequency, which is an improvement of 50 % compared to 40 kΩ of the standard MEA with TiN electrodes. Measuring the charge transfer (see Fig. 3) revealed a value of 10,1 nC at +1 V for CNT electrodes, which is an improvement of 72 % compared to 5,9 nC of TiN electrodes under the same conditions.

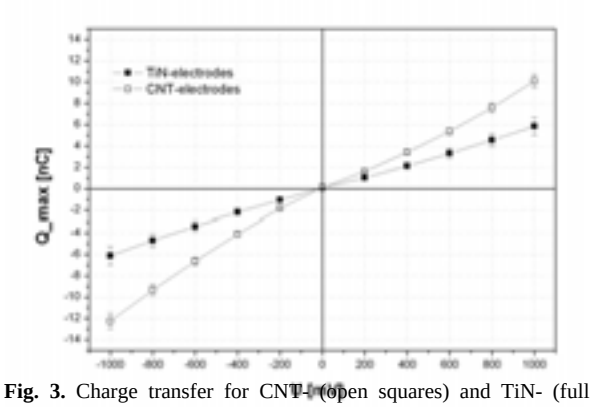

Fig. 3. Charge transfer for CNT- (open squares) and TiN- (full squares) electrodes under same conditions. The charge transfer of CNT electrodes is improved up to 72 %

The suitability of the CNT electrodes for recording purposes of neuronal cells was tested with dissociated cortical neurons from a rat. A cell culture was cultivated for a time period of 12 weeks, which proves the good substrate quality, long term stability and biocompatibility of the SiO_x insulating layer and not least of the CNT electrodes. During the 12-week cultivation network formation of the neurons was observed and neuronal spike activity (action potentials) was recorded (see Fig. 4) with a signal-to-noise ratio of up to 8.

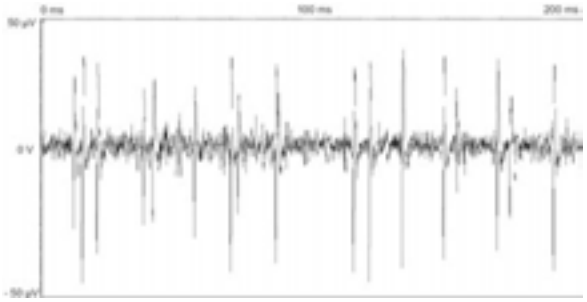

Fig. 4. Spike activity of dissociated cortical neurons, cultured on a CNT-MEA. The shown time period is 200 ms, the vertical window width is 100 µV.

Acknowledgement

This work was funded by Baden-Württemberg-Stiftung under grant MST II 12. The authors greatfully acknowledge the support of the clean room- and technical staff.

References

[1] Stett A., Egert U., Guenther E., Hofmann F., Meyer T., Nisch W., Haemmerle H. (2003). Biological application of microelectrode arrays in drug discovery and basic research. *Analytical and Bioanalytical Chemistry*, 377, 486-495.

[2] Keefer E.W., Botterman B.R., Romero M.I., Rossi A.F., Gross G.W. (2008). Carbon nanotube coating improves neuronal recordings. *Nature Nanotechnology*, 3, 434-439.

[3] www.multichannelsystems.com

[4] Stett A., Barth W., Weiss S., Haemmerle H., Zrenner E. (2000). Electrical multisite stimulation of the isolated chicken retina. *Vision Research* 40:1785-1795

A novel removable culture chambering system for multi-well MEAs

Marc P. Powell[1*], Ming-fai Fong[1,2], Steve M. Potter[1]

1 Laboratory for Neuroengineering, Department of Biomedical Engineering, Georgia Institute of Technology, Atlanta, GA, USA
2 Department of Physiology, Emory University School of Medicine, Atlanta, GA, USA
* Corresponding author, E-mail address: marc.powell@gatech.edu

Abstract
Multi-well microelectrode arrays (MEAs) are useful tools in extracellular electrophysiology, but geometric constraints of commercially-available multi-well MEAs restrict to cultures grown in these devices. In particular, the fixed culture chambering system prevents access of high-magnification objectives or intracellular recording electrodes to the cell layer. In this study, we sought to create a removable culture chambering system for multi-well MEAs. We designed a polydimethylsiloxane (PDMS) divider that provides pharmacological separation of cultures during an MEA recording experiment, but can be removed to improve access to the cellular layer. Here we report on the design and production of two prototypes and assess their efficacy in maintaining culture health.

1 Introduction

Multi-well MEAs provide significant advantages over the conventional single well MEA. The multiple arrays allow for many trials to be run simultaneously, thus sister cultures can be used under the same environmental conditions to reduce sources of variability in MEA experiments. The consolidation of multiple arrays onto one dish also eliminates the need for multiple pre-amps for separate test groups, significantly saving laboratory resources and reducing the number of animals used for tissue harvests. However, commercially available multi-well MEAs use a fixed divider with geometric constraints that cannot accommodate patch clamp experiments or high magnification imaging using an upright microscope (Fig. 1A). The aim of this project was to create a removable chambering system to facilitate patch clamp experiments on multi-well MEAs (Fig. 1B,C).

2 Materials and Methods

2.1 PDMS dividers

We designed and manufactured two types of removable PDMS culturing chambers. The first (Fig. 2A) was optimized for chamber volume, and the second (Fig. 2B) was optimized for adhesion to the MEA surface. In both cases, a thin film of 70% ethanol was used to adhere the PDMS to the MEA glass. Evaporation of ethanol yielded a tight but reversible seal. Teflon lids were used to enclose the main chamber of the MEA to prevent evaporation.

Dissociated cultures derived from E18 rat cortex tissue were grown in each chamber to assess viability.

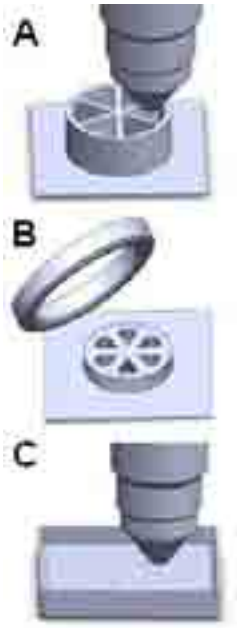

Fig. 1: Fixed versus removable dividers. (A) Solid model of the Multichannel Systems 6-well MEA and a Nikon CFI Fluor 40xW objective. The fixed divider is not compatible with high-magnification microscopy. **(B)** Solid model of one of our custom removable dividers and lid. **(C)** Solid model of MCS 6-well MEA after divider has been removed. In contrast with (A), there is ample space for high-magnification objectives. Note: MEA dimensions are 49mm x 49mm

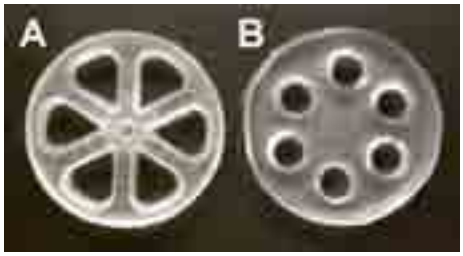

Fig. 2: Removable PDMS Dividers. (A) Tear drop well divider optimized for chamber volume. **(B)** Circular well divider optimized for adhesion surface area.

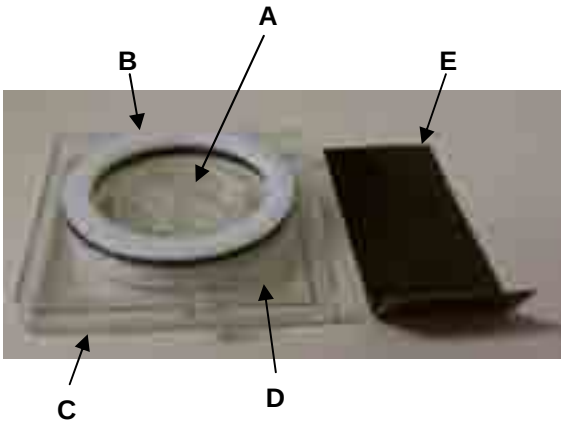

Fig. 3: Components of modifiable chambering system. (A) Removable PDMS divider **(B)** PDMS rimmed lid **(C)** MEA box **(D)** MEA **(E)** Removal tool

2.2 Chamber accessories

For using the PDMS divider during cell growth and MEA recording experiments, a modified MEA lid was created by putting a rim of PDMS along the bottom of a version of lids described in [1] with a larger diameter (Fig. 1B). The PDMS prevents movement of the lid on the MEA surface thus eliminating the possibility of the lid accidently removing the PDMS divider prematurely.

Once the PDMS divider has been removed for an intracellular recording experiment, there is no chamber to hold fluid which is critical for environmental control. To address this, the MEA is placed in a plastic MEA box (Fig. 1C, 3C). A thin layer of PDMS on the bottom of the container prevents MEA movement during the procedure. A tool was developed out of sheet metal to facilitate removal of the MEA from the box (Fig. 3E).

3 Results and Discussion

3.1 Adhesion and fluid retention

We examined whether the PDMS dividers could adhere to glass and retain fluid for two days in an incubator regulated at 35°C and 5% CO_2. Both divider prototypes successfully adhered to glass. Neither showed signs of leakage between chambers or to the surroundings.

3.2 Culture health and osmolarity

Neuronal cultures were grown for 29 days in both chamber types to test compatibility with living cells. Normal cell growth was observed under a phase-contrast microscope throughout the 29 days. Osmolarity was maintained within a viable range using the tear drop well divider in experimental conditions (Fig. 4). In contrast, the large surface area to volume ratio of the chambers in the circular well divider appeared to negatively affect osmolarity control (Fig. 4).

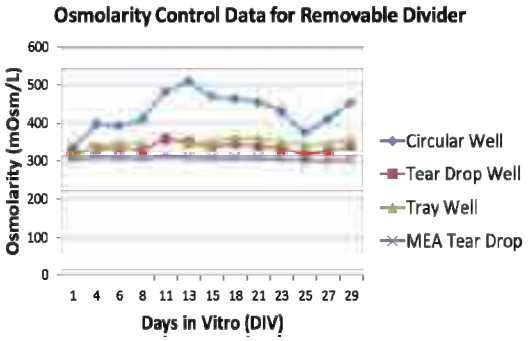

Fig.4: Osmolarity control data Each point represents the osmolarity of the fluid removed during each culturing media change. Fluid was replaced with media at 300 ± 6 mOsm/L. The tear drop divider used on an MEA with a Teflon lid [1] (MEA Tear Drop) had very consistent osmolarity control. When tested in a 6 well tray the circular well divider had poor osmolarity control compared to the tear drop divider which had similar results to the control well.

4 Conclusion

The removable divider reported here expands the experimental accessibility of commercially available multi-well MEAs compared to fixed rigid chambers. We have created a simple PDMS device that can be easily attached to and removed from MEA glass along with accessories to aid in the deployment of the device in its various uses. Together they provide a new tool for researchers seeking to conduct experiments that employ high-magnification microscopy using multi-well MEAs. The system is currently being tested to ensure its success during both an MEA recording experiment as well as a whole cell patch clamp experiment.

Acknowledgements

We thank Theodore French for his assistance in CNC machining, J.T. Shoemaker for his assistance in tissue harvesting, Gareth Guvanasen and Dr. Axel Blau for their insight into using PDMS, and Jonathan Newman for useful discussions. The work was supported by NIH NINDS Grant R01NS065992 to Dr. Peter Wenner (Emory University), the NSF EFRI grant 1238097 to S.M.P, the Petit Scholars Program Fellowship to M.P.P, and the NSF GRFP 09-603 Fellowship and Emory NI SPINR Fellowship to M.F.

References

[1] Potter, S.M., DeMarse. T.B. (2001) "A new approach to neural cell culture for long term studies." J. Neurosci Methods 110: 17-24.

High-resolution bio impedance imaging and spectroscopy with CMOS-based microelectrode arrays

Vijay Viswam*, Marco Ballini, Veerendra Kalyan Jagannadh, Branka Roscic, Jan Müller, David Jäckel, Andreas Hierlemann

ETH Zürich, Bio Engineering Laboratory, D-BSSE, CH-4058 Basel, Switzerland
* Corresponding author. E-mail address: vijay.viswam@bsse.ethz.ch

Abstract
Here we report on a new method for impedance spectroscopy based on a high-density microelectrode array (MEA), which can be used to determine the location of adherent mammalian cells by analyzing the impedance response within a frequency band from 10Hz to 10kHz.

1 Introduction

Impedance imaging and spectroscopy is an effective, non-invasive, electrical method of monitoring features of cultured cells, such as their position, morphology and cell-electrode adhesion. Here, we present a method for impedance measurements in a CMOS-based planar MEA.

2 Methods

We used an existing CMOS MEA system [1] featuring 11011 metal electrodes, 126 on-chip readout channels, stimulation units, and an analog switch matrix located directly underneath the electrode array. By means of the switch matrix an electrode can be connected to the stimulation buffer. The impedance can then be measured by applying an AC current (I_{Stim}) and sensing the voltage (V_{sense}) with a readout channel connected to the same electrode, as shown in Fig. 1. Since the input impedance (3.32pF) of the readout channels is approximately two orders of magnitude larger than that of the electrodes (|Z|= 4.6MΩ@1kHz), most of the AC current will pass through the electrode to the solution, which is held at constant potential by means of a reference electrode. Cells that are attached to the electrode surface change the measured impedance so that detection of cell adhesion on a large area at high spatial resolution becomes possible. On-chip analog-to-digital converters are used to digitize the signals, which are finally sent to a PC. The acquired signals are post-processed in Matlab to extract the spectra and to filter out the noise. Since the amplitude of the applied current sine wave is known [2], we can estimate the impedance of the electrode from the recorded amplitude. The procedure is repeated at different frequencies, from 10Hz to 10kHz, and then repeated for other electrode sets to cover the entire electrode area. Up to 42 electrodes can be measured in parallel reducing the measurement time for the full array.

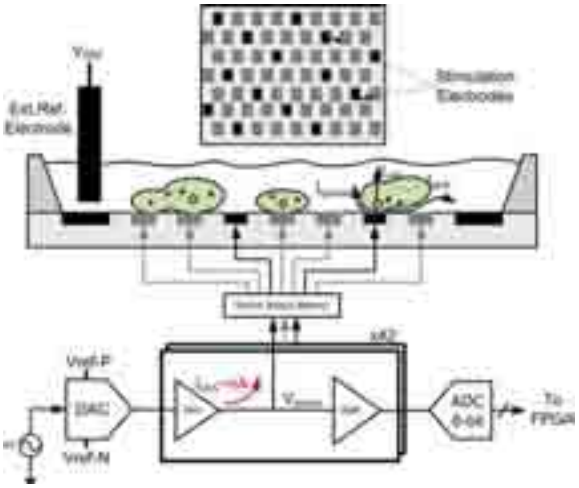

Fig.1 On-chip Impedance Measurement System.

An impedance image of the area is then assembled from the impedance values of each electrode.

3 Results

We tested the method by depositing Pt-black on half of the electrode array; the result is shown as an optical and a reconstructed impedance image in Fig. 2. Fig. 3 shows mammalian baby hamster kidney, BHK-21, cells cultured on the MEA for 3 days. From the impedance image, one can clearly see the position of the cultured cells on the electrodes. Both experiments were carried out using a 1kHz sine wave.

4 Conclusion

We have developed a method relying on a high density MEA to determine the location of adherent mammalian cells by analyzing the impedance response in a range between 10Hz and 10kHz. Preliminary experiments show the possibility to identify electrodes with Pt-black deposition or locate the distribution of BHK-21 cells on the electrode area.

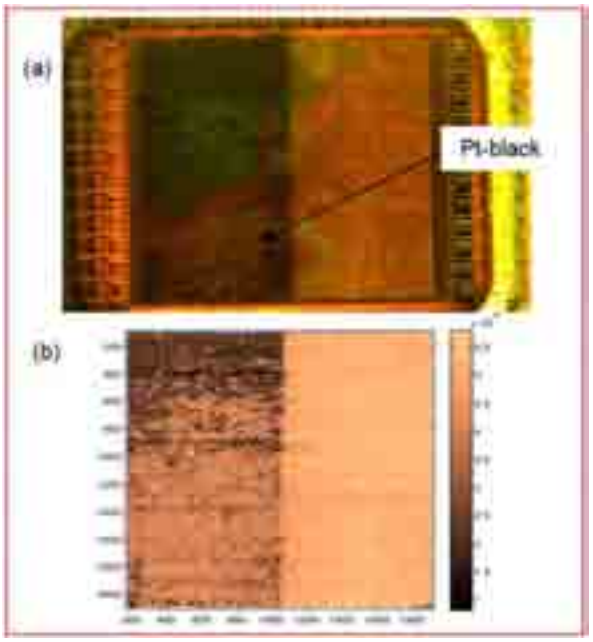

Fig.2 (a) Image of the array with Pt-black covering half of the electrodes; (b) Impedance image (color bar in MΩ).

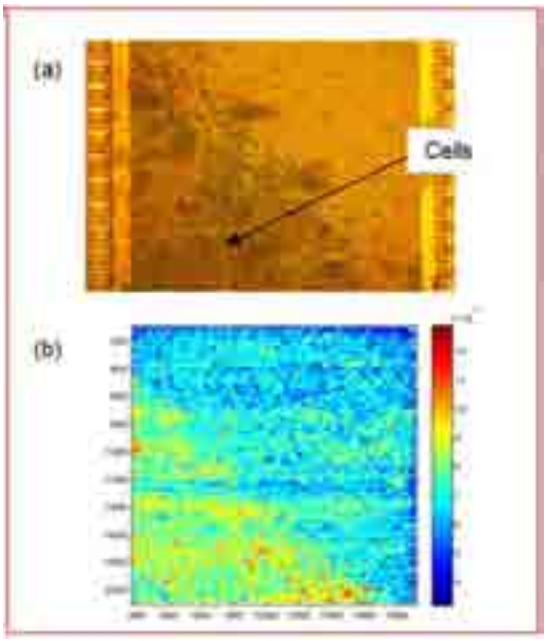

Fig.3 (a) Image of BHK-21 cells cultured on the MEA for 3 days; (b) Impedance image (color bar in MΩ).

Acknowledgement

This work has been conducted with financial support of the European Community through the ERC Advanced Grant 267351, NeuroCMOS.

References

[1] U. Frey, J. Sedivy, F. Heer, R. Pedron, M. Ballini, J. Mueller, D. Bakkum, S. Hafizovic, F. D. Faraci, F. Greve, K.-U. Kirstein, and A. Hierlemann, "Switch-matrix-based high-density microelectrode array in CMOS technology", *IEEE Journal of Solid-State Circuits*, Vol. 45, no. 2, pp. 467–482, 2010.

[2] P. Livi, F. Heer, U. Frey, D. J. Bakkum, and A. Hierlemann, "Compact Voltage and Current Stimulation Buffer for High-Density Microelectrode Arrays", *Proceedings of the IEEE International Solid-State Circuits Conference*, ISSCC, San Francisco, USA, 2010, pp. 240 – 241, 2010, ISSN 0193-6530, ISBN 978-1-4244-6034-2.

Interfacing with tens of neurons in acute neural tissue using an array of 61 extracellular micro-needles

Deborah E. Gunning [1*], John M. Beggs [2], Wladyslaw Dabrowski [3], Pawel Hottowy [3], Christopher J. Kenney [4], Alexander Sher [5], Alan M. Litke [5], Keith Mathieson [1]

1 Institute of Photonics, University of Strathclyde, Glasgow, G4 0NW, UK
2 Biocomplexity Institute, University of Indiana, Bloomington, IN47405, USA
3 Faculty of Physics and Applied Computer Science, AGH University of Science and Technology, Krakow, 30-059, Poland
4 SLAC National Accelerator Laboratory, Menlo Park, CA94025, USA
5 SCIPP, University of California Santa Cruz, Santa Cruz, CA95064, USA
* Corresponding author. E-mail address: deborah.gunning@strath.ac.uk

Abstract
Understanding information processing in the brain is one of the major goals of modern neuroscience. Even small-scale neural circuits are daunting in their complexity and require the development of new sensor technologies. We present a novel array of 61 micro-needle electrodes, of up to 200µm length and with 60µm hexagonally close-packed inter-needle spacing. The array allows an in-depth study of neuronal interactions by penetrating in to acute slices of brain tissue. Extracellular action potentials of up to 110µV are recorded from tens of neurons simultaneously. Furthermore, the electrodes can electrically stimulate individual neurons using charge-balanced current pulses. This has paved the way for the development of a 512-electrode system with the potential to record from hundreds of neurons simultaneously.

1 Introduction

This study involved the design, microfabrication, electrical characterisation and biological evaluation of an array of closely spaced micro-needles. The purpose of the array is to allow an in-depth study of neuronal interactions by recording from and electrically stimulating individual neurons in acute neural tissue.

Arrays of planar microelectrodes have been used very successfully to record the electrical activity of many neurons in vitro in 2-d structures (e.g. retina) [1]. This success has not been replicated in acute 3-d structures (e.g. acute cortical slices) as a consequence of a tissue slice's damaged surface layer. To address this problem, electrodes must penetrate beyond the damage. Extracellular wire electrodes or patch-clamps [2][3] bypass the damaged layer, however, the problem common to both techniques is the small number of neurons they detect. Here, a process was successfully developed to fabricate an array of 61 micro-needles to record from many neurons in an intact network. The novelty of this device over current technologies of this nature is the high-density, 60µm hexagonally close packed, array of electrodes (cf. 100µm [4] or 400µm [5]) and to allow recordings through a volume of tissue, multiple length needles are possible on a single array. Each needle has a small (10µm diameter) conducting tip with low impedance (~300kΩ ..ı). A first generation device with 61 needles recorded extracellular action potentials from ~20 individual neurons in rat cortex. Action potentials were recorded with amplitudes up to 110µV and a signal to noise of ~15:1. The electrodes were shown to be capable of eliciting action potentials with individual neuron precision via electrical stimulation using charge-balanced current pulses with ~1 to 2.9µA amplitudes. It is expected that the number of neurons detected by a second-generation 512-needle device will increase by an order of magnitude.

2 Method

The device is made using a novel combination of semiconductor fabrication techniques. The design is compatible with existing low noise pre-amplification and stimulation circuitry [6] that provides excellent temporal resolution (50µs). To fabricate the array, 61 high-aspect ratio tapered holes are etched in to silicon. A thick (2µm) thermal oxide is grown to form the needle sidewall passivation. A conformal tungsten deposition (low pressure chemical vapour deposition) ensures the tapered point of the etched hole is conducting (this will form the tip of the needle). The tungsten is selectively etched to electrically isolate each needle. For strength, the holes are partially filled with polysilicon. Aluminium is deposited and etched to form conducting tracks connecting each electrode to a bond pad for wire bonding to the readout PCB. The bulk silicon, on the backside of the wafer is chemically wet etched (tetra methyl ammonium hydroxide at 95^{o}C) to expose the oxide–coated needle tips. The size of the conducting tip is controllable in

size down to a few microns in diameter and is defined at this stage. The oxide is partially etched in hydrofluoric acid. The remaining silicon is etched as before, defining the length of the needle. A final oxide etch thins the sidewall insulation but completely removes the thinner oxide at the needle tip, exposing tungsten. This tungsten is electroplated with platinum black to lower the electrode/electrolyte impedance (Figure 1). The result is an array of closely spaced, low impedance, biocompatible electrodes with low noise at high spatial resolution. To quantify this: a typical electrode has, at 1 kHz, an impedance of 300 kΩ and ~5 μV RMS noise.

Fig.1 An array of hexagonally close-packed, 60 μm inter-needle spacing, 100 μm length needles (left) and the tip of a single needle electroplated with platinum to lower the needle impedance (right).

3 Results

In pilot experiments, acute slices of rat cortex were placed on to an array of needles. Using an artificial cerebrospinal fluid (using 5mM K^+) and precise temperature control (37°C), the slice was kept alive and the spontaneous activity of the cells was recorded. 300 μm thick slices were cut to allow perfusion of oxygen throughout the slice. Typically, signals from ~20 individual neurons could be detected (Figure 2) with both somatic and axonal action potentials being observed. Action potential amplitudes measured up to ~110 μV and the signal to noise ratio was ~15:1.

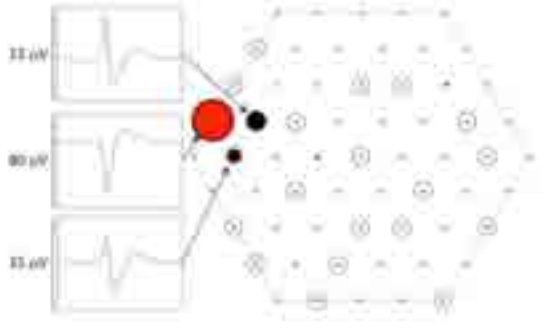

Fig. 2. The averaged signals of a neuron identified from its spontaneous activity. Each point in the hexagon represents an electrode's position on the array and the diameter of the point is proportional to the signal amplitude recorded on that electrode for a particular neuron. The seed electrode (red) is the electrode that records the highest amplitude waveform. The dashed circles indicate the locations of other neurons found in this preparation.

To verify the requirement of high-density electrodes, the data was sub-sampled (electrodes removed to create a 120μm spaced array) and re-analysed. For the dataset in Figure 2, the number of neurons identified decreased from 20 to 7. In a further six unique datasets (from different tissue preparations) it was found that the number of neurons, at best, was halved when the electrode spacing was increased and at worst was reduced to less than 10%.

Another important aspect of network studies is electrical stimulation. A range of current amplitudes from 0.4 to 4μA with 10% increments was applied to each electrode (50 iterations at each amplitude). The current pulse was triphasic and charge balanced with duration of 50μs/phase. It was found that ~8 neurons could be stimulated in a single preparation. The minimum stimulation current amplitude for 100% stimulation efficiency varied between 1.1 and 2.9μA.

4 Conclusions

As an important in vitro model of the brain, it is relevant to study network behaviour in acute slices. The challenge for microelectrode arrays is to bypass the damaged tissue that exists at the surface of an acute slice. A popular approach is to use arrays of micro-needles that can penetrate past the surface and make contact with healthy neurons in the intact network. In this study, an array of 61, 60μm spaced hexagonally close-packed needles was fabricated. It was shown to record action potentials from ~20 neurons in acute rat cortex across a 0.13mm^2 array area, with a signal to noise ratio of ~15:1 and signal amplitudes of 50-110μV. Furthermore, individual neurons were stimulated with 50μs/phase charge-balanced current pulses of amplitudes ~1.1 to 2.9μA (for 100% stimulation efficiency). This work represents a significant advancement in technologies for studying acute neural tissue in vitro with an unprecedented combination of spatial and temporal resolutions.

Acknowledgement

The work was funded by EPSRC grant EP/E039731/1 (DEG), NSF grants IIS-0904413, PHY-0750525 (AML) and IIS-0904912 (JMB), a Burroughs Wellcome Fund Career Award at the Scientific Interface (AS) and Polish Ministry of Science and Higher Education grants (WD). The device fabrication was done at the SNF, Stanford University, the JWNC, University of Glasgow and the Queen's University, Belfast.

References

[1] Field G.D. (2010): Nature, *467, 673-677*
[2] Castaneda-Castellanos D.R. (2006): Nature Protocols, *1, 532-542*
[3] Davie J.T. (2006): Nature Protocols, *1, 1235-1247*
[4] Heuschkel M.O. (2002): J. Neurosci. Methods, *114, 135-148*
[5] Nordhausen C.T. (1994): Brain Research, *637, 27-36*
[6] Hottowy P. (2008): Analog Integr. Circuits Signal Process, *55, 239-248*

Single cell recording and stimulation using a 0.18µm CMOS chip with 16,384 electrodes

R. Huys, D. Jans, A. Stassen, L. Hoffman, W. Eberle, G. Callewaert, P. Peumans, D. Braeken

Bio-NanoElectronics, Imec, Kapeldreef 75, Leuven, Belgium

1 Background/Aims

Electrophysiological methods are essential to increase our understanding of cellular network dynamics. A crucial improvement to meet this need is provided by multi-electrode arrays (MEAs) that enable large-scale non-invasive parallel electrical recordings. Major drawbacks of these *passive* MEAs, such as the limited amount of channels and the need for external amplification and filtering, inspired several groups in fabricating *active* MEAs based on CMOS technology. Hence, the reported systems offer significant improvements over conventional *passive* MEAs. We further increased the density and decreased the size of electrodes by using standard 0.18 µm CMOS technology in combination with in-house post-processing, aiming at single-cell addressability.

2 Methods/Statistics

We fabricated a high-density array of 16,384 micro-nail electrodes on top of the CMOS circuitry. The electrodes consisted of subcellular-sized tungsten rods (600 nm diameter) enclosed by a 300 nm SiO_2 layer. Every electrode was accessible for stimulation, recording and impedance sensing through software selection.

3 Results

The built-in impedance circuitry of the chip was used to characterize the electrical properties of the electrodes. The small tungsten electrodes had a characteristic capacitance of 7.5 ± 1.5 pF, large enough to allow measurement of extracellular electrical activity. After culturing primary cardiomyocytes on the chip for 4 days, we recorded spontaneous extracellular activity of cells on top of the electrodes (Fig. 1). Despite the submicron size of the electrodes, we obtained extracellular signals with signal-to-noise ratios of 15. Further, we demonstrated single cell electrical stimulation by overriding the inherent frequency of the spontaneous cardiac beating. The high-density electrode configuration allowed recording of individual cell action potentials and identifying the signal propagation through gap junction connections between neighboring cells.

4 Conclusion/Summary

This novel active MEA is a step forward to both fundamental cellular communication and pharmaceutical drug screening platforms, allowing high-throughput automated measurement with single-cell resolution.

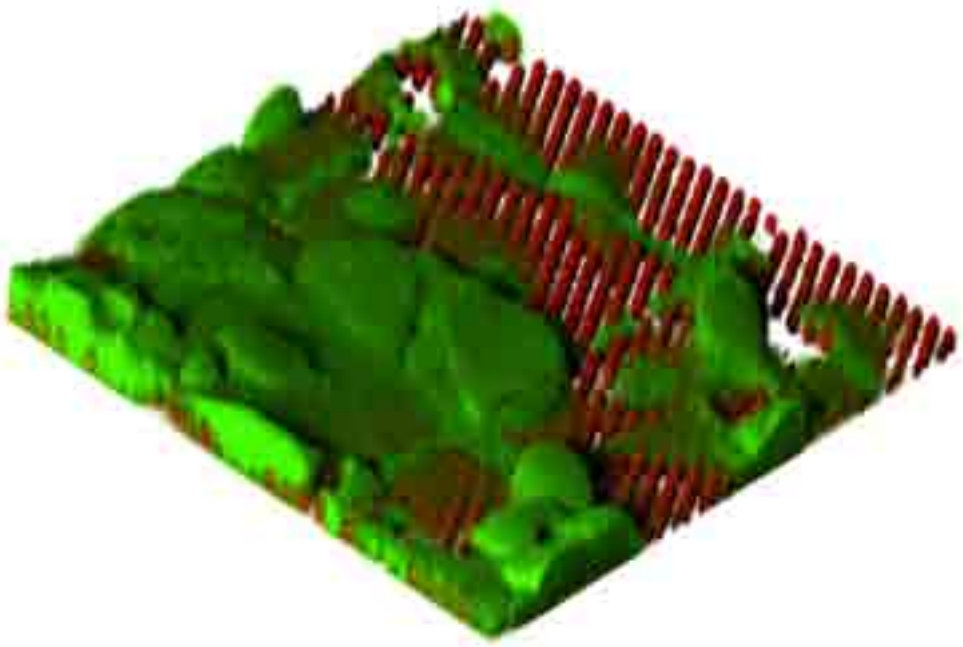

Fig.1 Reconstructed confocal image of cardiac cells growing on high-density active electrode arrays. Micronails are stained red; cells loaded with calcein green are stained green.

Sensors for Glass Cell-Culture Chips (GC^3)

M. Nissen[1], S.M. Buehler[1], S.M. Bonk[1], M. Stubbe[1], T. Reimer[1], W. Baumann[1] and J. Gimsa[1*]

1 University of Rostock, Chair of Biophysics, Gertrudenstr. 11 A, 18057 Rostock, Germany
* Corresponding author. E-mail address: jan.gimsa@uni-rostock.de

Background/Aims
Our glass cell-culture chips (GC^3) are equipped with Pt sensors for monitoring electrical signals, cell proliferation, and environmental conditions, such as medium temperature, pH and O_2 concentration.

1 Methods/Statistics

We designed five different integrated sensors for our glass cell culture chips (GC^3) [1, 2]: A temperature probe, pH- and O_2- sensors allow for the on line control of the environment within the glass chip. Interdigitated electrode structures (IDES) detect both the cell adhesion and proliferation, while multielectrode arrays (MEA) monitor their electric activity (Fig. 1). The cells can be located to the different structures by using dielectropheresis during cell seeding.

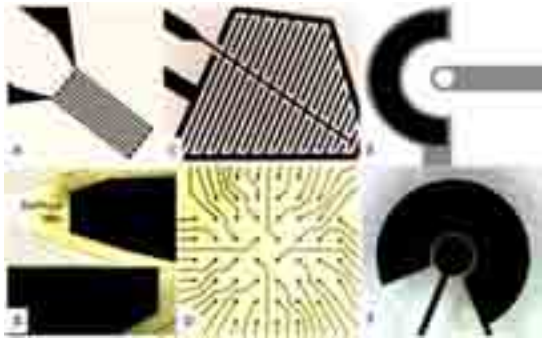

Fig. 1. Sensors of the GC^3: A) Temperature sensor, B) Mass electrodes, C) IDES, D) Multi-electrode array (MEA), E) Circular electrode for O_2 measurement*, F) Circular electrode for pH measurement*
**: Integration into the GC^3 is intended*

2 Results

The temperature probe was constructed following the principle of commercially available PT1000 temperature probes. It shows a linear behaviour in the range between 20 and 40 °C. However, an individual calibration is required for monitoring exact temperature values, as the resistance for 20 °C and the slope has a wide distribution.

Circular Pt electrodes were used for the O_2- sensor and with an additional Si_3N_4 layer as sensor substrate (20 - 60 nm) they were used as pH- sensors. The O_2 sensor typically shows a signal difference of 2 nA at -700 mV vs. Ag/AgCl comparing oxygen free and oxygen containing solution. In the pH range from 5 to 9 the pH sensor shows a linear response with a slope of up to -39.9 mV per pH step.

Electric impedance data of the IDES were used to calculate differential capacitance spectra. The number of cells growing on the IDES strongly correlated to the measured frequency peak values. Murine cortical cells were used to build active neuronal networks on the MEA structure. After 30 days, neuronal activity was measured with a MEA structure containing 52 electrodes. We tested different MEAs with electrode pad diameters of 15, 20, 25 and 35 µm.

3 Conclusion/Summary

Glass waver technology provides the tools to design microscopable chips with a huge variety of sensors to monitor cell culture conditions, cell growth and electric activity. Equipped with a cell-culture trough containing a medium volume of approximated 250 µl, it is possible to cultivate cells for up to 30 days. Our chips are more robust than conventional silicon chips and have a high rate of reusability. The GC^3 are autoclavable. Currently, we have a toolbox of five different sensor types for the design of specific GC^3. The new oxygen and pH sensors may complement our routinely used glass neurochip [3].

References

[1] Buehler S., Bonk S., Stubbe M., Reimer T., Nissen M., Gimsa J. (in prep.) Sensors for glass cell-culture chips (GC^3) for the replacement of animal experiments.
[2] Bonk S., Buehler S., Stubbe M., Tautorat C., Litwinski C., Klinkenberg E., Baumann W., Gimsa J. (in prep.). Design and characterization of pH, oxygen and adhesion sensors as well as electro-thermal micro-pumps (ETµPs) for sensorized cell-culture systems.
[3] Koester P., Buehler S., Stubbe M., Tautorat C., Niendorf M., Baumann W., Gimsa J. (2010). Modular glass chip system measuring the electric activity and adhesion of neuronal cells - application and drug testing with sodium valproic acid. *Lab Chip*, 10, no. 12, 1579–1586.

Fabrication of electroconductive polypyrrole coatings on platinum electrodes

Savolainen Virpi[1,2,*] Hiltunen Maiju[1,2,*], Albrecht Kevin[1,2,3], Nymark Soile[1,2], Kellomäki Minna[1,2], Hyttinen Jari[1,2]

1 Department of Biomedical Engineering, Tampere University of Technology, Tampere, Finland
2 BioMediTech, Tampere, Finland
3 Ilmenau University of Technology, Ilmenau, Germany
* Corresponding authors (equal contribution). E-mail addresses: virpi.savolainen@tut.fi, maiju.hiltunen@tut.fi

Abstract

Conducting polymers, such as Polypyrrole (PPy), can provide an efficient way to increase the effective surface area and thus the charge injection capacity of conventional metal electrodes. In this study, PPy coatings with two different thicknesses were fabricated on platinum (Pt) electrodes. The physical surface properties and electrical performance of coated electrodes were investigated. It was demonstrated that the impedance of coated electrodes with both coating thicknesses was significantly lower than impedance of bare Pt electrodes. The charge capacity of the electrodes with PPy coating was found to be clearly higher compared to the electrodes of bare Pt.

1 Introduction

Metals, e.g. platinum (Pt), are the most commonly used electrode materials showing good electrochemical properties. However, if the electrodes contact area is very small, its charge injection capacity is generally not high enough. A common approach to increase it is to physically increase the surface area by various processing methods. Another approach is to coat the electrode with electroconductive polymers, like polypyrrole (PPy). Due to its nodular surface structure, PPy increases the effective surface area of the electrode. The studies have shown that the actual surface area of PPy film can be 50 times greater than that of a smooth electrode of identical lateral dimensions and that such coatings lead to a remarkable reduction of the impedance at the electrode interface [1].

Properties of PPy can vary in broad range depending among others on the chosen counter ion and polymerization conditions [2-3]. Biocompatibility of PPy has been demonstrated with various cell types, but especially with neural cells [4].

The aim of this research is to provide promising electrode solutions for microelectrodes especially for ophthalmic applications. We are targeting towards electrodes that could be integrated e.g. into various implants by developing electrodes coated with active, biocompatible and electroconductive biomaterial that would enable better integration of the cultured cells onto the assessment system.

2 Materials and Methods

Electrodeposition of polypyrrole-dodecylbentzenesulphonate (PPy/DBS) coating on platinum (99.95%) surface was performed at room temperature in two-electrode electrochemical cell in aqueous solution containing pyrrole 0.2 M (Sigma-Aldrich, USA) and DBS 0.05 M (Acros Organics, USA) . The coating was potentiostatically grown at 1.0V using VersaSTAT 3 potentiostat/galvanostat (Princeton Applied Research, USA) controlled by VersaStudio software. The process was let to run until the charge density of 10 C/cm2 (thin film) or 90 C/cm2 (thick film) was obtained. After coating, the samples were washed in deionized water and air-dried.

The thickness and surface topography of the coatings was characterized using atom force microscope (AFM) (XE-100, Park Systems, USA). AFM image scans of 5 µm were conducted in air in non-contact mode using ACTA cantilever tips (Applied Nano Structures Inc., USA). The roughness value (R_a) was calculated from five parallel AFM images for both coating thicknesses using XEI image processing software.

Electrical properties of the coatings were characterized by electrochemical impedance spectroscopy (EIS) and cyclic voltammetry (CV). All the measurements were performed in a three-electrode cell at 37°C in phosphate buffer solution (pH 7.47). The impedance spectrum was measured using the Solartron Model 1260A Frequency Response Analyzer and 1294A Impedance Interface controlled by the SMaRT Impedance Measurement Software (Solartron Analytical, Hampshire, UK). The ZView modeling program (Scribner Associates inc., Southern Pines, NC) was used to analyze the impedance data. The recording of cyclic voltammetry (CV) data was conducted using the VersaSTAT 3 potentiostat/galvanostat.

3 Results and Discussion

Uniform, 68 and 531nm thick PPy/DBS coatings were achieved with charge densities of 10 and 90 C/cm^2, respectively. Mean R_a of thin films was 7 nm and thick films 9 nm. Both coatings showed nodular surface structure typical for PPys (Fig. 1).

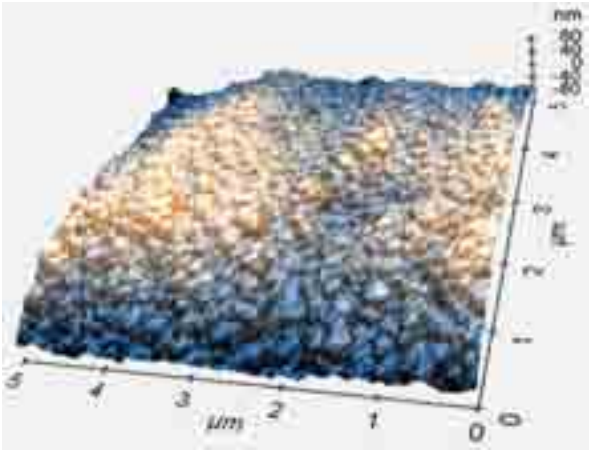

Fig. 1. Surface topography of a thick PPy/DBS coating.

EIS data showed that PPy/DBS coating improved the conductivity of the platinum by decreasing impedance values at low frequencies (Fig. 2). Impedance values of uncoated Pt electrodes varied between 28-60 kΩ at the frequency of 1Hz, while impedance values of Pt electrodes with PPy/DBS coatings varied between 8-15 kΩ. The coating thickness did not have effect on the impedance.

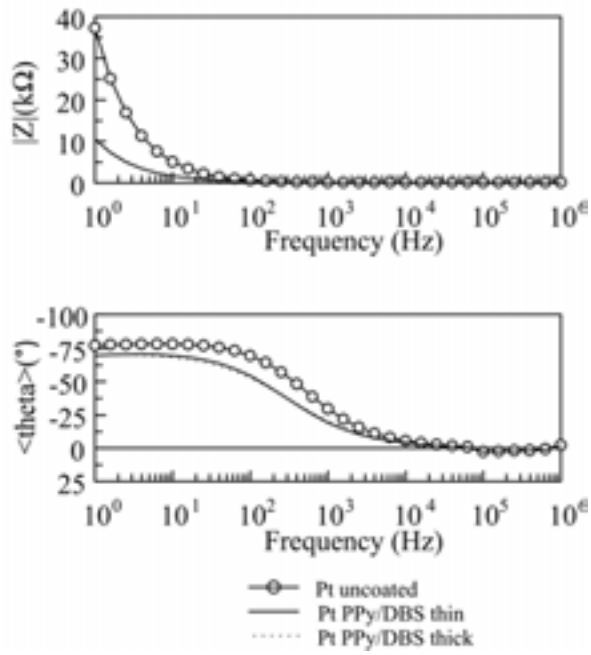

Fig. 2. Impedance plots of uncoated and PPy/DBS-coated platinum with two different coating thicknesses (average, n=4). Measurements were conducted using a 50-mV effective sine-wave alternating current at 31 discrete frequencies between 1 Hz and 1 MHz.

CV curves showed that PPy/DBS-coated Pt had greater charge capacity than uncoated Pt (Fig. 3). When comparing thin and thick coating, the thinner coating had greater charge capacities than the thicker one.

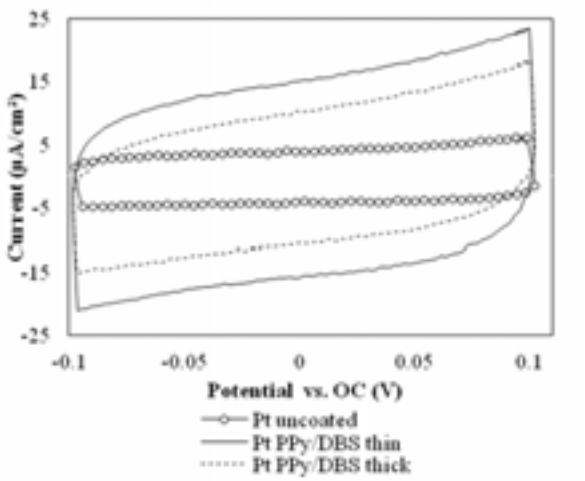

Fig. 3. Cyclic voltammetry measured with scan rate of 100 mV/s for uncoated platinum and PPy/DBS-coated platinum with two different coating thicknesses (average, n=2).

4 Conclusions

Our studies demonstrate that the electrochemical polymerization of PPy/DBS is a successful way to fabricate uniform, electrically conductive polymer coatings on Pt electrode surface. Furthermore, it is possible to control the coating thickness by controlling the accumulated charge density during the process. In our studies, the surface roughness of the coating remained at the same level despite the coating thickness. Our measurements showed that PPy/DBS coatings of Pt electrodes improved their electrical properties considerably and with claimed good biocompatibility these electrodes could provide improved stimulation and measurement capabilities. However, further studies are needed to characterize the long-term performance of PPy/DBS-coated Pt electrodes.

Acknowledgement

Financial support from the Academy of Finland (grant "Active Biomaterials for Retinal Prosthesis") and iBioMEP Graduate School (www.ibiomep.fi) are greatly appreciated.

References

[1] Cui et al. Sensors and Actuators A 93:8-18, 2001.
[2] Gelmi et al. Biomaterials 31:1974-1983, 2010.
[3] Thompson et al. Biomaterials 32:3822-3831, 2011.
[4] Wang et al. J Biomed Mater Res 68A:411-422, 2008.

The PharMEA Platform: A high throughput data acquisition instrument integrating real-time data analysis, data reduction, and wellplate-format microelectrode arrays

M. Heuschkel[1], T. Kauffmann[2], L. Sundstrom[3], J.-F. Beche[4], S. Gharbi[4], S. Bonnet[4], R. Guillemaud[4], P. Passeraub[5], D. Hakkoum[5], L. Stoppini[5], K. Georgy[6], J.-R. Péclard[6], H. Satizabal Mejia[6], A. Perez-Uribe[6], M. Kopanitsa[7]

1 Ayanda Biosystems SA, Lausanne, Switzerland
2 Bio-Logic SAS, Claix, France
3 Capsant Neurotechnologies Ltd., Romsey, UK
4 CEA-LETI, Grenoble, France
5 HES-SO HEPIA, Geneva, Switzerland
6 HES-SO HEIG-VD, Yverdon, Switzerland
7 Synome Ltd., Cambridge, UK.

1 Background/Aims

The PharMEA project (Multi-Electrode Array Technology Platform For Industrial Pharmacology And Toxicology Drug Screening) was a European research project aiming at the development of a novel drug-screening platform based on MEA technology including the following key features:

- ASIC-based integrated monitoring and stimulation hardware.
- Real-time data processing for the extraction of pertinent biological signals and reduction of the amount of data to handle, which allows to work with higher number of electrodes.
- Novel high-level data analysis software including graphical user interface and extraction of biological signal parameters.
- Novel 256-electrodes multi-well MEA biochips based on glass or porous polymer substrates allowing experimentation with dissociated cell cultures, acute tissue slices and organotypic tissue slice cultures.

2 Results

2.1 Hardware

The PharMEA platform is built around a commercial PXI chassis, which allows connecting several 256-channel amplifier interfaces within the same instrument. Two special plug-in modules, one for power supply and one for data acquisition that controls the operation of the amplifiers, are used for each 256-channel MEA interface. The amplification and stimulation electronics are based on a 64-channel ASIC. Four ASICs are used in each MEA interface in order to obtain a 256-channel MEA interface. On-board electronics allowing real-time data analysis of the biological signals as well as data reduction, i.e. elimination of noise signal without biological content, have been developed. The resulting PharMEA platform is shown in figure 1. Novel 256-electrode MEA biochips based on wellplate format (4, 8, 32 and 60 wells) were developed as well as porous polymeric MEA biochips intended for organotypic tissue slice cultures (see figure 2).

2.2 Software

New software controlling the PharMEA instrument has been developed. It includes the possibility to select electrodes to be monitored and electrode desired amplifier gain in a graphical map corresponding to the MEA used. It also enables real-time filtering of signals. Spike detection, signal parameters extraction, and extraction of complex features such as QT prolongation can also be achieved in off-line mode.

2.3 Biological platform validation

PharMEA platform validation was achieved with biological experiments addressing drug safety and drug screening applications. Embryonic chicken heart preparations were used for QT prolongation experimentation and were tested against Ivabradine, known to induce QT prolongation. The results obtained with the PharMEA platform confirm the QT

prolongation of Ivabradine. Organotypic and acute hippocampal tissue slices were used for drug screening validation, where spontaneous activity as well as stimulation induced burst activity could be recorded and analysed.

3 Conclusions/Summary

Working prototypes of the PharMEA instrument have been realised and instrument key features of real-time data analysis, data reduction, and use of multi-well format MEAs have been validated using heart preparations and hippocampal brain slices.

This research was supported via a grant from the European Community's Seventh Framework Program [FP7/2007-2013] under grant agreement n°232554.

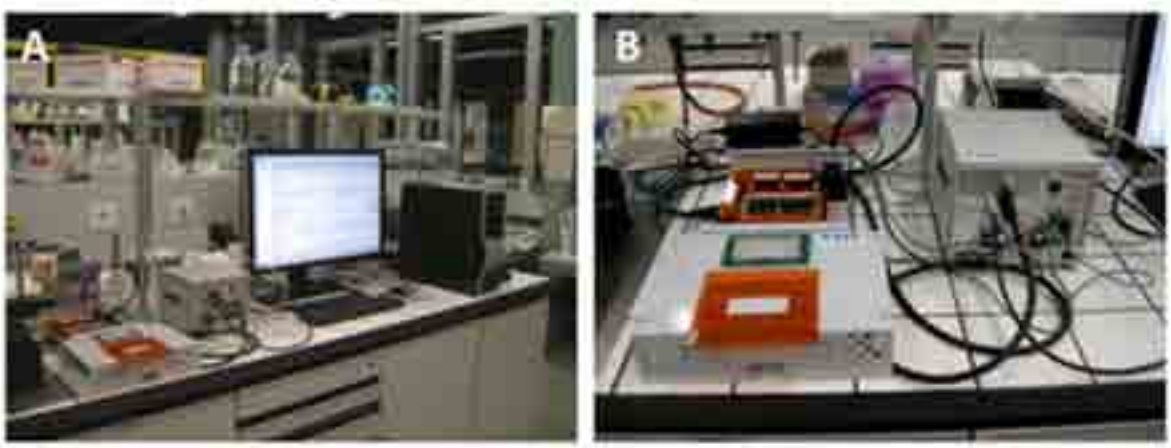

Fig.1: General view of the PharMEA platform prototype (A). It is made of a computer, a rack allowing the connection of several 256-channel amplifier units, and one 256-channel amplifier/stimulation interface. The amplifier/stimulation interface and the card rack are shown in (B).

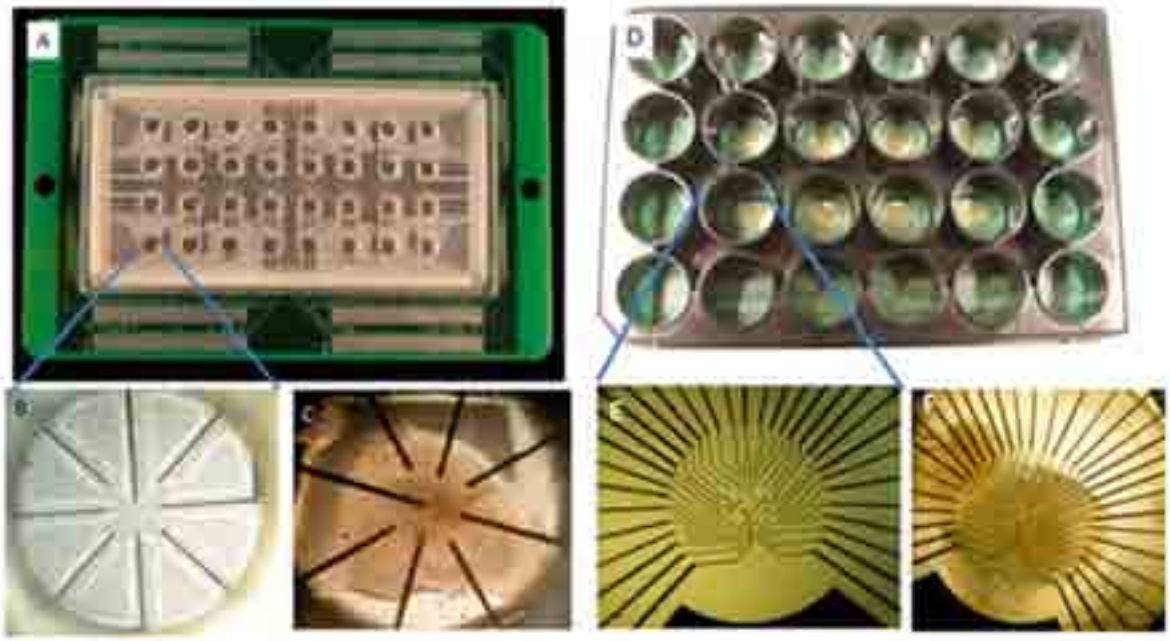

Fig.2: Pictures of porous 32-well MEA (A) and an 8-well porous polyimide substrate MEA (D). Each well consists of 8 silver-ink electrodes (B) or 32 platinum electrodes (E) that can be individually assigned as a recording or as a stimulating electrode. Hippocampal slice cultures laid down onto the 2 types of MEAs can be seen in (C) and (F).

A family of integrated circuits in submicron technology for in vivo and in vitro high density MEA experiments

Miroslaw Zoladz[1], Piotr Kmon[1], Pawel Grybos[1], Robert Szczygiel[1], Jacek Rauza[1], Marian Lewandowski[2], Tomasz Blasiak[2], Tomasz Kowalczyk[3]

1 AGH University of Science and Technology, DME, Mickiewicza 30, Krakow, Poland ,
2 Jagiellonian University, Dept. of Neurophysiology and Chronobiology, Gronostajowa 9, Krakow, Poland,
3 University of Lodz, Dept. of Neurobiology, Pomorska 141/143, Lodz, Poland
* Corresponding author. E-mail address: pgrybos@agh.edu.pl, zoladz@agh.edu.pl

1 Background/Aims

State of the art submicron technologies offer the possibility of multichannel application specific integrated circuits (ASICs) production for high-density MEA experiments. The ASICs can have more complex functionality and better performance (noise, power consumption, channel to channel uniformity, etc.) than existing solutions.

2 Methods

Based on our experience in design and practical applications of ASICs for neurobiology experiments comprising of hundreds recording sites [1-4], we propose a novel family of 64-channel ASICs designed in a submicron technology, which can be used both for in vivo and in vitro experiments. Thanks to the modern technology and implementation of an active digital control and correction circuits we obtained very good paramters and a complex functionality in a single 64-channel chip, namely:

- recording both LFP and spike signals with a wide range of a frequency band control, a low noise performance (3.7 μV), an ultra-low power consumption per channel (25 μW), and a very good uniformity of analog parameters from channel to channel (the gain spread 0.5%, the low cut-off frequency set below 0.1 Hz with a spread of only 30 mHz),
- stimulation in each channel with an effective artefacts cancellation and with a selection of different patterns.

3 Results

An exemplary member of this family is a chip called NRS64 (Neural - Recording - Stimulation 64-channel) which is shown with its main parameters in Fig. 1. The ability to control its gain, corner frequencies and stimulation parameters makes the this chip a good candidate for a wide range of neurobiology applications. The characteristic feature of this chip family is the ease of building dedicated measurement systems to suit various in vivo and in vitro experiments.

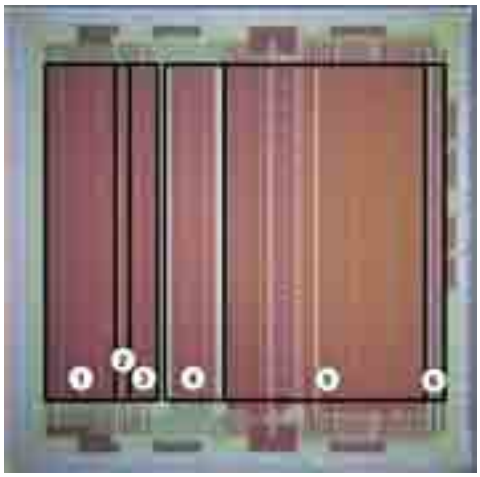

Fig.1 Photo of NRS64 chip: a) photo: 1 – stimulation block, 2 – control registers, 3 – artifact cancellation circuits, 4 – decoupling capacitors, 5 – recording channels, 6 - multiplexer.

Tab. 1. Main parameters of the NRS64 chip.

Tech / no. of channels	UMC 0.18 μm / 64ch
Gain	139 / 1100 V/V
Tuning low cut-off freq.	60 mHz - 100 Hz
High cut-off frequency	4.7 kHz / 12 kHz
Power per channel	25 μW
Input referred noise (3 Hz - 12 kHz) (100 Hz - 12 kHz)	 7.6 μV 3.7 μV
THD @ 1.5 mV	< 1%
Current stimulation with 8-bit resolution in six ranges	± (0.5; 2;8; 32; 128; 512)nA
Multiplexer frequency	5 MHz

Fig.2a presents a system with the NRS64 chip dedicated for in vivo experiments. The system is equipped with 10 mm long, 64-site electrodes from Neuronexus Technologies.

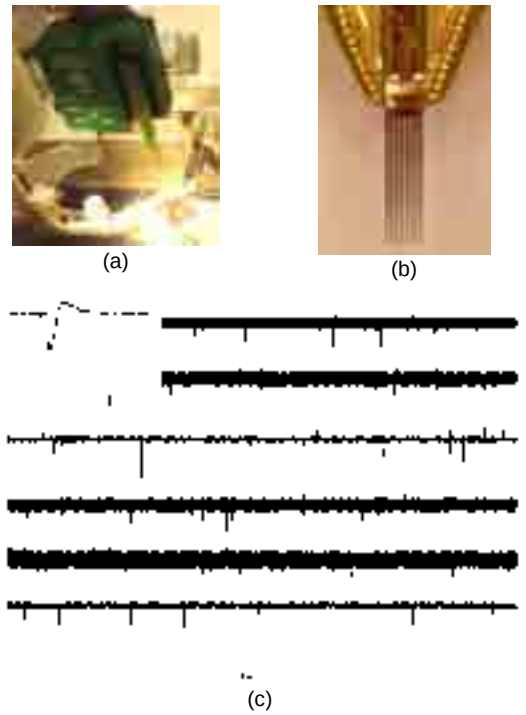

Fig.2 a) 64-channel system for in vivo recording, b) dedicated 10 mm long electrodes provided by Neuronexus Technologies, c) exemplary results of neuronal spiking in the intergeniculate leaflet of the rat lateral geniculate nucleus.

The experiment was performed on a rat under urethane anaesthesia. The electrodes were implanted into the brain to record infraslow oscillations at the level of neuronal spiking in the intergeniculate leaflet of the rat lateral geniculate nucleus. Signals from 64 channels were recorded for a few hours and the results from selected channels with the neuronal spiking are shown in the Fig. 2b.

Fig. 3a shows a 256-channel systems for in vitro experiments with 256 tip-shapes electrodes from Qwane Bioscience. In the test we used transverse hippocampal slice preparations. Fig 3b shows the epileptiform field activity evoked in hippocampal slices by tonic cholinergic stimulation (50 M bath perfusion). Note that epileptiform discharges recording is accompanied by a single unit activity. The lower panel of Fig 3b shows the burst of action potentials generated at the peak positivity of the field epileptiform discharge.

4 Summary

The development of high-density MEA experiments requires both tightly spaced electrodes and novel, highly reconfigurable multichannel integrated circuits which can both record and stimulate large neural networks at a single cell-resolution. We present a family of such ASICs and examples of their successful applications in both in vivo and in vitro experiments.

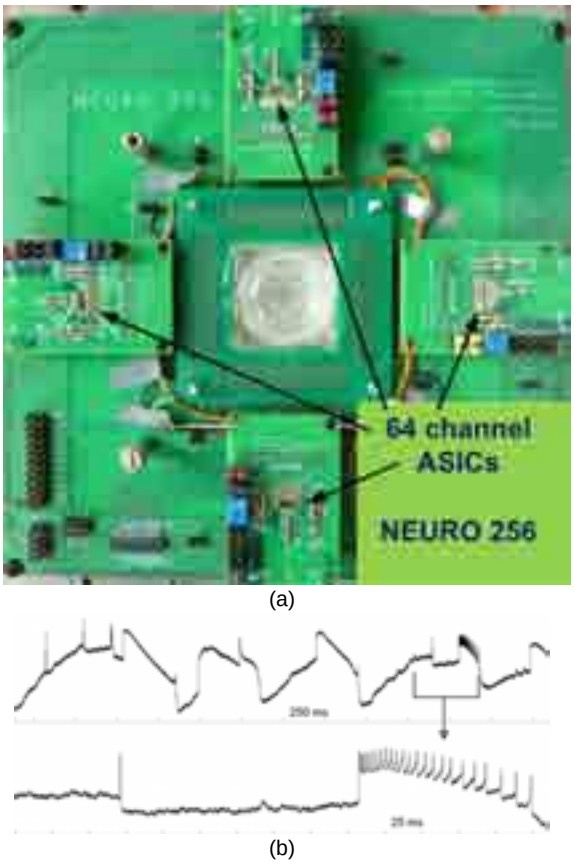

Fig.3 a) Highly reconfigurable 256-channel system for in vitro recording, b) burst of action potentials generated by a single neuron at the peak positivity of the field-recorded epileptic discharge.

Acknowledgement

This research and development project was supported by Polish Ministry of Science and Higher Education in the years 2008-2010 (NR 01-0011-04/2008). M. Zoladz thanks Polish Ministry of Science and Higher Education for financial support in the years 2010-2012 (project no N_N505559139).

References

[1] P. Grybos, et al., "NEUROPLAT64 - low noise CMOS integrated circuits for neural recording applications" Proc. 5th Int. Meet. Substrate-integrated MEA2006, 208-209, 2006, Reutlingen, Germany.

[2] W. Dabrowski, P. Grybos, A. Litke, "A low-noise multichannel integrated circuit for recording neuronal signals using microelectrode array", Biosens. Bioelectron. vol. 19, pp. 749-761, 2004.,

[3] P. Grybos, P. Kmon, M. Zoladz, R. Szczygiel, M. Kachel, M. Lewandowski, T. Blasiak, "64 Channel Neural Recording Amplifier with Tunable Bandwidth in 180 nm CMOS Technology", Metrol. Meas. Syst., Vol. XVIII (2011), No. 4

[4] M. Zoladz, P. Kmon, P. Grybos, R. Szczygiel, R. Kleczek, P. Otfinowski, "A Bidirectional 64-channel Neurochip for Recording and Stimulation Neural Network Activity", IEEE EMBS Neural Engineering Conference, 2011, Cancun, Mexico

3D capacitively coupled MEA on a 3D microstructure array with interface technology

Williamson, Adam[1]; Laqua, Daniel[2]; Klefenz, Frank[3]; Husar, Peter[2]; Schober, Andreas[1]

1 Technische Universität Ilmenau, FG Nanobiosystemtechnik, Germany
2 Technische Universität Ilmenau, FG Biosignalverarbeitung
3 Fraunhofer IDMT, Bio-inspired Computing, Ilmenau, Germany
* Corresponding author. E-mail address: adam.williamson@tu-ilmenau.de

Abstract
Biological components and computational concepts of realized BIO-ICT interactions have so far lacked the complexity of actual high level biological neural systems. Three key features are needed for the biological computational neuronal network: Complete 3D structures of neuronal cell networks, understanding of interactions of various types of neural cells, and organized, layered and patterned 3D neuronal tissue. We aim to construct an in vitro model of 3D neuronal networks using layered biomaterial and neural cells derived from human stem cells while stimulating and closely monitoring the evolution of cells and their connections with the 3D MEA array presented here.

1 Introduction

1.1 Motivation

The complex electrical activity of neuronal networks can be recorded with planar (2D) microelectrode arrays (MEAs). However, neuronal networks are inherently 3D networks. For the investigation of 3D neuronal networks special electrode arrays on 3D microstructures can be created for insertion into low-lying neuronal layers or cultured neuronal networks. Unfortunately the properties of electrode arrays, both 2D and 3D, are significantly diminished when in direct contact with biological tissue. Glial cells can build up around the electrode surface inhibiting signal measurement and in some cases the implant itself is (for example with silicon implants) rejected for biocompatibility reasons. The optimal solution for a sensor that is both 3D and biocompatible is for the implant to be of a material that is biologically neutral, such as glass, and for the electrodes on the 3D microstructures to be covered with an equally biologically neutral passivation, such oxide or nitride. Here we present initial results for exactly such a system.

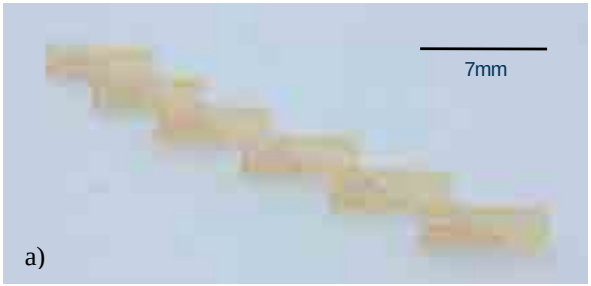

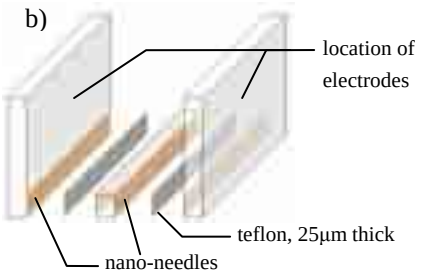

Fig. 1. a) MEA Sensors, when bonded together, create a 3D system of microstructures covered with multiple passivated electrodes as capacitive sensors. Strips of glass nano-neeldes are etched into each MEA chip. Individual chips are separated by glass spacers also etched with needles on both sides. Teflon strips are inserted between needle surfaces for bonding.

2 2D Systems

2.1 Fabricated 2D MEAs on Glass Wafers

Glass wafers are patterned with gold electrode arrays, seen in figure 1, making comb structures which are cut (along the red dashed lines) into individual fingers using a Nd:YAG laser (neodymium-doped yttrium aluminium garnet; Nd:$Y_3Al_5O_{12}$). Each finger of the comb, pictured in figure 1a, has two gold microelectrodes. In this design we evaluated the performance of six different electrode sizes. The six microelectrode surfaces themselves are covered by a mixed passivation stack of 66 nm of nitride, 66 nm of oxide, and finally another 66 nm of nitride. A cross section of a conducting shaft, which extends from the electrode surface to the interface circuitry, is seen in figure 2b. Using thin film technology a series of gold and nitride/oxide passivation layers are patterned on the glass wafer, resulting in a cross section resembling a coaxial cable. The passivated electrode surfaces cre-

ates a capacitive measurement across the passivation layer of each electrode with the complex electrical activity of the neuronal network on one side and the gold electrode on the other side.

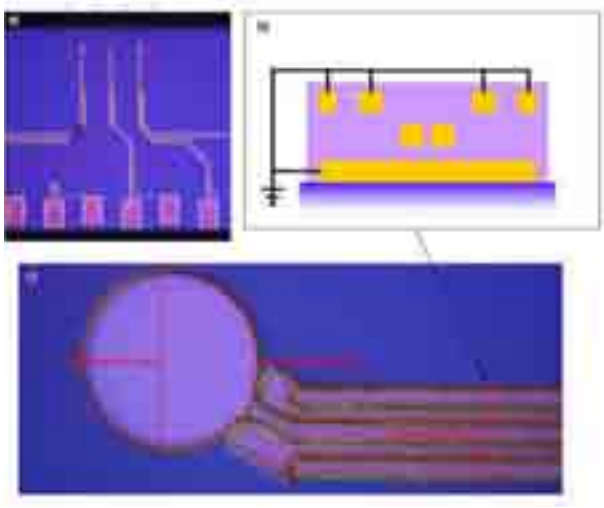

Fig. 2. a) The MEA Sensor with six different electrodes. Fingers are created by cutting along the red dashed lines with a Nd:YAG laser. A cross section of the electrode, in part b), shows the coaxial layout. Gold conduction lines run through the center of repeating layers of mixed nitride/oxide passivation stacks and are surrounded by grounded gold shielding lines.

3 Bonding for 3D Systems

3.1 The Glass Nano-needle/Teflon Interface

Here we demonstrate the ability to bond together several 2D glass structures, for example the above comb structures, using our glass nano-needles, 'glass grass' [1], and creating an ultra-strong glass nano-needle and Teflon interface, pictured in figure 3a. Data from pull-testing is seen in figure 3b. Nano-needle/Teflon interfaces (520 N/cm^2) significantly out perform the adhesion of bare glass to Teflon (90 N/cm^2) interfaces. An arbitrary number of 2D arrays can be stacked with this process.

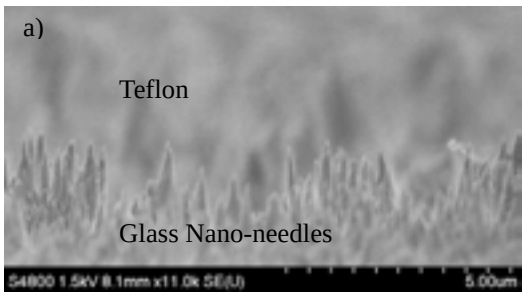

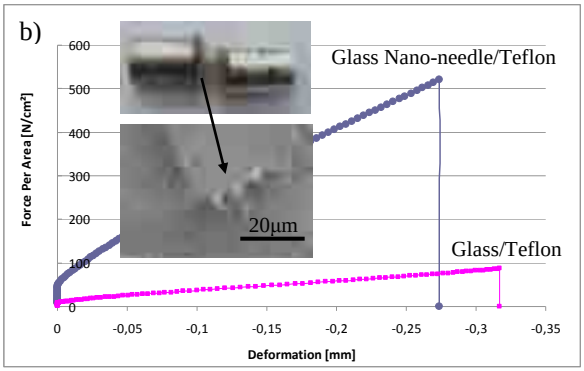

Fig. 3. Using a high pressure and temperature press, glass MEAs are bonded together with Teflon. a) Results of pull-tests show an extraordinary increase in adhesive strength between glass nano-needles (520 N/cm^2) and Teflon compared to bare glass and Teflon (90 N/cm^2). (*insert*) Pull-test carrier and SEM of result showing glass nano-needles embedded in Teflon.

4 Amplification and Output

4.1 Current 2D Results

Each electrode is connected to circuitry amplifying the measured (capacitively induced) voltage signal by a factor of 100. Using a Keithley wafer probe station test pins are landed on the passivated electrodes. Periodic, square, triangle, and saw-tooth wave signals with a peak-to-peak voltage down to 50 mV were tested and showed a 3 dB frequency of 12 kHz (amplification fallen to a factor of 70). Measured signals were in the volt range indicating that the initial capacitively induced voltage signals were in the mV range. Best results are obtained with the 50 µm diameter electrode.

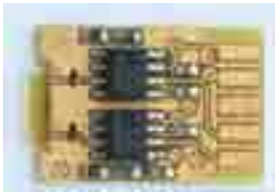

Fig. 4. Currently output is read from single chips connected to their own dedicated amplifiers. Test pins are landed on the passivated electrodes. Periodic sine square, triangle, and saw-tooth wave signals with a peak-to-peak voltage down to 50 mV were tested and show a 3 dB frequency of 12 kHz (amplification fallen to a factor of 70 from 100). Measured signals were in the V range indicating that the initial capacitively induced voltage signals were in the mV range.

Acknowledgement

We thank the European Commission under ICT FET OPEN FP7 "3DNeuroN" for funding.

References

[1] Katharina Lilienthal *et al* 2010 *J. Micromech. Microeng.* **20** 025017.

High uniformity of the main parameters of the integrated electronics dedicated to record broad range of the biopotentials

Piotr Kmon[1], Mirosław Żołądź[1], Paweł Gryboś[1], Robert Szczygieł[1]

1 AGH University of Science and Technology, Al. A. Mickiewicza 30, 30-059 Cracow, Poland
* Corresponding author. E-mail address: pgrybos@agh.edu.pl, kmon@agh.edu.pl

Abstract
Need to record large number of biopotentials involves building high density integrated electronic recording systems. Increasing the number of the recording sites allows one to observe greater explored area and thus to understand better its complicated functionality. In this paper we present approach of the recording channel that can be used in integrated systems where the number of the recording sites, the power consumption, the area occupation and the uniformity of the system parameters are the most important aspects. We describe measurement results of the 8-channel recording chip processed in the CMOS 180nm technology, that is dedicated to a broad range of the neurobiology experiments. Each recording channel is equipped with the control register that enables one to set the main channel parameters independently in each recording site. Thanks to this functionality the user is capable to set the lower cut-off frequency in 300 mHz – 900 Hz range, the upper cut-off frequency can be switched either to 10 Hz - 280 Hz or 9 kHz, while the voltage gain can be set either to 260 V/V or 1000 V/V. Single recording channel is supplied from 1.8 V, it consumes only 11 µW of power, and its input referred noise are equal to 4.4 µV.

1 Introduction

The aim of our work is to build multichannel recording system that will be able to adapt in a broad range of the neurobiology experiments that involve recording signals from hundreds of the recording sites. Having looked at the common biopotentials recorded either internally or from the skin (i.e. EEG, ECG, EMG, LFPs, neural spikes) it can be seen that these signals differ from each other in amplitudes values and frequency ranges [1]. Because many neurobiology experiments need to record different types of the biopotentials simultaneously, the recording electronics shall have a possibility to adapt its parameters for particular requirements of experiments. Having in mind that the designed system should have a multichannel architecture one also has to put a special attention to the uniformity of its main parameters from channel to channel. As we showed in our previous work [2] it is difficult to obtain concurrently large tuning range of the recording site and the low spread of the system main parameters together with addressing many other strict requirements (i.e. the low power consumption, the small area occupation, the low input referred noise). Problems with keeping the high uniformity in integrated multichannel systems was also reported by other groups [3-5]. We describe methods that we developed to overcome the problems mentioned above.

2 Results

To satisfy the requirements stated previously we designed an 8-channel recording chip. Its schematic idea is presented in Fig. 1. Each recording channel is configured by the on-chip digital register that allows one to set the lower and upper cut-off frequencies, the voltage gain and the channel offset of the recording channel. Additionally, to save the power consumed by the chip, the digital register allows to power up/down the channels that show no neuronal activity during the experiment. To overcome the problems with the uniformity of the lower cut-off frequency and to permit for large tuning range, the lower cut-off frequency is controlled by an 8-bit correction LF_DAC. Furthermore, there is an 8-bit correction OFFSET_DAC dedicated to control offset voltages of the recording channels. Its existence is especially important when the integrated electronics is fabricated in a modern submicron processes [6]. Additionally, there are FH and GAIN inputs that allow to control the upper cut-off frequency and the voltage gain of the recording channel independently. In order to limit the number of the chip lines, the outputs of the recording channels are connected to the 8:1 analogue multiplexer that is controlled by the on-chip LVDS receivers.

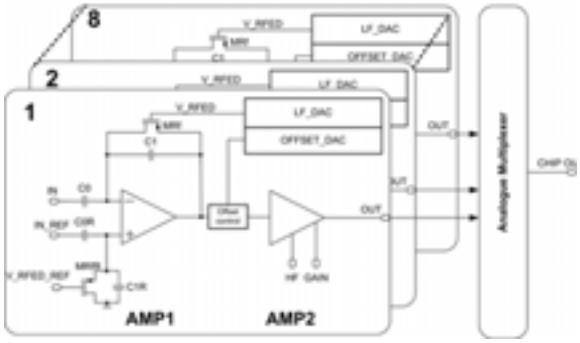

Fig.1 Schematic idea of the designed recording system.

3 Measurement Results

The 8-channel chip measurements are presented. The microphotograph of the bonded chip is presented in Fig. 2. Thanks to the on-chip digital registers that are implemented in each recording channel the user is able to set many operation modes. The presented chip main parameters are shown in Tab. I.

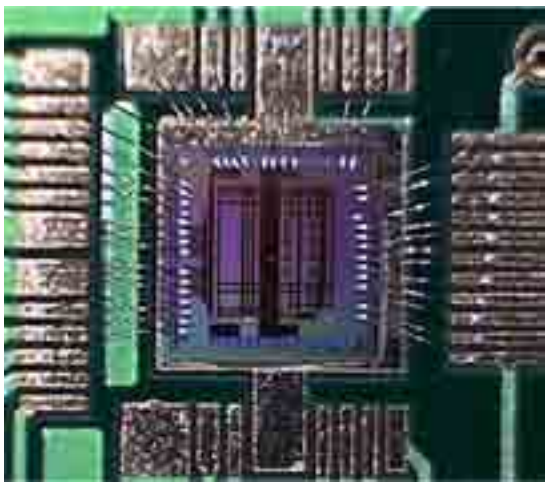

Fig.2 Microphotograph of the bonded chip.

Tab.I Main parameters of the presented chip.

Technology	CMOS 180nm
Gain [V/V]	260 / 1000
Lower cut-off frequency tunning range [Hz]	0.3 ÷ 900
Upper cut-off frequency tunning range [kHz]	0.01- 0.28 / 9
Input referred noise [μV]	4.4 (200 Hz – 9 kHz)
Single channel area occupation [mm^2]	0.06
Power consumption [μW]	11

4 Summary

Variety of operation modes of our chip, its low input referred noise, low power consumption, and small area occupation of the single channel make it a good candidate for applying in integrated recording systems comprising hundreds of recording sites. Additionally, up to our knowledge the power consumption of the single recording channel, the high uniformity of its main parameters in the broad tuning range, and the small area occupation are one of the best reported to date.

Acknowledgement

This research and development project was supported by Polish Ministry of Science and Higher Education in the years 2011-2013 (2011/01/N/ST7/01256).

References

[1] R. R. Harrison, “A versatile integrated circuit for the acquisition of biopotentials”, Custom Integrated Circuits Conference, 2007, CICC '07 IEEE, pp. 115-122

[2] P. Grybos, P. Kmon, M. Zoladz, R. Szczygiel, M. Kachel, M. Lewandowski, T. Blasiak, “64 Channel Neural Recording Amplifier with Tunable Bandwidth in 180 nm CMOS Technology”, Metrol. Meas. Syst., Vol. XVIII (2011), No. 4

[3] Brown, E.A., Ross, J. D., Blum, R. A., Nam, Y., Wheeler, B. C., DeWeerth, S. P., ‘Stimulus-artifact elimination in a multi-electrode system’, IEEE Transactions on Biomedical Circuits and Systems, 2008, Vol. 2, No. 1

[4] Perelman, Y., Ginosar, R., ‘Analog frontend for multichannel neuronal recording system with spike and LFP separation’, Journal of Neuroscience Methods 153, 2006, pp. 21–26

[5] Gosselin, B., Sawan, M., Chapman, C. A., ‘A Low-Power Integrated Bioamplifier With Active Low-Frequency Suppression’, IEEE Transactions on Biomedical Circuits and Systems, 2007, Vol. 1, No. 3

[6] M. Zoladz, P. Kmon, P. Grybos, R. Szczygiel, R. Kleczek, P. Otfinowski, ”A Bidirectional 64-channel Neurochip for Recording and Stimulation Neural Network Activity”, IEEE EMBS Neural Engineering Conference, 2011, Cancun, Mexico

A recording setup for long-term monitoring of *in vitro* neuronal networks on microelectrode arrays

Regalia G.[1*], Biffi E.[1], Menegon A.[2], Ferrigno G.[1], Pedrocchi A.[1]

1 Politecnico di Milano, Bioengineering Department, NeuroEngineering And medical Robotics Laboratory, Milan, Italy
2 San Raffaele Scientific Insitute, Advanced Light and Electron Microscopy Bio-Imaging Centre, Milan, Italy
* Corresponding author. E-mail address: giulia.regalia@mail.polimi.it

Abstract
We present the design of a custom recording front-end to monitor the spiking activity of neuronal networks grown on Microelectrode Arrays (MEAs). The circuit was specifically designed to be coupled with an autonomous environmental chamber, able to keep neuronal cultures under controlled temperature, osmolarity and pH. Preliminary simulations and tests on a single readout channel demonstrated that the defined circuitry is well suitable to process typical *in vitro* neuronal spikes. The pre-amplification stage of the 60-channel front-end was integrated inside the chamber in order to get a high signal-to-noise ratio (SNR) of the recordings. In this way, we recorded spontaneous neuronal electrical activity from hippocampal cultures grown inside the autonomous chamber for days. This system allows to collect multichannel data from neuronal cultures over long periods, providing an effective solution for long-term studies of neural activity.

1 Introduction

Neuronal cultures grown on Microelectrode Arrays (MEAs) are a powerful and widespread tool in a large variety of electrophysiological studies [1]. However, applications involving long-term analysis of network activity suffer from fluctuations in temperature, pH and osmolarity as well as mechanical perturbations occurring during recordings in the laboratory environment [2, 3]. To overcome these problems, we newly presented an innovative closed culturing chamber able to grow neuronal networks on MEA chips over weeks and to record their neuronal activity at the same time, by means of external commercial electronics [4]. However, problems related to the signal-to-noise ratio (SNR) of the recordings require to place the front-end as close as possible to the signal source. Here we present the development of a custom recording setup for this purpose and we demonstrate the feasibility of long-term recordings while maintaining neuronal cells inside the environmental chamber.

2 Methods

The proposed front-end

We devised a pre-amplification stage to be located inside the culture chamber and a following filter amplifier stage to be implemented on external boards.

The full front-end has to fulfill the following requirements: (1) high gain (max 60 dB), suitable for the amplification of typical *in vitro* neuronal spikes (20-400 µV peak to-peak) (2) three high pass filter poles (300 Hz), (3) three low pass filter poles (3 kHz), (4) low noise (less than typical thermal and background biological noise at the microelectrodes, i.e. <15-20 µV peak-to-peak), (5) input offset tolerance, (6) linear phase in the filter bandwidth. The band-pass circuit proposed consists of a pre-amplification stage, a Sallen-key high-pass filter, a Sallen-key low-pass filter and a RC circuit. Low noise (8 nV/$\sqrt{\text{Hz}}$), low supply current (400 µA) and precision amplifiers were chosen (OP1177, Analog Devices).

Assessments of the circuitry performance were made with both Spice simulations and measures from a single channel prototype. Inputs for the simulations consisted of sine waves and real MEA signals recorded in the standard setup with broadband (1 Hz-5 kHz) commercial equipment (Multi Channel Systems, MCS, GmbH). The frequency response gain of the prototype was obtained by providing 100 µV peak-to-peak sine waves with a wave generator (GFG-8210, Instek). The input-referred noise was determined by grounding the input, measuring the channel output and dividing it by the overall nominal gain. Measures were performed with an acquisition board (Ni USB-6009, 14 bit, 48 kHz, National Instruments).

Then, we implemented the 60-channel pre-amplifier on two 6.5x8.5 cm, 30-channel boards. These boards were designed to be piled up above the MEA chip inside the chamber and to contact MEA pads through gold pins. To minimize board sizes, surface mounting quad operational amplifiers and 0402 package passive components were used. A third board was developed to organize signals in a 68-pin socket compatible with MCS cables, inserted through the chamber top plate. These boards were tested in terms of gain, noise and cross-talk. The filter stage realiza-

tion is ongoing. Figure 1 depicts the full single channel front-end (top) and a schematic representation of the 60-channel recording front-end coupled to the environmental chamber (bottom).

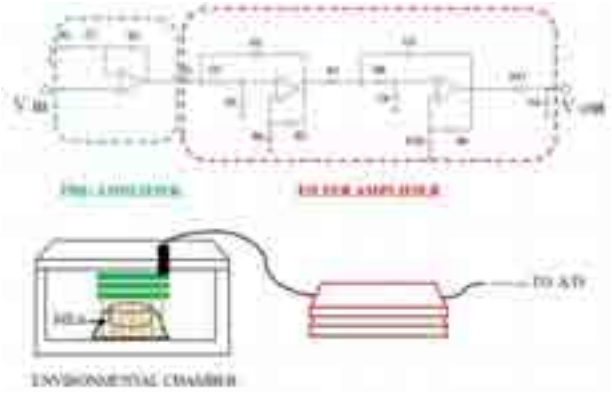

Fig. 1. Top: schematic for a single readout channel. Bottom: representation of the 60-channel recording front-end coupled to the environmental chamber housing a MEA chip.

Recordings of neuronal activity

The pre-amplification boards were covered with biocompatible silicon to protect them from the environmental high humidity level. Then, they were linked to external multichannel filter and data acquisition boards (MCS). The electrical activity of hippocampal neurons (CD1 mice, E17.5, 700 cells/mm^2) grown on standard MEA chips (MCS) put inside the chamber was recorded at different time points over the culturing period (21 days *in vitro*, DIVs). Activity of networks was recorded also with the standard MCS equipment to compare the two systems by means of standard signal processing [4].

3 Results

Electrical characterization

The defined front-end circuit demonstrated to be suitable for the analog processing of *in vitro* neuronal signals. Spice simulations confirmed requirements regarding frequency response morphology and provided expected output shape in response to real signals. Tests performed on the single channel prototype reported an experimental gain in agreement with calculations and Spice simulations (max 58.6 dB, Fig. 2). The measured input-referred noise level was nearly 10 µV peak-to-peak over the recording bandwidth, comparable to other custom equipments [5, 6].

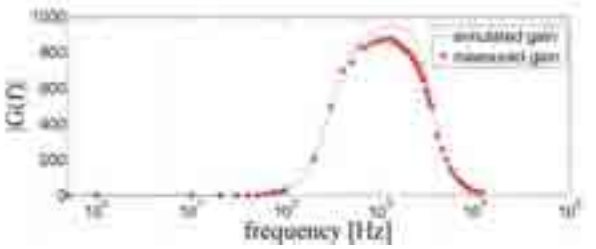

Fig. 2. Comparison between the full channel simulated gain (Spice) and the measured one.

Tests on the 60-channel pre-amplification board confirmed its gain and frequency behavior and reported a cross-talk comparable to results presented in the literature [7].

Neuronal activity recordings

Neuronal recordings performed with the custom board displayed a SNR high enough for successive spike detection and they were comparable to typical recordings with the standard setup in the short term (i.e. <2 hours). Moreover, we successfully recorded spontaneous electrical activity continuously over many DIVs. We never detected any spontaneous activity alteration nor any reciprocal interference between the internal electronics and the chamber environment over the recording sessions.

4 Conclusion and Discussion

The proposed analog front-end is suitable to be coupled with our autonomous culture system [4], both in terms of sizes and recordings performance. Our compact custom setup is cheaper and more easily replicable than commercial recording front-end devices or custom CMOS-based systems. Our final aim is to provide a compact technological platform for an electrophysiological laboratory, independent from both bulky incubators and expensive front-end equipments. This system provides new perspectives for *in vitro* long-term studies on neuronal cultures on MEAs.

Acknowledgement

Authors would like to thank people from the Alembic facility for their support and Roberta for animal dissection.

References

[1] Morin F., Takamura Y., Tamiya E. (2005). Investigating neuronal activity with planar microelectrode arrays: achievements and new perspectives. *J Biosci Bioeng*, 100, 131-143.

[2] Wagenaar D.A., Pine J., Potter S.M. (2006). An extremely rich repertoire of bursting patterns during the development of cortical cultures. *BMC Neurosci* ,7, art. no. 11.

[3] Blau A., Neumann T., Ziegler C., Benfenati F. (2009). Replica-moulded polydimethylsiloxane culture vessel lids attenuate osmotic drift in long-term cell cultures. *J* Biosci, 34, 59-69.

[4] Biffi E., Regalia G., Ghezzi D., De Ceglia R., Menegon A., Ferrigno G., Fiore G.B., Pedrocchi A. (2012). A novel environmental chamber for neuronal network multisite recordings. *Biotechnol Bioeng*, doi: 10.1002/bit.24526.

[5] Bottino E., Massobrio P., Martinoia S., Pruzzo G., Valle M. (2009). Low-noise low-power CMOS preamplifier for multisite extracellular neuronal recordings. *Microelec. J.*, 40, 1779-1787.

[6] Guillemaud R., Bêche J.F., Billoint O., Bonnet S., Gharbi S., Rostaing J.P., Trévisol M., Yvert B, Rousseau L., Goy F., Heuschkel M., David O., Saillet S., Charvet G. (2009). A Multi-channel platform for recording and stimulation of large neuronal structures. *Biomed Eng*, 30, 226-233.

[7] Rolston J.D., Gross R.E., Potter S.M. (2009). A low-cost multielectrode system for data acquisition enabling real-time closed-loop processing with rapid recovery from stimulation artifact. *Front Neuroeng*., doi:10.3389/neuro.16.012.2009.

Measurement of secondary responses in cellular co-cultures using the microelectrode array

Jessica Ka-Yan Law, Tobias Oberbillig, Dirk Saalfrank, Sven Ingebrandt*

Dept. of Informatics and Microsystem Technology, University of Applied Science Kaiserslautern, Zweibrücken, Germany
* Corresponding author. E-mail address: sven.ingebrandt@fh-kl.de

Abstract
A new encapsulation method for our standard MEA device is introduced in the present study. For fabrication of the devices we generally use 4" glass wafers, while the individual MEA chips are 11×11 mm^2. The planar MEA chips were in this study encapsulated such that the surface of the chips was almost at the same level of the surrounding PCB carrier enabling a larger area for cell culture. This design is now beneficial for the study of secondary responses of co-cultures where we use classical co-culture chambers with porous bottom membranes.

1 Introduction

Biological systems are complex and cell-cell interactions always play a significant role in communication between different parts of the body. For instance under fight-or-flight condition, the splanchnic nerve terminals of the sympathetic neurones release acetylcholine (Ach), which stimulate the cells to release catecholamines (e. g. adrenaline/ noradrenaline). The catecholamines released further act on target organs, mainly heart, sweat gland, and eye, for homeostasis [1]. A cascade of cellular events starts upon certain chemical or biological stimuli which the outcomes of events may be unpredictable. A tool for studying the outcomes of cell interactions is therefore important. The classical assay can be done by using standing cell inserts with porous bottoms to enable two cell types cultured separately.

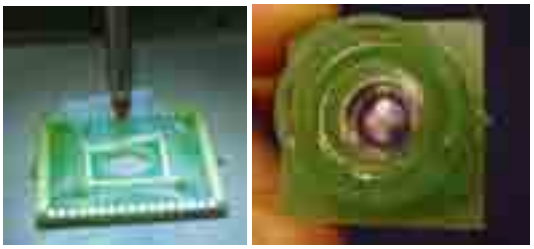

Fig. 1. Encapsulation process of our standard MEA devices by flip-chip gluing the 11×11 mm^2 chip directly to a PCB carrier.

Microelectrode arrays (MEA) have been extensively used in drug screening studies [2, 3]. In previous works conditioned medium has been used to study influences of released growth factors on the development of embryonic cardiomyocyte cultures [4]. However, to our knowledge none of the studies focused on direct secondary responses of drugs on cells. In the present study, we would like to demonstrate the feasibility of using the MEA to detect cardiac signal changes in response to stimulated secretory cells.

2 Methods

2.1 Chip encapsulation

In order to distinguish the secondary responses of the cells in the result of other cell types and for the purpose of co-culture, a new encapsulation procedure for our MEA chips was designed and fabricated. A planar MEA chip with 11×11 mm^2 size was located at the centre of the PCB board and a CAPTON foil (150 µm thickness) with gold connection lines was used to connect the bond pads with the PCB board via a flip-chip encapsulation procedure.

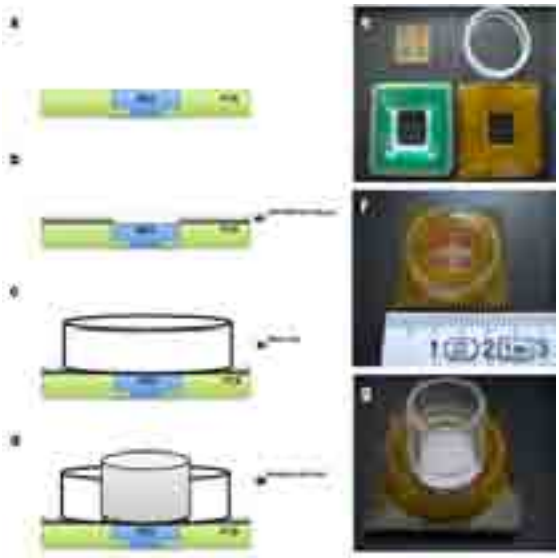

Fig. 2. Encapsulation process of the MEA co-cultures set-up. A planar MEA chip is located at the centre of the PCB board (a). The MEA chip is flip-chip bonded to the PCB board using a CAPTON foil (150 µm) with gold connection lines (b). The MEA chip is encapsulated together with a glass ring for culture medium (c). A commercial standing cell insert (Millicell®, 0.4 µm) can be placed on top of the MEA chip within the encapsulated glass ring (d, g). Different parts of a planar MEA chip (e). An assembled planar MEA chip with the size of 2.5×2.5 cm^2 (f).

In contrast to our previous encapsulation protocol (Fig. 1) a standing cell culture insert (diameter 13 mm; height 10.5 mm) can now be placed on top of the MEA chip (Fig. 2). Two different cell types were cultured separately with a vertical gap distance of 1 mm in between. A layer of cardiac cells was cultured on the MEA surface while another layer of catecholamines-releasing secretory cells was cultured on the membrane of the cell insert.

2.2 Cell culture

HL-1 cells (10^5 cells/cm^2) were plated on fibroectin-gelatin coated chips 3 days prior to the experiment and cultured in a supplemented Claycomb Medium (JRH Biosciences). The supplements were 10 %/ V fetal bovine serum, 100 U/ml penicillin, 100 µg/ml streptomycin, 0.1 mM norepinephrine and 2 mM L-glutamine. This medium was exchanged every day and 3 h before the experiment. On the day of experiment, the cells had formed a confluent layer on top of the chips.

3 Results

The basic function and the usability of the newly encapsulated, planar MEA chip was characterised by spontaneously active cardiac cells (Fig. 3). These cells were used as they have excellent signal-to-noise ratio, which allows a systematic and comprehensive characterisation of the MEA chips. Upon specific chemical stimulation of the secretory cell-containing layer, the secreted catecholamines were released to the cardiac layer through the permeable membrane of the commercial cell insert. The beat rate and conduction speed of the cardiac cells were measured directly from the MEA.

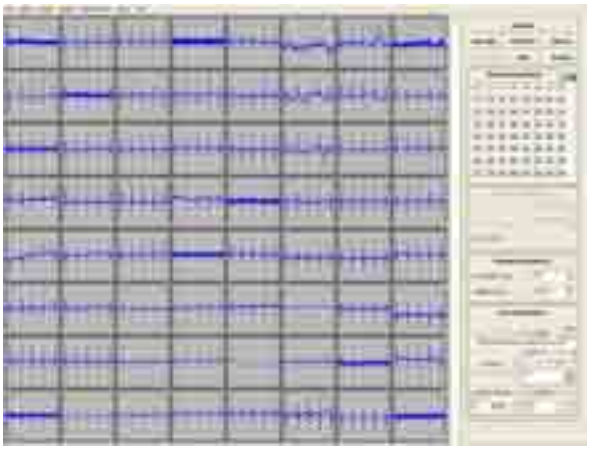

Fig. 3. Extracellular field potentials of cardiac cells recorded with the new co-culture MEA. HL-1 cells were cultured on the planar MEA chips and spontaneous signals were recorded after the cells were in culture for 3 days. Clear signals were observed from the MEA, which were encapsulated with the new method as described.

4 Conclusion

In our former studies we used a direct flip-chip bonding process of our MEA devices onto PCB carriers. This had the disadvantage that we needed to use glass rings of 9 mm inner diameter forming the active area available for cell culture. As a second disadvantage, the chip surface was lowered by the thickness of the PCB carrier compared to the present novel procedure; where a smaller step of 150 µm resulting from the thickness of the CAPTON foil is present. This procedure has now two important advantages: The effective size of the glass chip can be reduced enabling a more cost-effective fabrication of the devices. In addition we have now the possibility of combining our chips with classical insets with porous bottoms for standard co-culture studies. In future many secondary effects of cell-cell interactions will be feasible with our approach.

Acknowledgement

This work was supported by BMBF/AIF 17042X11 and BMBF/AIF 17N2110. The authors thank Alice Kasjanow (FH Kaiserslautern) for technical support during encapsulation of the MEA devices.

References

[1] Fulop T., Radabaugh S., Smith C. (2005). Activity-dependent differential transmitter release in mouse adrenal chromaffin cells. *Journal of Neuroscience*, 25, 7324-7332.

[2] Stett A., Egert U., Guenther E., Hofmann F., Meyer T., Nisch W., Haemmerle, H. (2003). Biological application of microelectrode arrays in drug discovery and basic research. *Analytical and Bioanalytical Chemistry*, 377, 486-495.

[3] Cui H.F., Ye J.S., Chen Y., Chong S.C., Sheu F.S. (2006). Microelectrode array biochip: tool for in vitro drug screening based on the detection of a drug effect on dopamine release from PC12 cells. *Analytical Chemistry*, 78, 6347-6355.

[4] Atkins D.L., Krumm P.A., Schutte B.C., Harrison J.D., Green S.H. (1997). Regulation of Rat Cardiac Myocyte Growth by a Neuronal Factor Secreted by PC12 Cells. *Pediatric Research*, 41, 832-841.

Budget prototyping of new MEA electrode layouts with film masks

Tomi Ryynänen[1*], Laura Ylä-Outinen[2], Susanna Narkilahti[2], Jukka Lekkala[1]

1 Department of Automation Science and Engineering, Tampere University of Technology and BioMediTech, Tampere, Finland
2 Institute of Biomedical Technology, University of Tampere and BioMediTech, Tampere, Finland
* Corresponding author. E-mail address: tomi.ryynanen@tut.fi

Abstract
In order to promote usage of custom designed microelectrode arrays (MEAs) we propose use of photoplotted film masks in the prototyping phase of fabricating and testing new MEA designs. Compared to conventional high quality glass masks, the film masks offer considerable costs savings. In our experience, phototoplotted film masks despite their lower resolution, can together with careful mask design be used in fabricating MEAs with quality and performance sufficient to measuring proper signals, for example, from neuronal cells.

1 Introduction

Several cell and tissue engineering studies can be well performed with the microelectrode arrays (MEAs) having the standard 8 x 8 electrode layout or one of a few other commercially available layouts. However, various novel research questions like controlled growth of neural cell networks, simultaneous multi drug experiments, advanced long term cell culturing environments, and even new material trials may benefit from electrode layouts differing from the traditional ones.

Commercial MEA manufacturers and several research groups have ability to produce custom designed MEAs, but the starting costs are relatively high due to expensive lithography mask sets needed for each custom electrode layout. To get the price of single MEA to a feasible level, the amount of similar MEA copies ordered, and at the same time also the total value of the order often gets unreasonably high. In addition, there is a risk that the design of the novel electrode layout would require some further optimization or that it even turns out to be totally unsuccessful to the intended purpose, causing a complete loss of money. Undoubtedly those reasons have decreased researcher's interest towards the custom designed MEAs, which in the worst case may have even slowed down the development in the field of cell and tissue engineering.

To make the utilization of custom MEAs more attractive, we propose prototyping the custom MEA designs at first with somewhat lower quality MEAs made by using photoplotted film masks which easily offer a remarkable lower price per MEA design compared with traditionally used glass masks. Once the cell or tissue experiments performed with the prototypes have proved the design to be optimal, placing expensive high quality MEA order is better justified.

2 Methods

We have tested 64 000 DPI and 40 000 DPI photoplotted film masks from Zitzmann GmbH (Eching, Germany) and Advance Reproductions Corporation (North Andover, MA, USA), respectively, in fabrication of standard 8 x 8 layout type of MEAs and customized MEAs with modified electrode sizes and/or locations. According to the film mask manufacturers the recommended minimum feature size with the film masks is about 10 µm, which sets certain limits to the microelectrode size and the width of the tracks. In our designs, the minimum track width has been 20 µm, and the microelectrode diameters of 30 µm or more have been used. The MEAs containing titanium [1] or ALD iridium oxide [2] microelectrodes have been tested in cell experiments where field potential signals have been measured from human embryonic stem cell - derived neuronal cells (hESC-N) as described earlier [3, 4] and also from human embryonic stem cell - derived cardiomyocytes (hESC-CM) [1].

3 Results

The major challenge with film masks is related to the mask design as the edges of the patterns in a film mask are not as sharp as in a glass mask, but as can be seen in Figure 1, include a few microns grey area which depending on process type (etching or lift-off) and mask polarity (negative or positive), may lead to wider or narrower patterns than designed. In addition to the nominal plotting resolution, the daily condition of the plotting machine and quality of the film used on plotting affect significantly on the width of the grey area. Another drawback related to film masks are the bubbles in the mask, which in the worst case might copy also to the thin film layers of MEA as unwanted dots or holes.

With a careful mask design it is, however, possible to achieve the wanted pattern widths after each masking step and thus use photoplotted film masks in fabricating highly uniform MEAs with sufficiently small feature size (Fig. 2). The performance of such MEAs has also been found feasible in several cell experiments. Figure 3 presents spontaneous hESC-N signalling measured with an ALD iridium oxide MEA that was fabricated using film masks.

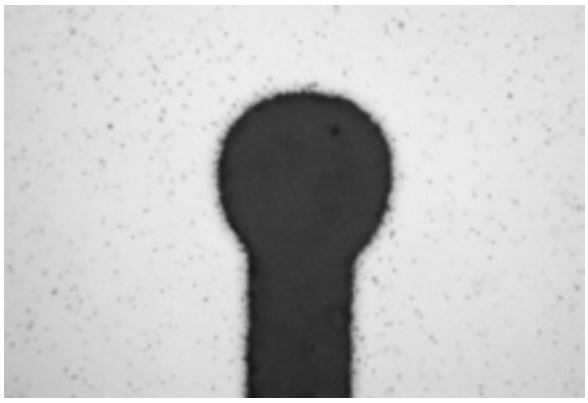

Fig. 1. MEA electrode pattern on photoplotted film mask. Electrode diameter is 38 µm.

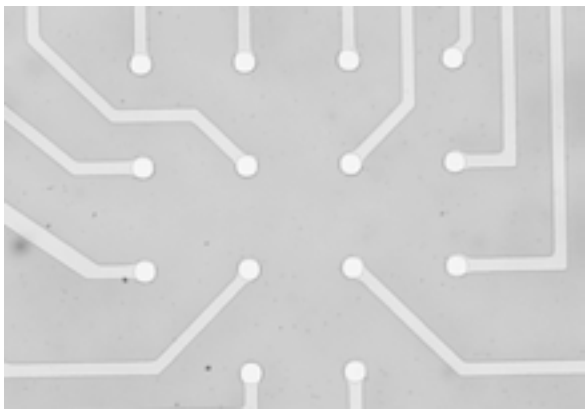

Fig. 2. MEA fabricated using photoplotted film masks. The diameter of the microelectrodes is 30 µm.

Fig. 3. Example of a spontaneous hESC-N signalling (cells on MEA for 14 days) measured with an ALD iridium oxide MEA fabricated using film masks.

Acknowledgement

This work was supported by the Academy of Finland (decision numbers 122959 and 123359), Tekes (decision numbers 40345/11 and 40346/11), the Finnish Cultural Foundation and its Pirkanmaa Regional Fund, and CHEMSEM graduate school.

References

[1] Ryynänen T. *et al*. (2011): All Titanium Microelectrode Array for Field Potential Measurements from Neurons and Cardiomyocytes—A Feasibility Study. *Micromachines* 2, 394.

[2] Ryynänen T., Ylä-Outinen L., Narkilahti S., Tanskanen J.M.A., Hyttinen J., Hämäläinen J., Leskelä M., and Lekkala J. (2012): Atomic layer deposited iridium oxide thin film as microelectrode coating in stem cell applications. *J. Vac. Sci. Technol. A* 30(4), Jul/Aug 2012.

[3] Heikkilä T. J. , Ylä-Outinen L., Tanskanen J. M. A., Lappalainen R., Skottman H., Suuronen R., Mikkonen J. E., Hyttinen J. A. K, and Narkilahti S. (2009):Human embryonic stem cell-derived neuronal cells form spontaneously active neuronal networks *in vitro*. *Exp. Neurol.* 218, 109.

[4] Lappalainen R. S., Salomäki M., Ylä-Outinen L., Heikkilä T. J., Hyttinen , J. A. K., Pihlajamäki H., Suuronen R., Skottman H., and Narkilahti S. (2010): Similarly derived and cultured hESC lines show variation in their developmental potential towards neuronal cells in long-time culture. *Regen. Med.* 5, 749.

Cardiac myocyte action potentials recorded with silicon nanowire transistor arrays

Xuan Thang Vu, Dieter Koppenhöfer, Sven Ingebrandt*

Dept. of Informatics and Microsystem Technology, University of Applied Science Kaiserslautern, Zweibrücken, Germany
* Corresponding author. E-mail address: sven.ingebrandt@fh-kl.de

Abstract
We present recordings of action potentials from primary heart cell cultures using robust silicon nanowire field-effect transistor (SiNW-FET) arrays. The SiNW-FET arrays were fabricated by a "top-down" approach in a wafer-scale level. The chips were then encapsulated to be capable for a long-term cell culture and for reliable functioning in cell culture medium. By the use of an electronic preamplifier with larger bandwidth compared to our previous reports, we succeeded to record action potentials of primary heart cells after 5 days in vitro. The devices are such robust that they can be cleaned and re-used for several repeated cell cultures.

1 Introduction

In the last decade, nano-scale devices gained increasing interest for biomedical applications due to novel properties of the sensor materials at the nano-scale level. In different studies, silicon nanowire field-effect transistor (SiNW-FET) devices have shown a higher sensitivity compared to corresponding micro-scale devices, due to an increased surface-to-volume ratio in the downscaled sensor version.

It has been shown that such devices can serve as a sensor platform for different biosensor approaches such as the electrical detection in biological affinity assays (DNA, viruses, bacteria) as well as for the functional coupling with electrogenic cells [1-5, 7]. In addition a very high special resolution of signal recordings from neuronal cultures can be achieved with SiNW-FET arrays [3]. In general, when working with cell cultures, the robustness and long-term stability of the devices is of major interest. In this work, we present the usage of SiNW-FET arrays to record the spontaneous action potential of cardiac myocytes after up to 8 days in vitro.

2 Material and Methods

2.1 Silicon nanowire arrays

The SiNW arrays were fabricated by a "top-down" approach on wafer scale as described earlier [5]. The devices consist of 28×2 individual addressable nanowires. The wire lengths in our design varied from 5 µm to 40 µm and the widths of the wires varied from 100 nm to 300 nm. The chips were encapsulated on 68 pin ceramic carriers (LCC0850, Spectrum, USA) and a glass ring formed a dish for the cell culture (Fig. 1).

2.2 Cell culture

The embryonic cardiac myocyte culture (Spraque Dawley rats, E18, Charles River GmbH, Sulzbach, Germany) was adapted from previously published protocols. The myocytes were plated onto the SiNW-FETs at densities of 60000 cells per chip. The chips were incubated for 5-8 days at 37 °C, and 5% CO_2. After 5-6 days in culture, the extracellular signals of the cardiac myocytes were recorded.

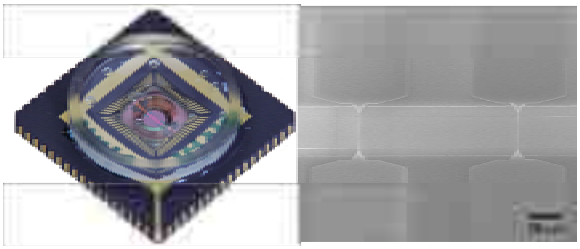

Fig. 1. Left: Picture of a SiNW chip readily encapsulated for cell culture assays. Right: SEM image of two SiNWs with their corresponding source drain connections.

2.3 Electronic amplifier

The electric signals were recorded simultaneously on 16 channels of the array by using a two-stage electronic amplifier setup (Fig. 2). The first amplifier stage converted the µA currents flowing through the SiNW-FETs to a voltage via a transimpedance circuit including a 1 MΩ feedback resistor. The DC part of the signal was filtered out by a feedback loop in the second amplifier stage and the signal was multiplied 100 times (Fig. 2). The output signals were then directly recorded by a National Instrument card (PCI 6071E) at a sampling rate of 10 kHz per channel. Action potentials were recorded after 5-8 days in vitro.

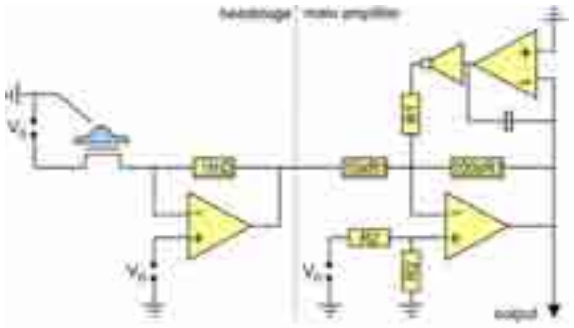

Fig. 2. Principle of the electronic amplifier circuit used for extracellular recording with SiNW.

3 Results

Figure 3 shows extracellular signals recorded with the SiNW array. The action potentials showed a typical signal shape with a beating frequency of about 60 beats per minute. The signal amplitude was about 2 mV, which is comparable to the signals recorded by standards micro electrode arrays (MEA) chip [6].

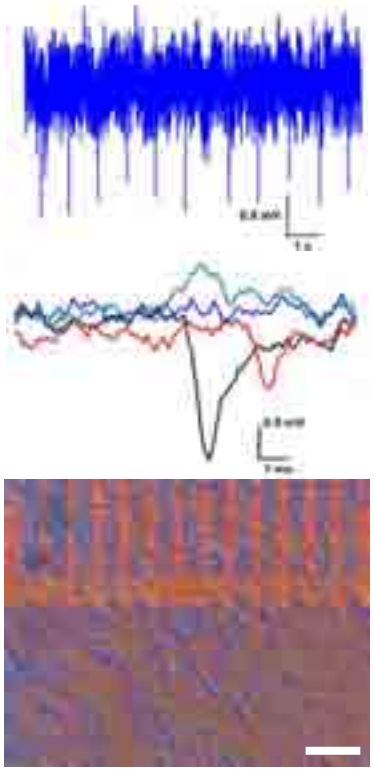

Fig. 3. Action potentials from a cardiac myocyte culture recorded by SiNW arrays (top). Zoom-in of a recorded action potential and comparison of signals from different channels of the arrays. Clearly a time delay between the recordings can be seen caused by the propagation electrical excitation in the tissue. A DIC microscopy image of the primary heart cell culture on SiNW chip (bottom – scale bar 100 µm).

However, the signals recorded by the SiNW-FETs were quite noisy with a noise level of about 0.5 mV. In addition, due to a limited bandwidth of the amplifier setup it was difficult to obverse the generally known slow components of the cardiac signals. The signal-to-noise ratio of our recordings was approximately 3:1, which is still lower compared to our MEA devices [6], but comparable to our previous report with rapidly growing HL-1 cell cultures [4]. The reason for this noise lies in the fabrication of the SiNW-FETs, where interface states at the Si/SiO_2 interface are altering the electrical transport of charge carriers inside the nanowires and implanted silicon contact lines are reducing the effective transconductance of the FETs due to the increased feed line resistances compared to other studies.

4 Conclusion

We have successfully recorded signals from primary heart cell cultures after 5 days in vitro with our SiNW-FET arrays. The implanted feed lines with passivation layers fabricated in an LPCVD process enable a high robustness of the devices. However, in our current design we suffer from a low signal-to-noise ratio, which is still too large to record neuronal signals. In future, we will focus on the technical improvement of the system as well as the SiNW devices to enable high density recordings from neuronal cultures.

Acknowledgement

We thank the Federal Ministry of Education and Reseach (BMBF), Germany for financial support via the project “Multifunktionales Pharmascreening mit Cell-Chip Hybridsystemen”, 17N2110. We thank A. Offenhäusser, R. Stockmann, J. Eschermann and coworker at Research Center Juelich, Germany, for supporting the fabrication of the SiNW-FET arrays.

References

[1] Cui Y., Wei Q., Park H., and Lieber C. M. (2003). Nanowire Nanosensors for Highly Sensitive and Selective Detection of Biological and Chemical Species. *Science*, 293 (5533), 1289-1292.

[2] Stern E., Klemic J. F., Routenberg D. A., Wyrembak P. N., Turner-Evans D. B., Hamilton A. D., LaVan D. A., Fahmy T. M., and Reed M. A. (2007). Label-free immunodetection with CMOS-compatible semiconducting nanowires. *Nature*, 445, 519-522.

[3] Patolsky F., Timko B. P., Yu G., Fang Y., Graytak A. B., Zheng G., and Lieber C. M. (2006). Detection, stimulation, and inhibition of neuronal signals with high-density nanowire transisotr arrays, *Science*, 313(5790), 1100.

[4] Eschermann J. F., Stockmann R., Hueske M., Vu X. T., Ingebrandt S., and Offenhäusser A. (2009). Action potentials of HL-1 cells recorded with silicon nanowire transistors. *Applied Physics Letters*, 95(8), 083703.

[5] Vu X. T., Stockmann R., Wolfrum B., Offenhäusser A., and Ingebrandt S. (2010). Fabrication and application of a microfluidic-embedded silicon nanowire biosensor chip, *Physica Status Solidi (a)*, 207(4), 850-857.

[6] Ecken H., Ingebrandt S., Krause M., Richter D., Hara M., and Offenhäusser A. (2003). 64-Channel extended gate electrode arrays for extracellular signal recording. *Electrochimica Acta*, 48(20–22), 3355-3362.

[7] Cohen-Karni T., Qing Q., Li Q., Fang Y., and Lieber C. M. (2010). Graphene and nanowire transistors for cellular interfaces and electrical recording. *Nano Lett.*, 10, 1098-1102.

Fabrication of a novel gold microelectrode with nanostructures using electrochemical deposition method

Kim Raeyoung[1], Nam Yoonkey[1 *]

1 Dept. of Bio and Brain Engineering, KAIST, Daejeon, Korea
* Corresponding author. E-mail address: ynam@kaist.ac.kr

Abstract
Low impedance and high charge injection limit of microelectrodes are essential factors to record and stimulate neural networks on a microelectrode arrays (MEA). In this study, we developed grain-like nanostructures ('nanograin') on microelectrodes using an electrochemical deposition method. 500 nm-diameter nanograins were formed on a planar gold surface of an electrode and 1 – 5 μm ellipsoidal nanograins were also formed along the boundary of the electrode. Nanograins reduced the impedance of electrodes by 69 fold versus the planar gold microelectrodes and current can be injected up to 50 ~ 60 μA without significant electrolysis. In addition, the nanograin electrodes had low noise levels, around 2.89 μV_{rms} for 10 μm electrodes, resulted in high signal-to-noise ratio. Spontaneous action potentials, ranging from 30 to 300 μV_{pp}, were recorded and biphasic current pulses (20 – 60 μA) could evoke action potentials from neurons adjacent to the stimulating electrodes. The nanograin electrodes will be useful for high-density MEAs with ultramicroelectrodes.

1 Introduction

Planar-type microelectrode arrays (MEA) provides a simple platform to record extracellular neural signals and stimulate nearby neurons simultaneously from dissociated neuronal networks. MEAs should have low impedance for high signal-to-noise ratio and large charge injection limit. Recently there have been reports on gold microelectrodes such as nanoflake[1], nanopillar[2], and gold spine[3]. In this work, we fabricated novel gold microelectrodes with nanograins by a simple electrochemical deposition method. Gold nanograin electrodes were characterized by SEM images, impedance measurements, charge injection limit estimation, neuronal cell culture and signal recording.

2 Materials and Methods

Electrochemical deposition was conducted with an aqueous solution containing 25 mM $HAuCl_4$ and 20 gL^{-1} polyvinylpyrrolidone. A two-electrode electrochemical cell with Ag/AgCl wire as a reference/counter electrode was used. A various sizes of gold microelectrodes (10, 30, 50 μm diameter) were tested. Customized MEAs were used. A range of fixed electrochemical potential (-0.25, -0.30, -0.35, -0.40 V) was applied using a DC power supply for 10 to 60 seconds. The electrical impedance was measured by LCR meter (E4980A, Agilent) in a 1x PBS with a large gold reference electrode. The input AC signal was 100 mV and the frequency range was from 100 Hz to 100 kHz. To test the neural recordings and stimulations, E18 rat hippocampal neurons were cultured (density 800 cells/mm^2). The MEA surface was coated by polydopamine ($C_8H_{11}NO_2$·HCl, 2 mg/ml) in 10 mM Tris buffer, pH 8.0, Sigma-Aldrich) for 1 hour. After treating with 1 minute air plasma, poly-D-lysine (0.1 mg/ml in 10 mM Tris buffer, pH 8.0, Sigma-Aldrich) coated for 1 hour. The electrical signal was recorded using MEA 1060 System (gain 1200, digital filter: 200Hz, High pass filter).

3 Results and Discussion

3.1 Gold microelectrode fabrication

The formation of gold nanograins was dependent upon the electrodeposition time. At the reduction potential of - 0.3 V, gold nanograin seeds, which were about 20 – 70 nm, were formed in 10 seconds. In 60 seconds, 500 nm of nanograins were formed on the planar surface of a gold microelectrode and 1 – 5 μm of ellipsoidal structures were constructed at the edge. The reduction potential and electrode size did not exert strong influence on nanograin formation.

3.2 Electrical characterization

When - 0.3 V was applied to 10 nm electrodes for 60 seconds, the impedance magnitudes decreased from 8740 kΩ to 126 kΩ, which impedance reduction ratio was 69.4. The impedance reduction was mainly due to the increased surface area of microelectrodes by nanograins. The electrode structure and the impedance value were not significantly different for the reduction potential from - 0.25 V to - 0.4 V, while inter-electrode variance was minimal at - 0.3 V, which was 20.0%.

The charge injection limit of gold nanograin electrodes was estimated. Negative-positive biphasic current pulses ranging from 5 μA to 60 μA were applied to nanograin electrodes for 400 μs. At 40 μA of pulse stimulation, the electorde potential response reached the electrolysis potential and the electrode was broken. The charge injection limit was 10.2 mC/cm^2 based on the geometrical area of the planar gold electrode (78.5 μm^2).

3.3 Neural network recording and stimulation

At 14 DIV, spontaneous extracellular spikes ranging from 22.7 to 292 μV_{pp} were readily recorded. The noise level was 2.89 μV_{rms} from 10 μm electrodes. The estimated SNR was 10 – 45. Occasionally, we recorded some large positive spikes from the electrodes. Biphasic current pulses with the level of 20 μA evoked action potentials from neurons neighbouring the electrode.

4 Conclusion

We fabricated a novel nanostructured microelectrode through a simple electrochemical deposition. By electroplating, we could form gold nanograins on specific electrodes without using additional templates or lithographic procedure. The gold nanograin structures efficiently reduced the impedance of microelectrodes which resulted in high SNR and charge injection limit compared to planar gold microelectrodes.

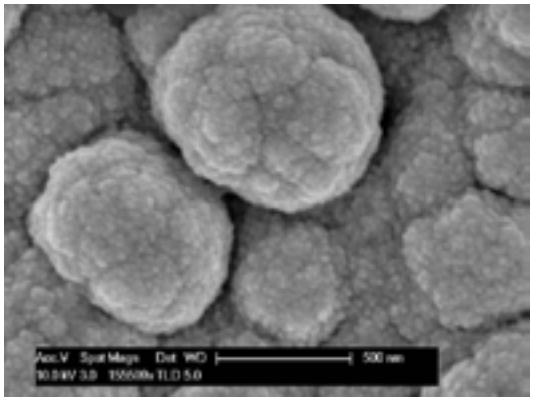

Fig. 1. SEM images of gold nanograin on a 10 μm electrode (- 0.3 V, 60 s)

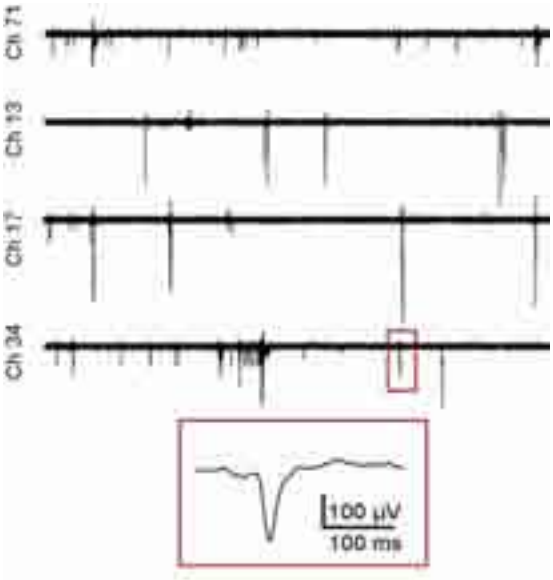

Fig. 2. Recorded spontaneous action potentials from hippocampal neuronal cultures using gold nanograin electrodes (14 DIV, 10 μm diameter).

Acknowledgement

This work was supported through NRF grant funded by the MEST (KRF-2008-313-D00614, No.2009-0080081, No. 2012007327) and the Industrial Source Technology Development Program (10033657-2010-12) of the Ministry of Knowledge Economy (MKE).

References

[1] Kim, J.-H., Kang, G., Nam, Y. & Choi, Y.-K. Surface-modified microelectrode array with flake nanostructure for neural recording and stimulation. *Nanotechnology* **21**, 85303 (2010).

[2] Brüggemann, D. *et al.* Nanostructured gold microelectrodes for extracellular recording from electrogenic cells. *Nanotechnology* (2011).

[3] Fendyur, A., Mazurski, N., Shappir, J. & Spira, M.E. Formation of Essential Ultrastructural Interface between Cultured Hippocampal Cells and Gold Mushroom-Shaped MEA- Toward "IN-CELL" Recordings from Vertebrate Neurons. *Frontiers in neuroengineering* **4**, 14 (2011).

Electrochemical deposition of polydopamine films for neural electrodes

Kyungtae Kang[1], Seokyoung Lee[2], Raeyoung Kim[2], Insung S. Choi[1*], Yoonkey Nam[2*]

1 Molecular-Level Interface Research Center, Department of Chemistry, KAIST, Daejeon, Korea
2 Department of Bio and Brain Engineering, KAIST, Daejeon, Korea
* Corresponding author. E-mail address: ichoi@kaist.ac.kr or ynam@kaist.ac.kr

Abstract
Neural electrodes are the core part of the neuron-material interfaces. Surface modification of the neural electrodes is highly required for the improved performance of the electrodes. In this study, we report a novel method for a site-selective biofunctionalization of neural interfaces by electrochemical synthesis of bare or bioactive polydopamine film. We devised an electrochemical deposition process that was only triggered on neural electrode surface by applying oxidation potentials to the electrodes under an adjusted pH condition. The thickness of deposited polymer film ('ePolyDA') was controlled by the oxidation time and surface properties were similar to polydopamine films. Biomolecules were covalently linked and the film promoted good neuronal adhesion and growth. Planar-type microelectrode arrays were used to investigate the site-selective deposition of ePolyDAs The spatially addressable biofunctionalization scheme would be potentially useful for integrating biomaterials with multichannel-type neural prosthetic devices in neural engineering fields.

1 Introduction

Recently, the biofunctionalization of the neural electrode interface has been actively reported to improve biocompatibility and the reliability of neural recording and stimulation. Detailed strategies include self-assembled monolayer coatings, layer-by-layer assembly, neurotrophin-releasing hydrogel coatings, co-deposition of polypeptide/polypyrrole, collagen conjugated polypyrrole/chondrotin sulfate, and poly(ethylenedioxythiophene) doped with laminin peptides and neurotrophinc growth factors. Although a variety of biomaterials (e.g. extracellular matrix (ECM) proteins, nerve growth factors, synthetic biopolymers) can be directly immobilized through covalent linking chemistry, most of the biofucntionalization studies have been led by synthesizing bioactive conductive polymer on electrode surfaces[1] and only a few efforts have been made toward the alternative biofunctionalization scheme[2].

In this work, we report an electrochemical biofucntionalization scheme that incorporated biomolecules into polydopamine film (PolyDA) using the electrochemical synthesis. As the electrochemical reactions occurred only at the surface of the electrodes, we could deposit the PolyDA films specifically at the voltage-applied electrodes. The electrochemically deposited polydopamine films were named 'ePolyDAs', and their chemical/physical properties were characterized and compared with the conventional polydopamine films. A 60-channel microelectrode array (MEA) was used to demonstrate the proposed site-selective biofunctionalization strategy. Rat hippocampal neurons were cultured to verify the biological functionality of the proposed.

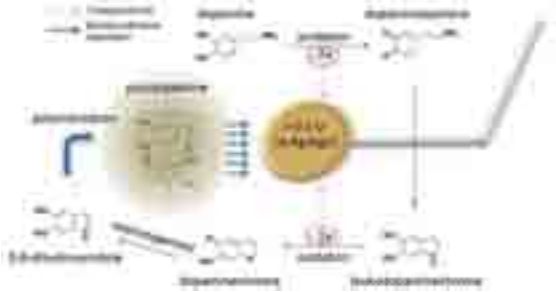

Fig. 1. A Mechanistic illustration of ePolyDA deposition.

2 Methods

For ePolyDAs, +0.5 V was applied to fixed area of the substrates in a buffered solution (10 mM sodium phosphate buffer (SPB) solution of dopamine, pH 6.0), with the platinum wire as a counter electrode, Ag/AgCl as a reference electrode. The pH difference made dopamine molecules not to be spontaneously polymerized without the voltage. After a desired reaction time, substrates were thoroughly rinsed with distilled water. In case of co-ePolyDAs, desired amount of biomolecules were mixed with dopamines in a pH 6.0 SPB solution, and the electrochemical synthesis was performed. Hippocampal neurons were plated onto the substrates at the density of 200-1000 cells/mm^2.

3 Results

For the co-deposition of ePolyDA and biomolecules, the identical electrochemical procedures were implemented in pH 6.0 mixed SPB solutions of dopamines and biomolecules. We chose 10:1 ratio between dopamines and biomolecules according to the results in previous section. Hippocampal neurons were cultured on 10:1 co-ePolyDA/PDL. Fig. 2a shows the fluorescence micrograph of hippocampal neurons, immunostained with anti-beta III tubulin (red) and hoechst 33342 (blue), targeting microtubules and nuclei, respectively. Neurons exhibited normal growth and development at 5 DIV, which was represented by well-spread somata, and elongated and branched neurites.

Fig. 2b shows the impedance measurement of TiN MEA (electrode diameter: 30 μm, electrode spacing: 200 μm) while targetting two electrodes. The impedance of all electrodes were measured at the time points of 5, 15, 25, and 40 min of the deposition (+ 0.5 V, co-ePolyDA/PDL (10:1)), by which we obtained the spatial distribution of the impedance increases at each time point. As shown at the above diagrams and the lower graph in Figure 5b, the impedance of two target electrodes increased 4.3 and 5.4 fold from the initial values, while non-target electrodes had 1.5 – 2 fold increase. The slight increase at the non-target electrodes appeared within the first 5 min, and the values remained same thorugh the entire reaction time. This global increase was presumably originated from the non-specific physisorption of PDL from the solution. The selective deposition of ePolyDAs at the target electrodes mainly occurred between 15 min and 25 min as there was no further increase at 25 min and 40 min. The increased electrode impedance was returned to the normal range (avg. |Z| = 119.9 kΩ @ 1 kHz) of clean TiN electrode when the electrodes were exposed to NaOH that is reported to dissolve polyDA films. The NaOH test confirmed that the large increase in targe electrodes was mainly due to the deposition of ePolyDA film.

4 Conclusion

In summary, we reported a novel method to biofunctionalize neural interfaces using electrochemically deposited PolyDA, which we named ePolyDAs. In addition, the codeposition of PolyDAs with biologically functional molecules and peptides was also reported as a novel scheme. The site-selective deposition of ePolyDA films was experimentally confirmed by measuring the impedance change of target electrodes in microelectrode arrays. Considering the versatility of PolyDAs and the site-selectivity of electrochemical strategy, we expect this method would be particularly advantageous for the sophisticated biofunctionalization of neural devices, and also improve the known PolyDA-based chemistry to be more versatile and practical.

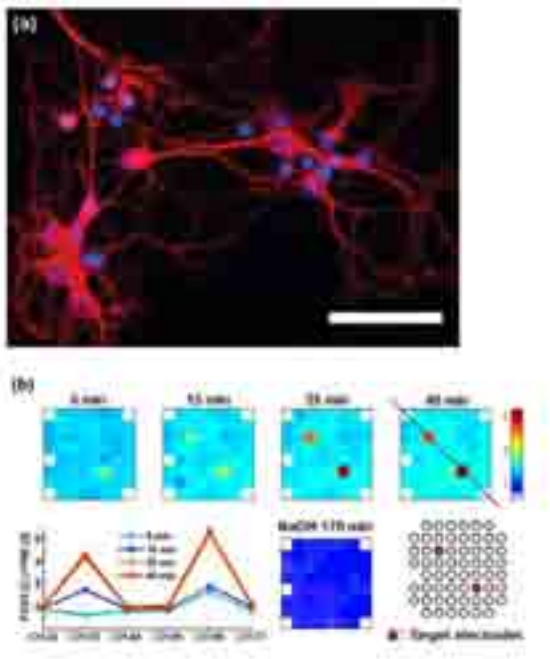

Fig. 2. (a) Fluorescence micrographs of hippocampal neurons on co-ePolyDA/PDL. The scale bar is 50 μm. (b) Spatio-temporal description of the impedance increases during 40 min-reaction. The numbers represent the ratio of the impedances compared with the ones before the reaction.

Acknowledgement

This work was financially supported by the grant from the Inudstrial Source Technology Development Program (10033657) of the Ministry of Knowledge Economy (MKE) of Korea, and the National Research Foundation of Korea (NRF) grant funded by the Korea government (No.2012007327).

References

[1] Kim, D.H., Richardson-Burns, S.M., Hendricks, J.L., Sequera, C., Martin, D.C. (2007): Effect of immobilized nerve growth factor on conductive polymers: Electrical properties and cellular response. *Adv Funct Mater*, 17, 79-86.

[2] Nam,Y., Branch, D.W., Wheeler, B.C. (2006): Epoxy-silane linking of biomolecules is simple and effective for patterning neuronal cultures. *Biosensors & Bioelectronics*, 22, 589-597.

Device development of miniature neuronal networks and analysis of spontaneous electrical activity

Lui Yoshida[1], Kenta Shimba[1], Kiyoshi Kotani[1], Yasuhiko Jimbo[1]

1 Graduate School of Frontier Science, The University of Tokyo, Japan

Abstract

To investigate the dynamics of neuronal networks, the device which is capable of multipoint simultaneous measuring and constructing multi-scale miniature neuronal networks was fabricated. The result of culturing rat embryo hippocampal neurons showed that the device is biocompatible and can be used successfully in long-term culture. Analysis of the electrical data obtained with the device suggested that, in miniature neuronal networks, there was neuronal avalanche which is considered very important to the process of storing and transforming information of a brain.

1 Background

In order to understand the operating principles of neural networks, it is necessary to associate the activity of each element neuron with dynamics of the whole network. However, with using optical imaging which possesses sufficient spatial resolution, in experiments with biological objects, brain slices and traditional dissociated cultures, a range of measurement is limited. Therefore it's difficult to comprehend the influences from other areas. One of approaches to those problems is to constructing miniature neural networks which fit within the microscopic field, but the knowledge about the dynamics of miniature neural networks is little known. The dynamics to be examined in this study are neuronal avalanches, the statistical phenomena of spontaneous activities, which are present *in vivo* and *in vitro*[1][2]. The probabilistic distributions of avalanche sizes and durations (described below) follow a power law and this fact suggests that neuronal activities optimize the transmission efficiency and the storage of information[1][3].

2 Material and Method

2.1 Device Fabrication

To build a group of miniature neural networks which consist of neurons from a few to several thousands, a unique device was fabricated (Fig. 1). The device was assembled with Polydimethylsiloxane (PDMS) structure and microelectrode arrays (MEA) with a one-of-a-kind electrode pattern. There are 3 types of circle-shaped compartments of cultures. The radius of those are 100μm(Type 1), 200 μm(Type 2), 400 μm(Type 3) and 4 compartments of each type have electrodes inside.

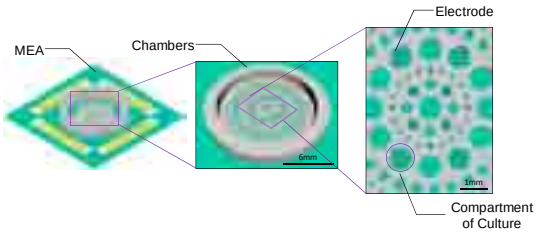

Fig. 1. Device for miniature neuronal networks

2.2 Cell Culture

Dissociated hippocampal neurons were obtained from hippocampus of embryonic Wister rats, at gestational day 19. They were disseminated to and maintained in the device containing 1.5ml of nutrient medium (i.e. Neurobasal® Medium (Invitrogen) supplemented with 2 % B-27 supplement (Invitrogen), 0.5 mM glutamax® (Invitrogen) and 1 % penicillin-streptomycin (Invitrogen)) and 1.5ml of conditioned medium. They are placed in humidified incubator having an atmosphere of 95% O_2 and 5% CO2 at 37 °C.

2.3 Data Processing

Extracellular Recording

The extracellular electrical signals of spontaneous activities obtained from the cultures were amplified twenty-fold with preamplifiers and filtered with a band-pass filter (100 Hz to 2 kHz), and then amplified thousand-fold with a main amplifier (NF Corp.). The signals were sampled at 25kHz with a resolution of 12 bits.

Spike Detection

The signals underwent a band-pass filter (300 Hz to 2kHz) and spikes were detected by amplitude thresholding[4]. The threshold is 5σ, σ is estimated

standard deviation by using median of filtered signals as $\sigma = median(|x|/0.6745)$ and x : filtered signals.

Neuronal Avalanche Analysis

The recordings were divided into bins which are time windows of duration Δt. A neuronal avalanche are defined as continuous sequence of bins which are sandwiched in between bins having no spikes (Fig. 2). An avalanche size is defined as the total number of spikes within the avalanche and An avalanche lifetime is defined as the duration of the avalanche. The probabilistic distributions of size and lifetime are calculated with all avalanches. To assess whether the distributions follow a power law, coefficients of determination were calculated by using least-square method with first 10 points. The recordings were analyzed at bin widths of 0.2, 0.4, 0.6, 0.8, 1, 2, 4, 8, 16 (ms).

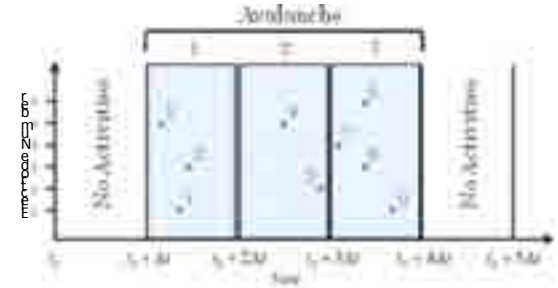

Fig. 2. Neuronal avalanche Analysis

3 Results

3.1 Extracellular Recording / Spike Detection

The signals were taken from 3 devices at 41 days *in vitro* (DIV). The raster plot showed that activities of cultures are independent of each other (Fig. 3). The spontaneous activities of cultures in the device at 41 DIV demonstrated that the device is biocompatible and can be used for long-term culture.

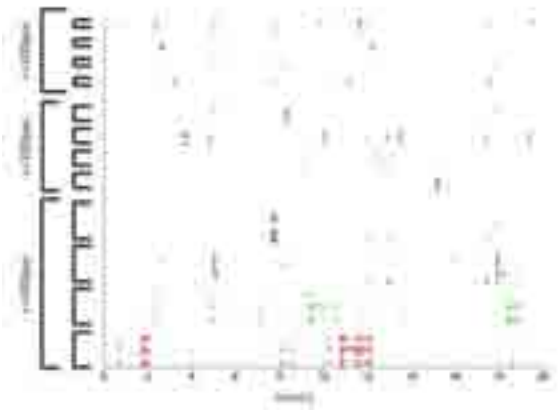

Fig. 3. Raster plot of spontaneous activities in the device

3.2 Neuronal Avalanche

The slopes of the distributions are stable when a bin width is more than 0.1ms (Fig. 4). The numbers of cultures whose distribution's coefficients of determination are more than or equal to 0.95 are listed in table 1. The result suggested that there are neuronal avalanches in all types of miniature neuronal networks. Therefore it is likely that neuronal avalanches are independent from the size of culture.

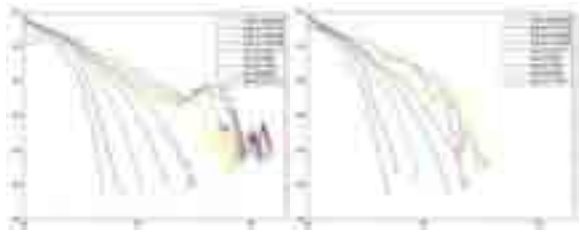

Fig. 4. Probabilistic distribution of one type 3 culture
Left is distribution of avalanche sizes and right is one of avalanche lifetimes. The number in brackets in legends is a total number of avalanches.

Table 1. Number of cultures whose distribution's coefficients of determination are more than or equal to 0.95
The result was described as "number of condition matched cultures/ number of total available cultures".

	Type 1	Type 2	Type 3
size	2/4	4/11	6/12
life-time	3/4	5/11	8/12

4 Conclusion

To investigate the dynamics of neuronal networks, a unique device which is capable of constructing multi-scale miniature neuronal networks was fabricated. The result of culturing rat embryo hippocampal neurons with the device showed that the device is biocompatible and suitable for long-term culture. The analysis suggested that there were neuronal avalanches in miniature neuronal networks.

Acknowledgement

This work was supported by Japan Society for the Promotion of Science(JSPS).

References

[1] J. M. Beggs and D. Plenz, "Neuronal avalanches in neocortical circuits" J. Neurosci, 23(35), pp. 11167-11177 (2003)
[2] T. Petermann, T. C. Thiagarajan, M. A. Lebedev, M. A. Nicolelis, D. R. Chialvo and D. Plenz, "Spontaneous cortical activity in awake monkeys composed of neuronal avalanches", Proc. Natl Acad. Sci. USA, 106, pp. 15921–15926 (2009).
[3] C. Haldeman, J. M. Beggs, "Critical branching captures activity in living neural networks and maximizes the number of metastable states.", Phys. Rev. Let., 94: 058101 (2005)
[4] T. Takekawa, Y. Isomura and T. Fukai, "Accurate spike sorting for multiunit recordings", European J. Neurosci., 31, pp. 263 272 (2010)

All-carbon-nanotube flexible neuronal electrodes

Moshe David-Pur[1,*] Lilach Bareket[1], Giora Beit-Yaakov[1,2], Dorit Raz-Prag[2] and Yael Hanein[1,2]

1 School of Electrical Engineering, Tel-Aviv University, Tel-Aviv 69978, Israel
2 Tel-Aviv University Center for Nanoscience and Nanotechnology, Tel-Aviv University, Tel-Aviv 69978, Israel
* Corresponding author. E-mail address: moshedav@post.tau.ac.il

Abstract
A new flexible neuronal micro electrode device, based entirely on carbon nanotube technology, is presented. Both the conducting traces and the stimulating electrodes consist of conducting carbon nanotube films. The nanotube films are embedded in a polymeric support and are passivated by an additional insulation layer. The use of carbon nanotubes bestows the device flexibility, durability, corrosion resistance, and excellent electro-chemical properties. As opposed to contemporary flexible neuronal electrodes, the fabrication process is simple and the resulting stimulating electrodes boast a record high specific capacitance. Recording and stimulation tests with chick retinas validated the advantageous properties of the electrodes and demonstrate their suitability for high-efficacy retinal stimulation applications.

1 Introduction

Successful in-vivo neuronal electrodes must be suitable to stimulate small and localized areas without causing electrode or tissue damage. The technological challenge is in simultaneously addressing two competing requirements: A geometric surface area which needs to be as small as possible and the impedance of the electrode which should be minimized [1]. Moreover, the need to realize the electrodes on soft, biocompatible materials further complicates the ability to form highly localized and safe electrodes.

As was previously demonstarted, carbon nanotube (CNT) with their three-dimensional structure bestows micro electrodes a huge surface area and therfore enable a reduction in the electrode size, while keeping the impedance low. Advantageous biological interaction between cells and CNT films further supports the motivation to explore CNT electrodes for in-vivo applications [2]. Since device performances in vivo are also determined by the tissue-electrode interface, the platform for the CNT electrodes should ideally be made of flexible, stretchable and bendable materials. A remaining challenge in using CNTs for neuronal applications, which we addressed in this work, is the integration of CNT technology onto flexible support while retaining the excellent properties of CNTs, as previously reported [2].

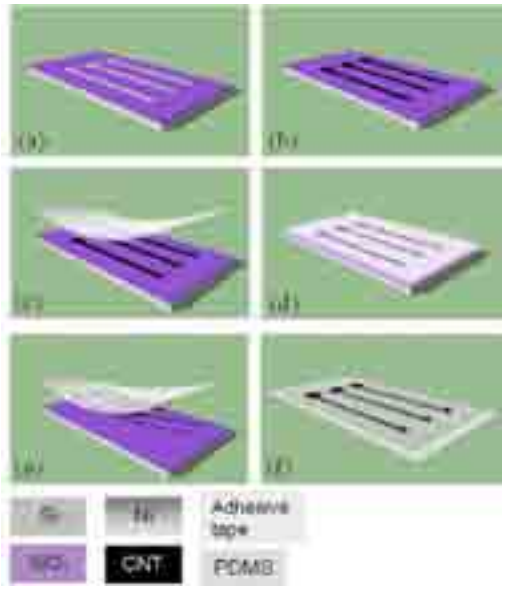

Fig. 1. Fabrication scheme. (a) After a photolithography step, a Ni layer is deposited on the substrate. (b) A CNT film is grown by CVD (c,d). An adhesive tape is attached and pressed lightly against the CNT film. (e) The CNT film is peeled off from the substrate. (f) The device is passivated with a holey PDMS membrane.

2 Results

The fabrication process is based on a transfer step of a chemical vapor deposition (CVD) grown CNT film to a flexible support. Figure 1 illustrates the flexible multi electrode array (MEA) process flow scheme using a medical tape (by 3M). Entire film structures can be faithfully transferred onto different types of substrates. Materials such as: PDMS (Poly(dimethylsiloxane)), polyimide, medical adhesive tape and sellotape were used. Spin coat or mechanical pressure coupling techniques were used to facilitate the nanotube transfer from the silicon dioxide substrate. Finally, the transferred nanotube film was aligned with a

passivation membrane made of PDMS to form a multi electrode array device.

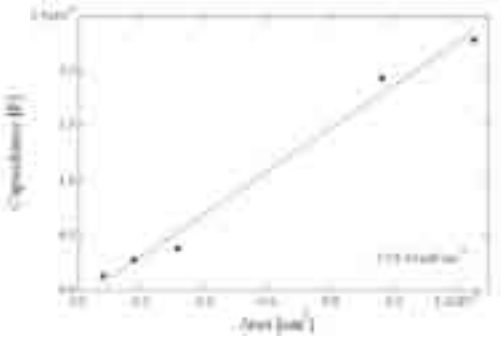

Fig. 2. Flexible CNT electrode capacitance versus electrode area.

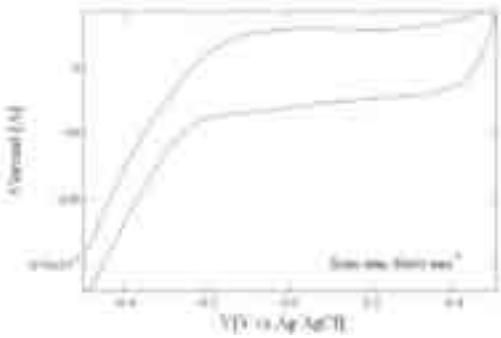

Fig. 3. Cyclic voltammetry scan measured in PBS. A capacitive behavior is demonstrated.

The entire device is based on CNTs including pads, traces and electrodes. Therefore, an optimization of the CNT film electrical resistance at different CVD growth parameters was performed. In average, a 400Ω/□ value was measured. Also, electro-chemical tests were performed to characterize the double-layer capacitance of the electrodes. Specific capacitance as high as 2 $mF \cdot cm^{-2}$ (Figure 2) was measured and the electrodes demonstrated almost pure capacitive behaviour, with no redox peaks seen within the scan range of ±0.5 V (Figure 3). Recording and stimulation were achieved owing to the excellent electro-chemical properties of the electrodes. Recording from embryonic chick retina (Figure 4) was achieved with signal to noise ratio of >10. Moreover, stimulation was achieved with threshold current of 4 nC for 30 μm diameter electrodes (Figure 5), similar to the threshold obtained by commercial TiN MEAs.

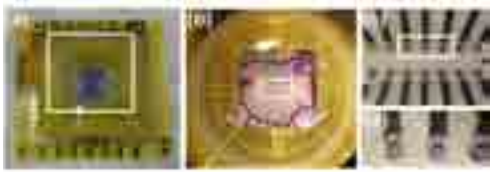

Fig. 4. (a) Fully packeged flexible MEA. (b) Retina flatted on the electrode sites. (c and d) Magnification of the electrode sites.

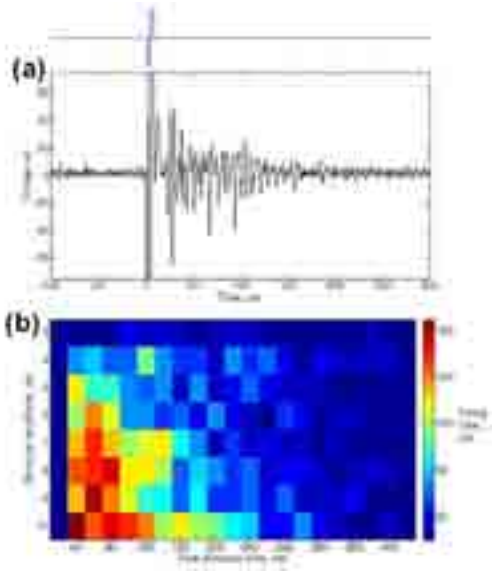

Fig. 5. Retinal responses recorded with a CNT electrode array. (a) A typical response evoked by stimulation (shown in blue) (b) Neuronal firing rate as a function of stimulation amplitude and post-stimulus time.

3 Conclusions

CNTs have many beneficial properties best suited for neuronal stimulation applications. Key features are: a three-dimensional morphology, high mechanical durability, a good electrical conductance and corrosion resistance. Growing loosely attached CNT films on SiO_2 substrate enabled us to utilize these qualities to form bio-compatible, flexible electrodes with superb properties. As opposed to contemporary neuronal electrodes, the device described here is based exclusively on nanotubes including the traces and the pads bestowing the technology simplicity, flexibility, durability, corrosion resistance and excellent electro-chemical properties.

References

[1] S. F. Cogan et al., *Neural stimulation and recording electrodes*., Annual review of biomedical engineering, 2008, 10, pp. 275-309,

[2] Tamir Gabay, Moti Ben-David, Itshak Kalifa, Raya Sorkin, Ze'ev R. Abrams, Eshel Ben-Jacob and Yael Hanein, *Electro-chemical and biological properties of carbon nanotube based multi-electrode arrays*, Nanotechnology, 2007, 18, pp. 035201-035206, 2007.

Diamond microelectrode arrays: A versatile tool for in vitro measurements

A. Pasquarelli[1], Z. Gao[1], S. Alsawafi[1], I. Izadi[1], E. Colombo[1,2], S. Gosso[2], A. Marcantoni[2], M. Ullmann[1], V. Carabelli[2], E. Carbone[2]

1 Institute of Electron Devices and Circuit, Ulm University, 89069 Ulm, Germany
2 Department of Neuroscience, NIS Centre, University of Torino, 10125 Torino, Italy
* Corresponding author. E-mail address: alberto.pasquarelli@uni-ulm.de

Abstract
Nanocrystalline diamond (NCD) is the functional material that we have been using during the last few years to realize microelectrode arrays in layouts of increasing complexity, targeting a variety of biological applications. This work presents an overview of such different designs and describes the potential application scenarios on the basis of both the theoretical predictions and the experimental results obtained so far.

1 Introduction

Microelectrode arrays (MEAs) became in the last decade a tool of primary importance for in vitro studies, including among others cell and tissue electrophysiology, genetic and degenerative diseases, prosthesis development and drugs screening [1-3]. The study of secretory cells activity was so far less impacted by the availability of MEAs, because their technology intrinsically limits their typical use to the stimulation and recording of electrical events (current and voltage). In fact the commonly used materials, e.g., titanium nitride and iridium oxide are excellent for low noise detection of action potentials, due to the large specific capacity, but show large background currents, rapid fouling, little chemical stability and ultimately short life-time, when operated in amperometric mode. Other materials like gold and platinum are chemically stable and therefore better suited for this application, but are opaque, thus limiting the observation of the biological samples and have anyway a strong tendency to fouling, due to their unspecific affinity for most biomolecules.

In recent years diamond emerged as good candidate for amperometric use [4]. Diamond electrodes show excellent chemical stability even in harsh environments [5], are transparent, little prone to fouling and can operate in a potential window of ~ 3 V, i.e. more than twice the potential of water electrolysis (1.23 V). The development of technologies for growth of synthetic nanocrystalline diamond (NCD) films on transparent substrates, the possibility of doping diamond with boron, thus obtaining conductive layers and the suitability of diamond for the typical microelectronic processes, made it possible to fabricate diamond-based MEAs [6-7], thus addressing the area of biological applications left uncovered by "mainstream" MEAs.

Moreover diamond electrodes are pH sensitive, when their surface is terminated with oxygen [8] and show low background noise. These additional properties can be exploited to detect both chemical and electrical potentials, thus expanding the range of applications for this outstanding material.

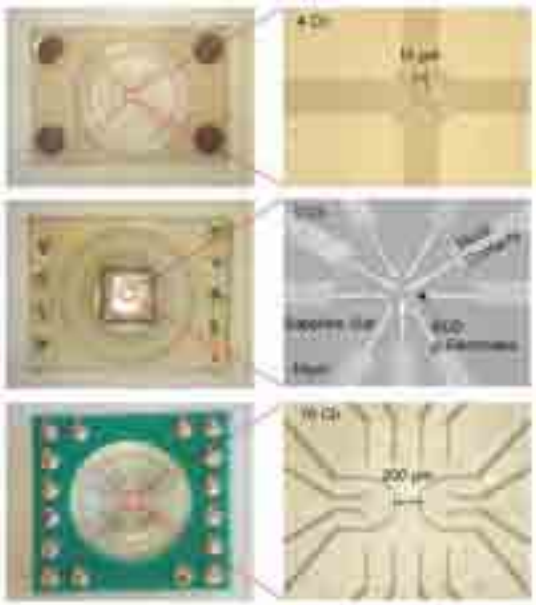

Fig. 1. MEAs of different layouts and complexity. The left column shows the whole chips and the right column shows the magnification of the sensing areas respectively. Top: 4 channel device with one single 100µm opening. Center: 9-channel array with 20µm diameter of the sensing opening. Bottom: 16-channel MEA with 18µm electrodes at the tip of the wires and 200 µm pitch..

2 Materials and methods

All devices presented here (Fig. 1.) share the NCD-on-Sapphire technology, which allows producing robust and reliable devices showing a transparency of more than 50 % in the green to red visible range, thus permitting, to a certain extent, the simulta-

neous detection of bioelectrochemical signals and fluorescence tracking of cellular activity.

Early devices were fabricated with a layout consisting in four microelectrodes arranged inside a single opening with diameter of 15 to 20 µm (Fig 1, top). Such devices were designed for single-cell observations with capability to localize the site of cell activity. Several layout variations of this basic quadrupolar array have been successively fabricated, including arrays with four individual single-cell openings or one larger opening to allow multiple cells detection at the expense of spatial resolution.

Subsequent technological developments followed two different directions: first we increased number and density of electrodes by designing 9-channel MEAs with all electrodes arranged in a sensing area of 20 µm in diameter (Fig. 1, center), in order to observe the activity of a single cell with an improved spatial resolution. In the second thread we increased the number of electrodes to a total of 16 units and their individual size to a diameter of 18 µm and arranged them on a 4x4 square grid having a pitch of 200 µm (Fig. 1, bottom). This latter device was targeted to simultaneous recordings from multiple cells, cell populations or whole tissues and study intercellular interactions.

Several experiment were carried out, first to characterize the behavior of the diamond electrodes in standard electrolytic solutions and then with different biological models. Due to the outstanding properties of diamond as type-0 electrode, large part of the validation work was focused on the amperometric method to study the activity of secretory cells. Here the comparison with the "gold standard" confirmed not only the qualitative but also the quantitative sensitivity of the diamond electrodes for this specific use [9].

More recently we started the investigations on the potentiometric sensitivity of diamond and possible exploitations thereof in the detection of bioelectric and biochemical potentials. Even though the electrode capacitance is only ~60pF (Fig 2), the accurate design of the electronic front-end allowed a signal detection efficiency of ~95%. Early results showing action potentials detected from cardiac tissue samples look very encouraging. Also variation of chemical potential could be clearly detected, in accordance with the property shown by oxygen-terminated diamond electrodes. A detailed description of experimental results obtained in all three operating modalities, is reported in another work also presented at this conference [10].

4 Conclusions

This work describes the technological progress achieved by our team in design, fabrication and characterization of diamond MEAs. This electrode material has proven to be very versatile and suitable for a wide variety of in vitro experiments, being excellent in amperometry and very promising for recording both electrical and chemical potentials. Furthermore the available transparency of diamond electrodes allows concurrent use of fluorescence and electrochemical methods.

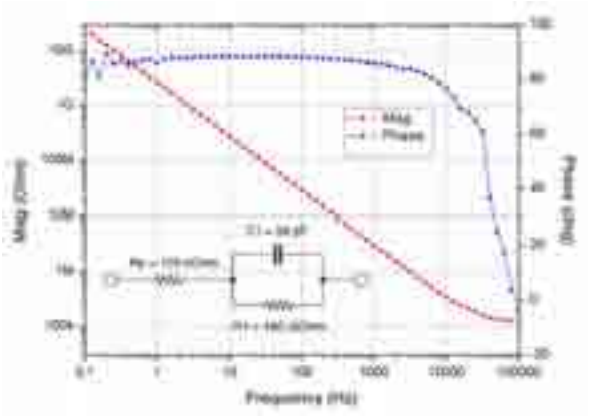

Fig. 2. Impedance spectroscopy of one electrode in the MEA16 device. The inset shows the fitted equivalent circuit. The moderate resistance and the dominant capacitive behaviour, together with a tailored electronic front-end, allow detecting potentiometric signals with a good sensitivity.

Acknowledgement

Work supported by BW-Stiftung, Regione Piemonte and Compagnia di S.Paolo grants.

References

[1] Stett A. et al., (2003). Biological application of microelectrode arrays in drug discovery and basic research. *Analytical and Bioanalytical Chemistry*, 377, 486-495.

[2] Johnstone A.F.M. et al., (2010). Microelectrode arrays: A physiologically based neurotoxicity testing platform for the 21st century. NeuroToxicology 31(4), 331-350.

[3] Eckhorn R. et al. (2006). Visual resolution with retinal implants estimated from recordings in cat visual cortex. Vision Research 46(17), 2675-2690.

[4] Show Y. et al., (2003). Characterization and Electrochemical Responsiveness of Boron-Doped Nanocrystalline Diamond Thin-Film Electrodes. Chem. Mater. 15(4), 879-888.

[5] Kraft A. (2007). Doped Diamond: A Compact Review on a New, Versatile Electrode Material. Int. J. Electrochem. Sci. 2, 355 - 385.

[6] Pasquarelli A. et al., (2011). Diamond microelectrodes arrays for the detection of secretory cell activity. International Journal of Environmental Analytical Chemistry 91: 150-160.

[7] Gao Z. et al., (2010). Transparent diamond microelectrodes for biochemical application. Diamond and Related Materials 19, 1021-1026.

[8] Denisenko A. et al., (2001). pH sensing by surface-doped diamond and effect of the diamond surface termination. Diamond and Related Materials 10(3-7), 667-672.

[9] Carabelli V. et al., (2010). Nanocrystalline diamond microelectrode arrays fabricated on sapphire technology for high-time resolution of quantal catecholamine secretion from chromaffin cells. Biosensors and Bioelectronics 26(1), 92-98.

[10] Gosso S. et al., (2012). Multi-purpose use of nanocrystalline boron-doped diamond MEAs for amperometric, potentiometric and pH recordings. This conference proceedings Book.

Multi-neural chip reader system for parallel neural activity monitoring of cultured neuronal networks

Myoung Joon Oh[1], Yoonkey Nam[1*]

1 Department of Bio and Brain Engineering, KAIST, Daejeon, Republic of Korea
* Corresponding author. E-mail address: ynam@kaist.ac.kr

1 Introduction

Planar-type microelectrode arrays (MEAs) have been proposed as a cell-based biosensor platform that can sense electrical activities from in vitro neural tissues such as brain slices or dissociated neurons. In order to utilize this system in high-throughput drug screening, massive parallel sensing platform is required. Here we designed a multi-neural chip recording system that is composed of glass chip, PCB chip adapter, SD memory card socket, and low-noise OP-AMP ICs.

2 Methods

MEAs were laid out on a 4 inch glass wafer and fabricated by photolithography, metal deposition, dry etching and plasma-enhanced chemical vapor deposition. Microelectrodes and insulators were made of gold (200 nm) and silicon nitride (500 nm), respectively. Neural amplifiers were designed with low-noise OP-AMP and amplified signals were digitized by USB6211 (National Instruments). Spike detection and analysis program was implemented using LabView. E-18 rat hippocampal neurons were cultured on poly-D-lysine treated MEAs for three weeks and neural recordings were performed.

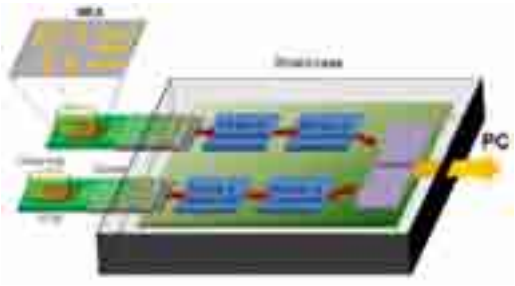

Fig. 1. Multi-MEA reader system using SD memory card socket.

3 Results

MEAs had 8 recording sensors (diameter: 50, 80 or 100 um) and 1 ground electrode (area: 25 mm2). The electrode impedance was 1.4MΩ, 700kΩ, and 400kΩ for 50, 80, 100 μm electrodes, respectively. The size of MEA chip was 1.5 cm x 2.0 cm and it was packaged with PCB adapter by gold-wire bonding and epoxy molding. Glass ring was installed to make a culture chamber on the MEA. The packaged MEA was connected with the amplifier unit through 9-pin SD memory card connector, which formed a simple and secure electrical interface between the MEA and amplifier unit. After 12 ~ 14 DIV, neural recordings were possible from multiple electrodes. From 100 um MEAs, background noise level was 1.87 μV(rms) and average spike amplitude was 30 ~ 100 μV. Despite the large size of the electrode, it was readily possible to obtain high SNR recordings above 10 dB (ratio > 3). Well-isolated single units and multi-units were recorded and spontaneously network bursting activity was recorded. In contrast to conventional MEA designs, it was not necessary to modify the electrode surface using platinum black, titanium nitride, or iridium oxide. Large electrodes provided low impedance values and noise level without compromising the capability of spike detection.

Fig. 2. Multi-MEA reader system using SD memory card socket. (Top) a packaged 8 ch MEA chip, (bottom) 2-chip system.

Fig. 3. Single-unit recording from flat gold electrodes (a) 100 μm, (b) 80 μm, (c) 50 μm in diameter.

Fig. 4. 2-Chip spike detection and processing system by LabView.

4 Conclusions

A compact multi-MEA system design was reported. Glass MEAs were packaged with PCB chips through wire-bonding and one-touch type electrical socket was employed for reliable electrical connections between the chip and amplifier unit. Low-noise amplifier units made it possible to obtain high quality neural recordings from two MEAs simultaneously.

Acknowledgement

This work was supported by System IC 2010 program funded by Ministry of Knowledge Economy, the National Research Foundation of Korea(NRF) grant (No. 2012007327) funded by the Korea government(MEST).

Design and fabrication of all-polymer transducers with different functional features for basic neuroscience and neuroprosthetics

Asiyeh Golabchi*, Rouhollah Habibey, Diego Scheggia, Francesco Difato, Francesco Papaleo, Axel Blau

Dept. of Neuroscience and Brain Technologies (NBT), Fondazione Istituto Italiano di Tecnologia (IIT), Via Morego 30, 16163, Genoa, Italy. *Corresponding author's email address: asiyeh.golabchi@iit.it

Abstract

Neural prostheses aim at recording or altering nervous system activity to partly restore motor, sensory or cognitive modalities that have been lost because of disease or trauma. Where appropriate, microelectrode arrays (MEAs) facilitate high-density recordings and local stimulation of neural activity in the brain. Their body integration, functionality and long-term stability may be improved by resorting to new, more tissue-like materials and conductors with low interface impedance and large charge transfer capacity. Recently, we presented an *in vitro* prototype of a highly flexible polymeric MEA made of a polydimethylsiloxane (PDMS) scaffold with microchannel tracks and electrodes which were coated with films of organic conductors or filled with a graphite-PDMS composite paste [1]. Here, we present an exemplary design concept for *in vivo* probes with carbon-PDMS conductors based on the same replica-molding technology. They were fabricated from laser-printed templates and feature a particular squeeze-clamping interconnection scheme based on rubber-like contact pads. This "soft contact" strategy alleviates stress-related twist and break found in classically bonded pads in ribbon cable-type wiring to external electronics.

1 Introduction

Microelectrode arrays (MEAs) are among the most commonly used neural interfacing technologies for the recording and stimulation of neural activity. They help in clinical therapy and basic neuroscience research [2]. Traditionally, MEAs are made of materials like glass, metals, or silicon [3]. However, the mechanical mismatch between these rigid substances and the brain tissue is disadvantageous, particularly in scenarios where devices may get displaced as a result of body movement [4]. PDMS is a commonly used flexible carrier that can alleviate this issue to some extent [5]. Despite major advances in neuroprosthetic device technology in recent years, in most cases, material-related failure limits the functional lifetime of an implant. In this study, we designed, fabricated and characterized a tough PDMS-based MEA prototype made from a simple laser-printed template. Its geometry is suited for the recording from within the medial longitudinal fissure in the prefrontal cortex (PFC) of mice.

2 Materials and Methods

2.1 Array design

The MEA µ-channels defining electrodes, tracks and contact pads were sketched with a MEMs CAD design software (Expert, Silvaco) and printed inversely on a laser transparency. They were then molded as 100 µm high µ-topographies using UV-curable nail polish, which was squeezed between a stack made of microscopy slides, the feature- and a black counter transparency and a 100 µm spacer transparency in between. The sandwich was exposed 2 min to UVA and developed for 5-30 min in 3-methylbutanol after removal of both the back-microscopy slide and counter transparency. The resulting µ-topography was used as a molding master for MEA production (*Fig. 1a*). An array consisted of 12 circular recording sites each with a radius of 80 µm and 310 µm vertical pitch. They were distributed over two square areas. Device dimensions are given in *Table 1*.

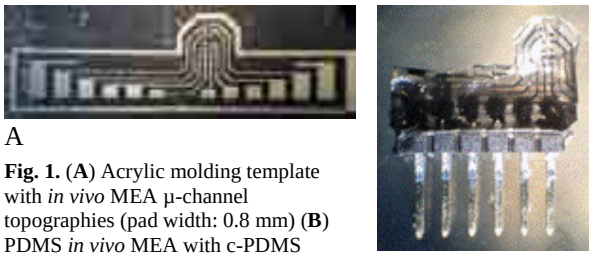

A B

Fig. 1. (**A**) Acrylic molding template with *in vivo* MEA µ-channel topographies (pad width: 0.8 mm) (**B**) PDMS *in vivo* MEA with c-PDMS conductor squeeze-clamped between standard 1.27 mm pitch double-row pin connector and sealed with PDMS.

2.2 Material selection and probe assembly

PDMS was chosen as the µ-channel insulator scaffold substrate because of its flexibility, good dielectric characteristics and low tissue response [5]. Carbon-filled PDMS (c-PDMS) was used as a flexible, readily available and easily processable electrical conductor to fill all scaffold voids. The c-PDMS composite was made by adding carbon powder to non-cured PDMS until the DC resistance dropped below 10 kΩ over the distance of about 1 cm. After

spreading c-PDMS into the voids, curing and selectively insulating wires with a thin PDMS backside coat, probes were folded along the shaft edge to slip their pads between standard double row connector pins. Pins had been dipped into c-PDMS to increase and stabilize pad-pin contact. Pad-pins were insulated by an additional coat of PDMS. To increase mechanical brain-insertion stiffness, probe shafts were coated with a thin gelatin film, which was solid at room temperature and slowly dissolved when in contact with water. Once the probe is inserted into the brain, the gelatin coat is expected to dissolve within minutes to hours and may furthermore act as a cell adhesion mediator.

Table 1 *Geometries of an in vivo MEA probe*

Parameter	Value
Total number of recording sites	12
Number of connected recording sites	8
Electrode diameter (µm)	160
Electrode pitch (vertical, horizontal) (µm)	310, 360
Shaft length (mm)	1.97
Maximum shaft width (mm)	2.95
Shaft thickness (µm)	< 130
Wire width (µm)	100

2.3 Probe characterization

A perfect recording electrode would feature maximum selectivity and low impedance. The electrical performance of probe electrodes was evaluated and compared by impedance spectroscopy between 1 Hz and 100 kHz in saturated KCl (Perstat 2273 potentiostat, Princeton Applied Research, USA). To ensure that the carbon-filled PDMS was non-toxic to neurons, its biocompatibility was assessed by comparing the health of rat cortex neurons cultured on autoclaved and poly-D-lysine/laminin-coated c-PDMS control MEAs with that of neurons on equally treated glass substrates following standard cell culture protocols.

3 Results

Absence of cytotoxicity was confirmed with cortex networks up to 14 days *in vitro* (DIV). In addition, neurons distributed homogeneously on flexible control MEAs without aggregation. Furthermore, cultures survived as long as control cultures on commercial MEAs. As the quality of neural signal recordings is affected by electrode impedance, impedance magnitude and phase were measured. All 8 microelectrodes of one out of three similar prototype probes were functional as exemplarily illustrated in *Fig. 2 & 3*.

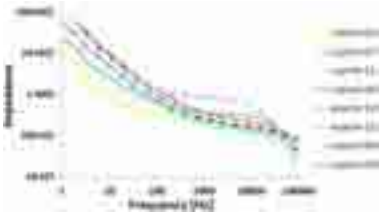

Fig. 2 *Impedances of non-coated MEA electrodes.*

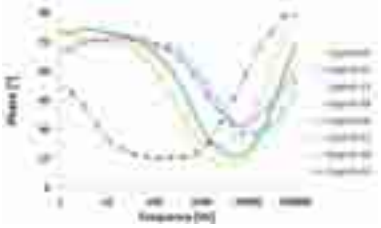

Fig. 3 *Phase characteristics of non-coated MEA electrodes.*

4 Conclusions

By using replica-molding microfabrication techniques, we designed and developed a prototype of a very flexible microelectrode array with 8 recording sites that can be implanted into the brain. We successfully tested a particular squeeze-connection strategy for establishing solderless pad-pin contact between the probe and a standard cable connector. To prevent buckling upon probe insertion into the brain, the flexible recording shaft was coated with gelatin to provide temporary insertion rigidity without need for any other delivery vehicle [6]. Impedance spectra indicate that the *in vivo* probe has a sufficiently low impedance of less than 1 MΩ at 1 kHz and mixed resistive and capacitive properties to allow for recording and electrical stimulation. The electrode arrays will be tested *in vivo* for their performance in chronic recording studies.

Acknowledgement

IIT intramural funding of this research line is greatly appreciated.

References

[1] A. Blau, A. Murr, S. Wolff, E. Sernagor, P. Medini, G. Iurilli, C. Ziegler, F. Benfenati (2011) Flexible, all-polymer microelectrode arrays for the capture of cardiac and neuronal signals, *Biomaterials*, 32, 1778-1786.

[2] B. A. Wester, R. H. Lee, M. C. LaPlaca (2009) Development and characterization of in vivo flexible electrodes compatible with large tissue displacements, *J Neural Eng*, 6, 024002.

[3] C. Hassler, T. Boretius, T. Stieglitz (2011) Polymers for neural implants, *Journal of Polymer Science Part B: Polymer Physics*, 49, 18-33.

[4] S. Lacour, S. Benmerah, E. Tarte, J. FitzGerald, J. Serra, S. McMahon, J. Fawcett, O. Graudejus, Z. Yu, B. Morrison (2010) Flexible and stretchable micro-electrodes for in vitro and in vivo neural interfaces, *Medical and Biological Engineering and Computing*, 48, 945-954.

[5] J. Subbaroyan, D. C. Martin, D. R. Kipke (2005) A finite-element model of the mechanical effects of implantable microelectrodes in the cerebral cortex, *J Neural Eng*, 2, 103-113.

[6] D. P. O'Brien, T. R. Nichols, M. G. Allen (2001) Flexible microelectrode arrays with integrated insertion devices, *Micro Electro Mechanical Systems, 2001. MEMS 2001. The 14th IEEE International Conference on*, 216-219.

Multi-purpose nanocrystalline boron-doped diamond MEAs for amperometric, potentiometric and pH recordings from excitable cells

S. Gosso[1], A. Marcantoni[1], D. Vandael[1], M. Turturici[1], S. Alsawafi[2], I. Izadi[2], E. Colombo[1,2], A. Pasquarelli[2], E. Carbone[1], V. Carabelli[1]

1 Department of Neuroscience, NIS Centre, University of Torino, 10125 Torino, Italy
2 Inst. of Electron Devices and Circuit, Ulm University, 89069 Ulm, Germany

Abstract
Here we show different biological applications of boron-doped nanocrystalline diamond microelectrode arrays (NCD-MEAs), fabricated according to previously described methods [1,3]. We constructed two prototypes with markedly different geometries: 9-channels NCD-MEA, with nine detecting microelectrodes arranged into a circular hole of 22 μm diameter for localizing secretory sites with high-spatial resolution within a single cell and a 16-channels NCD-MEA covering an area of 0.5x0.5 mm^2, ideal for measuring action potentials from networks of excitable cells and for detecting pH variations.

1 Materials and methods

1.1 NCD-MEAs realization

Starting from a single crystal double-polished 330 μm thick sapphire wafer, a Si-based nucleation layer was deposited by PECVD (Plasma Enhanced Chemical Vapor Deposition). The formation of nanodiamond nuclei was obtained by means of Bias Enhanced Nucleation (BEN) in a HFCVD (Hot Filament CVD) system and onto this substrate a 200 nm layer of intrinsic NCD was grown. Then we grew a quasi-metallic boron doped top layer (350 nm thickness) under the same parameters used for intrinsic growth. Finally, by means of photolithographic techniques and a Si_3N_4 passivation layer, we designed the active areas. The details of these processes are extensively described in [1-3].

1.2 Amperometric and potentiometric recordings

The 9-channels NCD-MEA has nine detecting microelectrodes patterned within a circular hole (22 μm diameter, Fig 1A), with the aim of increasing the spatial resolution of the recorded amperometric signals associated with the release of catecholamines from the secretory granules of adrenal chromaffin cells. In this way, we could resolve exocytotic signals within subareas of 16-32 μm2 of the total cell membrane surface (380 μm2). A single mouse (or bovine) chromaffin cell was placed onto the planar central hole by means of a patch-clamp micromanipulator. Exocytosis was triggered by perfusing the cell with an external depolarizing solution containing 30 mM KCl, or by applying short depolarizing pulses (2 V for 50 ms every 60 s) through the stimulating electrode. In this amperometric configuration, the NCD-MEAs were polarized to +800 mV to oxidize the released catecholamines.

The 16-channels NCD-MEA consists of sixteen round electrodes (20 μm diameter), separated by 200 μm pitch (Fig 2A). This geometry was addressed to detect synchronized action potentials (APs) from intact mouse sinoatrial node (potentiometric configuration), properly placed in contact with all 16 microelectrodes.

1.3 Cell preparation

Isolated chromaffin cells were obtained from adrenal glands of (1–3 months) old C57BL/6J male mice [4] or from adrenal glands of 6 months old cows [5]. Sino atrial node (SAN) was obtained from C57BL/6N adult (1-4 months old) mice [6].

2 Results

2.1 Quantal exocytic events detected using the 9-channels NCD-MEA (amperometric configuration)

Here, for the first time, we used the 9-channels NCD-MEAs for detecting quantal catecholamine release from chromaffin cells. Taking advantage of the high-density patterning of the array, amperometric signals could be independently detected from 9 different subareas of the same cell (Fig. 1). The recorded amperometric spikes had ms temporal resolution and pA sensitivity, in good agreement with kinetic parameters and amplitude recorded by carbon fibre electrodes (Fig 1B). The most significant innovation of the planar arrays, respect to classical amperometric approaches, is

that they could be used for spatially mapping the secretory sites by means of a MatLab routine, thus providing experimental evidence about the distribution of chromaffin granules over the cell membrane.

Our data show that, when a chromaffin cell is placed over the 9 electrodes, only some of the channels are preferentially activated during exocytosis (for example channels 2, 3, 6 in Fig. 1), indicating that chromaffin granules are not uniformly distributed within the overall cell membrane surface.

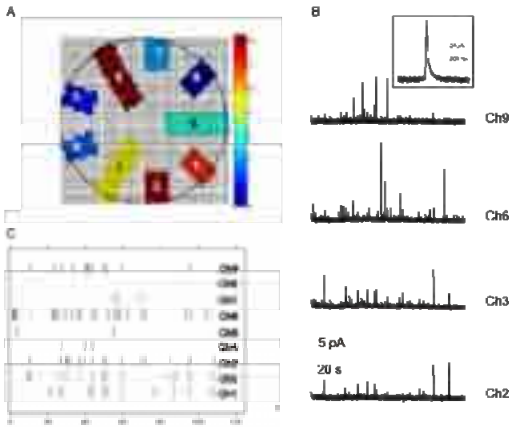

Fig. 1. The 9-channels NCD-MEA detects exocytotic events from different areas of a chromaffin cell. A) The 9 electrodes are patterned within a circular hole of 22 m diameter (comparable to the mean bovine chromaffin cell dimensions). The colorimetric scale to the right indicates the quantity of detected secretory events (blue = no secretion). Number of detected events has been normalized to the electrode dimensions. Threshold for amperometric spike detection was fixed to 8 pA. B) Representative secretory spikes from the indicated electrodes (channels, Ch). Inset: enlargement of an amperometric spike. C) Raster plot of measured spikes over 120 s recordings. Each bar represent an amperometric spike. Notice that no events have been measured by Ch 8.

2.2 Cardiac action potentials recorded using the 16-channels NCD-MEA (potentiometric configuration)

Extracellular APs from mouse sinoatrial node have been recorded by means of the 16-channels NCD-MEA (Fig 2). Oscillatory signals of 3 Hz mean frequency, 400 μV amplitude and ~150 ms duration were simultaneously detected by all the 16 electrodes.

Recordings had low background noise (<20 μV peak-to-peak over a bandwidth of 1 Hz to 1 kHz) and similar shape to those recorded using the classical TiN MEAs.

Finally, preliminary results indicated that 16-channels NCD-MEA can also detect localized changes of pH because of the high H+ sensitivity of oxygen-terminated diamond: during exocytotic events chromaffin cells release the acidic content of their granules (pH=5.5).

3 Conclusions

Our data demonstrate that: *i)* the two novel NCD-MEA prototypes are suitable for amperometric detection of quantal secretory events from excitable cells, with higher spatial resolution than classical carbon fibre electrodes. They allow the spatial mapping of secretory sites; *ii)* in the potentiometric mode, the NCD-MEAs can monitor the extracellular electrical activity of networks of excitable cells, and *iii)* in the potentiometric mode, NCD-MEAs detect changes of chemical potential associated to the extracellular pH variations during exocytic events.

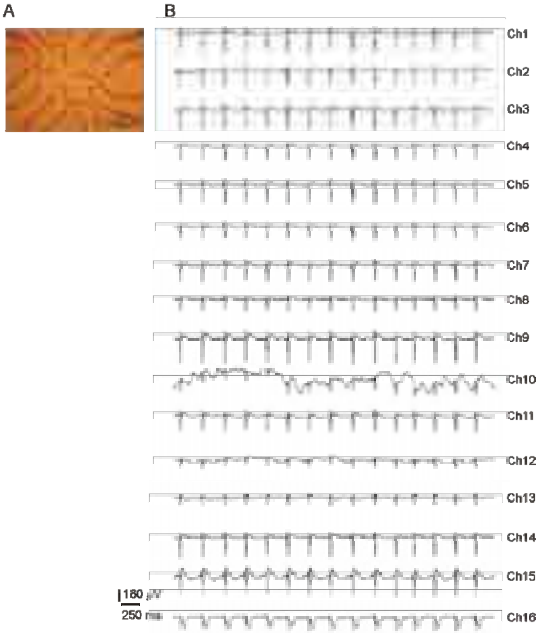

Fig. 2. The 16-channels NCD-MEA measures extracellular action potentials from a sino-atrial node tissue. A) Geometric arrangement of the 16-channels NCD-MEA. Detecting areas are indicated by black circles. B) Synchronized firing activity of sino-atrial node detected by the 16 microelectrodes. One trace was discarded from the analysis (10^{th} trace) due to its baseline noise.

References:

[1] Colombo E. et al, (2011). Fabrication of a NCD microelectrode array for amperometric detection with micrometer spatial resolution. *Diam Relat Mater.* 20:793-97.

[2] Alsawafi S. et al. 16. Channel NCD Microelectrodes Array to detect secretory activity of neuroendocrine cell populations. Diamond and Related Materials, under review.

[3] A. Pasquarelli et al. This conference proceedings Book.

[4] A. Marcantoni, V. Carabelli, D.H. Vandael, V. Comunanza, E. Carbone, (2009). PDE type-4 inhibition increases L-type Ca^{2+} currents, action potential firing, and quantal size of exocytosis in mouse chromaffin cells. *Pflugers Arch-Eur J Physiol.* 457:1093-110.

[5] Carabelli V., et al., (2001). Direct autocrine inhibition and cAMP-dependent potentiation of single L-type Ca^{2+} channels in bovine chromaffin cells. *J Physiol.* 532.1:73-90.

[6] Mangoni M. E., J. Nargeot, (2008) Genesis and regulation of the heart automaticity. *Physiol Rev.* 88(3):919-82.

Active multi-electrode arrays based on zinc oxide

Fabian J. Klüpfel[1*], B. U. Sebastian Schmidt[2], Alexander Lajn[1], Holger von Wenckstern[1], Josef A. Käs[2], Marius Grundmann[1]

1 Semiconductor Physics Group, University of Leipzig, Germany
2 Soft Matter Physics Group, University of Leipzig, Germany
* Corresponding author. E-mail address: fabian.kluepfel@uni-leipzig.de

Abstract
We present active multi-electrode arrays (MEAs) based on the optically transparent semiconductor ZnO. We characterize the stability of the devices and the sensitivity to electric signals in an electrolytic medium. This proof-of-principle study demonstrates the feasibility of transparent and active MEAs based on oxide electronics, allowing the simultaneous investigation of electrical and topological properties of cellular networks. This opens the research on active MEAs to the wide variety of materials and device types in the field of oxide semiconductors.

1 Introduction

Multi-electrode arrays (MEAs) are a valuable tool for monitoring the communication of neuron networks. Active arrays can reach a higher number of measurement electrodes and a higher spatial resolution than passive arrays due to on-chip multiplexing. Silicon-based devices are opaque and thus prohibit optical microscopy methods based on transmission. Moreover, the signal-to-noise ratio of silicon-based MEAs is so far much lower than that of passive arrays (e.g. [1]).

Electronic devices based on oxide semiconductors as ZnO-related compounds were undergoing rapid progress during the last years, partly driven by the needs of the display industry. Besides the optical transparency, properties like high mobility, low material costs and the possibility to fabricate electronic devices on glass or flexible polymer substrates add to the attractiveness of these materials.

Among the already demonstrated devices with ZnO-related materials are metal-oxide-semiconductor field-effect transistors [2,3], metal-semiconductor field-effect transistors (MESFETs) [4] and junction field-effect transistors [5]. We chose ZnO-based MESFETs as a starting point to evaluate the usability of oxide semiconductors for active MEAs, as MESFETs are generally considered to have lower noise than MOSFETs.

2 Experimental

The transistors consist of Mg doped ZnO channels with reactively sputtered Pt gate contacts on a sapphire substrate, as documented more detailed in [4]. We fabricated test chips with an extended gate design, where the electrode sites are located next to the transistors. The chips were covered with the epoxy-based photo resist SU-8, leaving holes with a diameter of 10 µm at the electrodes. The central part of the chip with several electrode/transistor pairs is shown in fig. 1.

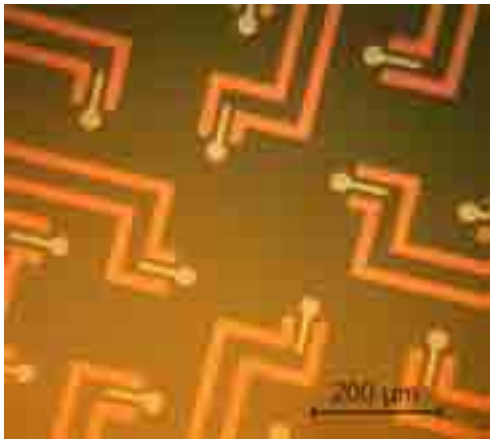

Fig. 1. Electrode area of the test chips. The circular electrodes are directly connected to the transistor gates. The ZnO channels are optically transparent.

Electric measurements have been performed using an Agilent semiconductor parameter analyzer 4155C and an Ag/AgCl electrode in 150 mM NaCl solution or Leibovitz L-15 medium on the chip.

The chip stability in contact with an electrolytic liquid has been studied by repeated capacitance and current measurements. After one week, no degradation of the electrical properties occurred. Studying the influence of the SU-8 layer on the transistor performance revealed an improvement of the transistor on-off-ratio, probably due to surface passivation.

By applying voltage pulses to the Ag/AgCl-electrode, it could be shown that the source-drain-current of the transistors is indeed very sensitive to voltage changes in the electrolyte (fig. 2). The noise level seems quite high so far. However, the setup has

not been optimized for noise measurements yet, so the contribution of the chip is up to now not clear.

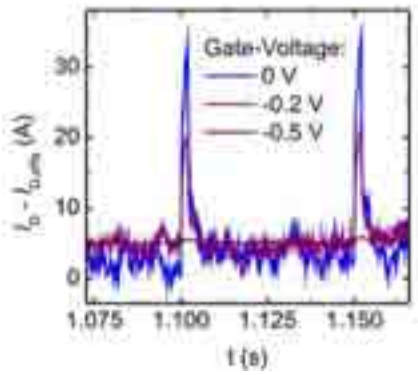

Fig. 2. Drain current response to square voltage pulses of 8 mV magnitude and 2 ms duration at the Ag/AgCl electrode.

Biocompatibility of the chips surface could be demonstrated by the growth of primary mouse neurons from cerebellum.

3 Conclusion

We fabricated multi-electrode arrays with MESFETs based on ZnO. We could show sufficient stability in electrolytic environment and that the modulation of the source-drain-current is possible by voltage changes in the medium. Next steps should be detailed signal-to-noise studies and test measurements with HL-1 cells or primary neurons to characterize the signal quality. Then optimization of the device layout and materials could take place.

Acknowledgement

We thank Monika Hahn and Holger Hochmuth for sample preparation, Thomas Claudepierre for providing the primary cells, and the Leipzig School of Natural Sciences – BuildMoNa (GS 185) for funding.

References

[1] Lambacher A., Jenkner M., Merz M., Eversmann B., Kaul R.A., Hofmann F., Thewes R., Fromherz P. (2004): Electrical imaging of neuronal activity by multi-transistor-array (MTA) recording at 7.8 µm resolution. *Applied Physics A*, 79, 1607-1611

[2] Nomura K., Ohta H., Ueda K., Kamiya T., Hirano M. Hosono H. (2003): Thin-Film Transistor Fabricated in Single-Crystalline Transparent Oxide Semiconductor. *Science*, 300, 1269-1272

[3] Fortunato E., Barquinha P., Gonçalves G., Pereira L., Martins R. (2008): High mobility and low threshold voltage transparent thin film transistors based on amorphous indium zinc oxide semiconductors. *Solid-State Electronics*, 52, 443 – 448

[4] Frenzel H., Lajn A., von Wenckstern H., Biehne G., Hochmuth H., Grundmann M. (2009): ZnO-based metal-semiconductor field-effect transistors with Ag-, Pt-, Pd-, and Au-Schottky gates. *Thin Solid Films*, 518, 1119-1123

[5] Schein F.L., von Wenckstern H., Frenzel H., Grundmann M. (2012): ZnO-Based n-Channel Junction Field-Effect Transistor With Room-Temperature-Fabricated Amorphous p-Type $ZnCo_2O_4$ Gate. *IEEE Electron Device Letters*, 33, 676-678

Towards real world applications: reproducible and stable PEDOT-CNT microelectrodes

Ramona Gerwig[1*], Kai Fuchsberger[1], Birgit Schroeppel[1], Gerhard Heusel[1], Alfred Stett[1] and Martin Stelzle[1]

1 Natural and Medical Sciences Institute at the University of Tuebingen, Markwiesenstrasse 55, 72770 Reutlingen
* Corresponding author. E-mail address: ramona.gerwig@nmi.de

Abstract
PEDOT-CNT microelectrodes can be fabricated in a reproducible and stable way. The material shows a porous morphology and exhibits extraordinary low impedances below 20 kΩ at 1 kHz (Ø = 30 µm) and exceptional high charge storage capacitances between 4 and 10 mF/cm^2. The low impedance and the superior charge transfer capacitance make them excellent candidates for recording and stimulation of excitable tissue.

1 Background and aims

For disorders of the central nervous system like epilepsy or Parkinson's disease, electrical signals from neurons as well as changes of the neurotransmitter concentration play an important role. To examine the cellular causes *in vitro* and *in vivo* with high spatial resolution, micro electrode arrays (MEA) are used [1-4]. Signal to noise ratio, stimulation and sensing properties as well as cell viability of the typically metal based electrodes [3, 5] are still to be improved. To this end, efforts have been made in the modification of the electrode surface using conducting polymers like poly(3,4-ethylene-dioxythiophene) (PEDOT) and carbon nanotubes (CNTs). Not only are CNTs biocompatible and biostable, but layers of CNTs exhibit large effective porosity and surface area resulting in very favorable charge transfer capabilities [6]. Exceptional viability of cells and their efficient integration with layers composed of CNTs has been observed [6-8]. On the other hand, PEDOT has shown to be one of the most stable conducting polymers. It has been reported in previous work that PEDOT is a suitable material for micro-neural interfaces [9]. Moreover, CNTs modified electrodes provide for enhanced sensing properties towards neurotransmitters such as dopamine [10]. Analyzing the "brain chemistry" could improve diagnosis of neuronal diseases ultimately leading to new and advanced therapeutic approaches. PEDOT-CNT composite materials are therefore considered as attractive candidates for the fabrication of electrodes in neuroprostheses as well as for *in vitro* diagnostics.

However, in order to address real world applications it is essential to establish robust technologies to fabricate mechanically stable PEDOT-CNT electrodes and to integrate them into neuroprostheses and biosensors. This is the main focus of this study.

2 Materials and Methods

To generate the PEDOT-CNT composite material electropolymerization was carried out using suspensions of ethylenediethoxythiophene (EDOT, 0.02 M), poly(sodium-p-styrenesulfonate) (PSS, $M_w \approx 70{,}000$ g/mol; 1 %) and carbon nanotubes (0.03 %). Pure PEDOT coatings were electropolymerized with the same concentrations in the absence of CNTs. PSS fulfills 3 different functions: it serves (i) as a conducting salt during electrodeposition, (ii) as dispersant for CNTs by polymer wrapping [11] and (iii) as a counterion for the positively charged PEDOT chains. The electrochemical deposition on 30 µm gold electrodes of a MEA (NMI-TT GmbH) was performed under ambient conditions in a three electrode system with galvanodynamic control applying a final current density of 2 mA/cm^2 and potentials of ca. 0.7 V vs. Ag/AgCl (chlorinated silver wire). Charge densities of 30-110 mC/cm^2 were passed during deposition in order to control the amount of deposited material on the electrodes. Employing an 8-channel potentiostat/galvanostat it is also possible to coat all 59 electrodes of the MEA in a fast and reproducible way. This method is highly promising allowing integration into commercial production processes.

Coatings were analyzed with scanning electron microscopy for surface analysis and imaging of the cross sections prepared by focused ion beam. Adhesion of the coatings was tested by the tape adhesion test (Cross-cut test ISO 2409:2007(E)) and optical as well as electrochemical characterization before and afterwards. Electrochemical characteristics were determined by impedance spectroscopy, cyclic voltammetry and voltage pulsing.

3 Results and Discussion

PEDOT and PEDOT-CNT electrodes show a homogeneous morphology with PEDOT-CNT showing higher porosity than PEDOT (Figure 1). As far as ad-

hesion is concerned, PEDOT and PEDOT-CNT electrodes withstand rinsing with solvents, autoclaving and plasma cleaning and can be used repeatedly in cell culture experiments.

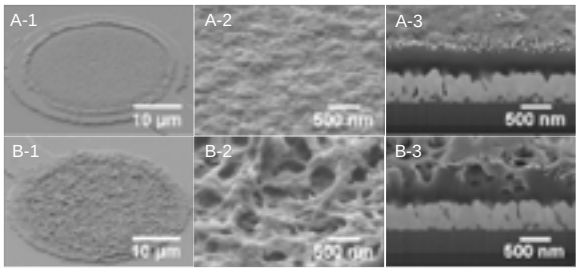

Fig. 1. SEM micrographs of (A) PEDOT and (B) PEDOT-CNT microelectrodes. (1,2) show top views and (3) cross sections prepared by FIB.

Electrochemical characterization reveals extraordinary low impedances below 20 kΩ at 1 kHz (Ø = 30 µm) and exceptional high charge storage capacitances between 4 and 10 mF/cm^2 depending on the film thickness. Figure 2 shows representative impedance spectra of different electrode materials (insert: corresponding phase angle).

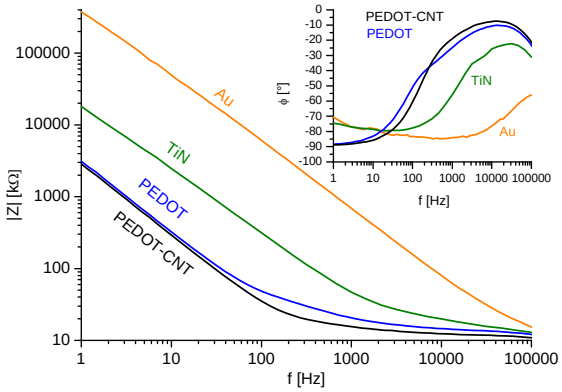

Fig. 2. Representative impedance spectra of different electrode materials (Ø = 30 µm). The insert shows the corresponding spectra of phase angle.

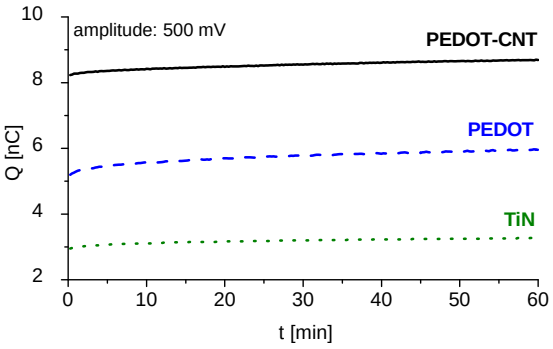

Fig. 3. Charge per pulse (anodic part) transferred over one hour of constant pulsing with biphasic, anodic first voltage pulses of 500 mV amplitude.

In Figure 3 the charge transferred with biphasic, anodic first voltage pulses (amplitude 500 mV, f = 1 kHz) over one hour is depicted. The charge transfer capacitance increases in the order of TiN, PEDOT, PEDOT-CNT. Electrodes are stable over one hour and 3,600,000 pulses. Impedance is not impaired by long term pulsing.

These highly reproducible electrical and unprecedented adhesion properties of PEDOT-CNT electrodes make them excellent candidates for neuronal recording and stimulation. Cardiac and neuronal recordings demonstrate the superior properties of PEDOT and PEDOT-CNT electrodes over TiN and Au.

PEDOT and CNT are known to be suitable for neuronal electrode material. It is now possible to produce microelectrode arrays from PEDOT-CNT electrodes in a stable and reproducible way so that they can be used in real world applications. Electrochemical measurements as well as *in vitro* experiments approve the superior properties over state of the art materials [12]. Further research will examine the integration into production processes as well as identify more applications for this material (See also the short paper and talk: Gerwig et al. “Advanced Cardiac and Neuronal Recording using PEDOT-CNT MEA”).

Acknowledgement

The support of Gordon Steve Link and NMI-TT GmbH is kindly acknowledged. Funding: BMBF Grant no. 01GQ0834 and Multi Channel Systems GmbH.

References

[1] A. Stett, U. Egert, E. Guenther, F. Hofmann, T. Meyer, W. Nisch, H. Haemmerle, *Analytical and Bioanalytical Chemistry* **2003**, *377*, 486-495.
[2] M. D. Johnson, R. K. Franklin, M. D. Gibson, R. B. Brown, D. R. Kipke, *Journal of Neuroscience Methods* **2008**, *174*, 62-70.
[3] D. R. Kipke, W. Shain, G. Buzsaki, E. Fetz, J. M. Henderson, J. F. Hetke, G. Schalk, *Journal of Neuroscience* **2008**, *28*, 11830.
[4] S. F. Cogan, *Biomedical engineering* **2008**, *10*, 275.
[5] K. D. Wise, D. J. Anderson, J. F. Hetke, D. R. Kipke, K. Najafi, *Proceedings of the IEEE* **2004**, *92*, 76-97.
[6] E. W. Keefer, B. R. Botterman, M. I. Romero, A. F. Rossi, G. W. Gross, *Nature Nanotechnology* **2008**, *3*, 434-439.
[7] V. Lovat, D. Pantarotto, L. Lagostena, B. Cacciari, M. Grandolfo, M. Righi, G. Spalluto, M. Prato, L. Ballerini, *Nano Letters* **2005**, *5*, 1107-1110.
[8] A. Mazzatenta, M. Giugliano, S. Campidelli, L. Gambazzi, L. Businaro, H. Markram, M. Prato, L. Ballerini, *Journal of Neuroscience* **2007**, *27*, 6931-6936.
[9] S. J. Wilks, S. M. Richardson-Burns, J. L. Hendricks, D. C. Martin, K. J. Otto, *Frontiers in Neuroengineering* **2009**, *2*.
[10] P.-Y. Chen, R. Vittal, P.-C. Nien, K.-C. Ho, *Biosens. Bioelectron.* **2009**, *24*, 3504-3509.
[11] M. J. O'Connell, P. Boul, L. M. Ericson, C. Huffman, Y. Wang, E. Haroz, C. Kuper, J. Tour, K. D. Ausman, R. E. Smalley, *Chemical Physics Letters* **2001**, *342*, 265-271.
[12] R. Gerwig, K. Fuchsberger, B. Schroeppel, G. S. Link, G. Heusel, U. Kraushaar, W. Schuhmann, A. Stett, M. Stelzle, *Frontiers in Neuroengineering* **2012**, *5*, 1-11.

Fabrication of microelectrode arrays with needle-type electrodes

Sebastian Roehler[1*], Jochen Held[1], Wolfgang Barth[1], Wilfried Nisch[1], Alfred Stett[1], Claus Burkhardt[1]

1 NMI Natural and Medical Sciences Institute at the University of Tuebingen, Reutlingen, Germany
* Corresponding author. E-mail address: sebastian.roehler@nmi.de

Abstract
We present two techniques to create a microelectrode array (MEA) with needle-type electrodes. The first method involves reactive ion etching of a negative tone resist (SU-8) on a glass substrate. For the second method silicon is wet etched to evolve arrays of pyramids which are then reproduced on a substrate by imprinting. Following this, in both cases the substrates are processed with optical lithography and thin film techniques to create electrodes, which can be addressed individually. Depending on the fabrication process the electrodes are shaped like 50 µm tall cones or pyramids.

1 Introduction

MEAs with substrate-integrated planar microelectrodes have been used for 50 years to stimulate and measure the activity of neurons in cell and tissue culture experiments. A lot of effort has been taken to improve these electrodes to yield measurements with high signal-to-noise ratio and stimulation experiments with low threshold and high spatial resolution. But in some cases the planar geometry implies disadvantages for example when recording from an acute tissue slice [1] or when the cells targeted for excitation are located inside a tissue volume [2]. To reduce the distance between the electrically active cells and the electrode for recording or between the stimulating electrode and the cell for stimulation, we developed a MEA with needle-type microelectrodes. These electrodes can be fabricated on different types of substrate which is an advantage to processes proposed by others which are bound to certain substrates like glass [3] or silicon [4-6].

2 Fabrication

We developed two processes to fabricate needle-type electrodes. For the first method (Fig. 1 a1-c1) we coat the substrate with a 50 µm thick layer of SU-8, an epoxy based negative tone resist. The resist is cross-linked and a 400 nm thick Ti-Au layer is sputtered onto it. This layer is patterned and serves as an etch mask for the SU-8. The SU-8 is dry etched using O_2/CF_4 plasma. The etch mask is removed in an ultrasonic bath.

For the second method (Fig. 1 a2-c2) we pattern silicon nitride etch masks on a (100)-oriented silicon wafer. The silicon is wet etched in potassium hydroxide until the pyramids under the nitride reach a height of 50 µm. A polydimethylsiloxane stamp is used to transfer this structure into OrmoComp, a UV-curable polymer.

The following process steps are identical for both methods. The material for the conductor paths is sputtered onto the substrates and patterned with thin film techniques (Fig. 1d).

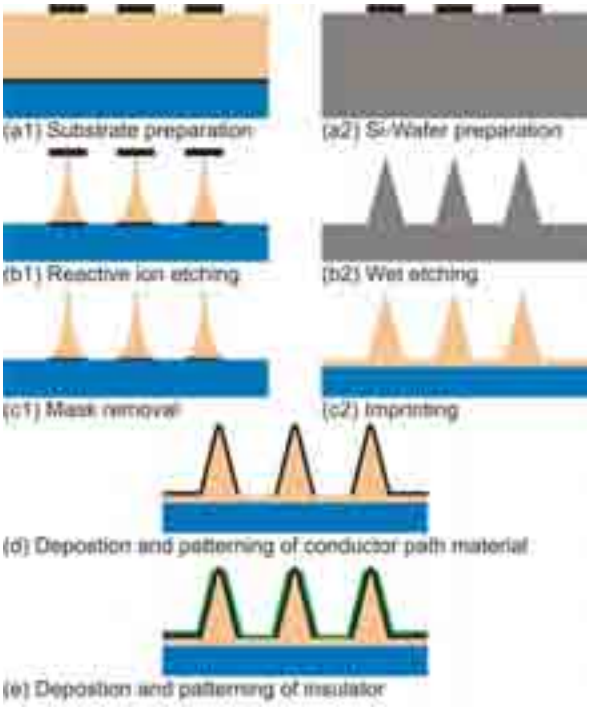

Fig. 1. Schematic overview of the fabrication process.

The insulator is deposited in a plasma enhanced chemical vapour deposition process. A maskless lithography step is used to remove the insulator at the tips of the needles. For this purpose the needles are embedded into a thick positive photoresist. The resist is removed only at the needle tips. To prepare the

deposition of the electrode material at the tip of the needle the insulator is etched in O_2/CF_4 plasma (Fig. 1e).

After opening the needle tips the resist is not removed but it is used for a lift-off process to cover the electrodes with nano-columnar titanium nitride (TiN, 600 nm). This ensures low impedances because of the high electrochemical surface area of TiN. The electrodes are rendered hydrophilic in O_2 plasma.

3 Characterisation

The microneedles were investigated in a focused ion beam (FIB) / scanning electron microscope (SEM). FIB preparation was used to investigate the layer structure at the needle tip and sidewall. This analysis revealed that there is a good electrical contact between the electrode at the tip and the conductor paths on the substrate.

Figure 2 and 3 show SEM images of arrays of 50 µm tall cones and pyramids fabricated by reactive ion etching and imprinting, respectively.

Fig. 2. SEM image of an array of 50 µm tall cones of SU-8 fabricated by reactive ion etching.

Fig. 3. SEM image of an array of 50 µm tall pyramids of Ormo-Comp fabricated by imprinting.

Figure 4 shows overlaid impedance spectra of an array of 59 electrodes fabricated by reactive ion etching. The mean impedance at 1 kHz is 115 kΩ with a standard deviation of 25 kΩ. The active geometric surface area of the electrode was approximately 580 µm^2. This impedance is slightly higher than that of a planar TiN electrode of the same area which exhibits an impedance of 30 to 40 kΩ at a diameter of 30 µm.

Measurements with tissue slices will be implemented soon.

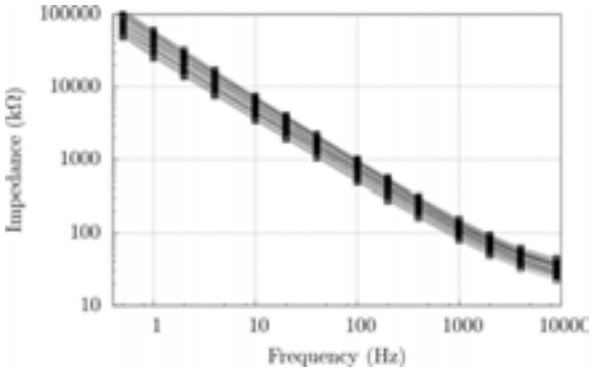

Fig. 4. Overlaid impedance spectra of an array of 59 needle-type microelectrodes.

4 Conclusion

In summary, we developed processes to fabricate arrays with needle-type microelectrodes on different substrates for recording and stimulating nerve cell activity inside of neuronal tissue. The height typically amounts to 50 µm. Typical values for the base diameters are 20 µm and a few microns for the tip radii. The part of the surface of the microneedle used as an electrode is defined by a maskless lithography step. Nano-columnar titanium nitride is used as electrode material.

Acknowledgement

This work was supported by the Federal Ministry of Education and Research (BMBF), grant 0312035A.

References

[1] Heuschkel M.O., Wirth C., Steidl E.-M., Buisson B. (2006). Development of 3-D Multi-Electrode Arrays for Use with Acute Tissue Slices, in *Advances in Network Electrophysiology*, M. Taketani and M. Baudry, Editors. Springer, 69-111.

[2] Djilas M., et al. (2011). Three-dimensional electrode arrays for retinal prostheses: modeling, geometry optimization and experimental validation. *Journal of Neural Engineering*, 8, 046020.

[3] Heuschkel M.O., Fejtl M., Raggenbass M., Bertrand D., Renaud P. (2002). A three-dimensional multi-electrode array for multi-site stimulation and recording in acute brain slices. *Journal of Neuroscience Methods*, 114, 135-148.

[4] Thiébaud P., Beuret C., de Rooij N.F., Koudelka-Hep M. (2000). Microfabrication of Pt-tip microelectrodes. *Sensors and Actuators B: Chemical*, 70, 51-56.

[5] Held J., Gaspar J., Ruther P., Hagner M., Cismak A., Heilmann A., Paul O. (2010). Design of experiment characterization of microneedle fabrication processes based on dry silicon etching. *Journal of Micromechanics and Microengineering*, 20, 025024.

[6] Charvet G., et al. (2010). BioMEA(TM): A versatile high-density 3D microelectrode array system using integrated electronics. *Biosensors and Bioelectronics*, 25, 1889-1896.

All diamond microelectrode array coated with carbon nanotubes

Clément Hébert[1,2*], Michel Mermoux[3], Catherine Villard[1], David Eon[1], Pascal Mailley[2], Franck Omnès[1]

1 Institut Néel, CNRS et Université Joseph Fourier, BP 166, F-38042 Grenoble Cedex 9, France.
2 CEA/INAC/SPrAM/CREAB 17 rue des Martyrs 38054 Grenoble Cedex 9, France.
3 Laboratoire d'Electrochimie et de Physicochimie des Matériaux et des Interfaces (LEPMI), UMR 5279, CNRS - Grenoble INP-Université de Savoie - Université Joseph Fourier BP75. 38402 Saint Martin d'Hères, France
* Corresponding author. E-mail address: clement.hebert@grenoble.cnrs.fr

Abstract
We present the development of diamond MEA coated with partially embedded carbon nanotubes (CNTs). Electrochemical characterizations of coated and non-coated diamond electrodes are reported. The results suggests a higher reactivity of carbon nanotube coated compare to bare diamond electrodes due to the large active surface of the CNTs as well as a lower impedance.

1 Diamond/CNT MEA: motivation and manufacturing

Carbon nanotube are thought to be one of the most promising materials for neural interfacing. However they might be toxic when dispersed into the body. Thus we developed a way to anchor the carbon nanotube to the diamond which is one of the best biocompatible electrode available. The first implementation of the anchoring in a diamond MEA and their performance are presented.

An insulating diamond layer is nucleated and deposited on a silicon substrate in a chemical vapor deposition reactor assisted by microwave plasma. This layer is then covered with a conductive diamond layer (boron doped diamond at $5.10^{21}cm^{-3}$). The conductive diamond is etched by oxygen plasma to pattern the surface with 121 addressable electrodes (60µm of diameter each) connected by diamond wires. The electrodes are separated by a distance of 150 µm. A selective diamond growth is performed to insulate the diamond wires. Finally the electrodes were coated with partially embedded carbon nanotubes grown in a Hot Filament CVD reactor. Scanning electron microscopy and raman were performed on the MEA in order to assesst diamond quality and doping

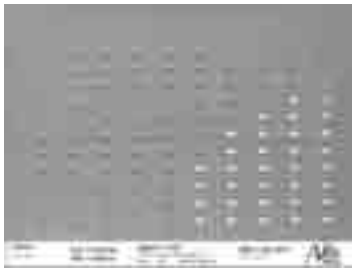

Fig.1 Microelectrode Array (white points : diamond, dark points :CNTs)

2 MEA characterization

Fig.2 Electrochemical impedance spectroscopy (Nyquist diagram) on bare and carbon nanotube coated diamond electrode in Fe^{2+}/Fe^{3+}.

Both carbon nanotube coated diamond electrodes and diamond electrodes were characterized by cylic voltammetry and impedance spectroscopy in Fe^{2+}/Fe^{3+}. The intensities collected with carbon nanotube electrodes were 100 times higher thanks to the large active surface offered by the nanotubes. The impedance was also seen to be reduced.

Neuron culture are currently carried out to assets the performances of such electrodes for neural interfacing.

Cell and Tissue Culture

Formation of one-way-propagated cultured neuronal networks using micro-fabrication and –fluidics techniques

Yuzo Takayama[1, 2*], Naoki Kotake[3], Tatsuya Haga[1], Takafumi Suzuki[4], Kunihiko Mabuchi[1]

1 Graduate School of Information Science and Technology, University of Tokyo, Tokyo, Japan
2 Research Fellow of the Japan Society for the Promotion of Science, Tokyo, Japan
3 Department of Fisheries Distribution and Management, National Fisheries University, Yamaguchi, Japan
4 Center for Information and Neural Networks, National Institute of Information and Communications Technology, Osaka, Japan
* Corresponding author. E-mail address: yuzo_takayama@ipc.i.u-tokyo.ac.jp

Abstract

Random structure of reconstructed cultured neuronal networks disturbs regulated electrical signals in it, and thus is one of the major problems for testing with neuronal network in vitro. To overcome this problem, we previously reported a simple method for regulating neurite direction in cultured neuronal network by combining micro-fabrication and –fluidics techniques (Takayama et al., J. Biosci. Bioeng., in press, 2012). In this paper, we attempt to further analyze the morphologies and functions of the patterned cultured neuronal networks by immunofluorescent study and modeling of fluid dynamics.

1 Introduction

Cultured neuronal network is a promising model system for studying neuronal network dynamics [1, 2]. Randomness in a reconstructed network structure, however, disturbs regulated electrical signal transmissions in it. Therefore, a method for precisely controlling structures and functions of cultured neuronal networks is required. To do this, we previously reported a simple method for regulating neurite direction in cultured neuronal network by combining micro-fabrication and –fluidics techniques [3]. In this study, we attempt to further analyze the morphologies and functions of the patterned cultured neuronal networks by immunofluorescent study and modeling of fluid dynamics.

2 Methods

The microfluidic neuronal culture device was fabricated by attaching the poly(dimethylsiloxane) (PDMS) sheet with a U-shaped cell trapping array onto a glass substrate (Fig. 1a). The master mold for the microfluidic culture device was fabricated by patterning two layers of negative photoresist, SU-8 3005 and 3050, on a silicon wafer. After curing the PDMS, the PDMS sheet was sealed onto a glass substrate which was pre-patterned with 0.1 % polyethyleneimine and 1 % pluronic F-127 solutions for regulation of neurite devleopment. Then, rat cortical neurons were inserted and cultured in the microfluidic culture device under culture medium flow condition with a rate of 0.5 μl/min. The effects of medium flow around the microstructures were simulated using fluid flow computing tool (Gerris for Linux) (Fig. 1b). Immunofluorescent visualization of neurons was also carried out.

3 Results

After one day in vitro (DIV), the effect of medium flow on the direction of neurite elongation was analyzed. We confirmed that neurites significantly extended to the medium flow direction in the samples cultured under a medium flow condition. In contrast, neurites extended to the flow direction and the opposite directions equiprobably in the samples without medium flow. This indicated that the chronic medium flow affected the direction of neurite development. By fluid flow simulation, we thought that this effect was caused by non-uniform distribution of fluid dynamics around cell trapping micro structures (Fig. 1b). We also confirmed that neurites from a microwell reached to the next microwell after 6 DIV and attempted to identify axonal growth and synapse formation by immunofluorescent studies (Fig. 1c).

References

[1] Wagenaar D.A., Pine J., Potter S.M. (2006). An extremely rich repertorie of bursting patterns during the development of cortical cultures. *BMC Neuroscience*, vol. 7, art no. 11.
[2] Takayama Y., Moriguchi H., Kotani K., Jimbo Y. (2009). Spontanesous calcium transients in cultured cortical networks during development. I*EEE Transactions in Biomedical Engineering*, vol. 56, pp. 2949-2956.
[3] Takayama Y., Kotake N., Haga T., Suzuki T., Mabuchi K. (2012). Formation of one-way-structured cultured neuronal networks in microfluidic devices combining with micropatterning tecnniques. *Journal of Bioscience and Bioengineering, in press*.

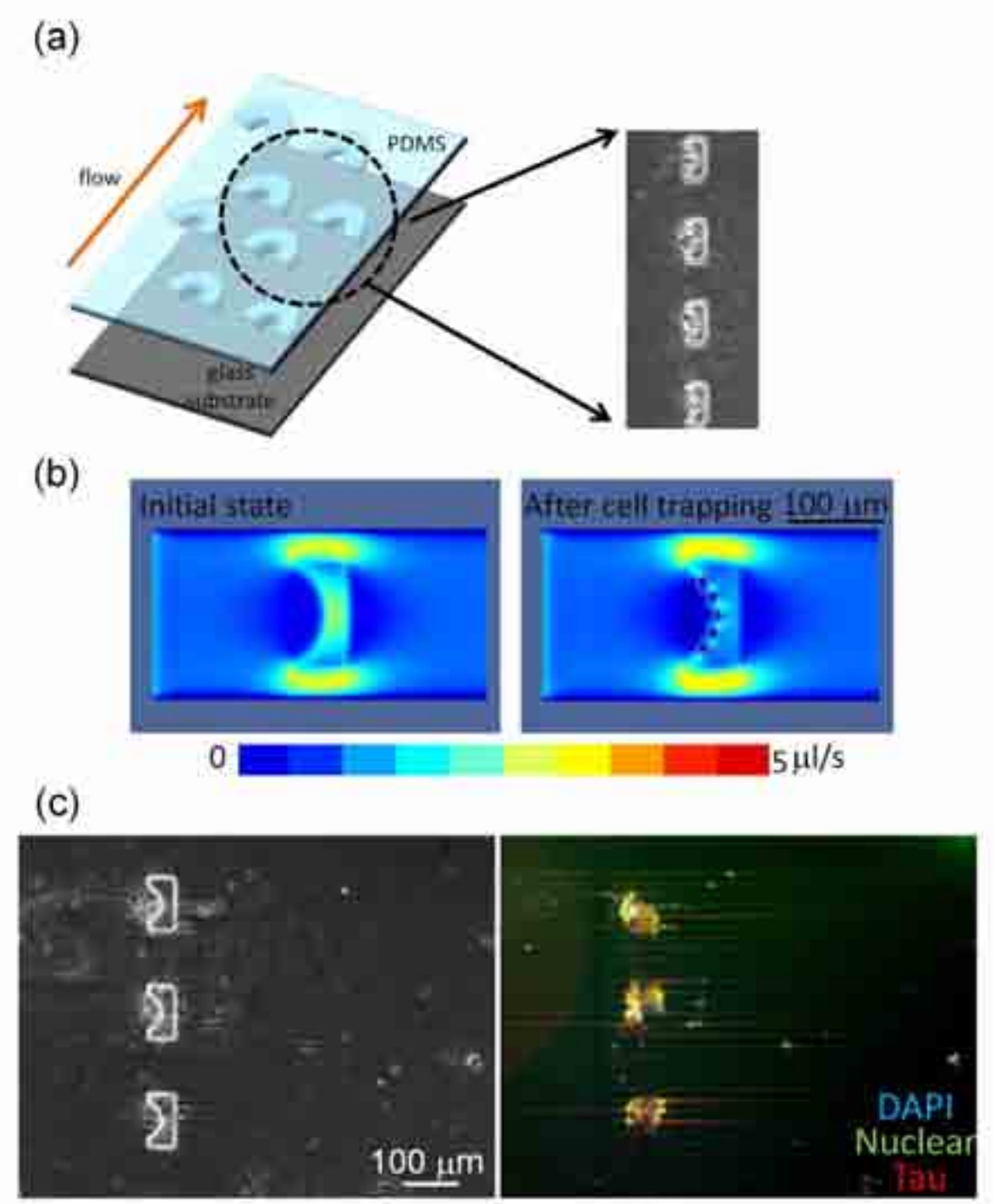

Fig. 1 Microfluidic-modulation of cultured neuronal network (a) Concept design of the microfluidic neuronal culture chamber (b) Modeling the effects of medium flow around the microstructures. The fluid velocity was simulated here. (c) Immunofluorescent identification of constructed cultured neuronal network.

Can cells self-porate their membrane to adjust intracellular osmolarity?

Matthias Gerhardt*; Monika Ehlert; Carsten Beta

Biological Physics/ Institute of Physics and Astronomy/ University of Potsdam
* Corresponding author. E-mail address: matthias.gerhardt@uni-potsdam.de

Abstract

During impedance spectroscopy studies, we observed that cells of the social amoeba *Dictyostelium discoideum* can produce spikes similar to action potentials known from nerve cells. To date, no voltage gated ion channels have been identified in the cell membrane of *Dictyostelium*. Therefore, the mechanism underlying the observed spikes remains unclear. We measured the spikes by an extracellular recording technique based on microelectrode arrays (MEAs). Our first results indicate that spikes are chemically triggered by particular buffer conditions, which we plan to investigate in more detail to derive a mechanism that explains the spikes.

1 Introduction

In the presence of sufficient nutrients, the social amoeba Dictyostelium discoideum lives in a single-celled vegetative state. If nutrients are depleted, the individual cells aggregate into a multi-cellular organism called pseudoplasmodium. The mechanism of self-organized cellular aggregation is well understood. In particular, the transition from individual cells to the pseudoplasmodium is mediated by chemotaxis in gradients of extracellular cAMP. Owing to this behavior, Dictyostelium discoideum is a popular model organism to study eukaryotic chemotaxis. To date, no voltage gated ion channels have been identified in the cell membrane of Dictyostelium. We observed that Dictyostelium discoideum can display rapid changes of the membrane voltage (spikes) similar to action potentials known from nerve cells. In this study, we present our first results, indicating that particular buffer conditions are responsible for triggering spikes that were measured by an extracellular recoding technique based on microelectrode- arrays (MEAs).

2 Methods

Dictyostelium discoideum AX2 wild type cells were grown in shaking culture using HL5 (FORMEDIUM HLG0102) over 48-72h until the cell density reached 107 cells per ml. Then the cells were harvested by dilution to get a final cell density of 2×106 cells per ml. 4×106 cells were given into the culture chamber of a HD30/10iR-ITO microelectrode array (MEA). The MEA device was subsequently mounted onto a MEA1060-Up-BC amplifier, which itself was installed in the light path of an upright video microscope. For data acquisition a MC_Card 64 and the MC_Rack software was used. Via the MC_RACK protocol, one of the MEA electrodes was connected with a trigger detector to trigger a LED that was additionally mounted into the image plane of the video microscope. The LED allowed for identification of those images, where cells were causing spikes because it was flashing each time the signal recorded from a particular electrode was exceeding a threshold of 35 µV.

After the cells were incubated for 30 min in the MEA culture chamber, the HL5 medium (240 mOsm) was exchanged either by Sørensen buffer (36 mOsM: 14.7 mM KH2PO4, 2.3 mM Na2HPO4 @ ph 6.4) or by a 360 mOsM buffer solution (340 mM Glucose, 0.35 mM KH2PO4 mM, 0.011 mM Na2HPO4). Using the microscope, we checked which of the MEA electrodes was occupied by cells. An electrode that contained at least one cell was selected for triggering the LED. We used a custom written software for controlling the video microscope to collect an image every 0.25 sec. After the experiment, the images were analysed. Based on the LED signal, we were able identify those images that correspond to the spike events of the trigger-coupled observation electrode.

3 Results and Discussion:

Despite the fact that up to now no voltage gated ion channels have been found in Dictyostelium, we measured extracellularly rapid changes (spikes) in the membrane voltage if the cells were located on top of a recording MEA electrode. The probability of such spikes dramatically increased after the osmolarity of the buffer solution surrounding the cells was decreased or increased. In the case of decreased osmolarity, each observed spike was followed by a kind of compensation wave. The amplitudes of the spikes were in the range of 50 µV and the pulse duration times around 300 ms. The compensation wave occurred with an amplitude similar to the spikes but with a duration longer than 1000 ms. In the case of increased osmolarity, the observed spikes were characterized by an amplitude of up to 200 µV and durations

shorter than 300 ms. A compensation wave was not observed in this case. The time during which a significantly increased probability for spike formation was observed, was found to be ~60 min in the case of increased osmolarity and ~30 min if osmolarity was decreased. After this time had elapsed, the probability to observe a spike decreased significantly. We found this behaviour to be reproducible, if once more the osmolarity was changed.

To investigate the reason for the occurrence of spikes, we used a custom modified video microscope to observe the cells at the same time when the spikes were detected. With our versatile setup we were able to exclude a broad range of artefacts, which might have also been responsible for causing the spikes. We assembled all recorded spikes together with the corresponding images showing the flashing LED and subsequently analysed these image sequences. By now, we are considering three possible scenarios that may cause the spikes: In scenario 1, a cell is changing its seal of the microelectrode against the buffer environment; in scenario 2, more than one cell is located on the same electrode causing also changes of the seal; and in scenario 3, the cell is changing its membrane voltage. From Van Dujin et al. 1990 we know that Dictyostelium discoideum can build up a membrane voltage, generated by an electrogenic proton pump, and that a poration of the cell membrane can rapidly change this membrane voltage. In our present work, we have observed that a change of the buffer osmolarity was causing transient spiking of a cell, where overall 5-20 spikes could be observed in a time window of 20 min. Therefore, we conjecture that Dictyostelium discoideum may exhibit an unknown mechanism for self-poration of its membrane to quickly adjust the osmolarity of its intracellular space against the extracellular environment. To further motivate this hypothesis, we simulated the membrane voltage [Gerhardt et al. 2011] of sphere shaped cells based on the cable equation using a COMSOL-Multiphysics workstation. We found that, indeed, a hole in the cell membrane can cause a rapid change of the membrane voltage leading to a travelling front of depolarization along the cell body. Due to the Helmholtz barrier layer at the microelectrode surface, the recorded signal corresponds to the first derivative of that membrane voltage. We thus calculated the first derivative of the simulated membrane voltage for comparison with the experimental results. Both experimental and numerical results are displayed in Fig. 1 below. The qualitative agreement between both time traces supports scenario 3.

4 Conclusion

To investigate the ability of Dictyostelium discoideum cells to generate spikes similar to the well known action potentials of nerve cells, we combined a video-microscopy setup and a MEA-system. Furthermore, we added a LED to the light path of the microscope to identify those images that coincide with the instances in time when a spike signal occurs. Using this method, we were able to relate the spike events to the corresponding images. We propose a mechanism to explain the occurrence of spikes based on self-poration of the cell membrane. Such self-poration events would equilibrate differences in the osmolarity and cause a depolarization wave, which can be extracellularly recorded with microelectrodes. Future investigations will focus on the use of fluorescent dyes to confirm the self-poration events. Furthermore, we will focus on the actin cytoskeleton and its role in controlling the process of self-poration.

Acknowledgement

This work was supported by the Europäische Fonds für Regionalentwicklung (EFRE) in the framework of the grant “Mehrkanal-Impedanzspektroskop zur Untersuchung chemotaktischer Motilität“.

References

[1] Van Duijn B, Vogelzang SA, Ypey DL, Van der Molen LG, Van Haastert PJ. “Normal chemotaxis in Dictyostelium discoideum cells with a depolarized plasma membrane potential.” J Cell Sci. 1990 Jan; 95 (Pt 1):177-83

[2] Gerhardt M, Alderman J, Stett A. “Electric field stimulation of bipolar cells in a degenerated retina--a theoretical study.” IEEE Trans Neural Syst Rehabil Eng. 2010 Feb;18(1):1-10. Epub 2010 Jan 12

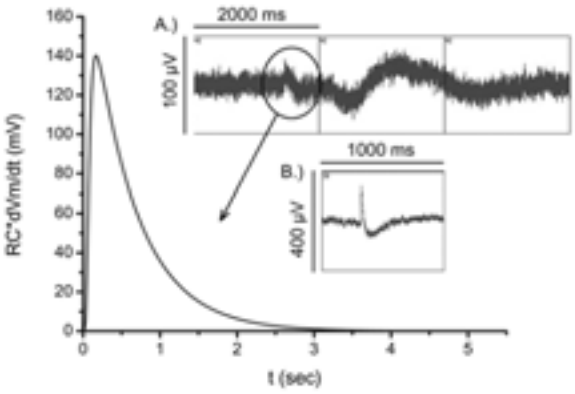

Fig. 1. Comparison of simulated and experimentally generated results. Experimental results shown in section A.): were recorded if osmolarity was decreased and the results shown in section B.): were recorded if the osmolarity was increased.

Functional connection between differentiated and primary neurons

Kenta Shimba[1*], Atsushi Saito[1], Akimasa Takeuchi[1], Yuzo Takayama[2], Kiyoshi Kotani[1], Yasuhiko Jimbo[1]

1 Graduate School of Frontier Sciences, The University of Tokyo, Chiba, Japan
2 Graduate School of Information Science and Technology, The University of Tokyo, Tokyo, Japan
* Corresponding author. E-mail address: shimba@bmpe.k.u-tokyo.ac.jp

Abstract
Regenerative medicine is expected to be a potent therapeutic option for the disorders or injuries of central nervous system (CNS). Many studies have been performed with animal models of some CNS diseases. However, the interaction between the implanted cells and the recipient tissue is still not well-understood at the cellular level. In this study, we examined the direction of functional connection between stem cell-derived neurons and primary cultured neurons. Results suggest that stem cell-derived neurons and primary cultured neurons form functional connection bidirectionally *in vitro*.

1 Introduction

Regenerative medicine is expected to be a potent therapeutic option for the disorders or injuries of the central nervous system (CNS). Many earlier studies have been performed with animal models of some CNS diseases to investigate effects of stem cell transplantation. Some reports showed that stem cell transplantation improved cognition and motor function [1]. However, little is known about the interaction between the implanted cells and the recipient tissue at the cellular level.

In this study, pluripotent P19 embryonal carcinoma cell-derived neurons (P19-neurons) and mouse cortical neurons were cultured with a co-culture device, which consists of a ring shaped polydimethylsiloxane (PDMS) chamber and a microelectrode array (MEA). In order to evaluate the functional connection between the two components, we recorded spontaneous activity and evoked response from substrate-embedded electrodes.

2 Materials and Methods

Fig. 1 shows the image of co-culture system. The co-culture device consists of an MEA substrate and a ring shaped PDMS chamber, which were photolithographically fabricated. The PDMS chamber has two culture compartments interconnected with 36 micro tunnels and allows co-culture of two neuronal populations. The MEA using our experiments comprises 64 indium tin oxide electrodes, half of which are for recording the activity of cortical neurons and the others are for the P19-neurons. The PDMS chamber was placed on the poly-ethylene-imine and laminin coated MEA substrate. Mouse cortical neurons were seeded into outside of the chamber. P19-neurons were seeded into the inside 4 days after plating cortical neurons.

Spontaneous activity was recorded from substrate-embedded electrodes. Electrical stimulation was delivered from each electrode to co-cultured neuronal network, and evoked responses were recorded. Spike trains were detected from the raw data by simple threshold method [2]. Network bursting was detected from spike trains by previously developed method [3].

3 Results and Discussion

Four or more days after beginning co-culture, P19-neurons and cortical neurons were morphologically interconnected through micro tunnels. Furthermore, neuronal networks were immunologically stained. Fluorescent images indicate that the networks formed synaptic connection through the micro tunnels.

Six days after plating P19-neurons, synchronized activity was observed between P19-neurons and cortical neurons. Synchronized bursting was detected from spike trains of co-cultured neuronal network, and we studied signal propagation within the neuronal

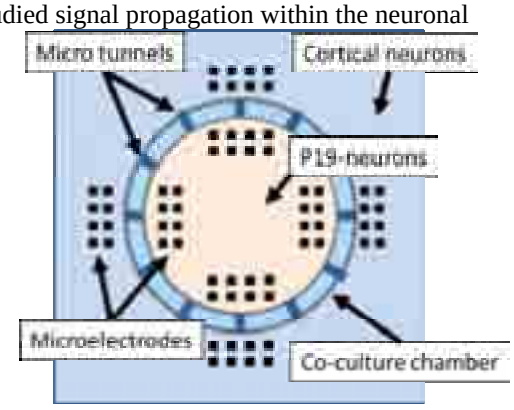

Fig. 1. Image of co-culture system.

network. Fig. 2 shows a pattern of signal propagation in a network bursting. The spatio-temporal patterns of

spontaneous firing suggest that functional connections were formed between cortical neurons and P19-neurons.

In order to evaluate the direction of the functional connection, cu-cultured neuronal network was stimulated electrically. Evoked responses of cortical neurons were observed from some recording sites several hundred milliseconds after P19-neurons were stimulated on the stimulation site shown in Fig. 3A. Moreover, propagation from cortical neurons to P19-neurons was observed (Fig. 3B). The results suggest that the functional connection was formed between cortical neurons and P19-neurons bidirectionally.

4 Conclusion

A co-culture device composed of PDMS chamber and an MEA substrate was developed in order to understand network formation between stem cell-derived neurons and cortical neurons. Results suggest that P19-neurons and cortical neurons formed functional connection bidirectionally.

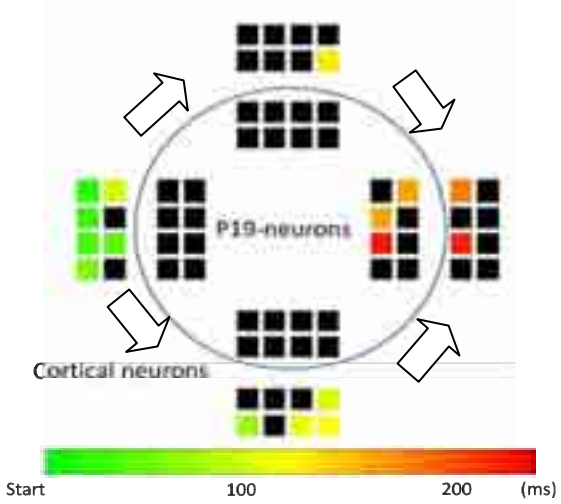

Fig. 2. Signal propagation in a synchronized bursting

Electrical signal was propagated from left site to right site for 200 ms. No signal ware detected from black electrodes (black closed square).

Acknowledgement

This work was supported by KAKENHI (23240065).

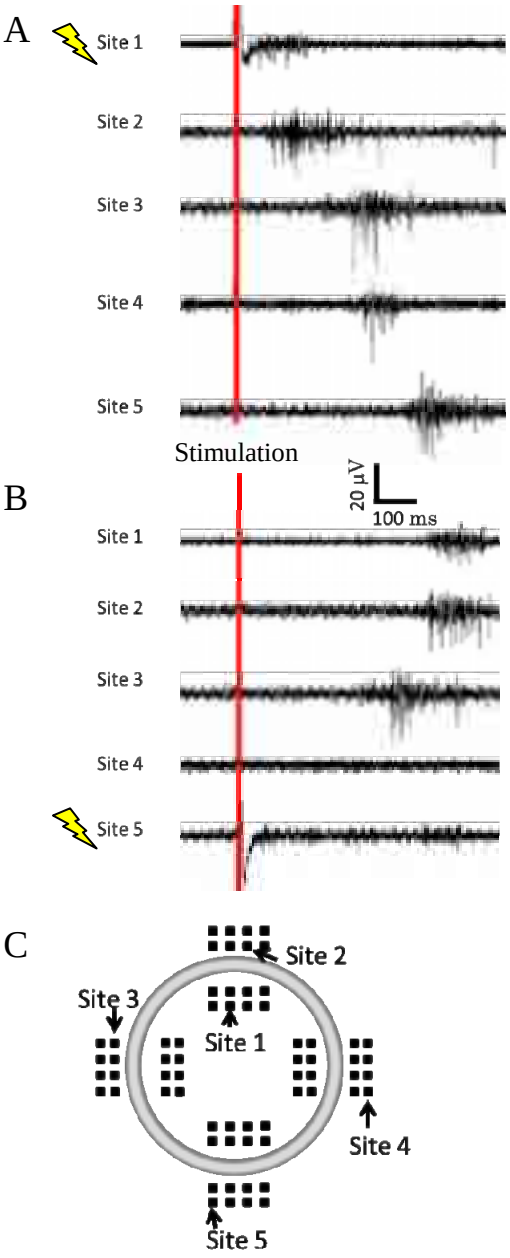

Fig. 3. Evoked responses to electrical stimulation. (A) (B) Responses to electrical stimulation on site 1 or site 5, respectively. Interactions between P19-neurons and cortical neurons were observed. (C) Electrodes position on MEA substrate.

References

[1] T. Ben-Hur, M. Idelson, H. Khaner, M. Pera, E. Reinhartz, A. Itzik and B. E. Reubinoff: "Transplantation of Human Embryonic Stem Cell–Derived Neural Progenitors Improves Behavioral Deficit in Parkinsonian Rats," *Stem Cells*, Vol. 22, pp. 1246-1255, 2004.

[2] E. Biffi, D. Ghezzi, A. Pedrocchi and G. Ferrigno: "Development and validation of a spike detection and classification algorithm aimed at implementation on hardware devices", *Comput. Intell. Neurosci.*, vol. 2010, Article ID 659050, 2010.

[3] M. I. Ham, L. M. Bettencourt, F. D. McDaniel and G. W. Gross: Spontaneous coordinated activity in cultured networks: Analisis of multiple ignition sites, primary circuits, and burst phase delay distributions, *J. Comput. Neurosci.*, 24, pp. 346 – 357, 2008.

Surface modification of Parafilm®: Characterization and applications in neuronal cultures

Yoo Sangjin[1] and Nam Yoonkey[1]*

1 Department of bio and brain engineering, Korea Advanced Institute of Science and Technology (KAIST)
* Corresponding author. E-mail address: ynam@kaist.ac.kr

Abstract
We propose the application of Parafilm® as neural cell culture substrate. Hydrophobic surface of the film can be easily coated by cell adhesion molecules or polyelectrolytes in order to cultivate the neurons. Viability and development of hippocampal neuron on the parafilm® substrate were analyzed. And micro patterns on the film surface were accomplished by using a conventional micro contact printing technique. We found significant increase of neurite outgrowth from the surface modified film substrate, and neuritis were sharply defined against the non patterning film surfaces. Moreover, it is easy to handle and simple to produce a high throughput culture chips. The film served as convenient and high efficiency substrate and it has potential to be a practical culture substrate for a neural chip platform.

1 Introduction

There have been many interests in the improvement of neural culture substrates for neurobiological studies and neuron-based biochips. In conventional neurobiological studies, glass coverslips or polystyrene, Petri dishes are the common substrate of choice [1]. While, hydrogel, elastomeric polymer, silicon, gold, carbon nanotube or nanowires were used in neuron-based tissue engineering and biochip design area. Here, we propose Parafilm® as a convenient neural culture substrate. It could be considered as a good candidate material due to its softness, flexibility, ease of handling and availability. We demonstrated the usability of Parafilm® substrate by showing the development of neural network, pattering with micro contact printing (μCP) and biochip platform. This presentation is a summary of recent publication [2].

2 Methods

Parafilm® M was used as culture substrate. In order to modify the surfaces, Parafilm® was coated with Poly-D-Lysine (PDL, 0.1mg/ml) or polyelectrolyte (PEL) multilayer composed of Poly allylamine hydrochloride (PAH, 20nM, pH 9.0) and Poly sodium 4-stirensulfonate (PSS, 60nM, pH 9.0,). PEL coating was done by layer-by-layer (LbL) technique. And dissociated hippocampal neurons from E18 rat hippocampi were cultured on the Parafilm® substrates (PSs). Calcein AM-live dead cell kit was used to quantify neuron viability and microtubules were stained by immunolabeling technique to measure the neurite growth. Micro contact printing technique was used to construct patterned neural networks on PSs.

3 Results

A hydrophobic Parafilm® surface was readily modified by PDL or PEL coating. Contact angles on the modified PSs were 28.10±1.62˚ and 68.38±0.72˚ for PDL and PEL, respectively. Compared with unmodified PSs, modified PSs promoted neuronal adhesion and neurite outgrowth. Cell viability was 32.69% and 34.11% for PDL and PEL modified PSs, respectively, while 5.11% for unmodified PSs. This viability values were similar with PDL coated glass (35.23%) and PEL coated glass (25.13%) substrates.

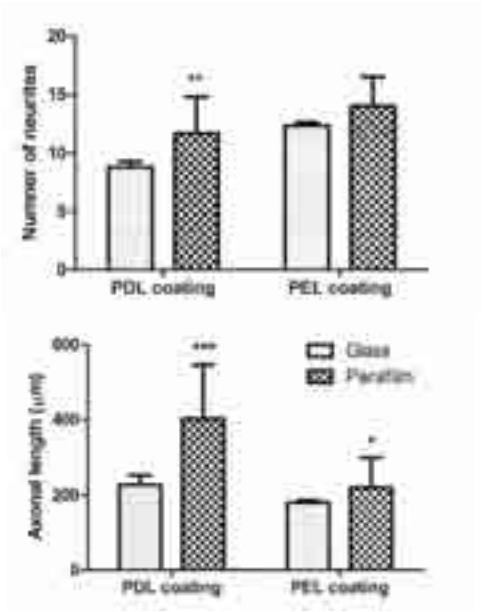

Fig. 1. Development of neurons on glass and Parafilm substrates. Data are presented as mean±SEM, n=45.50, α=0.01. upper and lower data were collected at 3DIVand 6DIV, respectively.

Moreover, development of neuron was improved from the film substrates. For example, the number of neuritis was increased from surface modified film substrates, and axonal length was also longer than glass substrates (Fig 1). When a PLL-FITC micro-pattern was printed on PSs, bare PS surface served as an excellent cell repelling material, which resulted in a well-defined patterned neuronal network (Fig 2).

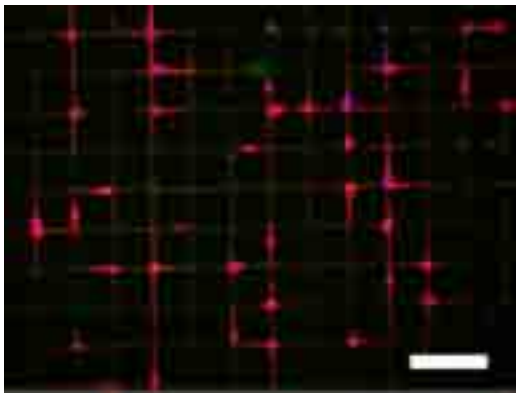

Fig. 2. Neural patterning on Parafilm substrate. Hippocampal neurons at 7DIV, Red: β-tubulin(III); blue: DAPI; Green: Poly L Lysine-FITC, Scale bar: 1000μm.

Long-term stable linear neuronal networks were obtained. Furthermore, it was easy to produce culture substrates in great quantities, which could be applied as a high throughput neural chip platform.

4 Conclusion

We presented a novel neural culture substrate using Parafilm®. Surface modified PSs showed not only good viability of neurons but also enhanced neurite outgrowth. As bare hydrophobic parafilm® surface did not support any neurite outgrowth, a good quality of neuronal patterning was possible using a micro-contact printing technique. Flexible and scratchable parafilm® could be high throughput substrate that has the same conditions. From these results, biocompatibility and utilization of the Parafilm® establish the feasibility of practical substrate for neural culture and cell chips.

Acknowledgement

This work was supported by the National Research Foundation of Korea(NRF) grant funded by the Korea government(MEST) (No. 2009-0080081, KRF-2008-313-D00614, 2012007327) and grants from the Brain Research Center of the 21st Century Frontier Research Program (No. 22-2009-00-002-00).

References

[1] Gary A. Banker et al. (1977). Rat hippocampal neurons in dispersed cell culture. *Brain Research*, 126, 397-425.

[2] Yoo SJ, Nam Y. (2012). Neurons on Parafilm: Versatile elastic substrates for neuronal cell cultures. *Journal of Neuroscience Methods*. 204, 28–34.

Directional neurite initiation and axonal outgrowth by surface geometry of cell adhesive micropattern

Min Jee Jang[1], Yoonkey Nam[1*]

1 Department of Bio and Brain Engineering, KAIST, Daejeon, Republic of Korea
* Corresponding author. E-mail address: ynam@kaist.ac.kr

Abstract
We investigated that the interaction between of surface cell adhesive regions and neuronal growth. Ten types of polygonal microscale patterns, so-called micropolygons, were contact-printed on glass coverslips and hippocampal neurons were cultured on it. We found that the shape of early adhered neurons resembled underlying micropolygons and neurites preferentially initiated from the vertex regions of micropolygons, especially a triangle. Moreover, a putative axon was preferentially protruded from the vertex angle of acute isosceles triangles.

1 Introduction

Axon guidance is crucial to construct functional circuits in the nervous system. Micro- or nanofabrication techniques have been introduced to control the development or growth of cultured neurons microsized surface adhesive patterns [1, 2] or topographical cues given by nanotubes [3] or nanofibers [4].

In this study, we investigate the geometric effect of surface adhesive micropatterns ('micropolygons') on neurite initiation and axonal outgrowth. According to the previous works that have reported the interaction between non-neuronal cells and surface micropatterns, cytoskeletons inside of cells were influenced by extracellular adhesive geometry. Based on these results, we hypothesized that the geometry of surface micropolygon would affect the arrangement of cytoskeletons and consequently result the directional initiation of neurite, especially axons.

2 Methods

We designed ten types of micropolygons whose sizes are comparable to the soma (~130 μm2). Each type of micropolygons was arranged as an array with 10 μm of distance between neighboring micropolygons. We fabricated these micropolygons on glass coverslips by means of micro-contact printing. All the printed micropolygons were composed of poly-L-lysine and synthesized laminin A chain. Hippocampal neuronsons dissociated from E18 S. D. rats were cultured on these patterned substrates and immunocytochemistry was used to label cytoskeletons. To quantitatively analyze results, we measured the anglele of neurite initiation and statistically compared the value to the expected vaue that was deduced from the following assumption, neurites are radially initiated and the chance of neurite intiation at each direction is equal. Furthermore, we investiaged the directional axonal outgrowth on triangular micropolygons by measuring the ratio of tau-1 labeled axons at each vertex.

3 Results

On the single cell level, adhered neurons were deformed like the underlying micropolygons. Neurites were preferentially initiated from the vertex regions of Triangle. This observation was statistically confirmed and only Triangles showed significantly higher ratio of neurite intiated from the vertex regions than the expected value. In addition, w found that the angle of vertex ('sharpness') is an important factor to induce neurites from the vertex. Using Hexagon and two star-shapes, which had the same position but different angle of vertices, we confirmed that only Star-60 showed the significant effect of neurite initiation from the vertex regions. These results suggest that the sharp vertex of surface adhesive regions had a significant effect on cytoskeleton dynamics, resulting directional neurite initiation.

Based on the previous reesults, we investigated that the effect of angularity on axonal outgrowth. Compared to the regular (Triangle) or obtuse isosceles triangle (Wide triangle), the direction of growing axons was biased to the vertex angle of acute isosceles triangles (Long triangle and Very long triangle). We further demonstrated that micropolygons could selectively guide multiple axons on the one substrate. The diretion of axons was determined by the direction of micropolygons where the neurons adhered (Fig. 1).

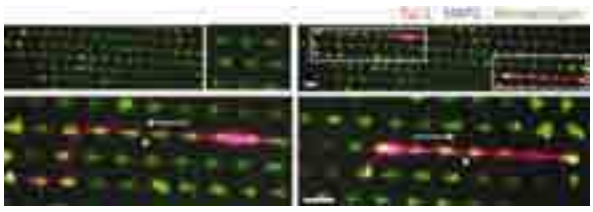

Fig. 1. Individual and simultaneous axon guidance of two neurons to the different way on the same substrate.

4 Conclusion

Here we investigated the interaction between neuronal growth and the geometry of surface adhesive regions. We fabricated soma-sized micropolygons by micro-contact printing and cultured hippocampal neurons. As results, we found that surface adhesive geometry influenced the cytoskeleton arrangement and consequently induced the deformation of cell bodies. In addition, growing neurites were initiated from the vertex regions of Triangle and this effect was caused by the sharp angle of vertices. Based on these results, we further investigated that acute isosceles triangles, which have one sharper vertex than others, had an effect on guiding axonal outgrowth from the vertex angle. Finally we demonstrated that the micropolygon could individually guide several axons. As micropolygons are easy to be fabricated on a culture substrate and only one is required to guide an axon, it would be a useful tool for designing neuronal circuits in vitro.

Acknowledgement

This work was supported by the National Research Foundation of Korea (NRF) grants (2012007327, 2011-0019213) and the Brain Research Center at the 21st Century Frontier Research Program (22-2009-00-002-00) funded by Korea Ministry of Education, Science and Technology (MEST).

References

[1] Stenger D. A., Hickman, J. J., Bateman K. E., Ravenscroft M. S., Ma W., Pancrazio J. J., Shaffer K., Schaffner A. E., Cribbs D. H., Cotman C. W. (1998). Microlithographic determination of axonal/dendritic polarity in cultured hippocampal neurons. *Journal of Neuriscience Methods*, 82(2), 167-173.

[2] von Philipsborn A. C., Lang S., Loeschinger J., Bernard A., David C., Lehnert D., Bonhoeffer F., Bastmeyer M. (2006). Growth cone naviation in substrate-bound ephrin gradients. *Development*, 133, 2487-2495.

[3] Jang M. J, Namgung S., Hong S., Nam Y. (2010). Directional neurite growth using carbon nanotube patterned substrates as a biomimetic cue. *Nanotechnology*, 21, 235102.

[4] Gertz C. C., Leach M. K., Birrell L. K., Martin D. C., Feldman E. L., Corey J. M. (2010). Accelerated neuritogenesis and maturation of primary spinal motor neurons in response to nanofibers. *Developmental Neurobiology*, 70(8), 589-602.

Permeability surveillance system for epithelial cell monolayers

Alexander Brezina[1], Elisabeth Engleder[2], Michael Wirth[2], Heinz Wanzenboeck[1*], Emmerich Bertagnolli[1]

1 Institute of Solid State Electronics, Vienna Universitiy of Technology, Vienna, Austria
2 Department of Pharmaceutical Technology and Biopharmaceutics, Universitiy of Vienna, Vienna, Austria
* Corresponding author. E-mail address: heinz.wanzenboeck@tuwien.ac.at

Abstract
Electrochemical impedance spectroscopy is a powerful analysis method for non-excitable cells. For continuous measurement of the growth of an epithelial cell culture a microelectrode array with a cell culture system mounted on top was developed. This system proved successful for the simultaneous growth surveillance of up to 4 cell cultures. Vital parameters of the cell culture such as confluence and permeability of the cell layer were derived. The presented system allows monitoring of the impact of drugs on the cells' transport properties.

1 Introduction

The majority of the human body is composed of non-excitable cells that cannot generate action potentials. Although these cell types are electrically inactive they possess electrical properties that can be utilized for their damage-free characterisation. Electrochemical Impedance Spectroscopy (EIS) is acknowledged as versatile analysis method for the impedance of cell layers that yields information on the density and the porosity of cell layers [1].

Pharmaceutical studies on transport properties for drugs are relying on reliable information on the confluence and the permeability of the cell layers [2]. These parameters are desired to be measured continuously without influencing or damaging the biological system under investigation. Typically, this cannot be achieved with the standard labelling techniques (e.g. fluorescence labelling). The permeability of a cell layer influences its electrical conductivity and its dielectric properties. Electrochemical impedance spectroscopy is a label free method that allows a continuous in-situ characterisation without damaging the cell layer.

This work introduces a novel platform using microstructured interdigitated electrodes (IDES) [3] on a microelectrode array (MEA) to determine the cell growth and the influence of different pharmaceutical permeation enhancers on an epithelial CaCo-2 cell monolayer by impedance spectroscopy.

2 Methods

2.1 Fabrication of the Microelectrode Array (MEA)

The MEA consists of four microstructured gold interdigitated electrodes (IDES) fabricated on a transparent glass substrate (Fig.1a). IDES are best suited as they allow a surveillance of a large area of the cell layer. Each IDES has a sensing area of 20,01 mm². The width of a single electrode is 50 µm and the interelectrode distance is also 50 µm (Fig. 1b).

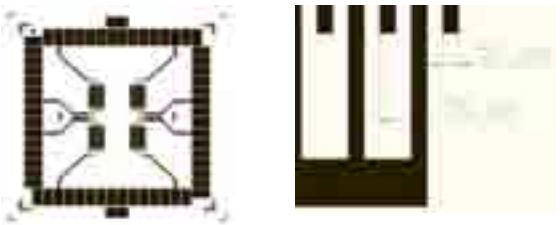

a) b)

Fig. 1. Multielectrode Array (MEA). a) MEA design with four interdigitated electrode sensors b) geometrical parameters of IDES

2.2 Fabrication of the cell culture system

The cell culture system consists of four individually cell culture chambers, each with a diameter of 5 mm and a height of approximately 8 mm. The cell culture system is made from an elastomer and is fabricated by soft lithography using a SU-8 master mould. Each reservoir can hold up to 157 µl RPMI cell medium.

2.3 Merging MEA and cell culture system

The cell culture system has to be aligned over the IDES either manually or by the aid of an microscopic alignment system (Fig. 2).

For a sealed, non reversible adherence the MEA and the cell culture system as well as the MEA Array was surface modified by an optimized plasma treatment before they become aligned to each other and merged together.

Fig. 2. MEA with cell culture system mounted on top. Each of the 4 IDES is equipped with an individual cell culture chamber.

2.3 Preparation of the cell culture

The fabricated MEA was sterilized at 120 °C and 1bar for 50 minutes. 7000 CaCo-2 cells suspended in 100 µl RPMI culture medium were seeded into each of the three cell culture chambers. The one remaining cell culture chamber was filled with cell-free RPMI culture-medium for reference purpose.

The CaCo-2 cells were cultured under defined ambient conditions at 37 °C, 95 % humidity and 5% CO_2. After 2 to 4 days the culture medium was removed from each well and replaced with fresh RPMI culture medium.

2.4 Impedance measurement

For measuring the impedance a commercial bioimpedance spectroscopy system from ScioSpec measuring in the range from 10 Hz to 10 MHz was employed. A multiplexer in the MEA holder allowed to sequentially measure impedance spectra of each of the four IDES sensors. For data interpretation the impedance changes with regard to the initial value were evaluated.

3 Results

Caco-2 cells are human epithelial cells that resemble the epithelium of the intestine [4]. The Caco-2 cells were adhering well on the used materials and on the cell culture system (Fig. 3).

Fig. 3. Optical transmission image of confluent Caco-2 cell layer grown on the interdigitated electrode sensor (IDES). The black stripes are the optically intransparent metal electrodes of 50 µm width.

This confirms the biocompatibility of all used materials and of the elastomer. Between seeding and confluence the cell number has been multiplying itself by a factor of 4 or more.

The impedance of cultured CaCo-2 was measured continuously. The impedance was recorded frequency and time resolved. The cell proliferation and the formation can be sensitively detected in all cell culture chambers at 300 kHz with the existing system.

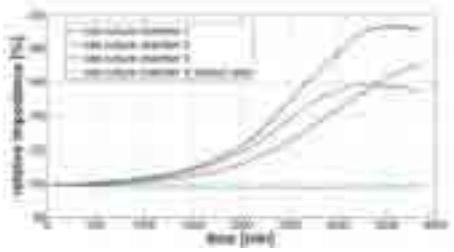

Fig. 4. Relative Impedance vs. culture time post-seeding. CaCo-2 cell growth can be detected electrically, proven by optical investigations (data not shown)

Permeability analyses of previously grown Caco-2 cell monolayers were carried out under the influence of permeation enhancers. The results of these permeation enhancement experiments showed that at correct dosage the influence and the consequent loosening of cell contacts can be electrically detected.

4 Conclusion and Discussion

Bioimpedance spectroscopy has been demonstrated to be a valuable tool for continuous online monitoring of cell growth, cell morphology, and cell adhesion. The proposed method is capable to monitor effects of drugs by the resulting impact on the electrical cell behaviour. The developed multiwell sensor allows for simultaneous study of 4 cultures for long-term measurement over many days.

References

[1] Lisdat, F., Schäfer, D., The use of electrochemical impedance spectroscopy for biosensing, Analytical and Bioanalytical Chemistry 391 (5) ,1555-1567 (2008)

[2] Yamashita, S., Furubayashi, T., Kataoka, M., Sakane, T., Sezaki, H., Tokuda, H., Optimized conditions for prediction of intestinal drug permeability using Caco-2 cells ; European Journal of Pharmaceutical Sciences 10 (3) , 195-204 (2000)

[3] Rümenapp, C., Remm, M., Wolf, B., Gleich, B. Improved method for impedance measurements of mammalian cells, Biosensors and Bioelectronics 24 (9) , 2915-2919 (2009)

[4] Mathieu, F., Galmier, M.-J., Pognat, J.-F., Lartigue, C. ; Influence of different calcic antagonists on the Caco-2 cell monolayer integrity - TEER, a measurement of toxicity?, European Journal of Drug Metabolism and Pharmacokinetics 30 (1-2) , 85-90 (2003).

Huge spikes recorded in microtunnels

Liangbin Pan, Sankaraleengam Alagapan, Eric Franca, Thomas DeMarse and Bruce Wheeler*

Pruitt Family Department of Biomedical Engineering, University of Florida, Gainesville, FL, USA.
* Corresponding author. E-mail address: bruce.wheeler@bme.ufl.edu

Abstract
Extracellular action potential signals recorded by MEAs are rarely greater than 200 µV as recordings are typically done in an open volume of conducting media. However, the signals may be significantly enhanced if the signal source is confined to a very. With this in mind, we have investigated how to best explain and utilize polydimethylsiloxane (PDMS) microtunnels devices on top of multi-electrode-arrays (MEAs) in order to enhance recorded action potential magnitude. The devices had two wells connected by microtunnels (3 µmx10 µmx400 µm). Rat cortical neurons were plated in one well followed by the second well seven days later in order to create unidirectional connectivity between the two wells as axons from the first well predominate in the connecting microtunnels. Due to the extremely limited space, the extracellular signals recorded in tunnels often reach 4 mV, 20 times greater than typical signals in the open culture systems. We report a statistical summary of amplitudes and impedances measured at the tunnel electrodes, finding a monotonic relationship between the two.

1 Background

Amplitudes of typical spikes recorded from somata by MEAs are usually smaller than 100 µV [1]. Those small signals which are on or even below noise leavel (around 10 µV)could not be recoreded, which would lead to loss of data and inaccurate analysis.

However, extracellular signals may be significantly enhanced if the signal source is confined to a limited volume. Clark and Plonsey [2] theoretically found that the magnitude of the extracellur potential from a nerve fiber within a nerve trunk could be 20 times greater than in infinite medium. Microtunnel structure is believed to be a proper tool to realize the signal enhancement. Microtunnel technology has been applied in neuroscience studies [3, 4, 5]. A typical tunnel is 3 µm x10 µm in cross-section and so is too small for cell bodies but allow axonal growth. The limited space within a microtunnel makes it ideal to enhance extracellular signals. Morales et al [6] reported large signals (around 2 mV) from axons in a 1 mm long microtunnel by using two separate electrodes outside the microtunnel. Dworak and Wheeler [4] studied the relationship between signal amplitudes and electrode impedances and suggested that signals in microtunnels could be 2.4 mV.

Given all these theoretical and experimental findings, we have investigated how to best explain and utilize polydimethylsiloxane (PDMS) microtunnels devices on top of new multi-electrode-arrays (MEAs) in order to enhance recorded action potential magnitude.

2 Methods

2.1 Microtunnel Device Fabrication

Photoresist SU-8 2002 (Microchem, Inc.) was spun on a silicon wafer at a nominal thickness of 3 µm, baked, exposed with the first mask, baked again and developed. Next, SU-8 2050 (Microchem, Inc.) was spun on at a nominal thickness of 120 µm and then baked. The second mask was aligned with the alignment marks of the first SU-8 film and then the second SU-8 film was exposed, baked again and developed. Mixed PDMS was poured on the wafer and then put on a hotplate for curing. Two wells for culture and another smaller circular well for reference electrode were punched out on the cured PDMS layer, as shown in figure 1.

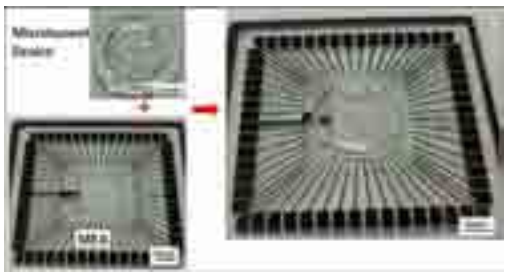

Fig. 1. Microtunnel device and MEA.

2.2 Cell Culture

Embryonic E18 rat cortical tissue was dissociated according to the vendor's protocol. Twenty µL of cell suspension (1,500,000 cells/ml) was added to Well A of a microtunnel device. The neurons extended axons through microtunnels (figure 2). Seven days later, cells were plated in Well B with the same density as Well A.

Fig. 2. Axons growing through microtunnels.

2.3 Measuring Electrode Impedances

AC pulses (10 mV @ 1 kHz) were applied between electrodes and reference electrode on an MEA combined with a microtunnel device holding 300 μL of Neurobasal media. Impedances of electrodes under microtunnels and in wells were measured.

3 Results

3.1 Huge Spikes of Axons in Microtunnels

Large extracellular spikes were recorded. Compared to regular spikes in open wells, the spikes in microtunnels are usually much larger. Examples were the two waveforms in figure 3.

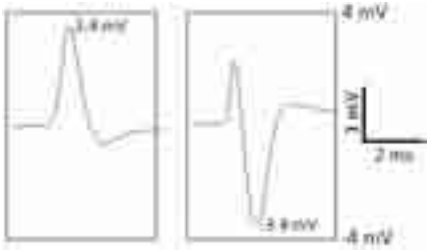

Fig. 3. Sample waveforms with large amplitudes.

The signals were so large that they even saturated the amplifier. So the real waveforms were clipped off and turned out flat tops. For the MCS MEA 1060 recording system, only waveforms smaller than 3.4 mV can be processed without being distorted. So the real amplitudes for these two signals could exceed 4 mV. With the noise level (30 μV) in microtunnels the signal-noise ratio is over 100.

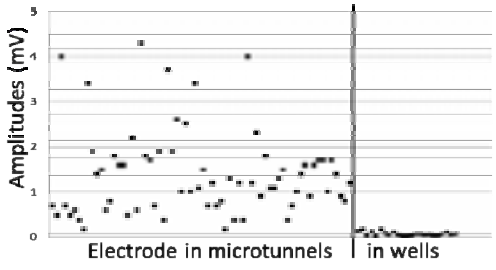

Fig. 4. Largest amplitudes in microtunnels and in open wells.

The largest spikes on each electrode were screened and measured. Figure 4 shows the largest amplitudes for all electrodes in microtunnels or open wells. The largest amplitudes in microtunnels are apparently much larger than those in wells. For the distorted waveforms, a simple geometric method was used to reconstruct the clipped parts in order to estimate their real amplitudes. Ten per cent of the largest waveforms of electrodes in microtunnels were larger than 3 mV, and even the smallest amplitudes are greater than 0.3 mV. However, for the electrodes in wells, most were smaller than 0.2 mV.

3.2 Huge Spikes and Electrode Impedances

The scatter plot in figure 5 shows the relationship between the amplitudes of huge spikes and the impedances of electrodes that recorded those signals in microtunnels. The monotonic trend means electrodes with higher impedance are more likely to record bigger spikes.

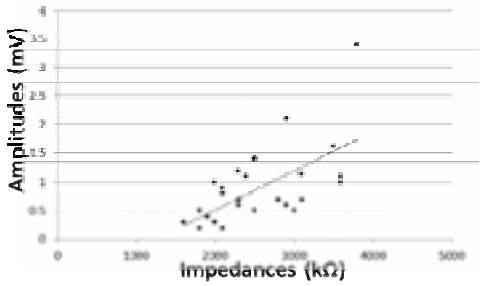

Fig. 5. Electrode impedances vs. the largest amplitude

4 Conclusions

We have recorded huge extracellular spikes from axons in microtunnels, which sometimes were over 4 mV, 20 times greater than the largest signals in open wells. The measurements of impedances of electrodes in microtunnels show their monotonic relationship with amplitude values. This report provides experimental and theoretical evidences for developing new recording technologies to obtain huge signals.

Acknowledgement

This work was supported in part by the National Institutes of Health research, grant NS 052233.

References

[1] Potter, SM. (2001). Distributed processing in cultured neuronal networks. *Progrress in Brain Redearch, 130, 49-62.*

[2] Clark, J. And Plonsey, R. (1968). The extracellular potential field of the single active nerve fiber in a volume conductor. *Biophysical J.*, 8, 842-864.

[3] Taylor, AM. et al., (2005) A microfluidic culture platform for CNS axonal injury, regeneration and transport. Nat. Methods, 2, 599-605.

[4] Dworak, BJ. and Wheeler BC. (2009) Novel MEA platform with PDMS microtunnels enables the detection of action potential propagation from isolated axons in culture. *Lab Chip*, 9, 404-410.

[5] Pan, L. et al., (2011) Propagation of action potential activity in a predefined microtunnels neural network. *J. Neural Eng*., 8, 046031.

[6] Morales, R. et al., (2008) Integrating multi-unit electrophysiology and plastic culture dishes for network neuroscience. *Lab Chip*, 8, 1896-1905.

Stem-3D “Multi-organs-on-a-chip”: tools for “Human-based in vitro testing systems”

L. Stoppini[1]; D. Hakkoum[1]; A. Sandoz[1]; P. Passeraub[1]; Fabien Moreillon[1]; W. Andlauer[2]; B Schnyder[2] ; KH Krause[3] ; M. Jaconi[3]; H. Keppner[4]; S. Brun[4]; J. Brossard[4]

1 Hepia, HES-SO Geneva
2 HES-SO Valais
3 University of Geneva
4 HES-SO Arc

1 Background/Aims

"Cell biochips" containing engineered tissue interconnected by a microfluidic network, allows the control of microfluidic flows for dynamic cultures, by continuous feeding of nutrients to cultured cells and waste removal. Thus, these types of systems can enhance functionality of cells by mimicking the tissue architecture complexities when compared to in vitro analysis but at the same time present a more rapid and simple process when compared to in vivo testing procedures.

Embryonic or adult stem cells have demonstrated the potential to self-renew and differentiate into a wide range of tissues including neurons, hepatocytes, cardiomyocytes, and cells of the intestinal lineage, depending on the culture conditions. The precise microenvironments required for optimal expansion or differentiation of stem cells are only beginning to emerge now, and the controlled differentiation of embryonic stem cells based on tissue engineering remains a relatively unexplored field.

2 Methods

We have developed a small-volume *in vitro* system in which intestine-like cells, hepatocyte cells and 3D micro-organs derived from embryonic stem cells (cardiomyocytes and neural cells) were cultivated in four separate porous membrane microchambers connected by microchannels with the presence of biosensors at the different levels. In a first step, we have used standard commercial membranes to obtain porous microchannel walls to supply nutrients and gases to cells cultured in 3D. Two types of electrodes were designed onto the porous membranes. Inter-digitized impedance electrodes were implemented to the first compartment to assess the tightness of the intestine epithelial cells. Two multi-electrode arrays (M.E.A.) were designed onto the porous membranes to record and stimulate electrophysiological activities from cardiomyocytes and 3D neural tissues. A dedicated perfusion system based on air pressure was used to allow the circulation of the culture medium to the different micro-organs through a microfluidic system.

3 Results

In a first series of experiments, we could record simultaneously action potentials from beating clusters of cardiomyocytes as well as spontaneous activities of neural 3D tissues both being derived from human embryonic stem cells using the same culture medium. We could also assess the functionality of intestine-like barriers using CaCo2 cells. Finally, hepatocyte cells (HepG2) grown in 3D were added to the biochip to check their long-term survival. Their functionality where characterized using the typical hepatic induced cytochrome-P450 (CYP1A) enzymatic activity profile in response to various toxic compounds in comparison to their already known analogue 2D activity. In order to increase the throughput we are developing a semi-automatic platform which will allow us to screen molecules on up to 12 biochips in parallel.

4 Conclusion

This human surrogate multi-organ biochip will enable the determination of toxicological profiles of new drug candidates. In addition, this chip should provide insight into inter-organ interactions resulting from exposure to pharmacological compounds, a capability which has not previously been demonstrated using previous in vitro systems. This system will thus be a more predictive tool in experimental pharmaceutical screening for efficacy and toxicity.

Acknowledgement

The research leading to these results has received a funding from the program Call HES-SO Switzerland.

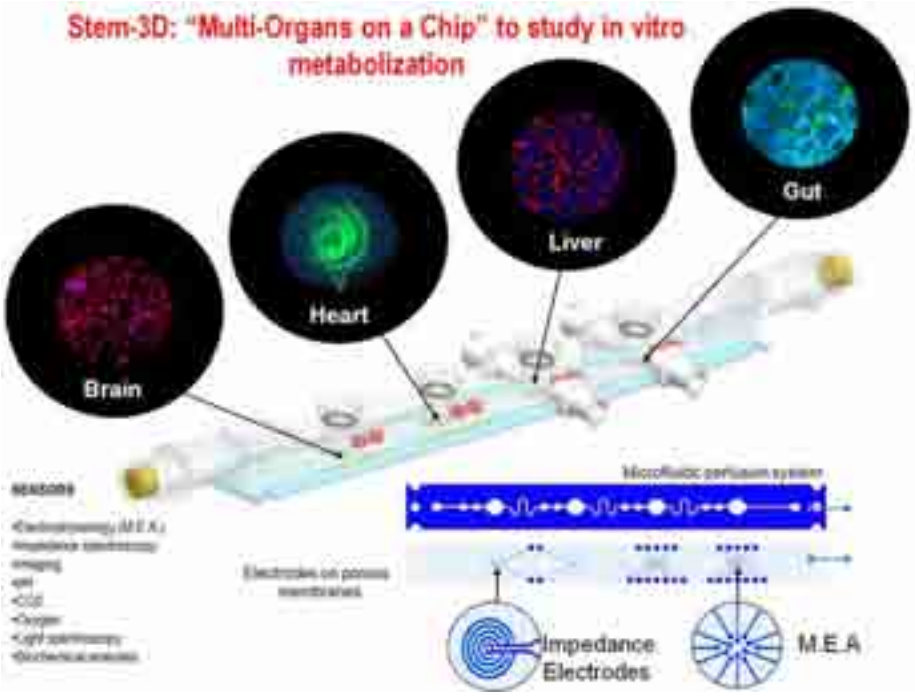

Fig.1: Scheme of the multi-organs biochip where four different tissue-like structures are represented by microphotography.

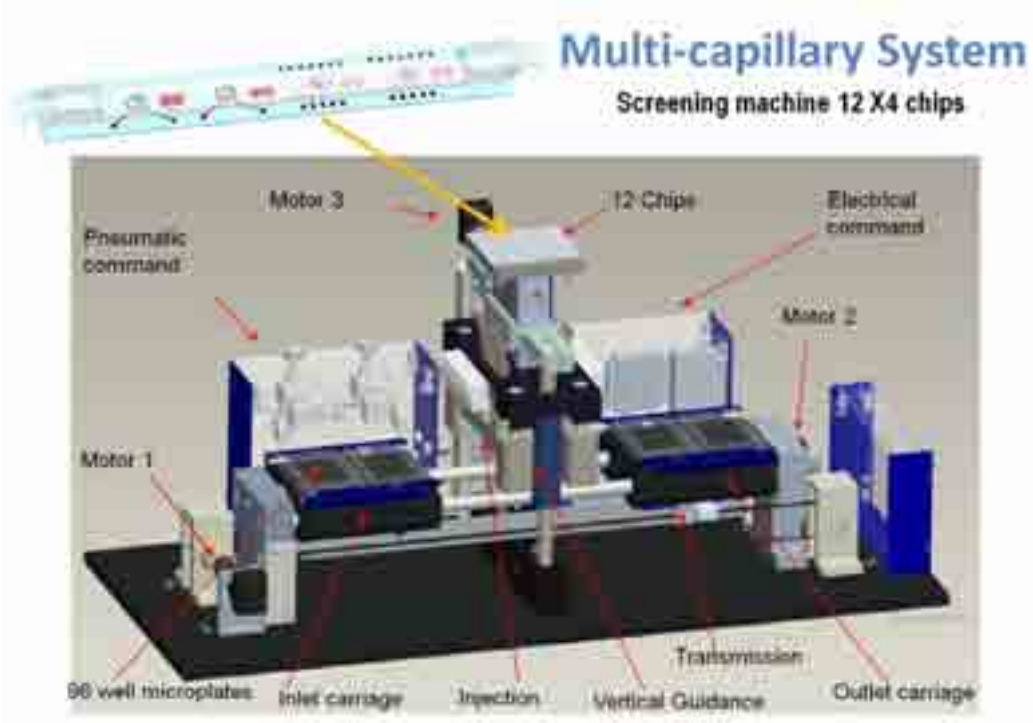

Fig.2: Scheme of the multi-organs platform where up to 12 biochips can be tested in parallel for molecule screening.

Design and fabrication of microchannel and cell culture scaffolds for neural guidance and enhanced optical accessibility of neural networks *in vitro*

Rouhollah Habibey*, Asiyeh Golabchi, Mario Cerino, Francesco Difato, Marina Nanni, Francesca Succol, Axel Blau

Dept. of Neuroscience and Brain Technologies (NBT), Fondazione Istituto Italiano di Tecnologia (IIT), Via Morego 30, 16163, Genoa, Italy. *Corresponding author's email address: rouhollah.habibey@iit.it

Abstract

Physical confinements and chemical cues are commonly applied to substrate surfaces to control neuronal attachment and growth. Temporal physical confinements can be produced with transparent polydimethylsiloxane (PDMS) microchannel tiles which stick reversibly to flat surfaces. In the present study, PDMS microstructures were overlaid on poly-D-lysine (PDL) and laminin-coated microelectrode arrays (MEAs) to let axons and dendrites grow through electrode-crossing microchannels. Three days after cultivation, neurites stated to grow into the channels to result in dense networks of axons and dendrites at 14 days *in vitro* (DIV), from which signals could be recorded at 17 DIV. The results showed that PDMS microchannels successfully force neurites to grow along defined pathways. The reversible bond between PDMS structures and the MEA surface makes such tiles a compatible tool for optical manipulation or staining studies.

1 Introduction

Low density culture and substrate patterning strategies are the methods of choice for controlling and tracing network connectivity on MEAs [1]. Several methods have been reported in the literature for patterning surfaces to control neuronal attachment and growth including chemical and topographical cues [2]. However, mechanical confinements usually require the substrates to undergo various pretreatments. And in most cases, the resulting structures are irreversibly fixed to the substrate. Finally, it is still difficult to combine such pre-patterned substrates with chemical patterning approaches [3]. We are therefore interested in exploring alternative concepts for the combined, but independent chemical and topographic patterning of networks.

1.1 Combination of chemical printing and physical confinement

Cell culture substrates such as Petri dishes or MEAs can be pre-patterned chemically by *e.g.*, polylysine (PL) through microcontact printing (μCP). Given that PDMS sticks to almost all flat surfaces without any glue, microchannel sheets with through-holes can be reversibly placed on these pretreated substrates. By design, the microchannels will thus be connecting individual through-holes laterally. In such setup, neurons can be seeded from above into these freely accessible through-holes, which simultaneously serve as cell culture microwells. Neural processes then have no other choice but to grow in these wells and interconnect through the microchannels. Depending on
the placing of the microchannel sheets with respect to the electrode matrix, different cell compartments may become accessible to MEA electrophysiology and/or optical manipulation in neural regeneration studies.

2 Methods

2.1 PDMS μ-channel molding

PDMS μ-channel tiles with overall heights of 200 μm were fabricated by replica-molding from bi-level SU-8 μ-structures on a 4" silicon wafer (*Fig. 1*). These structures featured four 200 μm-high oval-shaped reservoirs and 30 μm diameter columns for through-hole generation. Reservoirs were connected by an 8 × 8 matrix of 40 μm wide and < 70 μm high channels. Columns were located at the channel crossings. PDMS (Dow Corning, Sylgard 184) pre-polymer and curing agent was mixed (10:1), poured on an epoxy copy of the SU-8 master and cured at room temperature for 2 days applying slight pressure with help of a clamp. The resulting PDMS μ-channel tile was perforated by oval shape reservoirs with interconnecting channels.

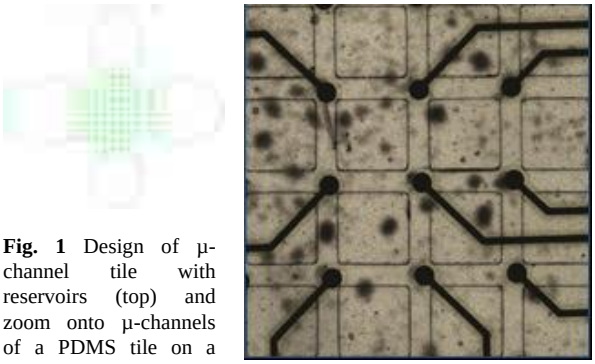

Fig. 1 Design of µ-channel tile with reservoirs (top) and zoom onto µ-channels of a PDMS tile on a 30/200 MEA (right).

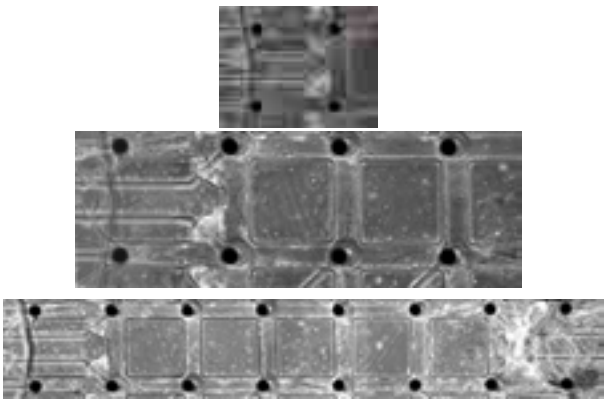

Fig. 2. Neurites are growing through 40 µm wide PDMS microchannels (5 DIV, 9 DIV and 14 DIV).

2.2 Cell culture

MEAs where hydrophilized by oxygen plasma (2 min, 50 W, 0.3 mbar O_2) and their surface coated with 0.1 mg/ml PDL and 0.1 mg/ml laminin (20 µl), which was allowed to dry. MEAs were washed twice with sterile ultrapure water and dried. To align the PDMS tiles with the MEA electrodes, a droplet of sterile water was used to temporarily decrease the physical adherence of PDMS to the MEA substrate (*Fig. 1*). After complete water evaporation, the reservoirs were filled with cell suspension (20 µl; 6000 cortical cell/µl, rat E18). Cells were allowed to settle on the PDL/laminin coat for 40 min in the incubator before 1 ml of serum-free medium was added (NBM, B27, Ala-Glu, Pen/Strep). Cultures were stored in a standard incubator (5%CO_2, 37 °C, 95% RH).

3 Results

Microscopic pictures were taken daily from 3 DIV onward to monitor neurite growth through the µ-channels (*Fig. 2*). At 3 DIV and 5 DIV, some neurites had reached the first channel junctions. The number of neurites in each channel and the number of channels with neurites increased with age (6 DIV - 14 DIV). After 14 DIV, axons from neurons in one reservoir had extended to the other reservoir (≤ 1.5 mm). The picture series furthermore revealed that neurites tended to change their positions within channels (*Fig. 2*). At 17 DIV, first signals could be recorded (not shown). This was late compared to unconfined control networks from which activity was recorded at 8 DIV. Because the overall channel cross section was large, some cells migrated into and within the channels and produced very low-density networks with growing axons or dendrites.

The shortest distance between two reservoirs was 1400 µm which showed that some axons can grow in PDMS channels over long distances. This will allow

4 Conclusions

PDMS µ-channel tiles were successful in guiding axons and dendrites along specific paths over MEA electrodes. Because the number of neurites per channel was rather low, their growth could be monitored easily by time-lapse photography. Some axons had crossed the shortest distance of 1400 µm between two reservoirs, which showed that even *in vitro* axons can grow over long distances. The presented PDMS µ-channel tiles will allow users to manipulate growing neurites by optical tools and evaluate their growth in detail. The tiles can be removed non-destructively after neurite ingrowth to perform any kind of classical optical manipulation or staining study. Current work focuses on the effect of different channel cross sections on growth rate and signal shape.

Acknowledgement

IIT intramural funding of this research line is greatly appreciated.

References

[1] S. B. Jun, M. R. Hynd, N. Dowell-Mesfin, K. L. Smith, J. N. Turner, W. Shain, S. J. Kim (2007) Low-density neuronal networks cultured using patterned poly-L-lysine on microelectrode arrays, *Journal of Neuroscience Methods*, 160, 317-326.

[2] G. Dos Reis, F. Fenili, A. Gianfelice, G. Bongiorno, D. Marchesi, P. E. Scopelliti, A. Borgonovo, A. Podesta, M. Indrieri, E. Ranucci, P. Ferruti, C. Lenardi, P. Milani (2010) Direct microfabrication of topographical and chemical cues for the guided growth of neural cell networks on polyamidoamine hydrogels, *Macromol Biosci*, 10, 842-852.

[3] E. Claverol-Tinture, M. Ghirardi, F. Fiumara, X. Rosell, J. Cabestany (2005) Multielectrode arrays with elastomeric microstructured overlays for extracellular recordings from patterned neurons, *J Neural Eng*, 2, L1-7.

MEA based neuromuscular junction assay

Tabassum Musa, Edward Keefer*

Plexon Inc, Dallas, USA
* Corresponding author. E-mail address: edk@plexon.com

Abstract
The neuromuscular junction is a primary target of many chemical warfare agents, including botulinum toxin and the full spectrum of organophosphorous nerve agents. Current techniques to differentiate between functional and non-functional toxins exhibiting diverse mechanisms of action are limited to the time consuming and expensive mouse lethal bioassay test, or in vitro targeted assays that require prior knowledge of the agent to be detected. We have reconstituted the NMJ system in vitro on MEAs, enabling a rapid, functional assay for compounds targeted to the cholinergic system or synaptic machinery. Our NMJ model is formed with embryonic murine spinal cord neurons and primary myoblasts spatially segregated with PDMS microtunnel structures to define the sites of functional neuromuscular junctions. NMJ formation at predetermined locations allows us to mimic the physiological situation of an intact organism in vitro with high reliability and reproducibility. Spatially patterning of the MEA electrodes allows us to measure the spontaneous or evoked firing of the motor neurons, axonal conduction velocities, and depolarization of the myocytes. This allows the system to detect any substance that modulates neuronal depolarization, vesicular secretion, cholinergic receptor function, or muscle depolarization. Functionally toxic compounds as well as those that kill cells can be detected. This is in contrast to current in vitro assays such as antibody or PCR based assays which detect only the presence of toxin molecules whether functional or not, or of most cell-based assays that are sensitive to cytotoxic agents only. The temporal profile of the NMJ responses to drugs or toxins can provide information on the relative concentration of the perturbing agent, yielding data beyond the binary nature of most current assays.

1 Introduction

Multi-electrode arrays have been used for over 30 years to monitor the electrical activity of neurons and other excitable cell types. Previous research with MEAs has measured the responses of primary neuronal cultures obtained from mice and rats to a spectrum of drugs and chemicals. This predicate work shows that EC50s determined with the neural cultures are in many instances very close to those obtained from in vivo or biochemical experiments. In addition to single cell type assays, MEAs offer an opportunity to create multi‐cellular constructs as mimics of in-vivo physiological systems. Neuromuscular transmission involves a complex series of molecular events that converts presynaptic neuronal excitation to post-synaptic muscular contraction. An in vitro system reconstituting that functional connectivity has application to a diverse set of problems.

2 Materials & Methods

PDMS devices with channels 10µm × 10µm (h × w) and length of 150 µm and 450 µm were made as described previously [1] and were placed on polycarbonate MEAs after Oxygen plasma treatment for 30 minutes followed by 15 minutes baking at 55ºC [Fig. 1]. One compartment of MEA surface was coated with 0.5% Gelatin overnight and Skeletal muscles from P3 mice were isolated and cultured in DMEM media with 10% FBS and 10% Horse serum. This media was replace with DMEM 5% Horse serum after 2 days.

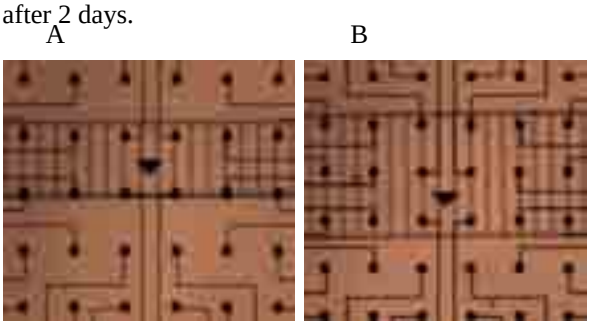

Fig. 1 PDMS Microchannel construct on Polycarbonate MEAs with channel length (A) 150 µm and (B) 450 µ

After 4 days of muscle cell culture, Spinal cord neurons from E16 mice were cultured on PDL coated compartment on MEAs.

3 Results & Discussion

Dissociated myocytes with single nuclei formed multi-nucleate muscle fibers overtime and each fiber was observed to be contracting independently and at different frequencies at div 7 [Fig. 2]. Axons from cortical neurons were observed to cross 150µm channels at div 4 and 450µm channels at div 8. This implies that longer channel length would allow to measure the electrical activity of muscle cells before and after formation of neuromuscular junctions.

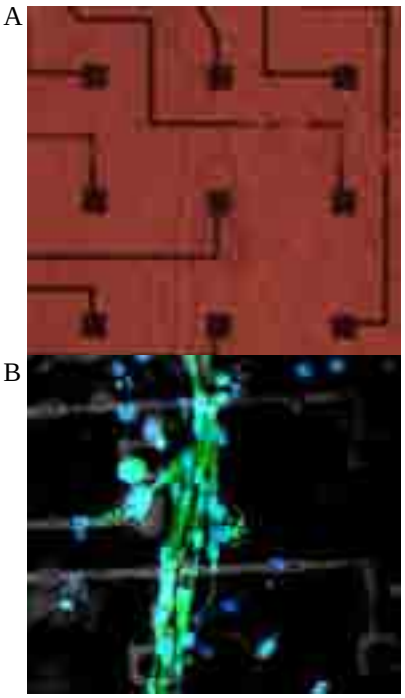

Fig 2 Skeletal muscle cells cultured from P3 mice on polycarbonate MEAs at DIV 7 (A) 20X Phase (B) Stained with Phalloidin and DAPI

Design optimization will attempt to maximize the focal nature or selectivity of electrical stimulation and explore improved signal to noise of recordings by integration of electrode contacts within microfluidic tunnels between wells. We are currently exploring the question if the spontaneous contraction of un-innervated myocytes with multiple, uncorrelated beat frequencies may mimic the in vivo condition known as muscle fibrillation, which is observed clinically on EMG testing subsequent to traumatic denervation. Use of disposable polycarbonate MEAs similar to described in previous study [2] with PDMS microfluidic construct can be cost effective tool for many applications.

Fig 3 Cortical neurons cultured from E16 mice at DIV 2.

4 Conclusion

By growing in vitro functional neuromuscular junctions, we can mimic the physiological situation of an intact organism with high reliability and reproducibility. Using substrate electrodes, we can monitor that function for long time periods without perturbation. Spatial patterning of the MEA electrodes allows us to measure the spontaneous or evoked firing of the neurons, axonal conduction velocities, and depolarization of the myocytes. Additionally, the system can be used to study clinically relevant problems such as chronic denervation-induced muscle atrophy subsequent to trauma or disease, or to screen for compounds which affect the regeneration and/or re-innervation by peripheral nervous system axons.

Acknowledgement

Fabrication of the multielectrode arrays was done in laboratory of Bruce Gnade, UT Dallas and financially supported by NSF PFI grant number IIP-1114211.

References

[1] Jeong Won Park, Behrad Vahidi, Anne M Taylor, Seog Woo Rhee & Noo Li Jeon, (2006). Microfluidic culture platform for neuroscience research. Nature Protocols; (4):2128- 2136

[2] Hamid Charkhkar, Gretchen L Knaack, Bruce E Gnade, Edward W Keefer, Joseph J Pancrazio,(2012). Development and demonstration of a disposable low-cost microelectrode array for cultured neuronal network recording. Sensors and Actuators B: Chemical; 161(1):655-660

Multi-Electrode Probes for In-Vivo Applications

Active, flexible brain computer interfaces for epilepsy

Brian Litt, M.D.

University of Pennsylvania, USA

Mapping epileptic networks is key to understanding and treating seizures in ~35% of the worlds 60 million people with epilepsy who cannot be controlled by medication. Until recently scientists conceived of these networks as contiguous volumes of brain spanning on the order of 3-10 cm^3. We now believe this view was promulgated by limitations of technologies used to map and remove these regions during epilepsy surgery. Grids of 10s of cm-scale, passive, platinum-iridium electrodes imbedded in Silastic are traditionally used to record from the brain's surface or penetrating into its depth. One wire is physically soldered to each contact, which limits the number of contacts that can be implanted. Signals are recorded with these electrodes traditionally at bandwidths of 0.1-70 Hz. Recent work by our group and others demonstrates that epileptic networks may be defined by high frequency oscillations (HFOs) and "micro-seizures" (μ-Sz) emanating from cortical domains on the scale of 10s of microns distributed in a "cloud like" configuration.

We present a multi-electrode array platform, made in collaboration with John Rogers at the Univ. of Illinois and Jonathan Viventi at the Polytechnical University of New York/ NYU designed to map and modulate these epileptic networks. Hundreds to thousands of contacts, each with its own amplifier and multiplexing transistors, are connected via silicon nanoribbons in a flexible, active array that is placed on the cortex. The resulting recordings demonstrate that epileptic spikes occur along specific pathways leading up to seizures, and that high frequency epileptic events may appear as spiral waves on the surface of epileptic brain, similar to cardiac arrhythmias. Efforts under way include making human scale arrays, adding electrical stimulation and other detecting/ effecting modalities, minimally invasive implantation, and wireless capability.

Disclosure: *The University of Pennsylvania and the University of Illinois have licensed the above technology to MC10, a start-up company in Boston, MA. As a result, Dr. Litt has equity in MC10.*

Compliant multi-electrode micro-channel array for recording afferent nerve activity.

Evangelos Delivopoulos[1*], Daniel J. Chew[2], Ivan R. Minev[3], James Fawcett[2], Stéphanie P. Lacour[3*]

1 Nanoscience Centre, Department of Engineering, University of Cambridge, Cambridge, UK
2 Brain Repair Centre, School of Clinical Medicine, University of Cambridge, Cambridge, UK
3 Laboratory for Soft Bioelectronic Interfaces, EPFL, Lausanne, CH
* Corresponding authors. E-mail address: evangelos.delivopoulos@gmail.com; stephanie.lacour@epfl.ch

Abstract
We have fabricated a compliant neural interface to record afferent nerve activity. Stretchable gold electrodes were evaporated on a polydimethylsiloxane (PDMS) substrate and were encapsulated using photo-patternable PDMS. The built-in microstructure of the gold film on PDMS allows the electrodes to twist and flex repeatedly, without loss of electrical conductivity. PDMS microchannels (5mm long, 100µm wide, 100µm deep) were then plasma bonded irreversibly on top of the electrode array to define five parallel-conduit implants. The soft gold microelectrodes have a low impedance of ~200kΩ at the 1kHz frequency range. Teased nerves from the L6 dorsal root of an anaesthetized Sprague Dawley rat were threaded through the microchannels. Acute tripolar recordings of cutaneous activity are demonstrated, from multiple nerve rootlets simultaneously. Confinement of the axons within narrow microchannels allows for reliable recordings of low amplitude afferents. This electrode technology promises exciting applications in neuroprosthetic devices including bladder fullness monitors and peripheral nervous system implants.

1 Introduction

The emergence of novel microfabrication technologies and materials is encouraging the development of neural-electrode interfaces for neuroprosthesis and rehabilitation [1, 2]. Until recently, silicon, metal and plastic were the primary materials used in neural probes [3]. However, softer materials such as hydrogels and silicones are now attracting substantial interest in neural engineering and neurotechnology, as they can be structured in three dimensional designs, while their mechanical properties match better the physical properties of the nervous system [4]. Compared to silicon and plastic, polymeric materials are 2-4 orders of magnitude softer and can conform to curvilinear neural tissue. Theoretically, neuroprosthetic implants prepared with such materials may present enhanced biocompatibility with an attenuated inflammatory and scaring response post-implantation.

In this study, we present a 3-dimensional neural interface comprised of microchannels (5mm long, 100µm wide, 100µm deep). At the bottom of the microchannels we have embedded stretchable gold electrodes [5]. The surface of the electrode thin gold film is covered with a network of microcracks (a couple of microns long separated by gold ligaments), which prevents the formation of large catastrophic cracks upon mechanical deformation. Thus, the continuity and conductivity of the metal film is maintained [6]. The electrode array is patterned using shadow-mask lithography and embedded in PDMS microchannels. Each microchannel is designed to host a nerve strand (<100µm diameter) from which neural activity is monitored. Our soft interface is evaluated in an acute setting using nerve strands from the L6 dorsal root of an anaesthetized rat. Cutaneous activity can be monitored in 5 distinct microchannels simultaneously. Our results demonstrate that the soft interface combined with the microchannel design allows for reliable recordings of small amplitude single fiber afferents. It is important to note that these data are obtained under saline conditions. We now aim at chronic implantation of our devices, in order to address their long-term reliability. We are particularly interested in addressing urinary incontinence and providing a viable long term bladder management option for patients with spinal cord injury [7, 8].

2 Methods

2.1 Electrode fabrication

Silicon wafers (Compart Technology Ltd) coated with a polystyrene sulfonic acid (PSS) water release layer were spun coated with PDMS (Sylgard 184 by Dow Corning, cross-linker to pre-polymer ratio 1:10 w/w) at 400rpm for 60sec (PDMS thickness 200 µm). Gold electrodes (2.5cm long, 150µm wide, 40nm thick) were evaporated through a polyimide shadow mask in a thermal evaporator. Two chromium adhesion layers (3nm/2nm thick, bottom/top) were also evaporated. Gold electrodes were encapsulated with photo patternable PDMS (PP-PDMS). This UV-sensitive PDMS is used as a negative photoresist [9].

PDMS microchannels were cast separately against an SU-8 mold containing rectangular recesses (5mm x 100µm x 100µm), peeled off then aligned and plasma bonded on top of the underlying microelectrode array on PDMS substrate. Assembled devices were then briefly exposed to an RIE plasma, which was found to reduce further the electrode impedance. Excess PDMS surrounding the devices on the wafer was cut and removed to expose the water soluble PSS layer underneath. The final device was released in water.

2.2 Electrode characterization

Devices were characterised in wet environment using an Autolab µIII frequency response (100Hz and 100kHz) analyser in potentiostatic mode. Reference and counter electrodes were Ag/AgCl and Pt mesh respectively. The working electrode was in contact to a gold pad on the PDMS via silver paste. Measurements were performed on electrodes encapsulated with PP-PDMS, with microchannels plasma bonded on top. Microchannels were filled with saline solution and degassed in a vacuum chamber to remove air bubbles.

2.3 Acute recordings

A female Sprague Dawley rat was anaesthetised with 1.5mg/kg of Urethane solution (Sigma Aldrich, Pool, UK) through the intra peritoneal route. A laminectomy was performed of the L1-L3 spinal vertebrae to expose the dorsal roots. The unilateral L6 dorsal root was rhizotomised 3mm caudal to the dorsal root entry zone of the spinal cord, and 100µm diameter strands of the proximal root were teased with fine No. 5 forceps proximally. Ethilon sutures (No.10, Ethicon) were threaded through the microchannels, tied to the cut ends of the proximal teased rootlets and pulled through the channels rostrally, threading the rootlets into the channels. The microchannel device was connected to an amplifier and filter module, through a pre-amplifier headstage (x1000) and an AC-DC amplifier (x10). Mains electrical interference was attenuated with a noise eliminator (Hum-bug, Quest Scientific). Signals were digitized using Power Micromax 1401 A/D converter hardware (50 kHz sampling rate) and recorded using Spike 2 software. Recordings were conducted under saline solution, in a tripole configuration where the two reference (outer) electrodes in the device are shorted together and connected to one input of the differential amplifier. The other input is connected to the central/main electrode of the microchannel (Figure 1 D). The animal and apparatus were connected to the ground of the amplifier head stage. Recordings were performed on a total of 3 different animals.

3 Results

3.1 Device fabrication and characterization

Figure 1 illustrates the device fabrication steps. The evaporated electrodes are encapsulated with photo-patternable PDMS (15µm thick) (Figure 1A). The encapsulation openings (300µm x 1000µm) have minimal footing (~5µm) and are accurately positioned (within a few µm) over the recording sites. PDMS microchannels are plasma bonded irreversibly to the underlying PP-PDMS layer (Figure 1B). The bonds that are formed across the entire length of the microchannel walls insulate each microchannel and prevent crosstalk between electrodes. Devices can be processed in parallel on 3'' silicon wafers (Figure 1C). A finalized device has maximum dimensions of 2.5cm x 1cm x 0.5mm. During acute recordings, the two reference electrodes (exposed area of each electrode 500µm x 150µm) at the exits of the microchannels are connected to the inverting input of a differential amplifier, while the main/central electrode of each microchannel (exposed area of each electrode 100µm x 200µm) is connected to the non-inverting input (Figure 1D). Electrochemical characterization of the device reveals an impedance of 200kΩ ± 13kΩ < 43º ± 1.4º, N=4, at 1 kHz for main electrodes (Figure 2A). The impedance of the two reference electrodes is 25kΩ < 55º and 30kΩ < 48º. Figure 2B depicts the modulus and phase of one of the two reference electrodes.

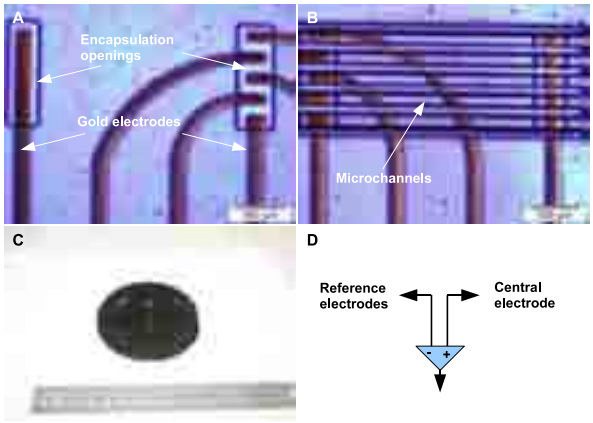

Fig. 1. Device fabrication. A) Encapsulation of gold electrodes with PP-PDMS. Each encapsulation window is 300µm x 1000µm. B) Air plasma bonding of separately cast PDMS microchannels to underlying encapsulated electrodes. C) Simultaneous processing of 3 devices on a wafer. D) Tripolar recording using a differential amplifier. Reference electrodes are shorted and connected to the inverting input, whereas the main electrode is connected to the non-inverting input of the differential amplifier.

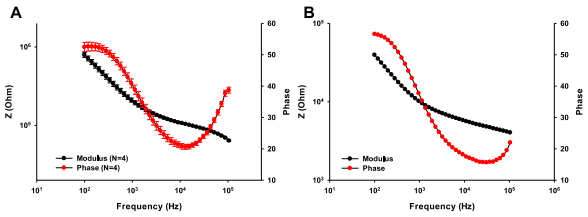

Fig. 2. Device characterization. A) Modulus and phase of 4 main electrodes. Data points represent the average modulus of 4 electrodes, while the error bars denote the standard error of means. B) Modulus and phase of 1 reference electrode. The other reference electrode has a similar modulus and phase.

3.2 Cutaneous recordings

The setup for in vivo recordings from the L6 dorsal root in saline solution is shown in Figure 2. Sutures are threaded into the microchannels (Figure 3A) and are tied to the proximal ends of transacted rootlets. The suture and rootlet are then pulled through the channel (Figure 3B). We recorded cutaneous activity from 3 channels simultaneously (Figure 4). Background noise was 20µV peak-to-peak, which is comparable to noise in hook electrode recordings under paraffin oil (15µV peak-to-peak, Figure 5). In the three channels we recorded 65µV, 130µV and 175µV biphasic spikes (negative then positive). Therefore, the signal to noise ratio (SNR) in each case is 10.24dB, 16.26dB and 18.84dB respectively. In comparison, the SNR in the hook electrode recording is 16.9dB. Activity occurs only while stroking the rat dermatome at the base of the tail and ceases once the stimulus is withdrawn. The duration of all spikes is approximately 1ms. After the experiment, rootlets were cut and left in the channels. No further activity could be recorded, during cutaneous stimulation of the dermatome. This verifies that prior acute recordings originated from a genuine response to applied stimuli and not other interference.

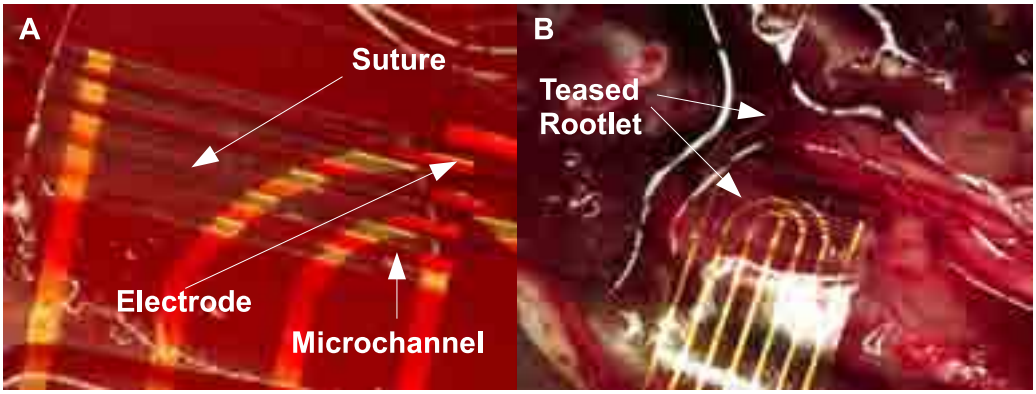

Fig. 3. In vivo L6 dorsal root recordings setup. A) Sutures threaded in the microchannels. B) L6 dorsal rootlets tied to the end of the sutures and pulled through the microchannels.

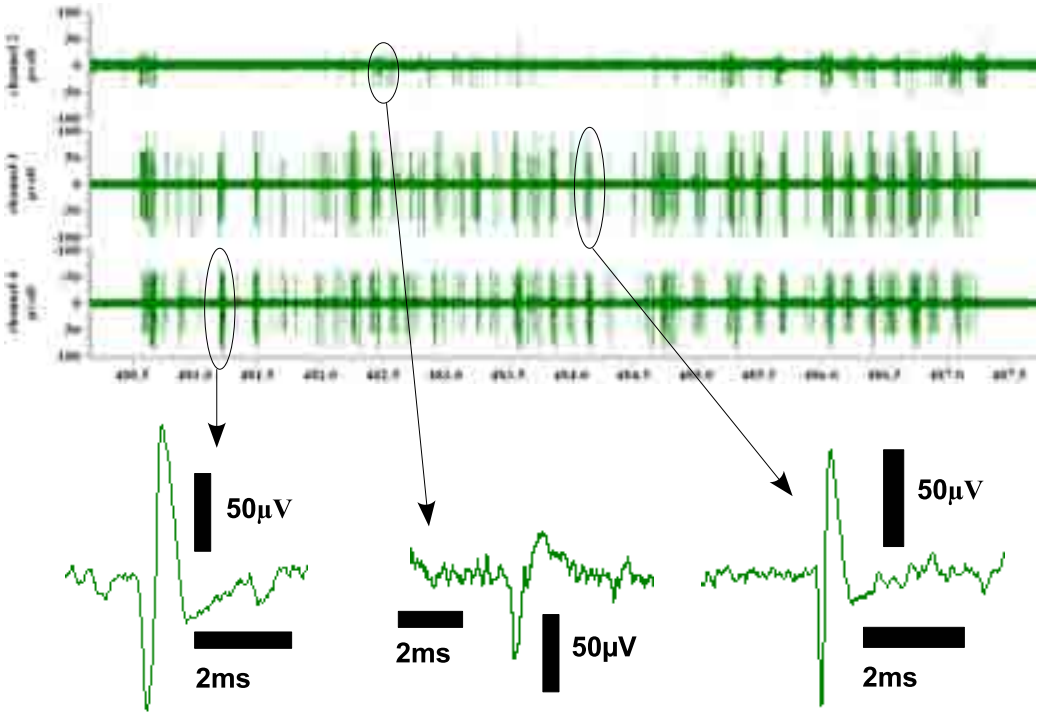

Fig. 4. In vivo L6 dorsal root recordings: Response to cutaneous stimulus, with high magnification traces from each channel. Channel 2, 3 and 4 peak to peak amplitudes are 65µV, 130µV and 175µV respectively.

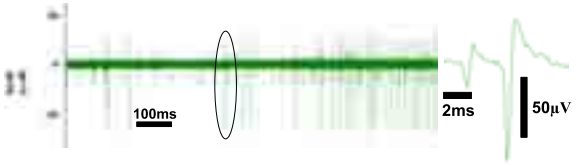

Fig. 5. Control hook electrode *in vivo* recording from the L6 dorsal root. Response to cutaneous stimulus, with a high magnification trace of the large amplitude biphasic spike. Peak to peak amplitude is 105µV. Background noise is approximately 15µV peak to peak.

4 Conclusions

We have developed a compliant, 3-dimensional PDMS neural interface with embedded electrodes and microchannels. Evaporated gold electrodes are mechanically compliant, so they can sustain the surgical manipulation without failure. These electrodes exhibit low impedance at 1 kHz. In an acute placement of the neural interface on an anesthetised animal, we recorded reliably under saline solution, afferent activity, generated from cutaneous stimulation. Our fabrication protocol should be scalable for implant batch processing. Our current goal is to proceed from this acute validation to a chronic implantation and validation of the integrated PDMS neural electrodes.

Acknowledgement

This research was funded by the EPSRC and the Royal Society.

References

[1] Minev IR, Chew DJ, Delivopoulos E, Fawcett JW, Lacour SP. High sensitivity recording of afferent nerve activity using ultra-compliant microchannel electrodes: an acute in vivo validation. Journal of Neural Engineering 2012;9(2):026005.

[2] FitzGerald JJ, Lago N, Benmerah S, Serra J, Watling CP, Cameron RE, et al. A regenerative microchannel neural interface for recording from and stimulating peripheral axons in vivo. Journal of Neural Engineering 2012;9(1):016010.

[3] Polikov VS, Tresco PA, Reichert WM. Response of brain tissue to chronically implanted neural electrodes. Journal of Neuroscience Methods 2005;148(1):1-18.

[4] Hassler C, Boretius T, Stieglitz T. Polymers for neural implants. Journal of Polymer Science Part B: Polymer Physics 2010;49(1):18-33.

[5] Lacour SP, Benmerah S, Tarte E, Fitzgerald J, Serra J, McMahon S, et al. Flexible and stretchable micro-electrodes for in vitro and in vivo neural interfaces. Medical and Biological Engineering and Computing 2010.

[6] Minev IR, Lacour SP. Impedance spectroscopy on stretchable microelectrode arrays. Applied Physics Letters 2010;97(4):043707.

[7] Delivopoulos E, Chew DJ, Minev IR, Fawcett JW, Lacour SP. Concurrent recordings of bladder afferents from multiple nerves using a microfabricated PDMS microchannel electrode array. Lab on a Chip 2012.

[8] Anderson KD. Targeting Recovery: Priorities of the Spinal Cord-Injured Population. Journal of Neurotrauma 2004 2011/10/30;21(10):1371-1383.

[9] Delivopoulos E, Minev IR, Lacour SP. Evaluation of negative photo-patternable PDMS for the encapsulation of neural electrodes. Neural Engineering (NER), 2011 5th International IEEE/EMBS Conference on; 2011 April 27 2011-May 1 2011; 2011. p. 490-494.

High resolution recordings of local field potentials with transistor needle chips in rat somatosensory and motor cortexes

Marta Maschietto[1], Stefano Girardi[1], Florian Felderer[2], Elisabetta Pasqualotto[3], Stefano Vassanelli[1*]

1 University of Padova, Dept. Biomedical Sciences, Padova, Italy
2 Max Planck Institute of Biochemistry, Martinsried, Germany
3 University of Padova, Dept. Information Engineering, Padova, Italy
* Corresponding author. E-mail address: stefano.vassanelli@unipd.it

Abstract

One of the major technological challenges in Neuroscience and application fields like Brain-Machine Interfacing and Robotics is to establish bi-directional communication (recording and stimulation) with the brain at high spatial resolution through innovative neuronal probes. In the present work, new implantable transistor needle chips (TNCs) featuring four Electrolyte Oxide Semiconductor Field Effect Transistors (EOSFETs) with a TiO_2 surface and a spatial resolution of 80 µm were used in single implants for interfacing with the somatosensory cortex of anesthetized rats. Local Field Potentials (LFPs) evoked by whiskers mechanical stimulation were recorded with TNC and the contributions of thalamic inputs to the cortical activity were isolated by application of the $GABA_A$ receptors agonist muscimol. Double implants of TNCs in somatosensory and motor cortexes allowed to record the simultaneous response of related brain areas.

1 Background/Aims

In the rat brain cortex sensory-motor signals are processed by large groups of interconnected neurons. Particularly in the S1 somatosensory cortex, neurons are arranged in column-shaped structures called barrels. Each barrel receives the sensory information from the corresponding whisker [1]. Tight interconnections between thalamus, S1 cortex and M1 motor cortex allow for a precise control of whisker movements. To have a thorough understanding of the neuronal networks in S1 and M1 by efficient brain-machine interfaces, multiple recording sites with a high spatiotemporal resolution are needed. At present, extracellular electrophysiological techniques based on single electrodes provide information about one or a few neurons with a low spatial resolution and a sparse sampling within the neuronal networks. Furthermore, the actual technologies featuring multiple recording sites integrated in microchips are based on metal electrodes, with a few recording sites and a low spatial resolution [2, 3].

In this work, new TNCs featuring four EOSFETs with a TiO_2 surface and spaced 80 µm were implanted both in S1 (single implant) and in M1 cortexes (double implant) of anesthetized rats. The devices, previously used to record neuronal activity from brain slices [4], were successfully used to record brain LFPs evoked by single whiskers stimulation. The application of muscimol as a $GABA_A$ receptors agonist allowed to suppress the intracortical activity, thus isolating the contributions of thalamic inputs. Altogether, the results demonstrate the reliability of the EOSFETs in recording signals from the rat brain cortex, thus paving the way to multi-transistor-arrays as new tools for large-scale high-resolution recordings from the living animal.

2 Methods

The TNCs featuring 4 EOSFETs with a TiO_2 surface and a pitch of 80 µm (Fig. 1, *left*) were fabricated according to [4]. Wistar rats (Charles River Laboratories) were maintained in the animal research facility under standard environmental conditions. P35 - P45 rats (100 - 145 g) were anesthetized with an induction mixture of Tiletamine and Xylazine (2 mg and 1.4 g/100 g weight, respectively). The anesthesia level was monitored throughout the experiment by testing eye and hind-limb reflexes and respiration, and checking for the absence of whiskers' spontaneous movements. Additional doses of Tiletamine and Xylazine (0.5 mg and 500 mg/100 g weight, respectively) were provided every hour to maintain a constant level of anesthesia. Surgical procedures were performed as described previously [5]. Briefly, under continuous monitoring of heartbeat and body temperature, windows in the skull over the right somatosensory cortex S1 (− 1 ÷ − 4 AP, + 4 ÷ + 8 ML) and/or motor cortex M1 (+ 1 ÷ + 4 AP, 0 ÷ + 3 ML) were made [6, 7]. Meninges were opened wide around coordinates − 2.5 AP, + 6 LM and +2.5 AP, +1.5 ML for S1 and M1, re-

spectively, for the subsequent insertion of the recording chips and diffusion of the drug (Fig. 1, *right*).

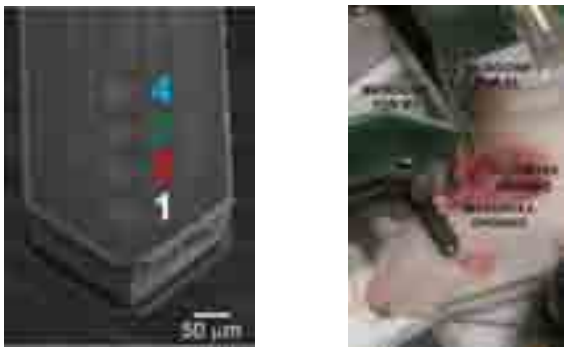

Fig. 1. (*Left*) SEM micrograph of the tip of the TNC, with the transistors (1-4). Scale bar: 50 µm. (*Right*) Magnification of the rat head with two chips, one for implant in S1cortex and the other in M1 cortex. The chips are shown in close proximity to the brain surface where the meninges have been cut. A tube connected to the piezoelectric bender for the insertion of the whisker and stimulation is visible on the bottom-right.

Contralateral whiskers were trimmed at 10 mm from the snout and individually deflected of ± 250 µm in the anterior-posterior direction with a piezoelectric bender (PICMA™ Multilayer Bender Actuator; Physik Instrumente). Each whisker was individually inserted into a tube connected to the piezoelectric bender (Fig. 1, *left*) and the response was checked in S1 cortex at -640 µm depth (corresponding to layer IV), in order to find the most responsive whisker (in terms of amplitude of signal) for the selected recording point. The so-called "principal whisker" (PW) was then chosen for the recording session. Evoked LFPs were recorded in all the layers by moving the chip down in the cortex. For each recording depth, 50 sweeps with 500 ms duration were recorded at 100 kHz sampling rate, and averaged by means of a custom-made software developed in LabView (National Instruments). For inhibition of intracortical activity, the $GABA_A$ receptors agonist muscimol (500 µM; Sigma-Aldrich) was applied as a gel onto the exposed brain. The diffusion of the drug was verified for a total time of 75 min, and the different contributions to the LFPs were studied by δ-source iCSD (inverse Current Source Density) analysis, as previously described [5].

3 Results

3.1 Recording of LFPs by means of TNC

Whiskers on anesthetized rats were mechanically deflected by means of a piezoelectric bender. The LFPs evoked by the PW were recorded with a 80 µm step by the TNC at different depths across all the layers of the S1 somatosensory cortex. In standard condition, i.e. without drugs application (Fig. 2, t=0), typical LFPs were recorded: in the central layers (IV-V) the signals showed a main negative peak about 15 ms after the stimulus onset. The main peak was anticipated by a minor positive peak only in the more superficial layers.

3.2 Inhibition of intracortical activity and isolation of thalamic inputs

It has been demonstrated that the application of the $GABA_A$ receptors agonist muscimol causes a generalized inhibition of intracortical circuits precluding their participation in sensory responses without eliminating synaptic inputs from the thalamus. As a consequence the recorded LFPs usually show a consistent reduction of amplitude [8, 9]. We applied a muscimol/agar gel (500 µM) on the surface of the exposed brain and the LFPs evoked under PW stimulation were recorded every 15 min (Fig. 2). Already after 15 min from muscimol application, the negative peaks at every depth were strongly reduced in amplitude, due to the inhibition of intracortical excitability. After 75 min, only the thalamo-cortical contributions persisted. Muscimol effect was visible also as a reduction in the spontaneous brain activity (represented by the large oscillations at t = 0) that became almost completely suppressed after 30 minutes.

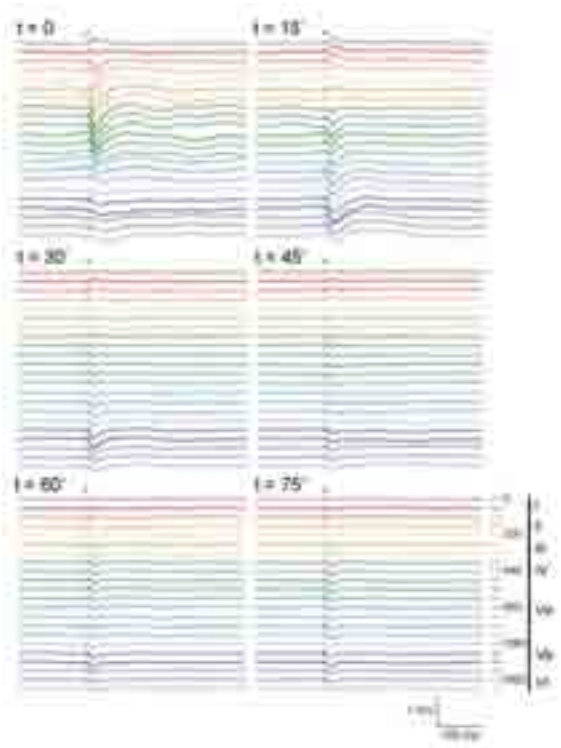

Fig. 2. Averaged LFPs (*n=50*) under whiskers stimulation and muscimol application. The stars indicate the stimulus onset. Scale bars (100 ms and 1 mV) refer to all the graphs. Depths in the cortex (in steps of 80 µm) and corresponding layers are shown at the bottom, right.

To study in detail the effect of muscimol diffusion through the somatosensory cortex, a δ-source iCSD analysis was performed (Fig. 3). This analysis allows to distinguish between inward and outward currents,

thus making it possible to study the propagation of the signals through the cortical layers. After 15 min of muscimol application the sinks (highlighted in yellow) were reduced, and new sources (coloured in red) appeared in upper layers. After 30 min, sinks persisted only in deeper layers with low amplitudes. The reduction of sinks was stable throughout the experiment and was accompanied by a reduction of sources. Residual sources and sinks denoted the inputs from the thalamus.

Fig. 3. δ-source iCSD analysis of averaged LFPs shown in Fig. 2, with highlighted sinks (yellow) and sources (red). Scale bars are expressed in μA/mm^3.

3.3 Double implant of TNCs in S1 and M1 cortexes for simultaneous recording of brain activity

As a prototype of experiment for the investigation of brain circuits involved in sensory-motor control, evoked LFPs were recorded simultaneously by two chips implanted in the S1 and M1 cortexes of anesthetized rats under mechanical single whisker stimulation. In Fig. 4 the plots of the two brain areas responses at the same depths and at the same time are shown.

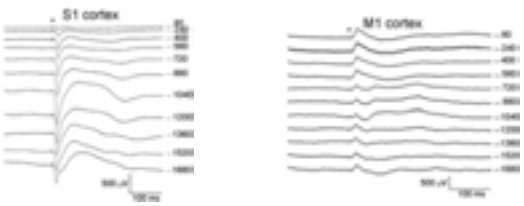

Fig. 4. Example of double recording with two chips from S1 (*left*) and M1 (*right*) cortexes. Scale bars: 100 ms and 500 μV. Stars indicate the whisker stimulus onset.

4 Conclusions

A thorough understanding of the neuronal activity in the brain is a basic requirement for the development of reliable brain-machine interfaces. To this aim, multiple recording and/or stimulation sites integrated at high spatiotemporal resolution are needed. The results presented in this work demonstrate the reliability of the TNCs in performing high-resolution recordings of evoked activity from the brain of anesthetized rats, thus paving the way to the application of EOSFETs multi-transistor arrays in brain-machine interfaces. The application of CSD to signals recorded in the presence of specific neuronal receptors agonists (like muscimol) or antagonists allows for the detailed analysis of the contributions to the cortical activity from different regions of the brain (like the thalamus).

Eventually, double implants demonstrated the possibility to record neuronal signals at the same time in two related regions, and open new perspectives on the use of TNCs in multiple implants to study the communication between correlated brain areas.

Acknowledgement

This work was funded by the European Commission, CyberRat project, Seventh Framework Programme (ICT-2007.8.3 Bio-ICT Convergence, 216528) and by the CA.RI.PA.RO. Foundation.

The authors are grateful to Prof. Peter Fromherz for providing them with the TNCs.

References

[1] Diamond M.E., von Heimendahl M., Knutsen P.M., Kleinfeld D., Ahissar E. (2008) 'Where' and 'what' in the whisker sensorimotor system. *Nature Review Neuroscience*, 9, 601-612.

[2] Prochazka A., Mushahwar V.K., McCreery D.B. (2001) Neural prostheses. *The Journal of Physiology*, 533, 99–109.

[3] Wise K.D., Anderson D.J., Hetke J.F., Kipke D.R., Najafi K. (2004) Wireless Implantable Microsystems: High-Density Electronic Interfaces to the Nervous System. *Proceedings of the IEEE*, 92, 76-97.

[4] Felderer F., Fromherz P. (2011) Transistor Needle Chip for Recording in Brain Tissue. *Applied Physics A*, 104, 1-6.

[5] Mahmud M., Pasqualotto E., Bertoldo A., Girardi S., Maschietto M., Vassanelli S. (2011) An automated method for detection of layer activation order in information processing pathway of rat barrel cortex under mechanical whisker stimulation. *Journal of Neuroscience Methods*,196, 141-150.

[6] Shimegi S, Akasaki T, Ichikawa T, Sato H. (2000) Physiological and anatomical organization of multiwhisker response interactions in the barrel cortex of rats. *The Journal of Neuroscience*, 20, 6241-6248.

[7] Swanson LW (2003) Brain Maps: Structure of the Rat Brain. Third ed. *London: Academic Press*.

[8] Wright N., Fox K. (2010) Origins of cortical layer V surround receptive fields in the rat barrel cortex. *Journal of Neurophysiology*, 103, 709-724.

[9] Roy N.C., Bessaih T., Contreras D. (2011) Comprehensive mapping of whisker-evoked responses reveals broad, sharply tuned thalamocortical input to layer 4 of barrel cortex. *Journal of Neurophysiology*, 105, 2421-2437.

Developing a thin-film electrode system to record *in vivo* cortical responses evoked by an artificial peripheral auditory device

Hiroyuki W. Kitamura[1], Jun Nishikawa[1], Takashi Tateno[1*]

1 Graduate School of Information Science and Technology, Hokkaido University, Sapporo, Japan
* Corresponding author. E-mail address: tateno@ist.hokudai.ac.jp

Abstract
In this report, we describe an extracellular recording system consisting of a 4-channel programmable amplifier on a chip and a thin-film electrode substrate. We first developed a soft and flexible 3-μm-thick polyimide film substrate supported on a 50-μm-wide square frame. Reducing the thickness of the substrate decreased its bending rigidity, potentially improving conformal contact with complex brain surfaces. For a microelectrode array recording system that can used *in vivo* and *in vitro*, we designed 4-channel programmable amplifier circuits on a 4.1 × 2.1 mm^2 chip using a 0.35-mm complementary metal–oxide–semiconductor (CMOS) process. We have characterized some of the individual components of the system and will evaluate the system as a whole in the near future. Finally, we describe possible applications of the system to detect small electrical signals from dissociated cortical neuronal cultures or *in vivo* brain tissue.

1 Introduction

Current auditory implants are effective for many individuals who are profoundly deaf or hard-of-hearing, particularly if cochlear or auditory brainstem implants are employed when patients are young. The sound quality obtained with current implants, however, is not optimal for many individuals. To help overcome this issue, we have developed a tool to record neural responses by artificially connecting acoustic sensors to the peripheral auditory nervous system and recording activity in the auditory cortex in response to electrical stimulation (Fig. 1). In this first report about our project, we address a sensing device and a CMOS large-scale integration (LSI) chip amplifier to record neural activity.

2 Materials and methods

A block diagram of the planned overall system is shown in Fig. 1. In this paper, we have focused on the last two blocks (thin film electrode and amplifier shown in gray).

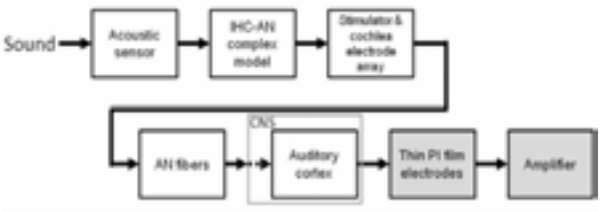

Fig. 1. Block diagram of an artificial peripheral auditory device and an *in vivo* recording system for the auditory cortex.

Recording electrode device

In conventional systems, thin electrode substrates (< 10 μm) are impractical for recording electrocorticograms from complex brain surfaces because the films are not sufficiently rigid and robust to be manipulated effectively during fabrication or recordings. In contrast to conventional wafer-based electronics, however, we used a 3-μm-thick polyimide film substrate that was soft and flexible with a 50-μm-wide, square supporting silicone frame (Fig. 2A). Reducing the thickness of the substrate decreased its bending rigidity, which may improve conformal contact with the surfaces of brain tissues.

Polyimide film substrates are fabricated using standard photolithography [1]. Briefly, a 100-nm-thick Al thin film was thermally deposited on Si substrates. This film functioned as a sacrificial layer for the flexible electrode array. The Al thin film was coated with polyimide (Photoneece, PW-1500, Toray) and ultraviolet lithography was used to pattern the substrate structure. The polyimide film was cured at 250°C for 2 hours under low-pressure conditions to avoid oxidizing the film. Electrodes were fabricated using a lift-off process. The surface was first coated with a lift-off photoresist (ZPN 1150, Zeon Corp.) and patterned to reflect the inverse structure of the electrodes. A thin indium–tin–oxide (ITO) film (thickness, 150 nm) was deposited on the entire region using radiofrequency magnetron sputtering. Then, 10-nm-thick Ti and 150-nm-thick Au films were deposited to cover the region occupied by the integrated electrodes. The thin films were patterned by dissolving the photo-

resist. The surfaces of the electrodes except for the contact pads were insulated with a coating of the polyimide film. Polyimide was removed from the contact pads via the ultraviolet lithography of the polyimide film. The insulation layer made of the polyimide film was cured at 250°C for 2 hours. We etched the sacrificial layer of aluminum film. Finally, the 200-μm-thick Si substrate in the sensing area was removed using deep reactive ion etching, whereas the 50-μm-wide supporting frame remained.

Four-channel CMOS amplifier

We also designed 4-channel programmable preamplifier and postamplifier circuits on a 4.1 × 2.1 mm^2 chip using a 0.35-μm CMOS process for a microelectrode array recording system that can be used *in vitro* or *in vivo*. The power consumption was 6 mW per channel, although it is not still satisfied. The cut-off frequencies of the high- and low-pass filters were selected to be 16 equal steps in the ranges of 1–100 Hz and 2–10 kHz, respectively. The gain of the preamplifier was 0, 20, or 40 dB, whereas that of postamplifier was 0, 6, 14, or 20 dB. The parameters of the LSI chip can be set using a personal computer and digital serial peripheral interface bus.

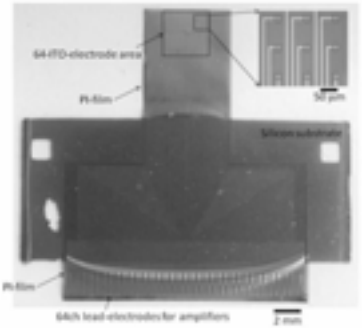

Fig. 2. Polyimide film substrate (3-μm-think) with a 50-μm-wide supporting frame and 64 ITO sensing electrodes.

3 Results

Recording electrode device

The thin polyimide film with a multielectrode array was fabricated using standard photolithography [1]. On the polyimide film substrates, a transparent, conductive ITO layer was deposited to form the electrode-array patterns via etching. In the standard pattern, electrode terminals were arranged in an 8 × 8 square grid (Fig. 2). In different versions of the polyimide film substrate, each terminal was a square with sides that were 10–50 μm in length, and neighboring terminals were separated by 50–250 μm. The different versions were intended to match the size of the primary auditory cortex in various rodents, including rats, mice, and guinea pigs. The ITO interface impedance in each channel was 2.0–2.5 kΩ at 1 kHz, whereas the reference/ground electrode impedance in the center of sensing area was 40–50 Ω at 1 kHz. Deep reactive ion etching was the most difficult part of the process because sensing electrodes were damaged by long periods of etching.

Four-channel CMOS amplifier

The CMOS LSI chip is shown in Fig. 3A. Amplifier circuits for electrical neural signals should be low-noise devices because extracellular signals are usually no more than a few hundred μV in the frequency range of 0.1–20 kHz. In our *in vitro* recording environment [2], the noise level of each channel in the system was 100–200 μV. The level was larger than we expected and is relatively high for the detection of neural activity.

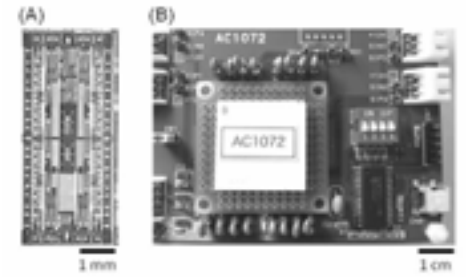

Fig. 3. (A) Four-channel programmable amplifier (4.1 × 2.1 mm^2 CMOS LSI chip). (B) Evaluation board to test characteristics of the device.

4 Conclusion

We have developed a bio-interface system containing a 3-μm-thick polyimide film and an ITO multielectrode array. The system is soft and flexible compared with conventional wafer-based electronic devices. Reducing the thickness of the substrate decreased the bending rigidity, which may improve conformal contact with brain surfaces. Next, we plan to employ this system to record evoked neural responses in the primary auditory cortices of rodents using both electrocorticography and optical imaging of voltage-sensitive dyes. The noise level in the current recording system, however, is larger than expected, and initial efforts will focus on resolving this issue.

Acknowledgements

This work was supported by the Funding Program for Next Generation World-Leading Researchers (NEXT program).

References

[1] Jimbo Y, Tateno T, Robinson HP. (1999): Simultaneous induction of pathway-specific potentiation and depression in networks of cortical neurons. *Biophys J, 76(2), 670–678.*

[2] Jimbo Y, Kasai N, Torimitsu K, Tateno T, Robinson HP. (2003): A system for MEA-based multisite stimulation. *IEEE Trans Biomed Eng, 50(2), 241-248.*

Fabrication and characterization of different electrode configurations on neural probes

Thomas Hertzberg[1*], Víctor Gordillo-González[2], Elena Tolstosheeva[1], Andreas Kreiter[2], Walter Lang[1]

1 Institute for Microsensors, -actuators and -systems, University of Bremen, Bremen, Germany
2 Brain Research Institute, University of Bremen, Bremen, Germany
* Corresponding author. E-mail address: thertzberg@imsas.uni-bremen.de

Abstract
This work presents the design, fabrication and characterization of neural probes. 15 different electrode configurations on multi-electrode-probes have been investigated. Additionally to the classic linear approach, there are configurations with tetrodes and electrodes at the border of the shaft. For packaging of the probes a rigid flex board with ZIF connector is used. A number of electrodes are currently in use for in-vivo measurements.

1 Introduction

Designing multi-electrode-probes for recording brain activity [1] leads to the challenge of placing a high number of electrodes into the brain cortex. In order to reduce mechanical impact on the brain, the size of the needles should be decreased to a minimum. However, in order to gather more information from the cortex, the number of electrodes should be as large as possible. The aim of this work is to find a balance between required space and gathered information.

2 Design and Fabrication

2.1 Electrode Layout

Needle electrodes with different electrode configurations have been designed and fabricated: linear, tetrode and border (Fig. 1).

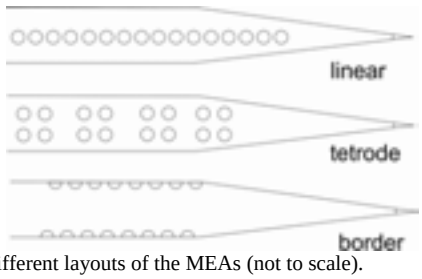

Fig. 1. Different layouts of the MEAs (not to scale).

Each shaft (length: 2.6mm, width: 140µm) contains 16 electrodes and one contact at the tip which acts as a reference electrode. Moreover, during implantation it is used to detect the moment when the probe penetrates the cortex and to monitor the implantation depth. The linear configuration is a classical approach which provides information on the depths of the cortex layers. Furthermore, the tetrode configuration adds a possibility to range the neurons via triangulation and the novel border configuration increases the span of measurable neurons by those situated on the back of the probe (Fig. 2 & 3).

Fig. 2. Active zone of electrodes.

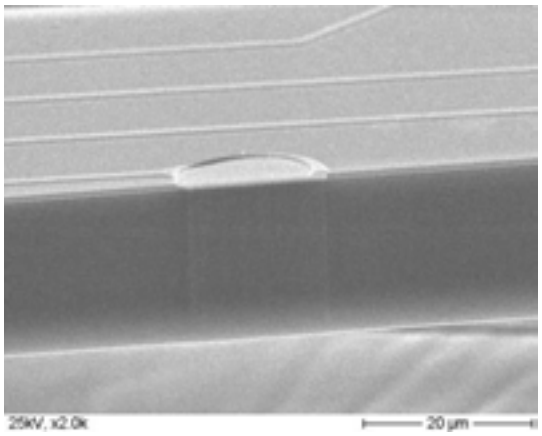

Fig. 3. SEM picture of border electrode at MEA edge.

There are 3 electrode sizes (100µm^2, 150µm^2 and 314µm^2). Additionally, the distance between the tetrode electrodes (d_1 in Fig. 4) is altered between 45µm, 65µm and 85µm whereas d_2 is kept constant at 200µm. This leads to 15 configurations.

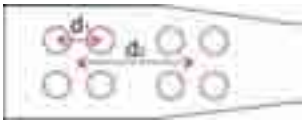

Fig. 4. Distances between tetrode electrodes.

2.2 Electrode Fabrication

SOI wafers (20µm device layer on 400µm handle wafer) are isolated with LPCVD silicon nitride. A 250nm platinum layer is sputtered and structured with a stack of chromium, gold and photoresist (PR) by combination of wet etching and physically etching (PC340, Ar plasma). After the platinum is structured, the conductors are isolated with a PECVD silicon nitride (thickness and stress of both nitrides are chosen to minimize the remaining stress on the probe shaft). The PECVD silicon nitride is opened at the electrode sites (Fig. 3) and the bondpads. After DRIE etching the front and back and wet etching the oxide layer, the probes are separated.

Each probe is glued (Delo Katiobond GE680 [2]) to the edge of a rigid flex board (left image in Fig. 5). The 17 contacts are Al-wire bonded and coated in epoxy (Delo Katiobond GE680, right image in Fig. 5). The rigid flex board containing the MEA is electrically ZIF connected to a headstage (Plexon HST/8o50-G20-TR) via an adapter (Fig. 6). Thus the ZIF connectors replace soldering of connectors to every probe. The flexible cable additionally offers more flexibility during characterization.

Fig. 5. MEA glued at tip of rigid flex board.
Left: before bonding, right: bonded and coated.

Fig. 6. MEA at tip of rigid flex board, with OMNETICS adapter for headstage (not mounted).

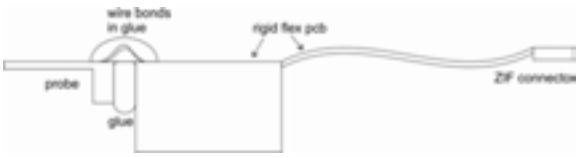

Fig. 7. Schematic view of the mechanical and electrical connection of the probe to a rigid flex board (not to scale).

3 Results

The electrodes were characterized using electro impedance spectroscopy. Results for one electrode are shown in Fig. 8.

All electrodes are currently being characterized in-vivo to evaluate the influence of electrode size and configuration on signal quality during acute recordings in rats.

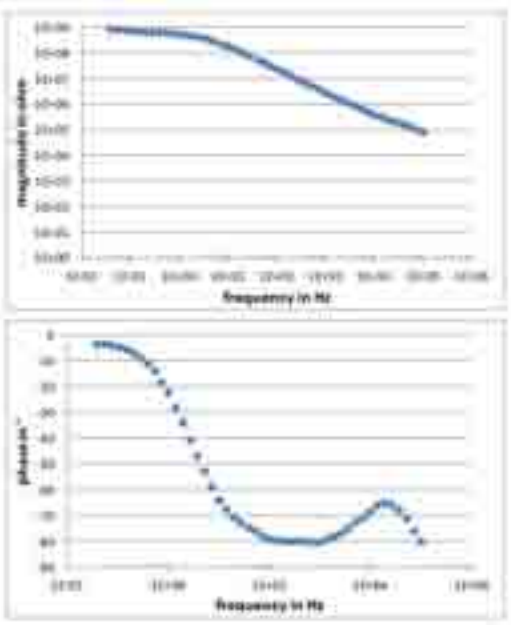

Fig. 8. EIS measurement of one electrode.

4 Conclusion and Outlook

A number of electrode configurations are fabricated, electrically characterized and are currently in use for in-vivo measurements.

The usage of rigid flex boards saves time and effort by replacing soldering with ZIF-connectors.

The next step will be replacing the rigid flex cable by a flexible polyimide cable to allow miniaturization of the cable and long-time implantation.

Acknowledgement

We thank the University of Bremen for subsidizing this work within the Forschungsschwerpunkt Neurotechnologie.

References

[1] Norlin P., Kindlundh M.G., Mouroux A., Yoshida K., Hofmann U.G. (2002). A 32-site neural recording probe fabricated by DRIE of SOI substrates. *J. Micromech. Microeng*. 12, 414–419.

[2] Delo Katiobond GE 680 http://www.delo.de.

High density micro-electrocorticography (µECoG) using flexible silicon electronics

Dae-Hyeong Kim[1], John A. Rogers[2], Brian Litt[3,4], Jonathan Viventi[5,6*]

1 School of Chemical and Biological Engineering, Seoul National University, Seoul, Korea
2 Department of Materials Science and Engineering, Beckman Institute for Advanced Science and Technology and Frederick Seitz Materials Research Laboratory, University of Illinois at Urbana-Champaign, Urbana, Illinois, USA
3 Penn Epilepsy Center, Department of Neurology, Hospital of the University of Pennsylvania, Philadelphia, Pennsylvania, USA
4 Department of Bioengineering, University of Pennsylvania, Philadelphia, Pennsylvania, USA
5 Department of Electrical and Computer Engineering, Polytechnic Institute of New York University, Brooklyn, New York, USA
6 Center for Neural Science, New York University, New York, New York, USA
* Corresponding author. E-mail address: jviventi@nyu.edu

Abstract
Current implantable brain devices for clinical and research applications require that each electrode is individually wired to a separate electronic system. Establishing a high-resolution interface over broad regions of the brain is infeasible under this constraint, as an electrode array with thousands of passive contacts would require thousands of wires to be individually connected. To overcome this limitation, we have developed new implantable electrode array technology that incorporates active, flexible electronics. This technology has enabled extremely flexible arrays of 720 and soon thousands of multiplexed and amplified sensors spaced as closely as 250 µm apart, connected using just a few wires.

1 Introduction

Due to the prior technological limitation of wiring each electrode individually, it has not been possible to record high density, 2-dimensional (2-D) µECoG. In initial experiments using a 360-sensor array (10 mm x 9mm) we discovered recurring spatio-temporal (ST) patterns in a feline model of epilepsy, motivating new analytical methods for studying µECoG signals and continued electrode development towards higher density arrays with broader coverage.

Fig. 1. High-resolution (500 µm spacing), flexible, active electrode array with 360 amplified and multiplexed electrodes. Only 39 wires are needed to sample from all of the 360 electrodes simultaneously.

2 Methods

Using a 360 channel, high-density active electrode array with 500 µm resolution, we explore ST patterns of local field potential spikes that occur within the surface area traditionally occupied by a single clinical electrode. We record subdural micro-electrocorticographic (µECoG) signals in vivo from a feline model of acute neocortical epileptiform spikes and seizures induced with local administration of the GABA antagonist picrotoxin. To analyze the data, we employ a clustering algorithm to separate 2-D spike patterns and to isolate distinct classes of spikes unique to the ictal state. Our findings indicate that the 2-D patterns can be used to distinguish seizures from the non-seizure state.

3 Results

We find two statistically significant ST patterns that uniquely characterize ictal epochs. Additionally, we present the most recent development of our array technology and examples of retinotopic and tonotopic maps produced from in vivo recordings.

4 Conclusion

New high density micro-electrocorticographic (µECoG) devices yield an unprecedented level of spatial and temporal resolution for recording distributed neural networks. Our characterization of 2-D spikes demonstrates that millimeter-scale ST spike dynamics contain useful information about ictal state. Further work will investigate whether patterns we identify can increase our understanding of seizure dynamics and their underlying mechanisms and inform new electrical stimulation protocols for seizure termination. µECoG is only one of the many possible applications of this technology, which also include cardiac, peripheral nerve and retinal prosthetic devices.

Acknowledgement

This material is based upon work supported by the National Science Foundation under grant DMI-0328162 and the U.S. Department of Energy, Division of Materials Sciences under Award No. DE-FG02-07ER46471, through the Materials Research Laboratory and Center for Microanalysis of Materials (DE-FG02-07ER46453) at the University of Illinois at Urbana-Champaign. J.A.R. acknowledges a National Security Science and Engineering Faculty Fellowship. Work at the University of Pennsylvania is supported by the National Institutes of Health Grants (NINDS RO1-NS041811, NINDS R01 NS 48598), the Dr. Michel and Mrs. Anna Mirowski Discovery Fund for Epilepsy Research and the Julie's Hope Award from Citizens United for Research in Epilepsy (CURE). J.V. is supported by a Taking Flight Award from Citizens United for Research in Epilepsy (CURE) and NYU WIRELESS.

Author Index

Author Index

Light Solutions for Electrophysiology

Rapp OptoElectronic

Pattern and Movable Spot Illumination Devices for Microscopy

IDEAL FOR MEA APPLICATIONS!

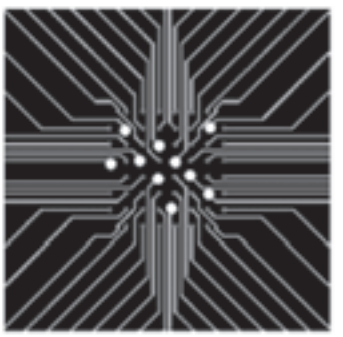

Versatile modular systems

Shown: MicroMATRIX – DMD based pattern illumination device on Zeiss AxioObserver

Simultaneous or sequential illumination of selected areas

Optical design and customized solutions

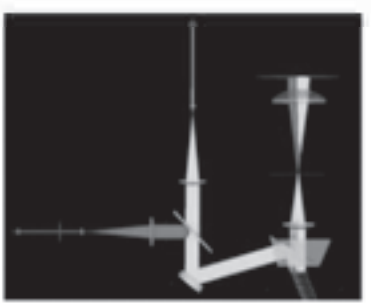

Electrophysiology combined with:

- Photostimulation
- Photoactivation
- Photoconversion
- Optogenetics
- Drug Photorelease
- Photolysis/Uncaging

Rapp OptoElectronic GmbH
Tel. +49 4103 701 890

www.rapp-opto.com
info@rapp-opto.com

Wireless *in vivo* System

Wireless-System

- All-in-one solution
- 4, 8 or 16 channels
- Sampling rate: up to 40 kHz per channel
- Resolution: 16 bit

multichannel systems

Innovations in Electrophysiology

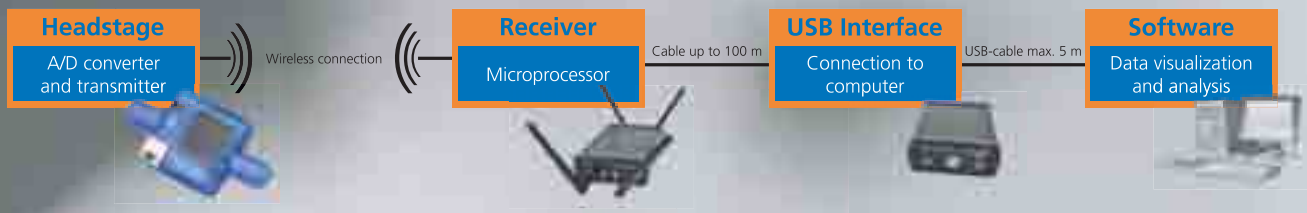

Visit us at our booth and see our latest products

New Generation of MEA-Systems

MEA2100-System

- Flexible contact unit
- 120 recording channels
- Integrated stimulation
- Gain and bandwidth adjustable via software

High Density MEAs with 256 Electrodes

256MEA30/8iR-ITO

- 256 electrodes
- 30 µm interelectrode spacing
- 8 µm electrode diameter
- High density array for detailed analysis of electrical activity

www.multichannelsystems.com

ISSN 2194-5519